CORRELATION OF COAL LIQUEFACTION REACTIVITY WITH COAL PROPERTIES

R. M. Baldwin

Chemical and Petroleum-Refining Engineering Department
Colorado School of Mines
Golden, Colorado 80401

S. L. Durfee and K. J. Voorhees

Chemistry/Geochemistry Department
Colorado School of Mines
Golden, Colorado 80401

ABSTRACT

A narrow suite of bituminous coals chosen from the DOE/Penn State sample bank has been hydrogenated in a batch stirred autoclave. Rates of conversion to THF-solubles have been measured, and the data modeled using a pseudo-second order rate expression. Extent of conversion and rate of conversion of the coals in the suite have been correlated to coal compositional parameters and structural features. Recent data on reactivity correlations with information from pyrolysis/mass spectrometry and C-NMR are presented.

INTRODUCTION

The relationship between coal composition and hydrogenation reactivity has been studied extensively for over 60 years. As early as 1920, Bergius (1) recognized that coal with less than 85% carbon (daf) made poor liquefaction feedstocks. Francis (2) suggested that reactivity was related to rank, and many other researchers have attempted to correlate reactivity with rank (3,4,5). Neavel (6) has shown that a relationahip does exist between rank and rate of coal hydrogenation to benzene solubles. Fischer (7) and his co-workers at the Bureau of Mines in Bruceton developed mathematical models for coal liquefaction reactivity based on a petrographic analysis of the parent coal. This concept was expanded and greatly elaborated upon by Given et al. (8,9,10,11), who established reactivity ensamples by statistical factor analysis of a large number of samples. Recently, Furlong et al. (12) studied the use of different definitions for coal reactivity, and demonstrated the utility of a definition based on kinetic parameters when ranking coals of very similar properties.

All studies relating coal properties to coal hydrogenation reactivity are hampered by the crude tools available for chemical and structural analysis of the prime reactant. Pyrolysis, followed by mass spectroscopy (Py/MS) of the products at low energy levels provides a new tool for coal analysis that can provide data on structural features that previously could not be obtained (13). Voorhees et al. (14), and Meuzelaar et al. (15) have recently reported correlations of structural data from coal Py/MS and coal hydroliquefaction reactivity.

EXPERIMENTAL

A series of bituminous coals from the DOE/Penn State sample bank were hydrogenated in a batch stirred autoclave reactor into which coal was injected. Table 1 presents data on coal properties in the suite. All coals were low sulfur, in order to minimize catalytic effects due to H_2S and iron pyrite. Details of the run procedure and reaction equipment used have been presented elsewhere (12). Coal samples were pyrolysed using a Fisher Curie-Point pyrolyser in conjunction with an Extranuclear SpectrEL mass spectrometer. Curie point wires composed of Ni (510 C final temperature) and low energy (14 ev) electron impact were used throughout for data acquisition. Mass spectral data were collected on a Hewlett-Packard 2100 S computer, and the data then analysed using ARTHUR (Infrometrix Inc., Seattle, Wa.). Solid state ^{13}C-NMR was performed at the NSF Regional Center for NMR at Colorado State University, Department of Chemistry.

DISCUSSION AND RESULTS

Rate data on coal conversion to THF-solubles was reduced using a pseudo-second

order kinetic model of the form:

$$\frac{dC}{dt} = -k_f C^2 + k_r P^2$$

Here k_f and k_r (with units: mass fraction · min^{-1}) are the forward and reverse rate constants for the reaction:

$$C \underset{k_r}{\overset{k_f}{\rightleftharpoons}} P$$

As previously, coal (C) was defined in these expressions as THF-insoluble organic matter, which included unreacted coal as well as high-molecular-weight moieties and coke produced by free radical recombination and condensation reactions. Parameter P was defined as all products soluble in THF.

Using conversion (X) defined as the fraction of coal reacted to THF-soluble materials, the mass balance may be rewritten as a function of the conversion:

$$\frac{1}{k_f} \frac{dX}{dt} = (-X)^2 - \left[\frac{1}{K}\right] X^2$$

Here C = 1 - X, P = X, and K, the equilibrium constant for the reaction, is given by k_f/k_r. Data for each of the 11 coals which were successfully run were processed by non-linear parameter estimation methods (16) to obtain values for the parameters k_f and k_r in the second-order model. These data are given in Table 2 as are values for the equilibrium constant K. Also in Table 2 are values for the 60 min conversion to THF-soluble materials (X(60)).

Data on the aliphatic-to-aromatic carbon ratios in the parent coal samples plotted against kinetic reactivity (k_f) are shown in Figure 1. With one exception, the correlation is one of increasing reactivity with increasing aliphatic to aromatic carbon ratio. This was to be expected, as it has been well established that the more aliphatic coals convert more readily in comparison with the more aromatic coals. The correlation with rate of conversion (Figure 1) is fairly good, thus substantiating the importance of aliphatic carbon-carbon bonds in coal hydrogenation. Aliphatic/aromatic carbon ratio also correlates fairly well with extent of reaction (X(60)), but not with reactivity as measured by the pseudo-equilibrium constant (K) from Table 2. Overall however, the correlation of aliphatic to aromatic carbon is the best with reactivity as defined in a kinetic fashion by the forward rate constant.

Coals from the reactivity suite shown in Table 1 were run in triplicate on the Py/MS, and an average spectrum obtained which represented a composite spectrum for 9 of the 11 coal hydrogenated. Data from Py/MS of the coal suite were reduced by ARTHUR, and a statistical factor analysis performed on the entire data set. From the factor analysis, 4 factors were identified which accounted for over 72% of the variation in the data set. The factors and the percent of total variation explained were as follows:

FACTOR	VARIATION ACCOUNTED FOR	CUMULATIVE VARIATION
1	24.3%	24.3%
2	23.1%	47.4%
3	14.8%	62.1%
4	10.0%	72.2%

These factors were utilized in Karhunen Loeve (K-L) plots obtained from ARTHUR, in order to ascertain whether any clustering into reactivity groupings could be obtained. As shown in Figure 2, a plot of K-L factor 3 vs K-L factor 2 does produce such a clustering, with the higher reactivity coals in the suite falling towards the upper right hand corner of the plot, and the less reactive coals clustering in the lower left. These data may indicate the utility of pyrolysis/mass spectrometry as a rapid screening tool for coal reactivity.

The data set from Py/MS of the coal suite can be rotated towards any other factor, and composite spectra calculated which demonstrate relationships between chemical moieties in the spectrum and the chosen factor. Such correlations have

recently been reported by Baldwin (17) on a suite of coals with a very broad geographical and rank distribution. Further analysis of this data set was performed by rotating the composite spectra towards reactivity, with reactivity defined in each of the three manners listed above (k_f, X(60), and K). The results of these analyses are presented in Figures 3-5. As before, the only meaningful correlation seems to be when reactivity is defined as a kinetic reactivity. Figure 3 indicates that a strong positive correlation exists between a homologous series of high molecular weight naphthalenes and coal reaction rate. Further analysis of Py/MS data set is continuing, and will be presented later.

LITERATURE CITED

1. Graham, J. L. and Skinner, D. G., J. Soc. Chem. Ind., 1929, 48.
2. Francis, W., Fuel, 1932, 11, 171.
3. Petrock, A. J., Gaigher, B. and Groenewoud, P., J. Chem., Met. Min. Soc. South Africa, 1937, 38.
4. Wright, C. C. and Sprunk, G. C., Penn State College, Mineral Ind. Exp. Sta. Bull., 1939, 28.
5. Fisher, C. H., Sprunk, G. C., Eisner, A., Clarke, L., Fein, M. L. and Storch, H. H., Fuel, 1940, 19, 132, 162.
6. Neavel, R. C., Fuel, 1976, 55, 237.
7. Fisher, C. H., Sprunk, G. C., Eisner, A., O'Donnell, H. J., Clarke, L. and Storch, H. H.,"Hydrogenation and Liquefaction of Coal, Part 2 Effect of Petrographic Composition and Rank of Coal", U. S. Bureau of Mines Technical Paper 642, 1942.
8. Given, P. H., Cronauer, D. C., Spackman, W., Lovell, H. L., Davis, A. and Biswas, B., Fuel, 1975, 54, 34.
9. Given, P. H., Cronauer, D. C., Spackman, W., Lovell, H. L., Davis, A. and Biswas, B., Fuel, 1975, 54, 40.
10. Abdel-Baset, M. B., Yarzab, R. F. and Given, P. H., Fuel, 1978, 57, 89.
11. Yarzab, R. F., Given, P. H., Spackman, W. and Davis, A., Fuel, 1980, 59, 81.
12. Furlong, M. W., Baldwin, R. M., and Bain, R. L., Fuel, 1982, 61, 116.
13. Masters, W. L., Van de Meent, P., Schuyl, P. J. W., De Leeuw, J. W., Schenck, P. A., and Meuzelaar, H. L. C., "Analytical Pyrolysis", Elsevier, 1977.
14. Voorhees, K. J., Durfee, S. L., and Baldwin, R. M., "Proc. ACS Conference on Macromolecular Secr. Symp.", Atlanta, 1981.
15. Meuzelaar, H. L. C., McClennen, W. H., Tomlinson, J. H., and Pope, D. L., "Proc. Int. Conf. Coal Science", Dusseldorf, 1981.
16. Bard, Y., "Non-Linear Parameter Estimation", IBM Share Program No. 360D-13.6.003.
17. Baldwin, R. M., DOE Principal Investigators Conference, Pittsburgh, 1982.

Table 1 Parent coal analyses

Coal				Ultimate analysis (wt % dmmf (Parr))					Maceral comp. (vol % dmmf)			Sulphur (wt % daf)	
PSOC No.	Rank	Seam	State	C	H	N	O	Min. matter	vit	iner.	lipt.	pyr.	tot.
001	hvAb	Upper Elkhorn	KY	84.36	5.46	1.54	8.64	4.71	54.8	21.7	23.5	0.10	0.81
056	hvCb	Arizona No. 2	AZ	77.37	5.90	1.34	15.39	6.92	83.9	12.8	3.3	0.01	0.45
071	hvCb	Rogers	WA	78.00	5.88	1.68	14.44	7.41	86.5	7.7	5.8	0.07	0.58
107	hvBb	Brazil Block	IN	81.97	5.07	1.37	11.59	6.42	62.4	14.6	23.0	0.11	0.53
151	hvCb	Lower Blue	NM	78.37	5.87	1.24	14.51	5.80	78.6	10.8	10.6	0.05	0.47
437	hvAb	Utah B	UT	80.26	6.20	1.47	12.07	5.63	92.1	6.0	1.9	0.11	0.51
444	hvBb	Colorado E	CO	78.87	6.47	1.57	13.09	2.46	94.4	3.9	1.7	0.06	0.46
456	hvAb	Blind Canyon	UT	79.49	6.43	1.58	12.50	4.91	88.7	10.2	1.1	0.06	0.37
577	hvCb	(unnamed)	TX	79.97	5.68	1.32	13.04	25.51	87.2	11.7	1.1	0.17	1.17

Table 2 Estimated second-order rate parameters

Coal (PSOC No.)	k_f*	k_r*	K	a	X (60)
001	0.0672 ± 0.0103	0.0094 ± 0.0069	7.17	0.728	0.724
056	0.1655 ± 0.0319	0.0107 ± 0.0080	15.51	0.797	0.828
071	0.1358 ± 0.0253	0.0068 ± 0.0066	20.01	0.817	0.837
107	0.0839 ± 0.0064	0.0018 ± 0.0023	45.94	0.871	0.810
151	0.1673 ± 0.0265	0.0143 ± 0.0076	11.71	0.774	0.801
437	0.1997 ± 0.0253	0.0082 ± 0.0046	24.34	0.831	0.850
444	0.1057 ± 0.0162	0.0002 ± 0.0039	485.33	0.957	0.872
456	0.2174 ± 0.0363	0.0055 ± 0.0051	39.81	0.863	0.884
577	0.1369 ± 0.0169	0.0157 ± 0.0063	8.74	0.747	0.769

* 95% confidence limits on k_f and k_r estimates.

Rate constants have units of (mass fraction min^{-1})

FIGURE 1

ALIPHATIC/AROMATIC CARBON RATIO VS FORWARD RATE CONSTANTS

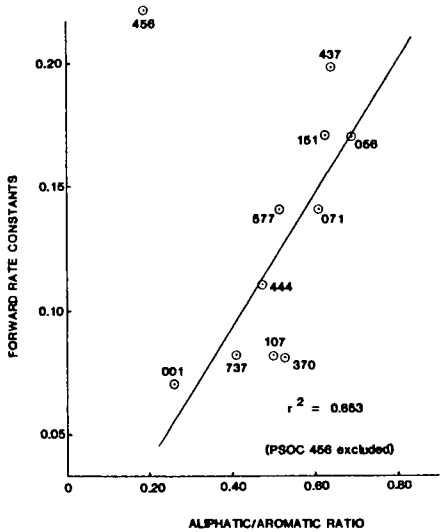

FIGURE 2

KARHUNEN-LOEVE PLOT

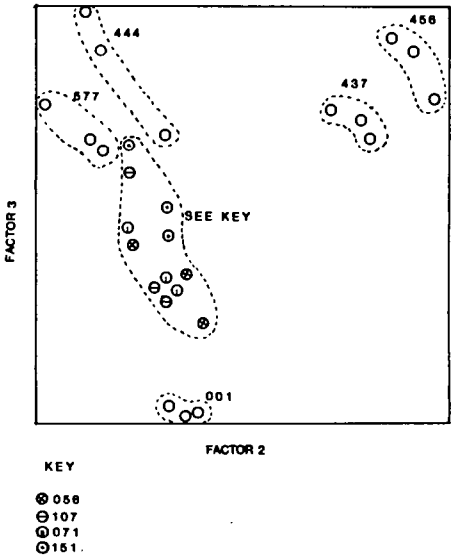

FIGURE 3

FACTOR SPECTRUM, KINETIC REACTIVITY

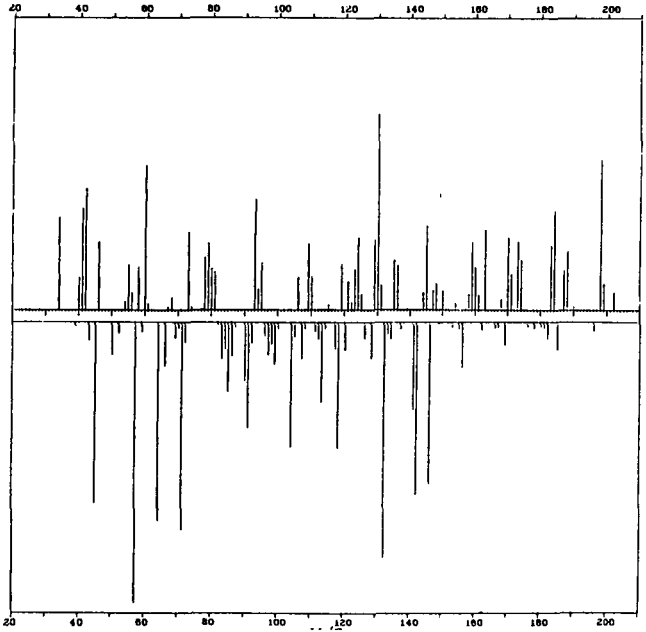

FIGURE 4

FACTOR SPECTRUM, X(60) REACTIVITY

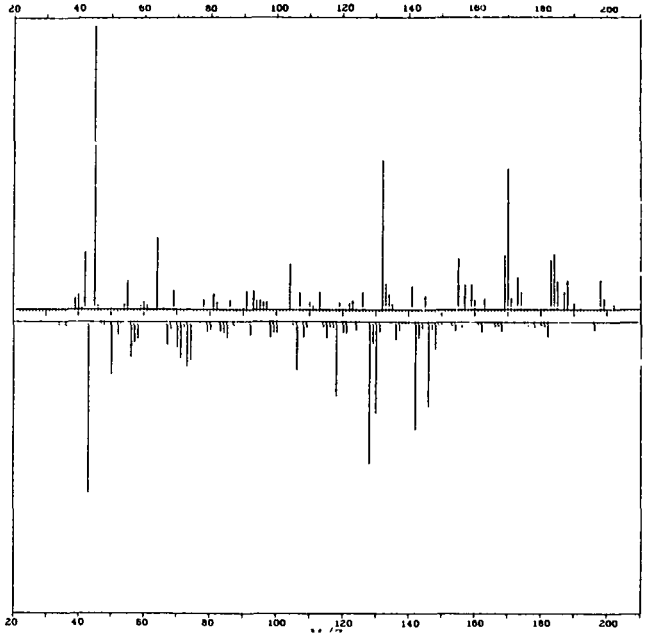

FIGURE 5

FACTOR SPECTRUM, EQUILIBRIUM REACTIVITY

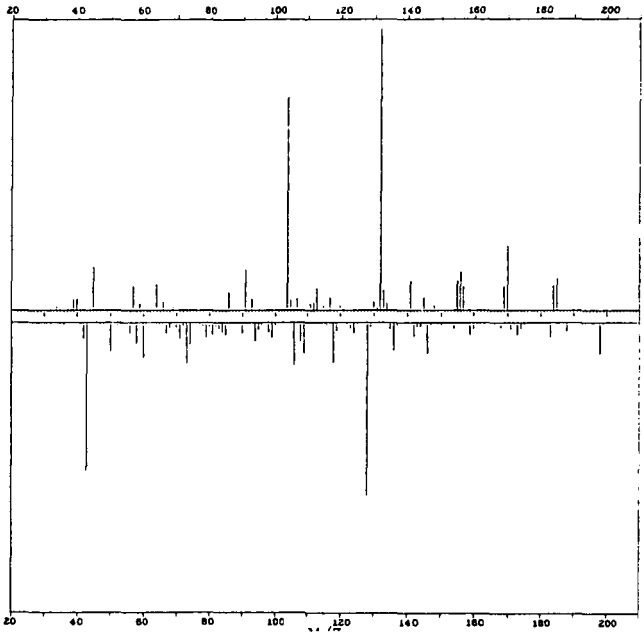

CHARACTERIZATION OF SHORT CONTACT TIME DISSOLUTION PRODUCTS FROM A SERIES OF VITRINITE-RICH COALS

Randall E. Winans, Hsiang-Hui King, Robert L. McBeth and Robert B. Botto

Chemistry Division, Argonne National Laboratory, Argonne, IL 60439

The objective of this study is to identify the transformations that occur in coal organic structural units during liquefaction. To ensure that mainly primary reactions are being observed, the study has focused on short contact time dissolution in donor solvent media. It has been shown by Neavel that under SCT conditions a significant amount of bituminous coals can be dissolved (1). Whitehurst et al. have reported an in depth study of the SCT reaction on several coals. In our study we have examined the relationship between the compositional parameters of the coals and both their reactivity and product chemical characteristics. Given and his co-workers examined the effects of coal characteristics on longer contact time liquefaction (3-5). This work by Given is one of the first applications of statistical analysis to this type of problem. However, either benzene (3) or ethyl acetate (4,5) was used to extract the products and conversion was calculated from the weight of the insoluble residue. Since the benzene insoluble, pyridine soluble fraction, often called asphaltols or preasphaltenes, is a key intermediate in the initial stage of coal liquefaction (6,7), we would like to correlate the solubility in hexane, benzene/ethanol, and pyridine with compositional parameters.

We have recently studied the SCT reaction of separated coal macerals (8). In order to separate the macerals by density gradient centrifugation it was necessary to demineralize the coals with HCl and HF and grind them to less than 3 microns. It has been shown that mineral matter exerts a beneficial and possibly unpredictable effect on the coal dissolution (2,9-11). To examine the effects of the demineralization and grinding, a series of 21 of the treated unseparated coals were studied. The original raw coals were obtained from the Penn State Coal Sample Bank. It was observed using multivariate analysis that product solubility, which was used to determine conversion, can be predicted from linear combinations of carbon, hydrogen, density and exinite content.

After considering these results, we felt that in order to make the study more complete, it would be useful to study another set of coals which had not been demineralized. Dr. Richard Neavel consented to supply us with a set of 25 coals from the Exxon Coal Library. These samples are essentially "premium" coals which have been protected from oxidation and are homogeneous. The preparation and some of the properties have been described (12). An advantage of using this set of coals is that other structure studies are in progress in other laboratories and in the Fundamental Chemistry of Coals program at ANL. This information will be useful in interpreting the results from the SCT reaction.

Experimental

SAMPLES Analytical data for the demineralized coals are given in Table 1. The Exxon coals are described in reference 12.

SCT REACTION Typically, 100 mg of coal sample and 300 mg of tetralin were transferred to a thick wall glass tube flushed with nitrogen, sealed, and plunged into a preheated fluidized sand bath at 419°C for 6 minutes. For the demineralized coals 60 mg coal and 240 mg of tetralin were used. After the glass tube was cooled in air and opened, the contents were washed out with hexane, agitated in an

ultrasonic bath, and centrifuged. The supernatant was removed and the insoluble part was washed with three portions of hexane. The hexane insoluble fraction was then extracted successively with portions of benzene/ethanol (1:1) mixture, and pyridine. Each insoluble fraction was dried under vacuum at 60°C (80°C for the pyridine insoluble fraction) and weighed. Conversion was calculated as follows:

$$\text{conversion } (\%,\text{daf}) = \frac{\text{wt. of coal} - \text{wt. of insoluble fraction}}{\text{wt. of coal } (1-\%\text{ ash})} \times 10^4$$

The benzene solubility was dropped for the Exxon coals when it was found that with the demineralized coals only a few percent more were soluble in benzene compared to hexane.

Approximate molecular weight or size distribution was determined by gel permeation chromatography for the benzene-ethanol soluble products for both the series of demineralized coals and for the Exxon coals. The samples were eluted with THF through a set of three ultra-styragel columns (Waters Associates) having 1,000, 500 and 100 Å nominal pore diameters respectively. The size exclusion limit was approximately 10,000. This set of columns was calibrated using several polymers and large nonpolymeric molecules that could be found in coals. The samples were detected using a UV spectrometer set at 254 nm, and the output digitized and stored using a microcomputer (DEC LSI 11/23). The data was further processed on a DEC VAX 11/780 computer.

Proton NMR data were obtained on the benzene/ethanol soluble product from the reactive Exxon coals. Pyridine-d_5 was used as the solvent and spectra were obtained on a Nicolet 200 MHz instrument. Using the measured areas under the aliphatic and aromatic regions, the fraction of aromatic carbons (fa) was determined from the Brown-Ladner equation (11).

RESULTS AND DISCUSSION

For both sets of coals the first aspect of the data which we examined was the relationship between composition of the whole coal and the yield of the soluble products. The benzene-ethanol solubility data which was calculated on a wt% of coal (dmmf) is shown in Figure 1 as a function of carbon content. A multivariant analysis was performed on this data using the Statistical Analysis System (SAS) package. The correlations observed for these samples were much poorer than those obtained for the set of demineralized coals. Some representative R^2 values are given for a selected combination of variables.

	Hexane		Benzene/EtOH		Pyridine	
	DC	Exxon	DC	Exxon	DC	Exxon
C	0.919	0.781	0.843	0.130	0.565	0.027
C,H	0.957	0.841	0.918	0.490	0.781	0.477

DC = demineralized coals.

A plot of predicted and observed benzene-ethanol solubility is shown in Figure 2. This difference found between the two sets of coals may be due to at least two reasons. First, the Exxon coals were not demineralized, and the effects of mineral matter on SCT dissolution may be critical and unpredictable. It should be emphasized that the Exxon coals were processed to give low mineral matter content and in the multivariant analysis, inclusion of the high mineral matter coals did not significantly affect the analysis. Secondly, there is a difference in particle

size, which should influence the variations in yields to a lesser degree. One would expect the smaller particle size samples to give a higher solubility, but it is difficult to deduce why the difference in correlation with composition results. It has been reported by Whitehurst et al. (2) that demineralization increases yields at short contact times especially for lower rank coals.

It is apparent from Figure 1 that for the lower rank coals the demineralized ones are more reactive than the untreated coals. This could account for the more predictable behavior with rank of the demineralized coals. For the Exxon coals in this study and as has been shown in other studies (2) the lower rank coals are less reactive under SCT conditions compared to the high volatile bituminous coals.

Variations observed in molecular size distribution as a function of composition appears to be more similar between the two sets of coals. A relative molecular weight or size distribution was obtained for all the coal products under identical conditions. The absolute values determined for the molecular weights cannot be trusted for coal derived materials. However, comparisons of the results from coal products run under standard conditions can be useful. An example of one of the chromatograms is shown in Figure 3. Most of the chromatograms had inflection points at molecular weights of approximately 300 and 700. All of the chromatograms were divided into three areas at 0-300, 300-700, and 700-10,000, and the relative areas of the three regions determined.

In the initial SCT study of the maceral concentrates, it was observed that the average molecular weight decreased with decreasing conversion (8). In both sets of whole coals this trend is followed. In order to look at the results in a more quantitative way, principal component analysis has been applied to these data. This approach has been eloquently described by Yarzab et al. (4). The objective of this analysis is to identify variables, such as original coal composition and molecular weight distributions, which change in a parallel fashion. The variables that meet this criteria are assigned to a "factor". A coefficient is calculated for each variable in each factor. The closer the coefficient or loading is to ±1.0 the better the variable correlates with that factor. Loadings with opposite signs indicated that these properties are inversely correlated.

The results of the principlal component analysis are shown in Tables 2 and 3 for the demineralized and Exxon coals respectively. Coefficients of less than ±0.5 have been left out since they are less significant and it makes it easier to see the correlations. In both sets of data the carbon content is directly correlated with the LMW band and inversely with the HMW. The reverse is true for the oxygen content and for the Exxon set, volatile matter, which inversely correlates with LMW and directly with HMW. The MMW band is independent of any of the variables used in this analysis and was assigned the 4th and least significant factor. The values at the bottom of each table indicate the contribution made by each factor in explaining variance observed. It appears that the molecular distribution of the products in SCT dissolution is a function of rank. A plot of the high molecular weight area as a function of carbon content in Figure 4 appears to confirm this observation.

The fa values were determined by NMR for the benzene-ethanol solubles from the Exxon coals. Factor analysis indicated that the fa values inversely correlated with hydrogen content of the coals and with solubilities in both benzene-ethanol and pyridine. A plot of fa's as a function of hydrogen content is shown in Figure 5. These results indicate a problem with using solubility to determine conversion. As expected the more aliphatic products tend to be more soluble. The same amount of bond cleavage in a more aromatic coal could have a lower yield by solubility. From this analysis it could be expected that fa values of the products should approximately follow the solubility. This is what is observed in Figure 6. Although there is significant scatter in the points the trend is apparent.

Conclusions

Apparently yields from SCT dissolution of finely ground, demineralized coals can be more accurately predicted than with the dissolution of raw coals. Gross product chemical characteristics do not seem to differ to a large extent. Presently we are examining more detailed chemical characteristics of the various products using pyrolysis mass spectrometry with precise mass measurements.

Acknowledgements

The authors thank the Pennsylvania State University Coal Sample Bank, Professor J.C. Crelling of Southern Illinois University, Professor L. Anderson of the University of Utah, and Dr. R. Neavel of Exxon Research and Engineering Company, for providing the whole coal samples. We are also grateful to Dr. G.R. Dyrkacz and Ms. C.A.A. Bloomquist for demineralizing the coals, Ms. K. Henriksen for obtaining the CPC data, and Mr. A. Kostka for the NMR results. Work performed under the auspices of the U.S. Department of Energy, Fossil Energy program under contract W-31-109-ENG-38.

References

(1) Neavel, R.C., Fuel 55, 237 (1976).
(2) Whitehurst, D.D., Michell, T.O. and Farcasiu, M., "Coal Liquefaction," Academic Press, NY p. 161 (1980).
(3) Abdel-Baset, M.B., Yarzab, R.F., and Given, P.H. Fuel 57, 89 (1978).
(4) Yarzab, R.F., Given, P.H., Spackman, W. and Davis, A. Fuel 59, 81 (1980).
(5) Given, P.H., Schleppy, R. and Sood, A. Fuel 59, 747 (1980).
(6) Farcasiu, M., Mitchell, T.O. and Whitehurst, D.D. CHEMTECH 7, 680 (1977).
(7) Neavel, R.C., "Coal Plasticity Mechanism: Inferences from Liquefaction Studies," in Coal Science, Vol. 1, Ed. M.L. Gorbaty, J.W. Larsen, and I. Wender, Academic Press, NY P. 1 (1982).
(8) King, H.H., Dyrkacz, G.R. and Winans, R.E. (submitted to Fuel).
(9) Guin, J.A., Tarrer, A.R., Prather, J.W., Johnson, D.R. and Lee, J.M. Ind. Eng. Chem. Proc. Des. Dev. 17, 118 (1978).
(10) Guin, J.A., Tarrer, A.R., Lee, J.M., Lo, L., and Curtis, C.W. Ind. Eng. Chem. Proc. Des. Dev. 18, 371 (1979).
(11) Garg, D. and Givens, E.N. Ind. Eng. Chem. Proc. Des. Dev. 21, 113 (1982).
(12) Neavel, R.C., Smith, S.E., Hippo, E.J., and Miller, R.N., Preprint, Fuel Division, ACS 25(3), 246 (1980).; Proceedings of International Conference on Coal, Dusseldorf, 1981, P. 1 (1981).
(13) Brown, J.K. and Ladner, W.R. Fuel 39, 87 (1960).

TABLE 1

Analytical Data for Demineralized Coals

Coal	%C[a]	%H[a]	%N[a]	%S[a]	%O[a,b]	%Ash	%E[c]	%V[c]	%I[c]	Density
PSOC-106	80.0	4.4	1.3	0.8	13.5	0.4	19.0	35.1	45.9	1.328
PSOC-107	78.7	4.7	1.5	0.4	14.7	0.1	13.1	69.5	17.3	1.301
PSOC-124	82.8	6.9	1.2	1.0	8.1	1.2	56.5	14.6	28.8	1.195
PSOC-151	75.0	4.9	0.8	0.4	18.9	0.3	5.5	83.9	10.5	1.322
PSOC-236	86.9	4.6	1.9	0.5	6.1	0.2	0.2	95.6	4.2	1.280
PSOC-240	67.5	5.0	1.2	1.7	24.6	0.4	4.4	92.1	3.5	1.376
PSOC-268	83.5	4.9	1.4	1.1	9.1	0.4	7.2	82.4	10.4	1.275
PSOC-285	77.5	4.9	1.4	4.4	11.8	3.3	3.0	91.5	5.6	1.276
PSOC-297	79.7	5.6	1.7	1.6	11.4	1.4	19.0	62.8	18.2	1.285
PSOC-380	89.5	3.4	1.1	0.6	5.4	0.2	0	88.6	11.4	1.357
PSOC-403	85.7	4.8	1.8	0.5	7.2	0.2	2.4	91.6	6.0	1.287
PSOC-409	87.1	4.2	1.9	1.5	5.3	1.1	6.5	86.9	6.6	1.317
PSOC-592	77.4	4.9	1.3	2.0	14.4	0.4	12.5	53.0	34.4	1.316
PSOC-594	75.0	4.8	1.2	2.7	16.3	0.5	5.1	88.5	6.6	1.322
PSOC-629	91.0	3.2	0.8	0.7	4.3	0.8	0	90.6	9.4	1.401
PSOC-852	75.3	5.0	1.7	0.4	17.6	0.0	1.9	94.0	4.2	1.309
PSOC-975	69.0	4.6	1.0	0.5	24.9	0.2	4.6	91.6	4.0	1.393
PSOC-1005	69.6	4.5	0.9	0.4	24.6	0.0	1.6	95.5	2.9	1.405
PSOC-1109	70.9	6.6	1.6	1.5	19.4	1.3	70.7	21.4	7.8	1.228
U1	77.3	5.7	1.5	0.7	14.8	1.0	10.2	85.2	4.6	1.244
SIU-744A	81.4	4.7	1.3	0.8	11.8	0.1	4.6	93.8	1.6	1.300
SIU-744B	82.2	5.1	1.4	0.8	10.5	0.3	15.4	71.0	13.6	1.271

[a] dry and ash free basis.

[b] by difference.

[c] E=exinite, V=vitrinite, I=inertinite.

TABLE 2. DEMINERALIZED COALS, VARIMAX ROTATED FACTOR PATTERN FOR PRODUCT MOLECULAR WEIGHT DISTRIBUTION

	Factor 1	Factor 2	Factor 3	Factor 4
Carbon	-0.80550			
Hydrogen		0.89706		
Sulfur		0.73940		
Oxygen	0.85843			
Nitrogen	-0.81678			
HMW	0.90740			
MMW			0.94011	
LMW	-0.96976			
Density		-0.91986		
Exinite		0.85784		
Vitrinite		-0.72136		
Inertinite		0.86206		
Pyridine Sol.	0.89258			

Variance explained by each factor:
Factor 1, 4.836022; Factor 2, 3.347514; Factor 3, 1.793194; Factor 4, 1.681776

TABLE 3. EXXON COAL VARIMAX ROTATED FACTOR PATTERN FOR PRODUCT MOLECULAR WEIGHT DISTRIBUTION

	Factor 1	Factor 2	Factor 3	Factor 4
Carbon	-0.85545			
Hydrogen		0.91672		
Sulfur		0.65336	0.53082	
Oxygen	0.79685			
VM	0.89172			
MM		0.93145		
Inert		0.70451		
HMW	0.91429			
MMW			0.96824	
LMW	-0.88076			

Variance Explained by Each Factor: Factor 1, 3.980301; Factor 2, 2.006584; Factor 3, 1.756227; Factor 4, 1.258782

Figure 1. Product solubility in benzene-ethanol as a function of carbon content.

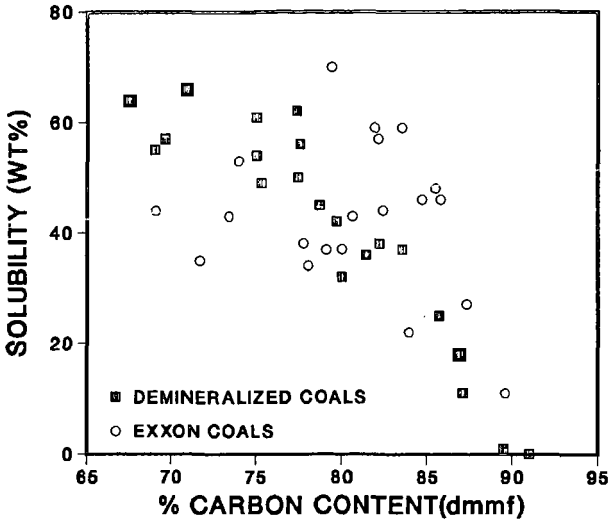

Figure 2. Predicted benzene-ethanol solubilities from multivarient least squares analysis using C and H content.

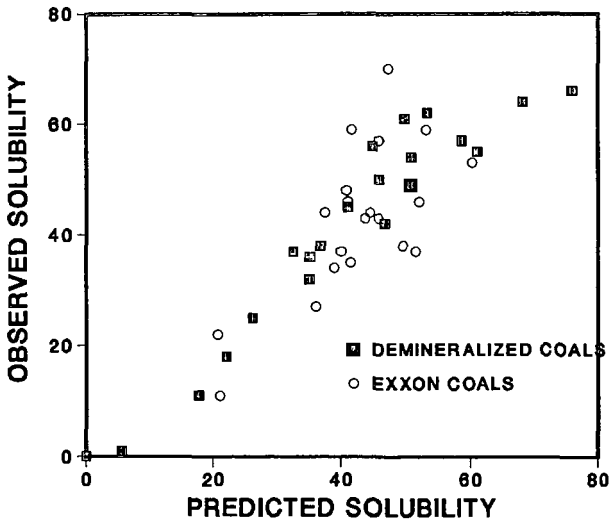

Figure 3. GPC of the benzene-ethanol soluble portion from a demineralized coal(psoc 107).

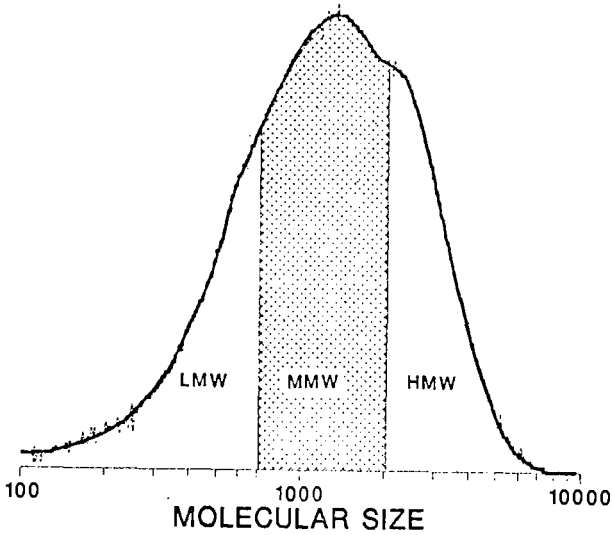

Figure 4. The change in relative amounts of high molecular species with carbon content of the coals.

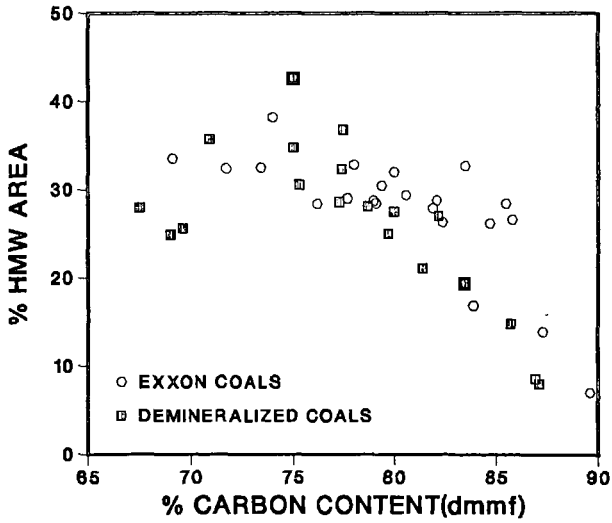

Figure 5. Variation of the fa of benzene-ethanol solubles with hydrogen content for Exxon coals.

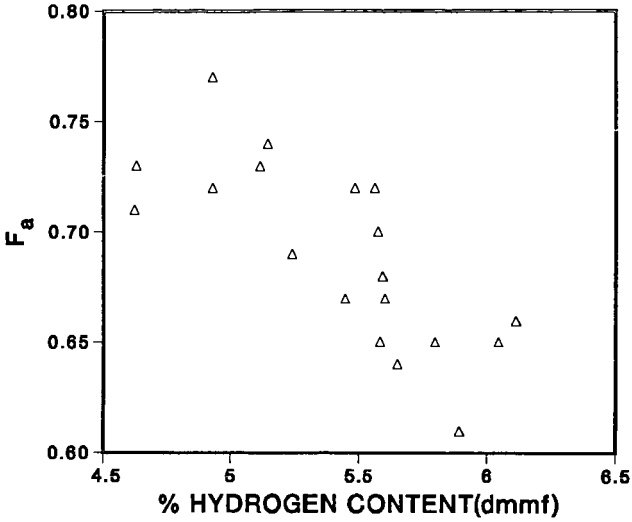

Figure 6. Variation of fa with benzene-ethanol solubility for the Exxon coals.

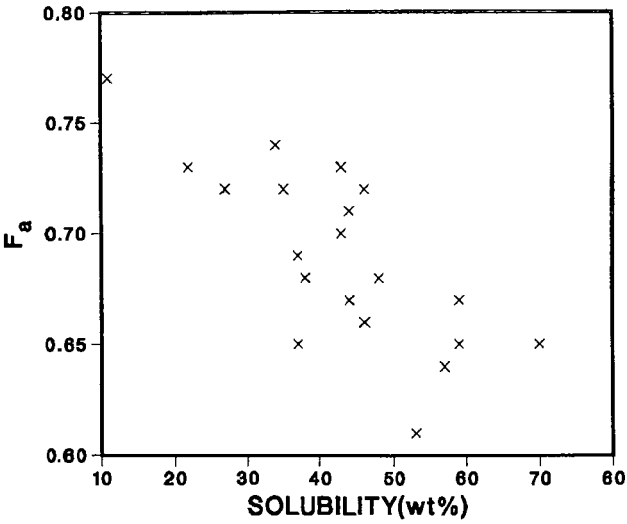

CHANGES IN HYDROGEN UTILIZATION WITH TEMPERATURE DURING DIRECT COAL LIQUEFACTION

D.H. Finseth, B.C. Bockrath, D.L. Cillo, E.G. Illig, R.F. Sprecher, H.L. Retcofsky, and R.G. Lett

Pittsburgh Energy Technology Center
P.O. Box 10940
Pittsburgh, PA 15236

INTRODUCTION

The role of hydrogen is of particular interest in direct coal-conversion chemistry. The presence of high pressure gaseous hydrogen is beneficial in virtually any direct conversion experiment, even under low severity conditions where the net hydrogen incorporation is nil. The hydrogen chemistry is extremely important in process design due to the large impact of hydrogen consumption on the process economics. An ideal process would consume a minimum of hydrogen while breaking the coal into soluble fragments. A reliable means of monitoring the major pathways of hydrogen utilization, in contrast to only measuring net hydrogen consumption, would be very useful for process optimization. The goal of this work was to develop an analytical approach for quantitatively distinguishing hydrogen consumed in hydrogenation from that utilized to stabilize thermolysis fragments.

The current view on the involvement of hydrogen in coal liquefaction is that it is consumed in direct hydrogenation and in the "capping" of thermolysis fragments.[1] In the capping mode, the hydrogen may be transferred by means of solvent intermediates such as hydroaromatics. The direct hydrogenation of aromatics is reasonably well understood, but the mechanism of hydrogen transfer is less clear. Upon homolytic thermolysis of a labile bond in the feed slurry, two free radicals are formed, which then stabilize by abstraction of hydrogen from nearby groups, by rearrangement, or by coupling. Rearrangement and coupling reactions of radicals can often result in hydrogen being eliminated from the fragment rather than consumed by it. In the complex, high molecular weight, slurry environment, all these routes to radical stabilization are accessible.

If coals were simple solid hydrocarbons (C_xH_y) without mineral matter or heteroatoms, there would be little interest in liquefaction, since a major goal of liquefaction is the removal of N, O, S, and mineral matter from the coal. Heteroatom removal is one of the most important roles for hydrogen in coal liquefaction, and it can be considered a subcategory of the thermolysis stabilization reactions just described.

Experimental evidence shows that the simple picture of bond thermolysis/radical stabilization outlined above is a gross oversimplification of direct coal conversion chemistry. In liquefaction experiments under an atmosphere of deuterium, the label is found in virtually all positions in the product. Positions α to aromatic rings are usually preferred, but a significant portion of the label appears in aromatic positions.[2] The methane produced also contains significant concentrations of deuterium, and dideuteromethane often predominates.[3] The presence of coal strongly catalyzes isotopic scrambling in a number of model systems.[4] These results are difficult to rationalize using the very simple model for hydrogen utilization.

Reference in this report to any specific commercial product, process, or service is to facilitate understanding and does not necessarily imply its endorsement or favoring by the United States Department of Energy.

Also, considerable conversion of coal to soluble products can occur under mild conditions where no net hydrogen is consumed. In this case, any hydrogen consumed must be compensated for within the slurry system. The ability of coal to act as a hydrogen donor is well documented.[5]

In a realistic direct conversion process, the distinction between coal and solvent is somewhat artificial. The slurry vehicle in a continuous unit operating at a steady state is a subfraction of the product from a previous cycle, making it impossible to clearly distinguish "solvent" from product oil in the reactor effluent. There is substantial evidence that solvent quality is enhanced by inclusion of certain high molecular weight components.[6] The solvent in these systems is intimately involved as a reactant and not as a neutral diluent. Thus, it may be preferable to consider the total feed slurry as a reactant mixture rather than as coal plus solvent.

Formulation of Analytical Approach

The fact that it is difficult to understand the detailed, molecular-level mechanism of hydrogen incorporation in complex liquefaction systems does not preclude improvements in understanding the net chemistry. It is reasonable to assume that hydrogen consumption will involve either hydrogenation or bond scission reactions. Conversely, both aromatization, the reverse of hydrogenation, and condensation, the reverse of bond scission, are potential sources of hydrogen. Exchange and isomerization reactions do not affect the net hydrogen balance.

Since stoichiometries of the two classes of hydrogen incorporation reactions differ, it is possible to construct a model that discriminates between the two. Such a model requires determination of the change in total hydrogen, the change in aromatic hydrogen, and the number of hydrogens incorporated during bond cleavage. The relationship between these quantities will be expressed as

$$\Delta^{H}_{Total} = \Delta^{H}_{Cleavage} + \Delta^{H}_{HYD} \qquad (1)$$

where Δ^{H}_{Total} is the total change in hydrogen,

$\Delta^{H}_{Cleavage}$ is the hydrogen consumed in bond cleavage, and

Δ^{H}_{HYD} is the hydrogen consumed in hydrogenation of the slurry.

This relationship describes only the reactions of hydrogen with the organic portion of the feed slurry. Focusing attention only on the organic reactions alleviates, to some extent, problems in the interpretation of total hydrogen balances. In total hydrogen balance calculations, it is impossible to distinguish H_2S and H_2O arising from organic reactions from those produced by inorganic sources in the coal. Although NH_3 presents less of a problem, some ammonia may be liberated from certain clays upon heating. The analytical problems associated with measuring small changes in the huge excess of gaseous hydrogen normally present under direct conversion conditions are also eliminated, since only carbonaceous products are analyzed.

Assuming that the total change in hydrogen (Δ^{H}_{Total}) can be determined by classical elemental analysis, then a method for measuring either the hydrogen consumed upon hydrogenation or bond cleavage is needed to use Equation 1. Since no satis-

factory method is available to count bonds before and after reaction in a coal liquefaction system, it is necessary to concentrate on determination of Δ^H_{HYD}. Although research efforts are underway to determine hydrogen speciation in solid coals, it is doubtful that any of the current methods are sufficiently quantitative for the present purpose.[7] One analytical tool that can be applied with reasonable confidence to both solids and liquids is ^{13}C nuclear magnetic resonance (NMR). Fortunately, it provides an indirect measurement of the hydrogen consumed in hydrogenation. Hydrogenation of organics results in incorporation of one hydrogen for every carbon reduced. Thus if a sample is hydrogenated without structural changes from an aromaticity of 0.80 to 0.70, then 10 carbons per 100 have been reduced and 10 hydrogens have been incorporated. The ratio of 1 hydrogen per carbon reduced does not hold exactly if there is significant reduction of aromatic nitrogen heterocycles, but the 1:1 stoichiometry is a good approximation if these reactions can be neglected. Combining elemental analysis and ^{13}C NMR data, the amount of hydrogen consumed in bond scission can be determined by difference.

Bond scission can be further divided into three categories, those resulting in (1) heteroatom elimination as H_2O, H_2S, or NH_3, (2) C_1-C_4 hydrocarbon gas production, and (3) breakdown of the coal matrix to yield nonvolatile (solid or liquid) products.

$$\Delta^H_{Cleavage} = \Delta^H_{NOS} + \Delta^H_{C_1-C_4} + \Delta^H_{Matrix} \qquad (2)$$

If a quantitative measure of the hydrogen used in these three bond scission modes can be obtained, it would be very useful in monitoring changes in liquefaction chemistry with reactor conditions such as temperature, pressure, catalyst, residence time, and feed composition.

In many respects, the direct conversion reactor is an inefficient coal gasifier that converts 5-20% of the coal to C_1-C_4 hydrocarbons while producing a by-product liquid (20-80%). Since C_1-C_4 hydrocarbon gases usually constitute a significant product stream, they must be carefully analyzed if the approach just described is to succeed. If accurate gas analyses are available and it is assumed that all hydrocarbon gases are generated by cleavage of alkyl substituents from aromatics, an estimate of the hydrogen consumed in gas production can be obtained. One mole of hydrogen is incorporated for every mole of light gas formed.

The most difficult term to evaluate in Equation 2 is Δ^H_{NOS}, the hydrogen consumed in heteroatom removal. The difficulty arises because of the variety of heteroatomic structures present and the different hydrogen stoichiometries involved in their elimination. If the organic sulfur in the feed slurry can be assumed to be primarily thiophenic, two hydrogens are incorporated per sulfur removed as H_2S:

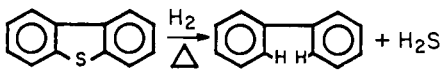

Removal of heterocyclic nitrogen proceeds through the fully hydrogenated nitrogenous ring system (5- or 6-membered).[8] There is a net incorporation of one hydrogen per nitrogen eliminated:

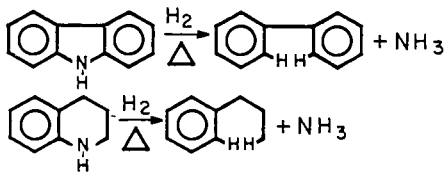

If amine functions exist in the feed, elimination of one amine nitrogen actually decreases the hydrogen content by one hydrogen:

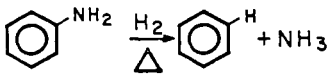

If the discussion is confined to bituminous coals, the majority of the organic oxygen will reside in either phenolic or ether structures.[9] Removal of ether oxygen results in the net incorporation of two hydrogens per oxygen removed, and removal of phenolic oxygen results in no net change in hydrogen:

$$R-O-R' \xrightarrow[\Delta]{H_2} R-H + HR' + H_2O$$

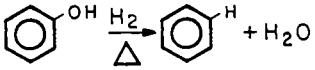

Under mild conditions where only minimal heteroatom removal occurs, the question of hydrogen stoichiometry is unimportant. However, under severe processing conditions significant heteroatom reduction can occur and an average stoichiometry must be assigned. For the present purposes, it has simply been assumed that on the average one hydrogen is incorporated into the carbonaceous product per heteroatom removed from the organic portion of the feed slurry.

Combining Equations 1 and 2 yields

$$\Delta^H_{Total} = \Delta^H_{HYD} + \Delta^H_{C_1-C_4} + \Delta^H_{NOS} + \Delta^H_{Matrix} \qquad (3)$$

The term Δ^H_{Matrix} can be determined by difference. Using Equation 3, only elemental analyses, carbon aromaticities, and quantitative gas analyses are required to partition the hydrogen consumption into that used in gas production, hydrogenation, heteroatom removal, and matrix bond cleavage. In reactions producing significant CO or CO_2, a correction must be applied to Equation 3, but in the experiments described below, both CO and CO_2 were negligible.

Experimental

The model just described was initially applied to a single steady-state period 800 hours into a long-term liquefaction experiment (FB-62) on the 400 lb/day coal liquefaction unit at PETC.[10] The unit was operated at 450°C under 4,000 psig H_2 pressure while feeding a 35% slurry of West Virginia (Ireland Mine) HvAb coal in centrifuged liquid product from a previous period of the run. Subsequently, a series of liquefaction runs on a 10 lb/day continuous coal liquefaction unit at PETC was investigated.[11] In the latter unit, a 40% coal slurry prepared from Homestead, Kentucky, HvAb coal and centrifuged liquid product produced from the same coal in the 400 lb/day unit was liquefied under 2000 psig H_2 at programmed temperatures between 375°C and 450°C. More recently, two series of experiments have been studied involving liquefaction of reactive (Illinois No. 6) and refractory (Blacksville No. 2) coals in the presence of SRC-II distillate in a stirred autoclave under 2000 psig H_2 over the temperature range 300°C to 450°C.

Elemental analyses of the organic material in the feed slurries were obtained from separate analyses of the vehicles and coal. Elemental analyses of the vehicles were done by classical microanalytical procedures, including direct oxygen determinations. The feed coals were analyzed by both microanalytical and standard

ASTM coal methods for moisture, ash, and sulfur forms. Product gases were analyzed by low resolution mass spectrometry of grab samples and gas chromatography. The products were split by Soxhlet extractions into methylene chloride soluble and insoluble fractions, which were then analyzed separately. The carbon aromaticity change across the reactor was determined by ^{13}C NMR, using the CP/MAS techique on the insoluble fractions and high resolution ^{13}C NMR in CD_2Cl_2 for the soluble fractions.

Results and Discussion

A comparison of the net changes in composition of the feed slurry and total product for Run FB-62 on the 400 lb/day unit is presented in Table 1. Combined with the gas make (8 wt% maf), the data in Table 1 allow application of Equation 3 to determine the modes of net hydrogen utilization in the reactor shown in Table 2.

Table 1. Analysis of feed slurry and total product, Run FB-62.

	Elemental Analyses (atoms/100 carbon atoms)					Carbon
	C	H	N	O	S	Aromaticity (f_a)
Feed Slurry	100	96	1.3	4.3	0.8	0.70
Total Product	100	106	1.3	2.6	0.6	0.67
Net Change	---	+10	0	-1.7	-.2	-0.03

Table 2. Net hydrogen utilization in Run FB-62.

Mode of Hydrogen Utilization	H Consumed/100 C
Gas Make	2
Heteroatom Elimination	2
Hydrogenation	3
Matrix Cleavage	3
Total	10

The results indicate nearly equal consumption of hydrogen by each of the four pathways considered at 450°C in the 400 lb/day unit.

Products produced at various temperatures in the 10 lb/day unit were then analyzed to determine if this analytical approach would detect changes in hydrogen utilization as reactor conditions changed. A plot of total product aromaticity vs. programmed reactor temperature is shown in Figure 1. The actual reactor temperatures vary somewhat from the programmed temperatures, but for simplicity, Figure 1 uses the programmed temperature. The three data points at each temperature correspond to three different hydrogen flow rates (80, 103, and 125 SCF/hr). The spread in values at a given temperature arises from experimental errors in the f_a determination and from sampling errors, as well as any real effect of hydrogen flow rate. Current work is being directed toward reduction of the data scatter. In this work the data points are all presented with no statistical justification of the indicated curve. Since other analyses show little, if any, effect of hydrogen flow rate in this range, the f_a values at each temperature can be averaged to yield an estimate of the actual best value indicated on the plot as a star.

The horizontal dashed line in Figure 1 indicates the carbon aromaticity of the slurry feed, obtained as a weighted average of the aromaticities of the slurry components. At low temperatures, where no chemical reaction takes place, the reactor would simply be mixing the slurry components. At the other extreme in temperature (450°C), the liquid product aromaticity is expected to again approximate the value for the solvent, since this is a requirement for steady-state recycle operation. Figure 1 indicates that the total aromaticity has nearly returned to the slurry line at 450°C, and the liquid product (CH_2Cl_2 solubles) has an aromaticity (0.69) that compares well with that of the vehicle (0.68). The most distinctive and surprising feature in Figure 1 is the apparent minimum in the carbon aromaticity at 400°C. This minimum suggests very significant changes in product hydrogen distribution upon going from 375°C to 400°C. This change is observed, although there is still little net hydrogen incorporation, no gas production, and relatively little heteroatom elimination at these temperatures. The only heteroatom lost under these conditions is oxygen, and part of this apparent loss may well be due to simple water loss rather than elimination of organic oxygen.

Applying the model to the average f_a data in Figure 1 results in the hydrogen utilization pattern shown in Table 3. As anticipated, little net hydrogen chemistry has occurred at 375°C. The only directly measurable change is the loss of one oxygen atom per 100 carbon atoms, requiring one hydrogen from matrix bond formation for balance. At 450°C, a hydrogen utilization profile much like that observed for Run FB-62 in Table 3 would be expected, and in general, that is what is found. The only difference is that the net hydrogenation is apparently less in the smaller 10 lb/day reactor that was operated at the lower hydrogen pressure. The term "apparently" should be stressed, since the absolute accuracy of f_a measurements on such samples is probably no better than $\pm$ 0.03. At 400°C, Table 3 indicates a significantly higher consumption of hydrogen by hydrogenation, 7 hydrogens/100 carbons, while the total net hydrogen incorporation is only 3 hydrogens/100 carbons. Since 2 hydrogens/100 carbons are consumed in heteroatom removal, this indirect analysis indicates consumption of 9 hydrogens/100 carbons in the 400°C slurry, while elemental analysis indicates an incorporation of only 3 hydrogens/100 carbons overall. The model then forces assignment of a negative value to matrix cleavage consumption, implying that the net change in number of bonds across the reactor is an increase. This suggests that under these conditions, internal condensation of the slurry components is producing hydrogen that compensates for that consumed in bond cleavage, heteroatom removal, and hydrogenation. It must be emphasized that this treatment considers only net chemistry, making it impossible to determine if the internally produced hydrogen or the hydrogen atmosphere provides the consumed hydrogen.

Table 3. Hydrogen utilization during liquefaction of Homestead, Kentucky, coal in the 10 lb/day unit.

Mode of Hydrogen Consumption	Hydrogens Consumed Per 100 Carbons in Feed		
	375°C	400°C	450°C
Gas Make	0	0	4
Heteroatom Removal	1	2	4
Hydrogenation	0	7	1
Matrix Cleavage	-1	-6	3
Total	0	3	12

Table 3 indicates that as the temperature of the reactor increases from 400°C to 450°C, the total hydrogen incorporation per 100 carbon atoms increases dramatically from 3 to 12, but the net consumption in hydrogenation actually decreases from 7 to 1. This effect is probably due to increasing hydrogen production via

aromatization with increasing temperature. This is not unexpected, since low temperatures tend to favor hydrogenation, while high temperatures favor aromatization. Higher temperatures also tend to favor thermolysis over hydrogenation, and this expectation is also confirmed in Table 3, where the net bond-breaking consumption (gas make, heteroatom removal, and matrix cleavage) changes from -4 hydrogens/100 carbons at 400°C to +11 hydrogens/100 carbons at 450°C. However, even at 450°C, only 3 hydrogens/100 carbons are consumed in breaking down the slurry matrix bonds. This indicates that bond breaking predominates over condensation by only about 1.5 bonds/100 carbons.

Using the approach outlined, a reasonable picture of the changes in hydrogen utilization with temperature emerges. At low temperature (375°C), physical changes and minor internal hydrogen redistribution occur with little net hydrogen chemistry and no net consumption. At 400°C, there is still only a small hydrogen consumption, but there is also evidence of significant internal hydrogen chemistry, with hydrogenation and condensation proceeding to approximately the same degree. At high liquefaction temperatures, a more conventional view of hydrogen utilization emerges, significant net consumption being utilized primarily in bond cleavage reactions, gas make, heteroatom removal, and matrix breakdown.

An additional series of autoclave experiments on the liquefaction of Illinois No. 6 and Blacksville No. 2 coals is currently being investigated to determine if this approach can distinguish differences in hydrogen utilization between coals of different reactivity over the temperature range 300°C to 450°C. Although analyses of these runs are not yet complete, preliminary results indicate there are distinct differences between the coals in the product aromaticity versus temperature relationship.

Although the approach presented appears to be useful on the basis of the results accumulated to date, a discussion of potential problems is appropriate. Analytical errors associated with the various measurements and the assumptions of the model both contribute to uncertainty in the results. The NMR determination of f_a is a prime source of error. For this number to have any utility, all the feed and product carbons must be observed and carefully quantified. The problem of observing all of the carbon in the soluble material is not too serious if the "soluble" material is not colloidal or suspended. If the correct NMR parameters are used, the largest source of error is then in the integration of peak areas. The problem of quantitatively determining f_a for the insoluble fractions, which requires the ^{13}C-CP NMR technique, is more serious. This technique will not observe liquid-like entrapped material and may not observe carbons that are too far removed from hydrogen for the efficient transfer of polarization. The lower inherent resolution of the solid phase NMR spectra also introduces a larger error in measurement of overlapping peak areas. Another potential source of error is the quantitative determination of gas yield and composition. This measurement is important due to its large impact on both total hydrogen consumption and net product aromaticity. The determination of organic oxygen in coal and coal-derived products is always a problem, and errors in this determination translate directly into errors in hydrogen in heteroatom removal. The determination of organic sulfur in the feed slurry requires distinguishing between organic and mineral sulfur in the coal.

Conclusions

The approach outlined yields a rather detailed description of the net utilization of hydrogen during direct liquefaction, partitioning it into contributions from gas generation, heteroatom removal, hydrogenation, and matrix breakdown. Preliminary results indicate that internal hydrogen reorganization, with little consumption, predominates at low temperatures, with hydrogenation being compensated for by the hydrogen liberated in condensations. As the temperature is increased, bond cleavage reactions and aromatization reactions appear to become more important,

and the net hydrogen consumption increases. Additional studies of the assumptions in the model and of uncertainties in the required analytical data are needed to critically evaluate the utility of this approach.

References

1. Gorin, E. In Chemistry of Coal Utilization, Second Supplementary Volume, M.A. Elliot, ed., pp. 1845-1881, Wiley-Interscience, New York, 1981.

2. Schweighardt, F.K., Bockrath, B.C., Friedel, R.A. and Retcofsky, H.L. Fuel, 48 (8), 1254-1255 (1976).

3. a. Heredy, L.A. In Proceedings of the International Conference on Coal Science, Düsseldorf, pp. 332-337, Verlag Glückauf GmbH, Essen, 1981.
   b. Wilson, M.A., and Vassallo, A.M. Ibid., pp. 338-343.

4. King, H., and Stock, L. Fuel, 61(3), 257-264 (1982).

5. Wender, I., Heredy, L.A., Neuworth, M.B., and Dryden, I.G.C. In Chemistry of Coal Utilization, Second Supplementary Volume, M.A. Elliot, ed., pp. 435-437, Wiley-Interscience, New York, 1981.

6. Derbyshire, F.J., Odoerfer, G.A., Varghese, P., and Whitehurst, D.D., Fuel, 61(10) 899-905 (1982).

7. Kuehn, C.W., Snyder, R.W., Davis, A., and Painter, P.C. Fuel 61, 682, (1981).

8. Katzer, J.R., and Sivasubramanian, R. Catal. Rev.-Sci. Eng., 20(20), 155-208 (1979).

9. Ruberto, R.G., and Cronauer, D.C. In Organic Chemistry of Coal, J.W. Larsen, ed., pp. 50-70, ACS Symposium Series 71, American Chemical Society, 1978.

10. Lett, R.G., Finseth, D.F., Schmidt, C.E., and Retcofsky, H.L. PETC/TR-82/13 (DE82018232), July 1982.

11. Klunder, E.B., Cillo, D.L., DOE/PETC/TR-82/9, (DE82012441), April 1982.

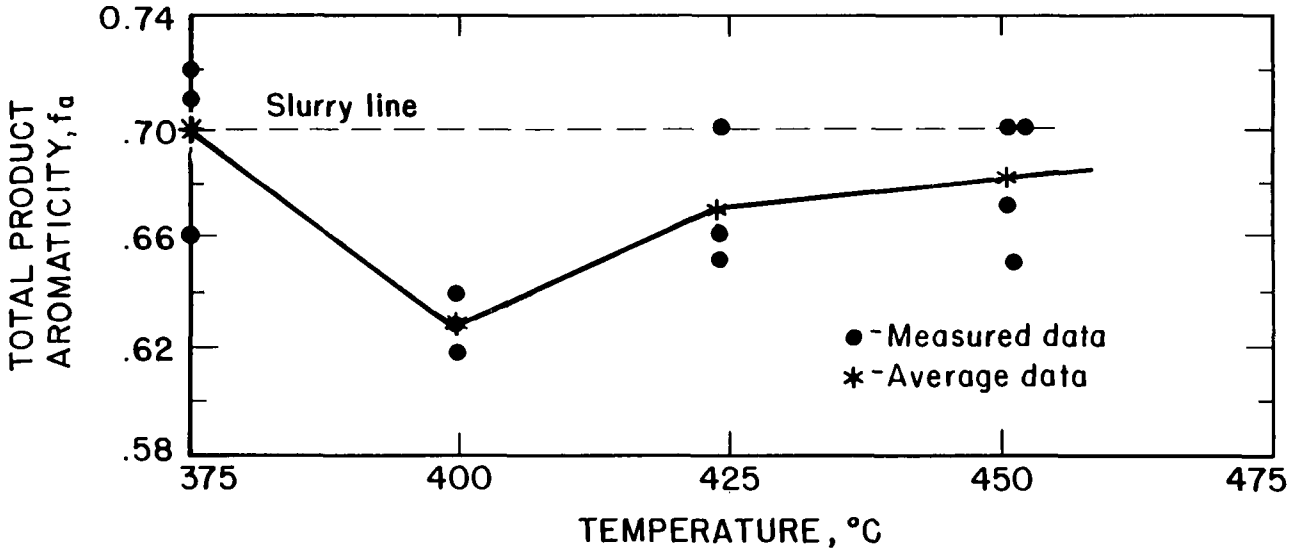

Figure 1 - Dependence of total product aromaticity on temperature.

BSI/1617-A

CHARACTERIZATION OF ARTIFACTS PRODUCED FROM TETRALIN DONOR VEHICLE UNDER COAL LIQUEFACTION CONDITIONS

Muthu S. Sundaram* and Peter H. Given
Coal Research Section
College of Earth and Mineral Sciences
The Pennsylvania State University
University Park, Pa. 16802

ABSTRACT

The hexane-soluble oil fraction of the heavy liquids produced from the liquefaction of coal using tetralin donor vehicle was fractionated by high pressure liquid chromatography. Three fractions were obtained: saturates, aromatics and polars. Each fraction was individually characterized via capillary column gas chromatography/mass spectrometry. Several binaphthyls and binaphthyl derivatives, produced from the donor solvent tetralin under coal liquefaction conditions, were identified in the aromatic fraction. These artifacts make up an important fraction of the whole aromatic fraction. There is a fairly clear tendency for the concentration of binaphthyls and derivatives to decrease with increasing rank of coal. A stepwise multiple regressional analysis shows that the clay minerals and pyrite present in coal independently catalyze one or more of the types of artifact formation.

INTRODUCTION

Partially hydrogenated aromatic solvents such as tetralin, hydrophenanthrenes and hydropyrenes are used as process solvents in several coal liquefaction processes. An important function of these solvents is to donate hydrogen necessary for capping the thermally produced free radicals from coal thereby preventing char formation. The effect of hydrogen donor concentration on the conversion of coal to THF or pyridine-soluble products has been throroughly investigated (1,2) and several modern analytical techniques have been applied to characterize the ensuing products of liquefaction. Combined gas chromatography-mass spectrometry (GC/MS) has been extensively used in the characterization of liquefaction products from coal conversion processes (3-6). However, only a limited amount of work has been done on the identification of artifacts produced from the donor solvent itself under the coal liquefaction conditions (7-9). A knowledge of the artifacts generated from the process solvent will be very helpful in developing methods for down-stream processing of the coal-derived liquids. In this paper, we describe the identification of the artifacts produced from a process using tetralin as the hydrogen-donor solvent for liquefaction of coal and the influence of coal characteristics on the concentration of the artifacts is also discussed.

---

*Current Address: Process Sciences Divison, Brookhaven National Laboratory, Upton, NY 11973.

EXPERIMENTAL

Coal Samples:

Selected characteristics of the coals used in the liquefaction studies are shown in Table 1. The set of coals covers a wide range of rank and geologic province; the mineral matter content varies from a low of 6% to a high of 34% and a wide variation in the sulfur content can also be noted. Other characteristics of the coals, such as macerals content, calorific value, composition of the mineral matter are available from the Penn State/DoE coal data base. The aromaticities were determined by Gerstein, et al. using CP-MAS ^{13}C nmr (10).

Liquefaction:

The liquefaction runs were performed in duplicate in tubing bombs under the following conditions: 2.5 gm coal + 7 ml tetralin, 425°C, H_2 pressure (at temperature) 1400 psi, 30 min reaction period and agitation at 400 min $^{-1}$. After the gases had been vented, the products were rinsed out of the reactor into a Soxhlet thimble with ethyl acetate. Extraction was continued in the Soxhlet apparatus for 24 hours. After evaporation of the ethyl acetate, the residue was weighed to determine the total conversion and then mixed with 500 ml hexane and left to stand overnight, after which it was filtered. After removal of the hexane, the soluble portion was distilled at about 70°C and 5 mm Hg pressure to remove naphthalene and excess tetralin and the monomeric by-products formed from them during the process. The undistilled material was weighed and is reported as "oil".

Analytical Procedures:

i) HPLC Separation:

Prior to GC/MS analysis, group type separation of the hexane-soluble oil was performed using a Waters Model ALC/GPC-201 HPLC (Waters Associates, Milford, Mass.). The instrument contained of the following accessory hardware: Model 6000A solvent delivery system, a Model 660 solvent programmer, a Model U6K septumless injection system, a Rheodyne Model 7010 backflush valve and a Model 440 absobance detector with inter-changeable UV filters.

Typically, 20 microliter of the oil was injected on to a semi-preparative (8mm ID X 30 cm length) micro-Bondapak-NH_2 column (Waters Associates, Milford, MA.). The mobile phase was spectral quality n-hexane distilled in glass (Burdick and Jackson, Muskegon, MI) and a flow rate of 6.0 ml min^{-1} was used. Saturates are not retained in the column and are eluted first followed by aromatic hydrocarbons. Polars have greater affinity towards the stationary phase which makes the analysis time longer. Hence after the elution of the aromatic hydrocarbons, solvent flow through the column was reversed using the backflush valve and the eluting material was collected as the polar fraction. UV detector response at 254 nm was recorded for the aromatic and polar fractions.

The three fractions--saturate, aromatic and polar--were collected in separate flasks and excess hexane from the fractions was distilled off in a rotary evaporator. Further concentration was effected by blowing a gentle stream of nitrogen using a Sillivap concentrator.

ii) GC/MS Characterization:

Identifications of individual components in each fraction were performed on an integrated GC/MS/Computer system. The instrument used was a Finnigan Model 4000 automated EI/CI mass spectrometer equipped with a quadrupole ion detector and interfaced with a Finnigan Model 9610 gas chromatograph and a dedicated LSI computer with 16K memory.

Several stationary phases coated on glass capillary columns were tested for their application which included SP-2100, SP-2250 (both from Supelco Inc., Bellefonte, Pa.), SE-30, SE-52, SE-54 and Dexsil 300 (all from Applied Science Lab., State College, Pa.). A 30 meter SE-54 (methylphenylsilicone) stationary phase coated-glass capillary column (film thickness, 0.25 micrometer) was found satisfactory for the analyses of both aromatic and polar fractions.

The operating conditions used for the GC were: injector temperature 250°C; carrier gas, helium; flow-rate, 1 ml/min. The sample was quantitatively introduced into the capillary column by purged splitless injection technique (11). The oven temperature was initially programmed to increase from 50° to 100°C at 20°C min^{-1} and then to 300°C at 5°C min^{-1}.

The mass spectrometer was operated in the electron-impact mode (70eV electron energy). Chemical ionization mass spectra (methane reagent gas) of the eluting components were obtained when necessary. Spectral data acquisiton was performed at appropriate scanning intervals and the mass spectra were recorded on magnetic tapes for later retrieval. Specific compound identification was made from the characteristic mass spectral splitting patterns. Retention time data and response factors were obtained for representative compounds. By monitoring the specific ion current (single ion monitoring), detection of compounds present at trace levels was considerably improved.

RESULTS AND DISCUSSION

Tetralin has been widely used as a hydrogen donor solvent in many coal liquefaction studies. In addition to the transfer of hydrogen from the hydroaromatic ring to coal free radicals, tetralin undergoes the following changes under coal liquefaction conditions:

1. Isomerization: Tetralin rearranges (isomerizes) to produce methylindans. This reaction is temperature dependent (12) and is catalyzed by pyrite (13).

2. Fragmentation: In this case, tetralin decomposes to produce a mix of smaller molecules which is mainly made up of alkylbenzenes. Curran et al. reported that the decomposition of tetralin to C_4 benzenes was enhanced in the presence of coal extracts (14).

3. Adduction/Polymerization: From deuterium labelling studies, Franz et al. showed that both 2-tetralyl and 1-tetralyl radicals are produced in competitive amounts when a low-rank coal is heated in tetralin (15). The tetralyl or naphthyl radical intermediates can react with free racidals generated from coal or they can recombine among themselves leading to polymerized products such as binaphthyls and their derivatives.

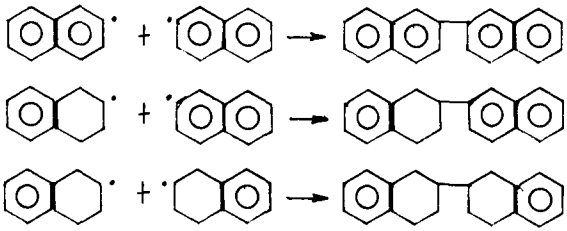

Various other isomers of the above representative compounds are also possible.

On the basis of their results from the flash pyrolysis of 1- and 2-tetralyl radical precursors in vacuum, the above authors suggested that the hydroaromatic radical intermediates 'may prefer disproportionation over combination pathways as temperatures increase'. While this is true for pyrolysis experiments at high temperatures and short residence times, it can not be generalized for coal liquefaction experiments at intermediate temperatures (400-450°C) and considerably long residence times (ca. 30 min.). Our results indicate that the dimerization of solvent radical intermediates occurs to a significant extent in a coal-tetralin system and that the concentration of the resulting artifacts seems to be affected by the coal characteristics.

A representative HPLC separation of an oil product is shown in Figure 1. Figure 2 shows the reconstructed Total Ion Chromatogram (TIC) of the aromatic fraction of the oil from PSOC-739. The large peaks at scan numbers 370 to 410 in the TIC in figure 2 are due to binaphthyls and related compunds, which evidently make up an important fraction by weight of the whole aromatic fraction. Similar results were obtained with other coals. Figure 3 shows the Specific Ion Chromatograms (SIC) for m/e values of 254, 258 and 262 corresponding to the molecular ions of binaphthyl and its tetrahydro and octahydro derivatives. The peaks are numbered and identified by number in Table 2. It will be seen that, in peaks height, 2,2'-binaphthyl and its derivatives predominate, indicating the higher reactivity of the 2-position compared to that of the 1-position.

When all the peaks are examined at the same attenuation, it is seen that binaphthyls and hydrogenated derivatives account for over 70% of the dimeric artifacts formed in the hydrogenation of all coals but that of highest rank, PSOC-801 (Stigler seam, Oklahoma). Having regard to the small size of other peaks in the TIC, it is unlikely that binaphthyls generated from the coals account for much of the peak heights observed. Philip et al. reported the presence of two isomers of octahydrobinaphthyls in a sample from the liquefaction of a Texas lignite using tetralin as the hydrogen-donor solvent (16). The actual amount of these and other products, however, was not specified. Schultz et al. identified 2,2'-binaphthyl (only) among the aromatic hydrocarbons in a SRC pilot plant product with a mixture of Kentucky Nos. 9 and 14 coals as feedstock, but only in trace amount (6). Thus the binaphthyls found in our work are indeed very largely artifacts of the solvent. In what follows, all of the compounds named are assumed to be derived entirely from the solvent.

In addition to the binaphthyls discussed, a number of phenyl naphthalene were identified: C_1-, C_2- and C_4-phenyl naphthalenes, and a phenyl tetralin. Only the sum of these compounds are shown in Table 3, under the heading $\Sigma\phi$-ν. Furthermore, a number of alkyl naphthalenes and either alkyl indans or alkyl tetralins (or a mixture) were found (C_1-C_4). Again, only the sum of the concentraitons of these compounds is shown in Table 3, under the heading $\Sigma\ C_n$-ν . The part of the HPLC fraction 2 (aromatics) accounted for by solvent artifacts is shown as a percentage in the final column of Table 3.

There is a fairly clear tendency for the concentration of binaphthyls and derivatives to decrease with increasing rank. The concentration of phenyl naphthalenes, whose formation involves ring-splitting, tends to increase with rank, as does the concentration of alkyl napthalene/indan derivatives, whose formation involves isomerization. As mentioned before, the isomerization of tetralin to methyl indans is catalyzed by pyrite (13); yet there is no correlation between the concentration of these derivatives and pyrite content. In fact, it is reasonable to suppose that many factors determine the yields of the various kinds of artifacts. This is substantiated by an equation developed by stepwise multiple regression:

$$\text{Concentration of artifacts (\%)} = 0.919\ MM + 14.5\ S_{pyr} - 9.81\ f_a + 38.2$$

The variables provided for the regression were: contents of C, O, S_p, S_{tot} and MM, and the aromaticity, f_a. The fraction of variance explained by this regression, R^2, is 0.851. The equation suggests that both clay minerals and pyrite independently catalyze one or more of the types of artifact formation. Abdel-Baset (13) found that clay minerals catalyze transfer of hydrogen from hydroaromatics to aromatics. Thus the significance of f_a in the equation may lie in the fact that it indicates the number of C atoms available for accepting H atoms and hence (presumably) for generating free radicals in the solvent (admittedly this term may be not very significant since the range of values of f_a is small).

In comparing the yields and composition of the products of liquefaction experiments, it might be considered desirable to subtract out the components derived from the solvent. The aromatic fraction of the oil (HPLC fraction 2) can be corrected as follows:

$$\% \text{ aromatics (corr.)} = \% \text{ aromatics (HPLC)} \times \frac{100 - \% \text{ artifacts}}{100}$$

Consequential changes are needed in other figures characterizing the product distribution. Thus:

% hexane-sol. oil (corr) = % sat. + % arom. (corr.) + % polars
% benzene-sol. total liquids (corr.) = % oil (corr.) + % asph.
% gases (corr.) = % conversion - % total liquids (corr.)

The corrected and uncorrected yields of various fractions obtained from the liquefaction of coals listed in Table 1 are shown in Table 4. From the table, it is clear that the adjustment of the figures for hexane-soluble oils and for the aromatic HPLC fraction makes a quite appreciable difference to the data and ought to be determined before product distributions for any batch system are evaluated.

CONCLUSION

An important fraction by weight of the whole aromatic fraction of the oils obtained from the liquefaction of coal using tetralin as the hydrogen-donor solvent was made up of binaphthyls and related compounds. The concentrations of these artifacts were affected by the coal characteristics. Both clay minerals and pyrite seem to independently catalyze one or more of the types of artifact formationfrom tetralin. This is a somewhat unexpected effect of coal characteristics on the composition of liquefaction products. Other donor solvents, such as partially hydrogenated phenanthrene or a commercial recycle oil, are obviously likely also to undergo changes during processing, whose magnitude and nature will vary with the feedstock, and whose effects on product composition will be appreciable.

ACKNOWLEDGEMENT

The coals used in this study were kindly supplied by Dr. William Spackman, Professor of Palaeobotany and Director of the Coal Research Section in this College. This work was supported by Contract No. DE-AC22-81-ET 10587 from the U.S. Department of Energy.

REFERENCES

1. Epperly, W. R., "EDS Coal Liquefaction Process Development, Phases IIIB/IV", Technical Progress Report, DoE, FE-2893-1T (1978).

2. Whitehurst, D. D., Mitchell, T. O., and Farcasiu, M., "Coal Liquefaction", Academic Press, New York (1980).

3. Bertsch, W., Anderson, E., and Holzer, G., J. Chrom., 126, 213-224 (1976).

4. White, C. M., Sharkey, Jr., A. G., Lee, M. L., and Vassilaros, D. L., in "Polynuclear Aromatic Hydrocarbons", Ed. Jones, P. W., and Leber, P., Ann Arbor Science Pub. Inc., Ann Arbor, MI. (1979).

5. White, C. M., and Lee, M. L., Geochim. Cosmochim. Acta, 44, 1825-1832 (1980).

6. Schultz, R. V., Jorgenson, J. W., Maskarinec, M. P., Novotny, M., and Todd, L. J., Fuel, 58, 783-789 (1979).

7. Cronauer, D. C., Jewell, D. M., Shah, Y. T., Modi, R. J., and Sheshadri, K. S., Ind. Eng. Chem. Fundam., 18, 368-376 (1979).

8. Cronauer, D. C., Jewell, D. M., Shah, Y. T, and Modi, R. J., ibid.,153-162 (1979).

9. Ruberto, R. G., Fuel Proc. Tech., 3, 7-24 (1980).

10. Gerstein, B.C., Murphy, P.D., and Ryan, L.M., in "Coal Structure", ed. R.A. Myers, Academic Press, New York, p. 112 (1982).

11. Grob, K., and Grob, K., Jr., J. High Res. Chro., 57 (1978).

12. Whitehurst, D. D., Farcasiu, M., and Mitchell, T. O., EPRI Annual Technical Report No. AF-480-RP-410-1 (1977).

13. Abdel-Baset, M., in "The Relation of Coal Characteristics to Coal Liquefaction Behavior", by Given, P. H., Spackman, W., Davis, A., Walker, P. L., and Lovell, H. L., Report No. 2 to RANN Division of Nat. Sci. Foundation, under Grant No. GI-38974, pp. 50-52.

14. Curran, G. P., Struck, R. T., and Gorin, E., Ind. Eng. Chem. Proc. Des. Dev., 6, 166 (1967).

15. Franz, J. A., and Camaioni, D. M., Fuel, 59, 803-805 (1980).

16. Philip, C. V., and Anthony, R. G., Preprints ACS Fuel Div., 24(3), 204-214 (1979).

17. Given, P.H. and Yarzab, R.F., in "Analytical Methods for Coal and Coal Products", ed. C. Karr, Academic Press, New York, Vol. 2, pp. 3-41 (1978).

Table 1

Selected Characteristics of Coals Used

PSOC No.		Province*	ASTM Rank	% C dmmf	% S dry	% MM,† dry	f_a**
833	Fort Union Bed, Mont.	3	Lig	70.43	0.55	16.26	0.68
791	A Pit, Texas	6	LIg	72.13	0.81	20.78	0.55
785	Lower Wilcox, Texas	6	sbb	73.21	1.06	14.29	0.54
240A4	Big Dirty, Wash.	5	sbb	74.34	0.39	17.82	--
240A1	Big Dirty, Wash.	5	sbb	75.11	3.36	33.98	--
866	G Seam, Colo.	4	HVC	76.97	0.50	22.22	0.64
548	Wolf Creek, Colo.	4	HVC	78.98	0.52	13.11	0.64
680	Indiana No. 6, Ind.	2	HVC	80.61	3.58	14.23	--
854	Juniata C, Colo.	4	HVB	81.64	0.40	6.71	0.63
739	Kentucky No.12, Ky.	2	HVB	83.29	2.72	15.05	0.70
773	Ohio No.6, Ohio	1	HVB	83.29	2.83	9.30	0.75
808	Croweburg, Okla.	2	HVA	84.71	3.20	6.57	0.73
821	Pittsburgh, W. Va.	1	HVA	84.92	2.56	6.00	0.70
801	Stigler, Okla.	2	MV	88.35	4.65	13.83	0.79

* Key to province numbers: 1, Eastern or Appalachian; 2, Interior; 3, North Great Plains; 4, Rocky Mountain; 5, Pacific; 6, Gulf.

** Data from ^{13}C nmr, kindly provided by Professor B. Gerstein, University of Iowa, now published by him (10).

† Calculated by a modification of the Parr formula (Given and Yarzab, 17).

Table 2

Identification of Peaks in Specific Ion Chromatograms of Figure 3

Figure 3(a):	1. 1,1'-binaphthyl 2. 1,2'-binaphthyl 3. 2,2'-binaphthyl
Figure 3(b):	1. 1,2,3,4-tetrahydro-1,1'-binaphthyl 2. 1,2,1',2'-tetrahydro-2,2'-binaphthyl 3. 1,2,3,4-tetrahydro-2,2'-binaphthyl 4. 1,2,3,4-tetrahydro-2,1'-binaphthyl (three other unidentified peaks)
Figure 3(c):	1. 1,2,3,4,1',2',3',4'-octahydrobinaphthyl 2. 1,2,3,4,1',2',3',4'-octahydro-1,2'-binaphthyl 3. 1,2,3,4,1'.2',3',4'-octahydro-2,2'-binaphthyl

Table 3

Concentrations of Solvent Artifacts in the Aromatic HPLC Fraction of Some Coals

percent of total fraction

PSOC No. C	Binaphthyls	Tetrahydro-binaphthyls	Octahydro-binaphthyls	Binaphthyl derivatives (total)	* $\Sigma\phi$-ν	Σ C_n-ν	Total artifacts
833	15.6	7.6	15.8	38.9	1.9	5.5	46.3
791	17.7	13.3	13.4	44.4	0.7	7.8	52.9
785	10.3	12.4	15.6	38.3	0.7	5.4	44.4
240A4	14.0	20.2	8.4	42.5	1.5	3.5	47.5
240A1	19.1	22.4	16.7	58.2	1.2	4.4	63.8
866	16.0	12.5	15.1	43.6	1.8	6.7	52.0
548	8.7	9.7	10.4	28.8	2.2	15.5	46.6
680	6.1	7.9	9.5	23.5	3.9	11.1	38.5
854	12.6	12.7	9.7	35.4	3.5	4.2	42.7
739	7.1	6.7	7.7	21.6	2.8	11.1	35.5
773	7.1	9.4	7.1	23.5	3.9	9.3	36.8
808	3.9	4.5	5.9	14.3	3.3	15.5	33.0
821	5.7	6.9	10.6	23.2	3.4	5.5	32.0
801	4.9	6.2	5.7	16.8	4.1	38.2	59.0

* Total phenylnaphthalenes.

** Total alkyl-tetralins and naphthalenes.

Table 4

Product Distributions from Coal Liquefaction,
Corrected for Artifacts from Solvents

(% of dmmf coal)

PSOC No.C	Total conversion	Total liquids		Gases (by diff.)		Asphal-tenes	Hexane-sol. oil		Sat. HPLC frac.	Polar HPLC frac.	Aromatic HPLC fraction	
		uncorr.	corr.	uncorr.	corr.		uncorr.	corr.			uncorr.	corr.
833	50.3	28.4	24.8	21.9	25.6	16.2	10.3	8.6	0.1	6.5	3.7	2.0
791	57.8	39.7	35.6	18.1	22.2	21.4	18.4	14.3	0.2	10.4	7.8	3.7
785	57.5	38.3	34.9	19.3	22.6	21.5	16.8	13.4	0.8	8.4	7.6	4.2
240A4	59.3	38.5	35.9	20.8	23.4	25.1	13.4	10.8	0.6	7.3	5.5	2.9
240A1	70.1	45.1	40.6	25.0	29.5	22.2	18.0	13.4	0.4	10.4	7.2	2.6
866	49.1	37.3	34.7	11.8	14.4	25.7	11.6	9.0	0.2	6.3	5.2	2.5
548	52.0	42.5	39.2	9.5	12.8	24.8	17.8	14.4	0.6	9.9	7.3	3.9
680	56.9	49.3	47.1	7.6	9.8	33.3	15.9	13.8	0.1	10.1	5.8	3.6
854	53.3	44.0	42.4	9.2	10.9	31.7	12.3	10.7	0.8	7.6	4.0	2.3
739	52.0	43.6	42.0	8.4	10.0	31.4	12.3	10.7	0.9	6.8	4.6	3.0
773	55.4	47.7	46.1	7.7	9.4	35.9	11.8	10.1	0.4	6.9	4.5	2.9
808	45.4	40.2	39.0	5.2	6.4	29.2	11.0	9.8	0.3	6.8	4.0	2.7
821	58.4	52.2	50.5	6.2	7.9	39.1	13.2	11.4	0.5	7.2	5.5	3.7
801	28.5	25.0	21.3	3.6	7.3	15.7	9.3	5.5	0.3	2.7	6.2	2.5

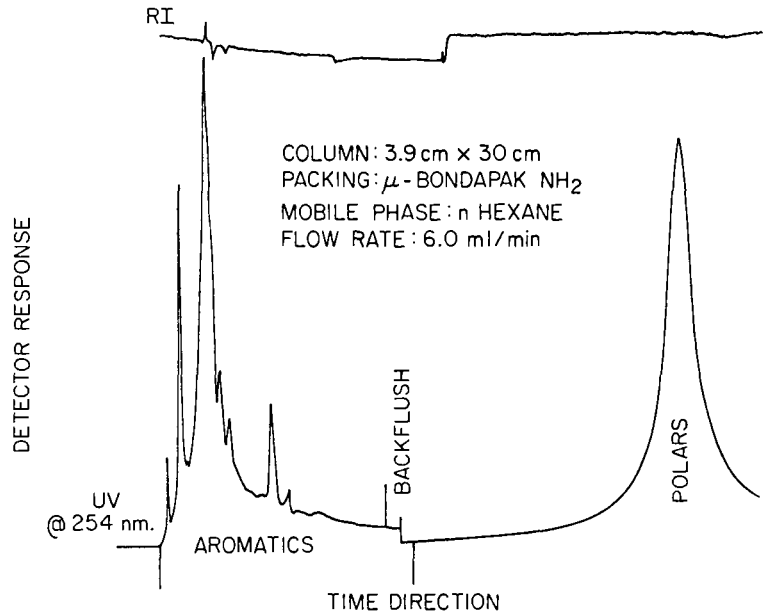

LIQUID CHROMATOGRAPHIC SEPARATION OF A VACUUM-STRIPPI
OIL INTO SATURATE, AROMATIC AND POLAR FRACTIONS

Figure 1

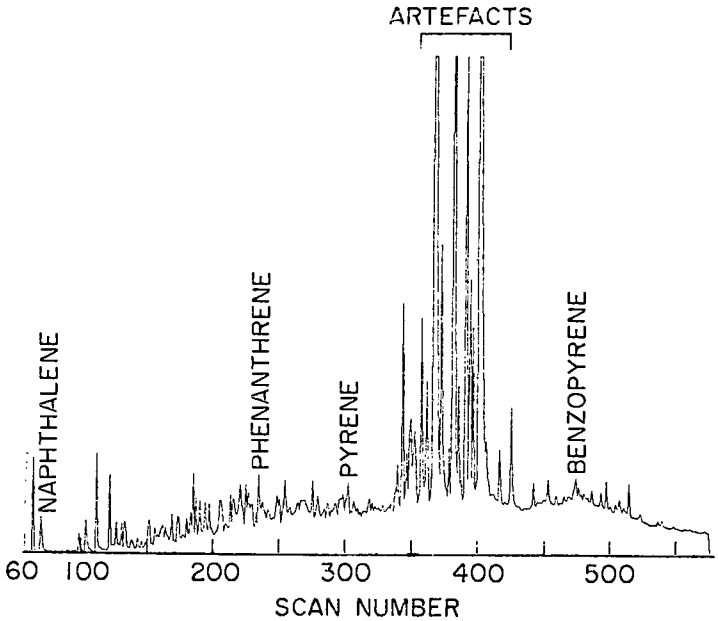

CAPILLARY GAS CHROMATOGRAM OF AROMATIC FRACTION FROM PSOC-739 (hvB, KENTUCKY #12)

Figure 2

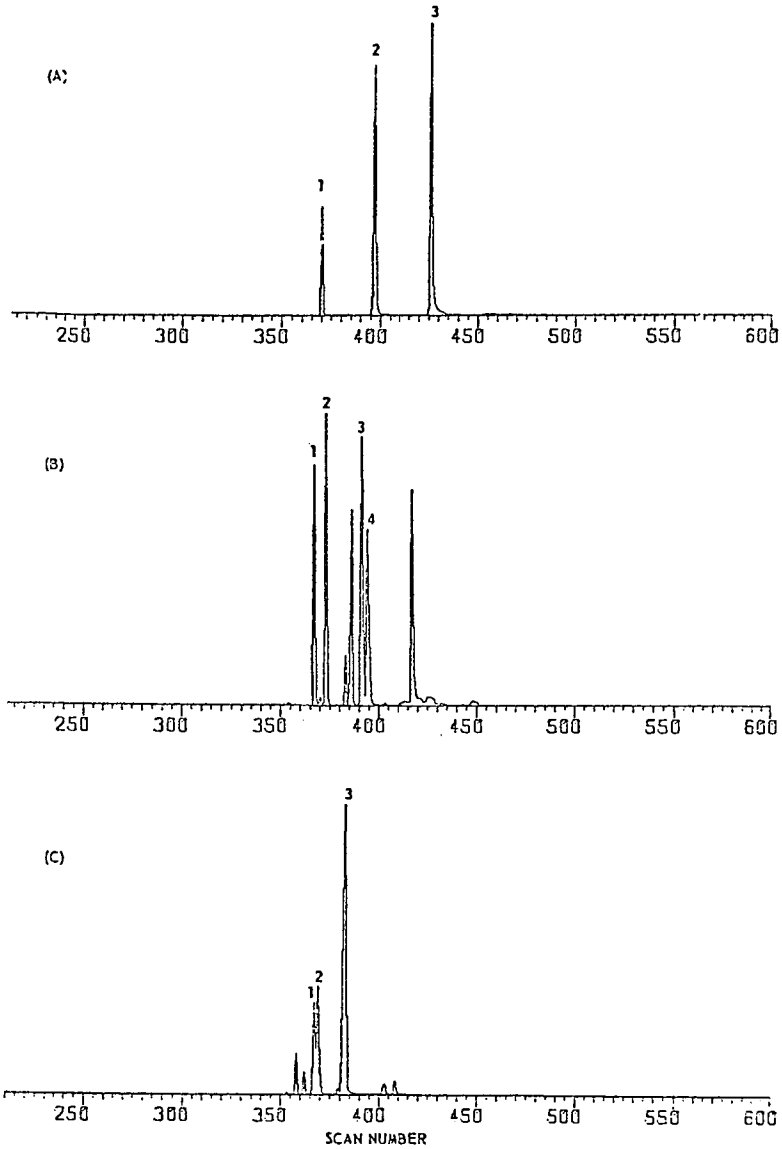

Figure 3 SINGLE ION CHROMATOGRAMS FOR HPLC FRACTION 2 FROM PSOC-739 (KENTUCKY NO. 12)
(A) m/e = 254, (B) m/e = 258, (C) m/e = 262

FATE OF SELECTED 1-, 2-, AND 3-RING COMPOUNDS DURING RECYCLE COAL LIQUEFACTION OPERATION

D. C. Cronauer, R. I. McNeil, D. A. Danner

Gulf Research & Development Company
P.O. Drawer 2038, Pittsburgh, PA 15230

and J. H. Wieland, and J. S. Abichandani

Department of Petroleum & Chemical Engineering
University of Pittsburgh, Pittsburgh, PA 15261

INTRODUCTION

To observe the adduction, isomerization, and cracking of labeled solvent species, a series of coal liquefaction runs was undertaken using a bench-scale unit capable of continuous recycle operation. These experiments were made with ^{13}C-labeled solvents including octahydrophenanthrene, phenanthrene, methylphenanthrene, dimethyltetralin, and mesitylene. This work served as an extension of previously reported[1-3] laboratory-scale experiments using similar labeled model liquefaction solvents.

EXPERIMENTAL

The recycle runs with labeled compounds were performed using a continuous, bench-scale, coal liquefaction unit, a schematic of which is shown in Figure 1. In summary, the unit consisted of feed and product systems, a preheater of 8 min nominal space time, and a 1 L stirred autoclave of 60 min space time.

The operating procedure consisted of preparing a feed slurry in a heated, stirred tank separate to the unit. The feed was made up of Powhatan No. 5 Mine coal, a portion of recycle heavy product slurry from the previous period, and a process solvent generated during previous SRC-II runs in the GR&DC P-99 PDU[4] feeding the same coal. The analyses of the solvent and coal are given in Table I. This feed blend was introduced into the bench-scale unit every 4 h.

The ^{13}C-labeled compounds were prepared under the direction of Professor E. J. Eisenbraun of Okalhoma State University with a portion of the analyses of intermediates and products being done at GR&DC. A detailed description of the techniques of synthesis and analyses of a portion of these compounds are reported by Seshadri et al.[5] and in Reference 3.

In addition to sample distillation and routine elemental analyses, samples of heavy product slurry were Soxhlet extracted using, in sequence, the solvents: pentane, toluene, and tetrahydrofuran (THF). The Soxhlet extractions with pentane and toluene were typically of 48 h duration, and the THF of 24 h. The solvents were stripped on a steam table (80°C) with a stream of

nitrogen prior to analysis. Selected samples of separator liquids (combined No. 2, No. 3, and ice traps) and pentane solubles were separated by HPLC into saturates, aromatics, and resin (polar) fractions. An in-house HPLC was used with Bio-Sil A silica gel (20-44 micron); a description of the operating procedure was reported by Suatoni and Swab.[6]

The level of ^{13}C-labeling in the product fractions was determined by the standard technique of combustion to CO_2 followed by use of a Varian MAT 250 MS to determine the ratio of mass 45 to 44 (stated sensitivity of $<2 \times 10^{-6}$). Isotopic compositions are reported as values, the definition of which follows:

$$^{13}C = \frac{R_S - R_R}{R_R} \times 1000\% \text{ (parts per thousand)}$$

where R_S and R_R refer to the $^{13}C/^{12}C$ ratio in the sample and reference, respectively. The reference is PDB (Peedee Formation carbonate [belemnite]) with a value of 0.0112372. Coal has a typical range of -20 to -30 parts per million (This analysis was done at GR&DC and at Global Geochemistry Corp.)

RESULTS

Overall Material Balance of Recycle Runs--Lined-out operation of the bench-scale unit was first established with a feed consisting of Powhatan No. 5 coal, process solvent (boiling point 400°-800°F), heavy recycle product slurry, and hydrogen. The product streams primarily consisted of gases, No. 2 and 3 condensates, and heavy product slurry. The reactor was run at conditions of 455°C, 1.0 h space time, and 13.8 MPa (2000 psig). After lined-out operation was achieved (34 h), a small sample of labeled octahydrophenanthrene (HPh) was introduced to the feed tank at a level of 26 g/5000 g charge. After 26 h, the next labeled compound, dimethyltetralin (DMT), was similarly charged, and the product streams were analyzed. For this and the remaining three labeled solvents, a 24-h period was used. The runs with labeled solvent were done in the following order: (89-1) octahydrophenanthrene (HPh), (89-2) dimethyltetralin (DMT), (89-3) mesitylene (MST), (89-4) methylphenanthrene (MePh), and (89-5) phenanthrene.

In all of the runs, it was assumed that the addition of the labeled solvent at a level of about 0.5 wt% once every 24 h would not affect lined-out recycle operation. Based on a detailed material balance of the second and fourth periods, this assumption appeared valid as shown in the Tables II and III.

Extraction of Process Samples from the Recycle Runs--To isolate concentrates for GC/MS and $^{13}C/^{12}C$-MS analyses, samples of both the combined condensates and heavy slurry products were separated into fractions using extraction and HPLC. The results for 89-1 and 89-5 are given in Table IV.

Calculated Material Balance of Labeled Species--To follow the course of the ^{13}C-labeled species during SRC-II type recycle runs, it was necessary to account for both slurry product withdrawal and losses due to vaporization. In the case of very volatile compounds, most of the ^{13}C-label was recovered in the light condensate collected in the traps. This material was not recycled, and, therefore, it was quickly lost from the system. In the case of essentially nonvolatile species, losses occurred by removal of a portion of the reactor effluent stream as heavy product. To account for vaporization losses, the reactor system was modeled using average material balances with a factor "XVAP" giving the fraction of ^{13}C-labeled compound that was lost during each reactor pass due to vaporization. Figure 2 is a plot of the calculated concentration of traced (^{13}C) of the slurry from the product tank as functions of time and losses due to vaporization.

Results of Analysis of Fluids for ^{13}C-Labeled Compounds--In addition to an analysis of the product slurries and condensate streams, individual samples of pentane solubles (oils), asphaltenes, and THF insolubles were analyzed for $^{13}C/^{12}C$ ratios to determine trends with time. Overall ^{13}C material balances were calculated to show how the labeled compounds were distributed between gases, condensates (Traps 1-3), heavy products (asphaltenes, etc.), and bulk product.

As shown in Figures 3 and 4 ($^{13}C/^{12}C$ ratios of slurries and condensates), the results show the trends predicted from Figure 2. Specifically, a concentration peak occurred at about 4-6 h into the cycle, and this went essentially to zero after 24 h. In addition, the curves for the phenanthrene (Ph) and octahydrophenanthrene (HPh) runs were similar, as would be expected from the closeness of their boiling points. The loss of labeled species into the condensates recovered in the various traps also followed expected trends. As indicated by ^{13}C analysis, about 11.8% of the highest boiling labeled compound, methylphenanthrene (MePh) was found in the condensates. However, the ^{13}C-labeled methyl group readily cracked as indicated by a high recovery (namely 46.9%) of labeled gases, primarily methane. The recovery of ^{13}C-labeled compounds in the condensates from the HPh and Ph runs was essentially identical at 32.9 and 34.2%, respectively. In the run with labeled dimethyltetralin, in excess of 80% of the label was observed in the condensate. Only a low recovery (about 10%) of the low boiling mesitylene was recovered in the condensates. From an analysis of the remaining streams, it appeared that this compound was lost from the heated feed tank.

The levels of labeled compounds in the heavy product fractions somewhat follow anticipated trends. The amount of HPh held in the asphaltene fraction, by chemical adduction, was 4.8% of that fed, while that in the THF insolubles was 0.5%. In the case of Ph, the respective levels were 1.5 and 0.7%. The level of adduction of MePh was intermediate between HPh and Ph at 2.9% in the asphaltenes and 0.3% in the THF insolubles. Considering the high level of MePh cracking, these latter values are consistent with those of HPh. Essentially no adduction of dimethyltetralin and mesitylene were observed in that the $^{13}C/^{12}C$ ratios of the heavy fractions from these runs were the same as those of the base case before label use.

Reaction Trends of Individual Phenanthrene Compounds--The aromatic cuts of condensates and slurry product streams were analyzed for Run 89-1 (HPh) and 89-5 (Ph). It is first noted that octahydrophenanthrene was present in the products at concentrations less than 0.03 wt%. This compound gave up at least a portion of its hydrogen very rapidly, and, therefore, it can be considered to be absent from a recycle system unless external catalytic hydrogenation is used. Within the accuracy of the GC/MS analysis, the concentrations of phenanthrene, dihydrophenanthrene (H_2Ph), and tetrahydrophenanthrene (H_4Ph) remained essentially constant through the run perids of Runs 89-1 and 89-5. The results are given in Table V.

It is first obvious that the results from Runs 89-1 and 89-5 are consistent. The total concentrations of phenanthrene plus hydrophenanthrenes averaged 2.9 and 2.8 wt% in the condensate and slurry, respectively. (Note that alkyl subsituted phenanthrenes are not included.) Due to boiling points, the relative distributions of hydrophenanthrenes to phenanthrenes were greater in the condensates than in the slurry. From an overall material balance, the conversions of coal to Ph, H_2Ph, and H_4Ph were about 0.7, 0.2, and 0.2 g/100 g MAF coal, respectively.

By a GC/MS analysis of the product fraction of Runs 89-1 and 89-5, it was found with the introduction of labeled Ph in SRC-II type operation, little of this component is hydrogenated to dihydro and tetrahydro species, In addition, an observed presence of labeled compounds of C_3-naphthalene and isomerized derivatives of octahydrophenanthrene confirms that ring opening and isomerization of hydroaromatics occurs at coal liquefaction conditions.

ACKNOWLEDGMENT

We are grateful for the funding of this project by the U.S. Department of Energy under DE-AC22-80PC30080. We acknowledge the suggestions of A. Bruce King, the laboratory work of H. K. Little, and the ^{13}C analyses of T. C. Ashbaugh, R. J. Drozd, and R. C. Burruss.

REFERENCES

1. McNeil, R. I., Cronauer, D. C., and Young, D. C., "Isomerization of Tetrahydroaromatic Groups Under Coal Liquefaction Conditions," Fuel, (scheduled April 1983).

2. McNeal, R. I., Young, D. C., and Cronauer, D. C., "Extents and Models of Adduction of Hydrocarbon and Nitrogen-Containing Solvents in Coal Liquefaction," accepted by Fuel.

3. Cronauer, D. C., McNeil, R. I., Young, D. C., and Ruberto, R. G., Final Progress Report, DOE Contract DE-AC22-80PC30080, September 1982.

4. McIlvried, H. G., "Summary of Results from SRC-II Runs Made on Process Development Unit P-99, Runs P99-15 to P99-85," Report No. 627RM101, DOE/ET/10104-42, November 1981.

5. Seshadri, K. S., Jewell, D. M., Bymaster, D. L., Dobbs, T. K., Brown, C. E., Vickery, E. H, and Eisenbraun, E. J., "Synthesis and ^{13}C-NMR Spectra of Some Substituted Benzenes, and Naphthalenes and Hydroaromatic Hydrocarbons," submitted to J Labeled Compounds.

6. Suatoni, J. C., and Swab, R. E., J. Chromat. Sci. (1976), 14, 535.

Table I

ANALYSIS OF COAL AND P-99 DERIVED PROCESS SOLVENT

Sample Designation	Powhatan No. 5 Mine Coal	Process Solvent
1. Proximate Analysis		
% Moisture	1.1	--
Ash	9.6	--
Volatile	39.6	--
Fixed Carbon	49.7	--
2. Elemental Analysis	(Dry)	
% Carbon	72.3	87.2
Hydrogen	5.1	8.7
Nitrogen	1.5	0.9
Oxygen	7.8 (diff)	2.8
Sulfur	3.6	0.4
Ash	9.7	--
	100.0	100.0

Table II

OVERALL MATERIAL BALANCE
Recycle Run 89

Feed (g/h)			Products (g/h)		
Run Period	89-2	89-4	Run Period	89-2	89-4
Coal	367.6	367.8	Gases (and H_2O)	98.9	97.5
Process Solvent	196.0	202.3	No. 2 Condensate	96.9	69.6
Heavy Product Slurry	661.6	656.0	No. 3 Condensate (plus ice traps)	95.1	141.8
Hydrogen (Consumption)	13.9	13.7	Heavy Product Slurry	900.5	882.3
Total	1239.1	1239.8	Total	1191.4	1190.2
			Recovery	96.1%	96.0%

Table III

NET PRODUCT YIELDS (MAF BASIS)
Recycle Run 89

Yield Component	89-2	89-4	Average
H_2 Consumption	-4.2	-4.2	-4.2
C_1-C_4	16.5	15.7	16.1
Other Gases(CO, etc.)	2.3	2.3	2.3
Water	5.9	5.9	5.9
C_5-380°F	15.5	16.8	16.1
380-550°F	9.1	13.0	11.1
550-900°F	10.3	7.6	9.0
C_5-900°F	34.9	37.4	36.2
380-900°F	19.4	20.6	20.1
900°F$^+$ P.S.	35.3	34.2	34.7
IOM	9.3	8.7	9.0
900°F$^+$ Organic	44.6	42.9	43.7

Table IV

HPLC EXTRACTION SUMMARY

Product Fraction	Saturates (wt%)	Aromatics (wt%)	Resins (wt%)	Hexane Ins. (wt%)
Run Period 89-1:				
a. Condensates	5.5 ± 1.6	50.1 ± 3.8	44.0 ± 4.0	0.4 ± 0.2
b. Oils (Slurry)	2.8 ± 0.5	64.7 ± 4.1	32.5 ± 6.5	
Run Period 89-5:				
a. Condensates	4.8 ± 2.4	53.0 ± 5.0	41.9 ± 3.7	0.3 ± 0.2
b. Oils (Slurry)	3.3 ± 0.3	69.0 ± 3.8	27.7 ± 3.8	

Table V

SUMMARY OF PHENANTHRENE CONCENTRATIONS, WT%

Component	89-1		89-5	
	Condensate	Slurry	Condensate	Slurry
Phenanthrene	1.66	2.10	1.85	2.25
H_2Ph	0.47	0.24	0.61	0.32
H_4Ph	0.67	0.33	0.51	0.30
H_8Ph	<0.03	<0.03	<0.03	<0.03

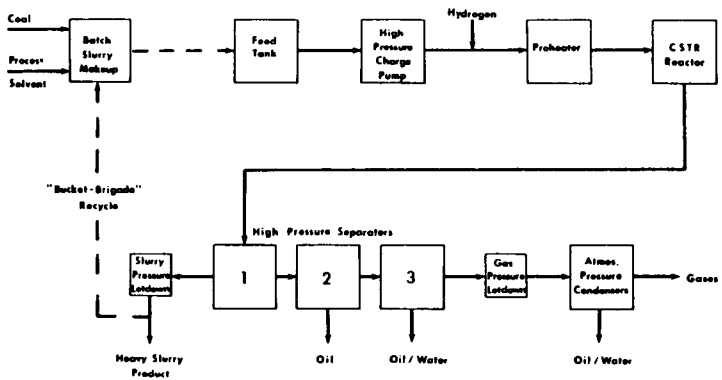

FIGURE 1: SCHEMATIC OF THE AI RECYCLE COAL LIQUEFACTION UNIT

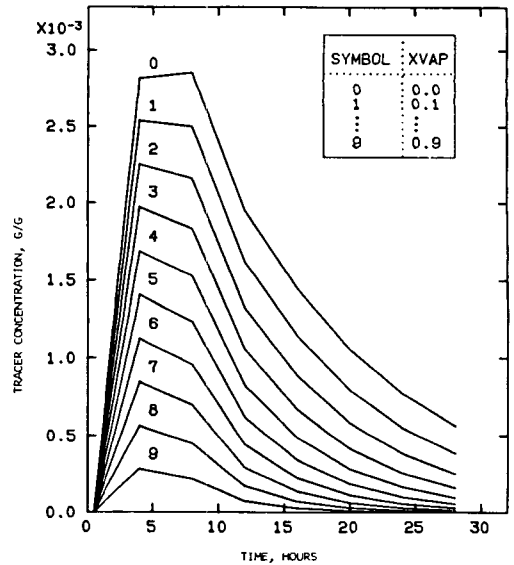

FIGURE 2: CONCENTRATION OF TRACER IN THE SLURRY PHASE AS A FUNCTION OF TIME ANDFRACTION OF TRACER VAPORIZED: SLURRY DENSITY=1.00

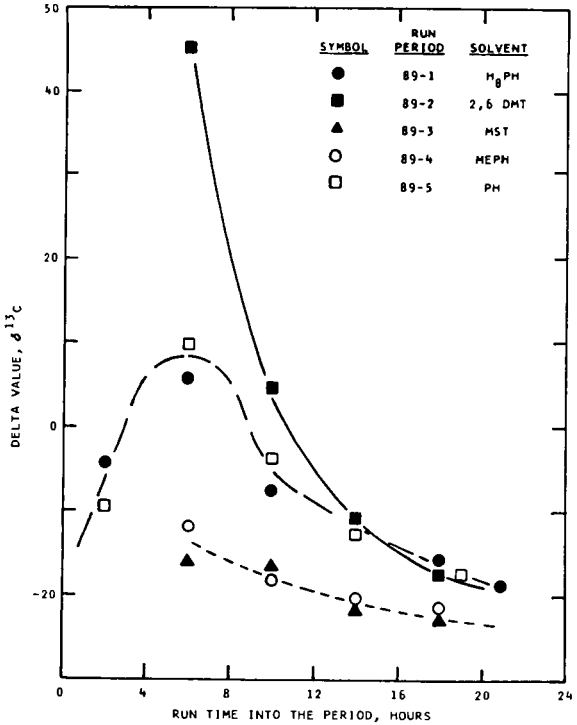

FIGURE 3: ^{13}C LEVELS IN THE CONDENSATE SAMPLES OF RUNS 89-1 THROUGH 89-5

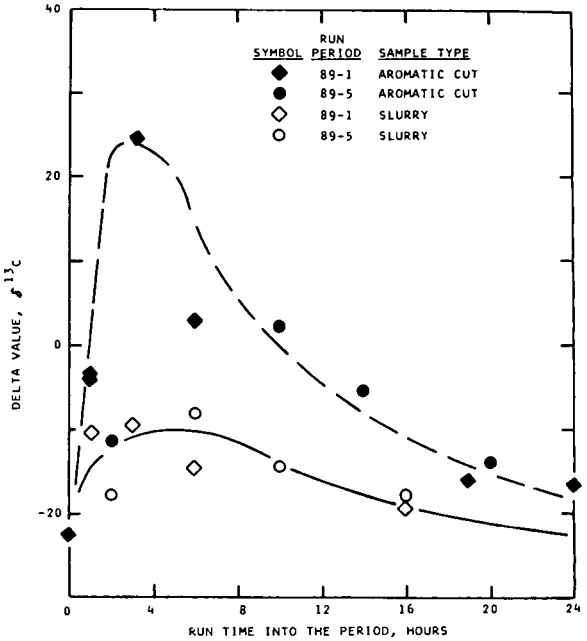

FIGURE 4: ^{13}C LEVELS IN SAMPLES OF PRODUCT SLURRY AND THE AROMATIC CUTS DERIVED FROM THE SLURRY

Correlation of Coal Quality to Coal Liquefaction

D. S. Hoover

International Coal Refining Company
P.O. Box 2752, Allentown, PA 18001

Introduction

A large-scale direct coal liquefaction plant will consume substantial quantities of coal as a feedstock material. Due to the nature of the coal mining industry this supply will be acquired from several mines operating in different coal reserves. Procurement of coal from multiple sources, over time will undoubtebly lead to variations in the characteristics of the plant feed. Physical and chemical coal properties are known to vary within a reserve due to the mechanisms of seam formation and subsequent geologic metamorphism. In addition, mining methods and physical beneficiation affect the organic and inorganic constituents in the mine product. Furthermore, the specification of a single seam, for example Ky #9 or Ill. #6 as the source for potential feed-coals, is insufficient since it has been shown that substantial variations in coal properties can exist within a single seam.

Although it is clear that variations in feed coal properties can affect plant operations and yields, few quantitative relationships have been developed. The difficulty in understanding the importance of coal characteristics is in part related to the complex nature of coal, and problems in the selection, characterization and testing of representative feedstock samples. The driving force for developing this understanding is directly related to the selection and procurement of the essential raw material for liquefaction processing. A scientifically based understanding of how to select coal sources from within a mining region and how to compensate for variations from an individual mine will improve the operability and economics of any direct liquefaction plant.

This study has investigated the degree to which coal properties change within a supply region and how these variations impact on yields and economics of an SRC-I type process. Statistical data analysis has isolated critical coal properties influencing liquefaction reactivity and quantitative prediction equations have been developed.

General Coal Characteristics Influencing Reactivity

Research work to identify the suitability of U.S. Coals for direct liquefaction were begun by the U.S. Bureau of Mines station at Bruceton, PA in the early 1940's[1,2]. These efforts investigated coals of varying petrographic composition and rank, concluding that these characteristics significantly affected the ease by which a coal could be liquefied. More recently, work has been completed by a number of investigators which confirms that the total reactive maceral content of the coal is related directly to its overall conversion to extractable products[3,4,5].

Although coal rank is recognized as a derived property related directly to a coal's composite organic chemical structure, its impact on liquefaction reactivity is not clearly understood. Most researchers are in agreement that coals higher in rank than high volatile A bituminous are poor candidates for liquefaction feedstocks due to low reactivity. This limitation presents little problem for the development of a coal liquefaction industry since these high rank coals represent only ten percent of the country's production. The

more abundant lower rank coals have displayed divergent reactivities depending upon the experimental conditions and method of investigation. Neavel[4] has shown that the coal conversion to benzene solubles plus gases is inversely proportional to the rank of the coal for residence times from 2.5 to 30 minutes. These results are generally in agreement with those of Whitehurst[6] and Yarzab[7] for long residence times. However, Whitehurst[6] has shown that in short residence time coal liquefaction, low rank coals are substantially less reactive than high volatile bituminous coals of similar petrographic composition. In processing coals under SRC-II conditions using disposable iron catalysts, Wright[8] has found that lignites and subbituminous coals have higher conversions and greater yields of distillate than high volatile bituminous Pittsburgh Seam coals. Thus, providing that reaction conditions are chosen correctly, the coal is prepared properly prior to liquefaction and sufficient catalyst is present, lower rank coals would appear to have higher reactivity than high volatile bituminous coals.

One coal characteristic not explained by measures of rank and petrographic composition is the nature of inherent mineral matter. Many authors have shown that mineral matter in coal can act as an inherent catalyst for improving liquefaction yields. The concensus of this work has been that iron sulfides, particularly pyrite, are the most effective catalysts present in the inherent coal mineral matter.[9] Although some differences in pyrite catalysis activity have been reported[10], most work has shown that the very high levels (up to 10% pyrite on coal) must be added to affect a significant change in the yield structure of Eastern Bituminous Coals.[11,12] Low iron subbituminous coals can be made more reactive with somewhat lower levels of pyrite addition.[13]

Experimental Investigation of Coal Reactivity

The International Coal Refining Company (ICRC) Research Group has been heavily involved with developing experimental data to support the SRC-I Demonstration Plant Project. A portion of this effort was to determine the effects of feed coal variation on plant performance. Although the majority of potential feed coals for this plant would come from a restricted area (Illinois Basin), it became clear in this program that three major technical areas would need investigation as follows:

- Coal variation from an individual mine,
- Coal variation within the reserve area, and
- Effects of these variations on liquefaction yields.

Due to design and operation considerations, a decision was made early in the demonstration plant program to consider only use of washed coals. This constraint significantly limited the number of mine operations which could be considered as suppliers.

An experimental program was established with the Institute of Mining and Minerals Research, University of Kentucky, to sample mining operations in a pattern to provide geographic and stratographic diversity. The sample locations, in relation to the mining regions are shown in Figure 1. Samples were collected from the run-of-mine coal as well as the washed coal. Several mining operations were studied for both long- and short-term variation in coal properties.

In the short term coal variability study, samples were collected from the operation daily and analyzed for changes in composition. Figure 2 shows the daily shifts in sulfur and ash content for a mine in the KY #9 seam. These results demonstrate that the coal cleaning plant is necessary not only to

reduce the amount of mineral matter in the coal, but also to buffer variations in composition due to mining. An additional benefit from coal preparation is an increase of approximately three percent in the total reactive maceral content of the clean coal, enhancing the liquefaction potential.

Based upon the results from the short term study, a five day period was selected as the time in which to composite a sample to define a plant's average output. Thus, once a month a five day period was sampled and composited for each of six months. These results (Figure 3) show that some long term shifts in clean coal composition can occur. The variations may result from changing characteristics of an individual coal reserve or changes in mine operations. A liquefaction processing plant will need the flexibility to deal with these changes if they would significantly affect operations.

The second portion of this project was to define the regional variation in coal composition. Table 1 shows the range in several clean coal properties across the region compared to the variation which might be expected from an individual plant. These results illustrate that the variation across the region is generally two to four times that which might be expected from an individual plant. Furthermore, the absolute ranges in variables, such as vitrinite reflectance, pyritic sulfur and total reactive macerals, are such that they will affect substantially coal liquefaction results. Therefore, despite the contention that coal supply from an individual mine will shift with time, there are probable advantages to selecting and blending coals from mines whose average composition is in the high reactivity range.

The third portion of this program was to test the set of clean coals to determine the effects of variations in properties on coal liquefaction. In this program the coals were liquefied in a 100 pound per day continuous bench scale process development unit (CPDU) under standard conditions as follows:

o Reaction Temperature	840°F
o Reaction Time	30 min
o Total Pressure	2000 psig
o H_2 Flow Rate	28,000 SCF/Ton Coal
o Coal Concentration	40 wt.% in Wilsonville Recycle Solvent

These are essentially the SRC-I standard process conditions with the exception of the shorter (30 min) residence time.. All samples from the process unit were analyzed by a standard workup procedure to determine the yields of products on a dry ash-free coal basis and hydrogen consumption.

Figure 4 shows the range in reactivity demonstrated by these coals as related to oils yield and hydrogen consumption. These two factors are useful for assessing coal reactivity since they are among the most sensitive economic parameters in a liquefaction plant. The results show a group of high reactivity coals (>25% oils yield), a group of average coals (15-25% oils yield), and one very low activity sample.

Ranges in coal reactivity of this magnitude impact both on plant operations and on revenue economics. Improvements to plant operation may include: improved solvent balance, less loss of preasphaltenes to the gasifier residue, and the flexibility to operate at lower severity. The advantages of operation at a decreased severity are lower duty on the fired preheater and better reaction stability. Of course, to operate with a high reactivity coal at high severity would require some additional hydrogen capacity and this element does impact on operations and economics.

Table 2 shows a yield and economic comparison of operating a hypothetical single-stage SRC-I type plant in a maximum heavy fuel oil mode. This analysis assumes that all the middle oil produced will be blended with the solid SRC and sold as heavy oil. The comparisons are shown on an identical plant case, operating with an average and, alternatively, a high activity coal. Although this assessement has been simplified and contains several assumptions, it is clear that using the high activity coal, including the hydrogen penalty, results in a significant (11%) improvement in revenues. Since these coals are sold currently on a fuel basis (cents/mm btu) there can be compelling economic incentives for choosing high activity coals.

The advantages in operations and economics for a simple thermal process (i.e. SRC-I) also appear to be present for more complex catalytic systems. Figure 5 shows the results of processing a low activity and a high activity coal, with and without a slurry phase catalyst. In this comparison, it is evident that the catalyst acts to provide an incremental improvement in oil yield over the baseline non-catalyst case. Rather than seeing the yield structures converge due to catalytic processing, they maintain approximately the same differential as the original coal reactivity. Although these results demonstrate that initial coal activity dominates in one stage thermal and catalytic processes, it is not clear what impact it has on integrated two-stage processing.

Analysis of Liquefaction Data

In order to realize an advantage due to coal reactivity in either operations or economics, it is necessary to understand methods of selecting high activity coals. One objective of this research program was to develop correlations between coal characteristics and liquefaction product yields. In order to develop these types of correlations it is necessary to have a homogeneous data set which provides a sufficiently broad, and normally distributed, pattern of variables. Although the current dataset is probably too small (13 coals) to develop highly correlated relationships, it is useful for determining trends in the data.

The coal characteristics and liquefaction yield data sets were both analyzed to detect and minimize strong statistical intercorrelations. This analysis resulted in the selection of four independent coal variables and five relatively independent liquefaction variables which were correlated against each other (Table 3). Based on the relationships detected from Table 3 the following empirical prediction models were calculated.

$$\text{Total Conversion} = (14.1\ (\text{Pyritic Sulfur}) + 4.1\ (\text{Vitrinite reflectance}) + 77.2) \times \text{Total Reactive Macerals}/100 \qquad \text{Eq. 1}$$

$$R^2 = 0.82$$

$$\text{Oil Yield} = 16.2\ (\text{Pyritic Sulfur}) - 1.2\ (\text{Volatile Matter}) + 13.6\ (\text{Vitrinite Reflectance}) + 52.9 \qquad \text{Eq. 2}$$

$$R^2 = 0.47$$

The multiple R-squared for equation #1 (0.82) is relatively good for complex multivariate relationships such as those existing in coal research. The constant term in this equation (77.2) is relatively large in comparison to

the values of the predicted variable and attempts to generate a strong relationship would work to reduce this value. The parity plot in Figure 6 of the observed conversion versus the predicted conversion shows there are no significant outliers (or large residuals) in this data set and that predictive relationship is reliable. Unfortunately, the R-squared for equation #2 is not as good (0.47). Figure 7 is the parity plot of oil yield observed versus oil yield predicted for this equation; it indicates that there are no single or patterned outliers. This suggests that an additional characterization factor is probably necessary to improve the prediction of oil yield.

This analysis of the data set resulted in the selecting of many of the same variables as those determined by the Pittsburg & Midway Coal Mining Co. for the prediction of SRC-II yield structures.[14] The relationship between pyritic sulfur in the clean coal and the conversion of total reactive macerals detected in the statistical analysis (correlation coefficient equals 0.902) is shown in Figure 8. This relationship shows that as pyritic sulfur drops below 1.10 wt. percent, the coal conversion reactivity decreases significantly. However, in another portion of the research program, experiments on the importance of coal preparation showed that levels of pyritic sulfur had little affect on liquefaction yields. The results from one of these experiments are shown in Figure 9. Despite coal samples which range in ash and pyritic sulfur in excess of those detected in the data analysis, the liquefaction yields are rather consistent.

The reconciliation of these seemingly diametrically opposed results appears to reside in the activity of the pyrite present in cleaned coals versus that in the run-of-mine and partially cleaned samples. A series of coals all cleaned to approximately the same ash level would be expected to contain approximately the same amount of pyrite, if it were distributed in the same manner in all the samples. The cleaned coals in the data analysis set (similar in preparation and ash content) ranged in pyritic sulfur from 1.42 to 0.65 percent, indicating that some of the samples probably contained pyrite which was finely dispersed in the organic matrix and was not removed by cleaning. Generally, these coals were those which had high activity for liquefaction. The pyrite that would be present in the level 1 and level 2 cleaning shown in Figure 9 would be comprised substantially of coarse material from seam partings and pyrite nodules. The experimental data on these samples indicate that this type of pyrite has little catalytic effect in the SRC-I liquefaction system. The majority of the catalytic activity appears to be provided by the finely dispersed pyrite retained in certain cleaned coals.

The importance of pyrite dispersion is also in general agreement with results determined in the disposable catalyst programs.[11,12,15] These workers found that additions of particulate pyrite at levels approaching 5 weight percent pyritic sulfur on coal were necessary to show much catalytic activity. However, when iron was added to the coal in a dispersed system, much lower levels resulted in high catalytic activity.[16] Hence, not only the amount, but more importantly the form of the pyrite in the coal appears to be the most important factor in controlling its contribution to the coal activity.

One can conclude also from the data analysis that the level of geochemical maturity, or rank of the coal as measured by vitrinite reflectance, is of significance to liquefaction yields. Although the range of rank in these samples is not as large as might be necessary to fully identify this effect, increases in rank correlate negatively with both oil yield and conversion. The subtle differences in the ranks of the coals in this sample suite do reflect changes in the structural chemistry of the coal macerals. In this range of geochemical maturity, coals lose oxygen and are believed to undergo

rearrangement and ring condensation. These reactions may tend to result in a more refractory organic phase to dissolution and liquefaction. A negative correlation of liquid yield and conversion with coal rank parameters was also reported by the P&M workers.[13]

Summary

It is clear from the preceeding discussion that variations in coal properties do affect liquefaction results. The observed differences between coals can be as large as those between Western Subbituminous compared to Eastern Bituminous, or as small as changes in coal within a single seam or individual mine. These variations in properties do affect liquefaction yields, plant operations and economics. Selection of coals, even from a restricted region, can be advantageous since critical properties vary more from source to source then from an individual mining operation.

Research at ICRC and elsewhere has shown that quantitative relationships can be developed between coal characteristics and yields. These efforts have shown that the amount of dispersed pyrite in the coal, the geochemical maturity and the petrographic composition are important coal parameters. Clean coals from this region with less than 1.10 wt. percent pyritic sulfur were found to have significantly reduced liquefaction reactivity. Unfortunately, the prediction of oil yield from coal properties has proven difficult and will probably require the addition of more fundamental parameters of coal chemistry to improve its precision.

An improved understanding of the relationship of coal properties to liquefaction results would be useful from a scientific point of view as well as a processing standpoint. The advantages of selecting and manipulating coals for improved processing results are self evident. The impact of pyrite dispersion in the organic matrix may indicate that initial dissolution reaction and associated hydrogen rearrangement, promoted by an in-situ catalyst, are instrumental in defining the final product distribution. The ability to better understand the mechanisms of coal dissolution from a fundamental point of view may lead to new improved processing concepts, as well as a better understanding of the U.S. coal resource.

Acknowledgement

The majority of the work reported in this paper was carried out by the International Coal Refining Company and the Institute for Mining and Minerals Research, University of Kentucky with support provided by the United States Department of Energy under Contract No. DE-AC05-78RO-3054.

References

1. Storch, H. H., Hirst, L. L., Fisher, C. H., and Sprunk, G. C., "Hydrogenation and Liquefaction of Coal", U.S. Bureau of Mines Tech. Paper 622, 1941, 110 pp.

2. Fisher, C. H., Sprunk, G. C., Eisner, A., O'Donnell, H. J., Clarke, L. and Storch, H. H., "Hydrogenation and Liquefaction of Coal. II. Effects of Petrographic Composition and Rank of Coal", U.S. Bureau of Mines Tech. Paper 642, 1942, 162 pp.

3. Davis, A., Spackman, W. and Given. P. H., "The Influence of Properties of Coals on Their Conversion to Clean Fuels", Energy Sources, 1976, pp. 55-81.

4. Neavel, R. C., "Liquefaction of Coal in Hydrogen Donor and Non-Donor Vehicles", Fuel 55, 1976, pp. 237-248.

5. Gorin, E., "Fundamentals of Coal Liquefaction", Chemistry of Coal Utilization, 1981, pp. 1845-1990.

6. Whitehurst, D. D., Mitchell, T. O., Farcasiu, M., Dickert, J. J., "The Nature and Origin of Asphaltenes in Processed Coals", EPRI Final Report AF-1298, 1979, 86 pp.

7. Yarzab, R. F., Given, P. H., Spackman, W., and Davis, A., "Dependence of Coal Liquefaction Behavior on Coal Characteristics. 4. Cluster Analyses for Characterization of 104 Coals", Fuel 59, 1980, pp. 81-92.

8. Wright, C. H., "Coal Rank Effects in the SRC-II Process", ACS Div. of Fuel Chem. Vol 27 #3-4, 1982, pp. 43-52.

9. Davidson, R. M., "Mineral Effects in Coal Conversion", IEA Technical Report, 1983, 100 pp.

10. Given, P. H., Spackman, W., Davis, A., Walker, P. L., Lovell, H. L., Coleman, M. M. and Painter, P. C., "The Relation of Coal Characteristics to Liquefaction Behavior III Mechanistic Studies, Product Distribution and Supportive Analytical Investigations, 1982, 104 pp.

11. Garg, D. and Givens, E. N., "Pyrite Catalysis in Coal Liquefaction", Ind. Eng. Chem. Process Des. Dev., 1982, pp. 113-123.

12. Killmeyer, R. P., "Coal Preparation for Syn-Fuels--Where Do We Stand?", Energy Progress Vol. 2 #1, 1982.

13. Alexander, B. F., and Anderson, R. P., "SRC-II Processing of Western Coals with Added Pyrite", ACS Div. of Fuel Chem. Vol. 27 #2, 1982, pp. 18-27.

14. Jones, G. L., "Effect of Coal Properties on SRC-II Yields and Relation to Relative Coal Reactivity", DOE/ET/10104-24, 1982, 27 pp.

15. Anderson, R. P., "Disposable Catalysts in the Solvent Refined Coal Process", American Inst. of Aeronautics and Astronautics, Vol. 2, 1980, pp. 1557-1561.

16. Garg, D., and Givens, E. N., "Effect of Catalyst Distribution in Coal Liquefaction", Fuel Processing Technology 7, 1983, pp. 59-70.

TABLE 1
COAL CHARACTERISTICS VARIATION IN SUPPLY REGION

	MEAN	VARIABILITY*	COEFFICIENT OF VARIATION	MAXIMUM COEFFICIENT OF VARIATION OF A SINGLE PLANT
ASH	9.2	±4.7	0.25	0.11
HEATING VALUE	12283	±1100	0.09	0.04
TOTAL SULFUR	3.1	±1.3	0.21	0.12
PYRITIC SULFUR	1.4	±1.0	0.36	0.23
T. R. MACERALS	93.3	±3.1	0.02	0.01
VIT REFLECTANCE	0.57	±0.18	0.16	0.04

*± 2 STANDARD DEVIATION

TABLE 2
YIELD AND ECONOMIC COMPARISON

PRODUCTS	AVERAGE ACTIVITY COAL YIELD*		HIGH ACTIVITY COAL YIELD*	
FUEL GAS	4.5		7.4	
LIGHT OILS	8.0	25.5	12.8	41.9
MIDDLE OILS	0.0		0.0	
HEAVY OILS	17.5		29.1	
SOLID SRC	44.8		27.1	
TOTAL PRODUCTS	74.8		76.4	
TOTAL REVENUE**	$ 8.90		$ 9.88	

*LBS OF PRODUCT/100 LBS DAF FEED COAL
**DOLLARS OF REVENUE/100 LBS DAF FEED COAL (1990 PRICES IN 1981 DOLLARS)

TABLE 3
CORRELATION OF INDEPENDENT COAL CHARACTERISTICS AND LIQUEFACTION YIELD DATA

	HYDROGEN CONSUMPTION	HYDROCARBON GASES	TOTAL OILS	CONVERSION OF TRM	ASPHALTENES/ PREASPHALTENES
DAF HYDROGEN	0.176	0.156	0.022	0.103	−0.191
DRY PYRITIC SULFUR	0.661	0.131	0.527	0.902	0.214
DAF VOLATILE MATTER	—	0.283	−0.243	0.121	−0.311
VITRINITE REFLECTANCE	−0.153	−0.289	−0.159	−0.360	−0.120

Figure 1
COAL SAMPLE LOCATION MAP

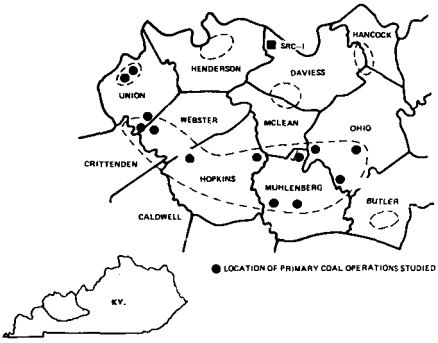

Figure 2
COAL FEED VARIABILITY

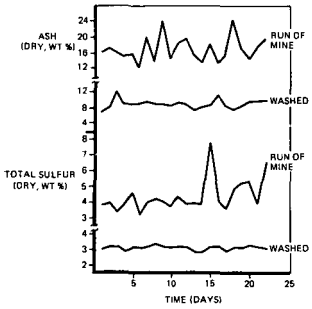

Figure 3
COMPOSITION VARIABILITY (CLEAN COAL)

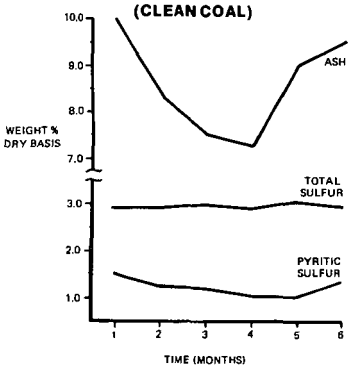

Figure 4
COAL SCREENING PROGRAM

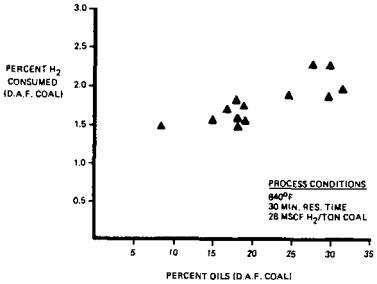

Figure 5
EFFECTS OF SINGLE STAGE CATALYTIC LIQUEFACTION

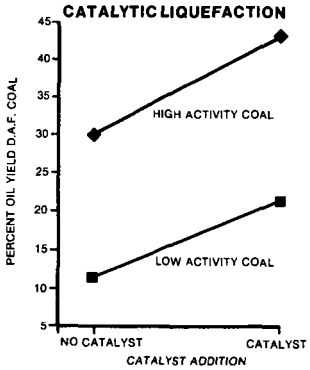

Figure 6
PARITY PLOT - PERCENT CONVERSION OBSERVED VS. PERCENT CONVERSION PREDICTED

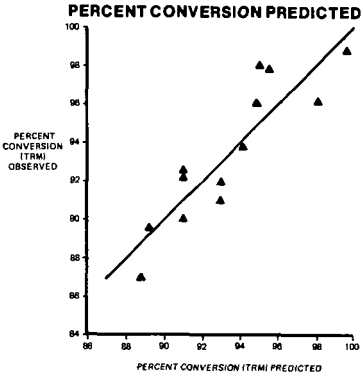

TRM — TOTAL REACTIVE MACERALS

Figure 7
PARITY PLOT - PERCENT OIL YIELD OBSERVED VS. PERCENT OIL YIELD PREDICTED

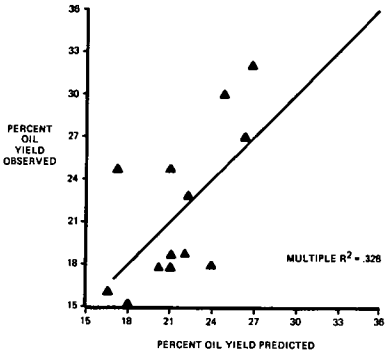

Figure 8
RELATIONSHIP OF PYRITIC SULFUR CONTENT TO COAL REACTIVITY

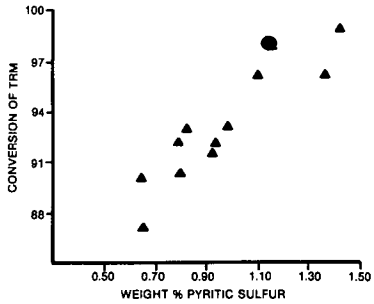

TRM — TOTAL REACTIVE MACERALS

Figure 9
EFFECTS OF COAL CLEANING ON SRC-I LIQUEFACTION

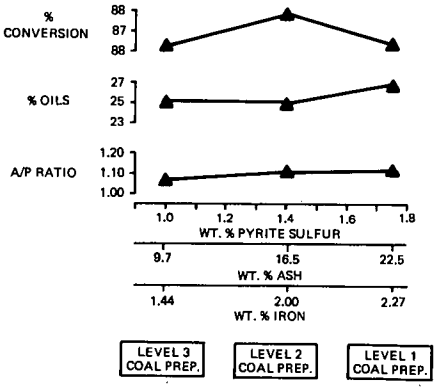

A/P ASPHALTENE/PREASPHALTENE

Correlation of Recycle Solvent Quality to Coal Liquefaction

F. K. Schweighardt

International Coal Refining Company
P. O. Box 2752, Allentown, PA 18001

INTRODUCTION

"Solvent quality" is a contrived solvent property used in coal liquefaction. It is assumed to be an important guide for expressing how well a recycle solvent will convert coal to products soluble in tetrahydrofuran (THF) or pyridine. Over the past 40-50 years, much has been written about the solvents used to prepare coal slurries, yet few solvent quality parameters have been quantified and related to process conditions or feedstocks.

For this report, solvent quality was measured by kinetic microautoclave test as used at the Wilsonville Advanced Coal Liquefaction Facility (1). The microautoclave method, originally developed by the Conoco Coal Development Company, has been used to quantify solvent quality at Wilsonville since 1978. This method (Note 1) defines solvent quality as the weight percent tetrahydrofuran solubles generated, based on weight percent moisture- and ash-free (MAF) coal. Traditionally, a solvent quality test result in the lower range (≈65) warned of potential preheater coking problems. More recently, solvent quality has been used to monitor the effects of adding light solvent refined coal (LSRC) and distillates to the solvent stream to enhance coal liquefaction and maintain solvent balance.

This study attempts to identify important independent and dependent variables associated with the solvent refining of coal (SRC) by relating plant operation to coal feedstock and product slate and by correlating the impact to changes in the results from the microautoclave solvent quality test.

PROPERTIES AND CHARACTERISTICS OF COAL LIQUEFACTION SOLVENTS

In SRC liquefaction, an effective process solvent should be (a) coal-derived to permit continuous plant operation; (b) a distillate with a nominal boiling range of 450-850°F; (c) able to sustain a 10-40 wt % coal slurry through feed pumps; (d) able to rapidly accept coal dissolution products in solution or suspension; (e) able to act as a hydrogen donor or shuttling agent for hydrogen transfer under a predominantly free-radical mechanism; and (f) capable of carrying the liquefaction product stream through solid/liquid separation processes and ultimately of being recycled to continue the process.

The chemical properties of recycle solvents have been well-documented by Whitehurst et al. (2), Burke et al.,(3) and Neavel (4). A recycle solvent generated under SRC-I process conditions exhibits a complex molecular composition. The solvent is composed of a mixture of alkyl (C_1-C_4)-substituted polynuclear hetero- and hydroaromatic compounds. Gas chromatography/mass spectrometry (GC/MS) data have revealed that 40 individual components comprise almost 60 wt % of the solvent. The remaining 40 wt % may include hundreds to thousands of individual compounds (5). The major molecular species are (5-30%) substituted naphthalenes and (5-10%) phenanthrenes.

During SRC-I liquefaction, each time the solvent/coal mixture passed through the reactor 0-30 wt% new solvent material is generated, on an MAF feed coal basis. Therefore, the molecular composition would be expected to constantly change and shift in response to processing conditions and feed slurry composition. At Wilsonville, the virgin distillate solvent exits the process at vacuum tower T102, trays 3 and 8 (see Figure 1 for a process flow scheme). The solvent is then held briefly in a holding tank (V178), from which daily samples are taken for solvent quality testing.

Recently, the solvent in V178 (originally V131A) has been mixed with LSRC or other product streams in tank V131B just before it is recycled into the process at V101A as a new coal slurry. The LSRC, a product stream from the critical solvent deasher, is added to the distillate solvent for several reasons. Most important to the overall process is that LSRC appears to enhance solvent quality by adding high-boiling compounds (6), and somehow promotes distillate yield so that solvent balance is maintained. Handling the LSRC in material balance calculations is a problem. If the LSRC is inert, it can simply be subtracted. However, if the LSRC is a reactant, its degree of conversion must be quantified before an oil yield can be computed (7). Because the addition of LSRC to the distillate solvent has not been continous for all coal types, solvent quality values from V131B samples are not included throughout this report.

Anthracene oil is sometimes added to the system at V178 to maintain solvent balance. For this study, data points were eliminated if more than 5% by volume anthracene oil was added to the V178 solvent within 5 days of a material balance period.

THE ROLE OF SOLVENT IN SRC-I LIQUEFACTION

Our current understanding of coal liquefaction is that bituminous coal, when mixed with solvent at 200-250°F begins to dissolve, but that most of the coal matrix is in suspension. The primary dissolution products are believed to be small molecules already trapped within the coal (8). Depending on coal type and rank, these compounds may represent 5-20% of the coal.

At Wilsonville, the feed slurry is held at 150-250°F (depending on the percent LSRC added) for 8-12 hr without hydrogen before it enters the preheater (B102) under partial hydrogen pressure. Under these holding conditions in tanks V101A and V101B, the recycle solvent must exhibit good dissolving power. That way, the solvent can extract and exchange with the small molecules trapped in the coal and fill other voids created by loss of water and swelling.

Thermal reactions, in which sissile bonds (9) break and initiate actual coal matrix liquefaction, do not occur until ~600°F. Such temperatures are first reached in the preheater (B102) under ~2,000 psi hydrogen pressure. At liquefaction temperatures, the nascent free radicals apparently rapidly combine with labile hydrogen from the feed coal during the first .1-5 min, forming a cresol- (or pyridine-) soluble product (4). When temperatures in the preheater reach 780°F, the recycle solvent appears to rapidly solvate the primary liquefaction product. After the process slurry stream enters the reactor, the exothermic reaction drives the temperature to almost 840°F during a residence time of 30-60 min. In the reactor the original recycle solvent and the new coal product components shuttle hydrogen to free-radical sites generated from splitting and cracking at reaction temperature (840°F).

The solvent, which is now modified in molecular composition by the addition of cracking and splitting products from 0-30 wt % MAF coal, can itself be rehydrogenated. This newly available, "donatable" hydrogen can be shuttled to more recently generated active sites formed in reactor R101 to further stabilize the system.

That portion of the solvent that is active in shuttling hydrogen to free-radical sites has been associated with the hydroaromatic content. Other hydrogen-transfer species have been suggested (2) to be active when hydroaromatic species were absent or depleted, including aromatic hydroxyl (e.g., β-naphthol) and alkyl (methyl) side chains like those found on 2-methylnaphthalene. Curran et al. (10) concluded that the liquefaction solvent needs sufficient donatable hydrogen to promote greater distillate yield and reduce coking, and that the hydrogen can come from many sources.

Correlation of Solvent Quality to Process Operation

A review of past operating reports from Wilsonville and interviews with Wilsonville staff resulted in an assemblage of 48 primary parameters that define a pilot plant run under the SRC-I first-stage regime (Note 2). Fifty-seven data points analyzed for these 48 variables span from 1978 (run 133) to 1982 (run 234). During this period, five major coal types were processed for 3-58 days on stream, per run. Usually one to three data points from each run were selected to represent a material balance at nominal steady-state conditions. These material balance points form the data base of this report.

In analyzing these data, we assumed that each coal type can be viewed independently, and that data for each coal type can be averaged. The reason for this assumption was that we believe the variability in coal reactivity changes the demand on the operating conditions, generates a coal-specific recycle solvent after line out, and would promote a unique product distribution. All coals or similar coal types are combined only when deemed necessary for general comparison purposes. The objective of this study is therefore to relate the microautoclave solvent quality test result to process factors that cause or are affected by a change in the solvent's role in SRC-I liquefaction.

The objectives of first-stage SRC-I liquefaction are assumed to be:

- Maximum conversion of coal to cresol (or pyridine) solubles
- Minimum hydrogen consumption based on MAF coal conversion
- Maintenance of process solvent in solvent balance
- Minimum hydrocarbon and maximum heteroatom gas production
- Minimum preasphaltene content in the vacuum tower (T102) bottoms

The major process variables considered are coal type, dissolver (R101) temperature and pressure, and coal space rate in the dissolver.

Reaction severity, i.e., the degree of coal conversion to distillate and gas, can be assessed from yield structure information, such as hydrocarbon and heteroatom gas production (total gas minus H_2O) and net hydrogen consumption.

Although total gas production may not seem to relate to the recycle solvent's physical or chemical properties, it is presumed to be affected by "solvent quality." Solvent quality in this case refers to the solvent's ability to shuttle hydrogen to those coal species that have split into large components and to minimize hydrocarbon cracking that forms C_1-C_4 gases.

The benzene solubles (SRC oils and asphaltenes) of the vacuum tower bottoms (T102) and the total SRC (pyridine solubles) of this same stream may be the best analyzed samples to quantify both product distribution and reaction severity. This T102 bottoms stream is "process-normalized" in that minor process excursions are averaged by the volume and throughput of the tower.

Process solvent is not measured, but it is determined by difference when calculating a material balance from laboratory distillation (450-end point) and subsequent gas chromatography results (450-850°F). We believe process solvent yield is neither a precise nor an accurate parameter to consider for correlation.

The light oils (C_5-450°F), which are quantified by gas chromatography data, provide another measure of liquefaction severity and solvent breakdown independent of total gas production.

Table 1 lists typical process parameters with the limits of the values accepted as equivalent in this study.

Table 1

Wilsonville SRC Process Conditions

Dissolver pressure	1,700 ± 100 psig
Dissolver temperature	825 ± 10°F
Dissolver volume in use	75%
Coal space rate	38 ± 3 lb/hr-ft^3
H_2 partial pressure (heater inlet)	1,470 ± 75 psi

Representative solvent quality test results for V178 (holding tank) solvent collected over the past 4 years are plotted as a function of time and coal type in Figure 2. Day-to-day variation can be as great as 10 units on the solvent quality scale. As an analytical test, solvent quality may be considered to have a precision of ±2.

RESULTS

Total Gas Production

Figure 3 plots the entire data set for total hydrocarbon and heteroatom gas production (MAF coal) vs. solvent quality for all coals. The distribution is clustered at 8 ± 2% total gas and 75 ± 6 solvent quality. Replotting total gas production from Kentucky #9 coal only gives four distribution curves, one for each mine. Figure 4 shows that each plot has distinct clusters and a few outlying data points. In Figure 4, the data points are coded to define common dissolver conditions (pressure, temperature, and volume used). Only in the Fies Mine Kentucky #9 coal is there an apparent shift to greater gas production at higher dissolver temperature and pressure. Figure 5 provides a different perspective by plotting total gas production data as a function of days on stream over 4 years. Note that because all data points are presented, process conditions varied more than the accepted limits given in (Table 1) for any one common preheater/reactor condition. Note that high gas production usually follows a change in coal type. This trend is apparently independent of reactor pressure, coal space rate, and almost independent of temperature (825-840°F).

Gas production is graphed as a function of total elemental hydrogen consumption in Figure 6; all data points are presented. If a total gas production range of 5-10% and a hydrogen consumption of 1.5-3% on MAF coal are arbitrarily set as lower and upper limits, the points outside these limits are mainly those from the material balance periods taken within 30 days after a change in coal type for SRC-I processing. These same points are the outlying data points in Figure 4.

Product Correlation to Solvent Quality

In order to analyze the data meaningfully and objectively, we related solvent qualities to product distribution by coal type at the selected material balance periods. Process variables such as preheater temperature and reactor pressure, temperature, and volume are documented in the discussion.

Dotiki Kentucky #9 Coal. The major differences in processing Dotiki coal occurred between Runs 202/203 and 204/206/208. The first set of runs was conducted at a lower dissolver temperature (825 vs. 840°F). Also, the pyrite content of the coal in runs 206B and 208 was less than 1.1%, whereas in run 203 it was 1.3%.

Figures 7A-7D plot solvent quality vs. specific product components. Figure 7A (pyrite content vs. solvent quality) identifies each point by run/ material balance number and can be used as a guide to identify the equivalent run in Figures 7B-7D.

Solvent quality does not appear to affect product yield. However, the percent pyrite in the feed coal appears to affect solvent quality; that is, if the percent pyrite is below 1.1 wt %, the solvent quality value deviates from the major distribution cluster. The operating conditions during runs 206 and 207 were upset because the high-pressure separator failed and nearly 70 vol % of the unit was filled with cresol-insoluble material. Run 208, which was short, however, had the highest solvent quality (70) and lowest (1.1%) pyrite content. This solvent quality value is unusually high; its cause is unknown and only one material balance (MB) sample was taken for this run. Daily solvent qualities measured before and after the 208AB MB were between 64 and 66.

Lafayette Kentucky #9 Coal. Runs 163 to 201 were conducted with Lafayette coal. Runs 163, 166, and 201 were at 75% dissolver volume at 1,700 psi and 825°F; dissolver pressure in runs 167, 168, 171, and 172 increased to 2,100 psi with only 50 vol % of the dissolver in use; and run 190 was performed at 2,100 psi, 825°F, and 75% dissolver volume. The largest volumes of anthracene oil were added to the system between runs 170 and 182. Solvent quality increased from 65 to 75, but fell to 68 after run 182 and remained there until the next coal type (Dotiki) was used. Figures 8A-8D illustrate the relationship for Lafayette coal. Note that most Lafayette feed coals had a pyrite content of less than 1.2 wt %.

Pyro Kentucky #9 Coal. Pyro Mine coal was run under dissolver conditions of 1,700 psi and 825°F for runs 151, 159, 160, and 161, and at 2,100 psi and 825°F for run 162. These process conditions are the most constant for the coals tested. Because run 151 was conducted with Indiana V solvent and processed 3 months before run 159, run 151 can be eliminated from each solvent quality correlation. Figures 9A-9D show the relationship between Pyro coal solvent quality and product distribution. Product yield ranged widely (±8%), but solvent quality changed only slightly (± 2). The range of product distribution is no less than that for other coal types that experienced solvent quality changes of more than ±10 from the average.

Fies Kentucky #9 Coal. Fies Mine coal was processed under the most varied conditions of all coal types (Note 2). Most Fies Mine coal was run at dissolver conditions of 2,100 psi, 840°F, and 75 vol %. Only three feed coals (229A, 229B, and 210AB) had a pyrite content below 1.1%. Anthracene oil was added only once, after run 210. Solvent quality was 75 and was not greatly affected (±2). The reason for this is not clear, but the optimum activity of hydrogenated anthracene oil may be 75 ± 2 as measured by the solvent quality test. Solvent quality and product distribution for Fies Mine coal are compared in Figures 10A-10D. In general, only total gas production (depicted earlier in Figure 4) shows any apparent correlation between solvent quality and dissolver temperature: lower dissolver temperature and higher solvent quality yield the lowest gas production.

Effect of Solvent Quality on the Attainment of Liquefaction Objectives

We assume solvents are primary products of the feed coals, therefore their compositions are affected first by the coal's structure, second by processing conditions, and third by addition of external material (LSRC), control of distillate boiling point distribution, or modification by chemical means.

Once a new steady-state process condition is reached and the solvent lined out, the solvent's new properties apparently allow a different product yield distribution to be maintained. The preheater and reactor temperatures have their greatest impact on the rate of formation of primary liquefaction products that place a demand on the solvent for rapid coal dissolution and hydrogen donation.

If the solvent is returned to the front end without addition from another stream (LSRC or distillate), we can at best anticipate an apparent steady-state solvent because the feed coal is constantly changing. Most importantly, the coal's pyrite content and distribution is more variable than the organic macromolecular structure. Figure 11 shows the range in solvent quality as a function

of coal type with and without LSRC addition, independent of process conditions, for all material balance periods. Circles represent average results, and the bars define the upper and lower limits of the solvent quality.

Next, we considered only those solvent quality results obtained from material balances more than 30 days after a change in feed coal type and more than 5 days after addition of anthracene oil. All data points were averaged by coal type with respect to their pyrite concentration (Figure 12).

Figure 12 shows that the Fies, Pyro, and Indiana V coals with >1.2% pyrite generated solvents with average SQ values above 72. The trend of Fies, Pyro, and Indiana coal data clustering together and Dotiki and Lafayette coal data clustering together was also observed for nearly all average product distributions (e.g., Figures 7-11) as well as other variables not included in this report.

Measurement of Liquefaction Behavior

Based on these observations, a logical approach to defining coal-derived recycle solvent quality is to react samples of the solvent, or the modified solvent, in the microautoclave test with the daily feed coal. This solvent quality test would involve comparison of the daily microautoclave product distribution (residue, preasphaltenes, and total benzene solubles) with the product distribution for a well-maintained standard coal of the same type. The primary liquefaction activity of the solvent would be determined under hydrogen-starved, solvent-rich conditions, to mimic the slurry tanks and the rapid coal dissolution process in the preheater at 750 ± 2°F. The secondary liquefaction activity of the solvent would be determined from a similar product distribution under hydrogen-rich conditions (2,000 psi), to quantify the sustaining hydrogen-transfer reactions in the reactor.

These two tests would be made within the same sand bath; at the same time, a third test microautoclave would be run. In this third bomb, the standard coal type would be reacted with a standard model compound solvent mixture. Together, all three results would provide internal checks on the reliability of the test (standard coal vs. standard solvent); optimum continued dissolution of process coal (feed coal vs. recycle solvent/no H_2); and optimum continued conversion to the desired product slate (feed coal vs. recycle solvent/ H_2).

Figure 13 summarize how this approach to measuring solvent quality could be used to predict liquefaction behavior of the next day's operation. Over a 3-month period in our laboratories, we have demonstrated that solvents from holding tank V178 yield different SQ values depending on whether they are tested with the feed coal that they will be slurried within the next run or a standard Indiana V coal. The greatest difference is the relative distribution of benzene solubles to preasphaltenes. Silver and Miller (11) were first to note similar coal conversion differences when using a solvent generated from Wyodak coal and reacting it with Kentucky #9 coal.

SUMMARY

The concept of quantifying solvent quality by a microautoclave test does have merit if the test is run with the same coal-type used for coal liquefaction. Correlation of the solvent quality result to preheater chemistry (rapid coal dissolution with minimum hydrogen shuttling) and reactor chemistry (rapid and sustaining hydrogen donation/shuttling) is apparently possible. As used at Wilsonville during runs 133-234, the microautoclave SQ result was of tangential significance for absolute day-to-day pilot plant operation. However, during the past 4 years the Wilsonville staff has collected SQ data under the most varied of conditions, e.g., changes in feed coal, addition of LSRC to the solvent, redefinition of solvent boiling range, and most recently, addition of hydrotreated material to the solvent. These SQ results do provide us with a relative measure of coal conversion behavior to solvent composition under pilot plant conditions to consider for future process design. The Wilsonville staff has prepared a topical report on solvent activity covering this subject (12).

From our SQ study of Wilsonville it is our opinion that bench-scale experiments comparing different coals with solvents of questionable parentage for single pass conversion are at best of limited relative value, and result in conflicting interpretations from lab to lab. Such experiments do define the kind of solvent composition that provides specific results. If such results or such solvents can be produced in situ is another question. Laboratory liquefaction experiments that may be the most meaningful (although the most time-consuming and expensive) are full recycle of the solvent for attaining apparent steady-state operation. We estimate 5-12 solvent passes are required for line-out depending on process conditions.

Note 1

Wilsonville Solvent Quality Test (#43080-60): Into a 30 mL bomb, add 1.5 g of standard Indiana V coal, 12 g of solvent, and a 1-in. steel rod. Place in sandbath (750°F) for 10 min and shake at 1,000 spm over 1.5 in. Extract the reaction products with tetrahydrofuran (THF) to determine THF insolubles. Calculate percent conversion on MAF coal. See Reference 12 for details.

Note 2

The full data base is available upon request from the author.

References

1. Wilsonville Pilot Plant, sponsored by U.S. Dept of Energy Contract #DE-AC22-82PC50041 and Electric Power Research Institute Contract #RP1234-1-2.
2. D. D. Whitehurst, T. O. Mitchell, and M. Farcasiu, "Coal Liquefaction," Academic Press, New York, Chapter 9, 1980.
3. F. P. Burke and R. A. Winschel, "Proceedings of the Science and Technology of Synfuels-I," Colorado Springs, Colo., March 1, 1982.
4. R. C. Neavel, Fuel, 55, 237 (1976).
5. D. M. Parees and A. Z. Kamzelski, J. Chrom. Sci., 20, 441 (1982).
6. D. D. Whitehurst, M. Farcasu, T. O. Mitchell, and J. J. Dickert, Jr., EPRI Report AF-480, July 1977.
7. D. Garg, Air Products and Chemicals, Inc., private communication.
8. M. Vahrman, Fuel, 49, 5 (1970).
9. H. W. Sternberg, R. Raymond, and F. K. Schweighardt, Prepr., Div. Pet. Chem., Am. Chem., Soc., 21, 24 (1975).
10. G. P. Curran, R. T. Struck, and E. Gorin, Ind. Eng. Chem., Proc. Des. Dev., 6, 166 (1967).
11. H. F. Silver and R. L. Miller, Proc. EPRI Contractors Meeting, 1978.
12. Catalytic, Inc., "Solvent Activity Studies," Topical Report No. 8, DOE Contract No. DE-AC22-82PC50041, EPRI Contract No. RP1234-1-2, Document No. Fe-10154-___, November 1982.

Acknowledgement

The author wishes to thank A. Rao and the Wilsonville staff for their assistance in data gathering and discussions, and the RTDD staff (D. Garg, E. Givens, D. Kang, R. Miller and D. Hoover) who provided the technical dialogue that tied many loose ends together.

FIGURE 1

WILSONVILLE PILOT PLANT PROCESS FLOW DIAGRAM

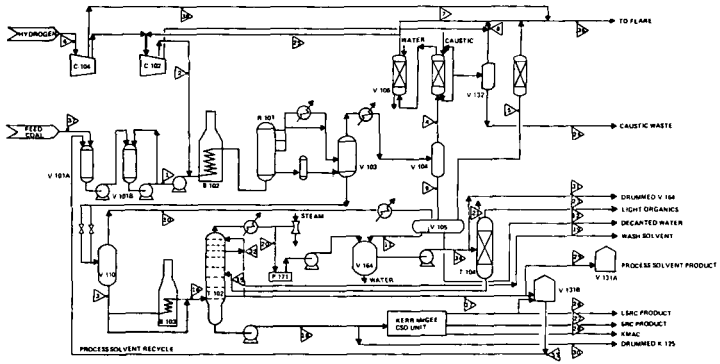

FIGURE 2

WILSONVILLE SOLVENT QUALITY (SQ)
VS.
COAL TYPE

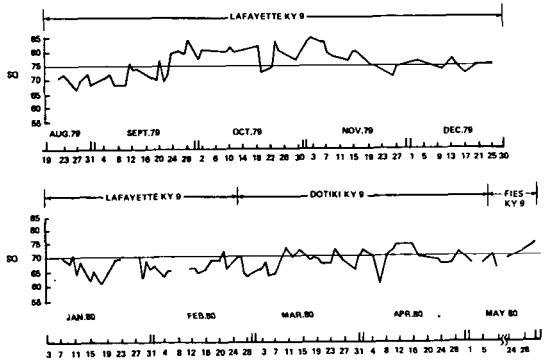

FIGURE 3

TOTAL GASES VS. SOLVENT QUALITY
ALL DATA POINTS

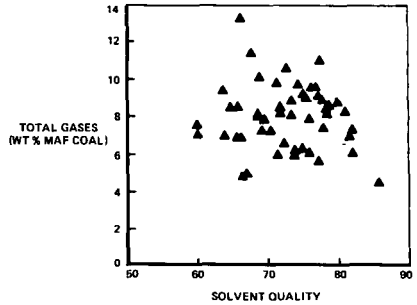

FIGURE 4

SOLVENT QUALITY VS. TOTAL GAS (WT % MAF COAL)

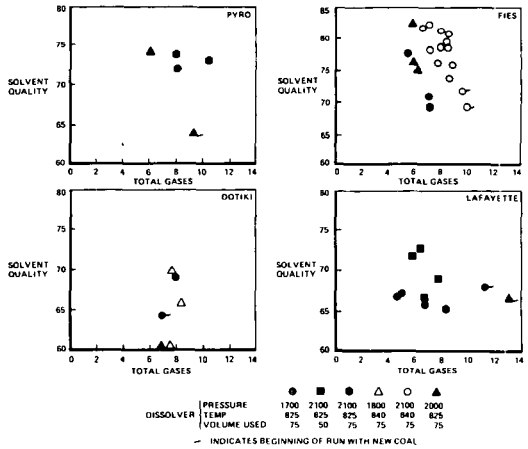

FIGURE 5

TOTAL GAS (HYDROCARBON + HETEROATOM)
AS A FUNCTION OF TIME

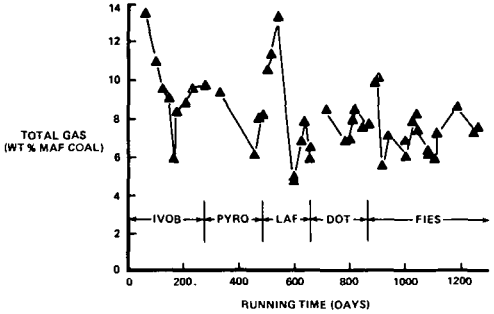

FIGURE 6

HYDROGEN CONSUMPTION VS.
TOTAL GAS PRODUCTION
ALL DATA POINTS

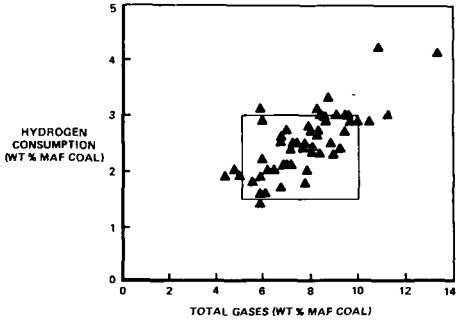

FIGURE 7

SOLVENT QUALITY VS.
PRODUCT YIELDS FOR DOTIKI COAL

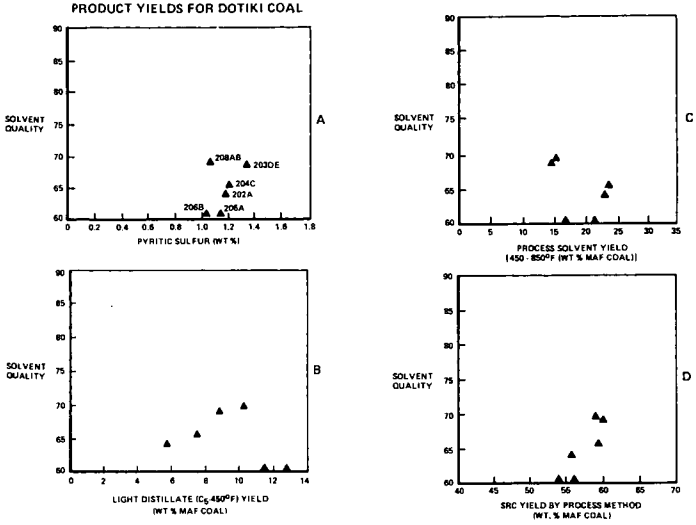

FIGURE 8

SOLVENT QUALITY VS.
PRODUCT YIELDS FOR LAFAYETTE COAL

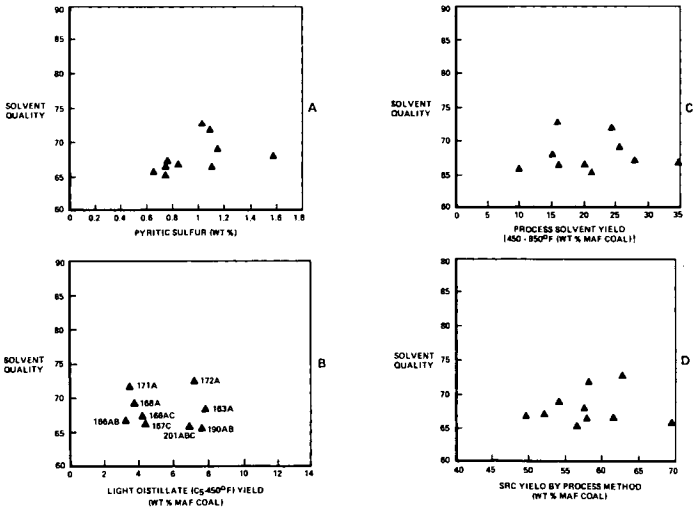

FIGURE 9

SOLVENT QUALITY VS.
PRODUCT YIELDS FOR PYRO COAL

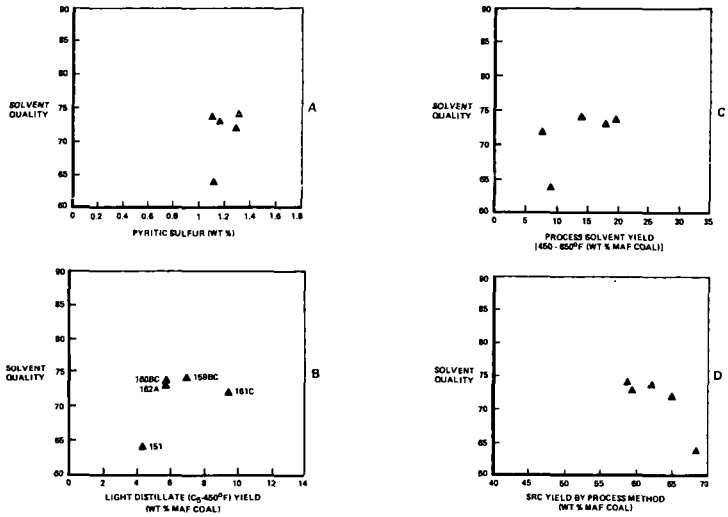

FIGURE 10

SOLVENT QUALITY VS.
PRODUCT YIELDS FOR FIES COAL

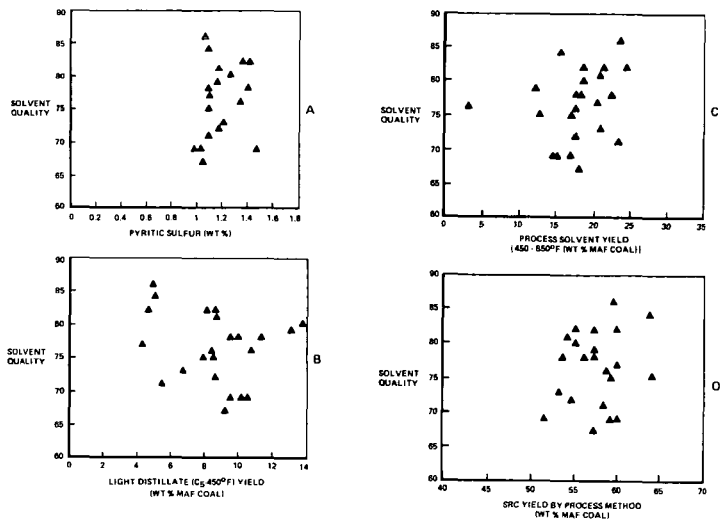

FIGURE 11

WILSONVILLE SOLVENT QUALITY (SQ) VS. COAL TYPE

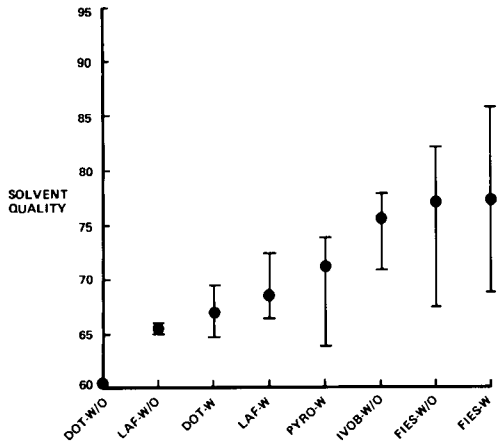

W : WITH LSRC ADDITION
W/O : WITHOUT LSRC ADDITION

FIGURE 12

COAL PYRITE VS. SOLVENT QUALITY BY COAL TYPE

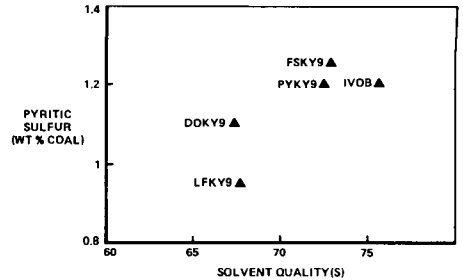

FIGURE 13

PROPOSED SRC-I SOLVENT QUALITY TEST

SOLVENT \ COAL	STO PROCESS COAL-TYPE (1)	DAILY TOTE-BIN NO H_2 (1)	DAILY TOTE-BIN H_2 (2)
STD SOLVENT TET/MN	QUALITY ASSURANCE TEST		
DAILY RECYCLE SOLVENT		PRIMARY COAL DISSOLUTION	SECONDARY PRODUCT - DISTRIBUTION
DAILY RECYCLE SOLVENT & ADDITIVE		PRIMARY COAL DISSOLUTION	SECONDARY PRODUCT DISTRIBUTION

(1) MICROAUTOCLAVE S/C (8/1); 10 MINUTES AT 750°F
DETERMINE: RESIDUE (THR) – PREASPHALTENES – BENZENE SOLUBLES

(2) TEST CONDITIONS TO BE DETERMINED

EFFECTS OF HEAVY RECYCLE SOLVENT COMPONENTS ON DIRECT COAL LIQUEFACTION

James R. Longanbach

Battelle Columbus Laboratories
505 King Avenue
Columbus, Ohio 43201

Introduction

The quality of the recycle solvent is critically important in all direct coal liquefaction processes. The fact that overall solvent quality can be greatly improved by adding some of the lighter nondistillable products to the solvent is one of the most important discoveries in direct coal liquefaction research in recent years.[1] Many recent studies have focused on the role of solvent in direct liquefaction. It has been shown that most hydrogen transferred to the dissolving coal during initial preasphaltene formation comes from the solvent rather than hydrogen gas.[1,2] The high molecular weight aromatic hydrocarbons in the recycle solvent are particularly adept at transferring hydrogen to coal and can retard retrogressive reactions which can lead to the formation of undesirable insoluble products. On the other hand, the coke formation reactions are also caused in large part by high molecular weight solvent components, particularly those containing phenolics and polyfunctional compounds.[4]

Other studies have focused on the role of nitrogen-containing aromatics in the recycle solvent. The lower molecular weight aromatics which contain basic nitrogen have been shown to be excellent hydrogen transfer agents[4] and may also readily penetrate the coal structure to react with reactive coal species before retrogressive reactions can take place.[5]

One of the problems encountered in all of these studies has been that when actual process derived solvents are used, they are so complex that the results are hard to assign unambiguously to particular chemical properties of the solvent, while the use of model compounds have simply not included materials of sufficiently high molecular weight to adequately represent the heavier species in true recycle solvents.

The purpose of this work is to further study the liquefaction chemistry of the heavier materials in a process derived liquefaction solvent. Solvents obtained from near equilibrium operation of the Lummus ITSL Process are being used because others have shown that this solvent is less complex than solvents from other processes.[6]

Experimental

Samples of SCT Recycle Solvent (2SCT16-1122), the solvent recycled to the short contact time coal dissolution step, and SCT Heavy Oil Product (2SCT16-1122), the 500^{+}F product from the same process step, were obtained from the Lummus ITSL Process pilot plant.

Both of these materials are black solids at room temperature. Analyses are listed in Table 1. Both have number average molecular weights (by vapor pressure osmometry) between 400-500 grams/mole. The SCT Heavy Oil Product, which is approximately a 1.8:1 mixture of reacted SCT Recycle Solvent and dissolved coal, has an H/C ratio of 0.80, slightly higher than the H/C ratio of the starting Illinois #6 coal and somewhat less than the H/C ratio, 0.95, of the SCT Recycle Solvent.

Illinois #6 coal used in the Lummus ITSL Process was also obtained and analyzed with the results shown in Table 2. The coal has been dried to approximately 4 percent moisture and ground to more than 70 percent -200 mesh for use in the process.

The procedure used for the liquefaction studies consists of mixing solvent and coal in a microautoclave (~18 cc volume) and pressurizing with either hydrogen or helium, containing a small amount of krypton as an internal standard, to 1000 psia (at room temperature). Standard reaction conditions are 800 F for 5 minutes. The autoclave is agitated with a wrist action shaker and heated in a fluidized sand bath. The autoclave is equipped with a thermocouple and recording pressure transducer. A typical pressure and temperature versus time curve is shown in Figure 1. The average heatup time, to 790 F, is 1.9 minutes. After reaction, quenching to 600 F requires ~0.5 minutes. This method gives excellent control of residence time at temperature.

The gases are transferred to storage in a 2-liter evacuated gas bulb for later analyses. The liquefaction products are washed from the autoclave with THF and the insolubles are extracted with THF in a Soxhlet extractor. Conversions of MAF THF insolubles are calculated using the weights of insoluble organic material (IOM) in the coal and solvent, the starting ash content of the solvent and coal and the moisture content of the coal. Excess THF is stripped from the THF solubles on a rotary evaporator and the resulting concentrated solution is slowly added to 20 parts of boiling heptane per part of THF to precipitate heptane insolubles. After the THF is distilled from the mixture, the precipitate is allowed to settle overnight and removed by vacuum filtration. The heptane is distilled from the filtrate and each of the fractions is dried in a vacuum oven overnight at 110 C, cooled and weighed. Net changes in the amounts of THF soluble-heptane insolubles (asphaltenes and preasphaltenes) and heptane solubles (oils) are calculated by subtracting blank extraction data for the starting solvent and coal to obtain differential solubility changes caused by liquefaction.

The gases are analyzed for H_2, CO, CO_2, CH_4, C_2's and Kr. After normalization to a standard krypton concentration, net yields (or losses of hydrogen) for each gas are calculated.

Results and Discussion

In order to study the chemistry of the 800^+F Recycle Solvent components, the SCT Recycle Solvent was separated by vacuum distillation into fractions with boiling points above and below 800 F (427 C). Liquefaction experiments using the 800^-F material serve as a baseline to allow a systematic study of the effects of addition of various fractions of the 800^+F materials to the liquefaction solvent. Additional chemical insight may be obtained by running reactions in the presence and absence of a 1000 psia (cold) hydrogen atmosphere. Also, the use of the same chemical class fractions obtained from the 800^-F and 800^+F fractions may help illustrate the effects of higher molecular weight on the reactions of the solvent.

The SCT Recycle Solvent sample has been distilled under vacuum to obtain 800^+F and 800^-F fractions with the results listed in Table 3. Approximately 36 percent of the sample distilled below 800 F. The 800^-F material has a higher H/C ratio and about 50 percent lower number average molecular weight. As expected, it is almost entirely heptane soluble. The 800^+F fraction contains 80 percent of the nitrogen, 84 percent of the sulfur and 76 percent of the oxygen in 65 weight percent of the sample. The heteroatom concentrations are not large, however, and total only about one heteroatom per molecule (containing an average of 34 carbon atoms).

Liquefaction experiments have been done using 6 g of either the total SCT Recycle Solvent or the 800^-F SCT Recycle Solvent fraction with 3 g of Illinois #6 coal under 1000 psia (room temperature) hydrogen or helium. The results are listed in Table 4.

Since both solvents and the coal are partially soluble in THF and heptane when exposed to the workup procedure before liquefaction at elevated temperature, the results have been corrected using blank extractions of the starting materials

to reflect the changes in the three solubility fractions before and after liquefaction. The results have also been corrected to remove the ash and moisture present in the starting coal. The reaction conditions have been chosen to obtain good, but not complete conversions so that differences due to the solvent and gas atmosphere can be seen. The reaction conditions gave nearly equal conversions of MAF THF insolubles, except for the 800⁻F SCT Recycle Solvent under hydrogen, which gave a significantly higher conversion. Most of the THF insoluble material is converted to THF soluble-heptane insolubles (preasphaltenes plus asphaltenes). Under helium there is a small net loss of heptane solubles (oils).

Hydrogen is produced on balance under a helium atmosphere while hydrogen is incorporated into the products on balance under a hydrogen atmosphere. The 800⁻F SCT Recycle Solvent may be exceptional in this respect and actually release a small amount of hydrogen, even in the presence of 1000 psig of hydrogen. The effects of different solvents and gas atmospheres on CO is negligible but more CO_2 is produced under helium and more CH_4 is produced under hydrogen.

The 800⁻F and 800⁺F SCT Recycle Solvent fractions are now being separated into chemical classes using the liquid chromatography method described by Later, et al.[8] Preliminary results from the separation of the 800⁺F SCT Recycle Solvent fraction are listed in Table 5.

Table 5. Separation of 800⁺F SCT Recycle Solvent Fraction by Liquid Chromatography

Solvent	Chemical Class	Recovery, Weight Percent
Hexane	Aliphatic hydrocarbons	4.9
Benzene	Aromatic hydrocarbons	27.9
Chloroform	N-Aromatics	4.8
THF-EtOH (10%)	OH-Aromatics	33.3
Total recovery		70.8

The 800⁺F material is approximately one-quarter aromatic hydrocarbons and 5 percent of aliphatic hydrocarbons and N-aromatics.

These separations will be extended to the 800⁻F SCT Recycle Solvent fraction and then these fractions will be added separately to the 800⁻F recycle solvent to determine the effect of various types of solvent molecules on the conversion and yields during the coal dissolution step.

Acknowledgement

The author gratefully acknowledges the receipt of samples from Harvey Schindler and James Chen of Lummus. Bruce Utz, DOE (PETC), provided all of the information needed to construct the microautoclave reactor system. Eneo Moroni, DOE (Germantown) has provided many useful insights to this work. Sayeed Akhtar, DOE (PETC) is the project monitor. This work was prepared with the support of the U.S. Department of Energy, Grant No. DE-FG22-82PC50783. However, any opinions, findings, conclusions, or recommendations expressed herein are those of the author and do not necessarily reflect the views of DOE.

Literature Cited

(1) Process Development for Improved SRC Options; Kerr-McGee Critical Solvent Deashing and Fractionation Studies. Final Report on EPRI Project 1134-2 by Kerr-McGee Corporation, July 1981.

(2) Neuworth, M.B. and Moroni, E.C., "Development of a Two-Stage Liquefaction Process", Adv. Coal Utilization Technology Symposium Papers, 345-58, IGT (1979).

(3) Thomas, M.G., Sample, D.G., and Floyd, J.L., Selectivity of Catalysts Towards Coal-Derived Products, NTIS Sand 79-182GC.
(4) Fundamental Studies in the Conversion of Coals to Fuels of Increased Hydrogen Content, Final Report on EPRI Project 1655-1 by Mobil Research and Development Corporation, November 1981.
(5) The Effect of Basic-Nitrogen Solvents on Coal Conversion, Proceedings of the Seventh Annual EPRI Contractors' Conference on Coal Liquefaction, May 12-14, 1982.
(6) "Advanced Coal Liquefaction", EPRI Journal, P. 31-34, May 1982.
(7) Wilson, B.W., Pelroy, R.A., Mahlum, D.D. and Frazier, M.E., Mutagenicity and Carcinogenicity Test Results on ITSL Process Streams, Proceedings ITSL Program Contractors' Project Review Conference, October 6-7, 1982.
(8) Later, D.W., Lee, M.L., Bartle, K.D., Kong, R.C. and Vassiloros, D.L., Chemical Class Separation and Characterization of Organic Compounds in Synthetic Fuels, Anal. Chem. 1981, 1612-20.

TABLE 1. ANALYSES OF SCT RECYCLE SOLVENT AND HEAVY OIL PRODUCT FROM THE LUMMUS ITSL PROCESS PILOT PLANT

Sample	SCT Recycle Solvent (2SCT16-1122)	SCT Heavy Oil Product (2SCT-1122)
Elemental Analyses, Wt %		
Ash	1.30	3.61
Carbon	86.77	85.87
Hydrogen	6.88	5.74
Nitrogen	0.94	1.02
Sulfur	0.53	0.99
Oxygen (by difference)	3.6	2.8
H/C	0.95	0.80
Distillation Data, Wt %		
800^{-}F	35.6	38.2
800^{+}F	64.4	61.8
THF Solubility, Wt %	96.4	88.6
Molecular Weight, g/mole	477	424

TABLE 2. ANALYSES OF ILLINOIS #6 COAL FROM THE LUMMUS ITSL PROCESS PILOT PLANT

Proximate Analyses, Wt %	As-Received	Dry
Moisture	3.99	-
Ash	9.72	10.12
Elemental Analyses, Wt %		
Carbon	69.73	72.63
Hydrogen	4.93	4.67
Nitrogen	1.18	1.23
Sulfur	2.88	3.00
Oxygen (by difference)		8.35
H/C		0.77
Particle Size Distribution, Wt %		
+70 mesh	0.07	
-70 +120	3.64	
-120 +200	18.90	
-200 +325	14.84	
-325	62.55	
THF Solubility, Wt %	13.7	

TABLE 3. ANALYSES OF 800⁻F AND 800⁺F FRACTIONS FROM THE DISTILLATION OF SCT RECYCLE SOLVENT (2SCT16-1122)

Sample	800⁻F	800⁺F
Weight % of Starting Material	35.6	64.4
Elemental Analyses, Wt %		
Carbon	90.96	87.88
Hydrogen	7.12	6.18
Nitrogen	0.57	1.30
Sulfur	0.23	0.69
Oxygen (by difference)	1.12	1.95
Ash	<0.01	2.00
H/C	0.94	0.84
Molecular Weight, g/mole	257	456
Solubilities, Wt %		
THF insolubles	0.0	5.5
Heptane insolubles	1.5	39.5
Heptane solubles	98.5	57.9

TABLE 4. SUMMARY OF MICROAUTOCLAVE LIQUEFACTION RESULTS WITH SCT RECYCLE SOLVENTS AND ILLINOIS #6 COAL

Run No.	7	15	9	17
Solvent	Total SCT Recycle Solvent		800⁻F SCT Recycle Solvent	
Gas Atmosphere	He	H_2	He	H_2
Conversion of MAF THF Insolubles, %	78.2	75.0	78.6	84.6
Net Change of Heptane Insolubles, % of Total MAF Products	19.0	17.8	18.0	19.2
Net Change of Heptane Solubles, % of Total MAF Products	-2.0	0.5	-0.0	1.1
Gas Analyses, Volume %				
H_2	0.85	-7.87	1.09	1.55
CO	0.16	0.12	0.13	0.14
CO_2	1.06	0.75	1.15	0.58
CH_4	0.77	0.98	0.75	0.90
C_2H_4/C_2H_6	0.49	0.39	0.35	0.34

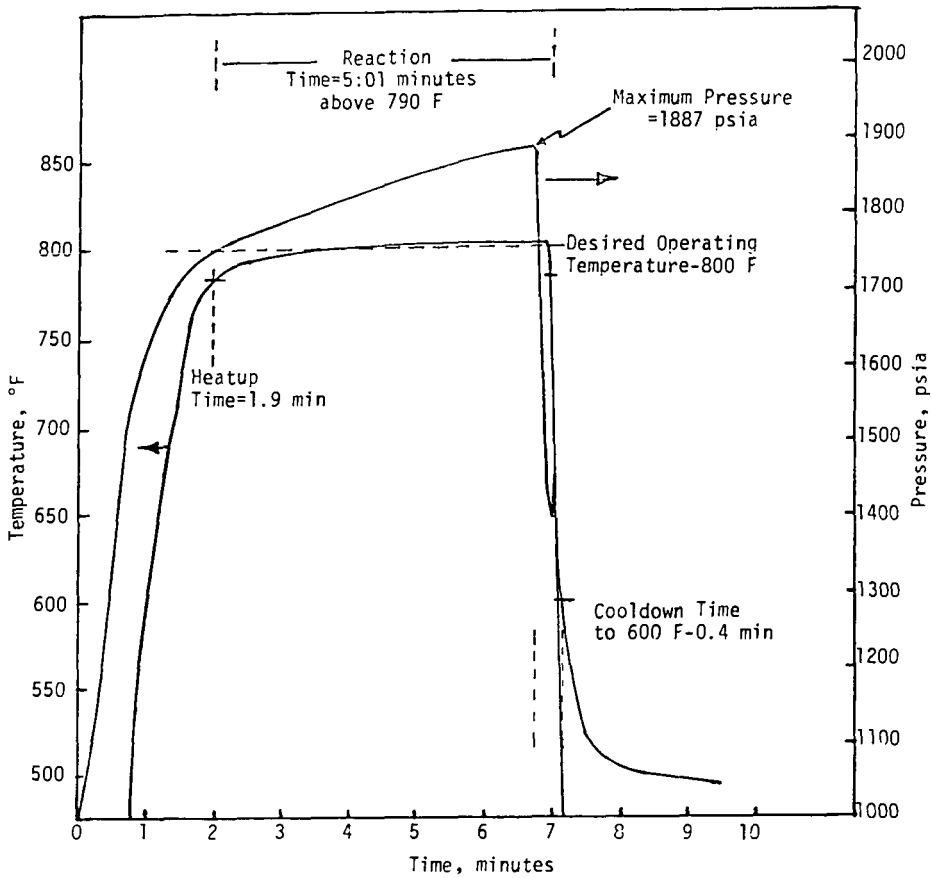

FIGURE 1. TYPICAL MICROAUTOCLAVE PRESSURE, TEMPERATURE VERSUS TIME CURVE FOR SRT COAL LIQUEFACTION

THE ORTHO-ALLYLBENZYL RADICAL: A SENSITIVE PROCEDURE FOR THE ASSESSMENT OF HYDROGEN DONOR SOLVENT REACTIVITY.*

James A. Franz, Russell D. Barrows and Donald M. Camaioni

Pacific Northwest Laboratory, P.O. Box 999, Richland, WA 99352

The thermal conversion of coal involves the decomposition of interconnected hydroaromatic structures into resonance stabilized benzylic radical fragments. Capping of these radicals with hydrogen from a donor solvent leads to the formation in high yields of lower molecular weight soluble and volatile products (1-5). In the absence of a donor solvent, the radicals abstract hydrogen from alkyl coal structures and depending on the supply of donatable hydrogen within the coal, conversion yields may be greatly affected (3, 6). In view of the great variety of radicals which must form during coal liquefaction and the many possible competing reactions which lead to products, the ability of a donor solvent to transfer hydrogen to coal radicals is undoubtedly of great importance.

Although much quantitative data describing the reactions of alkyl and heteroatom radicals with hydroaromatic donor solvents exists, (7-9) surprisingly little data is available on the reactions of resonance stabilized radicals with hydroaromatic donors (10-14). Realizing the importance of this data to the development of a basic understanding of coal conversion chemistry we have developed a procedure for the quantitative determination of hydrogen donor strengths toward benzyl radical. The method competes the rearrangement of o-allylbenzyl radical against hydrogen transfer to the radical from a donor solvent, see Equations 1 and 2. At this time, the method provides relative and estimated absolute rates of hydrogen atom transfer. Experiments are in progress which are designed to convert these relative rates to absolute rates with a high degree of accuracy and precision.

Experimental

Synthesis of o-allylazotoluene. o-allylbenzylazine was synthesized from o-allylbenzaldehyde and hydrazine sulfate according to the procedure of H. H. Hatt (15). The azine was reduced to its corresponding hydrazine derivative with Na-Hg(5%) in methanol. o-Allylbenzylhydrazine was oxidized to o-allylazotoluene according to the procedure of Cohen and Wang (16); m.p. 47.5-49.0°C; NMR ($CDCl_3$) , 7.33-7.20 (sharp m, 8H, aromatic-H), 6.25-5.75 and 5.15-4.80 (m, 6-H, olefinic-H), 4.96 (s, 4-H, benzyl-H to nitrogen atom, superimposed on vinyl region), 3.48 (d of t, 4-H, J = 6.2, 1.5Hz, benzyl-H to vinyl group); Analyses: Calc., C, 82.72, H, 7.64, N, 9.65; found, C, 82.6, H, 7.73, N, 9.58.

Determination of relative rates of hydrogen atom transfer to o-allylbenzyl radical. Solutions of the o-allylazotoluene, hydrogen donor, and sometimes an inert solvent such as benzene or phenyl ether, were degassed and sealed in pyrex tubes and then thermostatted for 20 minutes (approximately 2 half-lives). The concentration of azo compound was kept low (<.01M) to minimize radical induced decomposition and to minimize consumption of donor solvent (usually <5% consumed). The relative amounts of 2-methylindan (2MI) and

* This work was supported by the U.S. Department of Energy, Processes and Techniques Branch, Division of Chemical Sciences, Office of Basic Energy Sciences, under Contract DE-AC06-76 RLO-1830.

and o-allyltoluene (OAT) were determined by capillary gas chromatography analysis after they were separated from the unreacted azo compound by high performance liquid chromatography. In calculating k_{abs}/k_{re}, the room temperature concentrations of donor solvents were corrected to reflect the solution density at 160°C (17). We expect the error in these values to be ±5% due to lack of precise information about the actual liquid densities.

Results and Discussion

o-Allyazotoluene is a conviently prepared thermal source of o-allylbenzyl radicals. In donor solvents equilivant to or better than m-xylene it has a half-life of approximately 10 min at 160°C. Upon decomposition, a pair of o-allylbenzyl radicals form and undergo reactions of rearrangement, hydrogen abstraction and combination.

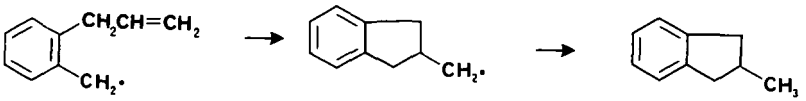

1)

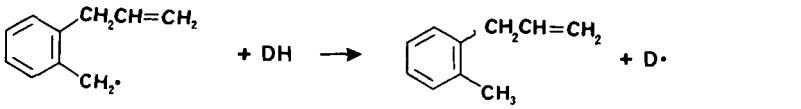

2)

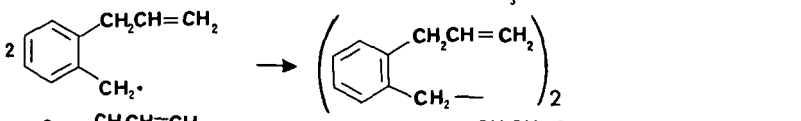

3)

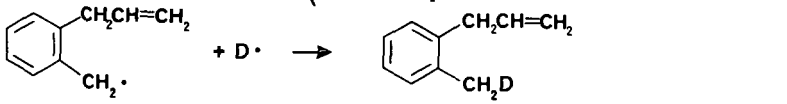

4)

The yields of products, 2-methylindan (2MI), and o-allyltoluene (OAT), formed from the competing reactions of rearrangement, Equation 1 and hydrogen atom abstraction, Equation 2, are observed to vary according to the hydrogen donor strength of the donor solvent (DH). Under the experimental conditions, the formation of 2MI and OAT are irreversible and the amount of DH consumed is small, so that the rate constant for hydrogen abstraction, k_{abs}, relative to rearrangement, k_{re}, for a given donor is provided by the expression,

$$\frac{k_{abs}}{k_{re}} = \frac{[OAT]}{[2MI][DH]n} \qquad 5)$$

where n is the number of donatable hydrogens per donor molecule.

The formation of 2MI is controlled by the unimolecular rearrangement of o-allylbenzyl and the rate constant, k_{re}, for this reaction is independent of solvent composition, such that the values, k_{abs}/k_{re}, provide a quantitative index of hydrogen donor strength. In Table I, index values for a series of hydrogen donor solvents and model compounds have been compiled from k_{abs}/k_{re} values. For convience of comparison, the values have been indexed relative to m-xylene for which k_{abs}/k_{re} is 2.53×10^{-3}.

Interestingly the index quantitatively bears out the expected relationship between donor strength and resonance stabilization energy of the radical formed from the donor molecule, i.e., 9,10-dihydroanthracene > allylbenzene > 9,10-dihydrophenanthrene > diphenylmethane > m-xylene. Diphenylmethane is

a much poorer solvent than dihydroanthracene because steric hinderance prevents both phenyl rings from being simultaneously conjugated with the radical site. Little steric hinderance is in effect for the radical derived from allylbenzene and therefore the radical experiences greater resonance stabilization than diphenylmethyl radical and exhibits a greater rate of hydrogen donation. Of the recyclable solvents, 9,10-dihydroanthracene is a far superior donor to tetralin or 9,10-dihydrophenanthrene.

The index quantitatively illustrates the astonishing effects of combined polar and resonance effects in accelerating atom transfer reactions, i.e., thiophenol > phenol > xylene. These results indicate that compounds such as naphthols and thiols are among the most important donors in high sulfur coals and oxygen rich medium ranked coals. It is clear that they play important and as yet relatively unknown roles in the formation of soluble conversion products and chars (18).

These results easily show the importance of establishing such a method for assessing donor solvent strengths. Furthermore, good methods for estimating the Arrhenius parameters for the absolute rate of rearrangement for o-allylbenzyl radical are at hand (19) and an experimental determination is in progress. Therefore, this body of data will be of great value both to researchers involved in developing thermochemical kinetic models of coal liquefaction and to investigators interested in understanding basic chemical transformations.

Table I. Hydrogen Donor Strength of Selected Solvents and Model Compounds Towards o-Allylbenzyl Radical.

Donor	Relative Donor Strength
m-xylene[a]	1
1,5-Cycloctadiene	11
Diphenylmethane	20
Tetralin	27
9,10-Dihydrophenanthrene	33
Phenol	76
Allylbenzene	114
9,10-Dihydroanthracene	635
Tri-n-butylstannane	3.2×10^5
1-Naphthol	1970
Thiophenol	1.10×10^6

(a) $k_{abs}/k_{cyc} = 2.53 \times 10^{-3}$

References

1. Curran, G. P.; Struck, R. T.; Gorin, E. Ind. Eng. Chem. Process Des. Dev. 1967, 6, 166.

2. Wiser, W. H. Fuel, 1968, 47, 475.

3. Whitehurst, D. D.; Mitchell, T. O.; Farcasiu, M.; Dickert, Jr., J. J. "The Nature and Origin of Asphaltenes in Processed Coals," EPRI Final Report AF-1298 (1979).

4. Neavel, R. C. Fuel, 1976, 55, 237.

5. Wender, I.; Friedman, S.; Proc. 13th IECEC (San Diego, CA., August 1978) Vol. 1, p. 457.

6. Derbyshire, F. J.; Whitehurst, D. D. Fuel 1981, 60, 655.

7. Ingold, K. U. in "Free Radicals" Kochi, J. K., Ed.; John Wiley and Sons, Inc; New York, 1973; Vol. 1, p. 74.

8. Schanne, L. F.; Haenel, M. W. Proceedings, Internation Conference on Coal Science, Dusseldorf, 1981, 416.

9. Le Roux, M., Nicole, D.; Delpuech, J.-J., Fuel, 1982, 61, 0000.

10. Bockrath, B., Noceti, R. P. Am. Chem. Soc. Div. Fuel Chem. Preprints 1981, 26, 94.

11. King, H. H.; Stock, L. M. Fuel, 1981, 60, 748.

12. Ross, D. S.; Blessing, J. E. Am. Chem. Soc. Symp. Ser. 1980, 139.

13. Gregg, R. A.; Mayo, F. R. Discuss, Faraday Soc. 1947, 2, 328.

14. Jackson, R. A. J. Chem. Soc. 1963, 5284; Jackson, R. A.; O'Neil, D. W. Chem. Commun. 1969, 1210.

15. Hatt, H. H. Org. Syn. Coll. Vol. II, p. 395.

16. Cohen, S. G.; Wang, C. H. J. Am. Chem. Soc. 1955, 77, 2460.

17. Reid, R. C.; Prausnitz, J. M.; Sherwood, T. K. "The Properties of Gases and Liquids", 3rd. Ed., McGraw-Hill Book Company: New York, Chap. 3.

18. Poutsma, M. L.; Dyer, C. W. in Ref. 8, p. 669.

19. Camaioni, D. M.; Barrows, R. D.; Franz, J. A., to be published in the Proceedings, International Conference on Coal Science, Pittsburgh, 1983.

THE USE OF o-TERPHENYL AND DIBENZO(c,g)PHENANTHRENE TO STUDY H-DONOR SOLVENTS

By

Eugene A. Kline
Tennessee Technological University
Cookeville, TN 38505

and

Bruce W. Farnum
Grand Forks Energy Technology Center
Box 8213, University Station
Grand Forks, ND 58202

The use of H-donors to increase yields of distillable liquids in direct coal liquefaction is well-documented (1,2,3). Several mechanisms have been proposed including the radical-trapping of hydrogen from the H-donors (4,5). Another mechanism suggested on the basis of thermochemical data (6) is a transfer of a hydrogen atom (radical) to an aromatic compound. This transfer is energetically favorable when specific atoms in the aromatic molecule are attacked. Phenanthrene, for example, is stabilized by 38 kcal/mole when attacked by a hydrogen radical to form the 9-hydrophenanthryl radical. This addition of hydrogen has not been studied to any extent at either of the model compound level or the process level.

Another reaction which may resemble the radical addition reaction was observed when 1,1'-binaphthyl was heated with an H-donor to form the thermally stable perylene (PER) (7). An H-donor was essential for coupling and different H-donors produced perylene in different yields. This reaction was used to study the relative ability of an H-donor to transfer its hydrogens at the high temperatures and pressures used in liquefaction. The coupling reaction appeared to have potential as a system to study this variety of H-transfer which may have important implications in the direct coal liquefaction process.

Problems encountered in this method of evaluating H-donors included the low yields of perylene and the low solubility of perylene in many solvents. Molar ratios of perylene to starting materials ranged from 1×10^{-2} to 28×10^{-2} after 1 hour reaction at 470°C. It was thought that a higher conversion of substrate would improve the reliability of the analytical method and would allow for shorter reaction times. One solution to the problem connected with the coupling to form perylene would be to find another molecule which would react by a similar mechanism but would give higher yields of a thermally stable product under similar reaction conditions. Copeland, Dean, and McNiel (8) reported that o-terphenyl (OTP) gave higher (60 pct) yields of coupled product, triphenylene (TP), than binaphthyl (18.7 pct) gave perylene when reacted with decalin at 490°C with a catalyst and hydrogen for 3 hours. Triphenylene was very stable and this reaction appeared to be a good alternative candidate for evaluation of H-donor reactivities. Several reactions were carried out with the o-terphenyl (Wiley Organics) and various H-donors at 470°C for 1 hour without hydrogen gas in small microreaction vessels. The results of these reactions are summarized in Table I and are compared to previously obtained results with 1,1-binaphthyl (7).

TABLE I

MOLAR RATIOS OF PRODUCT OF REACTANT FOR REACTIONS OF o-TERPHENYL AND 1,1'-BINAPHTHYL WITH H-DONORS AT 470°C FOR 1 HOUR*

H-Donor	TP/OTP x 10^{-2}	PER/BN x 10^{-2}
9,10-dihydrophenanthrene	2.05	3.1
1,2-dihydronaphthalene	2.47	3.4
1,2,3,4-tetrahydronaphthalene	2.51	1.3
fluorene	5.91	2.0
4,5-dihydropyrene	1.65	14.1
1,2,3,6,7,8-hexhydropyrene	--	28.0
indane	0.42	1.27
1,2,3,4-tetrahydroquinoline	0.37	--
1,2,3,4-tetrahydroisoquinoline	0.40	1.38
2,3-cyclohexenepyridine	0.88	--
indoline	--	3.84
5-indanol	0.49	1.24
indene	1.92	3.19

*Obtained by (Mole % coupled product)/(Mole % starting OTP or BN + sum of mole % of by-products)

The ratios of coupled product to starting materials were less satisfactory than those of binaphthyl in predicting H-donor ability. Some H-donors which promoted higher yields of perylene from binaphthyl also produced higher yields of triphenylene from o-terphenyl. There were exceptions including fluorene, 4,5-dihydropyrene and 1,2,3,6,7,8-hexhydropyrene which gave differing amounts of coupled product and in some cases even gave opposing trends. It was found with both substrates that many H-donors known to be good donors at lower temperatures did not give significant amounts of coupling at the higher temperatures used. This was particularly true of the heteroaromatic compounds with hydrogen attached to the heteroatom such as with 1,2,3,4-tetrahydroquinoline.

The conversion of o-terphenyl to triphenylene was not as great as expected based upon the three-fold yield of triphenylene over perylene (Equation 1). Moreover, very close to the peak of triphenylene in the gas chromatogram (using 6' x 2 mm ID 3 pct Dexsil 300 on Supelcoport 100/120 with programmed temperature) were several peaks analyzed by GCMS to be quatraphenyls (MW 306). Large amounts of biphenyl from the cracking of the terphenyl also reduced the possible yield of triphenylene and this complicated the analysis and the possible implications of the reactions to liquefactions.

Kinetics of the conversion of o-terphenyl to triphenylene were studied and compared with previous results of conversion of 1,1'-binaphthyl to perylene under similar conditions. The results are summarized in Table II.

TABLE II

PSEUDO FIRST ORDER RATE CONSTANTS FROM THE CONVERSIONS OF o-TERPHENYL AND 1,1'-BINAPHTHYL TO TRIPHENYLENE AND PERYLENE RESPECTIVELY

H-Donor	o-Terphenyl (k, min^{-1})	1,1'-Binaphthyl (k, min^{-1})
9,10-dihydrophenanthrene	7.0×10^{-3}	1.2×10^{-2}
1,2,3,4-tetrahydronaphthalene	7.4×10^{-3}	1.9×10^{-2}
1,2-dihydronaphthalene	---	---

The similarity between the products and the similar rate constants for each H-donor implied that the same mechanism was involved. When modeled as a first order reaction (Table II), o-terphenyl conversion was slower than binaphthyl conversion. It was interesting that 1,2-dihydronaphthalene formed no more coupled product with either binaphthyl or o-terphenyl after 45 minutes substantiating a similarity in the mechanism. The lower rate constants and the extra side products formed with o-terphenyl led to the conclusion that this system was less advantageous binaphthyl than coupling in the study of H-donor solvents.

Dibenzo(c,g)phenanthrene (DBP) (Equation 1) was investigated as another substrate likely to be a substitute for o-terphenyl and binaphthyl. Its structure suggested the possibility of facile coupling which could lead to enhanced rates and greater yields of coupled products. Dibenzophenanthrene was synthesized by coupling 1-tetralone to bis-dialin (BD) which was then reacted with maleic anhydride (9,10). The adduct was then brominated, dehydrobrominated, decarboxylated, and finally dehydrogenated to the desired dibenzo(c,g)phenanthrene, (Equation 1).

The low yield (7.5% overall) of dibenzophenanthrene was quite poor compared to that in the synthesis of binaphthyl (60%) from the common intermediate, 1,1'-dialin. The final product separated on an alumina chromatographic column with petroleum ether was 89% (VPC) pure. A small amount of this compound was reacted with 9,10-dihydrophenanthrene in the microreactor under the usual conditions. The yield of 8% coupled benzo(1,12)perylene (BP) product was an order of magnitude larger than either triphenylene or perylene. The retention time of the coupled product, benzoperylene, of 20.5 minutes was significantly longer than the retention times of other peaks in this reaction or of any component found in hydrogenated anthracene oil used as an experimental H-donor. There appeared to be no side reactions except some transfer of hydrogen from H-donor to the dibenzophenanthrene. Thus preliminary results indicate dibenzophenathrene might have distinct advantages over binaphthyl or o-terphenyl and would provide a very promising system to apply to the study of H-transfer reactions.

ACKNOWLEDGEMENT

This work was supported bu US DOE Contract No. DE-AC18-80FC10205.

LITERATURE CITED

1. Warrack C. Willson, Curtis L. Knudson, Gene G. Baker, Tom C. Owens, and Donald E. Severson, Technology in the Use of Lignite, Tenth Biannual Lignite Symposium, Grand Forks, ND, May 30-31 (1979) p. 170.

2. A.M. Souby, T.M. Owens, and D.E. Severson, Am. Chem. Soc. Div. Fuel Preprints, 25 (1) 233 (1980).

3. D.D. Whitehurst, T.O. Mitchell, and M. Farcasiu, Coal Liquefaction, Academic Press, New York, NY, (1980) p. 205.

4. F.J. Derbyshire, P. Varghese, and D.D. Whitehurst, Am. Chem. Soc. Div. Fuel Preprints, 26 (1) 88 (1981).

5. Everett Gorin, Chemistry of Coal Utilization; Supplementary Vol 2, Martin A. Elliott, Ed., John Wiley and Sons, Ney York, NY (1981) p. 1882.

6. Stephen E. Stein, New Approaches to Coal Chemistry, B. Blaustein, B. Bockrath, and S. Friedman, Eds., ACS Ser. #169, Am. Chem. Soc., Washington, D.C. (1981) p. 113.

7. Eugene A. Kline, Mark E. Harrison, and Bruce W. Farnum, Am. Chem. Soc. Div. Fuel Preprints, 27 (3-4) 18 (1982).

8. P.G. Copeland, R.E. Dean, and D. McNiel, J. Chem. Soc., 1687 (1960).

9. F. Bergmann, E. Eschinazi, and M. Neeman, J. Am. Chem Soc., 65, 179 (1943).

10. H.A. Weislich, Ber., 71,1203 (1938).

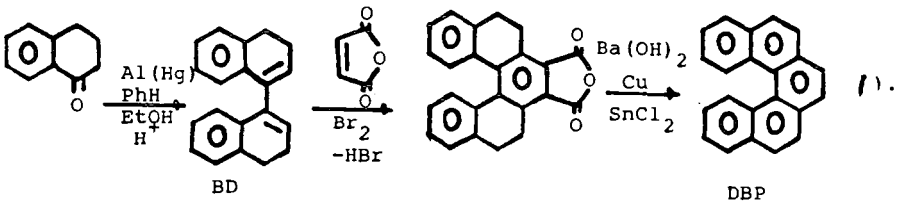

COAL STRUCTURE VS. FLASH PYROLYSIS PRODUCTS

W. H. Calkins

E. I. Du Pont de Nemours & Company
Central Research & Development Department
Experimental Station
Wilmington, DE 19899

The fast pyrolysis of coal produces tar, char and a range of low molecular weight gases in various proportions and amounts depending on the pyrolysis conditions (temperature, pressure) and the coal being pyrolyzed. Much research effort has been devoted to study of the reaction kinetics and effect of process variables, attempting thereby to elucidate the pyrolysis mechanism[1]. Less effort has been focused on coal chemical structure and its relationship to the pyrolysis reactions and pyrolysis products. It was to attempt to better understand coal structure and its influence on pyrolysis products and pyrolysis mechanisms that this project was undertaken. This paper will report only on that portion of the work concerned with the aliphatic hydrocarbon products and particularly the light olefins.

A continuous bench-scale pyrolysis apparatus (Fig. 1) was constructed similar to the design of Tyler[2]. The coal entrained in a nitrogen stream was injected into a sand bed fluidized with nitrogen and heated in a split furnace to the temperature desired. Volatiles emitted from the sand bed were passed into two cold traps in series containing cellulose thimbles to filter out the tar and char from the off-gas. Gas exiting the cold traps was vented through a wet-test meter with a side stream entering a Perkin-Elmer Sigma One computer-controlled gas chromatograph which analyzed for some 16 components. At the end of a pyrolysis run, the tar and char caught in the two thimbles were extracted in a soxhlet extractor with methylene chloride and methanol to obtain the weight of tar and char produced.

Figure 2 shows tar yields vs. temperature for a Texas Lignite. Figure 3 shows how the quantity and composition of the pyrolysis gas from the same coal varies with temperature. Only the major gases are shown. These curves are typical of many coals although the actual quantities vary[3]. From these two figures, it is apparent that the tar produced goes through a maximum at about 600°C and up to that temperature relatively small amounts of gases are evolved. Above 600°C, the production of the various gases increases rapidly while at the same time, the tar yield drops off. The inference can be drawn that the gas is coming from tar pyrolysis. That this is so, can be shown by pyrolyzing tar which has been produced at 600°C, at higher temperatures. Similar gaseous products are produced and in similar ratio as when coal is pyrolyzed at the higher temperature[4].

The yields of the hydrocarbon gases produced on coal pyrolysis vary greatly depending on the particular coal. This is shown for ethylene, one of the major products, in the first two columns of Table 1. The ethylene yield is related to the propylene

yield as shown by Figure 4. Similarly, the ethylene yield is related to the butadiene yield, suggesting that these gases have a common precursor. The methane and benzene, however, show no obvious relation to the ethylene yields. These products are apparently derived mainly from other components in the coal.

Coal Structure vs. Pyrolysis Products

To try to relate these yield differences to structural differences in the coals themselves, each coal whose pyrolysis behavior was studied was examined by ^{13}C NMR (with cross polarization and magic angle spinning). This work was done by E. A. Hagaman and H. Zeldes of Oak Ridge National Laboratory in a cooperative program with Du Pont. Typical pattern differences between a high ethylene-producing coal (PSOC 124), a low ethylene-producing bituminous coal (Sewickley) and two intermediate coals (Con Paso Blue 2 and PSOC 181), are shown in Figure 5. While the PSOC 124 coal shows high aliphatic character and the Sewickley shows the expected higher aromaticity, various other evidence suggests that aliphatic character alone is not the determining factor. The fractional area representing a chemical shift at 31 ppm, however, which is associated with methylene chains greater than 5 or 6 segments long, appears to correlate with the ethylene yield results. This peak which occurs at a chemical shift of 29 ppm in substances in solution is apparently shifted slightly to 30-32 ppm in solid coal. This was shown by running stearic acid in solution, and impregnated on to anthracite coal. The 29 ppm peak was shifted up field and broadened on the coal.

A plot of ethylene yield vs. the area fraction of the ^{13}C NMR spectrum at a chemical shift of 31 ppm, times the weight fraction of carbon in the coal is shown in Figure 6. The line is the least-squares fit to the points shown. While there is scatter in the data, a correlation is apparent (Correlation coefficient = .92).

Tar Structure Studies

Low temperature (600°C or less) pyrolysis of coal produces high yields of tar which on further pyrolysis produces the volatile hydrocarbon products we observe on high-temperature pyrolysis of coal. This shows that this tar contains the aliphatic precursors we observe in the coal itself, although they may be changed somewhat from the form in which they are in in the coal. A number of tars were therefore produced by pyrolysis of several different coals at 600°C in the laboratory coal pyrolysis unit for further study.

A ^{13}C NMR pattern for a solution of Millmerran tar (10% in $CDCl_3$) from 600°C pyrolysis is shown in Figure 7. It shows a very strong peak at a chemical shift of 29 ppm. The ^{1}H NMR spectrum was run on the same tar in $CDCl_3$ solution (Figure 8). It shows a strong peak at 1.2 ppm known to be due to methylene chains over 5 units long. By using a Dow Corning silicone DC200 fluid (%H=8.06) internal standard in the $CDCl_3$ solvent, quantitative determination of the $(CH_2)_n$ peak by ratio of its area to that of the 0 ppm silicone peak was possible. This showed 33.6 wt. % $(CH_2)_n$ in the tar. Similar patterns are shown by tars of other coals.

To quantify the assignment of the 1.2 peak in the proton NMR spectrum, a series of model compounds having long methylene chains was dissolved in $CDCl_3$ containing the silicone internal standard. In all cases, the 1.2-1.3 peak was very large and clearly detectable. Weight % $(CH_2)_n$ calculated for each compound are shown in Table 2. As can be seen from the Table, not all methylene groups appear in the proton NMR spectrum at 1.2-1.3 ppm. Only those (CH_2) groups shown in brackets in the structural formulas show up at that place. Those CH_2 groups conjugated with or close to the carboxyl groups or benzene rings appear at higher chemical shifts, and methyl groups appear at 0.7-0.8 ppm. This clearly identifies the 1.2-1.3 ppm peak as due to $(CH_2)_n$ but at the same time indicates that any analysis based on this method will not include all of the (CH_2) groups in coal. If the chains are long, however, most of the methylene will be included.

Table 3 shows the distribution of types of protons in 600°C pyrolysis tars from four different coals representing a wide range of olefin yields on pyrolysis. The Table shows that roughly 35% of the protons in the tar are polymethylene protons, the rest are divided between methyl groups, hydroaromatic hydrogens, hydrogens attached to aromatic carbons, and a small number of olefinic and some unidentified protons.

Table 4 shows the distribution of protons in tar from Texas Lignite pyrolyzed at various temperatures from 600°C to 920°C. This clearly shows that as the pyrolysis temperature is increased, the content of polymethylene in the tar decreases as do the hydroaromatic hydrogens. The aromatic hydrogens on the other hand increase rapidly to become the predominant species. This provides a convenient measure of the completeness of pyrolysis.

To try to isolate and purify larger quantities of the hydrocarbon precursors, a separation was made of the Millmerran tar by Preparative Liquid Chromatography. A number of fractions across the chromatogram were analyzed by FTIR and ^1H NMR and fraction 21 representing 38% of the original sample turned out to be high in $(CH_2)_n$ (concentration 68%). An Infrared spectrum of that fraction (Figure 9) showed a well resolved peak at $720cm^{-1}$, known to be characteristic of long methylene chains. This peak has a low extinction coefficient and is rarely descernible above background in coals themselves. A GC/MS pattern of that fraction (Figure 10) shows olefin/paraffin pairs of peaks from C_{17} to C_{24}.

The polymethylene compounds in pyrolysis tars are mainly present as linear paraffins or olefins, however, there are indications of lesser amounts of branched paraffins and olefins and alkylaryl compounds as well in the unfractionated tars. The form the polymethylene compounds have in the coal itself is not known, but extraction of various coals with methylene chloride for several days failed to remove more than 1% of the material, suggesting that the major part of the polymethylene compounds may be either chemically combined in the coal structure or else trapped.

Model Compound Pyrolysis

While it seemed likely on the basis of petroleum experience that polymethylene compounds would pyrolyze to form the low molecular

weight aliphatic hydrocarbons we observe on coal pyrolysis, known compounds as models of polymethylene and other structures in coal were pyrolyzed at similar temperatures and contact times as the coal.

Table 5 summarizes the results of pyrolysis of 7 model compounds. Products are only shown as major and minor. As can be seen by referring to the Table, under the pyrolysis conditions used, compounds containing methylene chains such as dodecane, octadecane, stearic acid, ethylbenzene, propylbenzene, butylbenzene, and phenyldodecane on cracking give substantial quantities of ethylene along with butadiene, propylene and other hydrocarbons in amounts roughly comparable to what we observe in coal pyrolysis. The aromatic portion in alkylaryl compounds appears to go mainly to toluene although small amounts of benzene and some styrene are produced as well. Some methane is also produced along with minor amounts of ethane, butane and other hydrocarbon. These results are quite consistent with what we find in coal pyrolysis and with petroleum cracking technology.

Interestingly, the methylaryl compounds investigated thus far do not produce methane on pyrolysis under the conditions we used. Toluene and the three xylene isomers apparently are only slightly converted at 850°C and 0.5 to 1.0 second contact time in the sand bed. 9-Methylanthracene and 3,6-dimethylphenanthrene produced no methane or other gaseous products, although they appeared to form tar or coke. This is consistent with the observations of Lang et al on methylnaphthalenes(5) which form condensation products but not gases under pyrolysis conditions.

Analysis for Polymethylene in Coal Itself

With ^{13}C NMR indication of the $(CH_2)_n$ moiety in coal and evidence of $(CH_2)_n$ in low and high temperature pyrolysis tars, as well as model compound pyrolysis information, it seemed important to devise a quantitative analytical method for $(CH_2)_n$ in coal itself. This raised the question whether coal could be liquefied under generally accepted solvent refining conditions and still retain undecomposed the polymethylene component? Also, if the $(CH_2)_n$ is liberated but not destroyed, can it be detected and quantitatively determined by proton NMR?

Figure 11 shows the proton NMR pattern of the liquefaction product of PSOC 124, a high ethylene yielding coal which was liquefied using 3 grams of coal, 3 grams of tetralin as donor solvent, 0.1 gram each of sodium sulfide and ferrous sulfide as liquefaction catalysts and 2000 psi pressure (cold) of hydrogen in a 10 ml shaker bomb. The liquefaction was run at 425°C for 2 hours in a sand bath with vertical shaking. The product liquid was washed out of the shaker tube with methylene chloride and filtered to remove the solids (ash, unconverted coal and catalysts). After removal of the CH_2Cl_2 by distillation, a weighed sample of the liquid was dissolved in deutero-chloroform containing a known amount of DC200 silicone fluid as internal standard. Examination of the NMR pattern clearly shows the $(CH_2)_n$ peak at 1.2 ppm and the CH_3 peak at about 0.8 ppm indicating that the polymethylene component of the coal is released from the coal matrix but not destroyed in the liquefaction process.

The rest of the NMR pattern (beyond 1.3 ppm) is heavily affected by the presence of the donor solvent and its dehydrogenation products so that this method is only useful for detecting the $(CH_2)_n$.

To develop a routine analysis based on coal liquefaction, first a series of batch shaker tube liquefaction runs were made in 10 ml shaker tubes using the same recipe as previously but varying the time, temperature and donor solvent. Tests were made with three different donor solvents [tetralin, dihydrophenanthrene (DHP), and tetrahydroquinoline (THQ)]. The $(CH_2)_n$ figures on the right hand 5 columns of Table 6 were obtained by separating the liquid from the solid by extraction with CH_2Cl_2, filtration to remove the solids, and distilling off the solvent (CH_2Cl_2). The $(CH_2)_n$ content of the liquid was determined by dissolving a weighed sample of liquid into a volumetric flask and making up to the line with CCl_3D containing a known quantity of DC-200 silicone internal standard. All conversions were 85% or more and usually above 90%.

In most cases, all three donor solvents gave similar results, but in a few cases the tetrahydroquinoline gave higher values. THQ was, therefore, selected for further investigation. Liquefactions were run, varying temperature and contact time. These results are shown in the three right-hand columns of Table 6 where results were reported for 400°C and 1.65 hours and 435°C for 4 hours. The lower temperature short contact time liquids were viscous and hard to work up. The high temperature longer time reactions showed little change over the 425°C/2 hour samples, so the latter conditions were selected as optimum.

The values obtained for $(CH_2)_n$ content of coals from coal liquefaction are reasonable based on the amount of ethylene produced in pyrolysis shown in column 1 and ethylene plus other hydrocarbons believed to come from the same source shown in column 2 of Table 6. These should represent minimum amounts in the coal. Column 3 shows the $(CH_2)_n$ found in pyrolysis tars calculated on the basis of the original coal which should also be a minimum since not all the tar is driven out of the coal at 0.5 seconds pyrolysis contact time.

For a number of reasons, it was desirable to be able to run this liquefaction analysis on a micro (<10 mg) scale. This would be much simpler to do if no added catalyst was required and hydrogen pressure was not needed. Experiments were, therefore, tried to see whether such an analysis could be developed under those conditions. Liquefactions were run in 3" long 3 mm pyrex glass tubes. Approx. 5 mg of (-200 mesh) coal samples (weighed to .01 mg) were charged to the tubes along with 10 mg of calcined clean sand, 1.1 times the weight of coal of the donor solvent and a 1 cm long 2 mm glass rod (for agitation) and the tubes purged with nitrogen and sealed.

Two such tubes were packed into each 10 ml shaker tube with steel wool packed around them. They were then subjected to 425°C for 2 hours in a sand bath with rapid vertical agitation with approximately 5 minutes heat up time to temperature and rapid cool down in a cold air stream.

The tubes were worked up by breaking in the middle and rinsing repeatedly with CCl_3D containing a weighed amount of DC-200 fluid, through a glass wool plug filter into a 1 ml volumetric flask. The contents of the flask were put into an NMR tube and run on the IBM NR-80 Fourier Transform NMR Spectrometer. The area of the 1.2 ppm peak was determined relative to the silicone peak and the weight % $(CH_2)_n$ calculated using the area ratio.

The results of these experiments are shown in columns 1, 2 and 3 in Table 7. They clearly show that low results are obtained with tetralin and dihydrophenanthrene under these conditions. This may be due in part to lower donor activity, but more likely due to low hydrogen content of the donor in the absence of a hydrogen atmosphere. The results with tetrahydroquinoline, however, appear to be about the same whether in the micro mode without hydrogen pressure or catalyst or in the macro mode with both. This system was, therefore, adopted as being simple, rapid and giving results equivalent to the macro system. Analysis of pairs of samples from some 40 coals by this method ranging in % $(CH_2)_n$ content by weight of from 0 to 17% (MF) showed a standard deviation of 0.59%. Table 1 column 3 shows these values for the coals previously discussed together with the ethylene yields. In view of the sampling problems with a heterogeneous material like coal and the small sample size, analyses were normally run in pairs. The coal was ground fine (-200 mesh) and well blended. Where greater accuracy is desired, more replicates can be easily run and the ^1H NMR can be run with more scans.

Ethylene yields (850°C) vs. $(CH_2)_n$ concentration for these coals are plotted in Figure 12 with the linear regression line shown. A correlation coefficient of 0.952 and a 0 intercept shows a good correlation.

Similarly plots of propylene and butadiene yields for the same coals, vs. $(CH_2)_n$ content also show strong correlations.

Conclusions

We conclude from the experiments described that the low molecular weight aliphatic hydrocarbons produced by flash pyrolysis of coal at temperatures of 700°C and over, result primarily from the cracking of long methylene chains which are part of the coal structure or trapped in it. Low temperature (600°C) pyrolysis of the coal drives off a portion of the coal as tar which contains these polymethylene moieties, primarily in the form of normal paraffins and olefins from C_{17} to C_{24} and higher. This polymethylene precursor(s) in coal is apparently destroyed during coalification, as it is essentially absent in anthracite and is much higher in lignite and subbituminous coals. However, even in low rank coals the concentration of the polymethylene moiety varies widely, probably determined by the types of plants from which the coals are derived. Cannel coals generally contain fairly large amounts of $(CH_2)_n$ (up to 17% or more). Some lignites and subbituminous coals contain as much as 10% $(CH_2)_n$.

Several other investigators[6-15] have reported the presence of aliphatic hydrocarbons in coal based mainly on solvent extractions. The amounts reported, however, have been generally much less than was found in this work. The difference presumably is that most of the polymethylene is chemically bound or trapped and non-extractable. Deno[16] reported the presence of long chain methylene compounds by chemical degradation of the coal, however, no quantitative conclusions could be drawn from that work.

The liquefaction method for estimation of $(CH_2)_n$ content of coals is being used to determine the $(CH_2)_n$ content of coal macerals and to explore the geochemical origins of the polymethylene components in coal.

Acknowledgements

The author wishes to acknowledge the important contributions by E. Hagaman and Henry Zeldes of Oak Ridge National Laboratory in ^{13}C NMR work on the coals studied in this project, and Penn State University for supplying many of the coal samples used.

REFERENCES

1. Howard, J. B., Chemistry of Coal Utilization, second supplement, Wiley Interscience, pps. 665-783

2. Tyler, Ralph J., "Flash Pyrolysis of Coals - 1", Fuel, 59, 218 (1980)

3. Tyler, Ralph J., "Flash Pyrolysis of Coals - 2", Fuel, 59, 218 (1980).

4. Tyler, Ralph J., "The Chemistry of Flash Pyrolysis; Secondary Cracking", 6th Anstradian Workshop on Coal Hydrogenation, November 13, 1981.

5. Lang, K. F. et al, Chem. B 89 2866 (1956).

6. Vahrman, M., Fuel 49 5 (1970).

7. Spence, J. A. and Vahrman, M., Fuel 49 395 (1970).

8. Rahman, A and Vahrman, M., Fuel 50 318 (1971).

9. Birkofer, L. et al, Bremmstoff Chemie 50 376 (1969).

10. Chauvin et al, Bull de la Soc. de France 11 3916 (1969).

11. Bartle, K. D. et al, J. Appl. Chem. 20 197 (1970).

12. Bartle, K. D. et al, Fuel 54 226 (1975).

13. Bartle, K. D. et al, Fuel 58 410 (1979).

14. Bartle, K. D. et al, Nature 277 184 (1979).

15. Zilm, K. N. et al, Fuel 58 11 (1972).

16. Deno, N. et al, Fuel 60 210 (1981).

FIGURE 1

-1 GM/HR COAL PYROLYSIS UNIT

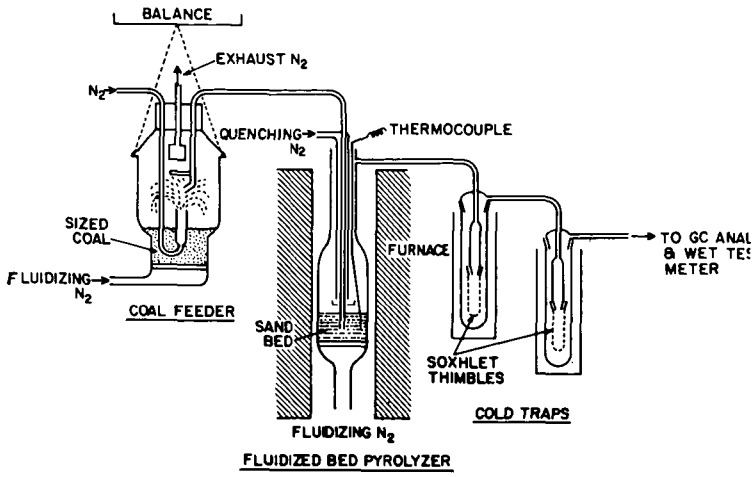

FIGURE 2

PRODUCT YIELDS FROM THE FLASH PYROLYSIS OF TEXAS LIGNITE

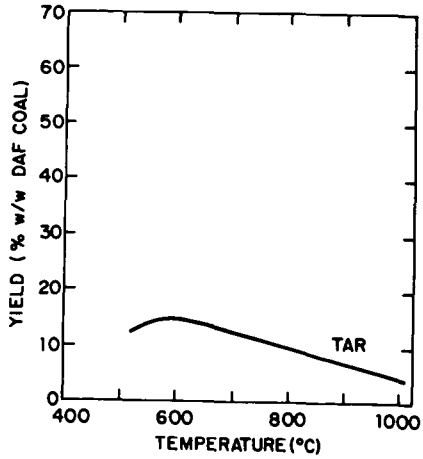

FIGURE 3

PYROLYSIS OF TEXAS LIGNITE
YIELDS OF PRINCIPAL GASES

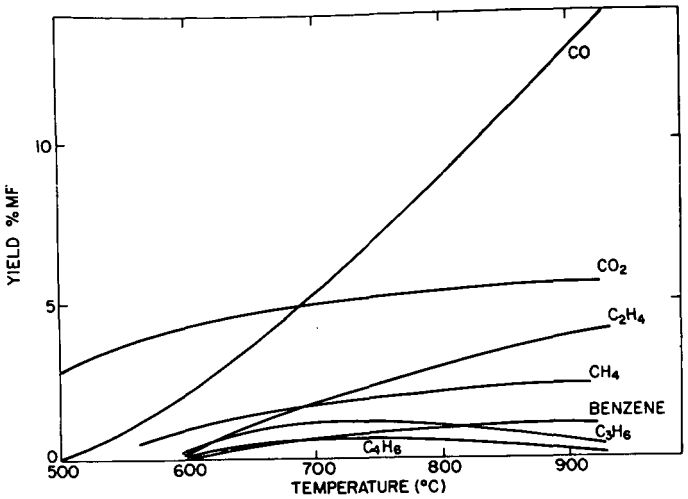

FIGURE 4

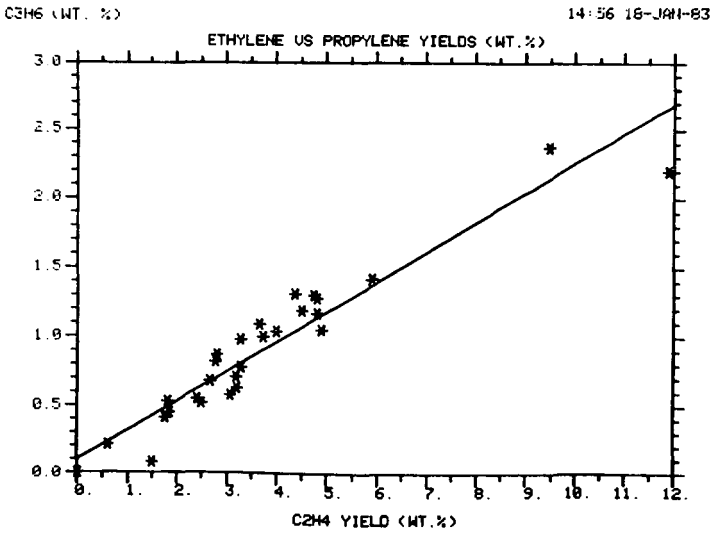

FIGURE 6

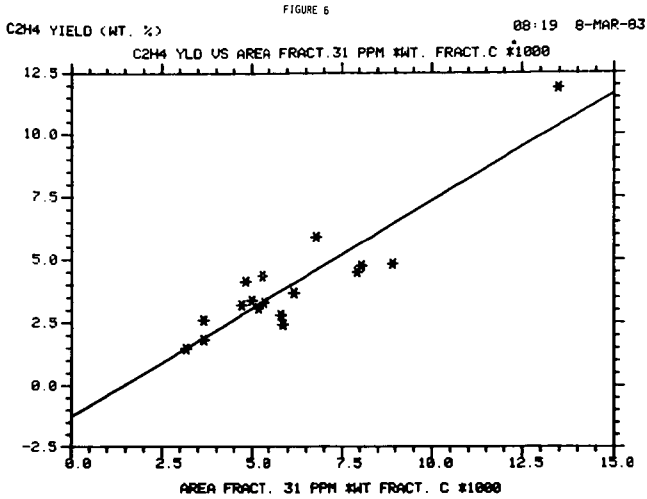

FIGURE 5

^{13}CNMR SPECTRA OF COALS PRODUCING DIFFERENT ETHYLENE YIELDS ON PYROLYSIS (850°C 4sec. CT)

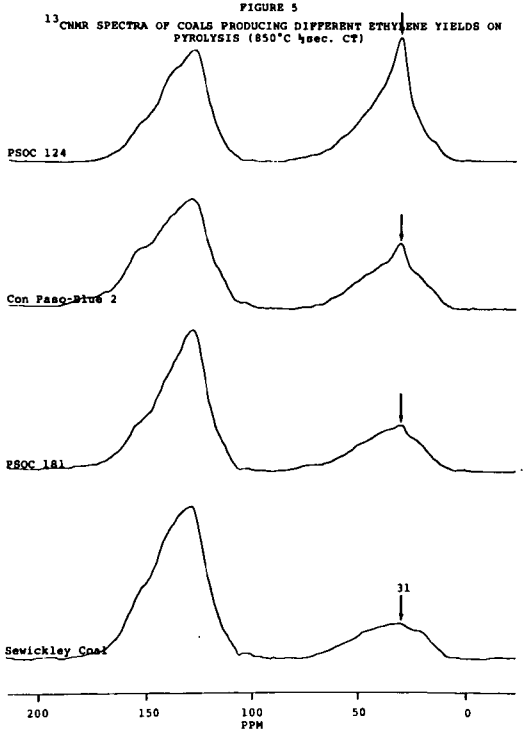

FIGURE 7

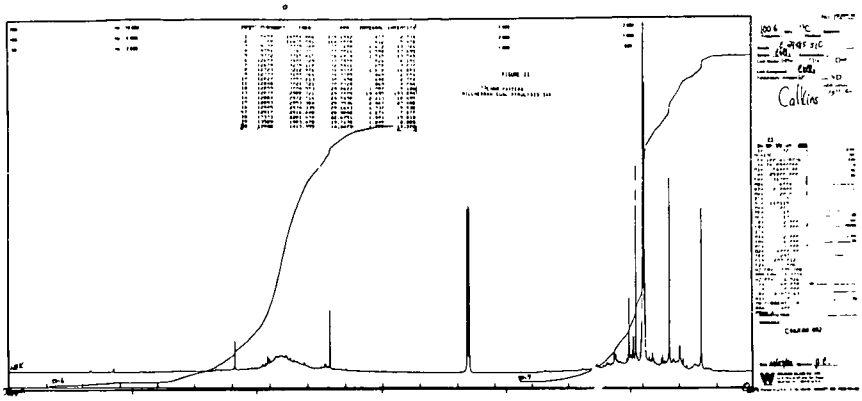

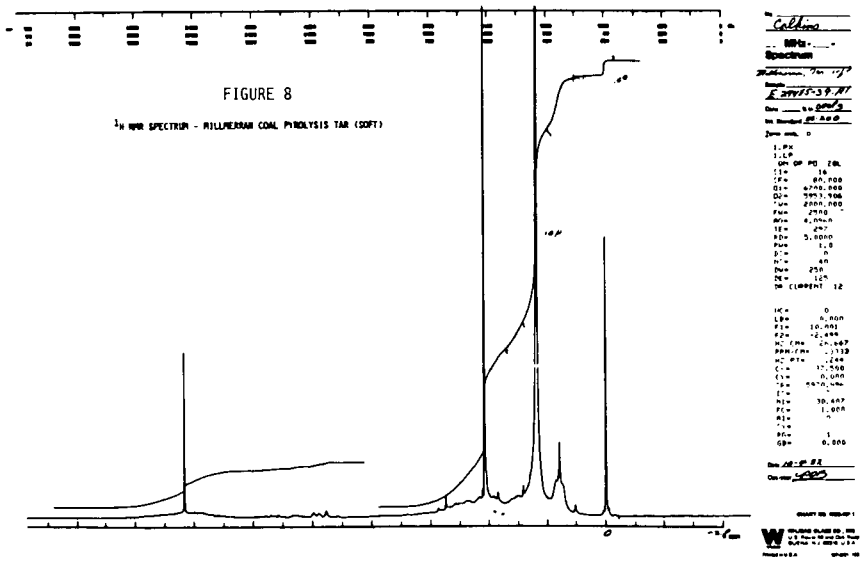

FIGURE 8

^{1}H NMR SPECTRUM - MILLMERRAN COAL PYROLYSIS TAR (SOFT)

FIGURE 9

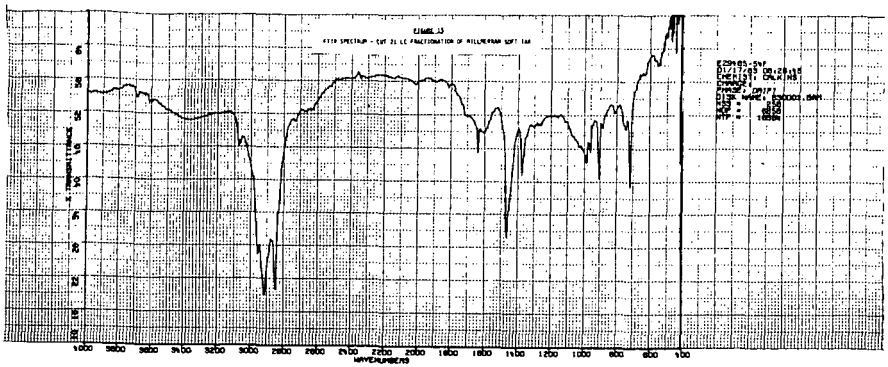

FIGURE 10

GC/MS SPECTRUM - CUT 21 LC FRACTIONATION OF MILLMERRAN SOFT TAR

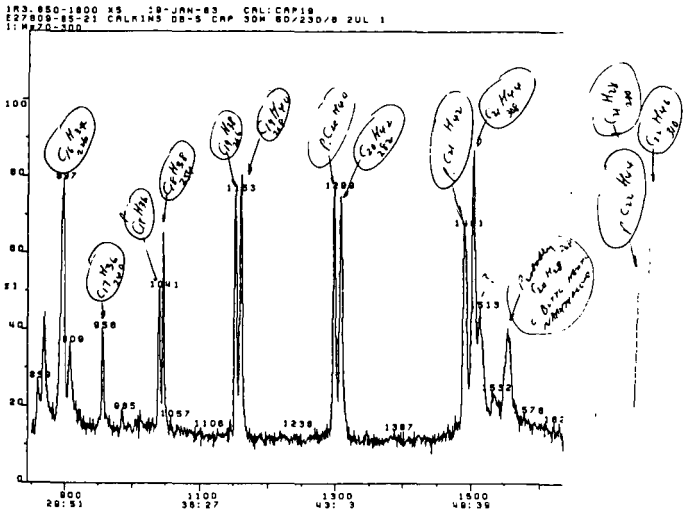

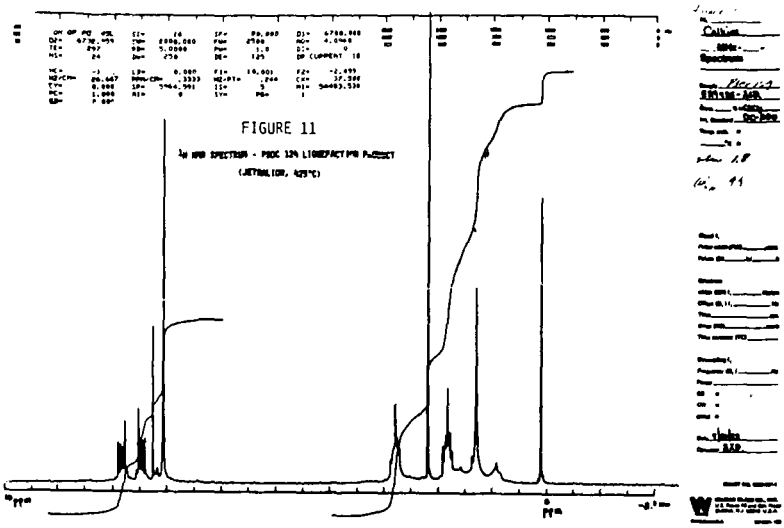
FIGURE 11

FIGURE 12

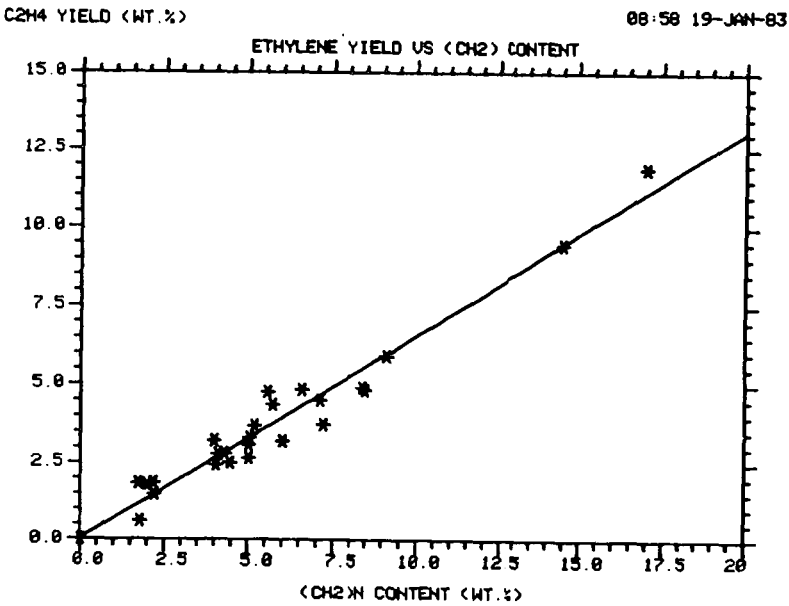
C2H4 YIELD (WT.%)
08:58 19-JAN-83
ETHYLENE YIELD VS (CH2) CONTENT
15.0
12.5
10.0
7.5
5.0
2.5
0.0
0.0
2.5
5.0
7.5
10.0
12.5
15.0
17.5
20
(CH2)N CONTENT (WT.%)

TABLE 1

ETHYLENE YIELDS IN COAL PYROLYSIS AND $(CH_2)_n$ CONTENT (WT. %)

(850°C 0.5 sec. CT.)

Coal	MF*	MAF**	$(CH_2)_n$ (MF)*
PSOC 124	11.9	13.1	17.0
King Cannel	9.47	11.04	14.5
Millmerran	6.08	7.01	9.65
Lovelady-L-2	5.91	7.94	9.11
Lovelady Y-4	4.90	6.68	8.40
Lovelady 81 VLL-92	4.82	7.00	8.48
Blind Canyon	4.82	5.07	6.56
PSOC 435	4.75	4.98	8.86
Emery	4.50	4.95	7.12
Con Paso-Blue 3	4.36	4.88	5.72
Con Paso-Blue 2	3.73	4.78	7.21
Con Paso-Yellow 4	3.67	4.17	5.18
Upper Hiawatha	3.30	3.65	5.03
Wyodak	3.21	3.52	4.0
Texas Lignite	3.20	3.59	6.01
PSOC 181	3.07	3.33	5.02
Con Paso-Yellow 6	2.80	3.05	4.31
PSOC 464	2.78	3.06	4.12
Lower Hiawatha	2.66	2.85	5.00
Pittsburgh 8	2.50	2.98	4.47
PSOC 1106	2.42	2.53	4.04
PSOC 657	1.85	2.28	2.18
Illinois 6-Burning Star	1.83	2.18	1.75
PSOC 833	1.77	2.01	2.00
Sewickley	1.48	1.75	2.20
Ohio 9-Egypt Valley	.61	.68	1.78
Anthracite	0.0	0.0	0.0

*Moisture Free
**Moisture and Ash Free

TABLE 2

$(CH_2)_n$ ANALYSIS OF KNOWN COMPOUNDS
(Proton NMR)

	Theory	Found
$CH_3[(CH_2)_{14}]CH_2CH_2-\overset{O}{\overset{\|\|}{C}}-OH$	64.0	62.6
$CH_3[(CH_2)_{10}]CH_3$	82.0	77.7
$CH_3[(CH_2)_{13}]CH_3$	85.8	81.8
$CH_3[(CH_2)_{17}]CH_3$	88.8	84.6
$CH_3[(CH_2)_{22}]CH_3$	91.1	91.7
$CH_3[(CH_2)_{23}]CH_3$	91.5	92.5
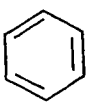 $CH_2CH_2[(CH_2)_9]CH_3$	51.2	49.1

TABLE 3

600°C. PYROLYSIS TARS - DISTRIBUTION OF TYPES OF H ATOMS

PPM	0.8	1.3	1.6-1.7	1.7-3.0	5.2	7.2
H TYPE	CH_3	$(CH_2)_n$		hydroaromatic or benzylic	olefinic	aromatic
COAL TYPE						
Texas Lignite	.085	.352	.077	.300	--	.187
Emery	.099	.331	.064	.263	.016	.232
PSOC 124	.110	.349	.170	.190	.010	.175
PSOC 435	.113	.220	.113	.267	.003	.166

TABLE 4

PYROLYSIS TARS - DISTRIBUTION OF H ATOMS
TEXAS LIGNITE PYROLYSIS VS. TEMPERATURE

PPM	.3 - .5	.8	1.3	1.6 - 1.7	1.7 - 3.0	5.2	6.5 - 8.0
H TYPE		CH_3	$(CH_2)_N$		HYDROAROMATIC	OLEFINIC	AROMATIC
PYROLYSIS TEMP. (°C)							
600	=	.110	.320	.048	.259	.044	.141
700	=	.100	.254	.036	.258	.048	.250
825	=	.067	.189	.027	.208	.053	.414
850	.009	.035	.078	.106	.159	.009	.566
920	.027	.018	.099	.117	.072	-	.577

TABLE 5

PYROLYSIS OF MODEL COMPOUNDS (LIQUIDS)
(0.3 ml/hr Liquid Feed in ca 2.1 l/min. N_2)
850°C 0.5-1.0 Sec. Contact Time

Model Compound	Gaseous or Volatile Products: Principal Products	Gaseous or Volatile Products: Minor Products
Stearic Acid	C_2H_4 C_3H_6 C_4H_6 CH_4 CO_2	Benzene C_2H_6
Dodecane	C_2H_4 C_3H_6 CH_4	C_4H_6 C_2H_6
Octadecane	C_2H_4 CH_4 C_3H_6	C_4H_6 C_2H_6
Ethyl Benzene	Styrene Toluene Methane	C_2H_6 Benzene C_2H_4
Propyl Benzene	Toluene Ethylene Styrene	Benzene Methane Ethyl Benzene
n-Butyl Benzene	Ethylene Toluene Ethyl Benzene Methane Styrene	C_2H_6 C_3H_6 Benzene
Phenyl Dodecane	Ethylene Propylene Methane Toluene Styrene	C_4H_6 C_2H_6 Benzene

TABLE 6

ESTIMATES OF $(CH_2)_N$ IN COAL (WT.%)

COAL	COAL FROM PYROLYSIS YIELDS		FROM 600°C PYROLYSIS TAR	FROM COAL LIQUEFACTIONS (MACRO) 2000 PSI H_2 (NA_2S, $FESO_4$ CATALYSTS)*				
	$\%C_2H_4$ 850°C	C_2H_4 plus other hydrocarbons	$\%(CH_2)_N$	TETRALIN 925°C/2 hrs	DHP***	THQ**** 400° 1.65 HR**	THQ**** 425° 2 HR	THQ**** 435°C 4 HR
PITTSBURGH 8	2.5	4.2	-	2.38	1.91	4.10	4.36	5.2
TEXAS LIGNITE	3.2	5.3	3.3	5.49	-	-	6.59	6.45
WYODAK	3.21	5.3	-	-	4.84	-	5.06	6.42
EMERY	4.5	7.5	5.2	7.77	-	8.77	7.3	8.60
PSOC 435	4.75	7.9	3.5	9.02	8.39	9.57	7.14	7.39
MILLMERRAN	6.10	10.2	4.4	-	-	-	9.65	12.35
PSOC 124	11.90	17.3	9.2	16.47	17.6	13.9	16.4	17.7

* ASSUMES 100% CONVERSION OF ORGANIC PORTION

** LOW CONVERSION, VERY VISCOUS PRODUCT

*** DIHYDROPHENANTHRENE

**** TETRAHYDROQUINOLINE

TABLE 7

COAL LIQUEFACTION ANALYSIS FOR $(CH_2)_n$ IN COAL (WT.%)

	Liquefactions (Micro) 425°C/2 hr.			Liquefactions (Macro) 2000 psi H_2
Coal	Tetralin	DHP	THQ	THQ 425°C/2 hr.
Pittsburgh 8	1.81	1.72	4.63	4.36
Texas Lignite	3.07	3.88	6.02	6.59
Wyodak			6.3	5.06
Emery	6.99	-	7.12	7.3
PSOC 435	4.82	5.19	7.73	7.14
Millmerran	4.31	6.57	9.13	9.65
PSOC 124	9.02	9.32	16.58	16.4

FLASH PYRDLYSIS OF COAL IN REACTIVE AND NON-REACTIVE GASEOUS ENVIRONMENTS

Muthu S. Sundaram, Meyer Steinberg and Peter T. Fallon
Department of Energy and Environment
Process Sciences Division
Brookhaven National Laboratory
Upton, L.I., N.Y. 11973

ABSTRACT

The objective is to obtain process chemistry for the rapid pyrolysis of coal with reactive and non-reactive gases for the production of liquid and gaseous fuels and chemical feedstocks. The gaseous products were analyzed via an on-line GC and the heavy liquids were characterized by HPLC, IR and GC/MS. The total carbon conversion was higher in the presence of reactive gases than in the presence of non-reactive gases. The heat-up rate of the coal particles in non-reactive gasifying media followed the order $He > N_2 > Ar$. The total carbon conversion from New Mexico subbituminous coal in the presence of these gases also followed the same order. Experiments were performed in a down-flow, entrained tubular reactor under a wide range of process conditions: 700° to 1000°C, 20-1000 psi, 0.5 - 5 sec. coal particle residence time. The effects of these process variables and the physical properties of the pyrolyzing gases on the yield and the quality of products from the pyrolysis of New Mexico subbituminous coal will be discussed.

INTRODUCTION

The flash pyrolysis of coal is a fast, gas-phase, non-catalytic, direct coal conversion technique for the production of gaseous hydrocarbons and significant quantities of aromatic liquid hydrocarbons for distillate fuels and chemical feedstocks. Pyrolysis is a complex process during which several chemical reactions occur simultaneously. A general concept of the pyrolysis process is shown in Figure 1.

Considerable amount of work has been done in the past on pyrolysis of coal which was summarized recently in a classic review by Howard (1). The experimental techniques, reaction conditions and the coal used were so diversified that the information available is of limited value in a process point of view. We have, therefore, undertaken a systematic generalized study to methodically develop and build a reliable data base on the flash pyrolysis of coals with reactive and non-reactive gases. The choice of inert gas is based on covering a range of physical property effects, i.e., heat capacity, thermal conductivity and diffusivity etc. The choice of reactive gas is based on the type of gases usually formed in the pyrolytic reactions of coal. The results obtained from the pyrolysis of New Mexico sub-bituminous coal in H_2, CH_4, He, N_2 and Ar atmospheres are presented in this paper.

EXPERIMENTAL

New Mexico sub-bituminous coal ground to less than 100 mesh and vacuum dried at 70°C was used in all pyrolysis experiments. The ultimate analysis of the coal is given in Table 1.

The experimental equipment used in these studies (Figure 2) is a highly instrumented 1-in.-i.d. by 8-ft-long entrained downflow tubular reactor system, which has been described in detail (2). Coal particles 150 micrometers or less in diameter are fed by gravity into the top of the reactor from a coal feeder enclosed in a high pressure vessel. The pyrolysis gas enters through a preheater, contacting the coal particles at the

top of the 8-ft reactor. The heat transfer, pyrolysis, and secondary reactions take place as the coal and entraining gas meet and flow concurrently down the reactor. Below the reactor is a 3-ft forced air cooling section in which the product-laden gases are cooled to 250° to 300°C. The char is removed from the effluent gas in a high pressure vessel which is maintained at 250° to 300°C to prevent liquid product condensation. The heavy liquid products in the effluent gas are removed in two condensers, one water cooled (15°C) and the other Freon cooled (-40°C). The remaining gases are then reduced to atmospheric pressure, measured via a positive displacement meter, and vented to the atmosphere.

The velocity of the coal particle through the reactor is calculated by adding its free-fall velocity based on Stoke's law to the down-flow gas velocity. The residence time is determined from the length of the reactor and the total coal particle velocity.

Product yields, as a function of coal particle residence time, are determined by sampling from taps located at 2-ft intervals along the length of the reactor. The product analysis is accomplished via an on-line, programmable gas chromatograph (GC) which determines CO, CO_2, CH_4, C_2H_4, C_2H_6, and BTX (benzene, toluene, and xylene) concentrations every 8 minutes. Products heavier than BTX ($>C_9$) can not be measured on-line because of condensation in the sample lines and the temperature limit (230°C) of the gas chromatograph. These products are collected in the condensers and analyzed at the end of each experiment. Selected liquid samples are subjected to elemental analysis and GC/MS studies.

The duration of an experiment is at least one hour and steady state is achieved in 3 to 4 minutes. Coal feed rates are usually about 500 g/hr. To facilitate uniform flow, 10% by wt Cab-O-Sil, a silica flour, is added to the coal. The non-reactive gases used were the inert gases, argon, helium and nitrogen. The reactive gases included hydrogen, methane and carbon monoxide. Yields are based on the percent of the carbon in the feed coal which is converted to products and determined as follows:

$$\% \text{ Carbon converted to product} = \frac{\text{Carbon in Product, g} \times 100}{\text{Carbon in Feed, g}}$$

A sum of the gaseous and liquid product yields, expressed as % carbon converted, will give the total carbon conversion due to pyrolysis. From feed rates, product yields, and an elemental analysis of the feed coal and char produced, a complete material balance can be made.

RESULTS AND DISCUSSION

Coal particles entering the reactor are heated to reaction temperature by convection from the preheated gas and by radiant heat from the reactor wall. In calculating the coal particle heat-up rate due to convection, a number of experimental configurations were considered for which heat transfer coefficients had been determined. These included heat and mass transfer from a falling water droplet (3), heat transfer to a fluidized-bed of particles (4), heat transfer to particles at Reynolds numbers greater than 500 (5), heat transfer in a distended bed of particles (6), and the theoretical heat transfer between a particle and a stagnant fluid. Since the Reynolds number for the coal particles falling through the gas in our work is very low, less than 10, neither the fluidized-bed nor the high Reynolds number work seemed appropriate. Also, the fluidized-bed work gave very low heat transfer coefficients, which were attributed to excessive bypassing of gas through the bed during the experiments (7). Since the work on distended beds showed good correlation of data from void fractions of 0.45 to 0.78, this appeared to provide the closest approach to our experimental conditions. The expression used is as follows (6):

$$Nu = 2.06\ N_{RE}^{0.425} N_{PR}^{1/3}$$

where Nu = Nusselt number $= \frac{h_g D_p}{K_g}$ (1)

N_{RE} = Reynolds number $= \frac{D_p V \rho_g}{\mu_g}$

N_{PR} = Prandtl number $= \frac{Cp_g \mu_g}{K_g}$

h_g = heat transfer coefficient for gas film,
D_p = diameter of particle,
K_g = thermal conductivity of gas,
V = velocity of particle through gas (free fall),
ρ_g = density of gas,
μ_g = viscosity of gas, and
Cp_g = heat capacity of gas.

By substitution

$$h_g = \left(\frac{2.06\ K_g}{D_p}\right)\left(\frac{D_p\ V\ \rho_g}{\mu_g}\right)^{0.425}\left(\frac{Cp_g\ \mu_g}{K_g}^{1/3}\right) \qquad (2)$$

and

$$M\ Cp_s \frac{dT_s}{dt} = h_g\ A_s\ (T_g - T_s), \qquad (3)$$

$$dT_s = \frac{h_g\ A_s}{M\ Cp_s}\ (T_g - T_s)\ dt,$$

$$t = \frac{M\ Cp_s}{h_g\ A_s}\ \ln\left(\frac{T_g - T_i}{T_g - T_s}\right), \qquad (4)$$

Where

Cp_s = heat capacity of coal
M = mass of coal particle
A_s = area of coal particle
T_g = temperature of gas
T_s = temperature of coal particle
T_i = initial temperature of coal particle
t = time to raise the particle temperature from T_i to T_s

Equation (2) was used to calculate the gas-film heat transfer coefficient between the coal particle and the preheated gases hydrogen, methane, carbon monoxide, helium, nitrogen, and argon. The values of gas-film heat transfer coefficient for various pyrolyzing gases under a set of arbitrarily chosen conditions are given in Table 2. Table 2 shows that for reactive gases, the heat transfer coefficient decreased in the following order: $H_2 > CH_4 > CO$; for non-reactive gases the order is found to be $He > N_2 > Ar$. Equation (4) was used to calculate the coal particle

temperature as a function of time and is plotted in Figure 3. Figure 3 shows that hydrogen gives the highest heat-up rate and argon the lowest; among the non-reactive gases, helium gives the highest rate. Although calculations of the final temperature of the coal particle were made, these should be considered as limiting values because chemical energy exchange and devolatilization also take place.

Calculations of the radiant heat transfer from the hot reactor wall to the coal particles indicate this contribution to be about 5 to 10% of the total heat transfer. Since these calculations are probably not accurate to better than ±10%, radiant heat transfer was not included in the coal particle heating rate or the temperature estimates.

When pyrolysis took place in the presence of non-reactive gases, the total carbon conversion followed the order: He>N_2>Ar. For example, at 900°C and 200 psi pressure of He, N_2 and Ar, the total carbon conversions were: 21.0%, 20.1% and 14.5%, respectively (Table 3). This includes the yields due to hydrocarbon gases, oxides of carbon, BTX and heavy liquids. In runs using N_2 or Ar as the pyrolyzing gas, difficulties were experienced in measuring the CO produced which arose as a result of inadequate resolution of this component from the solvent peak (N_2 or Ar). Hence, the CO yields from helium pyrolysis runs under identical conditions were used to determine the total carbon conversion in these cases. This could introduce some error in the total carbon conversion data for N_2 and Ar pyrolysis runs. In the case of reactive gases, the total carbon conversions were 37.6%, 30.4% and 17.5% respectively for H_2, CH_4 and CO atmospheres. There is a significant increase in total conversion in hydrogen and methane atmospheres over other inert gases. Though CO is a reactive gas, no enhancement in pyrolysis yields were noticed under the conditions investigated. The decrease in the gas film heat transfer coefficient for reactive and non-reactive gases and the total conversion both follow the same trend within each category. Thus, there appears to be a relationship between the heat transfer coefficient (or the heat-up rate of the coal particles) and total carbon conversion (Figure 4).

The effect of gas pressure on total carbon conversion was also investigated (Figure 5). As expected, hydrogen gave the highest carbon conversion. However, increasing the hydrogen pressure from 100 psi to 500 psi had little influence on the total conversion. The effect of pressure on total conversion was marked for all other gases. The maximum in the total carbon conversion and the pressure at which it occurs clearly seem to be dependent on the pyrolysis temperature. These differences indicate that a strong relationship exists between coal devolatilization and the transport properties of the pyrolyzing gases. More experiments are planned to understand these effects on coal pyrolysis in greater detail.

The flash pyrolysis of coal produces a wide range of gaseous and liquid products. The gas stream is mostly made up of methane, ethane, ethylene, CO and CO_2 besides the entraining gas. A typical pyrolysis product distribution is shown in Figure 6. Similar product distributions were obtained for other pyrolysis atmospheres and other conditons (8). Among these pyrolysis products, ethylene showed greatest variation in its yield. This is shown in Figure 7. Under all conditions, ethylene was produced in characteristically higher quantities in methane atmosphere (which we term "flash methanolysis") than in the presence of any other gas used. As high as 10.5% carbon in the feed coal was converted to ethylene at 825°C and 50 psi CH_4 pressure. This is approximately two times higher than that with the inert gases under similar conditions (10.5% with methane and 4.9% with helium). From several blank experiments, in the absence of coal, it was determined that homogeneous decomposition of methane does not occur in the reactor (8). A free-radical mechanism for the enhanced yield of ethylene during flash methanolysis of Douglas Fir wood, in the same pyrolysis reactor, was recently proposed (9). Figure 7 also reveals that in all cases, the ethylene yield decreased with gas pressure.

As expected, high yields of gaseous hydrocarbons were obtained when pyrolysis took place in hydrogen atmosphere. The total gaseous hydrocarbon yield ranged from 8.9% C at 800°C and 50 psi to 28.0% C at 900°C and 500 psi. The yields of both ethane and ethylene dcecreased with

increase in the pressure of hydrogen. In non-reactive gas media, no ethane was produced in measurable quantities in most instances. Among non-reactive gases, the yield structure was comparable between helium and nitrogen atmospheres and a representative case is shown in Table 3 in which the product yields from the pyrolysis of New Mexico coal in various gasifying media, under identical conditions, are compared. From the same table, it could be seen that in argon atmosphere, the yield of gaseous hydrocarbons and other products are considerably low.

The yield of CO_2 was about 1-2% C under all conditions in the presence of all gases with the exception of CO. Higher yields of CO_2 were obtained (7-9% C) when the pyrolyzing gas was CO. This is believed to be due to disproportionation of CO under the reaction conditions.

The liquid products (excluding process water) consist of two fractions: the "light oil" fraction, boiling between 60° and $150^{o}C$, and the "heavy liquid" fraction, boiling above $150^{o}C$. This classification is arbitrary, and various distillation ranges are used by different workers. In the BNL work, usually more than 90% by weight of the "light oil" is made up of benzene, toluene, and xylene, and the "heavy liquids" or "tars" contain condensed ring aromatic structures and high molecular weight compounds with high aromaticity (10).

"Light Oil" from coal is a potential source of some key chemicals such as benezene-toluene-xylene (BTX). Even though the exact mechanism of their production is not known, it is generally thought to consist largely of secondary pyrolytic reactions. Prolonged heating of the primary devolatilization products induces cracking and if hydrogen is available, stable lighter products are formed. Thus, the yield of light oil depends on the residence time of the tar vapor in the pyrolysis reactor and on the temperature. With longer residence times, more light oil is formed at the expense of the heavy liquids (tar). Too high a temperature ($>900^{o}C$) results in an increased yield of gases at the expense of both light oil and tar.

BTX yield ranged 1-3% C in the case of CO and non-reactive gases; up to 7% carbon in the feed was converted to BTX during flash hydropyrolysis and flash methanolysis experiments. The IR spectra of light oils, free from process water, obtained from a series of flash hydropyrolysis experiments with New Mexico sub-bituminous coal show (i) strong absorption in the low frequency range between 900 and 675 cm^{-1}, typical of aromatic ring C-H out-of-plane bending, (ii) strong absorption in the medium frequency range between 1600 and 1580 cm^{-1} due to C=C stretching, and (iii) moderate absorption between 3100 and 3000 cm^{-1} characteristic of the aromatic C-H stretch. Weak absorptions at 2926, and 2853 cm^{-1} ($\sigma_{C-H}CH_3$, ν_{as} CH_2, and ν_s CH_2, respectively) indicate that the extent of alkyl substitution is small.

Phenols, if any, were present only in very small amounts in the light oils produced from the flash pyrolysis of New Mexico sub-bituminous coal. The IR spectra of light oils produced at 900°C at 20, 60, and 200 psi showed absorption due to -OH groups to be present only in the 20 psi sample, and this spectrum was similar to the one obtained at 800°C and 200 psi. An increase in the hydrogen pressure or residence time of the volatiles tends to decrease the amount of phenols in the product stream, and temperatures above 900°C and hydrogen pressures above 50 psi favor the dehydroxylation/decompostion reactions of phenols. The light oil from the inert helium pyrolysis at 900°C and 50 psi had a composition qualitatively similar to that from flash hydropyrolysis under the same conditions, but for different reasons: In the presence of external hydrogen, the phenols initially formed undergo decomposition, but during inert gas pyrolysis the conditions are not favorable for initial phenol formation.

Heavy liquid or tar is an inherent product of coal devolatilization. Its composition is much more complex than that of light oils. Tar accounts for only a small amount of the carbon in the feed coal that is converted (0-5% C). Tars from selected runs were subjected to detailed investigation, but the data available at present are limited.

A basic problem in identifying the individual components in a tar is that compounds of widely varying polarities are present, precluding GC/MS analysis of the tar as such. By fractionating the tars on the basis of solubility in selected solvents and analyzing the fractions for individual compounds, valuable information could be obtained.

In one scheme of solvent fractionation, the tar is separated into oil (hexane soluble), asphaltenes (hexane insoluble but benzene soluble), and pre-asphaltenes (benzene insoluble). The yields of total tar and tar fractions from selected pyrolysis runs are shown in Table 4. The pre-asphaltenes, which include compounds of high polarity, comprise only a very small part of the tar. Except when the pyrolysis gas is methane, an increase in tar yield is accompanied by an increase in oil yield. The tar yield from flash methanolyis is between those from helium pyrolysis and from hydropyrolysis. In the case of helium pyrolysis, the tar yield tends to increase with increasing pressure.

The individual components in an oil sample from the flash hydropyrolysis of New Mexico sub-bituminous coal at 1000°C and 25 psi hydrogen pressure were identified with capillary GC/MS which is shown in Figure 8. The peaks are identified in Table 5. Naphthalene is the most abundant product in this tar; higher-ring aromatic compounds and heteroatom containing specie account for less than 10% of the total. No sulfur containing compounds were detected. The reason for the presence of relatively large amount of acenaphthylene in this tar is not known at present.

CONCLUSIONS

The conclusions which can be drawn from this work thus far are as follows:

1. Under the same conditions, the total carbon conversion was higher in the presence of reactive gases than in the presence of non-reactive gases. Among the reactive gases, the total carbon conversion followed the order: $H_2 > CH_4 > CO$. Among the non-reactive gases, the total carbon conversion followed the order: $He > N_2 > Ar$.

2. Pyrolysis in methane was characterized by high yields of ethylene and liquid products. As high as 10.5% carbon in the feed coal was converted to ethylene at 825°C and 50 psi. The ethylene yield during pyrolysis of coal with methane was approximately two times higher than that with the inert gases under similar conditions (10.5% CH_4 vs 4.9% with He at 825° to 850°C and 50 psi).

3. Phenols, if any, were present only in very small amounts in the light oil fraction of the liquid products. In the presence of external hydrogen, the phenols formed undergo decomposition, but during the inert gas pyrolysis the conditions are not favorable for initial phenol formation. An increase in the hydrogen pressure or residence time of the volatiles tends to reduce the amount of phenols in the product stream, and temperatures above 900°C and hydrogen pressures above 50 psi favor the dehydroxylation/decomposition reactions of phenols.

4. In the case of helium pyrolysis, the tar yield tends to increase with increasing pressure. The tar yield from methane pyrolysis is between those from helium pyrolysis and from hydropyrolysis.

5. The pre-asphaltenes, which include compounds of high polarity, comprise only a very small part of the tar. Except when the pyrolysis gas is methane, an increase in tar yield is accompanied by an increase in oil yield.

6. A correlation appears to exist between the total carbon conversion to gaseous and liquid products and the heat-up rate of coal particles for inert gases in the order of He > N_2 > Ar. Uncovering other effects of heat-up rate of coal particles on the pyrolytic behavior of coals require further investigation.

ACKNOWLEDGEMENT

This research was supported by the U.S. Department of Energy under Contract No. AC02-76CH00016. We would like to thank Dr. Clarence Karr, Jr., of the Morgantown Energy Technology Center, Morgantown, West Virginia, for his continued interest in this project.

REFERENCES

1. J. B. Howard, Fundamentals of Coal Pyrolysis and Hydropyrolysis, Chapter No. 12 in Chemistry of Coal Utilization, Ed. Elliot, M.A., John Wiley and Sons, New York, NY, p. 665-784 (1981).

2. P. Fallon and M. Steinberg, Flash Hydropyrolysis of Coal, The Design, Construction, Operation and Initial Results of a Flash Hydropyrolysis Experimental Unit, BNL 50698, Jan. 1977.

3. R.B. Bird, W.E. Steward, and E.N. Lightfoot, Transport Phenomena, Wiley, New York, 1960.

4. W.W. Wamsley and L.N. Johanson, Chem. Eng. Prog. 50, 347 (1954).

5. H.F. Johnstone, R.L. Pigford, and J.H. Chapin, Trans. AIChE 37, 95 (1941).

6. A. Sen Gupta and G. Thodos, AIChE J. 9, 751 (1963).

7. F. A. Zenz, and D. F. Othmer, "Heat Transfer in Particle-Fluid System", Chapter No. 13 in Fluidization and Fluid-Particle Systems, Reinhold Pub. Co., New York, NY, p. 421 (1960).

8. M. Steinberg, P. Fallon, and M. S. Sundaram, "Flash Pyrolysis of Coal with Reactive and Non-reactive Gases", Progress Report for October 1, 1981-Septemebr 30, 1982, To be published by Departemnt of Energy, Morgantown Energy Technology Center, Morgantown, W. Va.

9. M. S. Sundaram, Steinberg, M., and Fallon, P.T., "Flash Pyrolysis of Biomass with Reactive and Non-Reactive Gases", presented at International Conference on Fundamentals of Thermochemical Biomass Conversion, Estes Park, CO, BNL 32280 (October 1982).

10. M. S. Sundaram, M. Steinberg, and P. Fallon, "Flash Hydropyrolysis of Coals for Conversion to Liquid and Gaseous Fuels", BNL 51537, DOE/METC/82-48, (1982).

Table 1

Ultimate Analysis (Wt % Dry) of New Mexico Sub-Bituminous Coal Used in Pyrolysis Experiments

Carbon	59.3
Hydrogen	4.2
Oxygen[a]	16.8
Nitrogen	1.2
Sulfur	0.8
Ash	17.7

[a]) By difference.

Table 2

Calculation of Gas Film Heat Transfer Coefficients for Various Pyrolyzing Gases

Coal Particle Size - 100 micrometers
Coal Particle Initial Temp. - 20°C
Gas Conditions - 900°C and 1000 psi

Gas	h_g (Cal/cm^2-K°-sec)
Hydrogen	2.21×10^{-1}
Methane	2.02×10^{-1}
Helium	1.73×10^{-1}
Carbon Dioxide	9.9×10^{-2}
Carbon Monoxide	7.7×10^{-2}
Nitrogen	7.16×10^{-2}
Argon	4.96×10^{-2}

Table 3

Product Yields from the Flash Pyrolysis of
New Mexico Sub-bituminous Coal
at 900°C and 200 psi
Coal Residence Time: 2.4-4.6 sec.

Entraining Gas	He	N_2	Ar
% Carbon Conv. to Prod.			
CH_4	8.1	10.2	2.6
C_2H_4	3.5	0	3.3
C_2H_6	0	0.7	0
Total Gaseous H.C.	11.6	10.9	5.9
BTX	1.8	2.7	2.0
$>C_9$	1.2	0.4	0.8
Total Liquid H.C.	3.0	3.1	2.8
CO	4.4	(4.4)	(4.4)
CO_2	2.0	1.7	1.4
Total CO_x	6.4	6.1	5.8
Total Carbon Converted	21.0	20.1	14.5

( )CO could not be resolved from N_2 or Ar on the on-line GC. The values in paranthesis are CO yields from inert helium pyrolysis runs under identical conditions. This could introduce some error in the determination of the total carbon conversion.

Table 4

Composition of Heavy Liquids from
Flash Pyrolysis of New Mexico Sub-Bituminous Coals

Conditions												
Temperature (°C):	1000	1000	1000	800	1000	1000	900	900	900	900	900	900
Entraining gas:	He	He	He	H_2	H_2	H_2	CH_4	CH_4	CH_4	Ar	Ar	Ar
Pressure (psi):	20	100	1000	50	25	200	100	200	500	100	200	500
Product (%C Carbon Converted)												
Pre-asphaltene	0.29	0.10	0.47	0.20	0.05	0.04	0.03	0.06	0.0	0.02	0.03	0.04
Asphaltene	0.09	0.16	0.10	2.72	1.02	0.93	2.08	1.56	0.54	0.16	0.16	0.15
Oil	0.20	0.43	1.30	1.30	4.41	3.53	0.80	1.35	1.67	0.88	0.65	0.38
Total tar	0.58	0.69	1.87	4.82	5.48	4.50	2.91	2.97	2.25	1.06	0.84	0.57

Table 5

Composition of Heavy Liquids from the Flash Hydropyrolysis of New Mexico Coal

Peak No.	Component	% Peak Area
1	xylene	0.54
2	xylene	0.27
3	phenol	3.07
4	indene	6.45
5	naphthalene	60.80
6	quinoline	1.15
7	isoquinoline	0.29
8	C_1-naphthalene	1.25
9	C_1-naphthalene	0.32
10	biphenyl	0.03
11	acenaphthylene	14.98
12	acenaphthene	1.66
13	C_1-biphenyl/acenaphthene	1.79
14	fluorene	2.64
15	phenanthrane/anthracene	3.82

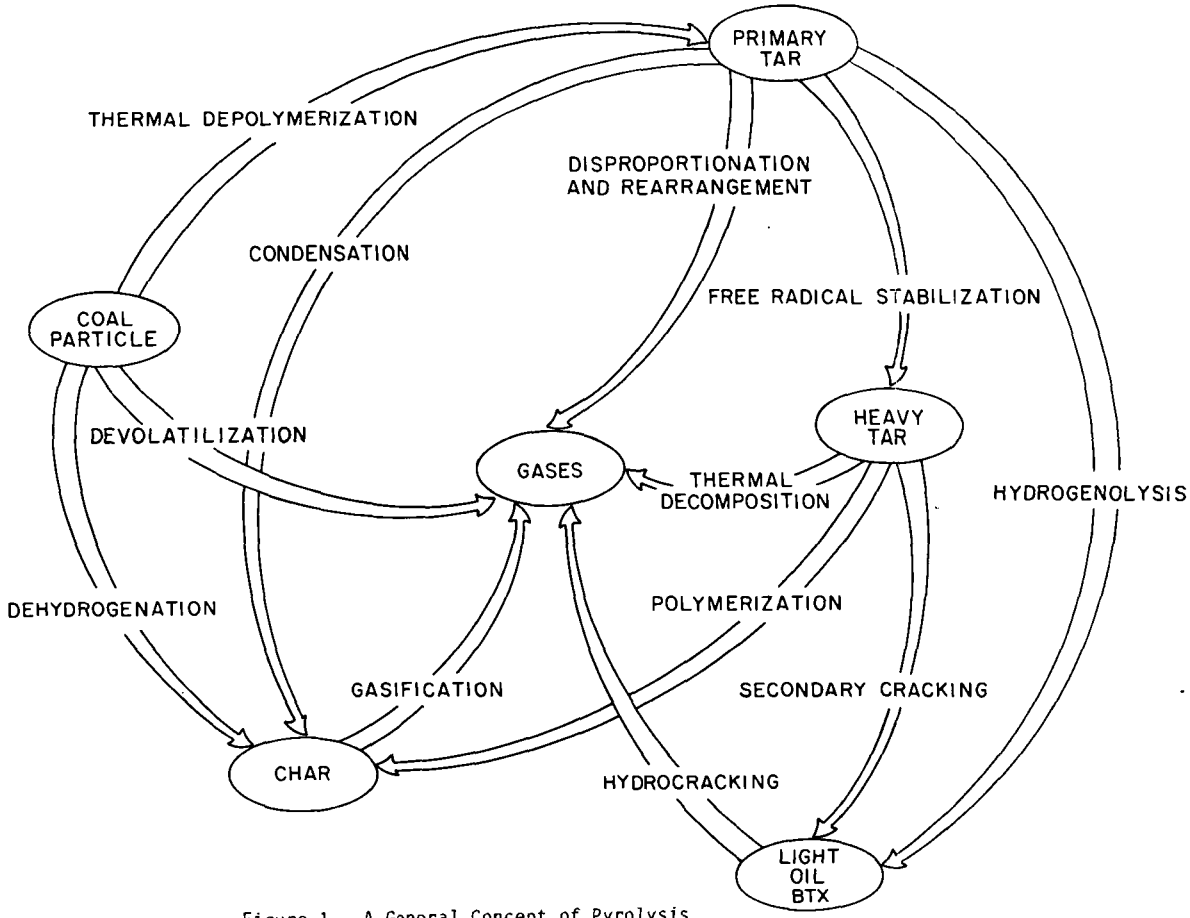

Figure 1. A General Concept of Pyrolysis

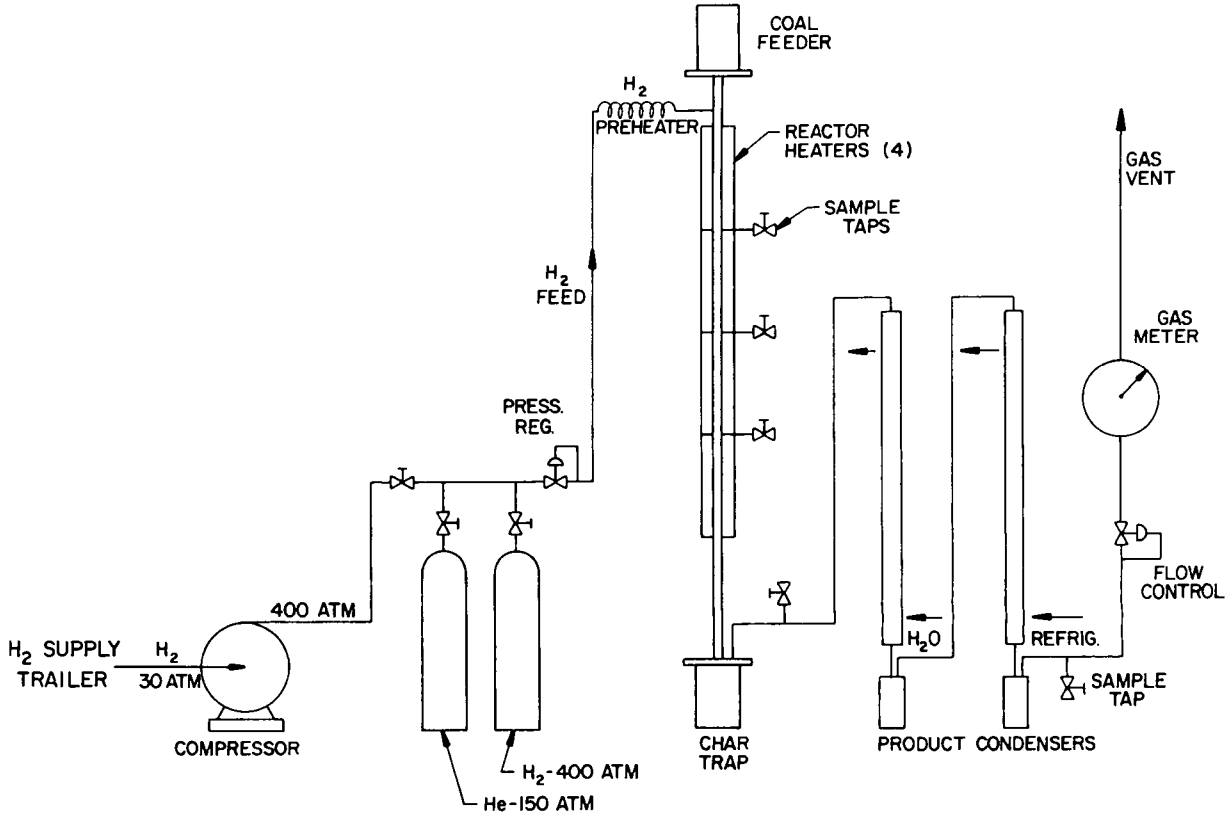

Figure 2. SCHEMATIC FLOWSHEET OF ENTRAINED TUBULAR REACTOR EXPERIMENT

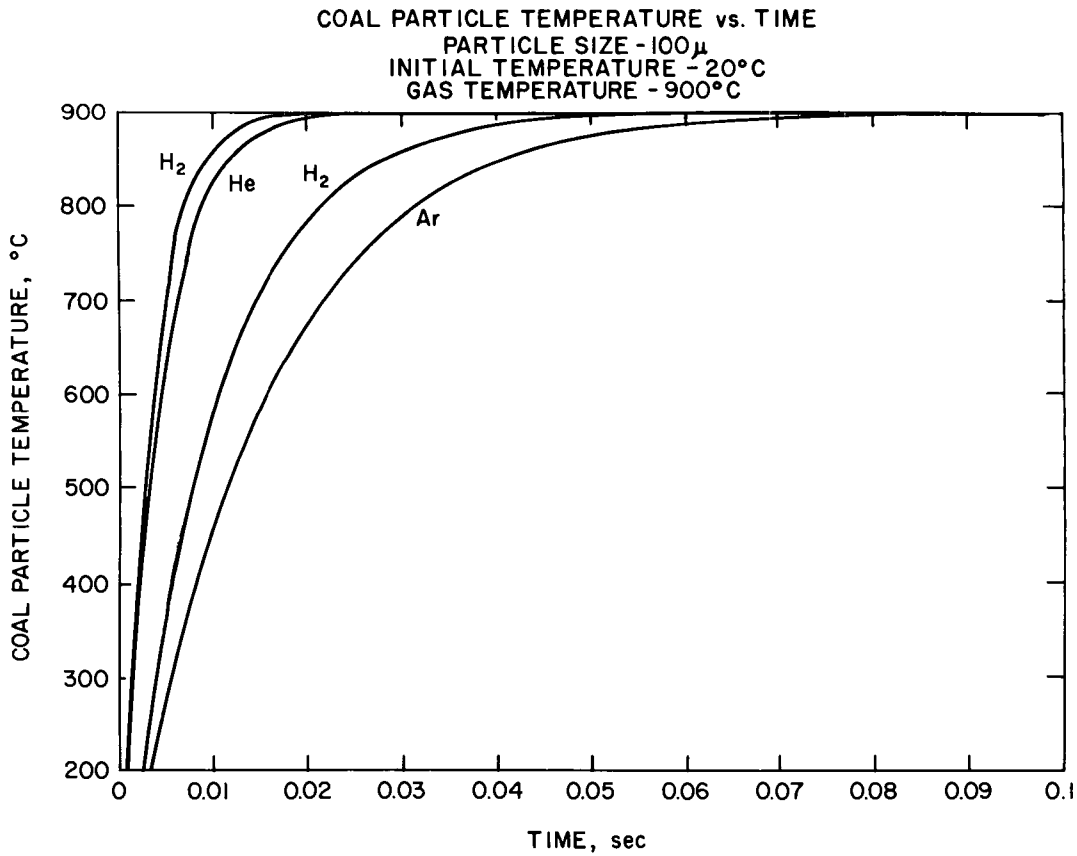

Figure 3. Coal Particle Temperature vs Time

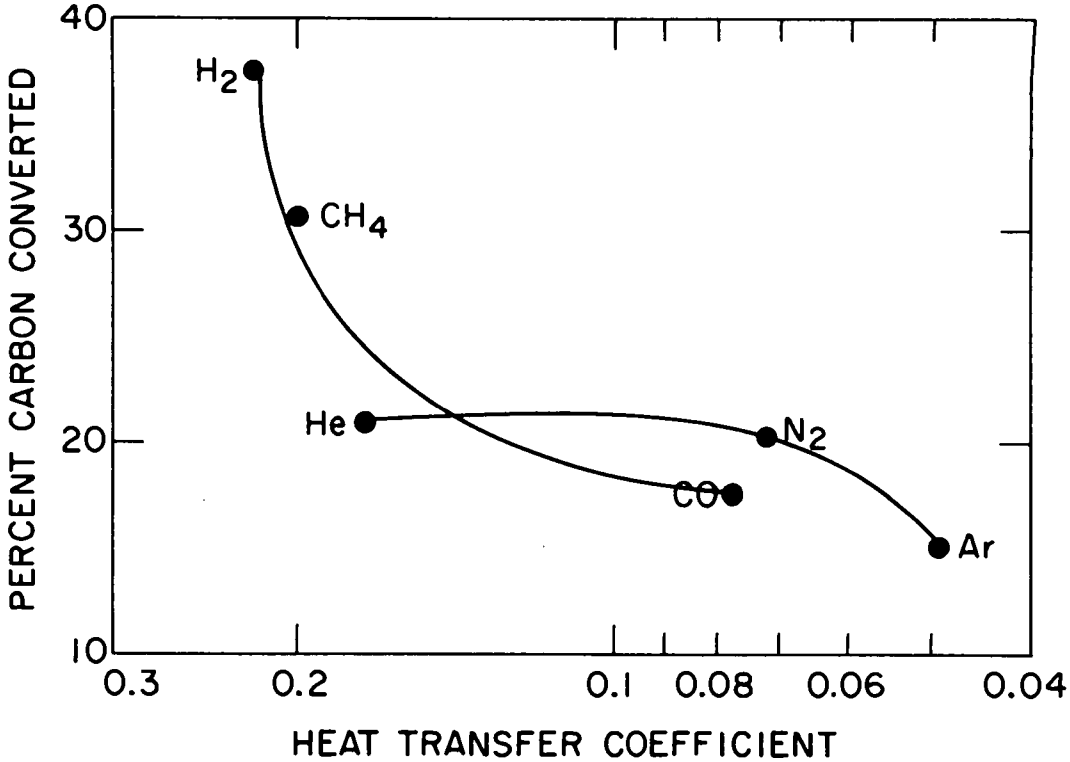

Figure 4. Percent Carbon Conversion at 900°C and 200 psi vs Heat Transfer Coefficient

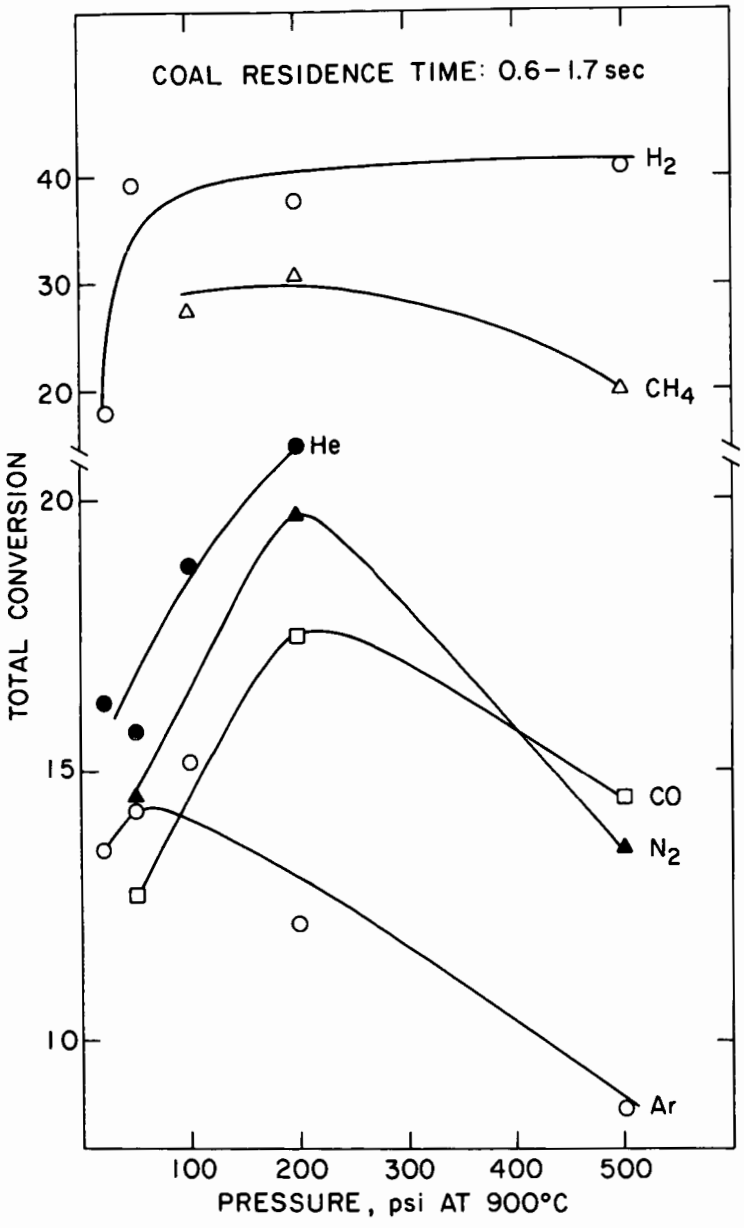

Figure 5. Total Conversion vs Pressure, at 900°C

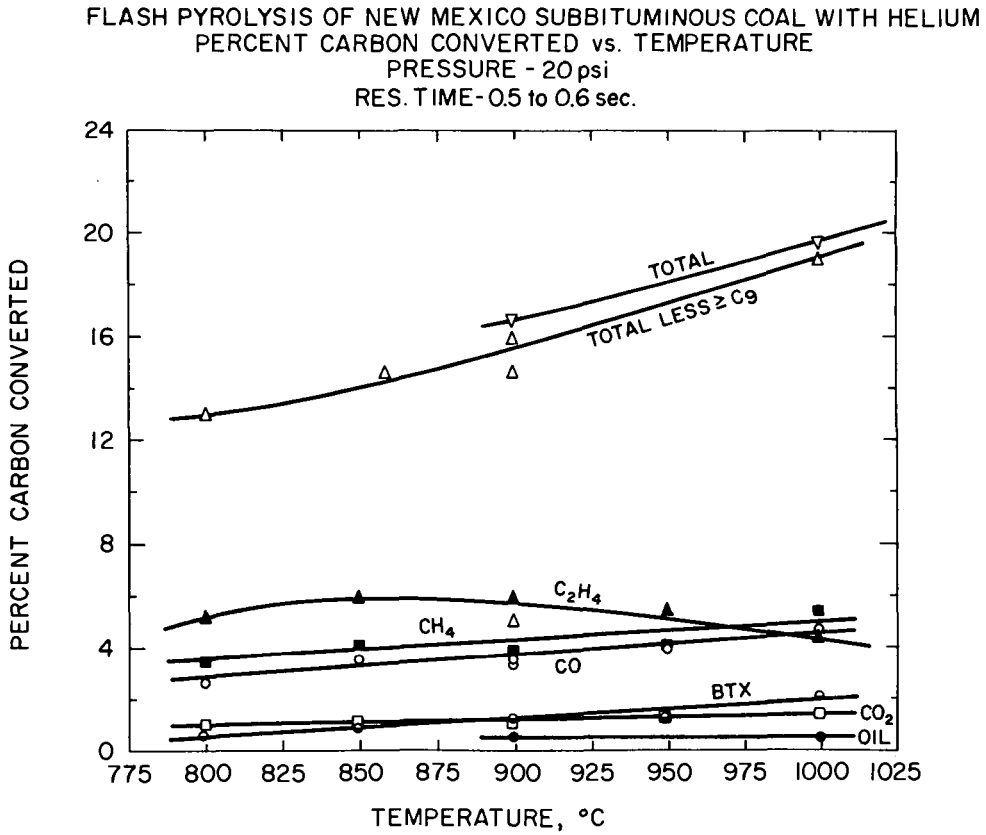

Figure 6. Product Yields vs Temperature at 20 psi He

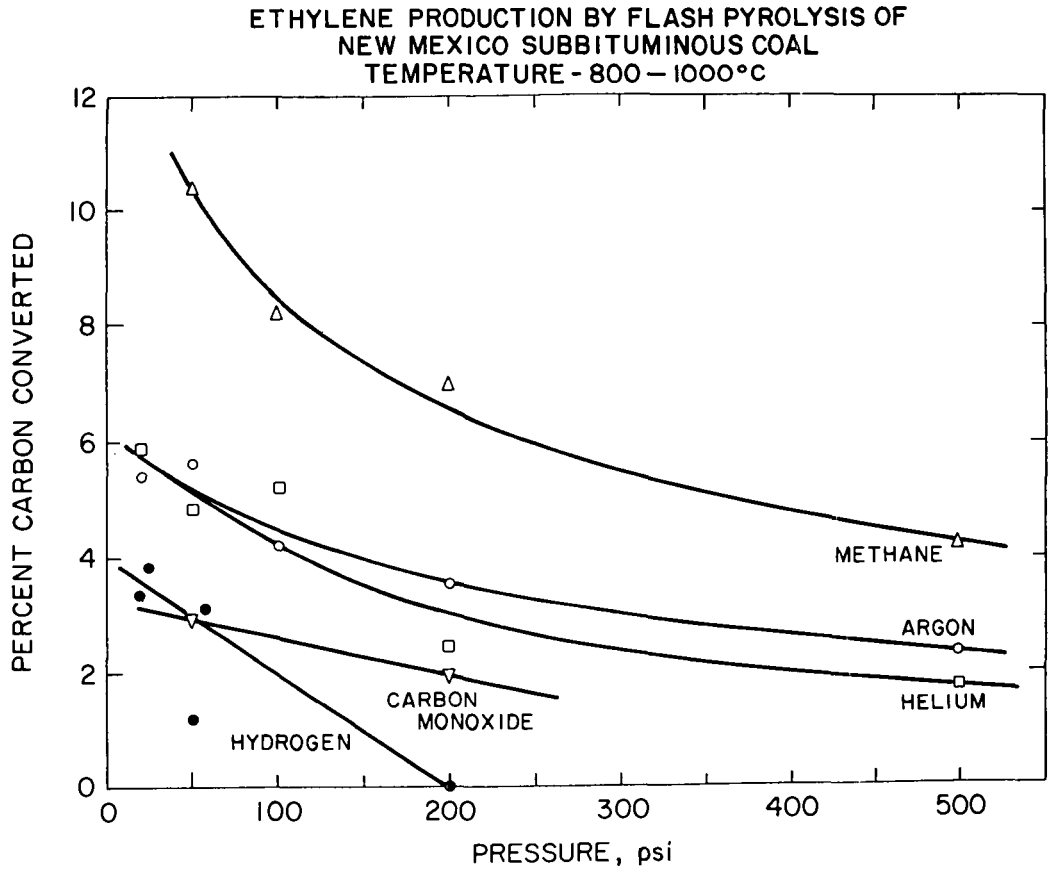

Figure 7. Ethylene Yield vs Pressure at 800° to 1000°C

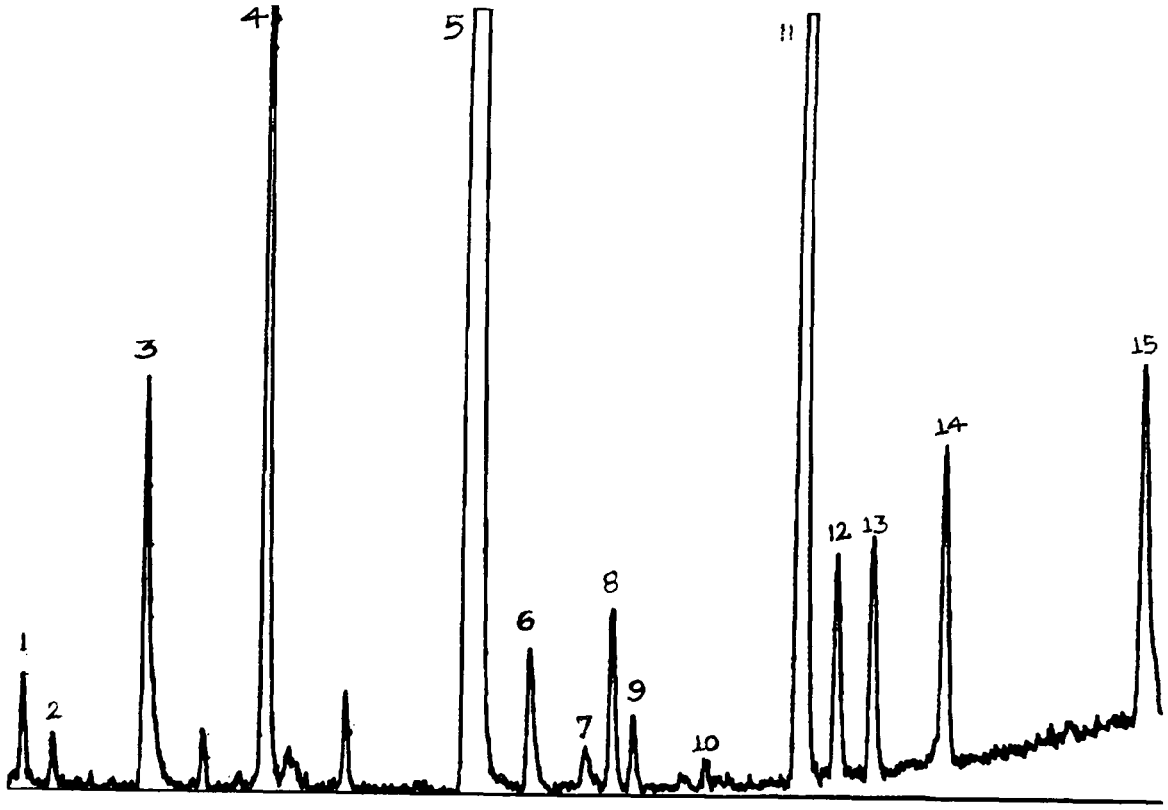

Figure 8. GC/MS Total Ion Chromatogram of a Pyrolysis Oil

CHARACTERIZATION OF COAL CHARS FROM A FLASH PYROLYSIS PROCESS BY CROSS POLARIZATION / MAGIC ANGLE SPINNING ^{13}C NMR

Mei-In M. Chou and Donald R. Dickerson
Illinois State Geological Survey
615 East Peabody Drive
Champaign, IL 61820

Dale R. Mckay and James S. Frye
Department of Chemistry
Colorado State University
Fort Collins, CO 80523

INTRODUCTION

In the last two decades, flash pyrolysis has been used to investigate the structure of coal and shale (1-4). Several coal conversion processes based on flash pyrolysis are under investigation in the United States (5-8), West Germany (9), and Australia (10,11,12). Studies of the molecular properties of the flash pyrolysis products have been confined to the liberated organic matter: volatile liquids and gases. Changes occurring in the organic structure of the chars are poorly understood.

The development of ^{13}C cross polarization (CP) (13) and Magic Angle Spinning (MAS) (14) Nuclear Magnetic Resonance (NMR) spectroscopy with high-power proton decoupling has allowed investigators to obtain spectra of the organic matter in solid coal (15-25). Sullivan and Maciel (26) and Dudley and Fyfe (27) have verified the quantitative reliability of this technique as applied to coal. ^{13}C NMR spectra of coal demonstrating the utility of both CP and MAS have been reported previously (15,16,18,21,22), however, there has been no reported investigation of ^{13}C CP/MAS NMR spectra of the chars produced by flash pyrolysis.

This paper reports the results of this technique applied to the study of chars produced by the flash pyrolysis of coal at progressively higher temperatures. The investigation has given valuable insight into the changes of organic composition of coal during carbonization as well as the optimum temperature for efficient conversion of coal into liquids and gases.

EXPERIMENTAL

A high-volatile C bituminous (HVCB) Illinois Harrisburg (No. 5) coal was used. The analyses of the raw coal sample are given in Table 1. The coal was flash pyrolyzed in a quartz tube under a flow of helium. The tube was heated at a ramp-rate of 75°C/msec to the desired final temperature with a 20 sec hold at the final temperature. Since only small quantities of coal were used for each run, a sample of sufficient size for NMR analysis and elemental analysis at each temperature was prepared by combining the products of replicate preparations.

Chars produced at 300°, 400°, 500°, 600°, 700°, and 800°C were studied. The ^{13}C CP/MAS NMR measurements of the chars were made on a JEOL FX60Q NMR spectrometer modified for CP and MAS. The spectra were recorded under standard conditions that have been described previously (26).

For the volatile analysis, the same sample of coal was heated in steps; first to 300°C, then successively to 400°C, 500°C, 600°C, 700°C, and to 800°C. The volatile matter was entrained in a helium flow of 35 mL/min and was analyzed by gas chromatography (GC) using a 2.5m x 3 mm stainless steel column packed with 3%

Table 1. Proximate and ultimate composition of the Illinois No. 5 (HVCB) coal sample. (moisture-free basis).

Proximate analysis	%	Ultimate analysis	%
Volatile matter	43.3	Hydrogen	4.72
Fixed carbon	44.3	Carbon	65.45
Ash	12.4	Nitrogen	1.13
		Oxygen (by diff.)	11.52
		Sulfur	3.91
		Low Temp. Ash	13.27

Dexsil 300 on 80/100 Chromosorb WHP connected to a flame ionization detector (FID). The column temperature was programmed from 50°C to 250°C at 8°C/min and held at the final temperature for 15 min.

RESULTS AND DISCUSSION

The GC traces of volatile products evolved at each charring temperature are shown in Figure 1. The evolution of decomposition products, gases and liquids, starts at 500°C, maximizes at 600°C, and completes at 700°C. At 800°C the main volatiles evolved are hydrogen and light hydrocarbon gases. The hydrogen to carbon atom ratios (H/C) of the coal and chars at each temperature are given in Table 2. There is little change in the H/C ratios at temperatures below 500°C. Above 500°C, the H/C ratios decrease as the temperature is increased. The data show a change in H/C value from 0.82 (highly benzenoid) at 500°C to 0.36 (highly graphitic) at 800°C. Based on similar results, polycondensation of the aromatic ring system occuring at the same time as dehydrogenation of the hydroaromatic and alicyclic systems has been suggested as a model for carbonization by early coal workers (28). However, ^{13}C CP/MAS NMR results give an insight into the changes of the organic matter of chars.

Table 2. The atomic ratio of hydrogen to carbon (H/C) for coal and chars at each temperature step.

Temperature (°C)	Raw coal	300	400	500	600	700	800
H/C	0.87	0.87	0.85	0.82	0.57	0.54	0.36

^{13}C CP/MAS NMR spectra of the raw coal and the six chars are illustrated in Figure 2. In general, the spectra exhibit two broad characteristic peaks. The chemical shifts are referenced to tetramethylsilane (TMS) with hexamethylbenzene (HMB) used as a secondary external standard. The chemical shift of the aromatic peak of HMB is taken to be 132.3 ppm relative to TMS. The peak at 129 ppm is assigned to sp^2 (mainly aromatic) carbon and the peak at 30 ppm is assigned to sp^3 (saturated) carbon.

The ^{13}C CP/MAS NMR spectra show (fig. 2) that the aliphatic carbon peak is progressively decreasing as the temperature is increased; while the aromatic carbon peak retains approximately the same height and shape. The peaks at 298 ppm and -37 ppm are spinning side bands (SSB). For a given temperature the NMR spectra provide a measure of the relative carbon distribution of the organic material remaining in the char. The relative percentages of aromatic (f_{ar}) and of aliphatic (f_{al}) carbons are calculated by dividing the integrated area of each individual carbon peak by the sum of the areas of the peaks. The f_{al} values of chars are shown in Figure 2. The f_{ar} of the raw coal is 67%. The initial stage

of heating (300°C) produces a char with 68% of f_{ar}, and successive heatings give chars with f_{ar} of 70% (400°C), 73% (500°C), 89% (600°C), 95% (700°C), and 96% (800°C). However, the actual amount of aromatic (w_{ar}) and aliphatic (w_{al}) carbon in char can be calculated by using the NMR measurements (f_{ar}; f_{al}), the organic carbon content of the char ($\%C_{org}$), and the weight of the char (w_{char}).

$$w_{ar} = \%C_{org} \times f_{ar} \times w_{char}; \; w_{al} = \%C_{org} \times f_{al} \times w_{char}$$

Figure 3 shows the calculated values and the weight of char based on 100 g of raw coal used in relation to temperature: the amount of aromatic carbon in char (w_{ar}) remains relatively constant at each temperature, while the amount of aliphatic carbon in char (w_{al}) is reduced during higher temperature charring. At 600°C, both a large reduction of the aliphatic-carbon content and a maximum weight loss occur.

This study shows that the aliphatic part of the organic matter in coal is substantially lost during pyrolysis at temperature greater than 500°C. Although, the loss of aliphatic-bound carbon from coal may involve several mechanisms, it may have been volatilized directly or it may have been converted to an aromatic form from which it could volatilize or could become fixed as part of the char. The maximum temperature for efficient evolution of volatiles from coal by heat is at 600°C to 700°C. Also, the amount of carbonaceous residue at 800°C can be estimated from the aromatic-bound carbon of raw coal. The usefulness of the ^{13}C CP/MAS NMR technique as a tool for coal process research is clearly demonstrated.

ACKNOWLEDGMENTS

Support of this work was provided by the US Environmental Protection Agency under Contract No. 68-02-2130 and the Colorado State University Regional NMR Center, funded by National Science Foundation Grant No. CHE 78-I858I. The authors gratefully acknowledge discussions with Dr. G. E. Maciel.

REFERENCES

1. Retcofsky, H. L., Schweighardt, F. K. and Hough, M., Anal. Chem. 49, 585 (1977).

2. Bartle, K. D., Rev. Pure Appl. Chem. 22, 79 (1972).

3. Van Grass, G., de Leeuw, J. W., and Schenck, P. A., in Advances in Organic Geochemistry 1979, 3d. A. F. Douglas and J. R. Maxwell, Pergamon, Oxford, pp 485-494.

4. Romovácek, Jirí and Jarolslav Kubát, Anal. Chem. 40, 1119-27 (1968).

5. Strom, A. H. and Eddinger, R. I., Chem. Eng. Prog. 67, 75 (1971).

6. Sass, A., Chem. Eng. Prog. 70, 72 (1974).

7. Sunberg, E. M., Peters, W. A., and Howard, J. B., Fuel 59, 405 (1980).

8. Che, S. C., Duraiswamy, K., Knell, E. W., and Lee, C. K., "Flash pyrolysis coal liquefaction process development," Occidental Research Corporation Final Report to the U.S. Department of Energy, Fe-2244-26, April 1979.

9. Peters, W., Gluckauf, 112, 8 (1976).

10. Collin, P. J., Tyler, R. J., and Wilson, M. A., Fuel 59, 479 (1980).

11. Tyler, R. J., Fuel 59, 219 (1980).

12. Collin, P. J., Tyler, R. J., and Wilson, M. A., Fuel 59, 819 (1980).

13. Pines, A., Gibby, M. G., and Waush, J. S., J. Chem. Phys. 59, 569 (1973).

14. Shaefer, J. and Stejskal, E. O., J. Am. Chem. Soc. 98, 1031 (1976).

15. Maciel, G. E., Bartuska, V. J., and Miknis, F. P., Fuel 58, 319 (1979).

16. Miknis, F. P., Sullivan, M., Bartuska, V. J., and Maciel, G. E., Organic Geochemistry, 3, 19 (1981).

17. Maciel, G. E., Sullivan, M. J., Szevereny, N. M., and Miknis, F. P., "Chemistry and physics of coal utilization-1980", Cooper, B. R., Petrakis, L., Eds., American Institute of Physics: New York, 66-81 (1981).

18. Zilm, K. W., Pugmire, R. J., Grant, D. M., Wood, R. E., and Wiser, W. H., Fuel 58, 11 (1979).

19. Maciel, G. E., Sullivan, M. J., Petrakis, L., and Grandy, D. W., Fuel 61, 411 (1982).

20. Zilm, K. W., Pugmire, R. J., Larter, S. R., Allan, J., and Grant, D. M., Fuel 60, 717 (1981).

21. VanderHart, D. L., and Retcofsky, H. L., Fuel 55, 202 (1976).

22. Retcofsky, H. L., and VanderHart, D. L., Fuel 57, 421 (1978).

23. Gerstein, B. C., Ryan, L. M., and Murphy, P. D., Prepr Pap.-Am. Chem. Soc., Div. Fuel Chem. 24, 90 (1979).

24. Wemmer, D. E., Pines, A., and Whitehurst, D. D., Philos. Trans. R. Soc. London Ser. A 300, 15 (1981).

25. Barron, P. F., Stephens, J. F., and Wilson, M. A., Fuel 60, 547 (1981).

26. Sullivan, M. J. and Maciel, G. F., Anal. Chem. 54, 1615 (1982).

27. Dudley, R. L. and Fyfe, C. A., Fuel 61, 651 (1982).

28. Wang, Z. and Shou, J. K., Prepr. Pap.-Am. Chem. Soc., Div. Fuel Chem. 25, 171 (1980).

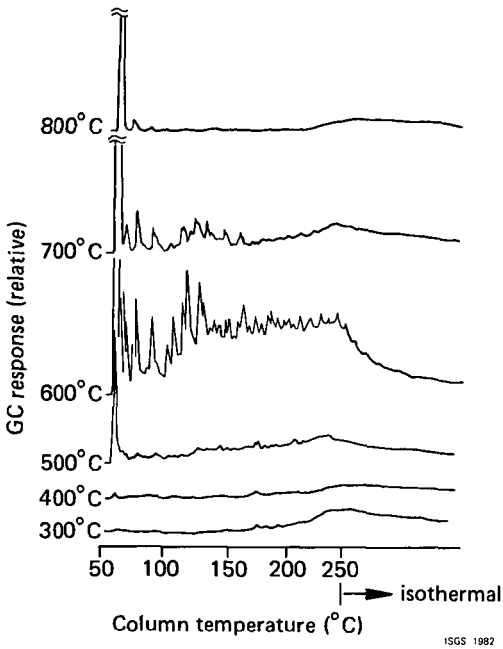

Fig. 1. The GC traces of volatile products produced at each charring temperature.

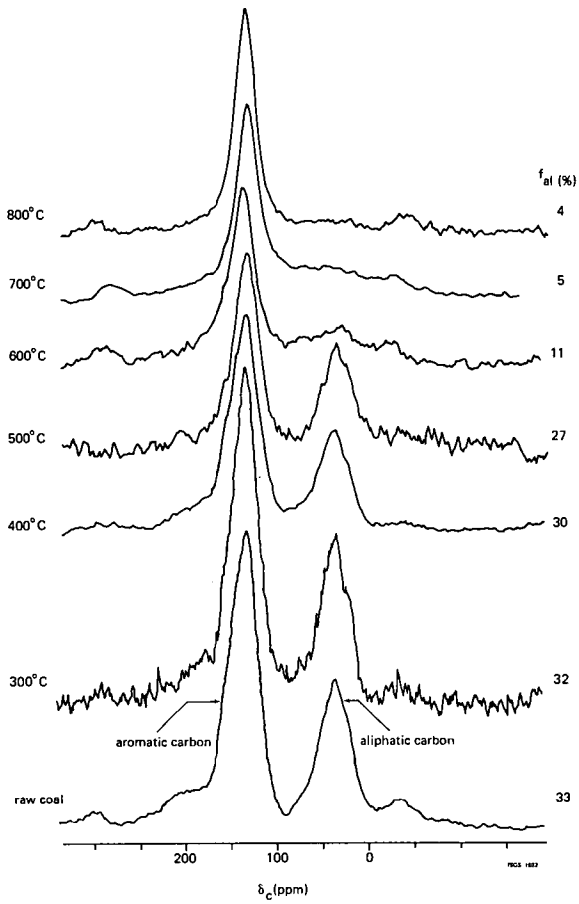

Fig. 2. ^{13}C CP/MAS NMR spectra of the raw coal and of the chars at the various charring temperatures.

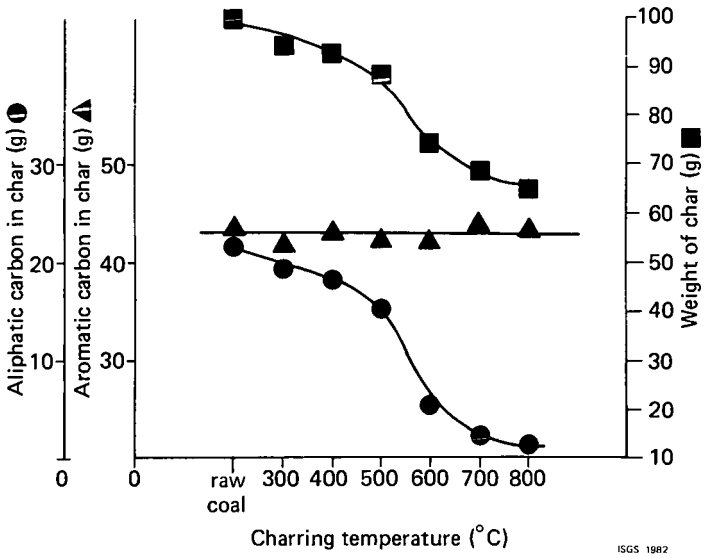

Fig. 3. The calculated amounts of aliphatic and aromatic carbon in char in relation to temperature and the weight of char based on 100 g of raw coal used.

DEPOSIT FORMATION IN HEAT EXCHANGER FROM COAL DERIVED NAPHTHA

L. G. Galya, D. C. Cronauer

Gulf Research & Development Company
P. O. Drawer 2038, Pittsburgh, PA 15230

P. C. Painter

Penn State University
University Park, PA 16057

and N. C. Li
Duquesne University
Pittsburgh, PA 15219

INTRODUCTION

Coal derived naphthas have been observed to produce deposits in hydrotreaters, heat exchangers, heaters, and reactor inlets which operate at approximately 400°C. These deposits are black in appearance and cause plugging of the reactor components. This results in a shutting down of the system. Such downtime is expensive due to both production losses and repair costs. If causes for deposit formation can be identified and a probable mechanism found, it should be possible to decrease or eliminate this expensive reactor downtime.

There are two main objectives for this study. 1) Determine what classes of compounds are responsible for deposit formation. This involves concentrating various classes of compounds by both distillation and chromatographic means and developing a way to indicate their potential for deposit formation. 2) Indicate a possible mechanism for deposit formation. This includes an examination of the deposit and the identification of secondary products of deposit formation.

EXAMINATION OF DEPOSIT

A deposit was formed in a pilot plant heat exchanger from a coal derived naphtha. The heat exchanger was run at approximately 400°C in an atmosphere consisting of vaporized naphtha and hydrogen. The formation of the deposit had resulted in shutting down the pilot plant. It was estimated that 10g of deposit was formed from 50 gallons of full range (66-204°C) naphtha. Therefore, only 0.006% of the original material was involved in deposit formation.

The deposit was drilled out of the plugged heat exchanger. It was insoluble in pentane, dichloromethane, chloroform, methanol, dimethyl sulfoxide, and pyridine. The elemental analysis of the deposit is given in Table 1, along with that of a typical naphtha feed. These analyses were performed by Micro-Analysis of Wilmington, Delaware.

The N/C ratio in the deposit relative to the feed increased by a factor of 15.0 while that of S/C and O/C increased by 9.9 and 1.8, respectively. Therefore, the nitrogen and sulfur compounds were heavily involved in deposit formation. The S/N ratio of the deposit was 0.11.

This indicates that the deposit was not comprised predominantly of ammonium polysulfides. These polysulfides have been observed as deposit materials in hydrotreatment runs.[1]

The fact that the O/C ratio only increased by a factor of 1.8 partially rules out an oxidative mechanism. The increase in oxygen could have been due to a small amount of oxidation which occurred after the deposit was collected. No precautions were taken at the time of collection to blanket it with nitrogen, and the deposit was several months old at the time of analysis.

CONCENTRATION OF DEPOSIT PRECURSORS

Coal liquid naphtha is a complex mixture. In order to identify the deposit precursors, they had to be concentrated. A combination of distillation and ion exchange chromatography was used to do this. The effect of these two concentration techniques was tested using TGA. From these experiments it was possible to identify the structural types responsible for much of the deposit formation.

The TGA experiment used to test concentrates for deposit formation consisted of heating the sample in a platinum boat from 25°C to 400°C, under nitrogen, at 20°/min. At 400°C the weight was recorded and the atmosphere switched to oxygen. The temperature was then increased to 700°C, and the material in the pan was burned off. This latter step allowed the tare of the balance to be checked.

It was determined that the residue remaining in the pan at 400°C was insoluble in common organic solvents. Herein, the insoluble residue is designated as "deposit."

It was shown in the pilot plant that the 177-204°C naphtha produced more deposit than the full range (66-204°C) naphtha. Therefore, various distillate cuts of the 177-204°C sample were prepared and tested for deposit formation. From these experiments it was found that the bottom 40% of the 177-204°C naphtha contained essentially all of the deposit precursors. The bottom 40% of the naphtha was used in the remainder of the experiments. It formed 1.73± .04 Wt.% deposit on heating to 400°C.

Because of the large amount of nitrogen seen in the deposit, the nitrogen containing compounds were concentrated on an ion exchange resin. Basic nitrogen compounds such as quinolines, pyridines and amines have been reported to be removed by Amberlyst-15 ion exchange resin.[2,3] The resin was prepared as described elsewhere[3] and it was used to remove the basic nitrogen compounds. It was ultimately decided that a ratio of 2.3:1::resin:bottom 40% was needed to lower the basic nitrogen content from 1.4% to 88 ppm, as determined by nonaqueous titration. This was the lowest basic nitrogen level that could be achieved.

While it was not possible to get the basic nitrogen content below 88 ppm, the deposit formation from the sample of ion exchange treated effluent was reduced to 34.7% of its original level. The correlation between deposit formation as measured by TGA and basic nitrogen level is shown in Table 3.

The material retained by the Amberlyst-15 ion exchange resin was desorbed by a solution of ammonia saturated methanol. The methanol was stripped off at 50°C under a stream of nitrogen. The resultant material was called the basic nitrogen concentrate. Examination of this material by ^{13}C NMR showed it to contain nitrogen heterocycles, such as pyridines and quinolines, and phenols. When heated to 400°C, the basic nitrogen concentrate gave 4.95% deposit as compared with 0.60% deposit from the effluent from the ion exchange resin. The weighted sum of the amounts of deposit from the basic nitrogen concentrate and that of the base-free material was 1.74%, which compares well with 1.73% deposit in the unseparated material. This indicates that there is no interaction between the basic and base-free material. The basic nitrogen concentrate was used in the remainder of this work.

The elemental analysis of the basic nitrogen concentrate, base-free material and bottom 40% of the 177-204°C naphtha is shown in Table 2. While the Amberlyst-15 concentrated the basic nitrogen compounds, it also carried along a large amount of oxygen in the basic nitrogen concentrate. An examination of the material boiling above 200°C by both ^{13}C NMR and Mass Spectrometry showed no evidence for molecules containing both basic and phenolic functionalities on the same molecule. It was not possible to completely separate this residual oxygen by caustic extraction.

EFFECT OF HEATING ON STRUCTURE

In order to arrive at an understanding of the mechanism of deposit formation, the effect of heating on the structure of the basic nitrogen concentrate was observed using FT-IR. Due to small amounts of deposit (~1-5mg) formed in the TGA pan, the use of other analytical techniques was not possible.

Samples were prepared by heating the basic nitrogen concentrate in the TGA at 400°C for a desired length of time. The deposit was recovered from the pan by soaking the pan with its contents in methylene chloride and evaporating the methylene chloride under nitrogen. The deposit was then made into KBr pellets as described previously.(4) Spectra were run on a Digilab 15B FTS System. Two hundred co-added interferograms at 2cm^{-1} resolution were taken for each sample.

Visual observation of the spectra showed changes in aromatic C-H, aliphatic C-H and hydroxyl bands at 3000-3100cm^{-1}, 2820-3000cm^{-1}, and 3100-3600cm^{-1}, respectively. These three bands were curve resolved and integrated using the methods of Painter, et al.(4) The integrated intensities for the three regions were plotted against heating time at 400°C and are shown in Figure 1. Substantial decreases were seen in all three of these regions with increased sample heating time.

MECHANISTIC CONSIDERATIONS

The decreases in aromatic C-H, aliphatic C-H, and hydroxyl bands described above have substantial implications for deposit formation. The loss of aliphatic C-H indicates a pyrolysis type of reaction. An analysis by gas chromatography of the TGA gaseous effluent shows the presence of light alkanes and alkenes as would be expected from a pyrolysis reaction.

The loss of aromatic C-H indicates a cross-linking of free radicals formed during pyrolysis with the subsequent formation of higher molecular weight molecules. The addition of octahydrophenanthrene to the basic nitrogen concentrate lowered the amount of deposit formed by 52%. Presumably, this is due to the capping of free radicals formed during pyrolysis.

The loss of O-H indicates either a loss of adsorbed water or a condensation reaction with a subsequent loss of water. The amount of water formed during heating was measured by gas chromatography. The adsorbed water in the feed was also measured. The amount of water produced during heating was substantially larger than the amount of adsorbed water on a molar basis. This indicates that some deposit formation occurs through condensation (phenol coupling) reactions. Reactions like these have been shown to occur upon heating naphthol to 400°C.[5] Silylation of the phenols with BSTFA resulted in a 24% decrease in the amount of deposit formed.

CONCLUSIONS

The heat exchanger deposit precursors are concentrated in the basic nitrogen concentrate obtained from the naphtha bottoms. This concentrate contains both heterocyclic nitrogen compounds and phenols. The primary reactions responsible for deposit formation were: 1) condensation of phenols, and 2) pyrolysis of alkylated nitrogen heterocycles.

ACKNOWLEDGMENTS

The authors wish to acknowledge helpful discussions with R. I. McNeil, J. Solash, D. C. Young and R. G. Ruberto, and assistance from M. K. Young and W. C. Zemla.

REFERENCES

1. Kara, S., Kobylinski, T. P., Beuther, H. Preprints Div. Petrol. Chem., 1982, 27, 849.

2. Jewell, D. M., Weber, J. H., Bunger, J. W., Plancher, H., Latham, D. R. Anal. Chem., 1972, 44, 1391.

3. Jewell, D. M., Albaugh, E. W., Davis, E. W., Ruberto, R. G. Ind. Eng. Chem. Fundam., 1974, 13, 1974.

4. Painter, P. C., Snyder, R. W., Starsinic, M., Coleman, M. M., Kuehn, D. W., Davis, A. Applied Spectroscopy, 1981, 35, 475.

5. Poutsma, M. L., Dyer, C. W., J. Org. Chem 1982, 47, 3367.

TABLE 1

ELEMENTAL ANALYSIS OF FEED AND DEPOSIT

ELEMENTAL	FEED	DEPOSIT
%C	83.92	73.63
%H	10.86	5.74
%O	5.14	8.22
%N	0.52	6.86
%S	0.23	1.83
%Ash	0.00	3.73
H/C	1.55	0.94

TABLE 2

ELEMENTAL ANALYSES OF BASIC NITROGEN CONCENTRATE, BASE FREE MATERIAL, AND BOTTOM 40% FRACTIONS

	Bottom 40%	Basic Nitrogen Concentrate	Base Free Material
% Carbon	79.67	78.25	80.30
% Hydrogen	8.44	7.95	8.94
% Nitrogen	1.54	3.54	0.14
% Oxygen	9.59	10.04	10.03
% Sulfur	0.65	0.22	0.58
H/C	1.27	1.22	1.34

TABLE 3

EFFECT OF BASIC NITROGEN ON DEPOSIT FORMATION

Basic N Content	Wt.% Deposit
88 ppm	.60%
173 ppm	.83%
280 ppm	1.40%
1.39%	1.73%

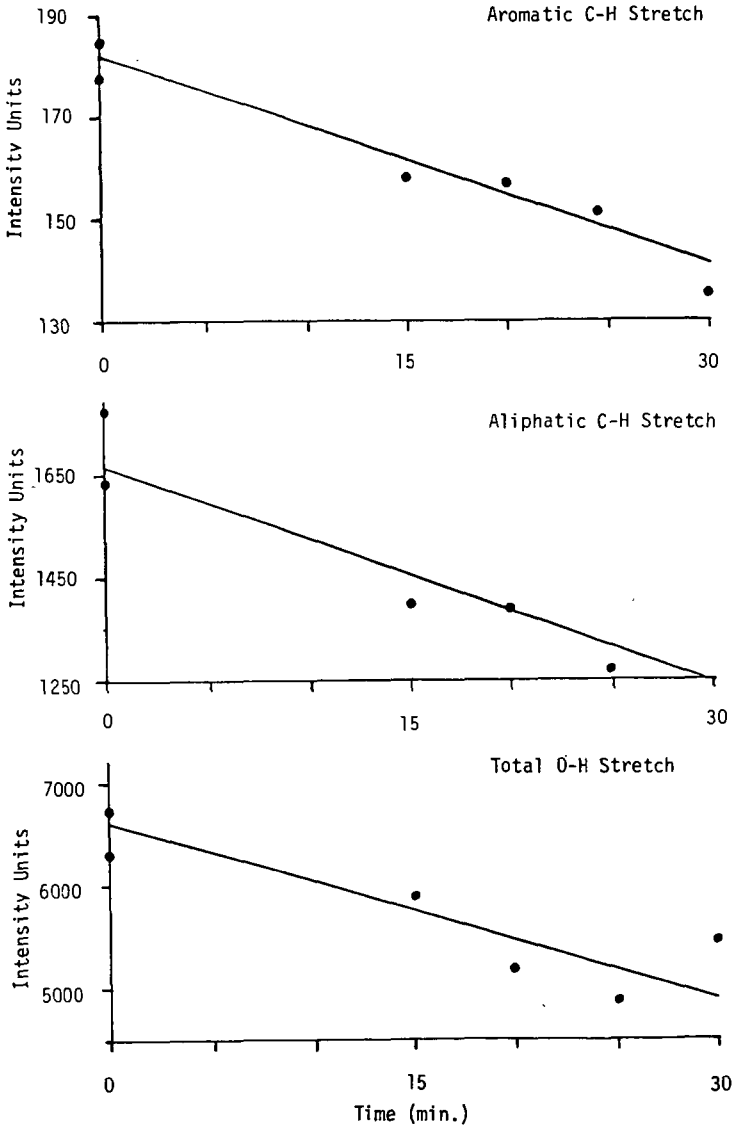

Figure 1. Integrated Intensities vs. Time at 400°C

Radical Initiation and Phenol Inhibition in the Thermal, Free Radical Decomposition of 1,3-Diphenylpropane(1), Dibenzylether(2) and Phenethylphenylether (3). Coal Liquefaction Model Studies

K.E. Gilbert

Department of Chemistry
Indiana University
Bloomington, IN 47405

Current thought on the structure of coal and the chemistry of coal liquefaction suggests that coal consists of large polycyclic clusters joined by short aliphatic links and that liquefaction reactions occur at these links. Much research has gone into the two atom links. We have been interested in the three atom links because in addition to the cleavage-abstraction reactions available to the two atom links, the three atom links may also react by radical chain reactions. These radical chain reactions can occur over a much wider temperature range than the cleavage-abstraction reactions and thus offer the possibility of a low temperature liquefaction process. Previous work has shown that 1, 2 and 3 decompose by free radical chain reactions as neat liquids or as solutions in hydrogen donating solvents in the temperature range of 300 to 400°C.(1)(Equation 1) Initiation of the radical chain process by benzylphenylether at 350° was demonstrated, but inhibition of the chain reactions by standard inhibitors, such as hindered phenols, was not studied. Herein we report on the effect of hindered phenols on the decomposition of 1, 2 and 3 at 350°, the development of methods for initiating these reactions at temperatures as low as 138°, the effect of hindered phenols on these reactions at lower temperatures and on the kinetic and thermodynamic barriers to these radical chain reactions.

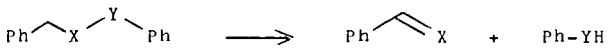

1)

1 X=Y=CH_2

2 X=O ; Y=CH_2

3 X=CH_2 ;Y=O

A large number of phenols, including 2,6-di-tert-butyl-4-methylphenol, have no effect on the decomposition of 1 at 350°. Stock has found that phenols catalyze the decomposition of 2 at 400°.(2) In order to understand the effect hindered phenols on radical chain processes the reaction of 1, 2 and 3 have been investigated at lower temperatures.

Prior to experimental work the thermodynamics of the overall reaction of 1 to toluene and styrene, 2 to toluene and benzaldehyde and 3 the phenol and styrene were investigated using the group additivity method of Benson (Table 1).(3)

Reaction of 1 is unfavorable at temperatures below 300°, thus initiation of this reaction should not occur at lower temperatures. Replacement of a CH_2 group by an oxygen greatly changes the thermodynamics and the decomposition of 2 and 3 are energetically favorable over the temperature range of interest.

The decomposition of 1 could not be effected by any of the low temperature initiators in accord with the thermodynamic calculations (Table 2). Reaction of 2 could be initiated by all of the low temperature initiators except AIBN, though this may not be a good experiment since AIBN is not very effective at hydrogen abstraction.(4) Reaction of 3 could be effected by di-tert-butyldiazene (TBD) at 180° but not by di-tert-butylperoxide (TPO) at 138° reflecting a kinetic barrier to reaction. In all cases the products were those expected from a radical chain reaction.

Reaction of 2 with TPO was found to be 0.68 order in 2 and 0.62 order in TPO (Table 3). The products were toluene, benzaldehyde and 1,2-diphenylethane(4) in the ratio of 1.1:2:0.65. The chain length, given by the ratio of benzaldehyde to 4, is 1.5. A mechanism consistent with this data is given in Scheme 1. Since the chain length is short both terms in the kinetic expression, derived using the steady state approximation, contribute thus accounting for the non-integral order in 2. The large amount of 4 formed suggests that hydrogen transfer from 2 to benzyl radical is slow at this temperature and controls the reaction path.

Addition of 2,6-di-tert-4-methylphenol to a mixture of 2 and TPO decreases the rate of reaction and surpresses the formation of 4. Toluene and benzaldehyde are the major products. The reaction order in 2 is 0.67 and -0.53 in phenol. A mechanism consistent with this data is given in Scheme 2. This is a general reaction scheme and under these experimental conditions k_5 and k_7 are small. The rate expression, using the steady state approximation, involves only first term under these conditions. Since $k_3 > k_2$ (5) while [2]>[ArOH] the two terms in the denominator are of similar magnitude. The data suggests that phenols function as inhibitors in this reaction by effectively competing with the substrate for initiator radicals, and by scavenging the chain carrying benzyl radicals.

Reaction of 2 with TBD at 180° to 200° was found to be 0.93 order in 2, 0.5 order in TBD with the products being toluene, benzaldehyde and 4 in a 6:8:1 ratio. The reaction mechanism of Scheme 1 accounts for this data with the recognition that the second term in the kinetic expression becomes more important at longer chain lengths. The increased temperature favors hydrogen transfer from 2 to benzyl radical at the expense of termination.

Addition of a 2,6-di-tert-butyl-4-methylphenol to the reaction of 2 and TBD decreases the reaction rate and surpresses the formation of 4 while still giving toluene and benzaldehyde. The reaction is first order in 2 and inverse first order in

phenol. The mechanism in Scheme 2 applies, except under these conditions k_5 is significant. This results in a two term rate expression. Phenol competes with 2 for initiator radicals and also for benzyl radicals. Reaction 7 is not yet important and hindered phenols continue to function as inhibitors at 180°C.

Reaction of 2 with 1,1,2,2-tetraphenylethane at 250° gives toluene and benzaldehyde in a reaction that is first order in 2. Addition of a hindered phenol has no effect on the reaction. Thus on going from 180° to 250° hindered phenols go from being inhibitors to being chain transfer agents.

In summary it should be noted that 2 is an excellent model compound. It decomposes over a wide temperature range to give stable products, can be initiated with a wide variety of initiators and allows the study of kinetic barriers to radical chain reactions. Finally the wide temperature range permits investigation of the temperature dependence of inhibition by phenols.

Conversely the all carbon system, 1, demonstrates a thermodynamic barrier to reaction with no reaction observed below 300°. This suggests that all carbon systems will not cleave to toluene and styrene by any process below 300° and that attempts to construct lower temperature coal liquefaction processes based on the thermal chemistry of all carbon systems will not be successful. That is the reactions of one and two atom links are limited to high temperatures by the energy required to cleave a C-C bond, while the three atom and higher number links are thermodynamically limited and would require higher temperatures to drive the reactions towards product formation. This might be circumvented by hydrogenating the alkenes formed, however this would probably require the use of catalysts and gets into subjects more complex than we wish to discuss here. This also suggests that free radical initiators will have no effect on coal liquefaction processes.

Acknowledgement This work was supported by the DOE office of Basic Energy Sciences under contract DEA CO2-10721A.

References

1. Gilbert, K.E. and Gajewski,J.J.,J Org Chem,(1982),47,4899.
2. Stock, L.M. and King, H-H.,Fuel,(1982),61,1172.
3. Benson,S.W.,"Thermochemical Kinetics",Wiley-Interscience:New York,1976.
4. Bartlett,P.D.;Fickes,G.N.;Haupt,F.C.;Hegelson,R.,Accts Chem Res,(1970),3,177.
5. Howard,J.A.;Ingold,K.U., Can J Chem,(1964),42,2324.

Table 1 Thermodynamics of the Reactions of 1, 2 and 3

					ΔG kcal/mol			
			ΔH	ΔS	100	200	300	400
1	⟶	$Ph-CH_3$ + Ph⟨	17.66	32.5	5.5	2.3	-.96	-4.2
2	⟶	$Ph-CH_3$ + Ph-CHO	1.23	53.0	-18	-24	-29	-34
3	⟶	Ph-OH + Ph⟨	10.30	33.9	-2.3	-5.7	-9.1	-12.5

Table 2. Reaction of 1, 2 and 3 with Various Initiators

Initiator/Temperature	1	2	3
AIBN/80°	NR	NR	NR
TPO/138°	NR	+	NR
TBD/180-200°	NR	+	+
$(Ph)_2CHCH(Ph)_2$/250°	NR	+	+
Ph⟨O-Ph/350°	+	+	+

Table 3 Reaction of 2 with TPO and TBD

[DBE]	[I]	[ArOH]	log R_i	Rxn Order
3.07	TPO/1.12	-	-4.07	
2.38		-	-4.15	
1.77		-	-4.19	.68
1.46		-	-4.29	
1.15		-	-4.37	
1.77	1.55	-	-4.11	
	1.12	-	-4.19	.62
	.61	-	-4.36	
1.77	1.12	.87	-4.85	
		.58	-4.68	
		.37	-4.52	-.61
		.29	-4.49	
		.14	-4.36	
2.38	1.12	.29	-4.41	
1.77			-4.49	.67
1.15			-4.62	
3.1	TBD/.51	-	-3.97	
2.0		-	-4.19	.93
1.3		-	-4.32	
2.0	.82	-	-3.95	
	.51	-	-4.19	.5
	.36	-	-4.27	
2.0	.51	1.15	-4.82	
		.89	-4.69	-1.10
		.57	-4.47	
		.29	-4.16	

Scheme 1

$$\mathrm{I\text{-}I} \xrightarrow{k_i} 2\ \mathrm{I}^*$$

$$\mathrm{I}^* + \mathrm{DBE} \xrightarrow{k_H} \mathrm{I\text{-}H} + \mathrm{DBE}^*$$

$$\mathrm{DBE}^* \xrightarrow{k_\beta} \mathrm{Ph\text{-}CH_2}^* + \mathrm{Ph\text{-}CHO}$$

$$\mathrm{Ph\text{-}CH_2}^* + \mathrm{DBE} \xrightarrow{k_H} \mathrm{Ph\text{-}CH_3} + \mathrm{DBE}^*$$

$$2\ \mathrm{Ph\text{-}CH_2}^* \xrightarrow{k_T} \mathrm{Ph}\text{—}\mathrm{Ph}$$

$$-\frac{\partial[\mathrm{DBE}]}{\partial t} = ek_i[\mathrm{I}] + \left(\frac{ek_i[\mathrm{I}]}{k_t}\right)^{1/2} k_H[\mathrm{DBE}]$$

Scheme 2

$$\mathrm{I\text{-}I} \xrightarrow{k_i} 2\ \mathrm{I}^*$$

$$\mathrm{I}^* + \mathrm{DBE} \xrightarrow{k_2} \mathrm{I\text{-}H} + \mathrm{DBE}^*$$

$$\mathrm{I}^* + \mathrm{ArOH} \xrightarrow{k_3} \mathrm{I\text{-}H} + \mathrm{ArO}^*$$

$$\mathrm{DBE}^* \xrightarrow{k_\beta} \mathrm{Ph\text{-}CH_2}^* + \mathrm{Ph\text{-}CHO}$$

$$\mathrm{Ph\text{-}CH_2}^* + \mathrm{DBE} \xrightarrow{k_5} \mathrm{Ph\text{-}CH_3} + \mathrm{DBE}^*$$

$$\mathrm{Ph\text{-}CH_2}^* + \mathrm{ArOH} \xrightarrow{k_6} \mathrm{Ph\text{-}CH_3} + \mathrm{ArO}^*$$

$$\mathrm{ArO}^* + \mathrm{DBE} \xrightarrow{k_7} \mathrm{ArOH} + \mathrm{DBE}^*$$

$$2\ \mathrm{ArO}^* \xrightarrow{k_T} \text{products}$$

$$-\frac{\partial[\mathrm{DBE}]}{\partial t} = \frac{R_i k_2[\mathrm{DBE}]}{k_2[\mathrm{DBE}]+k_3[\mathrm{ArOH}]} + \frac{k_5[\mathrm{DBE}]}{k_6[\mathrm{ArOH}]}\left(\frac{R_i k_2[\mathrm{DBE}]}{k_2[\mathrm{DBE}]+k_3[\mathrm{ArOH}]}\right)$$

MOLECULE-INDUCED HOMOLYSIS IN COAL CHEMISTRY: RADICAL INTERMEDIATES IN THE THERMAL DECOMPOSITION OF 1,2-DIHYDRONAPHTHALENE*

James A. Franz**, Donald M. Camaioni**, Robert R. Beishline***
and Don Dalling****

**Pacific Northwest Laboratory, Richland, WA 99352
***Weber State College, Ogden, UT 84408
****Department of Chemistry, University of Utah, Salt Lake City, UT 84112

Molecule-induced homolysis (MIH), the process by which two closed-shell molecules react to produce free radicals, has been recognized as an important contributing pathway to radical initiation during coal dissolution(1,2). The production of organic radicals by MIH and other pathways can lead in stepwise fashion to the production of highly reactive radicals to a significant degree at temperatures >400°C. In this paper, we summarize results which show that the decomposition of 1,2-dihydronaphthalene (DHN) involves both 1-hydronaphthyl (1HN) and 2-hydronaphthyl (2HN) radicals as well as 1-tetralyl radical and that the production of 1HN and 2HN leads to the scission of hydrogen atom (H•) and its participation in subsequent hydrocracking reactions.

Experimental. 1,2-Dihydronaphthalene (Aldrich) was purified by careful fractional distillation. 1,2-Dihydro-4-deuteronaphthalene(DHN-4-d) was prepared by treatment of 1-tetralone with lithium aluminum tetradeuteride. The 1-deuterotetralol (21g) was heated at 100°C for 20 minutes at reduced pressure with $KHSO_4$ (2g) followed by flash distillation. The crude product was dissolved in hexane, filtered through neutral alumina, and concentrated to give pure (99.7%) product in 66% overall yield. Thermal decomposition of DHN or DHN-4-d was carried out by degassing and sealing the reagents in pyrex tubes and placing the tubes in stainless steel vessels and surrounding the pyrex tubes with tetralin to balance internal pressure. Yields of products, naphthalene, tetralin and C_{20} compounds were measured by capillary gas chromatography (gc). The C_{20} products, 1-5 (Figure 1), were isolated from 16 hour reactions at 300°C by preparative gc and characterized by ^{13}C NMR (20 MHz) and ^{1}H NMR (300 MHz) and mass spectrometry for both DHN and DHN-4-d precursors. Compound 2 was subjected to an exchange of its benzylic hydrogen by heating in sodium dimsylate-d_5/DMSD-d_6 at 100°C. Reactions of DHN and the reagents of Table 1 were carried out at 425°C for 10 minutes and the product mixtures were analyzed by capillary gc for hydrocracked products. Products were identified by coinjection of authentic standards.

Results

Products of the thermolysis of DHN. When DHN is heated at 300°C the products, tetralin (40 ± 10%), naphthalene (40 ± 10%), C_{20} compounds, 1-5, (15% combined yield) and a variety of trace (5%) C_{20} products are formed. When heated at 425°C, C_{20} compounds comprise less than 5% of the products, naphthalene is formed in excess of tetralin and H_2 gas is formed.

Structures of Compounds 1-5. Compounds 1 and 2 each exhibited molecular weights of 260, four aliphatic methine carbons, 4 aliphatic methylene carbons,

* This work was supported by the U.S. Department of Energy, Processes and Techniques Branch, Division of Chemical Sciences, Office of Basic Energy Sciences, under Contract DE-AC06-76 RLO-1830.

4 unprotonated aromatic carbons along with the protonated aromatic carbons as determined by off-resonance decoupling techniques. ^{1}H NMR at 300 MHz revealed 12 fully resolved aliphatic hydrogens for each of 1 and 2. Compounds 3, 4, and 5 exhibited molecular weights of 262, 262 and 258. Homonuclear decoupling unambiguously established the structure of 1, as well as establishing the syn relationship of hydrogens b and h shown in the structure of 2. Deuterium exchange with compound 2 removed protons a, b, c, f, and g, but not d. When DHN-4-d was used to produce isomers 1-5, deuterium appeared only as shown in the product structures.

Hydrocracking Reactions. Table 1 presents hydrocracking reactants and products. The modest yields of products reflect the large number of competing reactions which consume H• and do not produce hydrocracked products.

Discussion

The principle initiation pathway for the DHN reaction is proposed to be that of Equation 1. The value of $\Delta H_f^o{}_{298}$ for 1HN assumes a DH^o for the 3-hydrogen

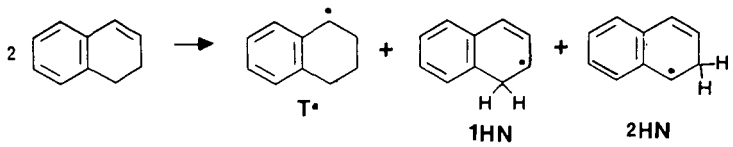

(1)

$\Delta H^o_{f,298}$ kcal/mole	30	35	56	60

of DHN to be 94.5 kcal/mole corrected for the difference in resonance stabilization energy (ΔRSE) between DHN and 1HN (ΔRSE), 16.7 kcal/mole, from Herndon's calculations (3). The value for 2HN assumes no resonance stabilization of DHN by the styrene-like olefinic portion of the molecule, giving a value of RSE of 12.4. Thus, the value of $\Delta H^{\neq}$ for reaction of the two molecules of DHN to give 1-tetralyl (T•) and 1HN is 31 kcal/mole, and 35 kcal/mole to produce T• and 2HN•. Other thermochemical values in Equations 1 and 2 are experimental values or estimates (4). Thus, appreciable concentrations of both 1HN and 2HN are expected at 300°C and above. Both 1HN and 2HN may undergo elimination of H• (Equation 2) with activation barriers of 30-35 kcal/mole, assuming 2-3 kcal barriers for H• addition to naphthalene.

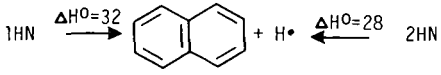

(2)

The structures of 1 and 2 are both consistent with the addition of 2HN to DHN followed by a second internal cyclization step and hydrogen abstraction from available donors (Equations 3, 4).

Both compounds 1 and 2 arise from face-to-face interaction of DHN and 2HN. The different products arise from the two different possible orientations of DHN in Equation 3. When DHN-4-d is used to produce 1 and 2, deuterium is predicted to occur at one methine and one methylene carbon, as observed. For possible structures arising from 1HN, two adjacent methine carbons would have been deuterated.

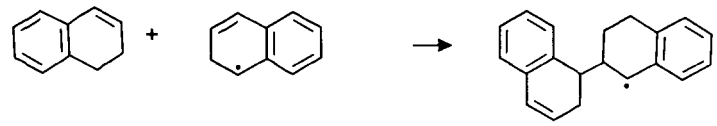

(3)

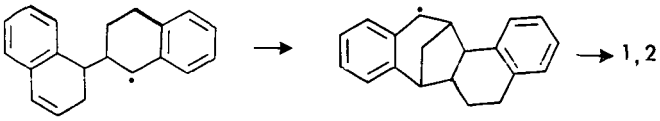

(4)

Compound 4, when produced from DHN-4-d, has deuterium solely at the position indicated. This dictates that 4 is derived from the symmetrical termination product of 1-HN which has undergone further reduction (Equation 5), as opposed to

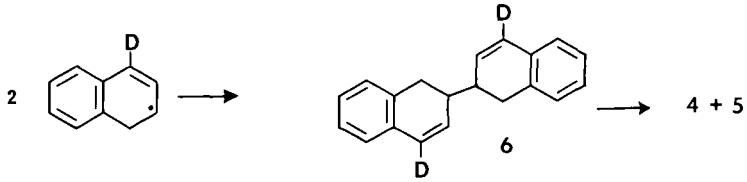

(5)

a pathway involving the adduct of 1HN to DHN, which would lead to 2 deuterated aliphatic carbons (only one deuterated methylene is observed). If intermediate 6 undergoes a net disproportionation, compound 5 is produced. Compound 3 arises from either the termination of T• and 1HN followed by reduction or the addition of T• to DHN followed by H• abstraction. Thus, these products provide convincing evidence that 1-tetralyl, 1-hydronaphthyl, and 2-hydronaphthyl radicals are important intermediates in the decomposition of DHN, consistent with the MIH pathway of Equation 1. It was previously established by Heesing and Muller (5) that the primary products, tetralin and naphthalene, were produced in a non-concerted reaction, but the intermediacy of 1HN and 2HN was not established because the structures of C_{20} products were not determined. Both 1HN and 2HN can of course be produced by H• abstraction from DHN.

At higher temperatures (>400°C), C_{20} products are insignificant and H_2 is formed in significant (10-30%) yields. The products of Table 2 are best explained by addition of H• (compare Benson's study of cyclohexadiene (6)) at the ipso position of the aryl group followed by departure of the substituent radical. The source of H• must be the elimination of H• from radicals such as 1HN and 2HN with modest barriers of 30-35 kcal/mole. Thus, the process of molecule-induced homolysis which occurs between structures which are relatively easily oxidized or reduced, together with chain decomposition steps, leads ultimately to hydrogen atoms, with no intermediate step requiring more than 35 kcal/mole. Partially oxidized or reduced structures in coal, or compounds capable of exceptionally stable radicals thus probably play an essential role in initiation pathways during coal dissolution leading ultimately to the cleavage of strong C-C bonds.

Table 1. Thermolysis of 1,2-Dihydronaphthalene in the Presence of Other Compounds.

Reagent (wt., mg)	DHN (wt., mg)	Products (% yield)[a]
Phenylether (450)	82	Phenol (1.4%)
Diphenylmethane (207)	35	Toluene (2.6%)
Tetralin (92)	13	n-butylbenzene (5.1%)
2,6-Dimethylnaphthalene (74)	24	2-methylnaphthalene (2.6%)

[a] Mole produced per mole DHN consumed.

References

1. H. H. King and L. M. Stock, Fuel, 1980, 59, 447-449 and ibid., 1982, 61, 257-264.

2. S. E. Stein, Am. Chem. Soc. Symposium Ser. 1981, 169, 97-129.

3. W. C. Herndon, J. Org. Chem. 1981, 46, 2119.

4. Sidney W. Benson, "Thermochemical Kinetics. Methods for the Estimation of Thermochemical Data and Rate Parameters," 2nd. Ed., Wiley-Interscience, 1976, New York, N.Y.

5. A. Heesing and W. Mullers, Chem. Ber. 1980, 113, 9-18 and see G. B. Gill, S. Hawkins and P. H. Gore, J. Chem. Soc. Chem. Comm. 1974, 18, 742.

6. S. W. Benson and R. Shaw, J. Amer. Chem. Soc., 1967, 89, 5351.

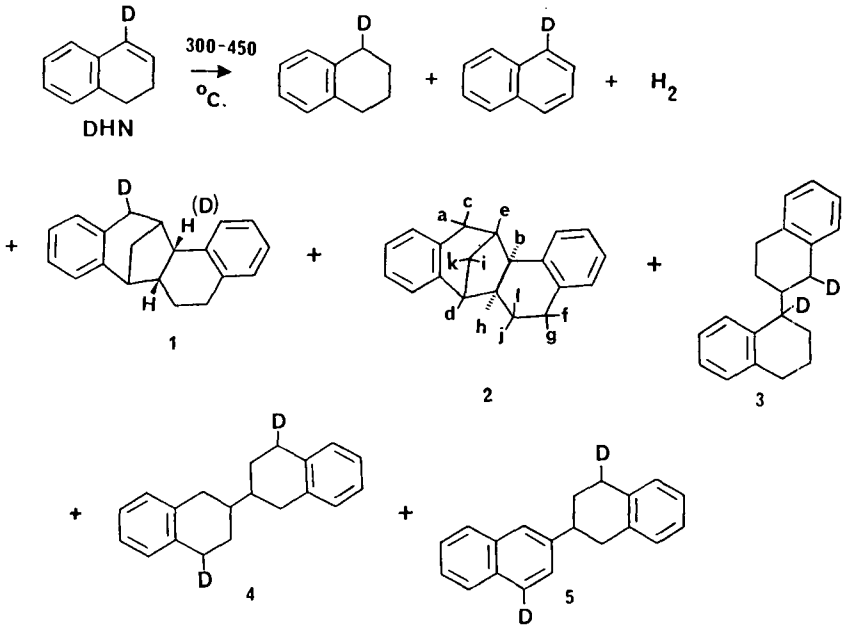

Figure 1. Major Products from the Thermal Decomposition of DHN. Deuterium atoms indicate label positions when DHN-4-d was used.

THERMAL CRACKING OF COAL MODEL DIARYL ETHERS IN TETRALIN SOLUTION

Y. Kamiya, E. Ogata, K. Goto, and T. Nomi

Faculty of Engineering, University of Tokyo
Hongo, Tokyo, Japan, 113

1. INTRODUCTION

Recently, the importance of aromatic ether structure(1,2) in coal molecule has been stressed, and so the thermal cracking of several aromatic ethers has been studied by several workers(3,4), in order to elucidate the coal liquefaction mechanism.

It is known that aliphatic ethers can be easily decomposed, but diaryl ethers such as diphenyl ether are quite stable at temperatures as high as 450°C.

Previously, we have reported that some diaryl ethers with polycyclic aromatic ring(5) were cracked relatively easily at 450°C.

In this paper, we wish to report the effect of ring structure of polycyclic aromatic ether as well as the effect of solvent on the thermolysis of diaryl ether, since aryl ether is one of key structures in coal liquefaction.

2. EXPERIMENTAL

Tetralin and other solvents were reagent grade and used after washing with sulfuric acid, alkali and water and subsequent distillation at 70°C under reduced pressure. Diaryl ethers were synthesized by refluxing a mixture of aryl bromide, phenolic compound, Cu_2O and γ-collidine for reaction time from 100 to 400 hr. According to repeated purification by SiO_2-Al_2O_3 column and recrystallization, diaryl ethers employed were of purities above 99%.

Solvent and diaryl ether were added to 90 ml magnetic stirring(1000 rpm) autoclave. After pressurizing with hydrogen, the autoclave was heated to reaction temperature within 25 min and maintained at the reaction temperature during the reaction time. At the completion of an experiment, the autoclave was cooled by electric fan to room temperature. The reaction products were subjected to gas chromatographic analysis to determine the yield of products.

3. RESULT AND DISCUSSION

3.1 Thermolysis of dinaphthyl ethers

The conversion of 1,2'- and 2,2'-dinaphthyl ethers in tetralin at 430°C was plotted against the reaction time in Figure 1. Almost linear relations indicate

that the conversion of ethers is of first order with respect to substrate concentration and the first order rate constants are calculated to be 4.7×10^{-5} and 2.8×10^{-5} sec^{-1} for 1,2'- and 2,2'-dinaphthyl ethers, respectively. The yield of naphthols was plotted against the residence time as shown in Figure 2. The ratio of 1-naphthol to 2-naphthol from 1,2'-dinaphthyl ether was 1 to 4, indicating that 2-naphthoxy radical is favorably formed.

1-Naphthol and 2-naphthol were confirmed to be not so stable at 430°C and their first order rate constants of conversion in tetralin were measured to be 4×10^{-5} and 3.5×10^{-5} sec^{-1} at 430°C respectively.

On the basis of the above rate constants the cracking rate constant of dinaphthyl ethers to naphthols can be calculated to be 2.3×10^{-5} and 1.25×10^{-5} sec^{-1} for 1,2'- and 2,2'-dinaphthyl ethers.

3.2 Effect of chemical structure of aryl ether on the reaction rate of thermolysis

Nine kinds of diaryl ether with phenyl, diphenyl, naphthyl, phenanthryl and anthryl groups were treated in tetralin solution at 430°C for 5 hr, as shown in Table 1. Diphenyl ether was very stable, but phenanthryl or anthryl ethers have shown very high conversion values.

Generally, the conversion rate constant of diaryl ethers increased with increasing the number of polycyclic aromatic ring of aryl structure.

The rate of conversion of phenyl aryl ether increased as the following order with respect to aryl group: Phenyl < Diphenyl < 2-Naphthyl < 1-Naphthyl < Phenanthryl < Anthryl.

Apparent ratio of the cracking rate of aryl-oxygen bond of diaryl ether can be calculated on the basis of the rate of formation of phenolic compound from ether along with the rate of elimination of corresponding phenolic compound. Because of very complex reaction system these calculated values in Table 2 can not be evaluated with high accuracy, but it seems to show that the bond dissociation energy of phenyl-oxygen bond is the highest and that of aryl oxygen bond decreases with increasing the number of polycyclic ring.

In order to make clearer the effect of aromatic structure on the rate of cracking, several diaryl ethers were treated in 1-methylnaphthalene, a poor hydrogen donating solvent, at 450°C for 2 hr as shown in Table 3. In this case, the color of solution after reaction was dark brown, indicating that polymerization reaction took place. The order of reactivity of diaryl ethers evaluated by the conversion rate constant was almost the same as the order in tetralin, that is, the rate constant increased with increasing the number of polycyclic aromatic ring of diaryl ether. However, the difference in the relative value of k was larger in tetralin than in methylnaphthalene.

3.3 Solvent effect

Above results lead us to further experiments on solvent effect in cracking

reaction.

As shown in Table 4, the effect of hydrogen donor solvent on the pyrolysis of 2,2'-dinaphthyl ether was most remarkable. In a poor hydrogen donor such as 1-methylnaphthalene, the conversion of dinaphthyl ether was only 23%, but it was increased to 39% in tetralin and to 93% in 9,10-dihydroanthracene. As for n-hexadecane, this compound itself was cracked remarkably at 430°C and so could be a good hydrogen donor because of radical and olefin formations. Decalin also could be a hydrogen donor for hydrogenation of naphthalene nucleus.

The effect of dihydroanthracene was outstanding, and so the conversion rate constant in dihydroanthracene was five times as large as in tetralin. Dihydroanthracene itself was comletely converted to other compounds by complex reactions involving dehydrogenation and disproportionation. The accelerating effect due to dihydroanthracene was so great that even diphenyl ether being the most stable diaryl ether was cracked to the conversion of 13.3% at 430°C in 5 hr. It was also observed that the conversion of 2,2'-dinaphthyl ether was proportionally increased with the concentration of dihydroanthracene in 1-methylnaphthalene.

The marked solvent effect by hydrogen donors on the conversion of polycyclic diaryl ethers can be attributed to the hydrogenation of aromatic rings by hydrogen transfer, because the hydrogen transfer reaction really occurs and the cracking of aliphatic ether proceeds very rapidly. A mixture of partially hydrogenated products from 2,2'-dinaphthyl ether by Pd-Pt catalyst was found to be cracked more rapidly than dinaphthyl ether.

Another interesting solvent effect was observed in the case of naphthol, that is, the rate constant of conversion of 2,2'-dinaphthyl ether was increased from 2.8×10^{-5} to 7.8×10^{-5} sec^{-1} by the addition of 26g of 1-naphthol.

It is known that hydrogen donor such as tetralin can partially hydrogenate aromatic nucleus(5) but not effective for the cracking of resulting aliphatic structure. Therefore, the main role of hydrogen donor solvent in coal liquefaction has been ascribed to the hydrogenation and stabilization of coal fragments being thermally produced.

If hydrogen donor only plays a role stabilyzing coal fragments, it would not be so effective for the thermal cracking of coal and the successive oil formation reaction.

The remarkable effect of hydrogen donor on the cracking of polycyclic aromatic ethers would be a good explanation for the effective degradation of coal molecule in the presence of hydrogen donor solvent.

4. CONCLUSION

Nine kinds of diaryl ether were thermally cracked at 430°C in tetralin or 1-methylnaphthalene solutions and the following conclusions were obtained.

1. The rate of conversion of diaryl ether increased with increasing the number of polycyclic aromatic ring of the ether.
2. The cracking reaction of diaryl ether was of first order with respect to ether concentration.
3. In the case of phenyl polycyclic aryl ethers, phenol was preferably formed rather than the other polycyclic aromatic phenols as cracking products.
4. Hydrogen donor solvent and naphthol accelerated remarkably the cracking reaction of diaryl ethers.

REFERENCES

1) Edited by M. L. Gorbaty, J. W. Larsen and I. Wender, " Coal Science Vol. 1 ", R. M. Davidson, Chapter 4, (1982), Academic Press.
2) Y. T. Shah, " Reaction Engineering in Direct Coal Liquefaction ", Chapter 2, (1981), Addison Wesley.
3) R. S. Schlosberg, W. H. Davis, Jr. and T. R. Asche, Fuel, 60, 201 (1981).
4) S. V. Panelker, Y. T. Shah and D. C. Cronauer, Ind. Eng. Chem. Fundam., 21, 236 (1982).
5) Y. Kamiya, T. Yao and S. Oikawa, ACS Symp. Series 139, p. 291 (1980), ACS.

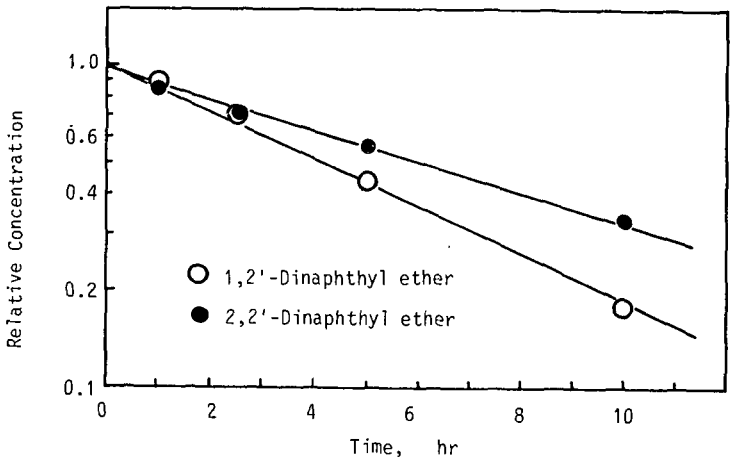

Figure 1. Thermal Cracking of Dinaphthyl Ethers in Tetralin at 430°C. (Ether 5.0g, Tetralin 30 ml, Initial P_{H_2} 50 kg/cm^2)

TABLE 1 THERMAL CRACKING OF DIARYL ETHERS IN TETRALIN AT 430°C FOR 5 HR

(Ether 5.0g, Tetralin 30 ml, Initial P_{H_2} 50 kg/cm^2)

Ether	Conversion(%)	k*1, 10^{-6}sec^{-1}	Relative Value of k	Products Yield(mole%)
Diphenyl ether	3.0	1.7	1.0	Phenol 0.84
4-Phenoxy diphenyl	7.6	4.4	2.6	Phenol 1.51 4-Phenylphenol 1.65
2-Phenoxy naphthalene	12.8	7.6	4.5	Phenol 4.64 2-Naphthol 1.16
1-Phenoxy naphthalene	38.0	26.6	15.7	Phenol 17.0 1-Naphthol 1.67
9-Phenoxy phenanthrene	53.0	42.0	24.9	Phenol 27.1 9-Phenanthrol 4.12
9-Phenoxy anthracene	(>99.9)	(>3840)	(>2260)	Phenol 72.8 Anthrone 0.53
2,2'-Dinaphthyl ether	39.2	27.6	16.3	2-Naphthol 12.8 1,2'-Dinaphthyl ether 4.7
1,2'-Dinaphthyl ether	57.0	46.9	27.8	2-Naphthol 19.5 1-Naphthol 4.6 2,2'-Dinaphthyl ether 2.2
2-Naphthyl-9-phenanthryl ether	66.1	60.1	35.5	2-Naphthol 19.1 9-Phenanthrol 4.4

*1; First order rate constant.

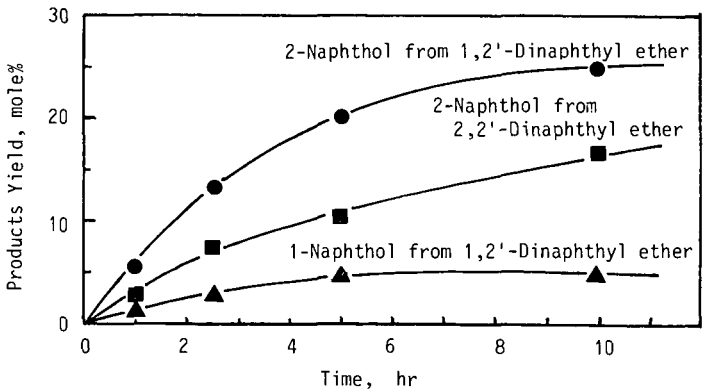

Figure 2. Reaction Products from Thermal Cracking of Dinaphthyl ether in Tetralin at 430°C.
(Ether 5.0g, Tetralin 30 ml, Initial P_{H_2} 50 kg/cm^2)

TABLE 2 THERMAL CRACKING RATE CONSTANT OF DIARYL ETHER

Diaryl Ether	Cleaved Aryl-Oxygen Bond	First Order Rate Constant k, 10^{-6} sec^{-1}
Diphenyl ether	Phenyl-Oxygen	0.52
1-Phenoxy naphthalene	1-Naphthyl-Oxygen	13.0
	Phenyl-Oxygen	1.7
2-Phenoxy naphthalene	2-Naphthyl-Oxygen	3.1
	Phenyl-Oxygen	1.0
1,2'-Dinaphthyl ether	1-Naphthyl-Oxygen	22.6
	2-Naphthyl-Oxygen	5.6
2,2'-Dinaphthyl ether	2-Naphthyl-Oxygen	12.5

TABLE 3 THERMAL CRACKING OF DIARYL ETHERS IN 1-METHYLNAPHTHALENE AT 450°C FOR 2 HR
(Ether 5.0g, Solvent 30 ml, Initial P_{Ar} 50 kg/cm^2)

Diaryl Ether	Conversion(%)	k, 10^{-5} sec^{-1}	Relative Value of k
Diphenyl ether	8.3	1.2	1.0
2-Phenoxy naphthalene	22.2	3.5	2.9
1-Phenoxy naphthalene	68.2	15.9	13.3
9-Phenoxy phenanthrene	81.1	23.1	19.3
2,2'-Dinaphthyl ether	38.7	6.8	5.7
1,2'-Dinaphthyl ether	80.0	22.4	18.7

TABLE 4 EFFECT OF SOLVENT ON THE THERMAL CRACKING OF 2,2'-DINAPHTHYL ETHER AT 430°C FOR 5 HR
(Ether 5.0g, Solvent 30 ml, Initial P_{H_2} 50 kg/cm^2)

Solvent	Conversion of Ether(%)	k, 10^{-6} sec^{-1}
1-Methylnaphthalene	23	14
n-Hexadecane	31	20
cis-Decalin	38	27
Tetralin	39	28
9,10-Dihydroanthracene	93	153

THE KINETICS OF CATALYTIC HYDROGENATION OF PYRENE--IMPLICATIONS FOR DIRECT COAL LIQUEFACTION PROCESSING*

H. P. Stephens and R. N. Chapman

Sandia National Laboratories, Albuquerque, NM 87185

INTRODUCTION

Although recycling heavy solvents has recently re-emerged[1,2,3,4] as a key to cutting the cost of direct coal liquefaction, little data for the hydrogenation of heavy solvent donors have been reported. This study addresses the kinetic and thermodynamic aspects of catalytic hydrogenation of pyrene, a donor solvent precursor thought to play an important role in coal liquefaction processes that use heavy recycle solvents.[5,6]

In the presence of a catalyst, pyrene (Py) is hydrogenated to di- (H_2Py), tetra- (H_4Py), hexa- (H_6Py), deca- ($H_{10}Py$) (Figure 1) and perhydro- ($H_{16}Py$) species via a complex mechanism involving a network of reversible parallel and series reactions. Though several studies have dealt with aspects of pyrene hydrogenation, including hydrocracking reactions,[7] reaction product distributions[8,9] and thermodynamic properties,[10] the kinetics of hydrogenation have not been previously reported.

EXPERIMENTAL

Thirty-six batch hydrogenation experiments were performed with solutions of 9.1 wt % pyrene in n-hexadecane, which approximated the concentrations found in integrated two-stage liquefaction recycle solvents.[11] To evaluate the effects of reaction conditions on the kinetics of hydrogenation, reactions were performed over a range of conditions: Temperatures of 348, 374 and 394°C, pressures of 500, 1250 and 2000 psig, and catalyst/pyrene weight ratios of 0.05, 0.15 and 0.45. Several experiments performed without catalyst confirmed that contributions of homogeneous reactions and reactor wall effects were insignificant. In addition, several catalyzed experiments performed with hexahydropyrene proved the existence of reversible reaction steps.

Materials. Pyrene, hexahydropyrene, and n-hexadecane were used as obtained from Aldrich Chemical Company. Modified Shell 324, a Ni-Mo/alumina catalyst currently used in the second stage of integrated two-stage pilot plant operations,[2] was added to the reactors as a -200 mesh powder. High purity hydrogen (99.999%) was used in all the experiments.

Apparatus and Procedure. The batch reactions were performed in stainless steel microreactors,[12] equipped with thermocouples and pressure transducers, with a liquid capacity of 3.6 cm^3 and a gas volume of 22 cm^3. Four reactors could be operated simultaneously. After the reactors were charged with 100 mg of pyrene, 1 g of n-hexadecane and 5, 15 or 45 mg of catalyst, they were pressurized with hydrogen (420, 1050 or 1850 cold charge), and heated to temperature (time to temperature = 1 min) in a fluidized sand bath while

* This work supported by the U.S. Dept. of Energy, Contract No. DE-AC04-76DP00789.

being horizontally shaken at 200 cycles/min. Temperatures and pressures were recorded with a digital data acquisition system during the course of the experiments. Following the heating period, the reactor vessels were rapidly quenched to ambient temperature (time of quench = 10 sec), and the products of the experiment were removed for analyses. It was estimated from the reactor heat-up and quench rates that the time at temperature could be determined to within 0.5 min. Temperatures could be maintained constant to within ± 2°C and pressures to within ± 20 psig during the heating period of the experiments.

Product Analyses. The products were washed from the reactor with toluene, filtered to remove catalyst and transferred to a volumetric flask. Following addition of an internal standard (2-methylnaphthalene), the product solution was brought to 50 ml with additional toluene and analyzed by gas chromatography (Hewlett-Packard 5840A with flame ionization detection FID) using the following conditions: 1/8 in x 10 ft column with Supelco 10% SP-2100 on 100/120 Supelcoport, temperature 220°C, nitrogen carrier gas 20 cc/min.

Gas chromatography/mass spectrometry techniques were used to identify the order of elution of components of the reaction mixture, which agreed with previously published results.[9] Quantitative analysis of the reaction mixture was accomplished using external and internal standards. The external standard, a solution of 2-methylnaphthalene, n-hexadecane, pyrene and 1,2,3,6,7,8-hexahydropyrene in toluene was used to obtain FID response factors for the components relative to the internal standard, 2-methylnaphthalene. These were 0.99 for n-hexadecane, 1.10 for hexahydropyrene and 1.04 for pyrene. The relative response for hexahydropyrene was used for the other hydropyrenes. The weights (W) of n-hexadecane, pyrene and hydropyrenes in each sample were calculated from their GC chromatogram areas (A), the response of 2-methylnaphthalene (R_{mn}) and their relative response (R_r).

$$W = R_r \cdot R_{mn} \cdot A$$

The concentration of pyrene and hydropyrenes was calculated on a molal, moles/1000 g hexadecane, basis. Concentration was normalized to initial pyrene concentration for the kinetic calculations.

CALCULATIONS

As a first step in delineating the overall reaction network for catalytic pyrene hydrogenation, the hydrogenation of pyrene to 4,5-dihydropyrene (equation 1) was analyzed:

$$Py + H_2 \underset{k_{-1}}{\overset{k_1}{\rightleftharpoons}} H_2Py \qquad (1)$$

The assumption that pyrene is not formed directly from hydropyrenes other than H_2Py and does not directly form hydropyrenes other than H_2Py is supported by reported studies of hydrogenation product distributions as a function of temperature and pressure.[9] Because the hydrogen concentration was in excess during the reactions (e.g., minimum of 26 moles of H_2 per mole Py), the rates can be modelled by pseudo first-order kinetics:

$$\frac{d[Py]_n}{dt} = k_{-1}[H_2Py]_n - k_1[Py]_n \quad (2)$$

$$\frac{d[H_2Py]_n}{dt} = f(t_n) \quad (3)$$

$[Py]_n$, $[H_2Py]_n$ ≡ molar concentrations of pyrene and dihydropyrene respectively, relative to the initial concentration of pyrene after n time intervals.

k_1, k_{-1} ≡ pseudo first-order rate constants.

$f(t_n)$ ≡ an empirical function derived by performing a least squares fit $[H_2Py]$ vs time data using piecewise cubic splines.

The values of k_1 and k_{-1} were determined by performing a minimization on F in equation (4):

$$F = \sum_j \left[\left([Py]_n \Big|_{t_n=t_j} - [Py]_j^* \right)^2 + \left([H_2Py]_n \Big|_{t_n=t_j} - [H_2Py]_j^* \right)^2 \right] \quad (4)$$

$[Py]_j^*$, $[H_2Py]_j^*$ ≡ experimental concentrations at time t_j.

$[Py]_n\Big|_{t_n=t_j}$, $[H_2Py]_n\Big|_{t_n=t_j}$ ≡ calculated concentrations at time t_j.

The values of $[Py]_n$ and $[H_2Py]_n$ were estimated by setting $[Py]_o = [Py]_o^* = 1$ and $[H_2Py]_o = [H_2Py]_o^* = 0$ and numerically integrating equations (2) and (3) using a fourth order Runge-Kutta algorithm.

RESULTS AND DISCUSSION

Qualitative aspects of the kinetics of pyrene hydrogenation may be obtained from curves of concentration vs time, at constant temperature and pressure, for the major species of the system. Figure 2 shows curves at 348°C and 1250 psig for the concentration of pyrene and 4,5-dihydropyrene (H_2Py) and Figure 3 for 4,5,9,10-tetrahydropyrene (H_4Py), 1,2,3,6,7,8-hexahydropyrene (H_6Py) and 1,2,3,3a,4,5-hexahydropyrene (I-H_6Py). As can be seen from the figures, the hydrogenated specie with the largest concentration is H_2Py followed by H_6Py, H_4Py and I-H_6Py. For these experiments, the concentration of deca- and perhydropyrenes was less than 1% of the product mixture.

The kinetics and thermodynamics of the formation of 4,5-dihydropyrene are discussed below with respect to the effect of catalyst/pyrene ratio, hydrogen pressure and temperature.

Catalyst/Pyrene Ratio. Figure 4 shows a plot of k_1 and k_{-1} vs catalyst weight for experiments performed at 348°C and 1250 psig pressure. As can be seen from Figure 4, k_1 for hydrogenation of pyrene and k_{-1} for dehydrogenation of dihydropyrene are proportional to catalyst weight, which is proportional to active surface area.

Hydrogen Pressure. From a plot of k_1 and k_{-1} vs H_2 pressure, Figure 5, it can be seen that while k_1 is linearly proportional to pressure up to 1250 psig, k_{-1} is relatively independent of pressure. This supports the assumption that equation (1) is the only reaction directly involving Py up to pressures of at least 1250 psig. However, the high forward rate constant at 2000 psig may indicate a change in reaction mechanism. In addition to the kinetic parameters, the pressure equilibrium constant and heat of reaction may be calculated for hydrogenation of Py to H_2Py. The pressure equilibrium constant K_p is defined as

$$K_p = \frac{1}{P_{H_2}} \frac{[H_2Py]}{[Py]} = \frac{1}{P_{H_2}} \frac{k_1}{k_{-1}} \qquad (5)$$

where P, the hydrogen partial pressure, is taken as the hydrogen fugacity. Based on the rate constants obtained at 348°C for 3 pressures and 3 catalyst/pyrene ratios, K_p was found to be $7.24 \times 10^{-4} \pm 0.61 \times 10^{-4}$ $psig^{-1}$. From K_p values obtained from the 374 and 394°C data, 4.77×10^{-4} and 3.14×10^{-4} $psig^{-1}$ respectively, the heat of hydrogenation ΔH of pyrene to dihydropyrene can be obtained from a van't Hoff plot shown in Figure 6. The enthalpy of hydrogenation was found to be -15 kcal/mole, which is comparable to values for hydrogenation of other polynuclear aromatics.[13]

Temperature. Figure 7 shows an Arrhenius plot of rate constants k_1 and k_{-1}. The apparent activation energies obtained from Figure 6 for the hydrogenation of pyrene and dehydrogenation of dihydropyrene were found to be 28 and 46 kcal/mole respectively for Shell 324 catalyst. As can be seen from Figure 7, although the forward and reverse rate constants are nearly equal at 348°C, the reverse rate constant is over twice that of the forward rate at 394°C. Therefore, although both reaction rate constants increase with temperature, dehydrogenation is favored over hydrogenation at temperatures above 350°C.

CONCLUSIONS

Ultimate application of this kinetic and thermodynamic data to direct coal liquefaction must take into consideration the conditions imposed by the particular process used. However, two generalizations may be made regarding hydrogen supplied by the dihydropyrene component of donor solvents: (1) Increasing hydrogen partial pressure increases both the rate at which H_2Py is formed and the equilibrium concentration of H_2Py. Therefore, pyrene rehydrogenation should be done at as high a pressure as is cost effective. (2) Although an increase in temperature favors the rate of attainment of equilibrium between Py and H_2Py, the position of the equilibrium is shifted toward pyrene. Temperature must therefore be adjusted to achieve an optimum trade-off between rate of formation and maximum possible concentration of H_2Py.

REFERENCES

1. "Recycling Solvents Works Wonders at SRC-I Plant", The Energy Daily, 11, No. 31, February 15, 1983.
2. H. D. Schindler, J. M. Chen, M. Peluso and J. D. Potts, "Liquefaction of Eastern Bituminous Coals by the ITSL Process", Proceedings of the 7th Annual EPRI Contractors' Conference on Coal Liquefaction, Palo Alto, CA, May 12, 1982, Electric Power Res. Institute, 1982.

3. T. W. Johnson, "Light SRC Recycle and Its Effect on Solvent Quality and the SRC Process", Proceedings of the 6th Annual EPRI Contractors' Conference on Coal Liquefaction, Palo Alto, CA, May 13, 1981, Electric Power Research Institute, October 1981.
4. L. L. Ansell, K. L. Trachte, and J. W. Taunton, "Bottoms Recycle Studies in the EDS Process Development", Proceedings of the 5th Annual EPRI Contractors' Conference on Coal Liquefaction, Palo Alto, CA, May 12-13, 1980, Electric Power Research Institute, 1980.
5. F. J. Derbyshire and D. D. Whitehurst, "Study of Coal Conversion in Polycondensed Aromatic Compounds", Fuel 60, 655 (1981).
6. F. J. Derbyshire, P. Varghese and D. D. Whitehurst, "Synergistic Effects Between Light and Heavy Solvent Components During Coal Liquefaction", Fuel 61, 859 (1982).
7. S. A. Qader, "Hydrocracking of Polynuclear Aromatic Hydrocarbons Over Silica-Alumina Based Dual Functional Catalysts", Chem. of Petroleum Proc. and Extraction II, p. 10 (1976).
8. J. Shabtar, L. Veluswamy and A. G. Oblad, "Steric Effects in Phenanthrene and Pyrene Hydrogenation Catalyzed by Sulfided Ni-W/Al_2O_3", Prep. Amer. Chem. Soc., Div. of Fuel Chemistry, 23 (1), 107 (1978).
9. L. R. Veluswamy, "Catalytic Hydrogenation of Coal-Derived Liquids and Related Aromatic and Heterocyclic Compounds", Ph.D. Dissertation, Univ. of Utah (1977).
10. K. P. Johnston, "Hydrogenation-Dehydrogenation of Pyrenes Catalyzed by Sulfided Cobalt-Molybdate at Coal Liquefaction Conditions", Fuel, in press.
11. B. R. Rogers, R. L. Jolly and R. M. Whan, "ITSL Solvent Quality Studies", Proceedings of the Dept. of Energy Integrated Two-Stage Liquefaction Meeting, Albuquerque, NM, October 1982.
12. R. J. Kottenstette, "Oil-Soluble Coal Liquefaction Catalyst Screening", SAND-82-2495, Sandia National Laboratories, Albuquerque, NM, March 1983.
13. E. Gorin, "Fundamentals of Coal Liquefaction", p. 1873, in Chemistry of Coal Utilization, 2nd Supplementary Volume, Martin A. Elliot, Ed., 1981.

FIGURE 1

STRUCTURES FOR PYRENE AND HYDROGENATED PYRENES

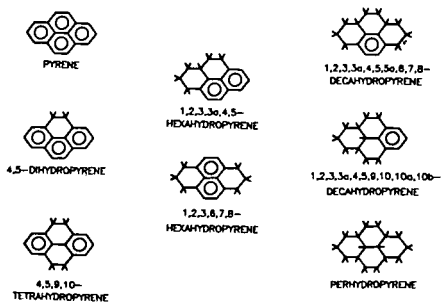

FIGURE 2

CONCENTRATIONS OF PYRENE AND DIHYDROPYRENE
(348 °C, 1250 PSIG, 15 MG SHELL 324)

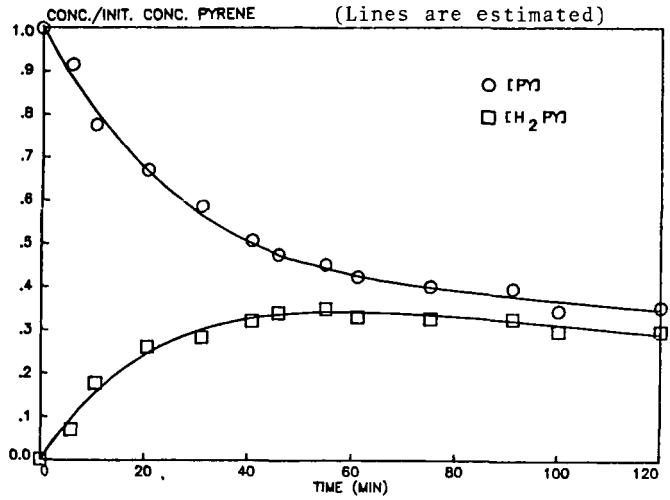

FIGURE 3

CONCENTRATIONS OF TETRA AND HEXA HYDROPYRENES
(348 °C, 1250 PSIG, 15 MG SHELL 324)

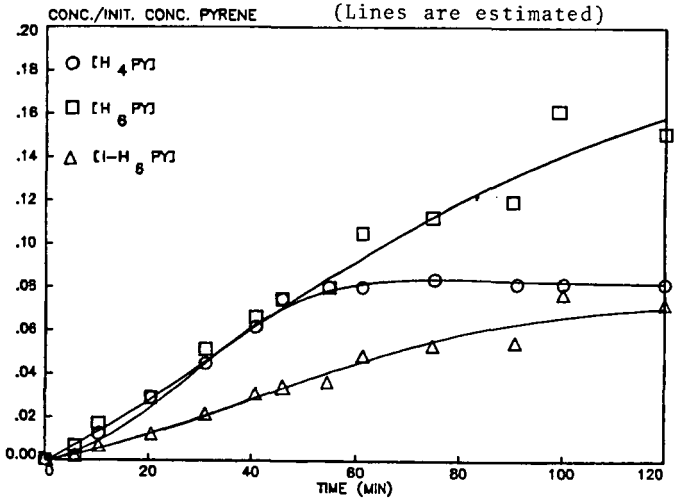

FIGURE 4

DEPENDENCE OF RATE CONSTANTS ON CATALYST LEVEL
(348 °C, 1250 PSIG, SHELL 324)

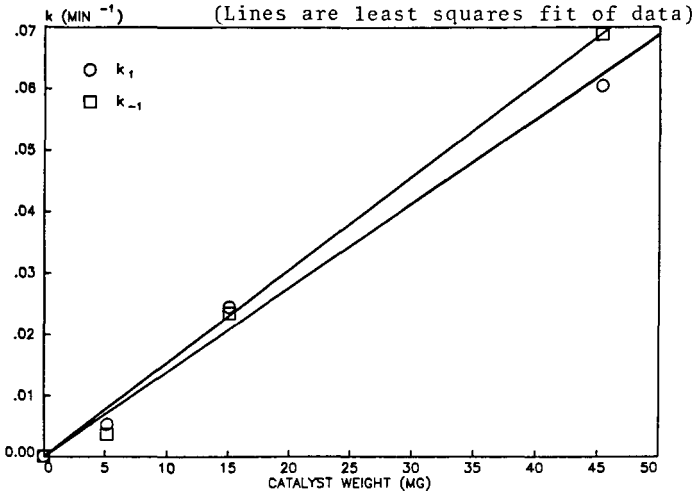

FIGURE 5

DEPENDENCE OF RATE CONSTANTS ON PRESSURE
(348 °C, 15 MG SHELL 324)

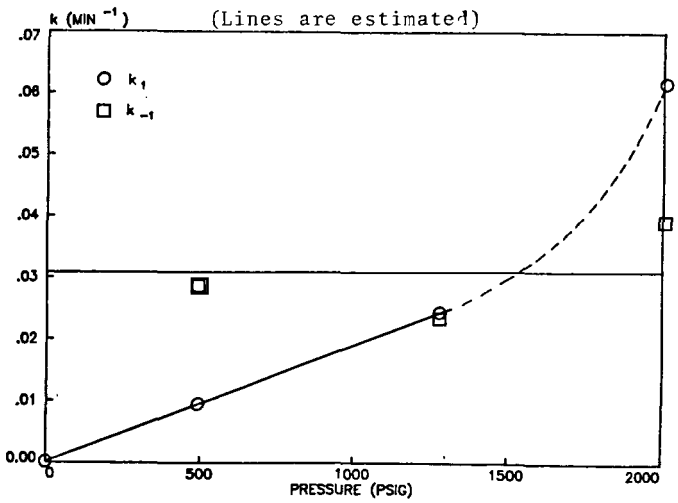

FIGURE 6

ENTHALPY OF HYDROGENATION REACTION
(348 °C, 1250 PSIG, 15 MG SHELL 324)

(Lines are least squares fit of data)

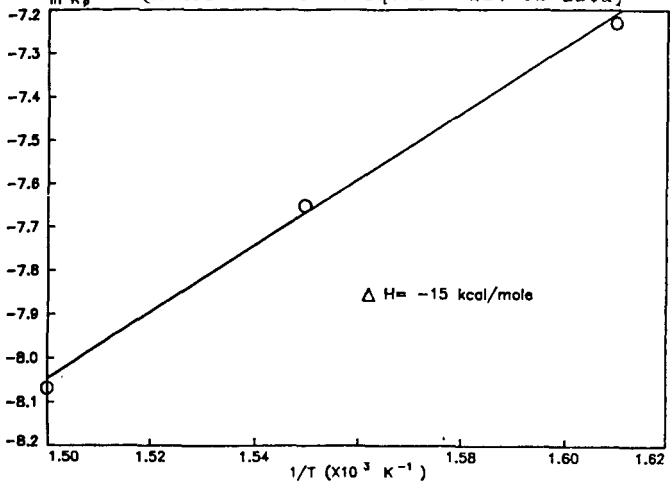

FIGURE 7

ARRHENIUS PLOT OF RATE CONSTANTS
(1250 PSIG, 15 MG SHELL 324)

(Lines are least squares fit of data)

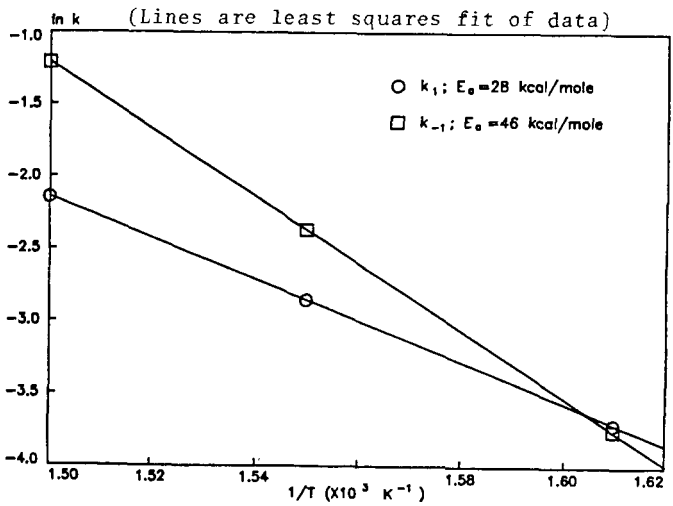

In-Situ Study Under Direct Coal Liquefaction Conditions of the Surface Interaction Between Iron Sulfides and Selected Number of Model Compounds

P.A. Montano, A.S. Bommannavar and Y.C. Lee

Department of Physics, West Virginia University
Morgantown, West Virginia 26506

Abstract:

The importance of iron sulfides in direct coal liquefaction has been noted by several investigators; an increase in coal conversion and quality of the products has been observed in their studies. In order to gain a better understanding of the role of iron sulfides in coal liquefaction we have investigated "in-situ" the interaction of FeS_2 and Fe_7S_8 with a series of model compounds. In our experiments 10% catalysts by weight were added to the model compounds. The model compounds studied were dibenzothiophene, pyrene, phenanthrene, 1,4-naphthoquinone, phenothiazine, and quinoline. The experiments were performed in nitrogen and hydrogen atmospheres. We find evidence of interaction between the pyrrhotites and some of the model compounds. The formation of intermediate iron oxides in 1,4-naphthoquinone indicates a strong interaction between the iron on the pyrrhotite surface and oxygen. The surface composition of pyrrhotite at 450°C was also studied in a UHV reaction chamber and the interaction with H_2, O_2 and CO was investigated using electron energy loss spectroscopy.

I. INTRODUCTION

Direct coal liquefaction is a process that has been known for a number of years. The liquefaction of coal is a complex process involving a close interaction between coal, hydrogen-donor solvent, and catalysts. The role of mineral matter and particularly iron sulfides in coal liquefaction has been the subject of several investigations (1-3). Mukherjee and Chowdbury observed an increase in coal conversion in the presence of mineral matter (2). Recycling the mineral matter tends to increase the reaction rate and enhance the conversion of pyridine-solubles to benzene solubles (4). The addition or presence of pyrite enhances the production of liquid products from coal (5). The specific effect of each mineral has not been well established (6) because some of the minerals occur in very small amounts. Some of the clay minerals may have only a simple physical effect (6). All the experimental results suggest the iron sulfides as the most actively involved minerals in coal liquefaction.

It has been observed that the conversion to liquid products for four different coals correlates with the stoichiometry of the pyrrhotites present in the residues (7). Stephens et.al. (8) carried out a series of experiments with various additives on an ILL#6 coal and observed an enhancement in conversion to benzene solubles with the addition of pyrrhotite and H_2S. Mössbauer studies (9,10) of the iron sulfides in coal indicate the existence of an interaction between coal components and the pyrrhotites at high temperatures. These experiments suggest an active role of the pyrrhotites in coal liquefaction. However, still many questions remain unanswered concerning the catalytic roles of H_2S and $Fe_{1-x}S$. Lambert points out that the catalytic activity observed for pyrite is solely due to H_2S acting as a hydrogen transfer catalyst (11).

More research is needed in order to clearly distinguish between the role of H_2S and the behavior of the pyrrhotites during coal liquefaction. In a complex material such as coal, it is difficult to identify the roles of vastly differing organic functional groups and their interaction with $Fe_{1-x}S$ and/or H_2S. A simpler approach

is the study of model compounds. Several studies have appeared in the literature on the effect of pyrite and pyrrhotite on model compounds. Guin et.al.(12) studied the hydrogenolysis of benzothiophene in the presence of pyrite. The main product was 2,3-dihydrobenzothiophene. When pyrite was used, the selectivity was shifted toward ethylbenzene. Pyrite seems to catalyze the hydrogenation of pyrene to dihydropyrene (13). Bockrath and Schroeder (14) observed that when pyrrhotite is heated in tetralin, only dehydrogenation is catalyzed. We report in the present work "in-situ" Mossbauer measurements of FeS_2 and Fe_7S_8 in six different model compounds. The behavior of the sulfide surfaces is also studied using electron energy loss spectroscopy. In addition, the changes taking place on the surfaces during reactions with simple gases are investigated using this technique.

Experimental

The "in-situ" Mössbauer measurements were carried out using the reactor shown in Figure 1. A more detailed description of this reactor can be found in Reference (9). The FeS_2 and Fe_7S_8 additives used were from natural mineral samples and were characterized by x-ray diffraction and Mössbauer spectroscopy. In the experiments with model compounds, 10% catalyst (200 mesh) by weight was added and mixed with 1 gm of the model compounds. The model compounds studied using Mössbauer spectroscopy were pyrene, phenanthrene, dibenzothiophene, 1,4-naphthoquinone, phenothiazine and quinoline. The experiments were carried out at 440°C in a nitrogen or hydrogen atmosphere. The reaction time was one hour. The residues were measured at room temperature. The stoichiometry of the pyrrhotites present in the residues was determined using the method described in references (7,15). Data acquisition and analysis were conducted on a microprocessor-based computer. The source was a 200 mCi ^{57}Co:Rh. All the isomer shift values are given in reference to α-Fe at room temperature. The surface properties of FeS_2 and Fe_7S_8 we studied using Auger and electron energy loss spectroscopy. The samples were mounted in an UHV chamber with a specially-designed high pressure reactor. In this reactor the samples were exposed to various gases (CO, H_2, O_2) and high temperatures.

II. EXPERIMENTAL RESULTS AND DISCUSSION

Mössbauer Measurements

The most important Mössbauer parameters in the study of the transformations and interactions of iron sulfides in coal are the isomer shift, the magnetic hyperfine and quadrupole splittings. The isomer shift (IS) results from the electrostatic interaction of the nuclear and electron charge distributions inside the nuclear region. The observed IS in the Mössbauer spectrum is the difference between the shifts in the source and absorber. The IS is given by the following relation:

$$IS = \frac{2\pi}{5} Ze^2R^2 \frac{\delta R}{R} \left(|\Psi_{abs}(0)|^2 - |\Psi_s(0)|^2 \right) \quad (1$$

The quantity $\delta R/R$ is a nuclear property and can be estimated using well characterized standards. The IS gives unique information on the valence state of the Mössbauer atom or ion. The range of IS values for iron compounds in reference to α-Fe covers values between -0.78 mm/sec for Fe^0 isolated in nitrogen to +1.9 mm/sec for Fe^+. (1 mm/sec = 0.48 x 10^{-7}eV for the 14.4 keV transition of ^{57}Fe.) The IS values reported include the second order Doppler shift (SODS). The SODS can

be easily distinguished by its temperature dependence. Its contribution to the present work is not large enough to justify the correction of the measured centroid.

The magnetic hyperfine splitting arises from the interaction of the nuclear dipole moment with a magnetic field due to the atom's own electrons. The Hamiltonian describing this interaction can be written as:

$$H_m = -\left(\frac{\mu}{I} M_I B\right) \qquad (2$$

where I is the spin of the nucleus, μ is the magnetic moment, M_I the magnetic quantum number, and B the magnetic field at the nucleus. For a pure magnetic interaction six transitions are possible between the 14.4 keV level (I=3/2) and the ground state (I=1/2). The presence of vacancies in the pyrrhotites results in a lower magnetic field at the iron ion; this feature is used to calculate the stoichiometry of the pyrrhotites in coal liquefaction residues. The atomic percentage of iron is calculated according to (15)

$$\text{at.\%Fe} = 100 \times \left[0.6836 \times 10^{-3} \times \bar{H}_{mhf} + 0.2881\right]$$

$$\bar{H}_{mhf} = \frac{1}{A_{Total}} \sum_i A_i H_i \qquad (3$$

$\bar{H}_{mhf}$ = average magnetic hyperfine field

A_{Total} = total Mössbauer spectral area

A_i = spectral area under i-th site

H_i = mhf on i-th site

The quadrupole splitting (QS) occurs when the Mössbauer ion electrons and/or the neighboring atoms produce an inhomogeneous electric field at the nucleus and when the nucleus possesses a quadrupole moment. The quadrupole splitting for the excited state 14.4 keV of ^{57}Fe is given by

$$QS = \frac{1}{2} e^2 qQ \left(1 + \frac{\eta^2}{3}\right)^{1/2}$$

where

$eq = V_{ZZ}$ = principal axis of the field gradient tensor

$$\eta = \frac{V_{XX} - V_{YY}}{V_{ZZ}} = \text{asymmetry parameter}$$

Q = quadrupole moment of the nucleus

The combination of IS and QS is very useful in the identification of minerals in coal. The procedure followed is to measure these parameters for standard well characterized compounds and to compare with the values obtained for the coal minerals.

The above Mössbauer parameters will be used to study the transformations and inversions of several model compounds with FeS_2 and Fe_7S_8.

A. Interaction and Decomposition of FeS_2 in the Presence of Model Compounds

Pyrene: Pyrite partially decomposes in the presence of pyrene even in the absence of hydrogen. The observed IS at 440°C for the sample in a nitrogen atmosphere is close to zero. The spectrum shows a well-defined doublet with a quadrupole splitting (QS) close to the value observed for pure pyrite. The spectrum of the residue shows the presence of a pyrrhotite with a stoichiometry close to that observed for Fe_7S_8, about 46% of the original pyrite remains unreacted. The conversion of pyrite to pyrrhotite is larger than the one obtained in the absence of pyrene. In the presence of H_2 the transformation of pyrite to pyrrhotite is complete. At 440°C the Mössbauer spectrum shows only a broad singlet with an IS = 0.35 mm/sec, this value is smaller than the one obtained for the pure pyrrhotites in the absence of pyrene (Table I). This is given as evidence of an interaction between the pyrrhotite and the gases present in the reactor. It is possible that what we observed in this experiment is an intermediate state of the iron on the pyrrhotite, probably interacting with molecular hydrogen and pyrene. The hexagonal pyrrhotite obtained after the reaction is very similar to the one observed in residues from coal liquefaction. H_2S apparently does not play any other role but that of controlling the H_2/H_2S ratio in the reactor.

Phenanthrene: The results of the Mössbauer measurements in a nitrogen atmosphere are very similar to those obtained for pyrene. There is partial conversion to $Fe_{1-x}S$ and the presence of a doublet with parameters close to those of pyrite at 440°C (no real evidence of an interaction). By contrast in the presence of hydrogen, the IS at 440°C is the same of pure $Fe_{1-x}S$. The conversion of pyrite to pyrrhotite is complete (Table II). We must again emphasize that the conversion of pyrite in the presence of the model compound is faster than in the absence of phenanthrene. If there is hydrogenation (1) of the phenanthrene, it is possible that the pyrrhotite does not play any direct role, or that the intermediates decompose faster than 10^{-7} sec (the lifetime of the Mössbauer level).

Dibenzothiophene: In the presence of this compound and in a nitrogen atmosphere, pyrite fully decomposes to $Fe_{1-x}S$. The pyrrhotite formed from this reaction has a stoichiometry close to that of Fe_7S_8 (Table II). There is evidence of interaction with DBZ at 440°C, a doublet is observed with IS close to zero and QS = 0.63 mm/sec (Figure 2). These values are similar to those of pyrite, however there is no pyrite left in the residues (Figure 3). In a hydrogen atmosphere the Mössbauer spectrum at 440°C is very different from that observed in nitrogen. A single Mössbauer line with an IS = 0.36 mm/sec is observed. The residue of this run is an hexagonal pyrrhotite. The present results indicate a reaction with the pyrrhotite. It is very probable that hydrogenation is the major catalytic role of the pyrrhotites in this system.

Phenothiazine: There is partial decomposition of pyrite in a nitrogen atmosphere, however in this case there is less decomposition than for pyrene or phenanthrene. Decomposition takes place in the presence of hydrogen but it is incomplete. The IS and QS at 440°C are clearly due to the unreacted pyrite (Table II). These measurements do not indicate any kind of strong reaction for FeS_2 or $Fe_{1-x}S$ with the model compounds. If any reaction occurs, it is very weak compared to pyrene, phenanthrene or DBZ.

Quinoline: There is only partial decomposition of pyrite to pyrrhotite in nitrogen or hydrogen atmospheres. The stoichiometry of the pyrrhotite present in the residues is very close to Fe_7S_8. In order to obtain such a stoichiometry, a high partial pressure of H_2S must be present in the reactor. The Mössbauer spectrum at 440°C can be attributed to FeS_2 alone; there is a very small contribution from the pyrrhotite and no evidence of reaction. These results suggest no active role for the pyrrhotite in catalyzing the hydrogenation of quinoline to tetrahydroquinoline

(THQ), only H_2S remains as a possible catalyst. We will come back to this problem when discussing the interaction with Fe_7S_8.

1,4-Naphthoquinone: A very interesting result is obtained when the reaction takes place in a nitrogen atmosphere. It is observed that Fe_3O_4 is present in the residue. In order for this to happen the pyrrhotite formed from the partial decomposition of pyrite must react with the oxygen present in the model compound. In a hydrogen atmosphere the magnetite is absent from the final products and full conversion of pyrite to pyrrhotite occurs. The present results indicate a strong affinity of the pyrrhotite surface towards oxygen, and indicates that breaking of oxygen bonds in coal is a possible mechanism by which coal conversion is enhanced.

B. Interactions and Transformations of $Fe_{7-8}S$ in the Presence of Model Compounds. (All the experiments in a hydrogen atmosphere.)

Pyrene: A single Mössbauer line is observed at 440°C with an IS ≈ 0.35 mm/sec. The residue shows the presence of FeS (troilite) and $F_{1-x}S$ with 48.2 at% Fe (Table III). Figures 4 and 5 show the Mössbauer spectra for this run at 440°C and room temperature respectively. The presence of troilite requires a very low partial pressure of H_2S in the reactor. This is not totally unexpected since the amount of free sulfur available from Fe_7S_8 is very limited. There is evidence of a reaction with the pyrene, but the sulfides obtained in this case differ markedly from those obtained for FeS_2. This difference may be attributed to the excess of H_2S when pyrite is the precursor of pyrrhotite.

Phenanthrene: The Mössbauer measurements in this case give very similar results to the ones obtained for pyrene. There is a reaction at 440°C; there troilite is present in the residues. These results contrast with the ones obtained when pyrite is added to phenanthrene. There is a marked difference between the behavior of the nascent pyrrhotite and Fe_7S_8. The excess of sulfur atoms on the pyrite surface is probably responsible for such a difference.

DBZ: There is evidence of a reaction at high temperatures (IS = 0.30 ± 0.06 mm/sec). The residue contains troilite. Since DBZ has sulfur, there must be a reaction between H_2S and the compound in order to effectively reduce the partial pressure of H_2S and allow the formation of FeS. There is evidence of active involvement of H_2S in the reactions.

Quinoline: There is some evidence of a reaction at high temperature (440°C), the IS = 0.40 ± 0.07 mm/sec close to that of pure pyrrhotite, but still slightly more negative. The residue of this run does not show any FeS, the pyrrhotite obtained has 48.2 at.% iron. We attribute this behavior to the presence of unreacted H_2S, otherwise FeS can be formed. This behavior is different from that observed for pyrite, again pointing out the difference between the nascent pyrrhotite (from pyrite) and Fe_7S_8.

Phenothiazine: Similar results to those obtained for quinoline, but in this case the at.% iron in the residues is lower (Table III). This last result is clear evidence of a higher partial pressure of H_2S in the reactor. This behavior contrasts with the one observed for DBZ. In both molecules sulfur is present, however in phenothiazine there is also nitrogen. It is tempting to attribute some reactivity to the pyrrhotite and nitrogen, although the present experimental evidence is insufficient to characterize pyrrhotite as an HDN catalyst.

1,4-Naphthoquinone: No troilite is observed in the residues; hexagonal pyrrhotite is obtained with 48.1 at.% iron. Results are very similar to the ones obtained for FeS_2.

In the present experiments we have studied the reactions of FeS_2 and Fe_7S_8 with

a selected number of model compounds. From the results of such experiments we suggest that one of the mechanisms by which pyrrhotite enhances coal liquefaction is through interactions with oxygen bonds in coal. There is also evidence from the present experiments as well as those reported in the literature that the pyrrhotites act as hydrogenation catalyst. However, the role of H_2S cannot be completely ignored. There is clear evidence of direct involvement of H_2S in the reactions. The reactions with nitrogen compounds are not very clear and more work remains to be done in this area of research. We are of the opinion that hydrodesulfurization has to be excluded as one of the roles of the pyrrhotites. In the following paragraph we will discuss the behavior of the pyrrhotite surfaces interacting with simple gases.

Electron Energy Loss Measurements

Normal incidence was used for the EEL measurements. The EEL spectra were measured in the second derivative mode for various primary electron energies (50 eV, 150 eV, 250 eV). A small modulation was applied to the CMA (v_{pp}=1 volt) and used as a reference signal. The major impurities were carbon and oxygen. The samples were subjected to Ar^+ ion bombardment for several cycles until a clean surface was obtained.

Electron energy loss spectroscopy is strongly surface sensitive. By varying the electron primary energy one is able to distinguish between volume and surface properties (16). Interband and intraband transitions can be identified with this technique. Ionization losses can be easily studied using electron energy loss spectroscopy. In the present work the major ionization losses studied are the $M_{2,3}$ and M_1 of sulfur and iron.

A. EEL Study of Fe_7S_8 At High Temperatures and in the Presence of CO, O_2 and H_2

Effect of Temperature: The effect of temperature on the EEL spectrum of a single crystal of Fe_7S_8 is shown in Figure 6 (Ep=150eV). One observes the transformation of the EEL spectrum as the temperature is increased, at 320°C there is iron enrichment of the surface. This is detected by the observed enhancement of peak C (surface plasmon of Fe). The peaks J,K are due to a 3p →3d transition ($M_{2,3}$ levels of iron). At 450°C the spectrum of the iron sulfide is different from that observed at RT with B peak shifted in energy from 5.1 to 6.2 eV. The new iron sulfide on the surface has a different electronic structure although some iron character is retained.

Interaction with Co, O_2 and H_2: The Auger spectrum of Fe_7S_8 after reaction with CO (4×10^{-4} torr) at 450°C is shown in Figure 7. One observes the presence of oxygen on the surface. This oxygen is bonded to the iron in the pyrrhotite. This is clearly seen in Figure 8 where the low energy iron Auger peak shows the characteristic shape of the oxide (a strong doublet around 50 eV). No carbon is detected on the surface; the absence of carbon can be explained only by the formation of some volatile species of carbon and sulfur (like CS_2). The electron energy loss spectrum at Ep=150eV is shown in Figure 9. The two strong peaks at low energies are characteristic of the Fe-O system. The Auger spectrum for Fe_7S_8 exposed to O_2 (4×10^{-4} torr, 450°C for five minutes) is shown in Figure 7. One can observe the strong similarities with the spectrum obtained for CO exposure. In Figure 9 the EEL spectrum for oxygen exposure is also shown. There is a great similarity to that of Fe_7S_8 exposed to CO. The lower J,K peak positions and sharpness are characteristic of iron oxides. If hydrogen is used instead of O_2 or CO one obtains the spectrum shown in Figure 9. This spectrum is that of an iron sulfide where some of the sulfur has been removed from the surface. The iron character of the surface is still retained as shown by the presence of the 3p →3d

transitions. If a combination of CO/H_2 (1:1) is used at 450°C the oxygen is totally removed from the surface (formation of H_2O). The iron sulfide surface is restored but with a stoichiometry different from that of Fe_7S_8. In all the experiments described here, a clean Fe_7S_8 sample was used as a starting material. An iron foil doped on the surface with sulfur was also studied using EEL spectroscopy. A very similar spectrum to that obtained at 450°C for Fe_7S_8 was measured. Such a result indicates a strong iron character of the pyrrhotite surface.

B. EEL Study of FeS_2 at High Temperatures and in the Presence of CO, O_2 and H_2

A typical energy loss spectrum of a pyrite single crystal surface is shown in Figure 10 (top). After heating the sample to 220°C one observes a dramatic change in the spectrum. We attribute this change to the presence of elemental sulfur, and probably some $Fe_{1-x}S$. At 320°C the spectrum of the surface is more similar to that of $Fe_{1-x}S$. It is noted that the 3p→3d transitions show the presence of more than two lines. This spectrum for the J,K transitions can be produced by the presence of two iron species ($Fe_{1-x}S$ and FeS_2). At 450°C the surface is that of pyrrhotite with no pyrite character retained. The spectrum is almost identical to that obtained at 450°C from Fe_7S_8 (Figure 7). We want to point out that the high temperature pyrrhotite is not Fe_7S_8.

The behavior of pyrite at 450°C in the presence of CO and O_2 contrasts markedly with that of Fe_7S_8 (see Figures 10 and 11). We believe that this difference in the EEL spectra between the two samples is related to the excess of elemental sulfur present on the pyrite surface at 450°C. This excess of sulfur does not permit the iron in the pyrrhotite to react with CO or oxygen. If H_2 is used as a gas instead of CO or O_2 a small change is observed in the EEL spectrum, probably due to the removal of the sulfur from the surface. If a combination of CO/H_2 (1:1) is used in the reactor, an EEL spectrum very similar to that observed for Fe_7S_8 is obtained. In this case elemental sulfur is removed from the surface and the surface behaves as that of a pure pyrrhotite.

In conclusion we find that the major difference in the behavior of the pyrrhotite and pyrite surfaces at high temperature is due to the presence of an excess of sulfur on the latter. We also observe that the pyrrhotite surface has a strong iron character and great affinity to oxygen. Although the present study is only on very simple gases, these gases are present in the reactor during direct coal liquefaction.

Acknowledgement: The authors want to acknowledge the financial support of the U.S. DOE.

REFERENCES

1. Davidson, R.M., "Mineral Effects in Coal Conversion," Report No ICTIS/TRZZ (1983). IEA Coal Research, London, Excellent review.

2. Mukherjee, D.K. and Chowdbury, P.B., FUEL (1976), 55, 4.

3. Hodek, W., Chemical and Physical Valorization of Coal, Roundtable Meeting, Liege EUR-5954-d/e/f/i, Luxembourg 87-103 (1978).

4. Granoff, B., Thomas, M.G., Baca, P.M., and Noles, G.T., ACS Div. of Fuel Chem. Preprints 23(1), 23 (1978).

5. Illig, E., "Disposable Catalysts in Coal Liquefaction," DOE, Albuquerque, NM (1978).

6. Gray, D., FUEL 57, 213 (1978).

7. Montano, P.A. and Granoff, F., FUEL 59, 214 (1980).

8. Stephens, H.P., Stohl, F.V., and Padrick, T.D., 368-373 "International Conference on Coal Science," Düsseldorf (1981), Verlag Glück Auf.

9. Montano, P.A., Bommannavar, A.S. and Shah, V., FUEL 60, 703 (1981).

10. Bommannavar, A.S. and Montano, P.A., FUEL 61, 523 (1982).

11. Lambert, J.M., Jr., FUEL 61, 777 (1982).

12. Guin, J.A., Lee, J.M., Fan, C.W., Curtis, C.W., Lloyd, J.L., and Tarrer, A.R., Ind. Eng. Chem. Process Des. Dev. 19, 440 (1980).

13. Derbyshire, F.J., Varghese, P., and Whitehurst, D.D., Proceedings of the International Conference on Coal Science, Düsseldorf (1981), Verlag Glück Auf, GMBH Essen, p. 336.

14. Bockrath, B.C. and Schroeder, K.T. in "New Approaches in Coal Chemistry," Eds. D.P. Blaustein, B.C. Bockrath and S. Friedman, ACS Symposium, Series 169, Ch11 (1981).

15. Montano, P.A., Magnetic Resonance Review, 7(3), 175-96 (1982).

16. Colavita, E., DeCrescenzi, M., Papagno, L., Scarmozzino, R., Caputi, L.S., Rosei, R., and Tosatti, F., Phys. Rev. B 25, 2490 (1982).

Table I

ISOMER SHIFT AT 420 °C

Sample	I.S. ($mmsec^{-1}$) (at 420 °C)
IL6	0.38 ± 0.05
KY 9/14	0.34 ± 0.05
Powhatan 5	0.35 ± 0.05
Blacksville #2	0.21 ± 0.05
Fe_7S_8	0.50 ± 0.03
FeS	0.51 ± 0.05

TABLE III

Compositions of the residues obtained from Fe_7S_8 + H_2 + model compounds

Dibenzothiophene	$Fe_{1-x}S$	(25%) : at.% Fe	48.2 ± 0.1
	FeS	(75%)	
Pyrene	$Fe_{1-x}S$	(11%): at.% Fe	48.2 ± 0.1
	FeS	(89%)	
Phenanthrene	$Fe_{1-x}S$	(23%): at.% Fe	47.7 ± 0.1
	FeS	(77%)	
1,4 Naphthoquinone	$Fe_{1-x}S$	(100%): at.% Fe	48.1
Phenothiazine	$Fe_{1-x}S$	(100%): at.% Fe	47.6
Quinoline	$Fe_{1-x}S$	(100%): at.% Fe	48.2

TABLE II

Mössbauer Parameters

COMPOUND	IS mm/s T=440°C	FeS_2 + N_2 QS mm/s T=440°C	RESIDUES at RT	IS mm/s T=440°C	FeS_2 + H_2 QS mm/s T=440°C	RESIDUES at RT
Dibenzothiophene	~ 0.0	0.63 ± 0.1	$Fe_{1-x}S$ at.%Fe 46.8	0.36 ± 0.05	-	$Fe_{1-x}S$ at.%Fe 48.2
Pyrene	~ 0.0	0.57 ± 0.1	FeS_2 (47%) $Fe_{1-x}S$(53%) at.% Fe 46.8	0.35 ± 0.05	-	at.%Fe 47.8
Phenanthrene	~ 0.0	0.45 ± 0.1	FeS_2 (24%) $Fe_{1-x}S$(76%) at.%Fe 46.8	0.50 ± 0.05		at.%Fe 48.1
1,4 Naphthoquinone	~ 0.04	0.57 ± 0.05	FeS_2 (70%) Fe_3O_4 $Fe_{1-x}S$ 46.7 at.%Fe	0.02 ± 0.05	0.53 ± 0.05	$Fe_{1-x}S$ at.% Fe 48.0
Phenothiazine	~ 0.04 ± 0.05	0.58 ± 0.05	FeS_2 (82%) $Fe_{1-x}S$ (18%) 46.8 at.%Fe	0.0	0.61 ± 0.05	FeS_2 (17%) $Fe_{1-x}S$ (83%)
Quinoline	~ 0.03 ± 0.05	0.56 ± 0.05	FeS_2 (73%) $Fe_{1-x}S$(27%) 46.7 at.%Fe	0.0	0.55 ± 0.05	FeS_2(64%) $Fe_{1-x}S$(26%) at.% Fe 47.8

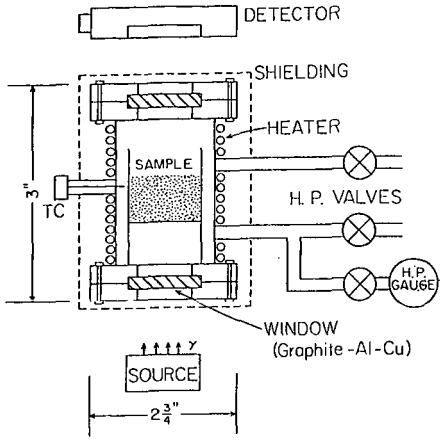

FIGURE 1 Reactor for Mössbauer "in-situ" measurements.

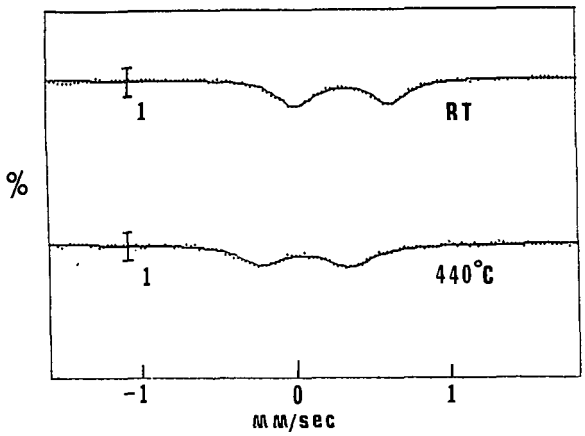

FIGURE 2 Mössbauer spectra at RT for a mixture of FeS_2 and DBZ.

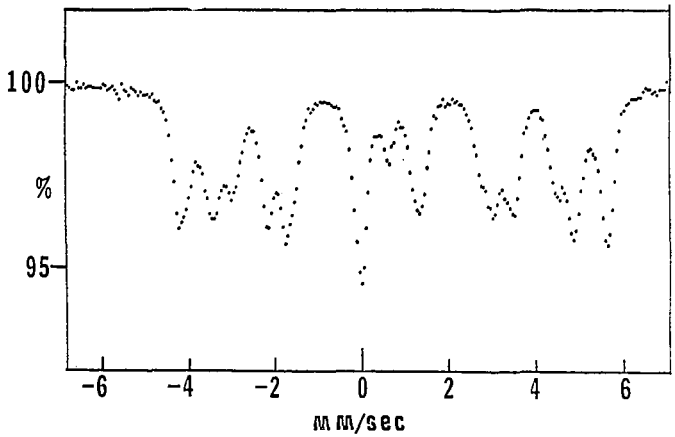

FIGURE 3 Mössbauer spectra at RT of the residue of the reaction of FeS_2 and DBZ.

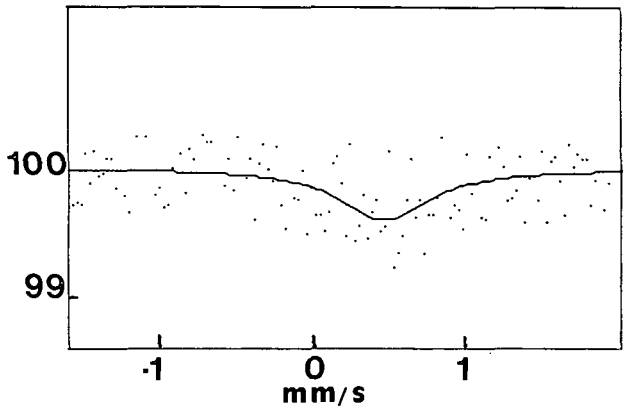

FIGURE 4 Mössbauer spectra at 450°C of Fe_7S_8 and pyrene in a hydrogen atmosphere.

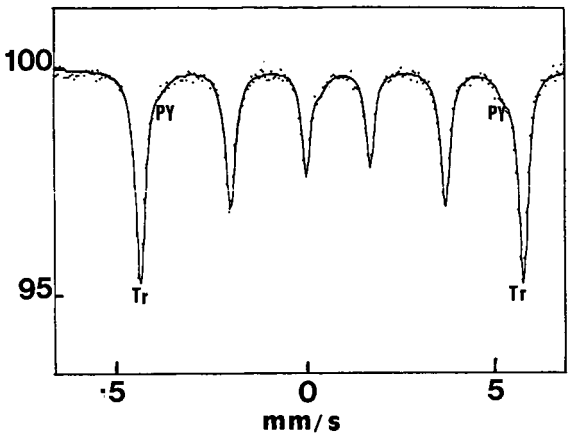

FIGURE 5 Mössbauer spectra of the residue of the reaction of Fe_7S_8 with pyrene. Tr: troilite
Pr: pyrrhotite

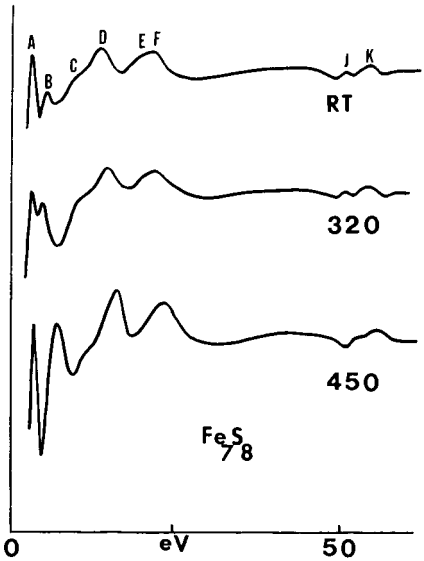

FIGURE 6 EEL spectra of Fe_7S_8 at various temperatures.

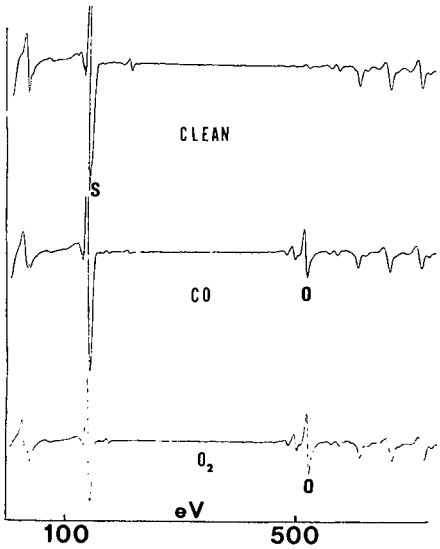

FIGURE 7 Auger spectra of Fe_7S_8 after a reaction with CO and O_2.

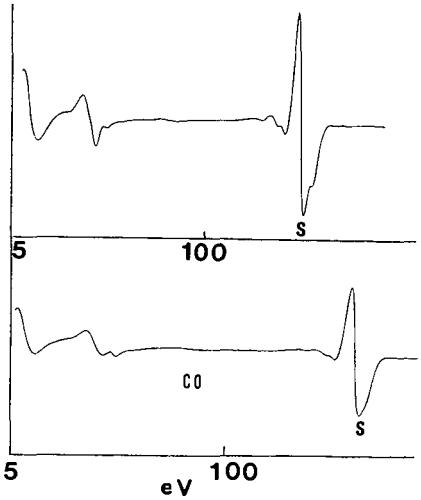

FIGURE 8 Auger spectra of Fe_7S_8 at low energies, clean and in the presence of CO (450° C).

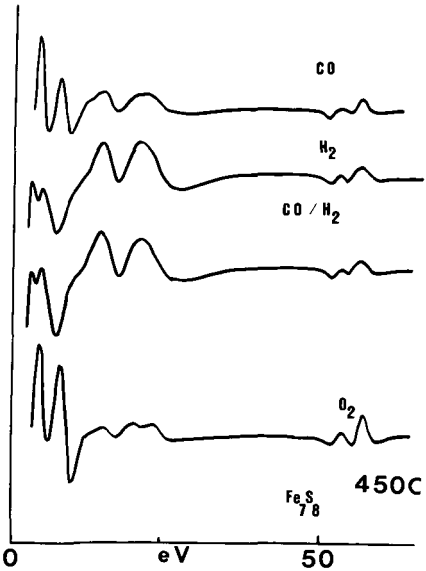

FIGURE 9 EEL spectra of Fe_7S_8 after reactions at 450° C with CO, H_2 and O_2.

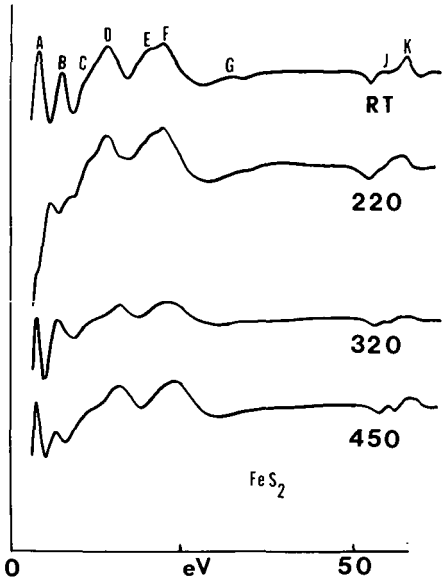

FIGURE 10 EEL spectra of FeS_2 after heating to various temperatures (RT to 450° C).

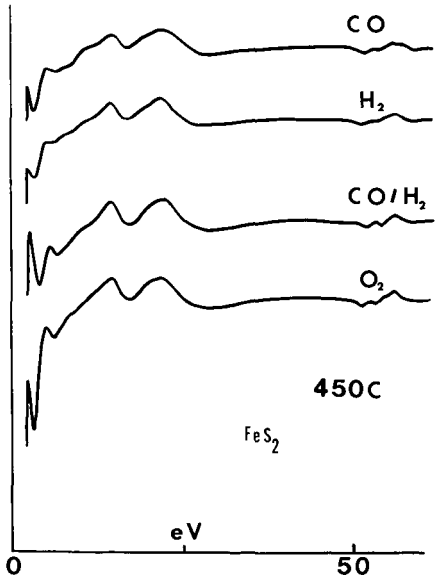

FIGURE 11 EEL spectra of FeS_2 after reaction with CO, H_2 and O_2 at 450° C.

IRON-BASED CATALYSTS, H_2S AND LIQUEFACTION

Virgil I. Stenberg, K. Tanabe, T. Ogawa, P. Sweeny and R. Hei

University of North Dakota, Grand Forks, North Dakota 58202

INTRODUCTION

One of the most promising advances of the past 50 years of coal liquefaction catalysis is learning of the iron and sulfur synergism. Now with the promotional effects of hydrogen sulfide demonstrated (1) and its mechanism of action being unveiled (2,3), the interaction of hydrogen sulfide with iron needs to be understood for explaining the basis of presulfiding catalysts and for new catalyst design. Presulfiding metal oxide hydrogenation catalysts has long been known to enhance liquefaction yields. However, the chemistry-based reason(s) for the enhancement is unclear. The metal oxides are probably converted to a mixed oxide-sulfide under sulfur-rich conditions. Using differential thermal analysis under high pressure for coal hydrogenation, Takeya (4) rates red mud + S at 297°C as having better catalytic activity than red red mud at 429°C. A combination of iron oxides and sulfur have been used for coal liquefaction effectively (5,6).

In related studies, Beardon and Aldridge have patented the pretreatment of coal with hydrogen sulfide to enhance conversions (7). Gatsis (8) utilized 4 to 8 volume percent hydrogen sulfide (based on hydrogen gas) to enhance the conversion of bituminous coal (Pittsburgh Seam Coal) into a more filterable, higher hydrogen content product using a solvent. The operating conditions in the extraction zone were 250°-500°C and 500 to 5,000 psig with a solvent to coal weight ratio of 0.2 to 10 and a residence time from 30 seconds to 5 hours. If hydrogen is not present in the extraction zone, then it is recommended that the H_2S amount be increased to 40% based upon the amount of coal fed into the extraction zone. Hettinger has shown that hydrogen sulfide causes a significant increase in hydrocracking (9). Goudrian et al. (10) and Satterfield and Model (11) conclude that hydrogen sulfide improved hydroliquefaction of bituminous coals using hydrogen gas and lignites using synthesis gas. Sondreal, Willson and Stenberg (1) have demonstrated the positive effect of H_2S on lignite liquefaction using synthesis gas. The product stream on the continuous flow unit has lower viscosity, lower gas yield and higher distillable oil yield. This enhancement could be due to the interaction of H_2S with the minerals present in coal.

EXPERIMENTAL

Diphenylmethane was purchased (Aldrich) and recrystallized from its ethyl alcohol solution, cooled and the purity of diphenylmethane determined by GC was over 99.9%. Sulfur (Aldrich) and H_2S (Matheson, Coleman and Bell) were used directly without purification. All the reactions were carried out in a 12-ml 316 stainless steel batch microautoclave (12). The heat-up time was at 2 minutes and cool-down time at 0.5 minutes, respectively. The reaction conditions were as follows: temperature, 300-425°C, mainly 425°C; time, 0-120 minutes, not including heat-up and cool-down times; the molar ratio of sulfur reactants are designated in each table. After the autoclave was cooled, the volume or pressure of gas was measured. The liquid products were washed out from the autoclave with ether, and then analyzed by GC. Instruments for identifying the products were GC-MS and ^{1}H-nmr. A gas chromatograph (Varian 2100) used for the separation of liquid products. Separation was effected by a column (0.64 cm x 183 cm) with 3% OV-17 supported on Suplecoport A.

RESULTS AND DISCUSSION

Diphenylmethane was selected as the model compound for these studies to exemplify the chemical reactions of an aromatic ring-aliphatic side chain in coal. Its chemical structure denies aliphatic elimination reactions. The aromatic-methylene-aromatic bonds apparent absence in SRL, SRC and the lower boiling liquids from coal liquefaction does not detract from diphenylmethane's theoretical value nor

prove its absence of its strucural relatives in coals. Its ability to reflect improved conditions for the liquefaction of coals in the ultimate criterion of value as a model compound. Its behavior under liquefaction conditions has already accurately reflected the H_2S enhancement of coal liquefaction.

The thermal stability of diphenylmethane is higher than bibenzyl and diphenylpropane. Diphenylmethane is thought to be one of the most thermally stable coal-related model compounds. This is bourne out by the data on the pyrolysis of diphenylmethane under various reaction conditions as illustrated in Table 1. Diphenylmethane does not decompose in the argon at the temperature of 425°C and reaction time of 60 minutes. Similar results were obtained in the presence of hydrogen sulfide. However, the decomposition of diphenylmethane was enhanced in the presence of either sulfur alone or a mixture of hydrogen sulfide and sulfur. In the pyrolysis reactions of diphenylmethane, sulfur functions as a reactant and 13 products are formed together with a polymer, cf. Table 1. With either elemental sulfur under argon or under H_2S atmospheres for 30 min, the conversions are 49.9 and 35.8%, respectively.

The presence of H_2S during the reaction of diphenylmethane with sulfur influences the product distribution. With H_2S, the yields of the low molecular weight products, toluene and thiophenol, are higher than those of the comparable reaction with S_8 despite the reduction in diphenylmethane conversion, cf. Table 1. The yield of high molecular weight products, classified as "polymer" in Table 1, was reduced which accounts for the difference.

The yields of gaseous and polymeric products increased with temperature and relative concentration of sulfur with little dependence on time, cf. Table 2. The amounts of gas evolved correlated with the yield of polymeric products under these conditions except when the S_8:diphenylmethane ratio was low. The reactions to form both gaseous and polymeric products are rapid and the yields appear to stabilize after 30 minutes.

Table 3 illustrates that diphenylmethane-S_8 product distribution does indeed change before 30 minutes even though the conversion did within experimental error. Tetraphenylethylene was the principal product in the initial stages of the reaction, and it vanished after 60 minutes reaction time. Benzene, toluene and thiophenol yields appear to be the main benefactors of these secondary reactions. Since the formation of tetraphenylethylene occurs largely within the 2-minute heat-up time, its formation is one of the principal primary reactions occurring in the diphenylmethane mixture. Its incomplete conversion into products is possibly due to either the diphenylmethane-S_8 reaction occurring only in the liquid phase at lower temperatures where sulfur-induced radical reactions are known to occur or a change in the chemical nature and reactivity of sulfur occurred with the reaction time.

In addition to tetraphenylethylene, tetraphenylethane and thiobenzophenone were detected at 300° and 350°C and their concentration decreases with increasing temperature. The low boiling products, benzene, toluene and thiophenol are not formed at 300° and 350°C. Therefore these must be categorized as secondary products.

In the hydrogen gas and/or the H_2S gas, the diphenylmethane conversion was about 4%. Benzene and toluene were formed in about equal amounts. On the other hand, the diphenylmethane conversion was enhanced in a H_2-H_2S mixture gas. The diphenylmethane conversion was H_2S concentration dependent, especially at lower H_2S concentrations, and independent of H_2 concentration under the conditions employed in this study. The main products with the H_2-H_2S mixture gas were again benzene and toluene. Several minor products were formed in less than 1% of the weight of diphenylmethane charged.

The results obtained in a presulfided reactor tube showed that the diphenylmethane hydrocracking was promoted in part by the metal sulfide layer formed on the stainless steel reactor wall. The reactor wall was sulfided with H_2S before the introduction of diphenylmethane which results in a black coating being formed on the reactor wall. Since the metal sulfide is being formed as the reaction proceeds in the nonsulfided metal reactor tube, it is difficult to be certain of the percentage, if any, of the hydrocracking which occurs in the gas phase.

With pyrrhotite, H_2 gas causes considerable hydrocracking of diphenylmethane which contrasts with its behavior in the absence of the iron sulfide. Benzene and toluene are the main products with benzene in excess.

The H_2-H_2S gas mixture over pyrrhotite enhanced the diphenylmethane hydrocracking reaction considerably more than H_2 alone did. Moreover, the diphenylmethane conversion in the presence of pyrrhotite was much higher than that in its absence. The effect of pyrrhotite particle size was not important.

Using pyrrhotite, the diphenylmethane conversion increases rectilinearly with increasing hydrogen pressure. A similar effect on conversion occurs when the hydrogen pressure is kept constant and the reaction time increased. As the rigor of the diphenylmethane reaction solution is enhanced by either increasing the hydrogen concentration or the reaction time, the benzene:toluene ratio increases from the value of 1.

The conversion of diphenylmethane is dependent on the H_2S concentration only until slightly more than a 1:1 mole stoichiometry is achieved whether or not pyrrhotite is present. The yields of benzene and toluene are similarly effected. The increasing concentration of H_2S inhibited the formation of products other than benzene and toluene. The amount of pyrrhotite present influences the conversion but not the product distribution. The pyrrhotite loading attained its optimum effect at a weight ratio to diphenylmethane of 0.5.

The thermal hydrocracking of diphenylmethane in the presence of initiating radicals has been suggested to proceed by reactions 1 and 2. In the absence of initiating molecules such as bibenzyl, the slow thermal decomposition reaction of

$$R^{\cdot} + H_2 \rightarrow RH + H^{\cdot} \qquad 1)$$

$$H^{\cdot} + Ph_2CH_2 \rightarrow PhH + PhCH_2^{\cdot} \qquad 2)$$

$$Ph_2CH_2 \rightarrow 2\,Ph^{\cdot} + PhCH_2^{\cdot} \qquad 3)$$

diphenylmethane, reaction 3 and the thermal decomposition data obtained under argon, provides the only source of $R^{\cdot}$ for reaction 1 with the consequence of slow kinetics of the thermal decomposition of diphenylmethane under hydrogen. Another reason for the slow kinetics of the diphenylmethane decomposition under hydrogen is the endothermic character of reaction 1. From bond dissociation data, one can expect this reaction to be endothermic by 0 to +25 kcal/mole depending on the nature of $R^{\cdot}$. The lack of hydrogen pressure dependence with no additives present is probably an artifact attributed to the low level of conversion and obscurred by experimental error.

With hydrogen sulfide and hydrogen present, the conversion and product yields are significantly higher. These results are consistent with reactions 4 and 5 becoming operational in the reaction mixture. The hydrogen sulfide pressure

$$R^{\cdot} + H_2S \rightarrow RH + {}^{\cdot}SH \qquad 4)$$

$${}^{\cdot}SH + H_2 \rightarrow H_2S + H^{\cdot} \qquad 5)$$

dependence is rationalized by reaction 4 and its maximum concentration optimum is controlled by reaction 5 which regenerates H_2S. The reaction sequence 4 and 5 is a thermodynamic stepwise alternative to the highly endothermic reaction 1. Thus, the hydrogen sulfide effect is suggested to take place by replacing reaction 1 with two potentially faster reactions which accomplished the same end result. Reaction 4 is estimated to be endothermic or exothermic by the range of -9 to +16 kcal/mole and 5 endothermic by +9 kcal/mole. Therefore, hydrogen sulfide functions as a H-transfer catalyst in a hydrogen-hydrogen sulfide gas mixture, and this results in an enhanced diphenylmethane hydrocracking reaction.

The significant changes on using pyrrhotite together with hydrogen and hydrogen sulfide is rate enhancement, hydrogen and hydrogen sulfide dependence and increased benzene formation. The rate enhancement can be attributed to a weakening of the SH bonds or outright dissociation of H_2S on the pyrrhotite surface which serves to enhance the rate of reaction 4. The hydrogen pressure dependence with pyrrhotite is attributed to the increased concentration of an active ${}^{\cdot}SH$ and reaction 5 becoming a significant factor in the reaction mixture. Since benzene is formed in higher yields than toluene and toluene is converted in low yield into benzene under these conditions in the absence of pyrrhotite, adsorption of diphenylmethane on the

pyrrhotite surface is indicated and the benzene in excess of a stoichiometric ratio with toluene formed from some adsorbed species.

Two factors were considered in the design of new iron oxide supported catalysts: (a) iron is the principal transition metal to be used based on the cost factor, and (b) the acidity of the support oxide should be varied to determine the optimum acidity. These metal oxides have been screened and the promising results published (3). Since then, we have continued work with these catalysts using sulfur additives and have obtained much more exciting results than those published, cf. Tables 5 and 6.

Diphenylmethane is converted into mainly benzene and toluene when exposed to reducing conditions at liquefaction temperatures such as 425°C (Table 5). When hydrogen is used in the stainless steel reactor with no added catalyst there is no conversion of the starting material. When metal oxide heterogeneous catalysts are added, the starting material is converted into the observed products to varying degrees (Table 6). All three newly designed and synthesized catalysts are active and compare favorably with the commercially available $CoO-MoO_3$. Table 6 gives data which demonstrate the positive effect of sulfiding the catalysts before or during use. The SiO_2- supported catalyst was selected for the present study on the basis of cost effectiveness.

ACKNOWLEDGEMENT

We gratefully appreciate the financial support of the Department of Energy through contract no. DEF62282PC50814.

REFERENCES

1. Sondreal, E.A.; Willson, W.G.; and Stenberg, V.I., Fuel, 1982, 45, 4250.
2. Stenberg, V.I.; Baltisberger, R.J.; Ogawa, T.; Raman, K.; and Woolsey, N.F., Fuel Division Preprints, American Chemical Society, 1982, 27, 22. Ogawa, T. and Stenberg, V.I., manuscript in preparation.
3. Stenberg, V.I.; Wettlaufer, D.; Baltisberger, R.J.; Knudson, C. and Woolsey, N.F., Fuel, submitted; Stenberg, V.I.; Srinivas, V.R.; Tanabe, K.; Jin, T. and Hattori, H., Chem. Lett., 1982, 1547.
4. Takeya, G., Pure and Applied Chemistry, 1978, 50, 1099.
5. Fischer, F.; and Dilthey, P., Ges. Abhandl. Kenntnis Kohle, 1930, 9, 512.
6. Bahr, H., ibid., 1930, 9, 514.
7. Beardon, R., Jr., and Aldridge, C.L., U.S. Patent 4,094,765, June 13, 1978.
8. Gatsis, J.G., U.S. Patent 3,503,863, 1970.
9. Hettinger, W.P.; Keith, C.D.; Gring, J.L. and Tetes, J.W., Ind. Eng. Chem., 1955, 47, 719.
10. Goudrian, F.; Gierman, H. and Vluger, J.C., J. Inst. Petrol., London, 1973, 59, (565)41.
11. Satterfield, C.N. and Model, M., U.S. NTIS, P.B. Rept., 1975, 248101.
12. Van Buren, R. and Stenberg, V.I., Chem. Ind. (London), 1980, 569.

Table 1 The Pyrolysis of Diphenylmethane with S_8 and H_2S/S_8[a]

Products[b]	S	H_2S/S
Benzene	1.1	1.0
Toluene	3.9	8.0
Thiophenol	6.9	9.0
Diphenyl sulfide	Trace	0.4
Unknown	0.0	0.7
Dibenzothiophene	0.0	0.8
Thioxanthene	0.7	2.0
Triphenylmethane	1.3	0.4
9-Phenylthioxanthene	Trace	Trace
9,10-Dihydro-9,10-diphenylanthracene	0.2	Trace
Tetraphenylethylene	0.2	0.0
12,13-Dihydrodinaphthothiophene	1.6	0.4
1,1,1-Triphenyl-2-phenylethane	0.3	Trace
Polymer	35.2	25.2
Conversion	49.9	35.8

[a]The reactions were done at 425°C for 30 min. at temperature with $H_2S:Ph_2CH_2:S$ ratio of 2.5:1:1. The sulfur reaction was done under an argon atmosphere.
[b]The results are given in mole percent based on the amount of starting material except for the amount of polymer. The latter is given in weight percent of Ph_2CH_2 plus S charged.

Table 2 The Reaction of S_8 with Diphenylmethane

Temp, °C	Time, min	Mole ratio $S:Ph_2CH_2$	Gaseous products, wt%[a]	Polymeric products, wt%[a]
300	30	1	1.0	14.8
350	30	1	2.7	29.8
425	30	1	6.6	35.2
425	60	1	7.0	33.6
425	120	1	6.8	34.0
425	30	0.5	4.6	9.9
425	30	2	18.1	44.2
425	0[b]	1	5.6	24.2

[a]Weight percent of total sulfur plus diphenylmethane charged.
[b]The heat-up time was 2 minutes with an immediate temperature quench.

Table 3 Time Dependence of S_8-Ph_2CH_2 Product Distribution[a]

Products[b]	Time at temperature, min			
	0[c]	30	60	120
Benzene	0.4	1.1	1.3	1.8
Toluene	0.6	3.9	4.2	3.3
Thiophenol	2.0	6.9	7.3	5.5
Unknown	1.2	0	0	0
Thiobenzophenone	0.9	0	0	0
Thioxanthene	1.3	0.7	0.9	0.7
Triphenylmethane	0.5	1.3	1.6	1.1
9-Phenylfluorene	0.9	0	0	0
9,10-Dihydro-9,10-diphenylanthracene	0.2	0.2	0.3	0.3
Tetraphenylethylene	7.6	0.4	0	0
12,13-Dihydrodinaphthothiophene	1.6	1.6	1.5	1.7
1,1,1-Triphenyl-2-phenylethane	0.2	0.3	0	0.3
Conversion	46.9	49.9	48.8	47.5

[a]The reaction temperature was 425°C; the S:Ph_2CH_2 mole ratio was 1; and the reactions were done under an atmosphere of argon.
[b]The results are given in mole percent based on the diphenylmethane charged.
[c]The heat-up time was 2 min with an immediate temperature quench.

Table 4 Diphenylmethane Conversion with S_8-H_2S[a]

Products[b]	Time at temperature, min				
	0[c]	15	30	60	120
Benzene	0	0.4	1.0	1.1	1.3
Toluene	0	6.7	8.0	6.9	6.7
Thiophenol	0	7.5	9.0	8.6	8.2
Diphenyl sulfide	0	Trace	0.4	0.2	0.4
Unknown	0	0.7	0.7	0.6	0.6
Dibenzothiophene	0	0.5	0.8	0.7	0.7
Thioxanthene	0.8	1.5	2.0	1.4	1.2
Triphenylmethane	0	0.2	0.4	0.3	0.2
Tetraphenylethylene	0.3	0	0	0	0
12,13-Dihydrodinaphthothiophene	0	Trace	0.4	Trace	Trace
Polymer	24.4	27.9	25.2	27.6	29.0
Ph_2CH_2 conversion	7.8	34.3	35.8	32.9	31.5

[a]The reaction temperature was 425°C and the H_2S:S:Ph_2CH_2 molar ratios were 2.5:1:1.
[b]The results are given in mole percent based upon the amount of starting material except for the amount of polymer. The latter is given in weight percent of Ph_2CH_2 plus S_8 charged.
[c]The heat-up time was 2 min with an immediate quench.

Table 5. Diphenylmethane Product Distribution Using the Fe_2O_3 - SiO_2 Catalyst[a]

Gases Added / Products	CO H_2O H_2S (P)	H_2 H_2S (P)	H_2 S	H_2[b] (U)	H_2 H_2S (U)
Benzene	1	83	71	43	105
Toluene	1	75	67	21	88
Cyclohexanes	0	3	7	0	5
Others	0	1	2	8	1
Conversion	1	88	81	41	100

P=presulfided
U=unsulfided

[a]The reactions were done in the 12ml rocking autoclaves at 425°C for 1 hr. H_2 (4.9 x 10^{-1} moles), H_2S (3.9 x 10^{-3} moles), and diphenylmethane (3 x 10^{-3} moles) were used. A 10 weight percent load of catalyst was used. The cited data is duplicate results. The presulfiding was done by exposing the catalyst to 250 psi H_2S, 1400 psi H_2 and raising the temperature to 425°C and keeping it there for 1 hr.

[b]The reaction temperatrue was 450°C.

Table 6. The Reaction of Diphenylmethane Using the Tanabe Newly Synthesized Catalysts[a]

	None	Fe_2O_3	Fe_2O_3 on ZrO_2	Fe_2O_3 on TiO_2	Fe_2O_3 on SiO_2	$CoO \cdot MoO_3$
$CO/H_2O/H_2S$	NA	Trace	4	2	Trace	34
H_2/H_2S	NA	30	82	98	100	99
H_2/S	9	30	92	95	81	99
H_2[b]	NA	5	45	16	23	96
$H_2/H_2S/H_2O$	NA	2	3	4	4	26

[a]The reactions were done in the 12ml rocking autoclaves at 425°C for 1 hr. H_2 (4.9 x 10^{-1} moles), H_2S (3.9 x 10^{-3} moles), and diphenylmethane (3 x 10^{-3} moles) were used. A 10 weight percent load of catalyst was used. The cited data is duplicate results. The presulfiding was done by exposing the catalyst to 250 psi H_2S, 1400 psi H_2 and raising the temperature to 425°C and keeping it there for 1 hr.

[b]The catalyst is presulfided for this run.

INCREASING THE ACTIVITY OF COAL MINERAL MATTER FOR HYDRODESULFURIZATION AND HYDRODENITROGENATION

Kindtoken H-D. Liu and Charles E. Hamrin, Jr.

Department of Chemical Engineering
and Institute for Mining and Minerals Research
University of Kentucky
Lexington, Kentucky 40506

Catalysis by coal minerals has been the subject of much work in recent years by Guin et al. (1,2), Granoff, et al. (3,4,5), Given and coworkers (6,7), and Mukhejee and Chowdhury (8) since its discovery by Wright and Severson (9) in 1972. Several studies using model compounds such as thiophene, benzothiophene, pyrrole, pyrrolidene, and n-butyl amine have also been published based on work performed at the University of Kentucky (10-16). It is the purpose of this paper to compare the hydrodesulfurization (HDS) and hydrodenitrogenation (HDN) activities of mineral matter modified by iron or nickel additions to the activities of untreated mineral matter.

EXPERIMENTAL - A pulse micro-reactor packed with mineral matter using hydrogen as the carrier gas was used to evaluate catalytic activity over the temperature range of 573 to 723 K at 101 kPa. Conversions were calculated from the total of C_4 gases detected in the product stream by gas chromatography. Details of the system are presented elsewhere (16). Modification of mineral matter was carried out by preparing physical mixtures of Ky #9 and Ky #11 with Harshaw Ni-4301 (6% Ni and 19% W as oxides on silica-alumina) and by evaporating various iron and nickel solutions containing Ky #9 and Ky #11. Physical mixtures were prepared in two different ways. In one method H_2-pretreated, -24+42 mesh particles of LTA and the Harshaw catalyst were combined to give 10 w/o nickel and loaded into the reactor for activity testing. The activity was between that of the LTA and the catalyst. A second physical method was used which gave more interesting results. The catalyst was ground in a mortar and pestle and combined with either of the LTAs, pressed, crushed to -24+42 mesh, and H_2 pretreated as for other test samples. The catalyst charged was 5×10^{-4} kg containing 10 w/o nickel (calculated).

Two grams of LTA were mixed with the corresponding amount of $Ni(NO_3)_2 \cdot 6H_2O$ to give 10, 25, and 50 w/o Ni mixtures. A small quantity of double distilled water (0.021) was added to dissolve the salt. If necessary, heat was added for about 30 seconds to carry out the dissolution. The slurry was then placed in a 383 K oven overnight to evaporate the liquid. The remaining solid was pressed, sieved, and pretreated as described earlier. Similar treatments were carried out with $FeCl_3 \cdot 6H_2O$, $Fe(NO_3)_3 \cdot 9H_2O$, and $NiCl_2 \cdot 6H_2O$.

RESULTS AND DISCUSSION - The HDN conversion for the combination of the Ky #11 LTA with the ground Harshaw catalyst is shown in Figure 1, along with the pure components. On the left is the Ky #11 LTA showing total conversion along with the amount of butane and unsaturates. This contrasts sharply with the catalyst which produces only butane, gives lower conversion, and loses activity as pulsing continues. The mixture (3rd graph from left) pro-

duces a mean conversion of 72.5 which is much higher than either of the components indicating a synergistic effect. The first pulse produced only butane but thereafter the butane accounted for about 12.5%, 1-butene for about 9%, and 2-butenes for about 51% of the total 72.5% conversion. Apparently, the hydrogenation sites are quite sensitive to nitrogen poisoning, but they do not affect the denitrogenation activity.

The effect is even more impressive when Ky #9 which was third lowest in activity was combined with the powdered catalyst. As shown in Figure 2, the mixture (right graph) gave a mean conversion of 77.2% which was the highest of any material tested. Again the first pulse gave pure butane; thereafter about 32% (of the 77.2%). After five pulses cis-2 butene appears and is about the same value as butane with the remainder trans-2-butene. No 1-butene was observed.

The catalyst produced from $Ni(NO_3)_2$ $6H_2O$ and Ky #11 evidenced quite stable performance with a mean conversion of 53.6% which is very close to the LTA value (Figure 1). Unsaturates make up almost all of the products.

Results for all of the Fe and Ni solution-type catalyst are presented in Table I which gives both HDN and HDS conversion. None of the mixtures improve the HDN conversion appreciably and the ferric nitrate decreases it by 26%. Very large changes in HDS conversion are apparent since the LTA gives $<1\%$ and the 50% Ni yields a value of 38.8%. The values of the surface area for the Ni treated mixtures give a mean value of 28.9 $m^2/g \pm 2.2$ which is slightly less than the untreated LTA value of 32.0. This indicates the added Ni is responsible for the increase in activity and the surface area is unaffected by the treatment. The iron treatment shows some improvement as does the nickel chloride, but the nitrate is by far the most effective treatment rivaling the Harshaw mixtures as shown in Figure 3. Here it is seen that 10% Harshaw with Ky #11 gives 23% conversion compared to 21% for the above treatment. The highest HDS conversion was 24.2% for the Ky#9-Harshaw mixture. It is also interesting to note that the Harshaw catalyst does not give a high concentration of n-butane as it did for HDN. Probably H_2S poisoning is responsible for the lack of hydrogenation.

The effect of temperature on HDS conversion for Ky #11 mineral matter, 25% Ni, and 50% Ni is shown on Figure 4. The 25% Ni mixture increases linearly by almost 3-fold from 600 to 700 K. The 50 w/o mixture increases 7-fold from 500 to 700 K. It is also obvious that the activity has increased significantly for the Ni-mixtures over the untreated mineral matter. One measure of this is the temperature required for the more active materials to give the same conversion as the mineral matter; i.e. 1% at 683 K. This requires considerable extrapolation, but it is estimated that the 25% Ni mixture would require a temperature of 523 K and the 50 w/o about 453 K.

Another comparison is shown in Figure 5 where log conversion is plotted against the reciprocal temperature. A previously reported curve is shown for presulfided Ky #11 LTA (Morooka and Hamrin, 10) which gave an activation energy of 58.6 kJ/mole. In this study a value of 57.5 kJ/mole was found for H_2-treated Ky #11 which is in good agreement with the earlier value indicating that pretreatment by H_2 or H_2S does not affect the activation energy. Shown on the figure are the data for the 25% Ni mixture which gave a value of 30.4 kJ/mole with a correlation coefficient ($r = 0.97$). For the 50%

Ni-LTA, a value of 30.3 kJ/mole (r = 0.97) was found. The Ni treatment cut the activation energy almost in half, but increasing the amount of Ni from 25 to 50 w/o had no effect on it.

Additional H_2-treatment on the Ni-modified LTA catalyst increases its HDS activity but decreased its HDN activity. Typical results are given in Table II for the 25% Ni mixture where the HDN activity decreased from 54.7 to 47.5 when additional H_2 treatment of 95 hours was carried out. This may be explained by the increase of cracking activity of the catalyst as the reduction of Ni sites proceeded.

The fact that Ni-added catalyst increased the HDS activity up to 56 times seems due to the high hydrogenation activity of Ni metal which plays an important role on the hydrocracking of thiophene as the first step to give 1,3-butadiene followed by hydrogenation to give n-butenes and butane. On the other hand, since the Ni added catalyst only keeps the HDN activity unchanged implies that the hydrogenation activity of Ni metal does not contribute to the n-butylamine conversion; therefore the n-butylamine HDN conversion is not a hydrocracking reaction but a cracking reaction in which dehydrogenation occurs.

Pyrrole and pyrrolidine pulsing on Ni modified Ky #11 LTA catalyst showed some poisoning effect on the n-butylamine HDN activity while thiophene pulsing increased the HDN activity from 41% to 51% but decreased the selectivity to n-butane.

ACKNOWLEDGMENT - This work was supported by the U.S. Department of Energy under Contract No. EX-76-C-01-2233.

LITERATURE CITED

1. Guin, J. A., Tarrer, A. R., Prather, J. W., Johnson, D. R., and Lee, J. M., Ind. Eng. Chem. Proc. Des. Dev., 17, 118 (1978).

2. Guin, J. A., Tarrer, A. R., Lee, J. M., Lo, L., and Curtis, C. W., Ind. Eng. Chem. Proc. Des. Dev., 18, 371 (1979).

3. Granoff, B. and Montano, P. A., in "Chemistry and Physics of Coal Utilization - 1980", ed. by B. R. Cooper and L. Petrakis, p. 291, Am. Inst. Phys., New York, 1981.

4. Granoff, B. and Traeger, R. K., "Coal Processing Technology", Vol. V, p. 15, A.I.Ch.E., New York, 1979.

5. Granoff, B. and Thomas, M. G., Am. Chem. Soc. Div. Fuel Chem. Preprints 22 (6), 183 (1977).

6. Given, P. H., presented at meeting of liaison board for coal liquefaction project, NSF-RANN, Penn. State Univ. (August 9, 1974).

7. Given, P. H., Spackman, W., David, A., Walker, Jr., P. L., and Lowell, H. L., "The Relation of Coal Characteristics to Coal Liquefaction Behavior", Report 3, NSF-RANN (1975).

8. Mukherjee, D. K. and Chowdhury, P. B., Fuel, 55, 4 (1976).

9. Wright, C. H. and Severson, D. E., Am. Chem. Soc. Div. Fuel Chem. Preprints 16 (2), 68 (1972).

10. Morooka, S. and Hamrin, Jr., C. E., Chem. Eng. Sci., 32, 125 (1977).

11. Morooka, S. and Hamrin, Jr., C. E., Fuel (London), 57, 776 (1978).

12. Morooka, S. and Hamrin, Jr., C. E., Chem. Eng. Sci., 34, 521 (1979).

13. Liu, K. H. D. and Hamrin, Jr., C. E., U.S. Patent 4,358,398, November 9, 1982.

14. Sakata, Y. and Hamrin, Jr., C. E., Ind. Eng. Chem. Prod. Res. Develop., June, 1983.

15. Johannes, A. H. and Hamrin, Jr., C. E., Fuel Process. Tech., in press (1983).

16. Liu, K. H. D. and Hamrin, Jr., C. E., Ind. Eng. Chem. Proc. Des. Dev., in press (1983).

TABLE I

Effect of Fe and Ni Modification of Ky #11 LTA
on HDN and HDS Conversions

Addition Compound	w/o Added Element	Surface Area m^2/g	Conversion* HDN	HDS
None	0	32.0	52.0	0.78
$Fe(NO_3)_3 \cdot 9H_2O$	10		38.6	1.98
$FeCl_3 \cdot 6H_2O$	10		48.0	0.96
$NiCl_2 \cdot 6H_2O$	10		48.8	4.73
$Ni(NO_3)_2 \cdot 6H_2O$	10	27.0	53.6	14.0**
$Ni(NO_3)_2 \cdot 6H_2O$	25	31.3	54.7	16.0
$Ni(NO_3)_2 \cdot 6H_2O$	50	28.3	60.7	38.8

* At 673 K, W/F = 2.91 g cat-hr/mole, 4 hr hydrogen pretreatment at 673 K.

** Extrapolated to 0 additional H_2 treatment.

TABLE II

Effect of Additional H_2 Treatment on
HDN Activity of 25% Ni-Ky #11 Mixture

	Additional H_2 Treatment at 673 K, hr			
	0	14	39	95
HDN Conversion From C_4's Produced, %	54.7 ± 0.9	51.0 ± 0.7	50.1 ± 1.3	47.5 ± 1.7
C_1 - C_3 By Cracking, %	6.0 ± 0.7	7.4 ± 4.1	11.0 ± 1.1	18.2 ± 1.9
Total Conversion, %	60.7	58.4	61.1	65.7
n-Butane in Total, %	7.9 ± 1.4	9.1 ± 1.1	16.5 ± 3.3	49.6 ± 12.0

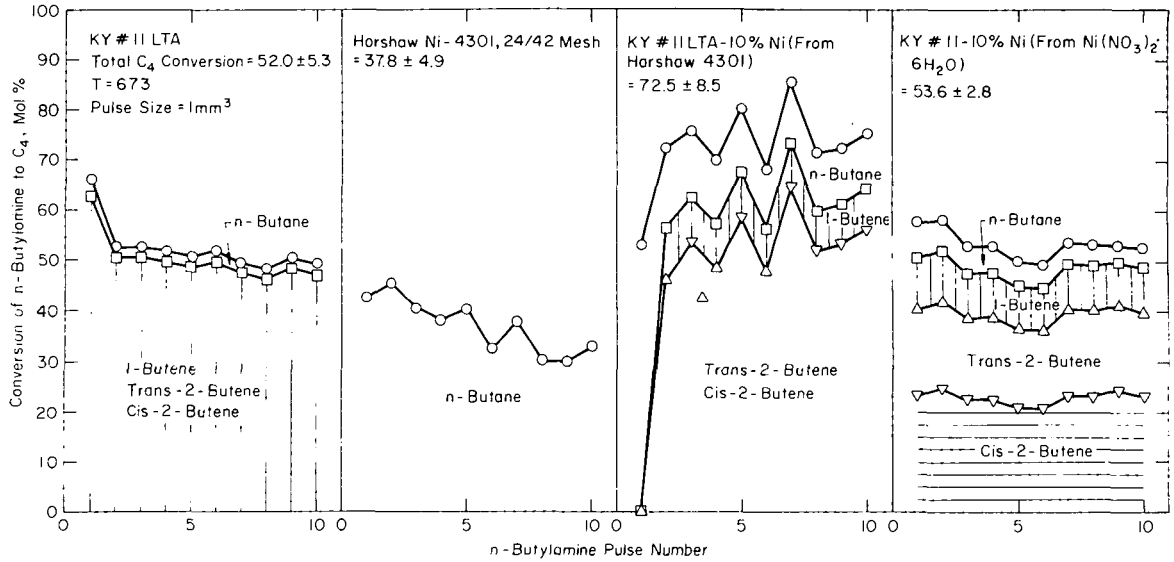

Figure 1. HDN Conversion and Selectivity for KY # 11 and Different Nickel Catalysts.

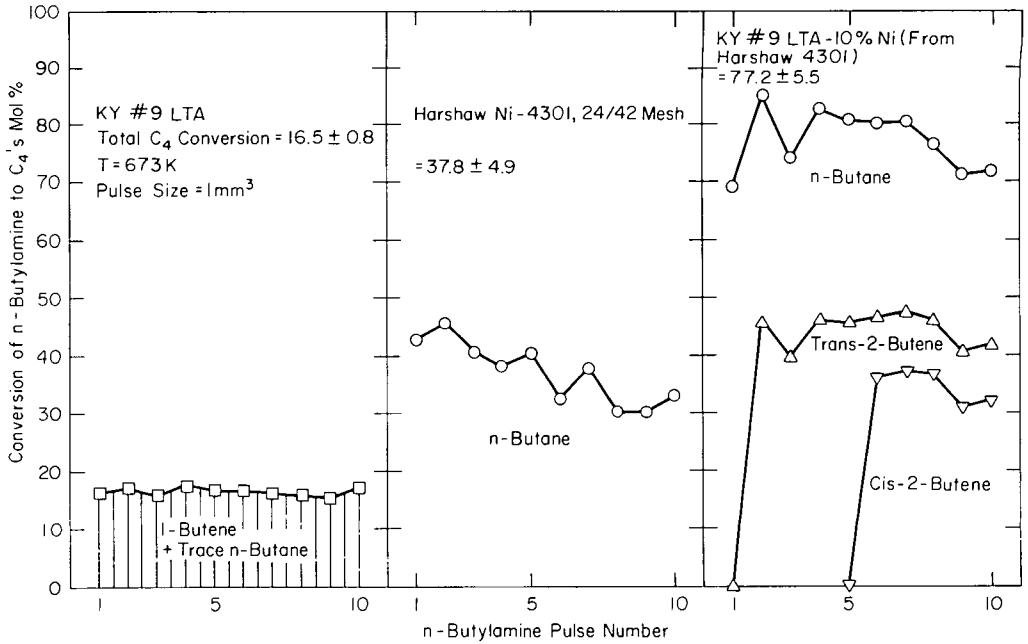

Figure 2. HDN Conversion and Selectivity for KY # 9 and Ni Catalysts.

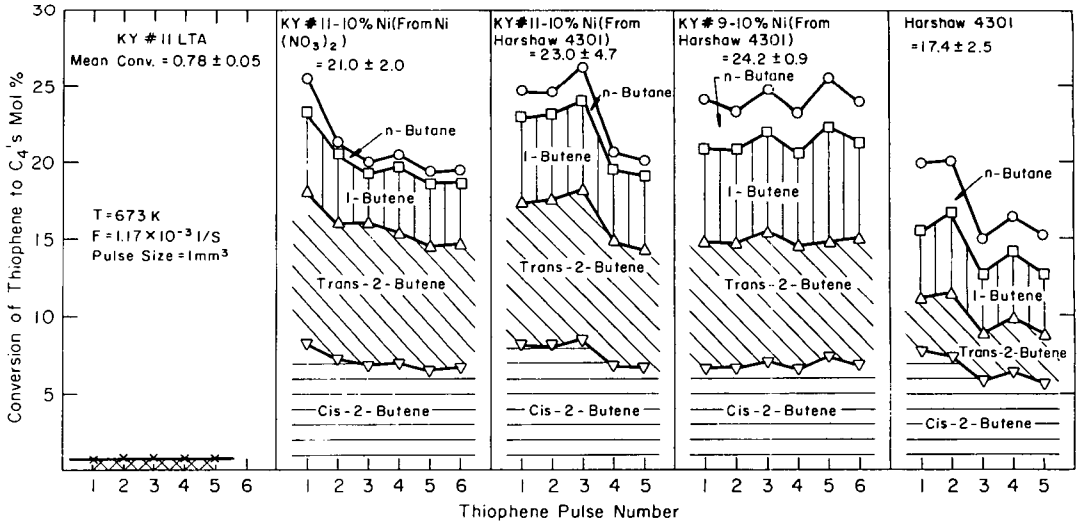

Figure 3. HDS Activity and Selectivity for KY LTA-Ni Mixtures with KY # 11 and Harshaw 4301.

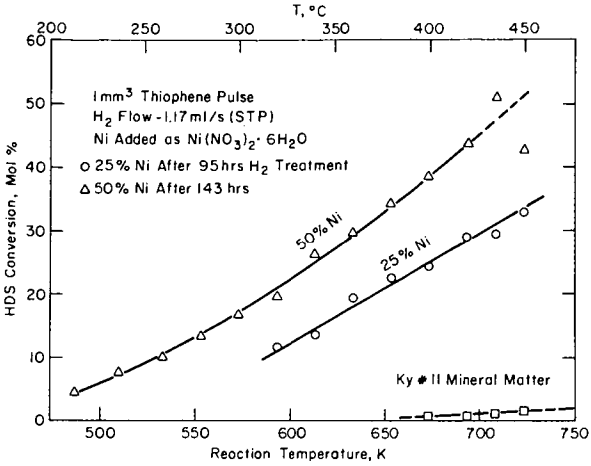

Figure 4. HDS Conversion versus Reaction Temperatures for KY # 11 with and without Nickel.

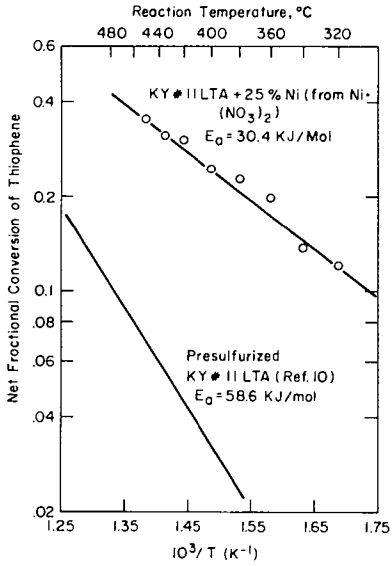

Figure 5. Comparison of Thiophene Conversion - Temperature Relationships for KY # 11 and KY # 11 - Ni Mixture.

Relative Activity of Transition Metal Catalysts in Coal Liquefaction

Diwakar Garg and Edwin N. Givens

Corporate Research & Development Department
Air Products and Chemicals, Inc.
P.O. Box 538, Allentown, PA 18105

Abstract

The catalytic activity of transition metals for coal liquefaction was studied and compared. Impregnation of coal with transition metals significantly increased the production of oils and the conversion of asphaltenes and preasphaltenes in coal liquefaction. Overall conversion of coal increased marginally with transition metals. The production of hydrocarbon gases decreased slightly with metals. Iron impregnation was more active in preasphaltenes conversion than cobalt, nickel, and molybdenum; whereas the other metals were more active in asphaltenes conversion than iron. Hydrogen consumption decreased with the use of metals. The quality of generated solvent decreased with iron, whereas it increased with other metals. Significant synergism was observed between iron and molybdenum. Simultaneous impregnation of coal with iron and molybdenum significantly increased the conversion of coal, asphaltenes, and preasphaltenes, and the production of oils compared to individual metals. The mixture of iron and molybdenum also decreased the hydrocarbon gas production over iron and molybdenum alone. In addition, the quality of generated solvent was higher with iron and molybdenum mixture compared to iron alone.

Introduction

Extensive research has been performed in the areas of catalytic and non-catalytic coal liquefaction. It is well known that in coal liquefaction, high-molecular weight compounds rupture thermally, producing unstable free radicals. These free radicals react with hydrogen donated by hydrogen donor species present in the process solvent to form stable species. Therefore, the presence of sufficient hydrogen donor compounds in the coal liquefaction reaction mixture is necessary to prevent the repolymerization of free radicals thereby aiding the production of lower-molecular-weight oils and asphaltenes. It has been speculated that mineral matter catalyzes the coal liquefaction reaction by enhancing the transfer of hydrogen from the gas to liquid phase thus maintaining the hydrogen donor capability of the process solvent.

The catalytic effect of mineral matter on hydrogenation of model compounds and coal has been investigated by a number of investigators.(1-12) Iron compounds which are abundant both in nature and as an article of commerce were studied extensively. The Germans found that adding iron sulfate and Bayermasse (iorn oxide containing material obtained from aluminum manufacture) to feed slurry improved coal liquefaction.(13) Numerous researchers who have studied the catalytic activity of iron as either iron pyrite or pyrrhotite in liquefaction have reported improved results.(14-22)

Like iron, molybdenum and several other transition metal have been shown to catalyze coal liquefaction.(13,23,24,25,26) Since transition metals are both expensive and scarce, their application in liquefaction will depend greatly on their activity at low concentrations. Interestingly, several metals have been shown to be very active in coal liquefaction at very low concentrations.(13,25,26)

In the present paper, the activity of iron, molybdenum, cobalt, and nickel in catalyzing the liquefaction of coal is discussed. The catalytic activity will be related to the product distribution which will include hydrocarbon gas make, oil yield, asphaltene and preasphaltene yields, and degree of coal conversion. The effect of iron and molybdenum mixtures was also studied. All the data reported in this paper refer to results in a continuous 100 pounds per day coal process unit.

Experimental Section

Materials. A low-ash, low-pyrite Eastern Kentucky Elkhorn #2 coal obtained from a mine in Letcher County was used in the study. The sample was treated in a coal preparation plant to reduce the ash and pyrite contents. This sample was purposely selected to minimize the influence of the coal ash and pyrite on the liquefaction. The coal sample was ground to 95% minus 200 mesh particles, dried in air and screened through a 150 mesh sieve prior to use. The detailed analysis of the screened coal is reported in Table 1.

SRC-II heavy distillate supplied by the Pittsburg and Midway Coal Mining Company was used as a process solvent. The chemical analysis of the process solvent is shown in Table 2. The solvent contained 93.8% pentane-soluble oils, 5.0% asphaltenes, 0.4% preasphaltenes, and 0.8% insoluble organic material (pyridine insolubles). The process solvent contained organic compounds boiling in the range of 550 to 850°F temperature.

Iron sulfate ($FeSO_4.7H_2O$) was received from Textile Chemical Company, Reading, Pennsylvania. The sample contained approximately 97% iron sulfate cyrstals and minor quantities of iron oxide, titanium dioxide and magneisum sulfate as impurities. Ammonium molybdate, nickel nitrate, and cobalt nitrate were reagent grade materials obtained from Fischer Scientific Company, Fair Lawn, New Jersey.

Metals Impregnation. A sample of coal was impregnated with 1% iron by adding a 10.0% ferrous sulfate solution in distilled water to ground coal. Three different samples of coal were impregnated with 0.02% molybdenum, nickel, and cobalt by mixing the samples with 0.5% ammonium molybdate, nickel nitrate and cobalt nitrate solutions, respectively. Since molybdenum, nickel, and cobalt are very expensive compared to iron, very low concentrations (200 ppm) of these metals based on coal were used. Another sample of coal was impregnated simultaneously with a mixture of 1 wt.% iron and 0.02 wt.% molybdenum based on coal. The impregnated coal samples were dried at 60°C for 72 hours and ground under nitrogen before use in liquefaction experiments.

Equipment. Process studies were done in a continuous 100 pound/day coal liquefaction unit equipped with a continuous stirred autoclave. The use of a stirred tank reactor ensured that solvent vaporization matched that of an actual coal liquefaction dissolver and that coal minerals did not accumulate.

Since there was no slurry preheater, all of the sensible heat was provided by resistance heaters on the reactor. Because of this high heat flux, the reactor wall was about 27°F hotter than the bulk slurry. Multiple thermocouples revealed that the slurry temperature inside the reactor varied by only 9°F from top to bottom. A detailed description of the reactor is presented elsewhere.(27)

The products were quenched to 320°F before flowing to a gas/liquid separator that was operated at system pressure. The slurry was throttled into the product receiver while the product gases were cooled to recover the product water and organic condensate. The product gases were then analyzed by an on-line gas chromatograph.

Procedure. Coal liquefaction runs were performed at 825°F, 2,000 psig hydrogen pressure, 1,000 rpm stirrer speed, hydrogen feed rate equivalent to 5.5 wt. % of coal, and a superficial slurry space velocity of 1.5 inverse hours. The coal concentration in the feed was 30 wt.%.

At least 10 reactor volumes of the product were discarded prior to collecting a product sample. A complete sample consisted of one 8-oz product slurry, one 1-L product slurry as back-up sample, a light condensate sample, and a product gas sample.

The product slurry from the continuous reactor was solvent separated into four fractions: (1) pentane-soluble material (oil), (2) pentane-insoluble and benzene-soluble material (asphaltene), (3) benzene-insoluble and pyrdine-soluble material (preasphaltene), and (4) pyridine-insoluble material. The latter contains insoluble organic material (IOM) and mineral residue. The overall coal conversion is calculated as the fraction of organic material (moisture-ash-free coal) soluble in pyridine.

Results and Discussion

Effect of Transition Metals - The impregnation of Elkhorn #2 coal with 1 wt.% iron had no effect on overall coal conversion but increased the production of oils from 12 to 25% (Table 3). The production of hydrocarbon gases decreased with iron; the decrease in the production of hydrocarbon gases is statistically significant at this level. The production of heteroatom gases changed marginally with iron impregnation. The preasphaltene concentration decreased from 44 to 36% with iron impregnation. Hydrogen consumption based on elemental hydrogen balance decreased from 0.6 to 0.4 percent with iron impregnation.

The hydrogen contents of the oil, asphaltene and preasphaltene fractions were lower with iron impregnation compared to the baseline run (Table 4). Apparently the dispersed iron system was not effective in hydrogenating the liquefaction products. This would be advantageous in that expensive hydrogen would not wasted in hydrogenating SRC (asphaltenes and preasphaltenes), which would be used ultimately as a boiler fuel. The SRC sulfur content was unchanged with iron impregnation. Likewise, the sulfur contents in the various fractions were unaffected with iron (Table 4). Nitrogen content in the oil and asphaltene fractions decreased slightly, whereas it increased in the preasphaltene fraction. The oxygen content of oils decreased slightly, but it increased

significantly in the asphaltene and preasphaltene fractions with iron impregnation. No definite conclusion could be drawn concerning deoxygenation because oxygen content was determined by difference.

The hydrogen distribution in the solvent generated by coal liquefaction was determined by proton NMR to determine the changes in solvent quality by iron impregnation. The hydrogen donor capability of a solvent was measured in terms of the combined concentration of H_a and H_o. The higher the combined concentration of H_a and H_o, the better would be the quality of the process solvent. Data in Table 5 revealed that the hydrogen donor capability of the solvent generated with no catalyst and with iron was lower than that of the original process solvent. The aromatic hydrogen content of solvent increased with both no catalyst and with iron. However, the increase in aromatic hydrogen content was more dramatic with iron. The decrease in the quality of the solvent generated with iron was contrary to the speculation made by several researchers that mineral matter improved coal liquefaction by enhancing hydrogen transfer from gas to liquid. In terms of actual plant operation, a decrease in solvent quality means a decrease in the liquefaction performance. Therefore, the generated solvent has to be hydrogenated externally to increase its hydrogen donor capability and to maintain the liquefaction performance of the iron catalyst.

The impregnation of coal with 0.02 wt.% (200 ppm) cobalt and molybdenum increased the coal conversion slightly. The magnitude of the increase in coal conversion was very similar to that obtained with 1 wt.% iron (Table 3). The coal conversion, however, decreased with nickel impregnation. The production of oils increased significantly from 12 to 20-21% with cobalt, nickel, and molybdenum. The increase was slightly lower than that obtained with iron. The production of hydrocarbon gases was higher with cobalt, nickel and molybdenum than iron but still lower than the base-line run. Preasphaltenes conversion increased with cobalt, nickel, and molybdenum, but it was much lower than that noted with iron. Asphaltenes yield was slightly lower with cobalt, nickel, and molybdenum than iron; asphaltene concentration decreased from 21 to 18 with cobalt, nickel, and molybdenum, whereas it decreased to 19 percent with iron.

Hydrogen consumption based on elemental hydrogen balance was lower with cobalt, nickel and molybdenum compared to baseline run (Table 3). Lower hydrogen consumption was due to lower production of hydrocarbon gases and lower hydrogen contents in the asphaltene and preasphaltene fractions (Table 4). Like iron, other metals were also found to be ineffective in hydrogenating asphaltenes and preasphaltenes. Nitrogen and sulfur contents in various fractions were very similar with and without metals. The hydrogen contents of the oil fractions obtained with metals were similar to the base-line run except for nickel (Table 4).

The quality of solvent generated with cobalt, nickel and molybdenum was higher than that generated either with iron or without metals (Table 5). The concentration of H_{AR} decreased and that of H_a and H_o either increased or maintained with cobalt, nickel and molybdenum. The increase in the quality of generated solvent is an indicative of enhancement of hydrogen transfer from gas to liquid phase with cobalt, nickel and molybdenum catalysts.

The above discussion showed that the impregnation of Elkhorn #2 coal with metals significantly increased oils production, increased preasphaltene conversion and decreased hydrocarbon gas make. The metals, however, did not change SRC sulfur content.

Comparing the activity of iron to that of other metals, it was found that iron impregnation yielded higher oils production and preasphaltenes conversion than other metals. However, other metals were more active in asphaltenes conversion than iron. The hydrogen content of generated solvent decreased with iron and nickel, whereas it was maintained with cobalt and molybdenum. The quality of generated solvent decreased with iron, but it increased with other metals.

Interaction of Metals in Coal Liquefaction - To utilize the selective activity of iron for the conversion of preasphaltenes and of other metals for the conversion of asphaltenes, a sample of coal impregnated simultaneously with iron and molybdenum was liquefied. The conversion of both asphaltenes and preasphaltenes increased with iron/molybdenum mixture compared to iron and molybdenum alone (Table 6). In addition, oils production increased significantly with the mixture compared to iron and molybdenum alone. Iron and molybdenum together not only increased oils production and asphaltenes and preasphaltenes conversion but also significantly increased the overall coal conversion from 87 to 91%. The production of hydrocarbon gas was lower with mixture than either alone. The SRC sulfur content changed slightly, but the change was within the limits of experimental error. These increase in coal conversion, oils production and asphaltenes and preasphaltenes conversion indicated a significant synergistic effect of the two metals.

Hydrogen consumption with the iron/molybdenum mixture was higher than molybdenum and iron alone (Table 6). The hydrogen content of the various fractions generated with iron/molybdenum mixture was very similar to that obtained with iron and molybdenum alone (Table 7). No significant differences were noted in the nitrogen and oxygen contents in the various fractions generated with iron and molybdenum alone or used together except for slightly lower nitrogen content noted in preasphaltene fraction obtained with iron/molybdenum mixture. The quality of solvent generated with iron/molybdenum mixture was higher than iron alone, but was lower than that obtained with molybdenum alone (Table 8).

The above discussion shows that a synergism exists between iron and molybdenum in the catalysis of coal liquefaction reaction. This synergism can be effectively utilized to increase the oils production and the conversion of asphaltenes and preasphaltenes. Furthermore, the increase in oil production can be obtained without significantly increasing hydrogen consumption by taking advantage of synergistic effect. The combination of iron and molybdenum, however, is ineffective in reducing SRC sulfur content.

Conclusion

The impregnation of coal with transition metals like iron, cobalt, nickel, and molybdenum increases the oils production by increasing the asphaltenes and preasphaltenes conversion. Metals impregnation also help in improving overall coal conversion except for nickel. The production of hydrocarbon gases decreases with metals. Likewise, hydrogen consumption decreases with metals. Iron is more active for the conversion of preasphaltenes and the production of oils than other metals, whereas it is less active for the conversion of asphaltenes.

These differences may partly be due to the use of higher concentration of iron than other metals. Since iron is rather inexpensive compared to other metals, it is economically feasbible to use higher concentration. On the other hand, it is not economically feasible to use higher concentration (greater than 200 ppm) of other metals. Simultaneous impregnation of coal with iron and molybdenum shows significant synergism in coal liquefaction. The conversion of coal, asphaltenes, and preasphaltenes and the production of oils are much greater with iron/molybdenum mixture than either of them alone. The mixture also results in lower hydrocarbon gas make than iron and molybdenum alone. The mixture, however, is ineffective in reducing the SRC sulfur content.

Literaure Cited

1. Mukherjee, D. K. and Chowdhury, P. B., Fuel, Vol. 55, No. 4, 1976.

2. Guin, J. A., Tarrer, A. R., Prather, J. W., Johnson, D. R., and Lee, J. M., Ind. Eng. Chem. Process Des. Dev., Vol. 17, pp. 118, 1978.

3. Guin, J. A., Tarrer, A. R., Lee, J. M., Lo, L. and Curtis, C. W., Ind. Eng. Chem. Process Des. Dev., Vol. 18, pp. 371, 1979.

4. Guin, J. A., Tarrer, A. R., Lee, J. M., VanBrackle, H. F., Curtis, C. W., Ind. Eng. Chem. Process Des. Dev., Vol. 18, pp. 631, 1979.

5. Gangwar, T. E., and Prasad, H., Fuel, Vol. 58, pp. 577, 1979.

6. Rottendorf, H., and Wilson, M. A., Fuel, Vol. 59, pp. 175, 1980.

7. Garg, D., Tarrer, A. R., Curtis, C. W., Lloyd, J. M., and Guin, J. A., Prepr. Div. Fuel Chem. Amer. Chem. Society, Vol. 24, pp. 631, 1979.

8. Gray, D., Fuel, Vol. 57, pp. 213, 1978.

9. Granoff, B., Baca, P. M., "Mineral Matter Effects and Catalyst Characterization in Coal Liquefaction," Annual Report (October 1977-September 1978), Sandia Laboratories (SAND-79-0505), Albuquerque, NM, April 1979.

10. Hamrin, C. E., Jr., "Catalytic Activity of Coal Mineral Matter," Interim Report for the Period April-September 1976, prepared for ERDA by University of Kentucky (FE-2233-2).

11. Tarrer, A. R., Guin, J. A., Pitts, W. S., Henley, J. P., Prather, J. W., and Syles, G. A., "Effect of Coal Minerals on Reaction Rates During Coal Liquefaction," Amer. Chem. Society Preprints, "Liquid Fuel from Coal," Academic Press, New York, 1977.

12. Granoff, B. and Thomas, M. G., "Mineral Matter Effects in Coal Liquefaction. 1. Autoclave Screening Study," Paper presented at the 85th National Meeting of AIChE, Philadelphia, PA (1978).

13. Wu, W. R. K., and Storch, H. H., "Hydrogenation of Coal and Tar", U.S. Department of Interior, Bureau of Mines Bulletin 633, 1968.

14. Wright, C. H., and Severson, D. E., Amer. Chem. Soc. Div. Fuel Chem. Prepr., 1972, Vol. 16, 68.

15. Seitzer, W. H., "Miscellaneous Autoclave Liquefaction Studies," Final Report prepared for EPRI by Suntech, Inc., under the contact EPRI AF-612 (RP-799-7), February 1978.

16. Moroni, E. D., and Fischer, R. H., "Disposable Catalyst for Coal Liquefaction", paper presented at the 179th national Meeting of Amer. Chem. Soc., Houston, Texas, March 1980.

17. Gray, D., and Neuworth, M. B., "Disposable Catalysts in Coal Liquefaction: The Effect of Iron Sulfides," Report prepared by the Mitre Corporation for the U.S. Department of Energy (DE-AC01-77ET10280), September 1981.

18. Given, P. H., Spackman, W., Davis, A., Walker, D. L., Jr., and Lovell, H. L., "The Relation of Coal Characterization to Coal Liquefaction Behavior," Reports Nos. 1 and 3 Submitted to National Science Foundation (RANN Division), March 1974 and September 1975.

19. Given, P. H., "Catalysis of Liquefaction by Iron Sulfide from Coals With Some Thoughts on Coal Mineral Analysis," paper presented at the Department of Energy Project Review Meeting on Disposable Catalysts in Coal Liquefaction held in Albuquerque, NM, June 1979.

20. Solvent Refined Coal (SRC) Process, Quarterly Technical Progress Report FE/496-155 Prepared for U.S. Department of Energy by the Pittsburg and Midway Coal Mining Company, Shawnee Mission, Kansas, March 1979.

21. Anderson, R. P., "Low Cost Additives in the SRC Processes." paper presented in the U.S. Department of Energy Project Review Meeting on Disposable Catalysts in Coal Liquefaction held at Albuquerque, NM, June 1979.

22. Garg, D., and Givens, E. N., "Pyrite Catalysis in Coal Liquefaction," Ind. Eng. Chem. Process Des. Dev., Vol. 21, pp. 113, 1982.

23. Ginsberg, H. H., Friedman, S., Lewis, P. S., Schlesinger, M. D., Stewart, A. J. and Hiteshue, R. W., "Hydrogenating Coal in a Pilot Plant with a Molybdenum Catalyst," U.S. Department of Interior, Bureau of Mines Report of Investigation 6573 (1960).

24. Moll, N. G., and Querderer, G. J., "The Dow Coal Liquefaction Process," Chemical Engineering Progress, pp. 46, November 1979.

25. Weller, S., Pelipetz, M. G., Friedman, S., and Storch, H. H., "Coal Hydrogenation Catalysts," Ind. and Eng. Chem., Vol. 42, No. 2, February 1950.

26. Pelipetz, M. G., Kuhn, E. M., Friedman, S., Storch, H. H., "Effect of Catalysts on the Hydrogenation of Coal," Ind. and Eng. Chem., Vol. 40, No. 7, July 1948.

27. Skinner, R. W., and Givens, E. N., "Effect of Solvent Hydrogen Content in the SRC Process," paper presented at the 179th National Meeting of American Chemical Society, Houston, March 1980.

Table 1

Chemical Analysis of Elkhorn #2 Coal Sample

	Weight %
Carbon	77.84
Hydrogen	5.24
Oxygen	7.20
Sulfur	1.08
Nitrogen	1.75
Moisture	1.55
Dry Ash	6.29
Distribution of Sulfur	
Total	1.08
Sulfate	0.04
Pyrite	0.25
Organic	0.79

Table 2

Analysis of SRC-II Heavy Distillate

Element	Weight %
Carbon	89.4
Hydrogen	7.2
Oxygen	1.7
Nitrogen	1.1
Sulfur	0.6

Table 3

Effect of Transition Metals on Coal Liquefaction

Catalyst	None	Iron	Cobalt	Nickel	Molybdenum
Metal Concentration, wt.% Coal	-	1.0	0.02	0.02	0.02
Feed Composition		70% Solvent + 30% Coal			
Temperature, °F	825	825	825	825	825
Pressure, psig	2,000	2,000	2,000	2,000	2,000
Hydrogen Flow Rate, MSCF/T	18.9	20.6	23.8	23.8	23.7
Reaction Time, Min.	35	32.8	36.7	37	36.5
Product Distribution, wt.% MAF Coal					
HC	5.2	3.5	3.8	4.8	4.1
CO, CO_2	0.7	0.6	0.7	0.7	0.7
H_2S	0.3	0.2	0.4	0.6	0.6
Oils	12.2	25.0	21.5	20.0	21.7
Asphaltenes	21.2	19.1	17.7	17.0	17.6
Preasphaltenes	44.2	35.8	40.2	38.5	40.3
I.O.M.	14.7	13.5	14.3	16.5	13.7
Water	1.5	2.3	1.4	1.9	1.8
Conversion	85.3	86.5	85.7	83.7	86.8
Hydrogen Consumption, Wt.% MAF Coal	0.64	0.40	0.39	0.33	0.40
SRC Sulfur, %	0.6	0.6	0.6	0.5	0.6

Table 4

Distribution of Elements in Various Liquefaction Reaction Fractions

Catalyst	None	Iron	Cobalt	Nickel	Molybdenum
Oil Fraction, wt.%					
C	89.5	89.9	89.6	89.8	89.5
H	7.2	7.1	7.2	7.1	7.2
O[a]	1.7	1.5	1.7	1.7	1.7
N	0.9	0.8	0.8	0.8	0.9
S	0.7	0.7	0.7	0.6	0.7
Asphaltene Fraction, wt.%					
C	85.9	85.6	85.6	85.0	85.3
H	6.3	6.0	5.8	5.9	5.9
O[a]	4.8	5.5	5.7	6.2	6.0
N	2.4	2.4	2.3	2.4	2.2
S	0.6	0.5	0.6	0.5	0.6
Preasphaltene Fraction, wt.%					
C	85.3	82.9	83.5	83.6	83.4
H	5.2	4.9	4.7	4.6	5.1
O[a]	6.2	8.9	8.9	9.0	8.3
N	2.2	2.6	2.3	2.3	2.6
S	0.6	0.7	0.6	0.5	0.6

[a] Oxygen is determined by difference.

Table 5

Distribution of Protons in the Oil Fraction

Catalyst	Process Solvent	Generated Solvent				
		None	Iron	Cobalt	Nickel	Molybdenum
Total Hydrogen, wt.%	7.2	7.2	7.1	7.2	7.1	7.1
H_{AR}	3.20	3.26	3.64	2.90	2.88	2.75
H_a	2.02	1.95	1.80	2.12	2.24	2.32
H_o	1.98	1.99	1.66	2.18	1.97	2.13

H_{AR} = concentration of aromatic protons

H_a = concentration of alpha protons defined as protons on carbon atoms immediately adjacent to an aromatic ring.

H_o = concentration of beta and higher protons defined as those protons residing on two or more carbon atoms removed from an aromatic ring.

Table 6

Synergistic Effect in Coal Liquefaction

Catalyst	Iron	Molybdenum	Iron + Molybdenum
Metal Concentration, wt.% coal	1.0	0.02	1.0 iron + 0.02 molybdenum
Feed Composition	70% Solvent + 30% Coal		
Temperature, °F	825	825	825
Pressure, psig	2,000	2,000	2,000
Hydrogen Flow Rate, MSCF/T	20.6	23.7	23.4
Reaction Time, Min	32.8	36.5	37.2
Product Distribution, wt.% MAF Coal			
HC	3.5	4.1	3.1
CO, CO_2	0.6	0.7	0.7
H_2S	0.2	0.6	0.6
Oils	25.0	21.7	36.3
Asphaltenes	19.1	17.6	15.2
Preasphaltenes	35.8	40.3	33.0
I.O.M.	13.5	13.7	9.3
Water	2.3	1.8	1.8
Conversion	85.6	86.8	90.7
Hydrogen Consumption, wt.% MAF Coal	0.4	0.40	0.59
SRC Sulfur, %	0.6	0.6	0.7

Table 7

Distribution of Elements in Various Liquefaction Fractions

Catalyst	Iron	Molybdenum	Iron • Molybdenum
Oil Fraction, %			
C	89.9	89.5	89.8
H	7.1	7.2	7.2
O[a]	1.5	1.7	1.6
N	0.8	0.9	0.8
S	0.7	0.7	0.6
Asphaltene Fraction, %			
C	85.6	85.3	85.1
H	6.0	5.9	5.9
O[a]	5.5	6.0	6.0
N	2.4	2.2	2.4
S	0.5	0.6	0.6
Preasphaltene Fraction, %			
C	82.9	83.4	83.7
H	4.9	5.1	4.9
O[a]	8.9	8.3	8.4
N	2.6	2.6	2.3
S	0.7	0.6	0.7

[a] Oxygen is determined by difference.

Table 8

Distribution of Protons in the Oil Fraction

Catalyst	Iron	Molybdenum	Iron + Molybdenum
Total Hydrogen, wt.%	7.1	7.2	7.2
H_{AR}	3.64	2.75	2.92
H_a	1.80	2.32	2.15
H_o	1.66	2.13	2.13

DISPOSABLE CATALYSTS IN TWO-STAGE COAL LIQUEFACTION

S.B. Reddy Karri and V.K. Mathur*

Department of Chemical Engineering
University of New Hampshire
Durham, NH 03824

Introduction

In Two Stage Liquefaction, coal is dissolved and partially hydrogenated in the short contact time first stage using process derived solvent as vehicle oil. The unreacted coal and ash are removed by antisolvent deashing and the product oil is upgraded in a separate catalytic reactor (Stage II). This scheme is proposed as a means of converting coal to distillate with higher yield, reduction in hydrogen consumption, and minimal catalyst poisoning since no catalyst is used in the first stage. A number of papers have been published discussing various aspects of this technique (1,2,3,4,5).

In this investigation a disposable ore catalyst consisting of a mixture of bauxite, limonite, and molybdenum ore concentrate is added to the first stage and its effect on the yield and quality of the product oil from the second stage is studied.

Rationale for the Use of Ores as Catalysts

Our research work (6,7) as well as a literature review reveals that cobalt and molybdenum are eminently suited catalysts for hydrogenation and hydrodesulfurization of coal, whereas nickel and molybdenum are good for hydrodenitrogenation. Other metals like iron, copper, tin, zinc, platinum, and tungston have also been found to be effective in coal liquefaction (8). The most inexpensive sources of these metals are their ores where they are present mostly as sufides or oxides.

A number of researchers (9,10) have shown iron pyrites to be an effective catalyst in coal liquefaction. Our earlier studies (11,12,13) have shown that mixtures of iron pyrites and minerals containing other catalytic active transition metals were better liquefaction catalysts than iron pyrites alone. The best ore catalysts tested, in terms of high liquid yield and low product oil viscosities, were mixtures of pyrites, molybdenum ore concentrate, and cobalt-containing ores.

In this study an acid treated (14) mixture of bauxite, limonite and molybdenum ore concentrate was used as a disposable catalyst in the first stage. In the second stage a commercial supported nickel-molybdenum catalyst was used for hydroprocessing.

*Inquiries should be addressed to this author.

Materials, Experimental Equipment, and Experimental Procedure

The major materials used in this study consisted of bituminous coal, a coal-derived heavy distillate, and a disposable ore catalyst. Bitminous coal from the Blacksville No. 2 mine, West Virginia (Pittsburgh seam) whose proximate and ultimate analyses are presented in Table I was used. The vehicle oil was distillate with a boiling range 232-455°C produced at the Ft. Lewis pilot plant running in the SRC-II mode.

A mixture of acid treated bauxite, limonite, and molybdenum ore concentrate (analyses of ores given in Table II) was used as a disposable catalyst in Stage I. A commercially available supported Ni-Mo-alumina catalyst from American Cynamid Co. (HDS-3) was used as a hydroprocessing catalyst for the Stage II. The catalyst and coal used were ground to minus 200 mesh. Hydrogen gas of > 99.95% purity was used.

Experimental Equipment

The hydrogenation reaction was carried out in a stainless steel liner placed in a high pressure internally stirred autoclave of one liter capacity. The experiments were carried out at a stirrer speed of 1000 rpm. The autoclave was provided with a cooling coil through which water could be passed to reduce the reaction temperature if so desired. The autoclave had an electric furnace controlled with a proportional temperature controller. The temperature of the reaction mass was continuously monitored by a temperature recorder. In addition, the autoclave was provided with a thermowell, a pressure gauge, a vent, a sampling valve, and a safety rupture disc. A compressor was used to pressurize the autoclave with hydrogen.

Experimental Procedure

Each of the experimental runs consisted of two stages. In the first, SRC-II distillate was used as the vehicle while in the second, the liquid product from the first stage was used instead. This procedure was followed to approximate the use of product oil from the Stage I for hydroprocessing in Stage II.

Stage I Liquefaction: Forty grams of crushed coal were placed in the liner. About 83.6 gms of SRC-II distillate (in approximately 1:2.1 ratio) were then added to the liner. A pre-determined amount of the disposable ore catalyst was next added to the contents of the liner. The stirrer assembly was fitted onto the autoclave and securely bolted. After testing for leakage, the autoclave was purged with hydrogen. It was then pressurized to a predetermined value so that a pressure of about 2000 psig (13.79 MPa) was reached at the reaction temperature. The heating was initiated thereafter. It usually took 65-70 minutes to heat the autoclave and its contents from room temperature to reaction temperature. The reaction was then allowed to proceed for a given period of time. The temperature was maintained at the reaction temperature during this period. After the elapse of reaction time, the reaction was arrested by turning off the power to the furnace and cooling the contents down rapidly by passing cold water through the cooling coil. The autoclave was allowed to cool down to room temperature by leaving it overnight. The lique-

Table I

Proximate and Ultimate Analyses of Coal Sample

Proximate Analysis	As Recd. %	Moist. Free %	Moist., Ash Free %
Moisture	1.2	N/A	N/A
Volatile	35.8	36.2	41.0
Fixed Carbon	51.5	52.1	59.0
Ash	11.5	11.7	N/A

Ultimate Analysis	As Recd. %	Moist. Free %	Moist., Ash Free %
Hydrogen	5.0	4.9	5.5
Carbon	72.0	72.9	82.5
Nitrogen	1.0	1.2	1.4
Sulfur	2.7	2.7	3.1
Oxygen	7.7	6.7	7.6
Ash	11.5	11.7	N/A
Btu/lbm	12,892	13,052	14,776

Table II

Mineral Ores and Their Percent Composition

1.	Limonite	Ni	1.1	Si	16.4
		Mg	9.8	Fe	20.2
		Al	1.4	Cr	0.5
2.	Molybdenum Oxide Concentrate (Moly. Corp.)	Mo	47.0	Ca	0.4
		Fe	2.8	Cu	0.5
		Si	3.5	Sn	0.4
		Mg	0.6	Zn	0.2
		Al	0.6	K	0.2
		S	0.4		
3.	Bauxite (Canada)	Mn	0.1	Si	1.9
		Ni	0.5	Ca	0.3
		S	0.1	Co	0.1
		Sn	0.7	Al	28.8
		Ti	10.1	Cr	0.3
		Mo	0.2	Cu	0.1
		Ag	0.1	Fe	5.6
		Na	0.6	K	0.3
				Mg	0.1

fied products were then taken out of the autoclave and hot filtered to remove unconverted coal, ash, and catalyst. The filtered liquid and residue were weighed and percent conversion and liquefaction calculated. Viscosity of the product liquid at 60°C was determined using a Brookfield viscometer.

Stage II Liquefaction: The same procedure was repeated using filtered product liquid from the Stage I. A commercial supported Ni-Mo catalyst was used for this stage.

Results and Discussion

The main objective of this investigation was to study the effect of addition of a disposable catalyst in the Stage I on the yield and quality of product oil from the Stage II. The percent conversion, percent oil yield and viscosity of the product oils are presented in Table III.

Percent conversion and liquefaction of coal are defined as follows:

Percent Conversion = {Original Coal (macf) - Residue (macf)} x 100/Original Coal (macf)

Percent Liquefaction = Liquid Products x 100/Original Coal (macf)

where macf = moisture, ash, catalyst free

Experiments S.N. 1 through 12 show the effect of addition of a disposable catalyst to Stage I. Experiments were conducted at reaction time of 30, 10, and 6.5 minutes for Stage I, whereas reaction time for Stage II was kept constant at 30 mintues. The other operating conditions were maintained the same as mentioned earlier under experimental procedure. It was found that percent coal liquefaction for all Stage I reaction time was about 10 percent higher when the disposable catalyst was used. Similarly, viscosity of product oil, from both Stage I and II, was lower for all Stage I reaction time when the disposable catalyst was used. Product oil from Stage II showed about 35 percent reduction in viscosity with the use of our disposable catalyst in Stage I.

In another set of experiments S.N. 13 through 16, effect of reaction temperature on product oil viscosity from Stage II was studied. Experiments were conducted at reaction time and temperature of 30 minutes and 400°C in Stage II, respectively, with and without the use of the disposable catalyst in Stage I. The first stage liquefaction was conducted at reaction time and temperature of 6.5 minutes and 425°C, respectively. The viscosity of product oil from Stage II was found to be lower by only about 20 percent as compared to 35 percent in earlier experiments S.N. 9 through 12. This is considered due to lower reaction temperature in Stage II.

Solvent analysis (15) was performed on product oil from Stage II for experiments S.N. 14 and 16. It was found that asphaltene content (cyclohexane insolubles) of product oil with no catalyst used in Stage I was 12.3 against 8.3 percent when liquefaction was conducted in Stage I in presence of the disposable catalyst. Preasphaltene (THF insolubles) content was found to be 0.3 percent in both the cases.

Table III

Liquefaction of Coal Using Two Stage Process

Serial Number	Name of Catalyst/Ore	Stage Number	%Catalyst (Based on maf coal/oil)	Reaction Time (mins.)	Reaction Temperature (C)	%Conversion	%Liquefaction	Viscosity, cp @60 C	Difference (% conv.-% Liq.)
1	--	I	--	30	425	85	70	28.5	15
2	Co-Mo Harshaw 0402T	II	1.0*	30	425	--	--	9.8	--
3	Limonite Moly. Oxide Conc. Bauxite	I	1.19 0.572 3.58	30	425	88	82	21.0	6
4	Co-Mo Harshaw 0402T	II	1.0*	30	425	--	--	6.1	--
5	--	I	--	10	425	83	69	42.4	14
6	Ni-Mo HDS-3 MTG-S-0658	II	1.0*	30	425	--	--	18.0	--
7	Limonite Moly. Oxide Conc. Bauxite	I	1.19 0.572 3.58	10	425	85	81	31.2	4
8	Ni-Mo HDS-3 MTG-S-0658	II	1.0*	30	425	--	--	11.0	--

Table III (cont.)

Serial Number	Name of Catalyst/Ore	Stage Number	%Catalyst (Based on maf coal/oil)	Reaction Time (mins.)	Reaction Temperature (C)	%Conversion	%Liquefaction	Viscosity, cp @60 C	Difference (% conv.-% Liq.)
9	--	I	--	6.5	425	83	69	68.0	14
10	Ni-Mo HDS-3 MTG-S-0658	II	1.0*	30.0	425	--	--	22.0	--
11	Limonite Moly. Oxide Conc. Bauxite	I	1.19 0.572 3.58	6.5	425	85	80	38.4	5
12	Ni-Mo HDS-3 MTG-S-0658	II	1.0*	30	425	--	--	14.25	--
13	--	I	--	6.5	425	84	70	66.0	14
14	Ni-Mo HDS-3 MTG-S-0658	II	1.0*	30.0	400	--	--	29.0	--
15	Limonite Moly. Oxide Conc. Bauxite	I	1.19 0.572 3.58	6.5	425	87	81	36.0	6
16	Ni-Mo HDS-3 MTG-S-0658	II	1.0*	30	400	--	--	23.0	--

* Percentage Catalyst Based on Product Oil from Stage I.

Conclusions

The disposable catalyst containing acid treated bauxite, limonite, and molybdenum ore concentrate when used in the first stage of the Two-Stage Liquefaction process improved the yield and quality of product oil. Coal liquefaction yield in Stage I increased by about 10 percent with the use of this catalyst. Similarly, the viscosity of product oil from Stage II showed a decrease of 20-35 percent when the disposable ore catalyst was used in Stage I.

References

1. Neuworth, M.B. and Moroni, E.C. "Fundamental Aspects of an Integrated Two-Stage Liquefaction Process," Presented at Int. Conf. on Coal Science, Dusseldorf, W. Germany, 1981.

2. Carson, T.C., Hastings, K.E. and Potts, J.D. "Two Step Coal Liquefaction is a Hydrogen Efficient Route to Distillate Fuels," Can. J. of Chem. Eng. 58, 703, 1980.

3. Chillingworth, R.S., Hastings, K.E., Potts, J.D. "LC-Finishing of SRC - A Logical Second Stage in Two-Step Coal Liquefaction," Presented at 87th AiChE National Meeting, Boston, 1979.

4. Schindler, H.D., Chen, J.M., and Peluso, M., "The Integrated Two-Stage Liquefaction Process," Presented at AIChE Annual Meeting, New Orleans, 1981.

5. Neuworth, M.B. and Maroni, E.C., "Development of a Two-Stage Liquefaction Process," Presented at Inst. of Gas Technology, Louisville, KY, 1979.

6. O'Leary, M.J., Stetson, D.C., Mathur, V.K., "Catalytic Coal Liquefaction by $CO-H_2O$," Coal Processing Technology, 5, 84, 1979.

7. Guttal, V., and Mathur, V.K., "Catalytic Desulfurization of Coal Using CO and Steam," Presented at the AIChE - IMIQ Meeting, Acapulco, Mexico, 1980.

8. Weller, S., Pelepetz, M.G., Friedman, S., Storch, H.H. "Coal Hydrogenation Catalysts," Ind. Eng. Chem. 42, 2, 330, 1950.

9. Thomas, M.G., Bickel, T.C., and Gramnoff, B. "The Effect of Catalysts on Short Contact Time Coal Liquefaction," ACS, Division of Fuel Chemistry, 26, 6, 173, 1981.

10. The Pittsburgh and Midway Coal Mining Co, "Liquefaction of Bituminous Coals with Added Catalysts," Technical Report No. DOE/PC/40005-20, 1982.

11. Mathur, V.K., "Disposable Catalyts in Coal Liquefaction," Presented at 64th CIC Coal Symposium, Halifax, Nova Scotia, 1981.

12. Mathur, V.K., Venkataramanan, V. "Mineral Ores as Disposable Catalysts in Coal Liquefaction," ACS 183rd National Meeting, Las Vegas, Vol. 27, 1, 1982.

13. Mathur, V.K., Fakoukakis, E.P., "Coal Liquefaction Using Ore Catalysts," Presented at AIChE Annual Meeting, Los Angeles, 1982.

14. Pratt, K.G., and Christoverson, V., "Hydrogenation of a Model Hydrogen - Donor System Using Activated Red Mud Catalyst," Fuel, 61, 5, 460, 1982.

15. Personal Communication, Pittsburgh Energy Technology Center, Pittsburgh (Pa), 1982.

COAL LIQUEFACTION WITH TIN OXIDE CATALYST

M. Mizumoto, H. Yamashita, and S. Matsuda
Hitachi Research Laboratory
Hitachi Ltd.
Ibaraki, Japan 31912

INTRODUCTION

In recent years, a large amount of work has been performed in the region of coal chemistry. Liquefaction of coal has been investigated widely not only of industrial application but also fundamental interests. Various catalysts are examined in a huge amount of papers reported. They are classified into many categories. One of them is metal oxide catalyst. Metal oxide catalysts are easily prepared and handled. Iron oxide catalyst and HDS catalyst have been tested in pilot scale experiments. In this paper, we examined the catalytic activity of metal oxide catalysts for direct liquefaction of coal.

It is useful to investigate the mechanism of the liquefaction of coal using model compounds which are typical of coal. In the latter part of this paper, we examine the hydrogenation of benzyl ether and discuss the reaction path of liquefaction.

EXPERIMENTAL SECTION

Figure 1 shows the experimental apparatus used in this work. The autoclave was made of stainless steel. Coal or model compounds were mixed with solvent and catalyst in the autoclave by continuous stirring. The autoclave was heated up to reaction temperature at a rate of 5°C/min under pressurized hydrogen.

Liquid products were seperated into three fractions by solvent extraction. That is, n-hexane soluble fraction was called oil, n-hexane insoluble and toluene soluble fraction was called asphaltene, and toluene insoluble fraction was called residue. Conversion of coal was calculated from the weight of residue (daf). Gas chromatography was used for analysis of gas and liquid products. Residue was analyzed by X-ray diffraction.

The composition of coals used in this work is shown in Table 1. Powdered coal (0.1 - 0.4 mm) was mixed with twofold of creosote oil. Catalysts were prepared by the following methods. That is, calcination of hydroxide (Fe_2O_3, TiO_2, MnO, ZnO, SnO_2) and impregnation method (Co-Mo-Al_2O_3, Ni-Mo-TiO_2). Powdered catalyst passed through a 200 mesh sieve was mixed with slurry in a ratio of 5 wt% to coal. Benzyl ether, phenyl ether, and dibenzyl were used as model compounds. They were added to 1-methylnaphthalene (MN) or tetralin and hydrogenated in the presence or absence of SnO_2 catalyst.

RESULTS AND DISCUSSION

Coals were liquefied at 450°C for 30 min under pressure of 150 atm. Pressurized hydrogen was allowed to flow at a rate of 300 l/hr (stp).

Figure 2 shows the conversion of Taiheiyo coal liquefied with various catalyts. It was found that SnO_2 catalyst showed the highest activity, and that the conversion of coal and yield of oil reached 100% and 75%, respectively. Consequently the reactions with SnO_2 catalyst were examined in detail hereafter.

At first, three kinds of coal were liquefied with SnO_2 catalyst under the same conditions mentioned above. Conversion of coal is shown in Figure 3. It was found that the conversion of coal increases with the content of volatile matter.

It was found that catalyst distributed in residue was reduced to metallic tin from X-ray diffraction analysis. Therefore it was considered that catalyst present in coal mixture under reaction conditions is melted tin metal.

The following scheme is well-known as the reaction path for coal liquefaction.

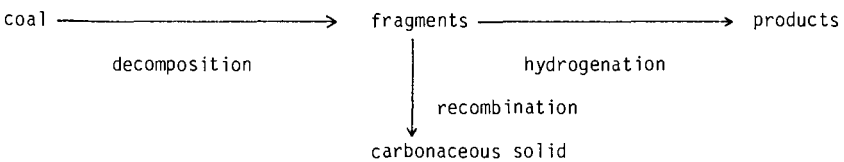

Scheme I

Coal is thermally decomposed to fragments followed by hydrogenation and recombination reactions. Fragments were recombined with each other to form carbonaceous solid which is one of the components of residue. When SnO_2 was used as catalyst, residue was not formed. It is considered that SnO_2 has higher selectivity for hydrogenation than for recombination. In order to confirm the reason we examined the hydrogenation of model compounds.

Benzyl ether was hydrogenated with or without SnO_2 catalyst under initial pressure of 150 atm. Figure 4 shows the gas chromatograms of products hydrogenated at 350°C in 1-methylnaphthalene. There are some differences in product distribution. In the presence of SnO_2 catalyst, benzyl ether decomposed to toluene and benzyl alcohol. Compounds which have higher boiling points than benzyl ether (called HBP compounds) such as fluoranthene were formed at low selectivity. On the contrary, the selectivity to HBP compounds increased in the absence of SnO_2 catalyst. Products from hydrogenation of benzyl ether with several catalysts are shown in Table 2. The selectivity to HBP compounds was found to be about 40% without SnO_2 catalyst, while in the presence of SnO_2 about 10%. It was also found that the selectivity was independent of the hydrogen donating property of solvent.

Phenyl ether and dibenzyl were hydrogenated under the same conditions. Compared with benzyl ether, conversions of them were low due to higher bond energy.

It was deduced that decomposition of benzyl ether takes place by the following scheme from the results of this work.

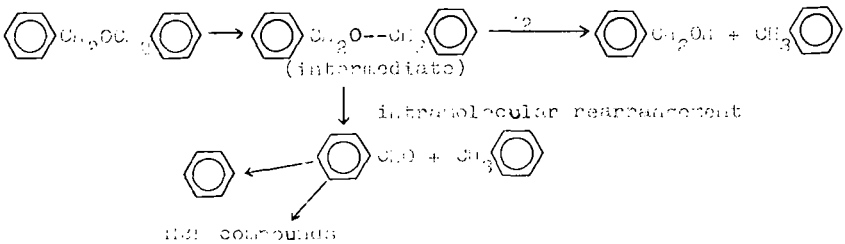

Scheme II

Benzyl ether decomposed to benzaldehyde and toluene accompanied with intramolecular rearrangement of hydrogen without SnO_2 catalyst. Benzaldehyde decomposed consecutively to benzene and reacted with solvent molecule to form HBP compounds such as fluoranthene. On the contrary, the reaction path seems to be different in the presence of SnO_2 catalyst. It was considered that the rate of hydrogenation of intermediate becomes higher than that of rearrangement with SnO_2. Therefore benzyl ether decomposed to toluene and benzyl alcohol with low selectivity to HBP compounds.

In this paper we discussed the reaction path of hydrogenation of coals and model compounds. It was concluded that tin interacts with fragments of coal and stabilized fragments to prevent recombination reaction.

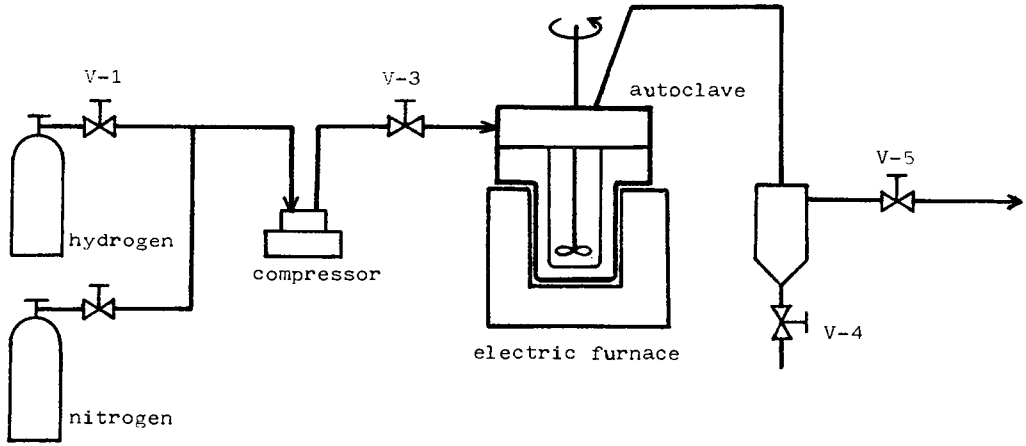

Figure 1. Experimental apparatus

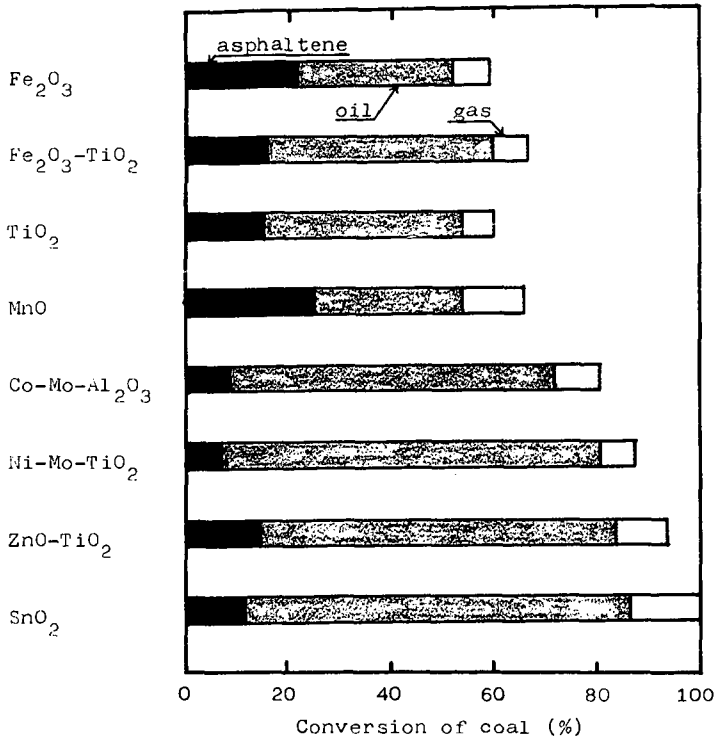

Figure 2. Liquefaction activity of catalysts. reaction temperature; 450 C, reaction time; 30min, H_2 pressure; 150atm

Table 1. Composition of coal.

coal	proximate analysis (%)				ultimate analysis (%)		
	ash	moisture	v.m.	f.c.	C	H	N
Taiheiyo	13.9	5.1	43.8	37.2	63.9	5.6	1.1
Mi-ike	16.2	2.6	37.2	44.0	68.8	5.0	1.1
Da tong	9.7	1.9	28.9	59.5	77.5	4.6	0.9

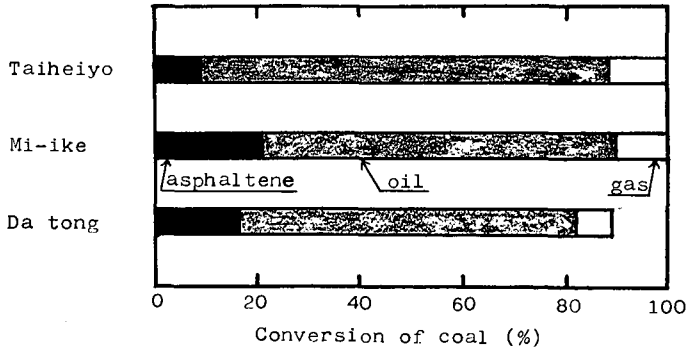

Figure 3. Reactivity of coal with SnO_2.
reaction temperature; 450°C, reaction time; 30min, H_2 pressure; 150atm

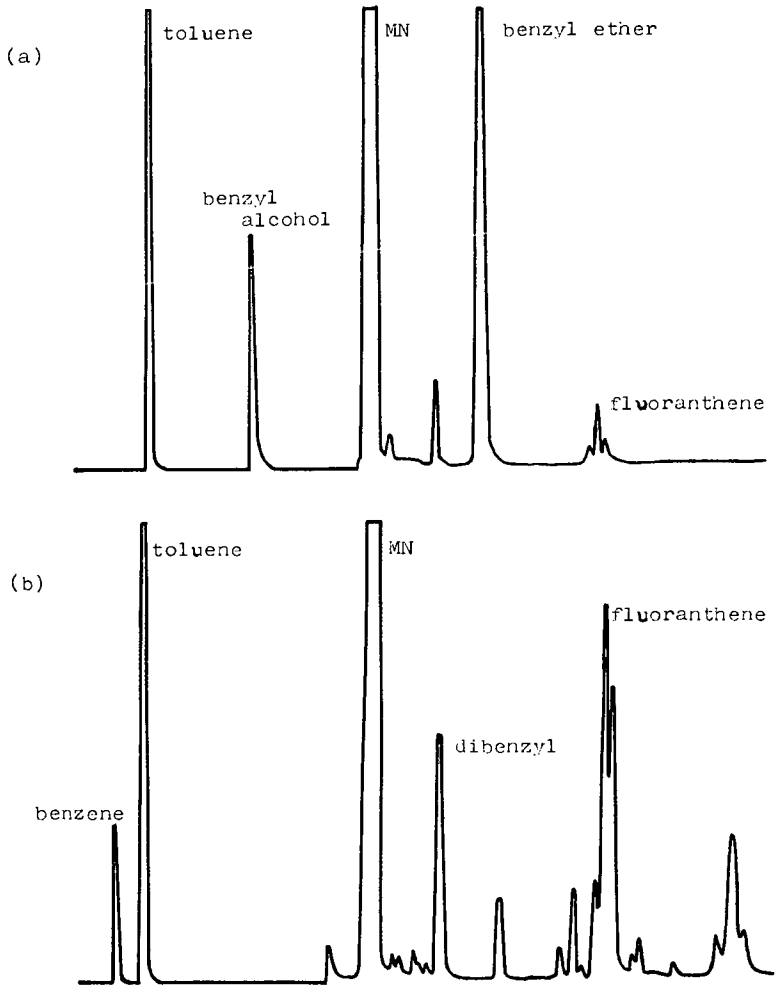

Figure 4. Gaschromatograms of products from hydrogenation of benzyl ether (a) with SnO_2, (b) without SnO_2. reaction temperature; 350°C, reaction time; 30min, initial H_2 pressure; 150atm

Table 2. Products from hydrogenation of benzyl ether.

catalyst	solvent	selectivity (%)			
		benzene	toluene	benzyl alcohol	HBP compounds[§§]
no	MN[§]	4.7	57.0	0	38.3
	tetralin	2.4	55.8	0	41.8
Ni-Mo-TiO_2	tetralin	9.9	45.6	0	44.5
SnO_2	MN	0	51.6	38.4	10.1

§ 1-methylnaphthalene

§§ compounds whose boiling points are higher than benzylether

A STRUCTURAL INVESTIGATION OF THE EFFECT OF CATALYSIS ON THE LIQUEFACTION PRODUCTS OF A BROWN AND A BITUMINOUS AUSTRALIAN COAL

M.G. Strachan,[A] A.M. Vassallo[B] and R.B. Johns[A]

A. Department of Organic Chemistry, University of Melbourne, Parkville, Victoria, Australia 3052.
B. C.S.I.R.O. Division of Fossil Fuels, North Ryde, N.S.W., Australia 2113.

INTRODUCTION

The effect of catalysts on the donor solvent hydrogenation of Australian coals, both brown and black, have been investigated by a number of workers (1-5). However, these studies have concentrated mainly on obtaining conversion, oil yield, asphaltene and preasphaltene data, rather than emphasising chemical structural analysis of the resultant products. To solely use the forementioned criteria as a basis for catalyst evaluation can and may be misleading, as the product quality is an unknown parameter, which can give much insight into both the effectiveness and mechanism of catalysis.

The paper reports a study comparing the effects of a single catalyst, Co/Mo, on two Australian coals of different rank at their uncatalyzed optimal oil yield temperatures (4)(8)(9) under donor solvent conditions. It was considered more appropriate to compare the products from the two coals at their respective optimal oil yield temperatures rather than at the same temperature. The former accounts and compensates for differing thermal reactivities with rank, thereby allowing a direct comparison of product qualities to be made.

The coals used for the study were a Victorian brown coal, LY1277, from the Loy Yang Field, a medium-light lithotype, and a N.S.W. high volatile bituminous coal from the Liddell Field. They were chosen because of their known liquefaction potential. They were reacted at 375°C and 425°C respectively, in batch autoclaves using a solvent (tetralin) coal ratio of 2:1, a catalyst concentration of 10% w/w coal and were reacted for 2 hours at temperature.

The total liquid product (TLP) (defined as CH_2Cl_2 solubles) was fractionated by a separation method (6) designed specifically to separate by functionality into chemically defined classes *viz.* acids, bases and neutrals. This method utilizes a sequence of ion-exchange resins and silica adsorption chromatography. A feature of the method is that it does not remove the donor solvent until all the polar material is absent, hence alleviating the risk of thermal alteration of the samples as may occur with an initial dissolution step. The method is very effective in class separation.

The TLP, residues and the resulting fractions have been investigated by a number of analytical and spectroscopic methods in an attempt to use chemical analysis as a probe for investigating the effectiveness, mode of action, and structural dependence of the catalyst. Although the TLP has been fractionated into its component classes the majority of the data reported here concerns mainly the TLP and residue.

RESULTS AND DISCUSSION

The effect of the Co/Mo catalyst on the two coals, as judged by normal liquefaction criteria is shown in Table 1. In both cases conversion increased with catalysis,

however the oil yields for the catalyzed (C) Liddell run was lower than for the uncatalyzed (UC), run, the converse of the Loy Yang case. The oil yield for the uncatalyzed Liddell run was much better than for both the Loy Yang runs, with the catalyzed Liddel run being only slightly lower in yield than the catalyzed Loy Yang run. On a conversion basis the catalyzed Liddell run gave 92% conversion compared to 62% for the uncatalyzed run, and 75% and 60% for the catalyzed and uncatalyzed Loy Yang runs respectively. Hence, on an oil yield/conversion basis the coals exhibit different liquefaction behaviour. Catalytic liquefaction of Liddell markedly increases conversion, but decreases oil yield. The increased conversion is at the expense of increased H_2O production and gasification. The gases being predominantly hydrocarbons. To determine the effect of catalyst, as to whether it primarily increases oil yield and/or conversion, or actually upgrades the products, the ratio of the H_2O and gases to oil yield must be taken. Clearly the ratio of H_2O/oil yield and gas/oil yield is very similar for the Loy Yang runs (Table 1), while it is markedly different between the two Liddell runs. These data indicate that in the Loy Yang runs the catalyst is not removing heteroatoms or upgrading the product, but rather interacting only with the coal and assisting its dissolution. However in the Liddell case the marked increase in the two ratios indicates both cleavage of alkyl side chains and heteroatom removal (i.e. the product is being affected by the catalyst).

Elemental analysis (Table 2) gives credence to these initial conclusions with H/C and O/C ratios being marginally higher for the uncatalyzed Loy Yang oil than the catalyzed oil, but still very similar. Whereas, the Liddell runs show the converse *viz.*, increased H/C and much decreased O/C for the catalyzed compared to the uncatalyzed oil. Data on the oils (Table 3) shows the composition (% w/w oil) of the LY1277 oils to be very similar (similar percentages of the various acidic, basic and neutral materials). This adds further to the hypothesis that the catalyst is primarily increasing the yield of product rather than upgrading it. If the catalyst had acted on the oil it would not be unreasonable to expect differences in the composition of the oils. This is indeed shown with the Liddell oils, where the uncatalyzed oil has 75% of its material as acids and bases (25% and 50% respectively), whereas in the catalyzed oil over 75% of the material is neutral, with less than 16% being basic. It is observed that nearly 70% of the oil exists as nonpolar neutrals which are predominantly aliphatic and aromatic hydrocarbons (7), whereas in the uncatalyzed oil this fraction represents only 14%. This is in marked contrast to the LY1277 oils where their respective percentages of nonpolar neutrals is very similar, as is the percentage of polar neutrals. Obviously this data shows quite markedly that for the Liddell oils the catalyst is acting not only on the coal but also on the resultant product, upgrading it via loss of functionalities to produce hydrocarbon neutral material. This data reaffirms the trends shown by H_2O/oil yield and gas/oil yield ratios.

Spectroscopic and molecular weight data further confirms these trends. A comparison of IR spectra (Figs. 1, 2), using semi-quantitative methods reveals only a minor decrease in the -OH absorption for the catalyzed LY1277 oil, whilst there is a marked reduction in the same absorption in the catalyzed Liddell oil. This is reinforced by the analogous reduction in the H_{OH} as shown by ^1H nmr. The aromaticities as determined by ^{13}C nmr (Fig. 3) of both catalyzed oils increased marginally over their uncatalyzed counterparts, with both the Liddell oils being much more aromatic than the LY1277 oils.

^1H nmr has shown there to be a reduction in the amount of aromatic protons (Har) for the catalyzed compared to the uncatalyzed LY1277 oil, the converse occurred for the Liddell oils (Table 4). Similarly, the percentage of methylene protons (Ho) and hence average side chain length increased for the catalyzed LY1277 oil compared to the uncatalyzed oil, whereas there was a marked reduction in both for the catalyzed Liddell oil. This is not surprising considering the high yield of

hydrocarbon gases from the latter, most probably formed from side chain cleavage. This view is further substantiated by the increase in the percentage of protons or carbons α to aromatic rings ($H\alpha$) compared to the uncatalyzed Liddell oil. However, with the catalyzed LY1277 oil there is a marked reduction in the percentage of $H\alpha$. This observation and the increase in Ho suggests that the catalyst may be operating in either of two ways: (a) hydrogenating aromatic rings or (b) enhancing the cleavage and hence ring opening of naphthenic rings in the coal structure. It is more likely the latter is occurring as the former was not observed for the Liddell oil, which also contains aromatic rings, and the structure of brown coal is suggested as having a large proportion of naphthenic rings and arene systems (10). This mode of action of the catalyst is more consistent with the other data, suggesting it is operating on the decomposition and dissolution of the coal rather than upgrading the oil. Modified Brown-Ladner equations (11) showed the LY1277 oils to both have a similar degree of substitution, whereas the Liddell oils were much lower in value with the catalyzed oil being substantially lower than that for the uncatalyzed oil. This trend is also shown by the Har/Car ratio, from both the modified Brown-Ladner method and directly from ^{1}H and ^{13}C nmr, (cf. Table 4) where the degree of condensation is much reduced for the uncatalyzed compared to the catalyzed Liddell oil, which in turn is similar in value to the LY1277 oils

This is suggestive of the catalyzed Liddell oil having a smaller average ring size and hence molecular weight than the other oils. Molecular weight data proves this to be the case, with the catalyzed Liddell oil having a MW less than half that of the uncatalyzed oil (169 and 379 respectively). The latter is slightly less than that found for the LY1277 oils which in turn have similar MWs (498 for the uncatalyzed and 512 for the catalyzed oil).

The semi-quantitative IR data agrees very well with that from ^{1}H nmr. The aromatic C-H bending region in the IR increases only marginally for the catalyzed Loy Yang oil (Fig. 1) but is markedly increased for the catalyzed Liddell oil (Fig. 2). The differences in the relative amounts of -OH stretchings are also reaffirmed by the amount of -C-O- IR spectral intensity, with the Liddell oils being less than the LY1277 oils, and the catalyzed Liddell oil being markedly reduced in the amount of -C-O- stretching while the LY1277 is only marginally reduced. Similarly the ^{13}C nmr also agreed with the ^{1}H nmr data, indicating that the $C_{aliphatic}/C_{aromatic}$ ratio decreases quite markedly between the LY1277 and Liddell oils (Fig. 3), but only slightly between the uncatalyzed and catalyzed oil from the same coal.

IR investigations of the residues revealed that the contribution of aliphatic $-CH_2-$, $-CH_3$ bending regions were greater in the catalyzed than in the uncatalyzed residues. CP-MASS ^{13}C nmr of LY1277 catalyzed residue (Fig. 4) showed it to have a lower aromaticity than the uncatalyzed residue, but still higher than the parent coal. For the Liddell case, hower, both residues had the same aromaticity which again were higher than the parent coal. The data from the LY1277 residues indicates that the catalyst, may in fact be hydrogenating aromatic rings whilst dissolving the coal. Why this occurs only for LY1277 and not for Liddell may be due to the selectivity of the catalyst, displaying structural dependence for the chemically very different starting materials. The result is surprising considering the previous data on the oils and the similar aromaticities, but not if the differing structures of the two coals are taken into account.

Pyrolysis-Gas Chromatography of the residues and the parent coals reaffirms previous observations that the catalyst does alter the organic structure of the residues. A main observation is the loss of the alkane/alkenes in the catalyzed Liddell residue, while they are present in the uncatalyzed residue. This agrees with the marked increase in hydrocarbon gas production in the former. The pyrograms of the Loy Yang residues, although differing in some components between

uncatalyzed and catalyzed residues, are not dissimilar, differing mainly in relative quantities of components.

This paper has attempted to show that there are definite advantages and disadvantages associated with the catalytic/non catalytic liquefaction behaviour of coals possessing a wide variation in rank. The use of catalyst, while appearing to only increase the oil yield/conversion for Loy Yang coal, markedly upgraded the product from Liddell coal - thereby indicating a quite different mode of action (reflecting a structural dependence) in each case. The possibility that the mode of action and reactivity of the catalyst may be temperature dependent (as the oils were produced at two different temperatures) cannot be overlooked. It was not the purpose of this paper to investigate such a possible phenomena. Rather it was to show, and it clearly has, the problems that may arise in product quality and upgrading if the only criteria for liquefaction are oil yield and conversion based.

ACKNOWLEDGEMENT

M.G. Strachan acknowledges the award of a University of Melbourne Research Scholarship.

REFERENCES

(1) Cudmore, J.F., *Fuel Proc. Technol.* 1977/1978, 1, 227.
(2) Jackson, W.R., Larkins, F.D., Marshall, M., Rash, D. and White, N., *Fuel,* 1979, 58, 281.
(3) Hatswell, M.R., Jackson, W.R., Larkins, F.P., Marshall, M., Rash, D. and Rogers, D.E., *Fuel,* 1979, 58, 783.
(4) Jones, D.G., Rottendorf, H., Wilson, M.A. and Collins, P.J., *Fuel,* 1980, 59, 19.
(5) Wilson, M.A., Rottendorf, H., Collins, P.J., Vassallo, A.M. and Barron, P.F., *Fuel,* 1982, 61, 321.
(6) Strachan, M.G., Johns, R.B. and Yost, R.S., *Anal. Chem.* Submitted for publication.
(7) Strachan, M.G., Chafee, A.L., Esdaile, R., Johns, R.B. and Yost, R.S., *Proc. 6th Aust. Coal Hydrogenation Workshop,* 1981, 7-16.
(8) Downing, P.G., Ph.D. Thesis, University of Melbourne, 1980.
(9) Charlesworth, J.M., *Fuel*, 1980, 59, 859.
(10) Durie, R.A., *Coal Research in C.S.I.R.O.,* 1959, 6, 12.
(11) Schwager, I., Farmanian, P.A. and Yen, T.F., *Adv. in Chem. Ser.,* 1978, 170, 66.

TABLE 1: PRODUCT DISTRIBUTION

Sample	Conversion %	Oil[A] yield	H_2O[A] yield	Residue	Gas[A]	H_2O/oil yield	gas/oil yield
LY1277 (uncat.)	60.30	45.92	6.52	40.72	6.84	0.14	0.15
LY1277 (cat.)	74.63	55.89	8.02	25.37	10.37	0.14	0.19
Liddell (uncat.)	62.22	59.57	1.48	37.78	1.17	0.03	0.02
Liddell (cat.)	91.75	54.71	8.25	8.25	29.53	0.15	0.54

A - g/100 g DAF coal

TABLE 2: ELEMENTAL ANALYSES

Sample	C	H	O*	N	S	H/C	O/C	N/C	ASH
		(DAF)							
LY1277	65.66	4.48	31.34	0.80	0.20	0.819	0.358	0.010	<1.0
Liddell	80.1	5.9	10.90	2.03	1.0	0.883	0.102	0.022	28.1
Total Oils									
LY1277 (uncat.)	81.72	7.49	9.79	1.00	-	1.10	0.089	0.010	
LY1277 (cat.)	85.08	6.85	7.83	0.24	-	0.966	0.069	0.002	
Liddell (uncat.)	87.80	6.15	3.94	2.11	-	0.841	0.033	0.021	
Liddell (cat.)	90.71	6.53	1.53	1.23	-	0.863	0.013	0.015	
Residues									
LY1277 (uncat.)	80.13	4.98	16.93	1.05	-	0.746	0.159	0.011	3.0
LY1277 (cat.)	69.66	4.95	24.51	0.889	-	0.853	0.264	0.011	17.9
Liddell (uncat.)	82.73	4.85	9.97	2.45	-	0.704	0.090	0.025	25.6
Liddell (cat.)	63.18	4.64	29.38	2.81	-	0.881	0.349	0.038	72.6

*By difference

TABLE 3: CHEMICAL CLASS COMPOSITION OF TOTAL LIQUID PRODUCT (w/w % of oil)

Fraction*	LY1277		Liddell	
	Uncatalyzed	Catalyzed	Uncatalyzed	Catalyzed
A1	22.09	23.51	11.63	1.69
A2	0.86	0.68	2.72	1.91
A3	1.03	1.36	2.48	0.42
A4	6.72	5.62	2.48	0.84
A5	1.55	1.19	0.01	2.12
A6	1.38	1.87	2.72	1.06
B1	2.80	4.77	2.97	0.21
B2	9.00	9.03	50.50	15.25
TN	54.50	51.97	24.49	76.50
NPN	31.07	34.76	14.45	69.84
PN	23.43	17.21	10.04	6.66

A series - acidic fractions from resins
B series - basic fractions from resins
TN = Total neutrals, i.e., NPN + PN: NPN = Nonpolar neutrals;
PN = Polar neutrals.
*See Ref. 6.

TABLE 4: ^{1}H-NMR DATA ON TOTAL LIQUID PRODUCTS

	^{1}H nmr Data											Mw Data[b]	
Sample	H_O	H_α	H_{ar}	H_{OH}	$\frac{H_{ali}}{H_{ar}}$	$\frac{H_{ali}}{C_{ali}}$	$\frac{H_{ar}}{C_{ar}}$	f_a†	δG†	$\frac{H_{aru}}{C_{ar}}$†	n†	$\bar{Mn}$	$\bar{Mw}$
LY1277 (uncat.)	29.0	32.9	27.1	11.0	2.3	1.71	0.45	0.66	0.74	1.75[c]	1.88	498	1049
LY1277 (cat.)	39.6	28.1	22.6	9.6	3.0	2.24	0.35	0.67	0.74	1.23	2.41	512	997
Liddell (uncat.)	35.7	23.4	31.2	9.6	1.9	2.49	0.43	0.75	0.54	0.58	2.52	379	758
Liddell (cat.)	21.3	29.3	45.1	4.3	1.1	2.27	0.60	0.78	0.35	0.76	1.73	169	240

† - Brown Ladner Method of ^{1}H nmr data analysis
b - GPC-HPLC method for molecular weight determination
c - High values due to high O/H ratio

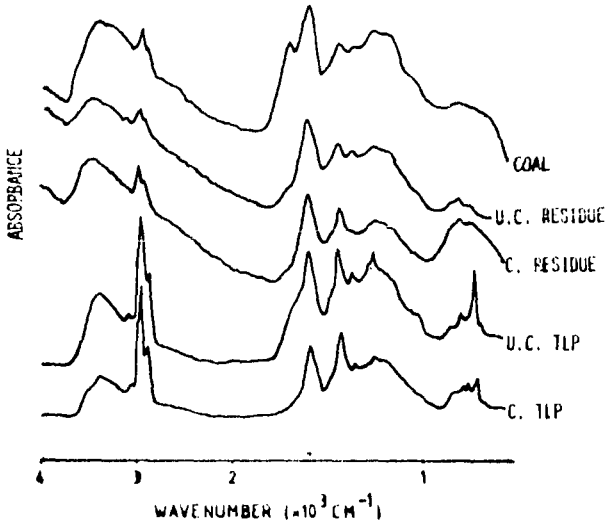

FIG. 1 I.R. SPECTRA OF LY1277 AND ITS LIQUEFACTION PRODUCTS

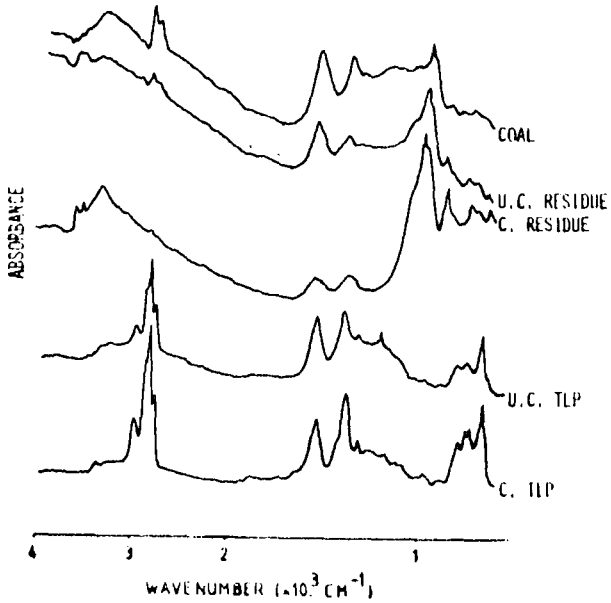

FIG. 2 I.R. SPECTRA OF LIDDELL AND ITS LIQUEFACTION PRODUCTS

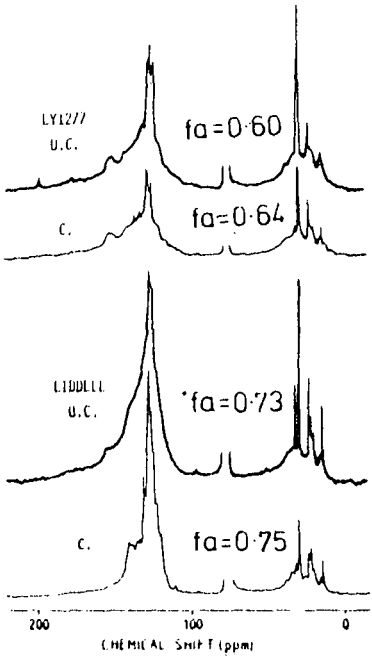

FIG. 3 25.0 MHz ^{13}C NMR OF TOTAL LIQUID PRODUCTS

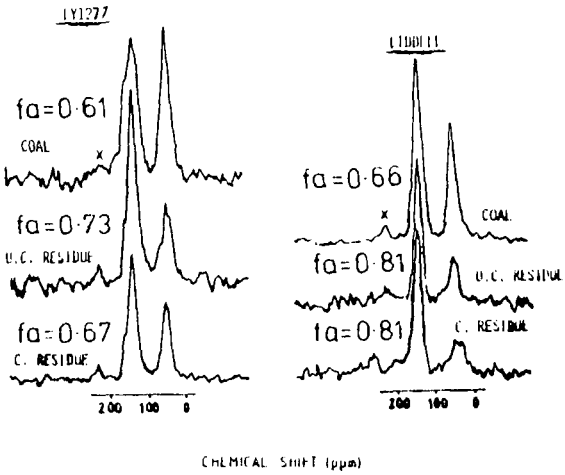

FIG. 4 SOLID STATE ^{13}C NMR OF COALS AND THEIR LIQUEFACTION RESIDUES

H-COAL® PROCESS MODELING AND SCALEUP

James B. MacArthur, Allen Li, and Anil S. Ambegaonkar

Hydrocarbon Research, Inc.
(A Subsidiary of Dynalectron)
P. O. Box 6047
Lawrenceville, New Jersey 08648

ABSTRACT

H-Coal® Process commercial viability has been confirmed by a highly successful, 2-1/2 year demonstration program at the Catlettsburg, Kentucky, Pilot Plant. A major accomplishment was the confirmation of scale-up of the H-Coal® Process chemistry in the well-mixed ebullated-bed reactor system. This paper describes the H-Coal® Process Model developed from bench scale and PDU testing and its relationship to the Pilot Plant operations. Kinetics, hydrodynamics, and overall process simulation are described.

PROCESS BACKGROUND

The H-Coal® Process is a direct catalytic coal liquefaction process developed by Hydrocarbon Research, Inc. for conversion of coal into high-quality, clean liquid fuels[1]. The process can be modified to produce a range of products from a heavy fuel oil to an all-distillate (C_4-650°F boiling range) syncrude. The novelty of the H-Coal Process resides in the use of the commercially proven ebullated-bed reactor in combination with other process steps to achieve C_4-975°F liquid product yields in the range of 40 to 55 weight percent on dry coal. Over twenty coal types have been evaluated in more than 70,000 hours of operation. The history development, and advances of the H-Coal® Process have been extensively documented. Some details of the process and HRI's ebullated bed reactor are appended to this paper.

H-COAL PROCESS SCALE UP

The development path for commercialization of the H-Coal Process is similar to that used by HRI for scale up of the commercial H-Oil™ residuum and heavy crude hydroconversion process. The H-Oil reactor system was successfully scaled up from the bench, through the PDU, followed by a pilot plant demonstration unit and finally to the commercial scale plant. The diameters of experimental reactors employed for collecting process, engineering and scale-up data are listed below. All reactors have operated at commercial design conditions.

	H-Oil Reactor Diameter	H-Coal Reactor Diameter
Bench Unit	3/4 in.	3/4 in.
Development Unit	8-1/2 in.	6 & 8-1/2 in.
Pilot Plant	4 ft. 6 in.	5 ft.
Commercial Plant	13 ft.	10-13 ft.

In addition, HRI has constructed two cold-flow reactor models for fluid dynamics studies and the development of improved reactor internals: a 6 in. x 12 ft glass column and a 5 ft x 24 ft. carbon steel vessel. These cold flow studies, combined with data collected from the various experimental units, have provided the information to scale the effects of equipment size, pressure and temperature on reactor fluid dynamics and vessel internals designs.

The performance of the H-Oil unit at the Kuwait National Petroleum Company's (KNPC) Shuaiba Refinery is evidence of this successful scale up technique. The KNPC H-Oil unit has two reactor trains, each operating on vacuum residuum at about 25,000 B/D. Both reactors have been operating since 1968.

The H-Coal reactor has been thoroughly tested in bench- and PDU-size systems and has recently completed a 2 1/2 year demonstration program at the Catlettsburg, Kentucky H-Coal Pilot Plant. The H-Coal Pilot Plant operation has achieved many significant results including:

- Confirmation of H-Coal process chemistry and equipment scale-up.
- Establishment of process mechanical operability and reliability in commercial-scale equipment
- Collection of engineering design and operating data on critical equipment
  - Slurry Preheater
  - Letdown valves
  - Slurry pumps
  - Reactor and internals
- Accumulation of about 7000 hours of on-coal operations with over 56,000 tons of coal processed.

H-COAL REACTOR IS WELL MIXED AND THERMALLY STABLE

To determine the degree of catalyst backmixing in an ebullated bed, a radioactively-tagged catalyst sample was charged to the PDU reactor in separate operations with Kentucky and Wyoming coals. The amount of tagged catalyst in the daily withdrawals and subsequent reactor catalyst bed dump was determined. The residence time distribution of catalyst in the ebullated-bed was then analyzed. A detailed discussion of the experimental procedures, and some of the test results were reported in the literature. The estimated reactor Peclet number reported by Bickel and Thomas[3] for the Kentucky coal operation was 0.451. Using a modified dispersion model and taking into consideration the fluid dynamics during the catalyst addition and withdrawal operations, the Peclet number for the Wyoming coal operation was estimated to be 0.248 (detailed analysis to be published). These low Peclet numbers indicate that the catalyst mixing characteristics in the PDU ebullated-bed reactor approximated that of the CSTR.

The axial temperature variation in an ebullated-bed reactor is significantly smaller than that in a plug-flow (fixed-bed or moving-bed) reactor at the same conversion level. The axial temperature gradient (ΔT) in an ebullated-bed reactor can be estimated using the following expression:

$$\Delta T = \frac{-\Delta Hr}{\rho C_p} \frac{1}{1+R} (C_{A_f} - C_{A_1}) \quad (1)$$

where,

C_{A_f}, C_{A_1} = concentration of reactant in the feed and in the reactor outlet, respectively.

ΔHr = heat of reaction

R = dimensionless constant related to recycle liquid/feed ratio and internal liquid backmixing. This constant ranges from 5-15 in ebullated-bed operations.

ρ, C_p = average fluid density and heat capacity, respectively.

The calculated temperature gradients from equation (1) are in agreement with PDU and Catlettsburg Pilot Plant data as shown below:

MEASURED VS. PREDICTED H-COAL REACTOR TEMPERATURE GRADIENTS

(Illinois No. 6 Coal, Burning Star Mine)

	PDU-5	Catlettsburg
Reactor Internal Diameter	0.71 ft.	5 ft.
Reactor Temperature	850°F	845-851°F
Reactor Pressure	2,700 psig	3,000 psig
Reactor Temperature Gradient		
Measured	16-20°F	11-18°F
Predicted	16°F	16°F

For a commercial-size H-Coal reactor operating at conditions similar to that of the Catlettsburg Pilot Plant, a temperature gradient of about 7°F was predicted. This lower reactor temperature gradient was due to increased backmixing in large size reactor. The same calculation procedure predicted temperature variations of 2-5°F in commercial H-Oil® reactors, which is consistent with commercial experience. The higher temperature gradients observed in H-Coal® reactors were caused by higher heat of reaction and lower ebullating recycle flow in the H-Coal® Process.

In plug-flow reactors, such as fixed beds and moving beds, the temperature gradient across the reactor for an exothermic hydrocracking reaction can be calculated using the following equation:

$$T_1 - T_f = \left(\frac{-\Delta Hr}{\rho C_p}\right)\left(C_{A_f} - C_{A_1}\right) \quad (2)$$

where subscripts f and 1 denote reactor feed and outlet conditions, respectively. Comparing equations (1) and (2), one can deduce that the axial temperature gradient in a plug-flow reactor is about one order of magnitude higher than that in an ebullated-bed reactor when both are operating at the same conversion level.

The well-mixed ebullating-bed reactor system enables commercial reactor systems to utilize the exothermal heat of reaction to preheat the H-Coal reactor feed. This enables the coal slurry preheater to operate at a low temperature (~700°F at the Pilot Plant). No coke was found in the slurry preheater after 2-1/2 years of Pilot Plant operation because of the mild preheater severities. The H-Coal reactor system is energy-efficient, cost-effective, and has the potential for highest plant on-stream factors of any direct coal liquefaction process.

H-COAL PROCESS MODELLING

The H-Coal® Process has been successfully demonstrated on the bench scale with over 20 coal types including bituminous, sub-bituminous, lignite and brown coal.

The H-Coal® Process offers considerable product slate flexibility, ranging from an all-distillate syncrude to a maximum heavy fuel oil production. The H-Coal® Process meets these requirements through manipulation of key process variables including:

- Coal space velocity
- Catalyst type and replacement rate
- Hydrogen partial pressure
- Reactor temperature
- Recycle slurry composition

HRI has developed a tool to predict the effect of these key process variables on H-Coal yields and product qualities for Illinois No. 6 coal. The H-Coal® Process Simulator is a comprehensive computer model of the H-Coal reactor system at steady-state conditions. The Simulator includes recently updated correlations for H-Coal product qualities, reactor vapor/liquid equilibrium "K" values, and an H-Coal kinetic model. All reactor feed and effluent streams, reactor composition, and product yields and qualities are depicted. Procedures are contained in the Simulator for elementally balancing yields and calculating reactor slurry composition as a function of recycle slurry and recycle gas feed stream rates and compositions. The reactor slurry composition is an important parameter in the H-Coal kinetic model for predicting product yields.

HRI has developed a semi-empirical kinetic model based on a back-mixed reactor system. The conversion reactions are assumed to be irreversible. The reactions are first order except for preasphaltene and asphaltene conversion. The reaction mechanism assumed is shown in Figure 1. Coal is made up of inert components (ash and inert organic material) and reactive components. The primary reactions involve the conversion of reactive coal to preasphaltenes and gases (including hydrocarbon and heteroatoms). Secondary reactions involve the conversion of preasphaltenes to asphaltenes, distillates (C_4-400°F, 400-650°F, and 650-975°F) and gases. Finally, in tertiary reactions, asphaltenes convert to distillates and gases, and distillates convert to lighter boiling components.

The kinetic model is incorporated into the H-Coal® Process Simulator. In the Simulator, empirical correlations are used to separate the distillate components into narrow (50°F) boiling range fractions. These components are utilized to obtain better estimates of reactor composition (through vapor/liquid equilibrium flash calculations), physical/chemical properties of the product streams, and for elemental balancing of the H-Coal® Process yields.

Table 1 summarizes the data base used to develop the H-Coal Kinetic Model for Illinois No. 6 Coal (Burning Star Mine). All process variables cover a wide range with the exception of temperature. The temperature effect has been modeled based on prior data obtained on a different Illinois coal (Monterey Mine).

TABLE 1. H-COAL KINETIC MODEL - RANGE OF DATA USED

COAL TYPE:	Illinois No. 6 (Burning Star Mine)
CATALYST:	HDS-1442A
NUMBER OF YIELD PERIODS:	140
PROCESS UNITS:	BENCH, PDU
PROCESS VARIABLE RANGES	
Coal Space Velocity	25 - 80 lb/hr/ft^3
Pressure	1450-2700 psia
Hydrogen Partial Pressure	1100-1900 psia
Temperature	840 - 852°F
Catalyst Age	0-600 hours
	0-3000 lb coal/lb catalyst
Operating Mode	Bottoms Recycle
Reactor Stages	Single

The H-Coal Kinetic Model components, correlating parameters, range of yield data, and standard deviations of the correlations are summarized in Table 2. Coal conversion is correlated as a function of coal space velocity, reactor temperature, and the concentration of reactive coal in the reactor. The Illinois coal is very reactive and coal conversion data covered a narrow range of 87-96 weight percent of MAF coal. Hydrogen partial pressure effects were not statistically significant. Although catalyst age and activity influence solvent quality, no catalyst impact on coal conversion could be correlated from available data. The standard deviation for the total bench and POU data base was 1.2%.

TABLE 2. REVISED H-COAL KINETIC MODEL

COMPONENT	FORM OF CORRELATION	RANGE OF YIELDS % MAF COAL	STANDARD DEVIATION
Coal Conversion	F_1 (SV,T,C)	87-96	1.2
Preasphaltenes	F_2 (SV,T,AGE,H_2PP,C)	1.3-20	-
Toluene Conversion	F_1-F_2		
Asphaltenes	F_3 (SV,T,AGE,H_2PP,C)	11-30	2.5
975°F$^-$ Conversion	F_1-F_2-F_3	45-80	2.0
650-975°F Liquid	F_4 (F_1,F_2,F_3,SV,C)	6-14	2.3
400-650°F Liquid	F_5 (F_1,F_2,F_3,F_4,SV,C)	5-30	2.1
C_4-400°F Liquid	F_6 (F_1,F_2,F_3,F_4,F_5)	10-40	3.1
C_1-C_3 Gas	F_7 (F_1,F_1,F_2,F_4,F_5)	5-15	1.7

Preasphaltene and asphaltene conversions were correlated as a function of coal space velocity, catalyst age, hydrogen partial pressure, reactor temperature, and reactor concentration. Statistical performance was significantly improved by correlating the toluene conversion (coal conversion minus preasphaltene yield) and 975°F$^+$ conversion (coal conversion minus preasphaltene and asphaltene yield). This eliminated data scatter associated with small differences between large numbers. Standard deviations of 1.8% and 2.0% were achieved for the toluene conversion and 975°F$^+$ conversion, respectively. Yields of distillates (C_4-400°F, 400-650°F, 650-975°F) were similarly correlated. The data, however, were more limited and data scatter more significant. Further data are required to confirm these reactions rate constants.

The H-Coal® Process Simulator includes empirical correlations of hydrogen consumption, and heteroatom (COx, H_2S, NH_3, H_2O) yields. Liquid product qualities are calculated by kinetic (for S,N) and empirical correlations.

The H-Coal® Process Simulator has been used extensively to predict H-Coal® Process performance over a wide range of operating conditions and to evaluate process improvements. Significant improvements have been made in increasing the recycle solvent boiling range (400°F$^+$ to 600°F$^+$) and extincting the heavy vacuum gas oil stream. This improves process economics when a transportation product slate is desirable.[4] Also, recent studies have shown that the hydroclones used for preparation of recycle slurry oil may be eliminated in most cases without sacrificing liquid yields. The Simulator has been used to verify Pilot Plant performance.

H-COAL PILOT PLANT YIELDS PREDICTIONS CONFIRMED

The H-Coal Pilot Plant had a successful 131 day run with Illinois No. 6 and HDS-1442A catalyst (Run 8) during the second half of 1981. The run was conducted with daily catalyst addition and withdrawal to maintain a target catalytic activity. During this run, 19,200 tons of dried coal were processed with the reactor processing coal or oil slurry 100% of the time and coal fed for 72% of the time. The data obtained at the Pilot Plant are felt to be representative of what would be achieved in long term commercial operations.

Yield data were obtained in both September and a four-day material-balance period (October 29-November 2). The yield data obtained during the material-balance period were considered most representative due to lined-out H-Coal operations at steady-state conditions during this period.

Table 3 presents a comparison of yields obtained at the PDU scale with those obtained during the four-day material-balance period at the Pilot Plant for the Illinois No. 6 bituminous coal. Table 4 presents similar data for Wyodak subbituminous coal. These data show equivalent yields at the two scales and confirm the scaleup of H-Coal® Process chemistry. The H-Coal Kinetic Model and Process Simulator closely predicted the demonstrated Pilot Plant performance. These results provide confidence in HRI's ability to project commercial scale plant performance based on results obtained in bench and PDU units.

TABLE 3. H-COAL PROCESS CHEMISTRY SCALE-UP ILLINOIS NO. 6 COAL

UNIT	PDU	PILOT PLANT
Nominal Size, T/D	3.5	200
YIELDS	PERCENT	PERCENT
C_1/C_3	10.68	11.77
C_4/400°F	18.74	22.41
400/975°F	28.33	25.27
975°F$^+$ Residuum	19.00	21.26
Unconverted Coal	5.78	3.46
Ash	11.51	11.31
Total Distillate Oil	47.07	47.68
Residuum Plus Coal	24.78	24.72

TABLE 4. H-COAL PROCESS CHEMISTRY SCALE-UP WYODAK COAL

UNIT	PDU		PILOT PLANT	
Nominal Size, T/D	3.5		200	
YIELDS	PERCENT	B/T	PERCENT	BTU
C_1/C_3	99.8	-	9.29	-
C_4/400°F	22.12	1.62	25.95	1.93
400/975°F	24.06	1.40	23.93	1.41
975°F$^+$ Residuum	11.27	0.51	10.65	0.48
Unconverted Coal	10.72	-	9.12	-
Ash	8.84	-	9.13	-
Total Distillate Oil	46.18		49.88	
Residuum Plus Coal	21.99		19.77	

SUMMARY

The H-Coal® Process follows the same successful development and scale up path used for the H-Oil Process. Results of reactor testing and modeling are in agreement with plant data, confirming that ebullated beds are well-mixed and highly stable. A kinetic model and overall process simulator have been developed and shown to accurately predict results from bench, PDU, and Pilot Plant scales. Pilot Plant results confirm scaleup of the H-Coal® Process chemistry. Data obtained in future bench and PDU units may be used with confidence for design of commercial scale plants.

REFERENCES

1. Eccles, R. M. and G. R. DeVaux, "Current Status of H-Coal® Commercialization", Winter National Meeting, AIChE, Orlando, Florida, March, 1982.

2. Li, A., and D. Lin, "Scaleup Performance and Thermal Stability Analysis of H-Oil and H-Coal Ebullated Bed Reactors", 32nd Canadian Society of Chemical Engineers Meeting, Vancouver, B.C., October, 1982.

3. Bickel, T. C., and Thomas, M. G., IEC Process Design and Development, Vol. 21, No. 3, July, 1982.

4. MacArthur, J. B., J. E. Duddy, A. S. Ambegaonkar, and A. V. Moomjy, "H-Coal Liquids-Upgrading Upstream or Downstream?" AIChE 1983 Spring National Meeting, Houston, TX, March, 1983.

FIGURE 1

H-Coal® Kinetic Model Reaction Mechanism

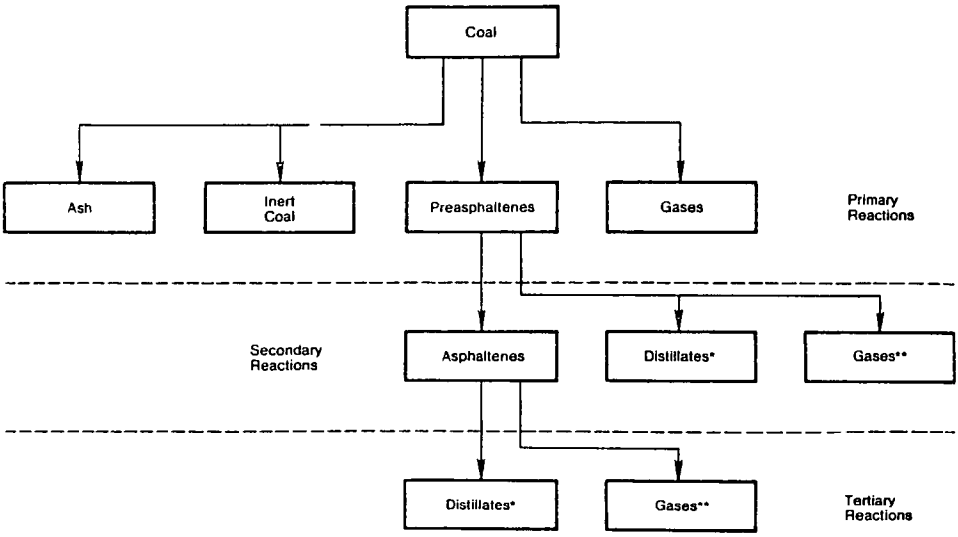

*Distillates are Separated into 3 Components Including C_4/400°F Naphtha, 400/650°F Middle Distillate, and 650/975°F Heavy Distillate.

**Gases Include Hydrocarbons and Heteroatom Compounds.

APPENDIX

H-COAL PROCESS DESCRIPTION

Figure 1 presents a simplified flow diagram of the H-Coal Process. Coal is slurried with a process-derived oil, pumped to reactor pressure, mixed with hydrogen, preheated and fed to the reactor. There, coal, recycle oil, and hydrogen react in the presence of a catalyst. Depending on the process severity selected, the net product yield can be all-distillate material or, at low severities, a distillate and a heavy fuel oil. The reactor typically operates at temperatures of about 800-850°F and pressures of 2500-3000 psig. A portion of the reactor effluent is treated to reduce its solids content. Low-solid-content oil is recycled as a slurry oil for the coal. The balance of the liquid is fractionated to produce an all-distillate product. The vacuum residuum, containing nondistillate oils, unconverted coal, and ash, can be fed to a partial oxidation unit to produce the hydrogen for the process.

EBULLATED-BED REACTOR DESCRIPTION

Figure 2 is a sketch of the ebullated bed reactor which is the heart of the H-Coal reactor design. The reactor feed and recycle streams from the ebullating pump enter the bottom of the reactor. The liquid flow causes the catalyst bed to expand and fluidize. The catalyst remains in the bed. The reactor products, including the unconverted coal and ash solids, leave the bed and are separated for further processing. Because the catalyst is constantly in motion, a portion can be withdrawn and replaced to maintain high catalyst activity. On a daily basis, about one or two percent of the catalyst inventory is removed for this purpose. The ebullated-bed reactor system has over 30 unit-years of commercial operations in HRI's H-Oil® petroleum residuum hydroconversion process. The H-Coal® catalyst now being used has also been demonstrated commercially in H-Oil operations.

The ebullated-bed reactor allows intimate contact between catalyst particles, hydrogen, and the coal-oil slurry to achieve essentially isothermal reaction conditions and provide low constant reactor differential pressure. Other major advantages of the H-Coal reactor system are that:

- High liquid yields and qualities are achieved in the presence of a synthetic catalyst and are not dependent on the catalytic effect of coal ash.
- Continuous catalyst replacement controls deactivation, provides constant product quality, will permit continuous catalyst regeneration, and provides for high on-stream factors.
- Operating conditions can be varied to meet flexible product slate requirements.

FIGURE A-1

Simplified H-Coal® Process Flow Diagram

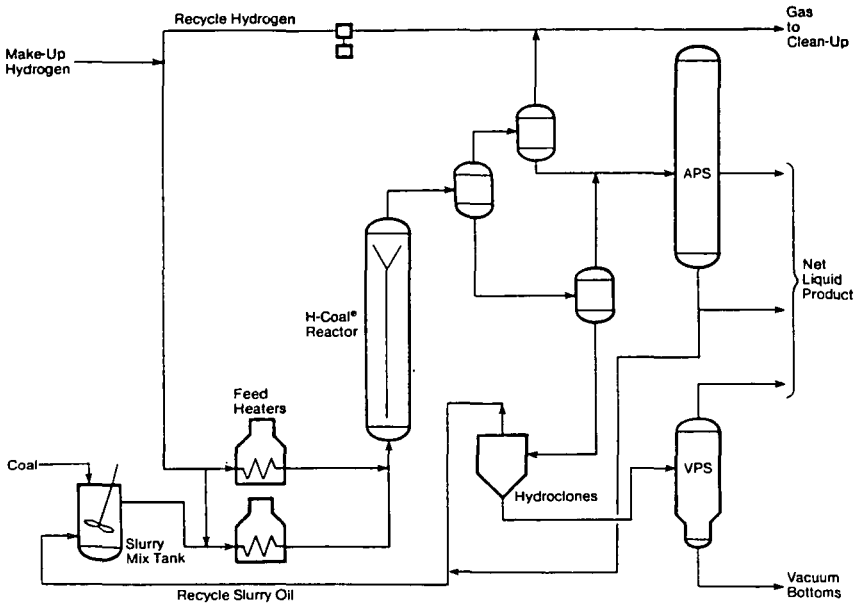

FIGURE A-2

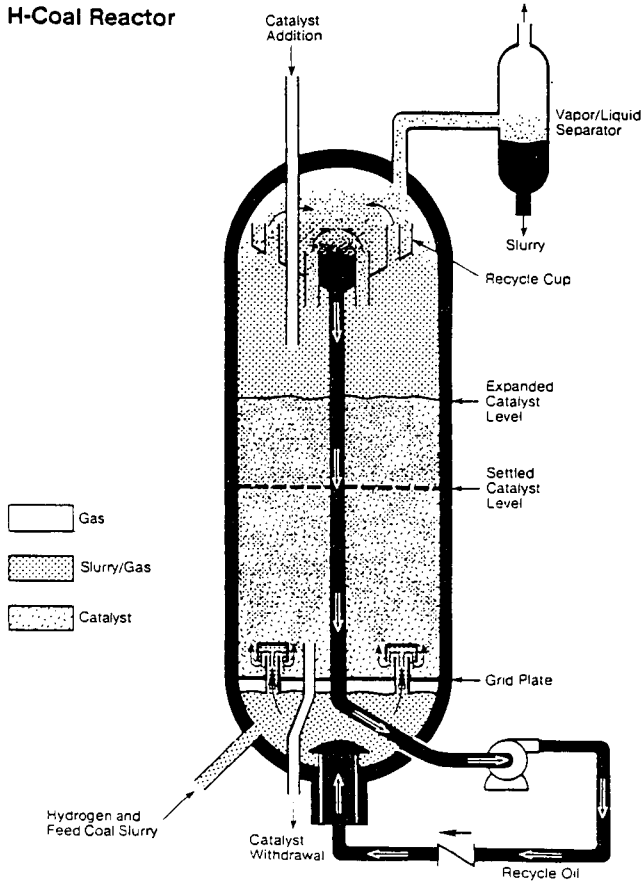
H-Coal Reactor
Catalyst Addition
Vapor/Liquid Separator
Slurry
Recycle Cup
Expanded Catalyst Level
Settled Catalyst Level
Gas
Slurry/Gas
Catalyst
Grid Plate
Hydrogen and Feed Coal Slurry
Catalyst Withdrawal
Recycle Oil

HYDROGEN AND METHANE SOLUBILITY IN SRC-II COAL LIQUID

Fu-Xin Ding, Shiao-Hung Chiang and George E. Klinzing

Chemical and Petroleum Engineering Department
University of Pittsburgh
Pittsburgh, PA 15261

INTRODUCTION

The most important steps in coal liquefaction processes are the dissolution of coal in the hydrogen-laden solvent and the subsequent hydrotreating of the coal derived liquid. A small amount of methane is usually formed during coal liquefaction. Thus hydrogen and methane solubility data are essential for the design and operation of coal liquefaction reactors.

A number of investigators studied vapor-liquid equilibrium in binary and multicomponent systems of heavy hydrocarbon liquids and light gases, including hydrogen and methane.[1-11] Only limited experimental data for methane-coal liquid and hydrogen-coal liquid mixtures have been reported in the literature.[5,7] An attempt was made in this study to obtain solubility data in the binary system of hydrogen-coal liquid (SRC-II) and the ternary system of hydrogen-methane-coal liquid (SRC-II) under conditions comparable to those encountered in coal liquefaction processes. Two specially designed in-situ hydrogen probes were adopted for monitoring hydrogen concentration/partial pressure in both vapor and liquid phase.

EXPERIMENTAL

The experimental set-up and procedure used in this study are essentially the same as that described in previous papers.[6, 7] A schematic flow diagram of the equipment is shown in Figure 1.

A one-liter autoclave was used as the equilibrium cell. The autoclave is made of stainless steel and equipped with an automatic temperature controller capable of maintaining constant temperature within ±1 K of the desired setting. A magnatic stirrer, driven by a variable speed motor, was installed in the autoclave. Two in-situ probes were used to measure the hydrogen partial pressure. The operating principle of these probes has been discussed elsewhere.[12]

Hydrogen and methane were supplied to the equilibrium cell from high pressure cylinders through gas feed lines. Liquid and gas samples can be withdrawn from the cell into the low pressure section. A Hewlett-Packard 5880A chromatograph system was used for sample analysis.

High pressure hydrogen (41 MPa) and methane (13 MPa) were used in this work with reported purity of 99.995% and 99.0%, respectively. The SRC-II coal liquid (supplied by the Gulf R&D Co.) was catalytically hydrotreated with Ni-Moly catalyst for four hours at 640°F.[7]

RESULTS AND DISCUSSION

Hydrogen-Coal Liquid Binary System. The hydrogen solubility data were obtained by measuring hydrogen partial pressure (using the in-situ probe) and by taking liquid samples at temperatures ranging from 420 to 681 K and total pressures from 4 to 11 MPa. Figure 2 shows the hydrogen solubility as a function of total pressure. When the total pressure is held constant, the hydrogen solubility increases with temperature to a maximum value and then decreases. The reason for this apparent solubility inversion is attributable to the rapid increase of coal liquid partial pressure with temperature, which causes a significant decrease in hydrogen partial pressure in the gas phase under constant total pressure. It can be shown that the hydrogen solubility increases monotomously with temperature if hydrogen partial pressure is held constant (Figure 3). In addition, hydrogen solubility data of this study are found to be in good agreement with the results reported by Lin et al[5] at temperatures below 550 K.

Hydrogen-Methane-Coal Liquid Ternary System. Experimental measurements were made at two temperatures, 591 K and 645 K, and at pressures up to 14 MPa. In order to determine the effect of methane on hydrogen solubility, methane partial pressure was varied from zero to 3.5 MPa. The experimental results are plotted in Figures 4 and 5. Under constant hydrogen partial pressure* and temperature, the hydrogen solubilty decreases dramatically with an increase in methane partial pressure. For example, at 645 K and constant hydrogen partial pressure (9.52 MPa), hydrogen concentration in the liquid phase falls from 0.136 to 0.0387 mole fraction when methane partial pressure increases from zero to 3.0 MPa. The methane solubility versus its partial pressure is shown in Figures 6 and 7. The results indicate a linear relationship between methane solubility and its partial pressure at constant temperatures and constant hydrogen partial pressures. A study of the effect of hydrogen partial pressure on methane solubility is underway and the result will be presented in a future paper.

CONCLUSION

Hydrogen and methane solubilities have been experimentally obtained in the binary hydrogen-coal liquid (SRC-II) and ternary hydrogen-methane-coal liquid (SRC-II) systems at elevated temperatures and pressures. In the binary system, hydrogen solubility exhibits a temperature inversion at constant total pressure due to the strong dependence of coal liquid partial pressure on temperature. In the ternary system, hydrogen solubility is affected considerably by methane partial pressure at constant temperatures. The methane solubility exhibits a linear correlation with its partial pressure when hydrogen partial pressure is held constant.

ACKNOWLEDGEMENT

Funding of this work provided by U. S. Department of Energy, under the contract No. DE-AC22-80 PC33014, is gratefully acknowledged.

*The hydrogen partial pressure was accurately measured by the in-situ hydrogen probe.

REFERENCES

1. Legret, D., Richon, D. and Renon, H., J. Chem. Eng. Data, 1982, 27, 165-169.
2. Simnick, J. J., Sebastian, H. M., Lin, H. M. and Chao, K. C., J. Chem. Eng. Data, 1979, 24, No. 3, 239-240.
3. Lin, H. M., Sebastian, H. M. and Chao, K. C., J. Chem. Eng. Data, 1980, 25, 252-254.
4. Simnick, J. J., Lawson, C. C., Lin, H. M. and Chao, K. C., AIChE Journal, 1977, 23, No. 4, 469-476.
5. Lin, H. M., Sebastian, H. M., Simnick, J. J. and Chao, K. C., Ind. Eng. Chem., Process Des. Dev., 1982, 20, 253-256.
6. Sung, S., "Phase Equilibrium of Hydrogen/Coal Liquid System" Ph.D. Thesis (1981), Univ. of Pittsburgh, Pittsburgh, PA 15261.
7. Kara, M., Sung, S., Ding., F. X., Klinzing, G. E. and Chiang, S. H., Proceedings of Thermodynamics Symposium at the Second World Congress of Chemical Engineering, Oct. 4-9, 1981, Montreal, Canada.
8. Simnick, J. J., Liu, K. D., Lin, H. M. and Chao, K. C., Ind. Eng. Chem., Process Des. Dev., 1978, 17(3), 204-208.
9. Li, Y. H., Dillard, K. H. and Robinson, R. L., J. Chem. Eng. Data, 1981, 26, 200-204.
10. Simnick, J. J., Sebastian, H. M., Lin, H. M. and Chao, K. C., J. Chem. Eng. Data, 1980, 25, 147-149.
11. Brainard, A. J. and Williams, G. B., AIChE Journal, 1967, 13, 60.
12. Gala, H., Kara, M., Sung, S., Klinzing, G. E. and Chiang, S. H., AIChE Journal, 1981, 27, 159-162.

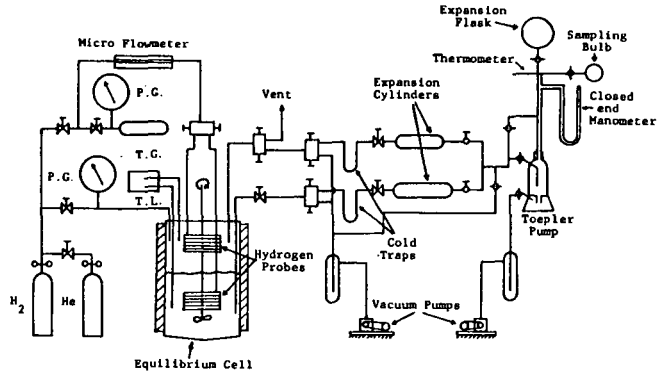

Figure 1 Schematic Diagram of the Experimental Set-up

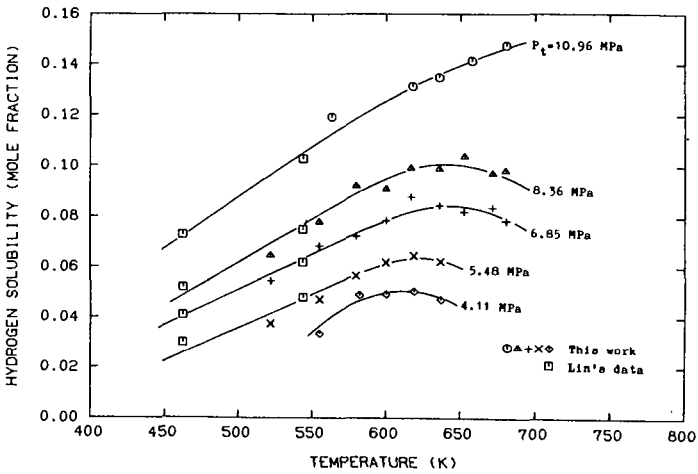

Figure 2 Hydrogen Solubility in SRC-II Coal Liquid vs. Temperature at Constant Total Pressure

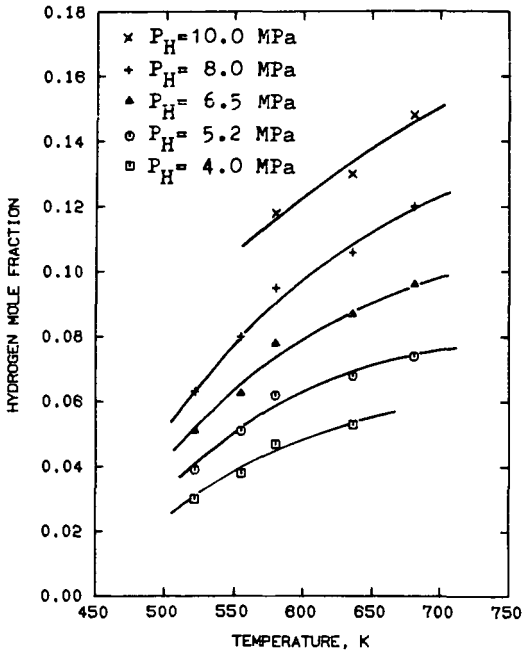

Figure 3 Hydrogen Solubility in SRC-II Coal Liquid vs. Temperature at Constant Hydrogen Partial Pressure

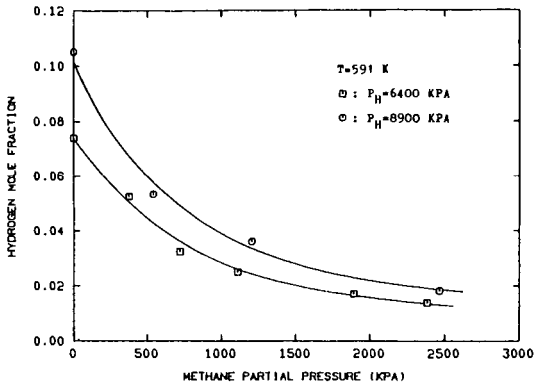

Figure 4 Hydrogen Solubility in SRC-II Coal Liquid vs. Methane Partial Pressure at 591 K

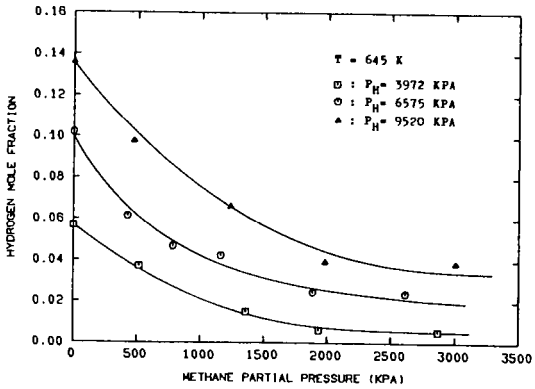

Figure 5 Hydrogen Solubility in SRC-II Coal Liquid vs. Methane Partial Pressure at 645 K

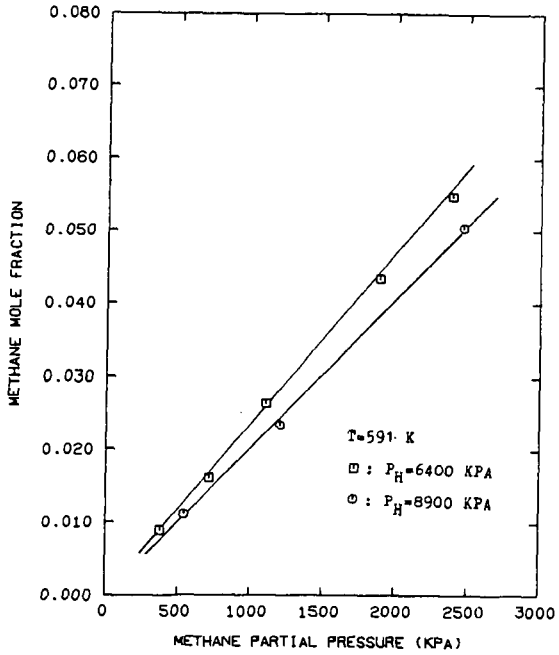

Figure 6 Methane Solubility in SRC-II Coal Liquid vs. Methane Partial Pressure at 591 K

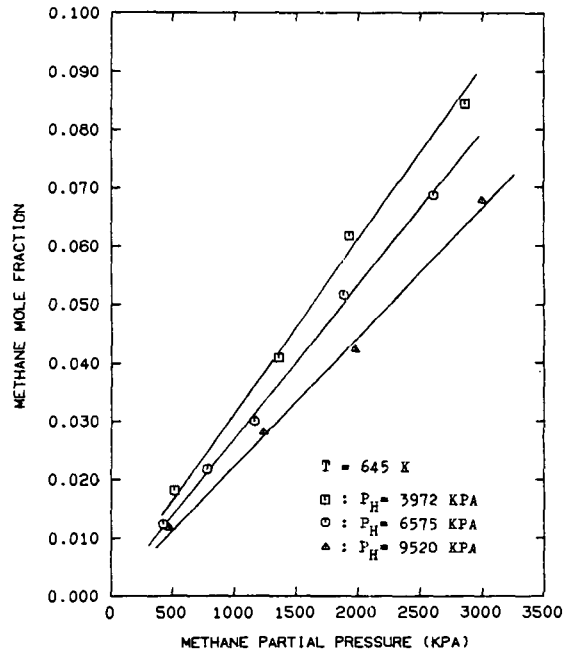

Figure 7 Methane Solubility in SRC-II Coal Liquid vs. Methane Partial Pressure at 645 K

DISSOLVING COAL AT MODERATE TEMPERATURES AND PRESSURES

Frank R. Mayo, Albert S. Hirschon, John S. Zevely and Karen Sundback

SRI International, 333 Ravenswood, Menlo Park, CA 94025

Introduction

The objective of the research reported here was to determine the kinds and proportions of breakable C-C and C-O bonds in the connecting links between the condensed systems in coal. Such information should tell us about the possibility of coal liquefaction under mild conditions. The kinds and proportions of C-O and C-C bonds were investigated by cleavage reactions. Cleavages of C-O bonds in esters and ethers by strongly basic amines, iodides, and acids are discussed first and then our results on the distribution of oxygen in coal are compared with the results of other workers. We then discuss the cleavage of C-C bonds in connecting links by oxidations of coal fractions and some differences among the oxidation products. In terms of C-C bonds to be broken by oxidation, the principal problem is determining whether the condensed aromatic systems are joined by single or multiple methylene groups. Our conclusions are compared with some in the literature. This paper is an expansion of a previous presentation.(1)

The above findings and conclusions are the foundation for a new program to prepare a coal product on a laboratory scale at a moderate temperature and pressure that will melt or dissolve in a cheap solvent at or below 100°C. Ash can then be removed and the product can be used as a clean fuel or processed more easily than coal to a liquid fuel. A progress report will be made.

Coal Preparation: Extraction of Coal With Pyridine

All of the work reported here was done with a beneficiated Illinois No. 6 coal, obtained from Pennsylvania State University as PSOC 25. This dried coal contained 76.0% C, 4.88% H, 1.46% N, 2.17% S, 1.71% ash, and 13.8% O by difference. Much of the work reported in this section was carried out with soluble coal fractions so that changes could be followed by number-average molecular weights ($\overline{M}_n$). Some of these fractions were prepared by extracting our coal exhaustively with pyridine at 100°C. About 16% dissolved, apparently without chemical reaction. About one-third of the pyridine-soluble material was soluble in toluene; it contained more hydrogen and less oxygen than the toluene-insoluble, pyridine-soluble (TIPS) fraction, which is a useful model for coal and was used in much of our work. The TIPS fraction is heterogeneous in molecular weight and chemical composition. One TIPS fraction of $\overline{M}_n$ 1100 (by vapor-phase osmometry) was fractionated by GPC; 76% of the total had $\overline{M}_n$ in the range 550-1550. After hydrolysis of a TIPS fraction by alcoholic KOH, the products were easily separated into fractions of $\overline{M}_n$ 350 to 1430, H/C ratios (a measure of aromaticity) of 0.98-0.74, and with different proportions of aromatic hydrogen.

Reactions of Coal Fractions With Amines

Strongly basic amines have long been known to dissolve more coal than pyridine.(2,3) We now attribute the high solubilities of coals in these solvents to chemical cleavage of C-O bonds in ester and ether groups. This conclusion comes from reactions of both TIPS and pyridine-extracted coal with $BnNH_2$. After these reactions, most of the free $BnNH_2$ was removed by vacuum distillation and the rest by washing with dilute aqueous HCl; the latter was then extracted by aqueous ammonia. Table 1 shows that close to one molecule of $BnNH_2$ becomes bound to the TIPS for each cleavage reaction or additional molecule formed. With both TIPS and pyridine-extracted coals, the extents of reaction increase with the severity of treatment. For the pyridine-extracted coal, we do not know how much $BnNH_2$ is incorporated per cleavage, but if the ratio is 1, there is about 350 in molecular weight units associated with each bound $BnNH_2$.

The amine extracts from long reactions of coal at 100° are apparently true solutions, but they become partly insoluble on drying. Thus, one EDA extract was

centrifuged and dried at 76° and 1 torr, but then only 90.5% was soluble in EDA and only 24% was soluble in pyridine on repeated extractions. In a $BnNH_2$ extraction, considered to be equivalent, the extract was centrifuged in an ordinary centrifuge. Another 1.5 hours at 30,000 g then produced no additional precipitate. Nearly all the solvent was then removed from the solution and 200 mL of pyridine was added to a 1-g sample. The total solubility in Table 2 is consistent with other extractions but the high solubility in pyridine was unprecedented. We think that this high solubility is due to the omission of the first drying, but the presence of a few tenths of 1% of $BnNH_2$ in the pyridine may also have had some effect. The drying may partly reverse the cleavage or cause condensation in other ways.

Other Cleavage of TIPS

Several other reagents, mostly halides or sources of halogen, but also acids and sodium, also cleave TIPS, presumably at C-O bonds as reported at the Houston meeting.(4) Table 3 gives the average numbers of molecules recovered from an original TIPS molecule, as measured by $\overline{M}_n$. After allowance for bound halogens, the carbon recoveries were usually 90-95%. We assume that the missing material was low molecular weight water-soluble or volatile material lost in the workup and therefore that the numbers in Table 2 are minimum values. However, to the extent that the products contain salts or other impurities (for which we have no evidence), the numbers in Table 2 are too large.

A TIPS fraction of $\overline{M}_n$ 1283 was treated for 7-15 days at 90°C with hydrogen iodide in solution in pyridine, toluene, or water. By GPC, the high-molecular weight peak in the TIPS disappeared almost completely and was replaced by low molecular weight peaks. Similar but incomplete changes occurred in toluene and water. The reaction of HI in pyridine resulted in recovery of 4.4 moles of product per 1283 g of TIPS and incorporation of 3.03 g-atoms of iodine per initial mole of TIPS. From the iodine content of the product, we would expect 4.03 molecules of product, in good agreement with the $\overline{M}_n$ data considering that there was 6% loss of carbon and that the iodide hydrolyses at room temperature.

Distribution of Oxygen in a TIPS Fraction

A TIPS fraction of M_n 1090, by reaction with alcoholic KOH, contains ~ 0.8 ester group per average molecule and reaction with HI or $ZnCl_2$ gives ~ 1.2 additional cleavages per TIPS molecule. The phenol content corresponds to 3.5 oxygen atoms per average molecule. The net result is that these three functional groups account for 64% of the 14.4% oxygen in our coal. These results are compared with results of others in Table 4. The principal difference is that we report as esters what others report as carboxyl groups.

Although there is little doubt about the cleavage of ethers by hydrogen iodide, or of esters by amines, the cleavage of ethers by EDA and $BnNH_2$ has no precedent in the literature. We have treated model ethers with these amines for long periods at 100°C, sometimes in the presence of an equal weight of coal, but we have found no evidence of reaction with benzyl phenyl ether, dihexyl ether, 4-hexyloxyphenol, or trimethylene oxide. However, since the amines and the halides produce similar effects, we see no alternative to ether cleavage by amines. Perhaps the involvement of condensed aromatic nuclei or the uneven concentration of phenol groups(9) makes the coal ethers more reactive.

Oxidations of Coal Fractions

We reported most of our work on coal fractions at the Atlanta Meeting.(10) We aimed at maximum recovery of "black acids", slightly soluble in weak aqueous base, with minimum loss of carbon. We expected investigations of these black acids, made with different oxidizing agents, to give us information on breakable C-C bonds in coal. For oxidations, we used mostly extracted coals in suspension, and aqueous NaOCl or oxygen in water at pH 13, adding sodium hydroxide to maintain the pH, or a suspension in 15-35% nitric acid. We obtained 65-80% yields on carbon of black acids with the reagents named, with $\overline{M}_n$ about 1000, and 12-20% loss of carbon. Five to 10% yields of water-soluble acids were also obtained. Although the nitric acid

oxidation products had the lowest H/C ratios (0.65 from 0.73 in pyridine-extracted coal) other differences among the black acids were not obvious.

Because the yields of black acids with the three main oxidizing agents were similar, we have compared the black acids with respect to molecular weight distributions and water solubility. We used both gel permeation chromtography (GPC) in dimethylformamide and high performance liquid chromatography (HPLC), starting the elution with 10 mL of 25% n-propanol in water, followed by neat DMF. GPC was done in a Waters column with 500 Å pores, packed in DMF. HPLC separations were done on a Hamilton PRP-1 column. With each column, the flow rate was 1 mL/min and a UV detector at 313 nm was used. Several known compounds were tested on the HPLC column: 2-naphthoic acid, trimellitic acid, pyromellitic acid, and phenyl benzoate eluted at 8-12 mL but everything else tested (mostly aromatic hydrocarbons, some with one oxygen atom) eluted at 24 mL or more. Thus the HPLC column is mostly a test for water solubility. The plots of UV absorption against retention time consist mostly of fairly sharp peaks with little absorption between well-separated peaks.

Results on 11 black acids are summarized in Table 5 arranged according to their origins. Several black acids from NaOCl oxidations of pyridine-extracted coal were combined, dissolved in dilute base, and fractionally precipitated by addition of hydrochloric acid. Sample F28D precipitated between pH 5.5 and 5.0, F29E between 5.0 and 4.66. As expected, by GPC 28-D contained more of the highest molecular weight (lowest retention volume) component at 5 mL and less of the lower molecular weight materials. Sample F29E suggests that the 5.0 mL GPC peak corresponds to the 4.3 ML HPLC peak, but the correspondence is poor with Sample F29D. We suspect that the 5.0 mL GPC peak is not as homogeneous as it appears and that the water-soluble components are polycarboxylic acids that are associated in DMF.

The 5.0 mL GPC component is the major GPC component in most of the black acids in Table 5. Exceptions are black acids T74B, U60B, and U85A, which show that degradations by sodium hypochlorite, 50% nitric acid, and Ce^{4+} are relatively severe. The most 5.0 mL component came from an oxidation with oxygen in water suspension at pH 13 and 50°C; this reagent is apparently the mildest and most selective of those that we have used. However, 35% nitric acid gave more lower molecular weight and water-soluble material without much sacrifice of carbon recovery.

By HPLC, five of the eleven black acids gave at least 46% of the 4.3 mL component and seven of the eleven have a 27.8 mL component that is either the largest or second largest component. Six of the black acids in Table 3 contain more than 70% of one component by either GPC or HPLC (underlined in the Table); two of them show more than 70% of one component on both columns. One of the latter black acids, T10B, represents 68% recovery of carbon in the coal fraction. Because of our high recoveries of soluble carbon and the different effects of oxidizing agents on the aliphatic and aromatic portions of coal, these chromatographic methods offer considerable potential for determining some average structures in unprocessed coal.

Oxidations with m-Chloroperbenzoic Acid (MCPA)

The objective of this work was to determine the proportion of single methylene groups as connecting links between condensed systems in coal. This problem evolved into a search for diaryl ketones in the black acid oxidation products of coal fractions. The diaryl ketones were expected to react with MCPA to convert them to esters, which were then saponfified. The critical measurement is a decrease in $\overline{M}_n$ on saponification of the esters. However, we could measure the $\overline{M}_n$ only on the water-insoluble products that we recovered from the saponification; the water-soluble products were presumably the lowest molecular weight material. In three out of four experiments deserving consideration, there was a 2-9% increase in $\overline{M}_n$ of the recovered acids. In one experiment, there was a decrease in $\overline{M}_n$ from 410 to 391, but these black acids represent only 18% of the carbon in a TIPS fraction that was oxidized with 50% nitric acid. We propose that this oxidation concentrated diaryl ketones in the black acids, but even then, their proportions were barely measurable by our MCPA method.

These results indicate that there are no important proportions of bridging methylene groups in our coal, but our method is insensitive. However, the next section shows that this conclusion is consistent with most of the evidence from the literature.

Cleavages in Diphenylalkanes

Literature data on breakdown of α,w-diphenylalkanes are summarized in Table 6. These hydrocarbons are designated by the number of methylene groups that they contain. The first reference shows that with $AlCl_3$ and H_2 at 325°C, 1,3-diphenylpropane is most reactive, followed by diphenylmethane and diphenylethane. All the hydrocarbons with 0 to 4 methylene groups were cracked; the extents of reaction ranged only from 32 to 83%. The second reference indicates that 1 has the most reactive bond in coal because a very small yield of dihydroxydiphenylmethane, in which both aryl-CH_2-aryl bonds were broken, was obtained. However, all the other references in Table 5 indicate that in the absence of $AlCl_3$ or BF_3 1 is the least reactive of these hydrocarbons and that there may not be much of this kind of bond present in coal anyway. Two references indicate that ether links break more easily than C-C bonds. In terms of bond energies, the phenyl-C bonds are strongest. In terms of our project objective, the C-C bonds that are breakable in conventional coal liquefaction appear to be mostly, perhaps entirely, in sequences of two or more methylene groups.

Summary and Conclusions

We have shown that 44% of the carbon in our beneficiated Illinois No. 6 coal can be dissolved by cleavage of ester and ether links by amines, acids, or iodides at 100°C and atmospheric pressure. Up to 80% of the remaining carbon can then be made soluble in weak aqueous base by oxidation at 60°C or below. One practical problem in coal liquefaction is now to try the use of cheaper reagents to break ester and ether links, and to determine what temperatures and pressures are required. Other practical problems are to reduce the consumption of base in oxidations with oxygen (pH 13 has been required) and to see if oxygen can replace part of the sodium hypochlorite or nitric acid used for oxidations. Some remarks on our progress are expected to be made at the meeting.

Acknowledgement

All of the work described here was supported by the U.S. Department of Energy through the Pittsburgh Energy Technology Center. The results reported here were supported by Contract No. 22-81ET11423.001 and the work in progress is supported by Grant No. DE-FG22-82PC50788.

References

(1) F. R. Mayo, A. S. Hirschon, and J. S. Zevely, Abstracts and Research Accomplishments of AR&TD Liquefaction Projects, Pittsburgh Energy Technology Center, p. 100 (September 1982).
(2) I.G.C. Dryden, Fuel, 31 176 (1952).
(3) D. W. Van Krevelen, Coal, Chapter X, Elsevier Publishing Co., New York, 1961.
(4) F. R. Mayo, D. H. Buchanan, and L. A. Pavelka, Preprints, Division of Fuel Chemistry, 25(2), 182 (1980).
(5) J. N. Bhaumik, A. K. Mukherjee, P. N. Mukherjee, and A. Lahirir, Fuel, 41 443 (1962).
(6) H. Wachowska and W. Pawlak, Fuel, 56, 422 (1977).
(7) H. Wachowska, B. N. Nandi, and D. S. Montgomery, Fuel, 58, 257 (1979).
(8) R. C. Ruberto and D. C. Cronauer, ACS Symposium Series, 71, 50 (1978).
(9) J. W. Larsen, P A. Nadar, M. Mohammadi, and P. A. Montano, Fuel, 61, 889 (1982).
(10) F. R. Mayo, L. A. Pavelka, Preprints, Division of Fuel Chemistry, 25(1), 31, 1981).
(11) N. D. Taylor and A. T. Bell, Fuel, 59, 499 (1980).

(12) L. A. Heredy, Adv. Chem. Series, 192, 179 (1981).
(13) B. M. Benjamin, V. F. Raaen, P. H. Maupin, L. L. Brown, and C. J. Collins, Fuel, 57, 269 (1980).
(14) L. W. Vernon, Fuel, 57, 507 (1980).
(15) D. C. Cronauer, D. M. Jewell, Y. T. Shah, and R. J. Modi, Ind. Eng. Chem., Fundamentals, 18, 153 (1979).
(16) E. Kuhlman, E. Boerivinkle, and M. Orchin, Fuel, 60, 1002 (1981).
(17) R. Liotta, K. Rose, and E. Hipps, J. Org. Chem., 46, 277 (1981).
(18) Y. Takemura, H. Itoh, and K. Ouchi. Fuel, 60, 379 (1981).

Table 1

REACTIONS OF ILLINOIS NO. 6 COAL WITH EXCESS $BnNH_2$

Pyridine extraction ⟶ 18.1% sol. + 81.9% insol.

TIPS (toluene-insol.,pyr.-sol.), yields corrected.

	% N	$\bar{M}_n$	Moles/1090g TIPS TIPS	$BnNH_2$
No extraction	1.68	1090	1.0	0
24 h at 23°	2.79	534	2.0	1.1
9 d at 100°	3.31	379	2.9	1.7

Pyridine-insoluble, yields corrected (%N)

4 h at 23° ⟶ 1.3% sol.(4.36) + 97% insol.(3.49)

16 d at 23° ⟶ 7.3% sol.(4.12)

11 d at 100° ⟶ 45.7% sol.(5.11)+ 52% insol.(5.13)

Table 2

EXHAUSTIVE EXTRACTION OF ILL. 6 COAL BY $BnNH_2$

	Carbon recoveries after correction for bound amine
Soluble in pyridine	42.7%
Soluble in $BnNH_2$, not in pyridine	1.5
Undissolved	54.2
Unaccounted for	1.6

Table 3

MOLECULES FORMED BY CLEAVAGE OF ONE MOLECULE TIPS
(mostly in pyridine solution)

Reagent	Molecules	Reagent	Molecules
$ZnCl_2$	3.1	$p\text{-}C_7H_7SO_3H$	1.6
$LiI \cdot H_2O$	3.1	Na in NH_3 + $BuNH_2$	1.6
$ZnBr_2$	3.0		
Pyridine·HI	2.7	Me_3SiI	1.5
MeI neat	2.0	$LiClO_4$	1.4
Benzylamine	1.8	HBr	1.3
$BnMe_3N^+I^-$	1.7	I_2	1.1

Table 4

OXYGEN DISTRIBUTIONS IN COALS

Coal	%C daf	%O	Distribution of O, % OH	C=O	CO_2H	Ether	Inert	Ref.
A	79.4	12.5	48	13	6	18	14	Blaumik HI 1962 5
B	83.0	8.4	50	6	2	26	16	
C	88.0	4.0	30	5	0	40	25	
K-I	78.2	15.1	16	4	5	8	67	Wachowska OH change 1977 6
K-II	81.1	11.7	11	4	4	5	76	
K-III	87.0	6.0		4	6	25	65	
K-N	87.9	4.5		8	8	61	23	
A	92.6	4.2			5	28	67	
Canadian	89.4	3.9	24		8	48	20	Wachowska 1979 7
Ill. 6	82.5	6.7	36	6	10	42	6	Ruberto 8 1978
Subbit.	77.3	16.2	35	6	27	6	26	
Ill.	76.0	14.4	36	ester16	12		36	This paper

Table 5

FRACTIONATIONS OF BLACK ACIDS BY GPC AND HPLC

Black Acid No.	Origin		Yield[a]	Retention Times, min.[b] GPC			HPLC		
T74B	TIPS	NaOCl	74	10.0	12.1	5.0	27.7	3.5	4.5
				45	28	27	54	18	14
T57B	EDA extract		43	5.1	7.7	8.1	23.7	4.8	4.3
				37	20	16	81	3	2
F28D	Pyr-extd.[c]			5.0	10.4	6.4	4.3	25.0	5.6
				88	10	2	46	28	7
F29E	Pyr-extd.[d]			5.0	6.8	7.0	4.3	27.9	31.1
				74	9	8	71	25	3
T33B	EDA-extd.		62	5.0	9.5	12.3	25.6	4.0	28.2
				56	41	3	53	27	6
R56B		O_2 in H_2O		5.0	7.1	9.9	24.9	3.8	4.1
				90	5	3	33	22	22
T10B	$BnNH_2$-extd.		68	5.0	11.0	8.2	4.3	27.6	31.0
				76	13	8	75	19	2
L23B	Pyr-extd.	15% HNO_3	68	4.8	7.9	9.7	27.8	3.9	29.0
				77	18	3	51	23	18
K23A		35% HNO_3	64	5.0	7.7	10.0	4.3	27.9	31.0
				53	32	15	62	36	2
U60B	EDA-extd.	50% HNO_3	18	8.1	10.5	9.7	4.6	28.0	31.1
				61	25	7	58	38	3
U85A	TIPS	Ce^{4+}	54	8.2	5.2	10.7	25.7	4.3	6.0
				58	20	17	40	34	9

[a] Yield of black acid from indicated substrate, on carbon.

[b] The numbers on the second lines for each retention times are the percentages of the total products, as measured by an ultraviolet detector.

[c,d] Combined black acids from NaOCl oxidations precipitated between pH 5.5-5.0[c] or 5.0 to 4.66[d].

Table 6

CLEAVAGES OF $Ph-(CH_2)_n-Ph$

Reagent	Temp., °C	Order of reactivity for n values	Reference
$AlCl_3 + H_2$ in C_6H_6, 90 m	325	3 > 1 > 2 ≥ 4 > 0	Taylor,[11] 1980
$PhOH + BF_3$	100	1	Heredy,[12] 1981
Tetralin, 18 h	400	3 > 2, 4	Benjamin,[13] 1978
Tetralin + H_2 30 m	450	2 > 1	Vernon,[14] 1930
Excess tetralin	450	2 > 4 >> 1	Cronauer,[15] 1979
Decalin + H_2 ± Ph_3SnCl, 1 h	<400 450	mostly ether splits 2, 3	Kuhlmann,[16] 1981
^1H NMR		No significant amount of 1 in THF-soluble products	Liotta,[17] 1981
$CO + H_2O$, 1 h	400	3 > 2 > 1 Ethers split more easily	Takemura,[18] 1981

APPLICATION OF CROWN ETHERS AS PHASE TRANSFER CATALYSTS IN THE ELECTRON TRANSFER REACTIONS OF COAL

Ramani Narayan and George T. Tsao

Laboratory of Renewable Resources Engineering
Purdue University
West Lafayette, Indiana 47907

INTRODUCTION

The electron transfer reactions of coal as exemplified by the Sternberg procedure (1) for reduction and reductive alkylation has been the subject of intensive investigation by a number of research groups (2-5). The reaction suffers from the problems of extended reaction time, side reactions, incorporation of the electron transfer agent and/or solvent into the coal. Further, in most cases, negligible quantities of soluble products were obtained on quenching the reaction immediately after the electron transfer step.

In view of this, the discovery by Pedersen (6,7) that certain macrocyclic polyethers called crown ethers have the ability to complex alkali metal cations, and the results of Dye (8), Kaempf (9) in the solubilization of alkali metals using these crown ethers, prompted us to envision the use of crown ethers to act as phase transfer catalyst in the electron transfer reaction with coal.

Thus, a stable solution of electrons can be prepared in an inert ethereal solvent like THF at room temperature because the equilibrium

$$M \rightleftharpoons M^+ + e^- \text{ solvated}$$

is shifted to the right by the complexation equilibrium

$$M^+ + \text{crown ether} \longrightarrow M^+ \text{ CE - complex}$$

The limitations of solubility, decomposition problems, reactivity and incorporation of the electron transfer agent can be overcome.

Another important facet of the crown ethers is that they have been successfully employed as reagents for direct solid-liquid phase transfer reactions (10). Thus, the problem of interphasic electron transport from solution to the aromatic substrate in coal would be solved, because the crown ether can function as a phase-transfer catalyst.

Further, the complexation of K by crown ether results in the metal cation being held inside the cavity of the crown ether and the resulting ion pair is loose. This would promote the irreversible electron transfer with bond cleavage (11).

EXPERIMENTAL

Coal: The Illinois No. 6 coal from the Burning Star No. 2 mine (courtesy of the Southern Company Services, Inc.) C-68.25%, H-5.30%, N-1.69%, S-3.62%, Ash-17.7% was used in the studies. It was demineralized, (12) extracted with Benzene:Methanol (3:1) to remove the trapped organic, and dried in vacuum at 100°C for 24 hours before use.

Reagents: The crown ether selected for study was the 18-crown-6, 1. This crown ether has a hole 2.6-3.2 A in diameter. The electron donor alkali metal selected for the study was potassium because its ionic diameter is 2.66 A and should, therefore, fit nicely in the crown ether hole resulting in a 1:1 complex. Using a 1:1 molar ratio of potassium to crown ether (CE), a 0.14 molar and 0.28 molar solution was prepared which was deep blue in color clearly indicating the presence of 'solvated electrons' in solution. This was reacted with different weights of coal under a blanket of nitrogen and the reaction quenched with water.

RESULTS AND DISCUSSION

Analysis: The percent g-atom of potassium consumed in the reaction of the K-CE reagent with coal was determined by measuring the difference in the volume of hydrogen evolved when the blank reagent and the reaction mixture was quenched with water after the same reaction period. To establish the accuracy of our analytical method and the validity of our reagent as an electron transfer agent, it was reacted with standard compounds and the mole of compound consumed per g-atom of potassium computed by the hydrogen evolution method. The values obtained compare favorably with those reported in literature (13) for the same compound using a different electron transfer agent and a different analytical method (Table 1).

TABLE 1

Compound	Mol of Compound Required per g-atom of Metal	Literature Value
Benzil	0.6	0.50
2-Butanol	1.29	1.1
Naphthalene	0.58	0.50

Effect of Electron Concentration and Time: The percent g-atom of potassium consumed in the reaction is a measure of the uptake of electrons by the coal resulting in the formation of the coal radical anion which undergoes cleavage at the ether and sulfur linkages. In the reaction of a 0.14 molar solution of K in THF with different weights of coal, the metal consumption increased with coal weight until it levelled off at the larger coal weights (Fig. 1).

One can deduce from this that for a given molar solution of metal, there is a certain concentration of electrons present which is going to be dependent on the amount of crown ether used. As the coal weight increases, the aromatic substrates available for electron transfer increases and more electrons are transferred to coal which is reflected in the amount of K consumed. This will continue till at a certain coal weight, all the available electrons get transferred. Any further increase in coal weight will still reflect the transfer of all the available electrons and the K consumed will be the same in each case. For the 0.14M solution, the minimum weight of coal required to be able to take up all the available electrons is 100 mg.

Increasing the K concentration to 0.31 molar showed a dramatic increase in the percent K consumed (Fig. 2) although the plot of percent K consumed against coal weight followed the same pattern as that obtained for the 0.14 molar solution. It is probably that at this increased electron concentration, a two electron transfer is taking place with the formation of the coal dianion and at the lower concentration, a one electron transfer occurs with the formation of the radical anion (Scheme 1).

Since complete electron transfer takes place at the 100 mg coal weight, it was selected for a time study. The K consumption increases very rapidly in the first thirty minutes and then levels off (Fig. 2). This suggests that the transfer of electrons proceeds very rapidly and is complete in thirty minutes with the electron concentration obtained from a 0.14M K/THF solution.

Solubility Studies: Based on the above studies, 1 g of coal was treated with 20 mmol of K in the THF with 20 mmol crown ether (0.2 molar in K), stirred for six hours and quenched with water. After rotaevaporating to dryness, the reacted coal was washed extensively with water to remove the K-salts and crown ether and extracted with THF. The degree of conversion was calculated as % solubility = wt of feed coal - wt of THF insoluble residue/wt of feed coal x 100. The elemental analysis and solubility of the feed coal and solubilized coal is summarized in Table 2.

TABLE 2

Sample	C	H	S	N	*THF Solubility	H/C	O (By diff)
Feed Coal	74.47	4.97	3.55	1.42	5.9%	0.8	15.59
Reacted Coal (1 g Coal/ 0.2M K-THF Solution)	74.41	7.39	2.0	1.40	52.%	1.12	14.80

*Based on coal residue insoluble in THF. Thus any error in the weight due to presence of moisture crown ether, etc., would only mean more THF solubility than obtained.

^{1}H and ^{13}C NMR Studies: The 470 MHz ^{1}H NMR spectrum of the solubilized coal is shown in Fig. 3, while the proton decoupled ^{13}C NMR spectrum is shown in Fig. 4. The integration in the ^{1}H NMR shows that the ratio of $H_{ar}:H_{sat}$ is 1:4. The broad peak around 3.4 ppm is assignable to the hydroxyl protons. The sharp resonance signals in the 1-1.6 ppm region are assigned to the R-CH_2-R grouping. These could also arise from methyl protons (CH_3-R), however, the absence of any methyl carbon resonances in the 11-22 ppm region rules out this possibility. Furthermore, the appearance of a group of signals in the 28-34 ppm region confirms the presence of methylene groups (-CH_2-) in a saturated ring system. This, in all probability, would be a saturated six-membered ring system joined to an aromatic ring system. The strong resonance signal at 69.7 ppm evidently comes from the C atom bearing the hydroxyl group (-CHOH) in the saturated ring. The aromatic ring carbons appear in the 125-145 ppm region. The 125-128 ppm signals are due to the protonated aromatic carbons and the 138-145 ppm signals due to quaternary mapthalenic type carbons.

Thus, by using a phase transfer catalyst 18-crown-6, rapid and effective electron transfer to coal has been achieved. This has resulted in the formation of coal radical anions or dianions depending on the concentration of the solvated electrons in solution (Scheme 1). These ions have undergone facile cleavage reactions (Scheme 2) resulting in depolymerization as demonstrated by the considerable increase in THF solubility from 5.9% for the starting coal to 52% for the reacted coal. The increase in the H/C ratio from 0.8 to 1.12 representing an uptake of 32H atoms per 100 C atoms is due in part to hydrogen pick-up from the capping of the cleavage coal radical or anion fragments. That this corresponds to reductive cleavage of the ether bonds in coal is supported by the presence of a large percent of hydroxyl groups in the solubilized coal as indicated by ^{1}HNMR. A Birch type reduction of the aromatics to hydroaromatics would account for the uptake of the remaining hydrogen atoms (Scheme 3) and is supported by the appearance of the R-CH_2-R grouping in both the ^{1}H and ^{13}C NMR.

REFERENCES

1. H.W. Sternberg, C.L. Delle Done, P. Pantages, F.C. Moroni, and R.E. Markbly, Fuel, 1971, 50, 423.

2. L.B. Alemany, S.R. King, and L.M. Stock, Fuel, 1978, 57, 738; (b) L.B. Alemany, and L.M. Stock, Fuel, 1982, 61, 256; (c) C.I. Handy and L.M. Stock, Fuel, 1982, 61, 700.

3. H. Wachowska and W. Pawlak, Fuel, 1977, 56, 216; (b) H. Wachowska, Fuel, 1979, 58, 99.

4. L. Lazarov, I. Roshkov and S. Angelov, Fuel, 1979, 57, 637; (b) L. Lazarov, M. Stefanova and K. Petrov, Fuel, 1982, 61, 58.

5. K. Niemann and H.P. Hombach, Fuel, 1979, 58, 853; (b) K. Niemann and U.B. Richter, Fuel, 1979, 58, 838; (c) Fuel, 1982, 61, 423.

6. C.J. Pedersen, J. Amer. Chem. Soc., 1967, 89, 7017.

7. C.J. Pedersen, J. Amer. Chem. Soc., 1970, 92, 386.

8. M.T. Lok, F.J. Tehan, and J.L. Dye, J. Phy. Chem., 1972, 76, 21.

9. B. Kaempf, S. Raynal, S. Boileau and J.M. Lehn, Agen. Chem. Internal. Ed., 1974, 13, 611.

10. G.W. Gokel and H.D. Durst, Synthesis, 1976, 168.

11. S. Bank and D.A. Juckett, J. Amer. Chem. Soc., 1975, 97, 567.

12. M. Bishop and D.L. Ward, Fuel, 1958, 37, 191.

13. K.W. Bowers, R.W. Giese, J. Grimshaw, H.W. House, N.H. Kolodny, K. Kronberger, and D.K. Roe, J. Amer. Chem. Soc., 1970, 92, 9.

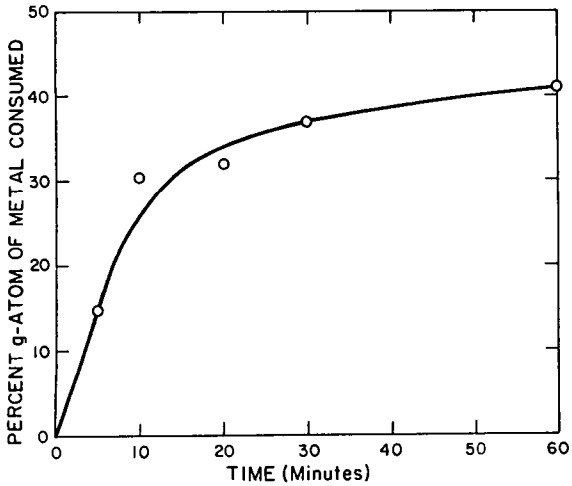

Figure 2.

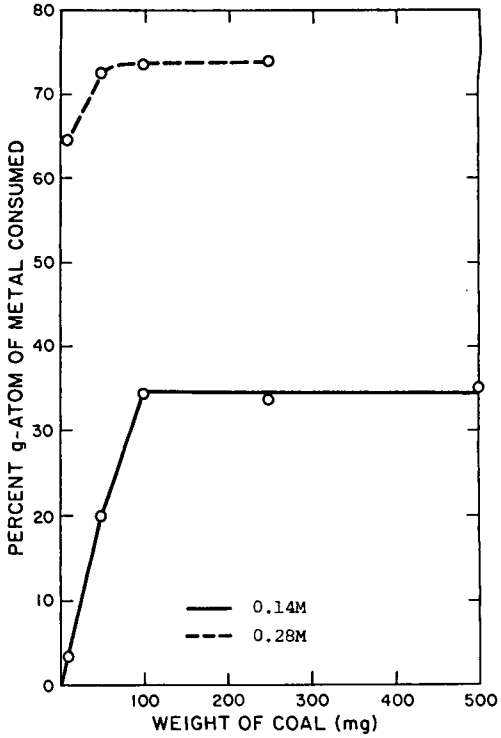

Figure 1.

Figure 4.

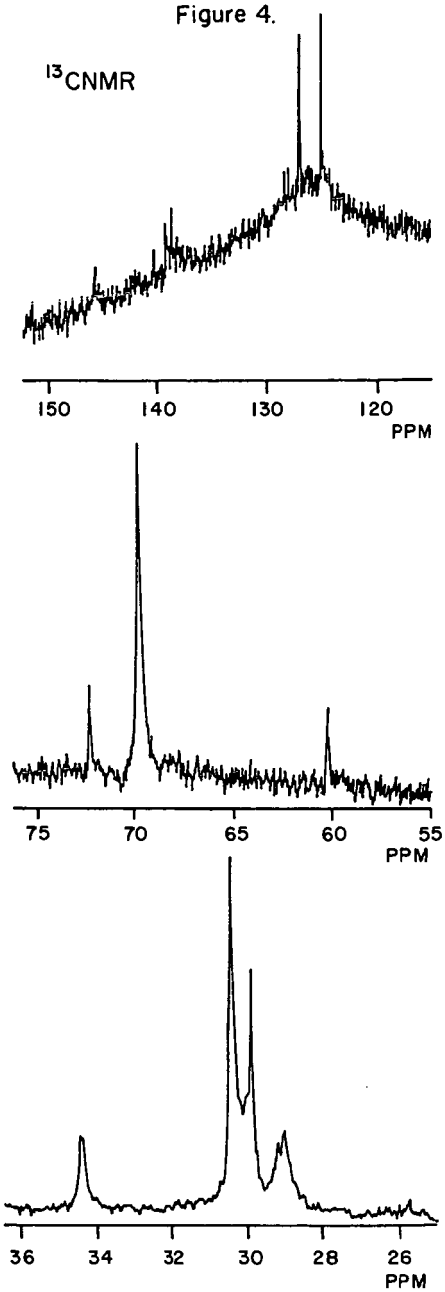

Figure 3.

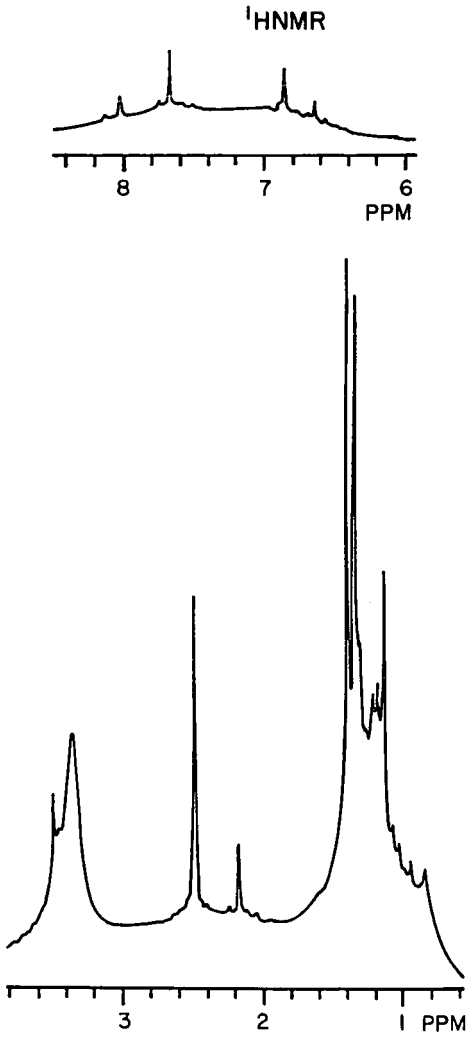

Scheme - 1

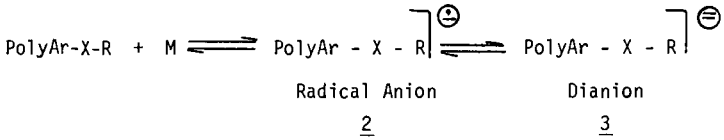

R = Aromatic,Hydroaromatic
- CH_2Ar, -S Ar
X = -O, S

CLEAVAGE (Scheme 2)

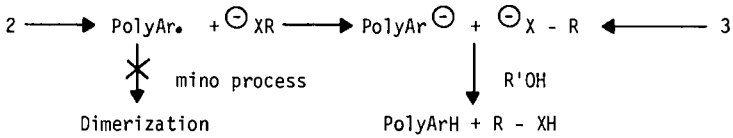

REDUCTION (Scheme 3)

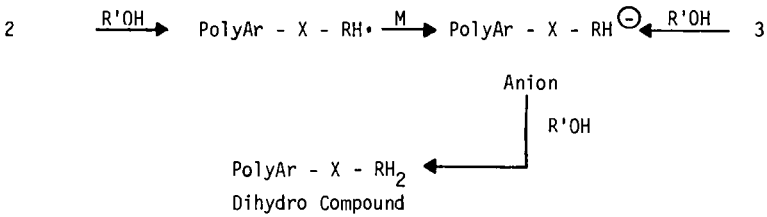

THE EFFECT OF LIQUEFACTION CONDITIONS ON THE TRACE ELEMENT CONTENT OF SOLUBLE COAL-DERIVED NON-VOLATILE PRODUCT

J. W. Hellgeth, R. S. Brown and L. T. Taylor

Department of Chemistry
Virginia Polytechnic Institute and State University
Blacksburg, Virginia 24061

INTRODUCTION

Trace element data on coal-derived products at the pilot plant stage are generally available. Several years ago the feed coal (Kentucky hvBb(1) and West Virginia hvAb(2)) and products from a single batch of a long-term liquefaction run on a 400 lb coal/day process development unit were sampled. Preferential removal of selected elements from the liquid product via centrifugation was observed in each case. Iron-containing minerals were preferentially removed if the West Virginia coal was employed; while, aluminum silicates were removed with Kentucky coal. Numerous elements (V, Cr, Mn, Ni, B, Be, Ti, As) did not show preferential removal upon centrifugation. Other elements were predicted to be associated with organic moieties.

Later multi-element analysis data on wet-ashed Amax feed coal, the chloroform-soluble solvent refined coal (Wilsonville, AL demonstration facility) derived therefrom and several size exclusion chromatographic fractions were obtained.(3) Appreciable metal concentration was found in practically all samples. For several elements, concentrations were higher in SRC than in its parent feed coal. This observation suggested the presence of organometallic species since these materials were soluble in a wide variety of organic solvents and had passed 5.0 μm filters.

Neutron activation analysis has been employed to obtain information on trace elements present in process streams of SRC I and SRC II (Tacoma, WA demonstration facility) products derived from a Western Kentucky coal.(4) In the SRC I process the filtered mineral residue was observed to be the sink for most trace elements with the exception of Ti, Cl, Br and Hg. The SRC I product was found to contain less than 2% of the elemental concentrations in the coal. The SRC II distillate product contained less than 1% of the elemental content of the feed coal. All elements were depleted in SRC I relative to the coal except Br.

A more recent study(5) has been concerned with SRC's which differ (from each other) either in feed coal source, conversion severity or method of residue removal. These materials originated at the Wilsonville facility and were directly analyzed as filtered pyridine solutions via atomic emission spectrometry. Of the metals observed, those which showed any significant concentration (10-1000 μg/g of SRC) were Al, B, Cu, Fe, Si and Ti. West Kentucky SRC from different mines (Lafayette and Fies) exhibited similar metal content with few exceptions. The effect on elemental concentration of mineral matter removal via filtration or critical solvent deashing was varied. The most significant changes were seen with Ca, Fe, Si and Ti. With the exception of Ti, the elemental concentration in the CSD product was two times or greater than the concentration of the filtered product. An increase in hydrogen pressure (2000-2100 psi) and temperature (418°-450°C) had a minimal effect on metal content. Only for Ca, Si and Ti was there greater than 50% reduction in concentration on going to more severe reaction conditions. Those metals which are expected to be most strongly organo-bound (i.e. transition metals) did not significantly change concentration as a function of processing conditions. Mineral-related elements such as Al, Ca, Mg and Si, on the other hand, appeared to fluctuate

in concentration with processing parameters.

As can be seen above, all trace element studies have involved coal-derived process solvents, pilot plant sampling, lengthy and rather severe reaction conditions and mostly bituminous feed coals. In several of these investigations analytical methods were applied to the ashed sample rather than to the unmodified material where less sample-handling and less opportunity for introduction of impurities are possible.

We wish to report soluble trace metal analysis data on an extensive number of "in-house" short-contact time SRC's prepared with various basic nitrogenous and non-basic model process solvents with both bituminous and subbituminous coals. Data are reported as a function of liquefaction time and temperature, method of residue removal and solvent solubility. In addition, size exclusion chromatography (SEC) of selected SRC's with metal-specific inductively coupled plasma atomic emission spectrometric (ICP-AES) "on-line" detection will be utilized to aid in determining the fate of trace metals during liquefaction.

RESULTS AND DISCUSSION

Trace metal analysis of 18 elements in pyridine via ICP-AES has been performed on numerous in-house SRC's in order to determine the effect of various conversion parameters on metal content. Table I list pyridine soluble SRC (Indiana V coal) metal concentrations as a function of process solvent. In order that some point of reference be established in comparing analyses, concentrations are expressed in μg of metal per gram of extracted moisture-free coal not of SRC. The numbers in each case are representative of two independent liquefaction runs and respective metal determinations. Relative standard deviations varied between 1% and 10% depending on the level of metal. Significant metal content is found for 12 of 18 metals monitored. The highest concentrations invariably are observed with Fe, Si and Ti regardless of the process solvent employed. In general, metal content does not appear to be greatly influenced by the various process solvents employed. Initially, one might have argued that the presence of a good ligand donor solvent such as THQ would complex and solubilize more metal than a poor ligand donor solvent. This is not the case with Indiana V SRC. A greater than ten-fold change in metal content with the four solvent systems is observed only with Ca (17.4-319.9) and Mn (3.73-48.4); while, Al (20.3-121.0) and Si (27.1-208.0) also reflect a rather large fluctuation in concentration. Those elements reflecting the greatest fluctuation in concentration are probably mineral related. Differences in both mineral particle size distribution and viscosity of the SRC extract (which would affect the separation achieved by centrifugation) could cause this variation.

Data were also obtained as a function of reaction time (10 and 30 minutes) for pyridine soluble SRC derived from Wyodak #3 coal. Increased reaction time lowers the content of most metals. Again, many of those elements decreasing in soluble metal concentration with an increase in reaction time could be mineral related (Ca, Mg, Si and Ti). A possible explanation for this observation is that a longer reaction time may more extensively de-complex these elements thereby removing them from the pyridine soluble SRC into the residue. This finding is somewhat surprising in that one might have reasoned that a longer reaction time would lead to more extensive metal solubilization (i.e. mineral matter converting to organometallics). This may very well be the case with Ag, Al, Cu and Fe which show an increase in concentration with reaction time.

The most dramatic change in SRC metal content is found with the extraction solvent employed. Table II compares the analysis of 9 elements obtained on toluene and pyridine soluble fractions (Wyodak #3 SRC). The

TABLE I

METAL ANALYSIS DATA OF SRC'S PREPARED WITH VARIOUS PROCESS SOLVENTS[a,b]

Element	TETRALIN/PYRENE (50:50) 86.4%[c]	THQ (100) 93.7%[c]	TETRALIN/MN (50:50) 91.9%[c]	TETRALIN/THQ/PYRENE (25:50:25) 92.8%[c]
Al	50.9	107.0	20.3	121.0
B	95.4	97.9	104.0	105.1
Ca	319.9	65.7	17.4	90.4
Cu	10.2	6.87	9.01	5.35
Fe	240.3	165.4	277.4	219.8
Mg	17.9	19.2	6.93	5.35
Mn	21.5	3.73	48.4	13.4
Ni	21.9	19.9	12.4	30.1
Si	132.9	201.4	27.1	208.0
Ti	133.4	113.7	116.2	199.9
V	6.17	5.06	4.82	9.04
Zn	40.8	19.2	15.4	27.3

[a]Indiana V Coal; S:C, 2:1, 400°C; 30 minutes; 7.5 MPa H_2

[b]<1 μg/g MF Coal measured for Ag, Ba, Cd, Cr, Mo, Sn. Units are μg/gMF coal.

[c]Pyridine Conversion (MAF)

TABLE II

METAL ANALYSIS DATA OF PYRIDINE AND TOLUENE SOLUBLE SRC'S[a]

	WYODAK #3[b]		INDIANA V[b]	
Element	Toluene Conversion[c] 77.85%	Pyridine Conversion[c] 82.59%	Toluene Conversion[c] 84.2%	Pyridine Conversion[c] 93.9%
Al	21.5	436.6	6.44	170.1
B	4.56	6.82	40.9	93.7
Ca	18.4	135.2	3.01	90.0
Fe	25.6	207.5	9.58	141.3
Mg	0.81	68.8	0.63	19.7
Ni	1.72	5.63	0.74	6.57
Si	17.9	775.6	16.9	314.5
Ti	15.9	130.0	7.48	43.9
Zn	3.71	8.83	6.74	15.1

[a]THQ; S:C, 2:1; 418°C; 7.5 MPa H_2; 30 minutes

[b]<1 μg/g MF Coal: Ag, Ba, Cd, Cr, Mn, Mo, Sn, V (Toluene)
<1 μg/g MF Coal: Cd, Mo, Sn (Pyridine)

[c]MAF basis

differences in concentration are large. In many cases metal concentrations are approximately one to two orders of magnitude higher in pyridine soluble SRC relative to toluene soluble SRC. Also, the number of elements appearing at concentrations less than 1 μg/g MF coal are 3 times more numerous for toluene soluble SRC relative to pyridine soluble SRC (9 versus 3) given nearly the same percent conversion. This observation is especially important in that it indicates that the metals concentrate themselves in the toluene insoluble-pyridine soluble products. Again similar findings (Table II) are observed with SRC derived from Indiana V. This finding has an implication regarding metal speciation. The greater concentration of metals in the pyridine soluble fraction suggests that the nature of many of these soluble coal-derived metals is more like a coordination complex rather than a true organometallic metal to carbon bonded species.

Trace metal analysis data are also available for SRC material derived from four different Wyodak coals, Table III. Identical liquefaction conditions were employed. Conversions are based on pyridine solubility which accounts for the relatively high metal contents found. A relatively wide variation (>200%) exists between high and low specific metal content for the four SRC's even though they are all derived from Wyodak coals. The highest metal content appears to be almost uniformly associated with SRC from Wyodak #4 coal (e.g. 13 out of 18 elements). Our Wyodak coals differ considerably from each other in ash content, fixed carbon, %C, %O and %S. Table IV lists ultimate and proximate analyses for these four coal samples. On a moisture free basis the ash content of Wyodak #3 is approximately double the ash content of the other Wyodak coals; yet, its SRC has the lowest metal content for half of the elements monitored. SRC from Wyodak #4 which contains the highest concentration of soluble metals has a feed coal of intermediate ash content and percent sulfur and the lowest percent oxygen. This lack of correlation between ash content and soluble SRC metal content supports the idea of organo-bound metals in coal-derived products. In fact SRC soluble metal content appears to not correlate with either ash, moisture, volatiles nor fixed carbon content. A general trend of metal content versus percent conversion is also not apparent.

Information regarding the number of groups of species for a particular metal and the effective molecular size of each group have been obtained via SEC-ICP-AES on both pyridine and toluene soluble Wyodak #3 SRC (Table II). In both cases the SRC was generated under identical liquefaction conditions. Seven common elements (Ca, Cu, Fe, Mg, Si, Ti, B) were chromatographically detectable in both SRC's employing pyridine elution (e.g. toluene soluble material was re-dissolved in pyridine and eluted from the column with pyridine) and a μ-styragel column. As might have been expected a greater overall concentration of metal is detected in the separation of pyridine soluble SRC than toluene soluble SRC. A greater concentration of larger "sized" material is also observed in pyridine soluble SRC (VR-85) relative to toluene soluble SRC (VR-39) as evidenced by the greater emission intensity of the earlier eluting metal-containing species in the respective metallograms. Totally size-excluded material (retention volume ≅ 3.5 mL) as well as selectively permeated metal species are apparent. This implies that there exists a group of organo-metallics of rather large size and another (usually broader) distribution of organometallics of considerably smaller size. This bimodal behavior is especially pronounced in the pyridine soluble fractions.

Metallographic comparison data are available on SRC's prepared at different reaction times. Pyridine extraction was employed; therefore, a greater number of chromatographically detectable metals was realized. Changes in reaction time do not appear to cause as extensive alterations in metal size distribution as changes in reaction temperature. The minor changes which are observed are not consistent from one metal to another. More specifically, B and Ca appear to have a greater concentration of large

TABLE III

METAL ANALYSIS DATA OF SRC'S PREPARED WITH DIFFERENT WYODAK COALS[a,c]

Element	Wyodak #1 72.3%[b]	Wyodak #2 84.7%[b]	Wyodak #3 85.4%[b]	Wyodak #4 83.3%[b]
Ag	1.57	-	0.97	5.75
Al	397.0	312.0	194.0	483.0
B	31.8	28.5	14.9	28.6
Ba	3.76	3.27	0.97	15.9
Ca	1567	1228	540.6	4069
Cd	-	-	-	2.02
Cr	1.17	2.35	1.70	4.28
Cu	5.64	4.07	6.92	13.1
Fe	125.0	171.0	157.9	180.0
Mg	391.0	258.0	90.5	320.0
Mn	19.6	21.9	7.12	17.0
Mo	-	-	-	4.35
Ni	13.8	17.6	20.6	53.0
Si	113.0	170.0	104.5	169.0
Sn	-	-	-	-
Ti	49.0	44.2	39.5	66.9
V	4.28	4.34	5.28	7.10
Zn	11.6	22.1	9.43	52.7

[a]50% tetralin/50% methyl naphthalene; S:C, 2:1; 400°C; 7.5 MPa H_2; 30 minutes.

[b]Pyridine conversion (MAF)

[c]Units are μg/g of MF coal

TABLE IV

ULTIMATE AND PROXIMATE ANALYSES

	Wyodak[a] #1	Wyodak[a] #2	Wyodak[a] #3	Wyodak[a] #4	Ind V[c]
%C	65.81	64.00	48.27	64.80	65.8
%H	5.15	5.34	4.47	5.59	5.0
%N	0.86	0.85	0.71	0.88	1.4
%O	21.19	20.97	24.32	17.52	7.6
%S	0.41	1.07	6.60	1.96	3.7
Ash	5.1	5.9	20.3	0.1	10.3
Moisture	9.9	8.1	7.0	7.6	5.1
Volatiles	36.1 (54.8)	37.7 (52.6)	35.0 (37.0)	39.4 (48.6)	37.4
Fixed Carbon	49.3 (40.1)	48.3 (41.0)	37.7 (41.4)	44.9 (42.6)	47.2

[a]Samples prepared by drying for 5 days, 133 Pa, 20°C to remove storage water.

[b]Numbers in parenthesis are proximate analyses on moisture free basis obtained in our laboratory.

[c]Data obtained from Kerr McGee Corp., Cresent, OK.

size species at the longer reaction time (30 minutes) than the shorter one (10 minutes). The reverse situation operates with Cu, Fe, Ti and Zn. An interpretation of these results suggest that B and Ca may incorporate with initial regressive reaction products; whereas Cu, Fe, Ti and Zn are tied-up more with the progressive reaction products. A longer reaction time should be conducive to both primary-secondary product progressive reactions as well as to regressive reaction behavior.

REFERENCES

1. R. G. Lett, C. E. Schmidt, R. R. DeSantis and A. G. Sharkey, "Screening for Hazardous Elements and Compounds in Process Streams of the 1/2 Ton Per Day SYNTHOIL Process Development Unit", PERC/RI-77/12, October, 1977.

2. R. G. Lett, J. W. Adkins, R. R. DeSantis and F. R. Brown, "Trace and Minor Element Analyses of Coal Liquefaction Products", PETC/TR-79/3, August, 1979.

3. D. W. Hausler, L. T. Taylor, J. Borst and W. B. Cooley, "Dev. At. Plasma Spectrochem. Anal. Proc. Int. Winter Conf.", R. M. Barnes, Ed., Heyden & Son, Inc. Philadelphia, PA (1982) p. 496.

4. R. H. Filby, D. R. Sandstrom, F. W. Lytle, R. B. Greegor, S. R. Khalil, V. Ekambaram, C. S. Weiss and C. A. Grimm, Proceedings DOE/NBS Workshop on "Environmental Speciation and Monitoring Needs for Trace Metal-Containing Substances from Energy Related Projects", F. E. Brickman and R. H. Fish, eds., NBS Special Publication 618, 1981, p. 21.

5. R. S. Brown, D. W. Hausler, J. W. Hellgeth and L. T. Taylor, ACS Symp. Ser., 205, 163 (1982).

ANALYTICAL CHEMISTRY OF PRODUCTS FROM PROCESS STRATEGIES DESIGNED TO REDUCE THE BIOLOGICAL ACTIVITY OF DIRECT COAL LIQUEFACTION MATERIALS

D. W. Later, C. W. Wright and B. W. Wilson

Pacific Northwest Laboratory
P.O. Box 999
Richland, Washington 99352

INTRODUCTION

The current status of understanding the chemical basis for the generally increased genetic activity of direct coal liquefaction materials, as compared to petroleum-derived products, has led to the investigation of a number of potential process strategies for reducing the biological activities of coal-derived liquids. Approaches that have been investigated include optimized fractional distillation, catalytic hydrotreatment, recycling of heavy-end and bottoms materials, and two stage liquefaction coupled with reduced liquefaction severity and improved quality hydrogen donor solvents.

Biodirected chemical analyses of coal liquefaction materials over the last several years have led to the identification of at least two important classes of compounds which are largely responsible for the biological response observed in laboratory systems upon exposure to these materials. The classical carcinogens in coal liquids are the polycyclic aromatic hydrocarbons (PAH), primarily those having from 4 to 6 aromatic rings. Kennaway, Cook and others in the early part of this century showed that certain coal-derived PAH could cause skin tumors in mice and rabbits (1,2,3). It has been found, in general, that genetic activity, particularly initiation of tumorigenisis, resides in high boiling heavy-end materials and correlates with overall PAH content better than with any other chemical class (4-6). More recently nitrogen-containing polycyclic aromatic compounds (N-PAC), specifically the amino-PAH, have been recognized as genotoxic constituents in several coal-derived materials. In quantitative terms, the amino-PAH occur at relatively lower concentrations as compared to the PAH. However, due to the increased sensitivity of the Salmonella typhimurium microbial mutagenicity test to amino-PAH, they are readily detected in the complex coal liquid mixtures by this biological assay (7-11). The possible contribution of amino-PAH to the etiology of any cancers induced in coal product workers is only now beginning to be understood. Amino-PAH such as 2-aminonaphthalene and 4-aminobiphenyl are recognized as human carcinogens (12). Furthermore, recent studies have demonstrated that the amino-PAH as a chemical class do contribute to the overall initiation of skin tumors in laboratory mice (13).

A common goal of the direct liquefaction process strategies considered in this study is the reduction of biological activity via reducing the concentration levels of the amino-PAH and the 4-, 5- and 6-ring PAH. In this report, coal liquefaction strategies such as distillation, bottoms recycle, hydrogenation, and two stage liquefaction will be discussed in terms of their effect on the chemical composition of process materials.

ANALYTICAL METHODS

The evolution and development of analytical methods at PNL (Pacific Northwest Laboratories) has been primarily directed by the requirement of determining the biologically adverse chemical classes and compounds in coal liquefaction materials. Accordingly, methods have been designed for the identification and quantification of not only homogeneous chemical classes, but also individual components. Figure 1 outlines the overall analytical approach currently used. An

initial separation of crude materials by adsorption column chromatography (14) enables the determination of gross chemical composition in terms of PAH and N-PAC content. Secondary chromatographic separations are achieved by HPLC methods (15) for the PAH, and a combination of adsorption and gel permeation chromatography (14,16) for the N-PAC. Finally, instrumental methods such as capillary column gas chromatography and mass spectrometry are used to provide detailed qualitative and quantitative chemical analysis of individual components in the separated materials.

During the last several years, the SRC (solvent refined coal) processes have received prime attention and consideration as potential direct coal liquefaction technologies. An illustration of the detailed data obtained from the previously described analytical procedures for the PAH fraction of a full boiling range SRC II end-product is provided in Figure 2 and Table 1. It should be noted at this point that all process materials investigated during this study and discussed in this paper were from process development units or pilot plants and may not necessarily be representative of products which will eventually be produced on a commercial scale.

RESULTS AND DISCUSSION

DISTILLATION

An effective process technique that has been used in the petroleum industry for the gross separation of end-products of refining according to volatility is distillation. Optimized fractional distillation has recently been applied to the products of direct coal liquefaction in an effort to effect a molecular weight separation and isolate the biologically active components in the higher boiling fractions (6). Bioassays of crude distillates and chemical class fractions from several direct liquefaction processes have shown that the majority (>99%)of genetic activity is contained in the distillate fractions boiling above 700°F (4-5). Figures 3 and 4 aid in understanding the chemical basis for this observation.

Figure 3A and 3B present chemical class weight distribution information for the 50°F distillate cuts of typical end-products from the SRC II and EDS (Exxon Donor Solvent) coal liquefaction processes, respectively. For each process, greater than approximately 80% of the material is distilled below 700°F. In terms of chemical class composition, there is a decrease in aliphatic hydrocarbon content and increasing levels of N-PAC and polar hydroxylated polycyclic aromatic hydrocarbons (HO-PAH) with increasing boiling point temperature. The neutral PAH portion of each distillate cut generally remains constant.

The effect of distillation temperature on molecular weight is shown in Figure 4 for the PAH fraction of the SRC II boiling point cuts. As a general trend, compounds of increasing molecular weight can be correlated with increasing distillation temperature. For example, pyrene, which is noncarcinogenic, is at a maximum concentration in the 700-750°F cut, while the potent carcinogenic compounds such as benzo(a)pyrene are distilled in the greater than 800°F cuts. This trend is also observed for the mutagenic N-PAC and amino-PAH components of the distillate fractions.

In summary, optimized fractional distillation in effect eliminates the bulk of components from the full boiling range material (Figure 1) which have a molecular weight greater than approximately 200 daltons and minimizes the levels of compounds that contain polar nitrogen and oxygen functional groups. Additionally, materials resulting from this process strategy would have a higher aliphatic hydrocarbon content and would be nominally biologically inactive.

BOTTOMS RECYCLE

Information from the distillation studies led to the suggestion that the greater than 700°F material, or bottoms, might simply be recycled continuously to extinction within the process to yield a non-biologically active end-product. Recently, experiments have been conducted with the SRC II process by the Merriam Coal Liquefaction Laboratory to determine the feasibility and applicability of this process strategy. Crude materials sampled from the SRC II process while operating in the bottoms recycle mode, with a recycle cut point temperature of 290°C (554°F) and assayed for microbial mutagenicity (S. Typhimurium, TA98) showed no detectable activity although these net products contained 5-10% (by weight) material boiling above the recycle cut point temperature. This work also demonstrated that an increased recycle of heavier-ends reduced the net yield of heavy distillate.

CATALYTIC HYDROGENATION

Catalytic hydrogenation has been considered both as an off-line post-production upgrading step, as well as an integral process in direct coal liquefaction technologies. Early results with catalytic hydrotreatment of an SRC II fuel oil blend material showed that mutagenic activity was substantially reduced by hydrogenation (17). This was explained by the reduced levels of amino-PAH due to deamination of the nitrogen functionality which occurs readily under the reducing conditions of hydrogenation processes. Furthermore, hydrogenation of the PAH components can lead to reduced aromaticity and/or carbon-carbon bond scission of higher molecular weight PAH. This again leads to a reduction in the biological potency of the end-products.

Several direct liquefaction technologies including EDS and TSL (two stage liquefaction) incorporate some form of catalytic hydrogenation step within the process. Table 2 lists the quantitative results for the major components detected in the PAH fraction of the 700-750°F distillate cut of end-products from the SRC II (no hydrogenation) and EDS (process solvent hydrogenation) processes. An obvious effect of the hydrogenation process is a general reduction in the EDS material of the concentration levels of parent PAH, for example pyrene and benzofluorene, as compared to other constituents of the fraction such as the hydroaromatics and alkylated species. In general, the EDS distillate cut is composed of several compounds within a fairly narrow concentration range, while the SRC II material has a few major components with other constituents at much lower concentration levels. Table 3 gives an estimate of the magnitude of the chemical differences that result from the hydrogenation process. The increased proportions of alkylated and hydroaromatic PAH in hydrotreated materials has the net effect of increasing the hydrogen to carbon ratio and enhancing the quality of both process products and recycle solvents.

TWO STAGE LIQUEFACTION

Two stage liquefaction processes such as the second generation integrated two stage liquefaction (ITSL) incorporate several process features which lead to both process streams and potential product materials which show reduced genotoxicity (18,19). It appears that the two most important features are reduced liquefaction severity in the first stage and catalytic hydrotreatment in the second stage. Low severity extraction depends upon the availability of high quality hydrogen-rich solvent which results from hydrotreatment. Severity in the initial liquefaction step is reduced primarily by lowering the residence time of the coal slurry in the first stage reactor. The improved solvation and hydrogenation properties of the higher quality solvent allows the coal to be solvated quickly and efficiently, thus minimizing the possibility of retrograde reaction which leads to the formation of polar materials and may cause polymerization or coking.

Reduction in nitrogen content of the distillates is the main reason for the lower genotoxicity of the ITSL materials as compared to the single stage processes. Figure 6 compares gas chromatograms of the nitrogen-containing PAH fractions after the first and second stages of the ITSL process. Deamination that is only partial in the low severity reactor is relatively complete in the hydrotreator product. This reduces the overall concentration of genotoxic amino-PAH in the process material and end-products. Similarly, hydrogenation and cracking occurs for the other PAH components in the process material resulting in the superior recycle solvent properties required for low severity liquefaction in the first stage and high quality end-products that are suitable for upgrading and refining.

CONCLUSION

The ability to perform detailed chemical analysis provides insights and understanding into both the areas of biological effects and process strategies. There are a number of chemical differences which have been discussed for the different products from direct liquefaction strategies, including hydrogenation, de-nitrogenation, and alkylation. The higher molecular weight genotoxic PAH and N-PAC which are minor constituents in most full range distillate coal liquids can be effectively reduced in concentration by optimized fractional distillation, bottoms recycle, or hydrogenation. Furthermore, two stage liquefaction with enhanced recycle solvents under low severity conditions coupled with hydrogenation reduces the aromatic and polar PAH content while increasing the hydrogen to carbon ratio of the process material. In general, the strategies investigated in this work result in higher quality process materials and end-products which are suitable either for refining or upgrading into usable products.

ACKNOWLEDGEMENT

This work was supported by the U.S. Department of Energy, Contract No. DE-AC06-76RLO 1830 with the Office of Fossil Energy.

REFERENCES

1. Cook, J. W., Proc. Royal Soc. B., 1932, 111, 455-484.
2. Kennaway, N. M.; Kennaway, E. L., J. Hyg., 1936, 36, 236-267.
3. Cook, J. W.; Hewett, C. J.; Heiger, I., J. Chem. Soc., 1933, 395-405.
4. Mahlum, D. D., J. Appl. Toxicol., 1983, (in press).
5. Later, D. W.; Pelroy, R. A.; Mahlum, D. D.; Wright, C. W.; Lee, M. L.; Weimer, W. C.; Wilson, B. W., In: "Proceedings of the 9th International Symposium on Polynuclear Aromatic Hydrocarbons," Battelle Press, Columbus, OH, 1982.
6. Wilson, B. W.; Willey, C.; Later, D. W.; Lee, M. L., Fuel, 1982, 61, 473-477.
7. Later, D. W.; Pelroy, R. A.; Lee, M. L.; Wilson, B. W., Mutat. Res., 1983, (submitted).
8. Wilson, B. W.; Pelroy, R. A.; Cresto, J. T., Mutat. Res., 1980, 79, 193-202.
9. Later, D. W.; McFall, T.; Booth, G. M.; Lee, M. L.; Tedjamulia, M.; Castle, R. N., Environ. Mut., 1983, (submitted).
10. Geurin, M. R.; Ho, C.-h.; Rao, T. K.; Clark, B. R.; Epler, J. L., Environ. Res., 1980, 23, 42-53.
11. Haugen, D. A.; Peak, M. J.; Suhrbler, K. M.; Stamoudis, V. C., Anal. Chem., 1982, 54, 32-37.
12. Radomski, J. L., Ann. Rev. Pharmacol. Toxicol., 1979, 19, 129-157.
13. Pelroy, R. A.; Later, D. W.; Mahlum, D. D., Environ. Mut., 1983, (submitted).
14. Later, D. W.; Lee, M. L.; Bartle, K. D.; Kong, R. C.; Vassilaros, D. L., Anal. Chem., 1981, 53, 1612-1620.

15. Lucke, R. B.; Later, D. W., Wright, C. W.; Weimer, W. C., Anal. Chem., 1983, (submitted).
16. Later, D. W.; Lee, M. L.; Pelroy, R. A.; Wilson, B. W., In: "Polynuclear Aromatic Hydrocarbons: Physical and Biological Chemistry," Cooke, M., Dennis, A. J.; Fisher, G. L., eds., Battelle Press, Columbus, OH. 1982, pp. 427-438.
17. Wilson, B. W.; Petersen, M. R.; Pelroy, R. A.; Cresto, J. T., Fuel, 1981, 60, 289-294.
18. Wilson, B. W.; Pelroy, R. A.; Mahlum, D. D.; Frazier, M. E., In: "Proceedings ITSL Program Contractors Project Review Conference," Albuquerque, NM, October 6-7, 1982.
19. Wilson, B. W.; Pelroy, R. A.; Mahlum, D. D.; Frazier, M. E.; Later, D. W.; Wright, C. W., Fuel, 1983, (submitted).

TABLE 1. Quantitative and Qualitative Analysis of the PAH in the SRC II Full Range Distillate[a]

Peak No.	Mol. Wt.[b]	Compound Identification	PAH Fraction (PPM (ug/g)[c]
	128	Naphthalene	730 ± 50[d]
1	142	2-Methylnaphthalene	15,040 ± 680
2	142	1-Methylnaphthalene	2,840 ± 130
3	156	2-Ethylnaphthalene	11,400 ± 540
4	156	2,6- and/or 2,7-Dimethylnaphthalene	12,500 ± 1000
5	156	1,7- and 1,6- or 1,3-Dimethylnaphthalene	8,260 ± 440
6	156	C_2-Naphthalene	
	152	Acenaphthylene	340 ± 20
7	154	Acenaphthene	7,990 ± 450
8	170	C_3-Naphthalene	
9	170	C_3-Naphthalene	
10	168	Dibenzofuran	13,360 ± 740
11	166	Fluorene	13,960 ± 1180
12	168	C_1-Acenaphthene and/or Dihydrofluorene	39,960 ± 4140
13	184	C_4-Naphthalene	
14	180	9-Methylfluorene	16,650 ± 3040
15	182	C_1-Dibenzofuran and/or C_2-Acenaphthene and/or C_1-Dihydrofluorene	
16	180	2-Methylfluorene	11,750 ± 680
17	180	1-Methylfluorene	9,830 ± 480
18	180,182,198	C_1-Fluorene and/or C_2-Acenaphthene and/or C_1-Dihydrofluorene, and/or C_1-Dibenzofuran	
19	184	Dibenzothiophene	12,290 ± 750
20	196	C_3-Acenaphthene and/or C_2-Dihydrofluorene	
21	178	Phenanthrene	44,640 ± 2840
22	194,196	C_2-Fluorene and/or C_2-Dihydrofluorene	
23	196	C_2-Dihydrofluorene	
24	192	3-Methylphenanthrene	9,300 ± 840
25	192	2-Methylphenanthrene	11,950 ± 800
26	192	1-Methylphenanthrene	3,680 ± 490
27	212	2-Chloroanthracene Internal Standard	
28	204	Dihydrofluoranthene	8,780 ± 100
29	202	Fluoranthene	3,820 ± 30
30	202	Pyrene	19,520 ± 470
31	204	Dihydropyrene	
32	218	C_1-Dihydrofluoranthene and/or Benzo(a)naphthofuran	
33	216	Benzo(a)fluorene	2,840 ± 230
34	216	Benzo(b)fluorene and/or 2- or 4-methylpyrene	10,360 ± 1110
35	218	Dihydrobenzo(b)fluorene and/or Benzo(b)naphthofuran	
36	216	1-Methylpyrene	2,650 ± 470
37	230	C_1-Benzofluorene and/or C_2-pyrene/fluoranthene	
38	228	Benz(a)anthracene	660 ± 60
39	228	Chrysene	1,110 ± 120
40	242	6- or 4-Methylchrysene	2,110 ± 210
41	252	Benzo(j or b)fluoranthene	250 ± 50
42	252	Benzo(e)pyrene	200 ± 60

(a) SRC II Full Range Distillate obtained from Gulf Research and Development Co., Merrian Coal Liquefaction Laboratory, Shawnee Mission, KS. An Amax Belle Ayr Mine subbituminous coal was used during run DOE 454RA which was made in the convention recycle mode.
(b) As determined by capillary column gas chromatographic-mass spectrometry.
(c) Determined from response factors of standard compounds.
(d) Based on three determinations; 10 mg/ml, 5 mg/ml, and 2.5 mg/ml dilutions.

TABLE 2. Concentrations of the Major Components of the 700-750°F Distillate Fractions of SRC II and EDS End-Products.

Compound	PAH FRACTION PPM (μg/g)[a] E.D.S.[b]	SRC II[c]
Dihydrofluoranthene	2,098 ± 36	21,822 ± 6,335
Fluoranthene	1,089 ± 16	30,210 ± 1,819
Pyrene	29,838 ± 976	275,991 ± 32,372
Dihydropyrene	6,391 ± 157	27,733 ± 8,413
Benzo(b)fluorene and/or 2- or 4-Methylpyrene	47,042 ± 11,610	257,629 ± 70,359
1-Methylpyrene	26,567 ± 6,371	34,335 ± 4,405
Benz(a)anthracene	308 ± 23	4,098 ± 942
Chrysene	1,554 ± 335	2,086 ± 561

(a) Concentration of components in the PAH fraction as determined from response factors of standards. Based on three determinations at 10 mg/mL, 5mg/mL, 2.5 mg/mL dilutions.
(b) EDS 50° distillate from a feed blend of naptha and process solvent of Illinois No. 6 coal; ECLP operations, Exxon Research and Engineering Co., Baytown, TX.
(c) SRC II 50° distillates from a feed blend of naptha and process solvent of Powhatan No. 5 mine coal; PDU P-99 operated by Gulf Science and Technology Co., Harmarville, PA.

TABLE 3. Concentration Ratios of Selected 4-Ring PAH in the 700-750°F Distillate Fractions of SRC II and EDS

Compound Ratio	EDS	SRC II
pyrene / 1-methylpyrene	1.1	8.0
pyrene / dihydropyrene	4.7	10.0
fluoranthene / dihydrofluoranthene	0.5	0.7

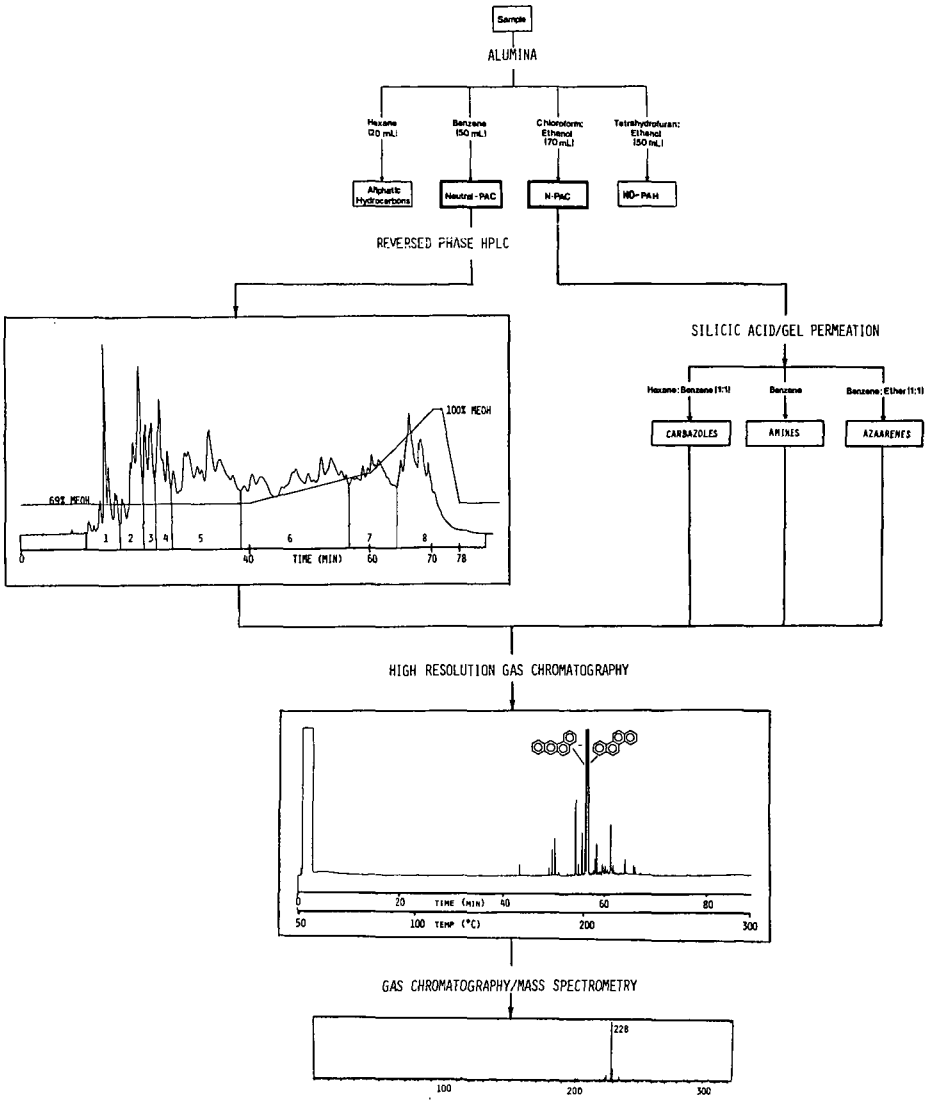

FIGURE 1. Overview of the analytical methodology used for the detailed chemical characterization of coal liquefaction materials.

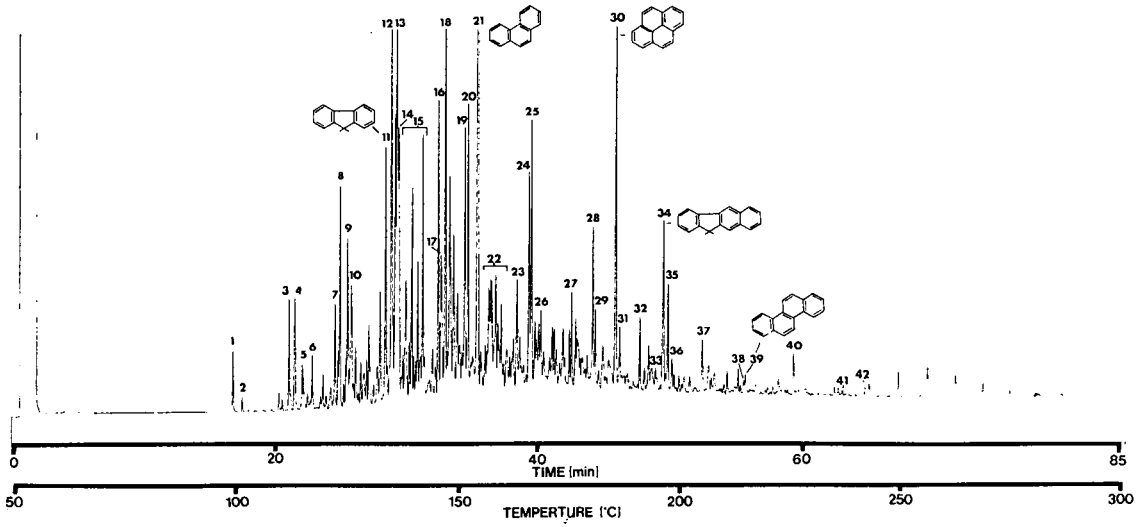

FIGURE 2. Capillary column gas chromatogram of the PAH fraction from SRC II full boiling range material. Peak numbers refer to compounds listed in Table 1. Conditions: 30 m x 0.25 mm Durabond 5 (J & W Scientific) fused silica column, temperature programmed from 50°C to 280°C at 4°C/min.

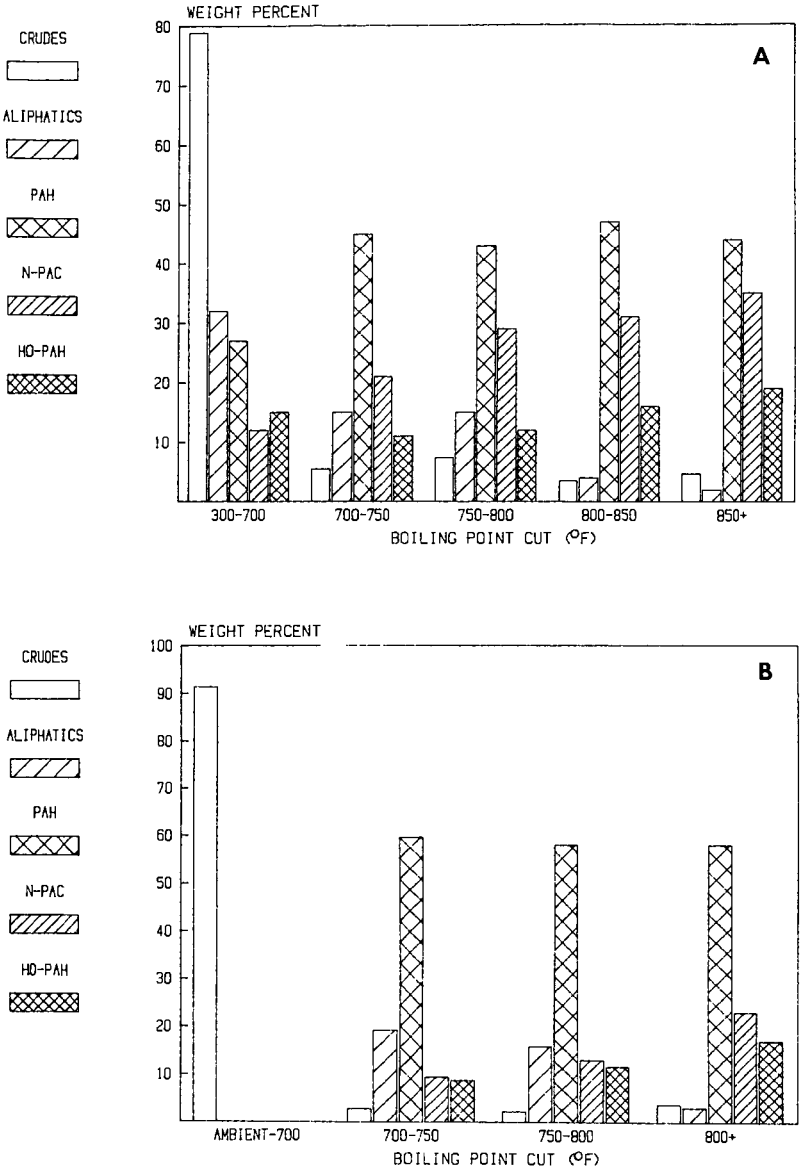

FIGURE 3. Weight distribution of chemical classes in the (A) SRC II and (B) EDS distillate fractions (see Table 2 footnotes for a detailed descritpion of these process materials).

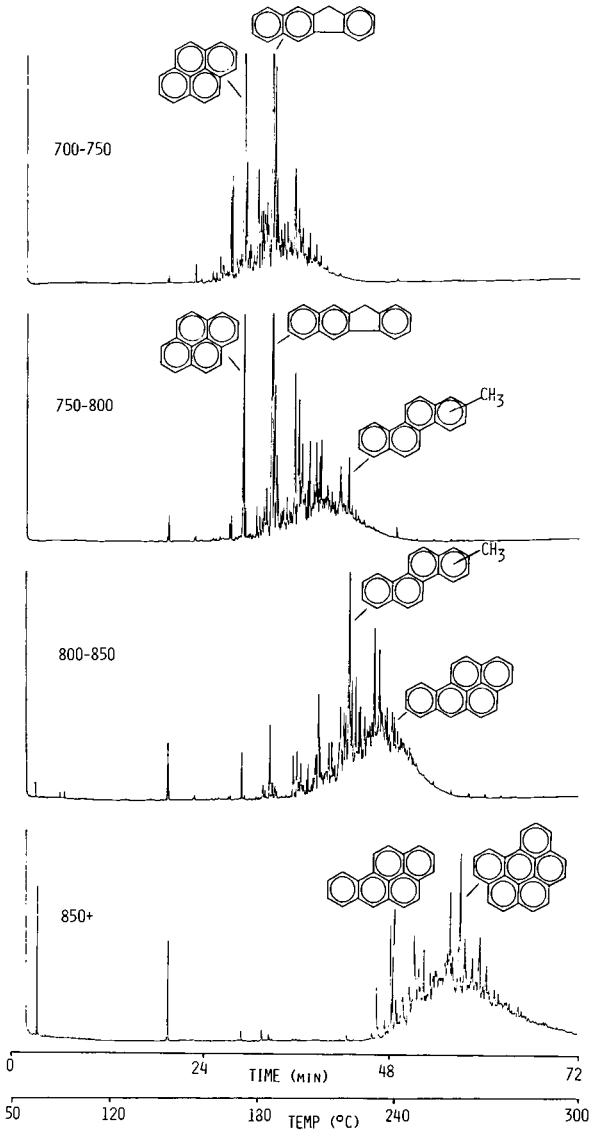

FIGURE 4. Capillary column gas chromatograms of the PAH fractions from the SRC II 50°F distillates fractions. (See Table 2 footnotes for a detailed description of this coal-derived material.) Conditions as in Figure 2.

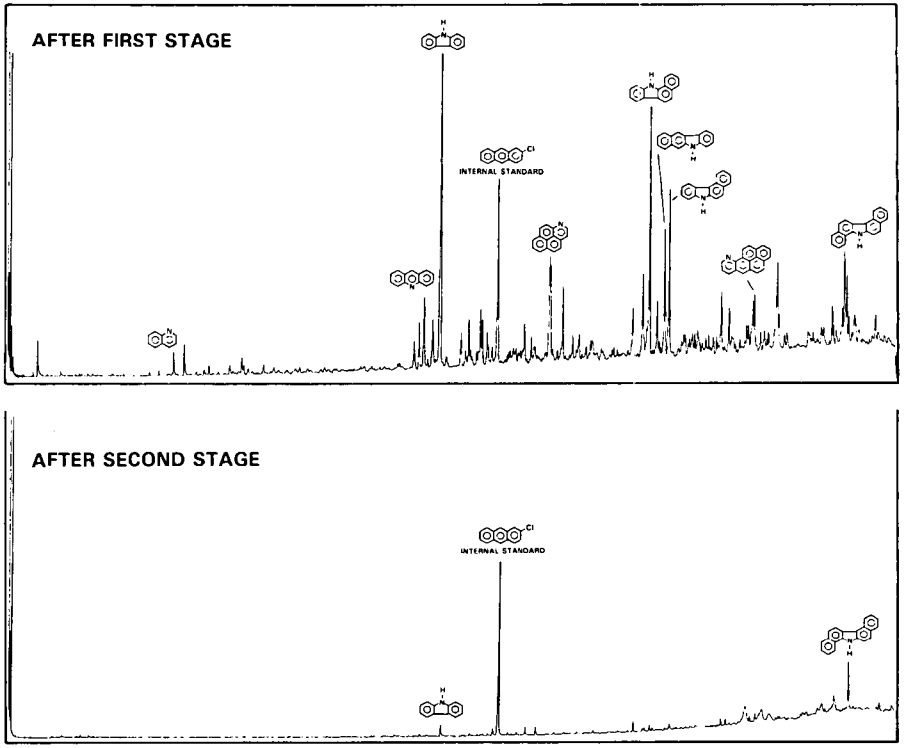

FIGURE 5. Process effects on the N-PAC content of two stage liquefaction products. Gas chromatographic condition as in Figure 2. Samples were from the ITSL process development unit operated by C. E. Lummus, New Brunswick, NJ.

ALTERNATIVE PATHWAYS FOR PYROLYSIS OF CELLULOSE

Fred Shafizadeh

Department of Chemistry, University of Montana
Missoula, Montana 59812

INTRODUCTION

Pyrolysis of biomass involves heterogeneous substrates and complex reactions. The substrate may contain various amounts of cellulose, hemicelluloses, lignin, extractives and inorganics with different thermal properties. The reactions involve alternative pathways and consecutive series, which are affected by pyrolytic conditions including the time and temperature profile, ambient atmosphere and catalysis by inorganic materials. Consequently, composition, yield and rate of formation of the products are highly dependent on the employed substrate and pyrolytic condition. This situation accounts for variation of the results, particularly on kinetic studies, which may range from kinetics of specific chemical reactions to global kinetics or modeling of an entire process. The latter may be based on a rate determining chemical step or even a physical process such as heat or material transfer. Pyrolysis of cellulose illustrates these points. The alternative pathways proposed for pyrolysis of this material is shown below (1,2).

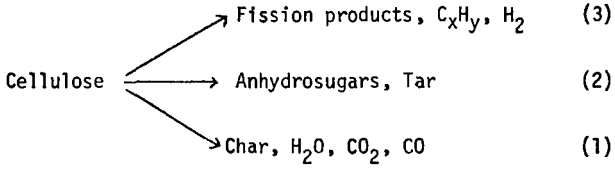

Pyrolysis at temperatures below 300°C involves depolymerization, dehydration, rearrangement and formation of carboxyl and carbonyl groups, evolution of CO and CO_2, development of free radicals and condensation to char. At temperatures above 300°C, these reactions are accompanied by the conversion of the glycosyl units to levoglucosan by transglycosylation. This reaction is preceded by the activation of the molecule, presumably through glass transition, which gives the required conformational flexibility. At still higher temperatures (above 500°C), the glycosyl structure of the levoglucosan or cellulose rapidly breaks down to provide a variety of low molecular weight fission products, including hydrocarbons and hydrogen as well as CO, CO_2 and H_2O obtained at lower temperatures. The pyrolysis products could further react to alter the composition of the pyrolysate. The secondary reaction may proceed in the gas phase as further decomposition of levoglucosan, in the solid phase as the condensation and crosslinking of intermediate chars to highly condensed polycyclic aromatic structures, or by interaction of both phases as gasification of char by reaction with H_2O and CO_2 at high temperatures to produce CO and H_2. In view of all these possibilities the kinetic data are valid only for specific chemical reactions or well defined systems. Generalization could be misleading and controversial, because of major differences in the results obtained under different conditions. These differences are shown in the following examples of pyrolysis of cellulose under different conditions.

KINETICS OF CELLULOSE PYROLYSIS

Global Kinetics

The global kinetics for isothermal evolution of volatile pyrolysis products from purified cotton linter cellulose, within the temperature range of 275-310°C, has been studied in air and nitrogen (3). The Arrhenius plot of the results on first order kinetics is shown in Figure 1. These data gave activation energies of 37 and 17 Kcal/mole in air and nitrogen. Figure 1 indicates a transition at ca. 300°C which reflects the existence of two different pathways. As seen in Figure 2, the rate of pyrolysis measured by weight loss under isothermal conditions, shows an initial period of acceleration and proceeds much faster in air than in inert atmosphere. As the pyrolysis temperature is increased, the initiation period and the differences between pyrolysis under nitrogen and air gradually diminish and disappear at 310°C when pyrolysis by the second pathway takes over.

Kinetics of the lower temperature pathway

The reactions in the first pathway, which dominates at lower temperatures, involve reduction in molecular weight or DP by bond scission, appearance of free radicals, elimination of water, formation of carbonyl, carboxyl and hydroperoxide groups (in air), evolution of carbon monoxide and carbon dioxide, and finally production of a charred residue. These reactions, which contribute to the overall rates of pyrolysis of cellulosic materials, have been individually investigated. Reduction in the degree of polymerization of cellulose on isothermal heating in air or nitrogen at a temperature within the range of 150-190°C has been measured by the viscosity method. The resulting data have been correlated with rates of bond scission and used for calculating the kinetic parameters. These calculations give an activation energy of 21 Kcal/mole for bond scission in air and 27 Kcal/mole in nitrogen, and indicate that at low temperatures a larger number of bonds are broken in air than in nitrogen.

The rates of production of carbon monoxide and carbon dioxide at 170°C are much faster in air than in nitrogen, and furthermore, accelerate on continued heating. It is instructive to compare the initial linear rates for the evolution of these gases with the rates of bond scission obtained for depolymerization at 170°C. As can be seen in Table I the rate of bond scission in air approximately equals the rate of production of carbon dioxide plus carbon monoxide in moles per glucose unit. In nitrogen, however, the rate of bond scission is greater than the rates of carbon monoxide and carbon dioxide evolution combined.

Table I. Initial rates of glycosidic bond scission and carbon monoxide and carbon dioxide formation at 170°C.

Reaction	Rate X 10^5 in N_2 mole/162 gm hr	Rate X 10^5 in air mole/162 gm hr
Bond Scission	2.7	9.0
CO Evolution	0.6	6.4
CO_2 Evolution	0.4	2.1

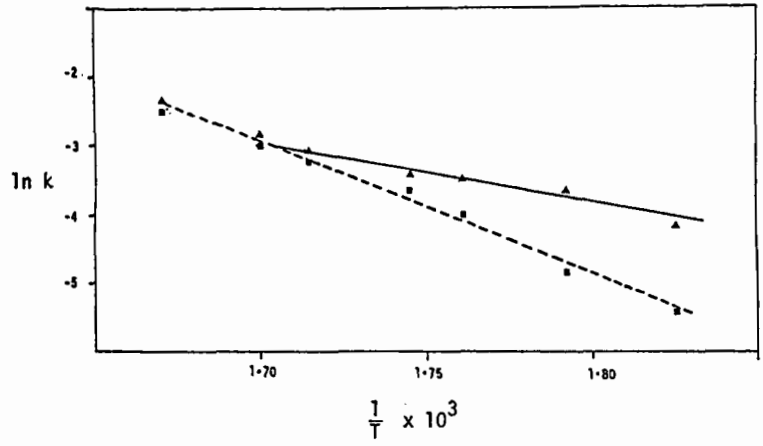

Figure 1. Arrhenius plots for first order reactions in the isothermal degradation of cellulose in air (--■--) and nitrogen (--▲--).

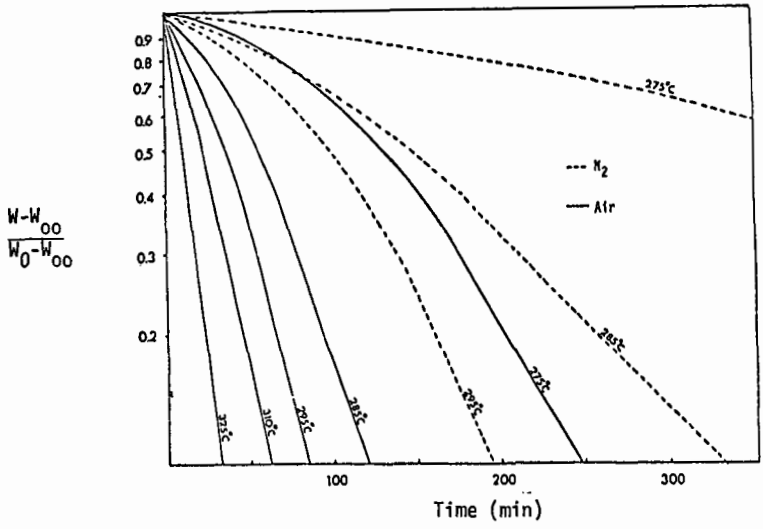

Figure 2. First order plot for the residual cellulose weight (normalized) versus time. Plots at 310°C and 325°C for air and nitrogen are similar.

On heating cellulose in air, hydroperoxide functions are simultaneously formed and decomposed, and their concentration climbs until a steady state is reached. At 170°C the steady state is reached in about 100 min. The decomposition of the hydroperoxide function appeared to follow first-order kinetics with a rate constant of $2.5 \cdot 10^{-2}$ min^{-1} at 170°C. From the steady-state concentration of $3.0 \cdot 10^{-5}$ mole/162 g min, the rate of hydroperoxide decomposition is therefore 7.5×10^{-7} mole/162 g min. When compared with the initial rate of bond scission in air at 170°C (Table I), it is apparent that hydroperoxide formation could make a significant contribution to bond scission.

Kinetics of the intermediate pathway

The primary reaction in this pathway involves depolymerization by transglycosylation forming a tar containing anhydrosugars (levoglucosan and its isomer), randomly linked oligosaccharides and various dehydration and fission products. As the reaction proceeds, the residue contains some glycosyl units that have been detected by CP/MAS ^{13}C-NMR and FTIR, and some char (4). The char is formed partly from direct decomposition of cellulose as discussed earlier and partly by decomposition of the tar. On raising the temperature the tar forming reactions accelerate rapidly and overshadow the production of char. At this time, it should be pointed out that evaporation of levoglucosan and the volatile pyrolysis products is highly endothermic. Thus, the increased oven temperature could raise the rate of heat transfer but not necessarily the temperature of the ablating substrate which is cooled by the heat of evaporation, especially under vacuum. In other words, at the higher temperatures, the pyrolysis process may be controlled by the rate of heat transfer rather than the kinetics of the chemical reaction. Material transport presents another major obstacle to the investigation of chemical kinetics, because if the products of primary reactions are not removed, they can undergo further decomposition reactions. Table II shows the difference between the yield of different pyrolysis products in vacuum, which removes the primary volatile products, and in nitrogen at atmospheric pressure which allows more decomposition of the anhydrosugars. It also shows the effect of inorganic catalysts in changing the nature of the reactions and products.

Table II. Analysis of the pyrolysis products of cellulose at 300°C under nitrogen and vacuum.

Condition	Atm. pressure	1.5 Mm Hg	1.5 Mm Hg, 5% $SbCl_3$
Char	34.2%[a]	17.8%[a]	25.8%[a]
Tar	19.1	55.8	32.5
levoglucosan	3.57	28.1	6.68
1,6-anhydro-β-D-glucofuranose	0.38	5.7	0.91
D-glucose	trace	trace	2.68
hydrolyzable materials	6.08	20.9	11.8

[a]The percentages are based on the original amount of cellulose.

In view of these considerations, the chemical kinetics of cellulose pyrolysis have been investigated within the limited temperature range of 260-340°C and under vacuum in order to obtain chemically meaningful data (5). Under these conditions, the chemical kinetics of cellulose pyrolysis could be represented by the three reaction model shown below.

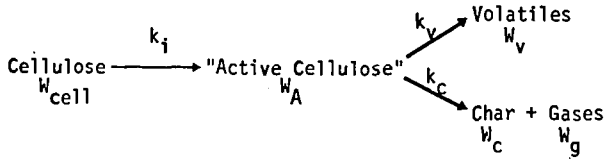

where

$$\frac{-d(W_{cell})}{dt} = k_i[W_{cell}]$$

$$\frac{d(W_A)}{dt} = k_i[W_{cell}] - (k_v + k_c)[W_A]$$

$$\frac{d(W_c)}{dt} = 0.35k_c[W_A]$$

$$k_i = 1.7 \times 10^{21} e^{-(58,000/RT)} \text{ min}^{-1}$$

$$k_v = 1.9 \times 10^{16} e^{-(47,300/RT)} \text{ min}^{-1}$$

$$k_c = 7.9 \times 10^{11} e^{-(36,000/RT)} \text{ min}^{-1}$$

In this model it is assumed that the initiation reactions discussed earlier lead to the formation of an active cellulose, which subsequently decomposes by two competitive first order reactions, one yielding anhydrosugars (transglycosylation products) and the other char and a gaseous fraction.

Partially pyrolyzed cellulose, in addition to the original sugar (glycosyl) units, contains new functionalities formed by dehydration, rearrangement, decarbonylation, decarboxylation and condensation. In the intermediate chars these functionalities include carbonyl, carboxyl, aromatic and aliphatic carbons as analyzed by CP/MAS ^{13}C-NMR (5). After complete pyrolysis of the glycosyl units (5 min at 400°C) a relatively "stable" char is left that contains about 70% aromatic and 27% aliphatic carbons. On heating at 500°C char is converted to a highly condensed and crosslinked material, containing about 90% polycyclic aromatic carbons.

CONCLUSION

Pyrolysis of cellulose proceeds by alternative pathways involving a variety of reactions which provide different products. The kinetics of these reactions are highly dependent on the experimental conditions.

ACKNOWLEDGMENTS

The author is pleased to acknowledge the contributions of Dr. A.G.W. Bradbury, and the support of the National Bureau of Standards and the National Science Foundation.

REFERENCES

1. F. Shafizadeh, Advan. in Carbohydr. Chem., 23, 419 (1968).

2. F. Shafizadeh, J. Anal. and Appl. Pyrol., 3, 283 (1982).

3. F. Shafizadeh and A.G.W. Bradbury, J. Appl. Polym. Sci., 23, 1431 (1979).

4. Y. Sekiguchi, J.S. Frye, and F. Shafizadeh, J. Appl. Polym. Sci., submitted for publication.

5. A.G.W. Bradbury, Y. Sakai, and F. Shafizadeh, J. Appl. Polym. Sci., 23, 3271 (1979).

KINETICS OF THERMAL DEGRADATION OF WOOD AND CELLULOSE BY T.G.A.

COMPARISON OF THE CALCULATION TECHNIQUES

C. VOVELLE, H. MELLOTTEE, J.L. DELFAU

C.N.R.S. - Centre de Recherches sur la Chimie de la Combustion
et des Hautes Températures
45045 ORLEANS CEDEX - FRANCE

INTRODUCTION :

Kinetics of thermal degradation of cellulosic materials has attracted widespread attention due to its importance in two main fields : synthetic fuel production from biomass and fire research. Usually, the results of kinetic studies have been expressed by means of an overall mass loss rate equation :

$$-\frac{dm}{dt} = A\ (m - m_f)^n \exp\ (-E/RT) \qquad 1)$$

with m = mass of material at time t, m_f = final mass, T = temperature, A = preexponential factor, n = reaction order, A = activation energy and R = perfect gas constant.

Several reviews (1), (2), (3) have pointed out that there is a great scatter in the values measured for the kinetic parameters : A, n and E. In particular, activation energies reported for wood are very often lower than those obtained for cellulose.

Recently (4), we have performed thermogravimetric analysis of cellulose and several kinds of woods and we have shown that this discrepancy was mainly related to the use of an overall equation to represent thermal degradation of wood. By calculating the mass variations by means of a simulation model allowing several reactions to be taken into account, we have reproduced with a good precision the experimental thermograms. For wood, in nitrogen, this agreement between experiments and calculations was obtained with a two-step degradation mechanism. The first step starts around 520 K and corresponds to the degradation of the mixture hemicellulose + lignin. The second step is observed around 620 K and is due to the pyrolysis of cellulose.

It is highly interesting to notice that for this second step of wood pyrolysis, the values of the kinetic parameters obtained with pure cellulose could be used.

The methods usually proposed for determining kinetic parameters from thermogravimetric analysis curves are based on the assumption that the mass loss rate can be interpreted by means of an overall equation. In view of the results that we obtained for wood, it was interesting to study how these methods could be applied to a two-step degradation mechanism and compare the precision of the results obtained with different methods. In this paper, we have reported kinetic calculations performed with the most commonly used techniques : FREEMAN and CARROLL (5), maximum point (6), ratio method (7), COATS and REDFERN (8) and BROIDO (9). These calculation techniques have been applied to thermograms measured for pure cellulose and three kinds of woods : fir, poplar and oak, the experiments having been performed under nitrogen.

EXPERIMENTAL :

A SETARAM thermobalance has been used. This apparatus allows simultaneous

TGA and DTA measurements. It is worth specifying that due to DTA requirements, the thermocouple used to measure the sample temperature was surrounded by the platinum sample holder, so that there is a good coupling between temperature measured by the thermocouple and the sample temperature.

A nitrogen flow rate equals to 120 ml/min has been used, and the heating were respectively : 16.2°C/min (cellulose), 12.9°C/min (oak), 13.0°C/min (fir) and 23.2°C/min (poplar). All the experiments have been performed with initial mass close to 25 mg.

Mass and temperature versus time curves were digitized by means of a H.P. plotter. Transformation and smoothing of the data to mass versus temperature curves and derivative calculations were performed by a H.P. 1000 computer.

RESULTS AND DISCUSSION :

We have plotted on figure 1 the thermograms obtained with cellulose and the three kinds of woods. Usually, from these curves, a conversion factor is defined by :

$$Y = \frac{m_o - m}{m_o - m_f} \qquad 2)$$

with : m = mass remaining at time t, m_o = initial mass and m_f = final mass.

The overall kinetic equation is expressed in term of this conversion factor :

$$\frac{dY}{dt} = A\,(1 - Y)^n \exp(-E/RT) \qquad 3)$$

or by using the heating rate : $\beta = dT/dt$

$$\frac{dY}{dT} = \frac{A}{\beta}\,(1 - Y)^n \exp(-E/RT) \qquad 4)$$

To use this equation for wood, it is necessary to define a conversion factor specific to each step of the degradation mechanism. If the step s is assumed to be observed between an initial value of the mass : $(m_o)_s$ and a final value $(m_f)_s$, this conversion factor is defined by :

$$Y_s = \frac{(m_o)_s - m}{(m_o)_s - (m_f)_s} \qquad 5)$$

These boundary values play an important role, since the variation of Y_s over a given temperature range can be modified by changing the values used for $(m_o)_s$ and $(m_f)_s$ and it can be considered that five kinetic parameters are needed to specify the thermal degradation : A, n, E, $(m_o)_s$ and $(m_f)_s$.

In order to get starting values for these boundary values of the mass, we have used the results obtained in the previous study carried out with the simulation model (4). These results have been reported in table I. When performing these calculations, the following assumptions had been made :

- wood is composed in equal proportion of cellulose and a so called "second component"
- for each component, several reactions can be observed, each reaction occurring between an initial value α_o and a final value α_f of the mass ratio $\alpha = m_k/(m_o)_k$ with m_k = mass of component k at time t and $(m_o)_k$ = initial mass of component k.

From the values reported in table I, it can be seen that the first step in the thermal degradation of wood, starting around 520K corresponds to the pyrolysis of the so-called second component, the pyrolysis of cellulose being responsible

for the second step observed at higher temperature. In fact, these two steps are not really successive and a progressive replacement of the first one by the second is rather observed. Owing to this overlapping, it seemed preferable to not use the intermediate part of the thermograms and in the following we have considered that:

- At the beginning of the first step, only the pyrolysis of the second component is observed. Assuming that this component represents 50% of the initial mass of wood and with the values of α_f reported in table I, the boundary values for the first step are equal to m_o and .7 m_o.

- Kinetic parameters of the second step can be calculated accurately only when the pyrolysis of the other component is achieved, so that the initial value of the mass is .7 m_o, while, from the values of α_f it is found that the final value is close to .33 m_o.

In fact , these values have been allowed to vary slightly in order to optimize the results.

In the following we have described the results obtained by applying successively the different methods.

FREEMAN and CARROLL method :

By taking the logarithm of both sides of equation 4 and differentiating with respect to temperature, the following expression is obtained :

$$\frac{d \log (d\Upsilon/dT)}{d \log (1-\Upsilon)} = n - \frac{E}{2.3\ R} \frac{d\ (1/T)}{d \log (1-\Upsilon)} \qquad 6)$$

By plotting the left hand side versus $\frac{d\ (1/T)}{d \log (1-\Upsilon)}$ a straight line must be obtained, with a slope equals to E/2.3 R and an intercept equals to n. The preexponential factor A is calculated thereafter by means of equation 4.

To illustrate the precision which can be expected when using this method, we have plotted the results obtained respectively for the first step and the second step of fir pyrolysis on figures 2 and 3. It can be seen on figure 2 that the points corresponding to the lowest values of $d(1/T)/d \log(1-\Upsilon)$ tends to be outside of the straight line, this deviation being due to the beginning of the occurrence of the second step. However, on the main temperature range of each step, the linear relationship is fairly well verified.

The values obtained for the second step of wood pyrolysis and for cellulose pyrolysis (table II) are in good agreement with the values that we calculated previously with the simulation model (table I). For the first step, on the other hand, the activation energies obtained for fir and oak are slightly higher than those calculated previously and some discrepancies are observed in the values of the order of reaction.

It is mainly interesting to notice that these calculations confirm that the kinetic parameters of the second step of wood pyrolysis keep the value obtained with pure cellulose.

A second remark can be done concerning the method of calculation. Due to the properties of logarithms and derivatives, the results are independent of the value chosen for $(m_o)_s$ and only $(m_f)_s$ is playing a rôle. For the second step of wood pyrolysis, the value of $(m_f)_s$ can be known with accuracy since it corresponds to the final value of the mass observed on the thermogram. Therefore, for the second step, the determination of the kinetic parameters by means of this method is not affected by errors resulting of a wrong estimation of the initial value of the mass.

Maximum point method :

From equation 4, the following relationship is obtained between the values

of the parameters corresponding to the maximum conversion rate :

$$E = n \frac{R\ T_m^2}{(1-\gamma_m)} \left(\frac{d\gamma}{dT}\right)_m \qquad 7)$$

where T_m, γ_m and $(d\gamma/dT)_m$ represent respectively the values of the temperature, the conversion factor and the derivative of the conversion factor at the point where the conversion rate is maximum.

The order of reaction is calculated by using one of the following expressions :

$$n = (1-\gamma_m)^{(1-n)} \quad \text{if} \quad n \neq 1 \qquad 8)$$

$$n = 1 \text{ if } (1-\gamma_m) = 1/e \qquad 9)$$

with e = basis of neperien logarithm.

The preexponential factor is calculated from equation 4.

This method cannot be applied to the first step of wood pyrolysis, since, due to the overlapping with the second step, there is no maximum in the conversion rate vs temperature curve.

The values obtained for cellulose and the second step of wood pyrolysis are reported in table III.

It can be observed that the kinetic parameters determined for wood are still very close to those calculated for pure cellulose.

However, in addition to its limitation concerning the treatment of the first step of wood pyrolysis, this method suffers a second disadvantage related to its accuracy. A small error in the estimation of the temperature corresponding to the maximum conversion rate entrains a large variation in the values of γ_m. This is illustrated by the following values measured for fir :

T K	635	636	637
$(d\gamma/dT)\ K^{-1}$	$2.77\ 10^{-2}$	$2.85\ 10^{-2}$	$2.82\ 10^{-2}$
γ_m	.612	.644	.672

Moreover, this method is directly dependent on the values chosen for $(m_o)_s$ and $(m_f)_s$ and it can be seen that if the values of n, A and E obtained for poplar are close to the values calculated with the other methods, the value used for $(m_o)_s$ seems abnormally elevated.

Ratio method :

This method has been formulated by MICHELSON and EINHORN (7). If equation 4 is written for two values of the temperature T_i and T_j, the following expression can be derived :

$$\log \frac{(d\gamma/dT)_j}{(d\gamma/dT)_i} = n \log \frac{(1-\gamma_j)}{(1-\gamma_i)} + \frac{E}{2.3\ R} \frac{T_j - T_i}{T_i\ T_j} \qquad 10)$$

where the subscripts i and j mean that the quantities have been measured at temperatures T_i and T_j.

If this calculation is repeated for couples of temperature such that the ratio $r = (1-\gamma_j)/(1-\gamma_i)$ remains constant, the plot of the left hand side versus $T_j - T_i/T_i\ T_j$ must be a straight line of slope equal to E/2.3 R. The order of reaction is calculated from the value of the intercept.

Values obtained by applying this method (table IV) are in close agreement with those determined with the FREEMAN and CARROLL method for pure cellulose as well as for the two steps of wood pyrolysis.

It is important to notice that the rôle played by the boundary values $(m_o)_s$ and $(m_f)_s$ in the calculation of the conversion factor is reduced to a minimum when to ratio method is used. Calculation of the order of reaction involves only $(m_f)_s$ while, for the activation energy, the values are totally independent of $(m_o)_s$ and $(m_f)_s$ since these two quantities vanish when the left hand side of equation 10 is calculated. This method is therefore particularly convenient for the kinetics of wood pyrolysis, especially for the first step, where, due to the relatively small value of the difference $(m_o)_s - (m_f)_s$, the conversion factor is very sensitive to a small change in the value estimated for $(m_f)_s$.

COATS and REDFERN method :

Equation 4 cannot be integrated directly. However, using an approximation for the integral of the exponential term several expressions can be derived. COATS and REDFERN (8) have obtained :

$$\log \left[\frac{-\log(1-Y)}{T^2}\right] = \log \frac{AR}{\beta E}\left[1 - \frac{2\,RT}{E}\right] - \frac{E}{2.3\,RT} \quad \text{if } n = 1 \qquad 11)$$

$$\text{and} \quad \log \left[\frac{1-(1-Y)^{(1-n)}}{T^2\,(1-n)}\right] = \log \frac{AR}{\beta E}\left[1 - \frac{2\,RT}{E}\right] - \frac{E}{2.3\,RT} \quad \text{if } n \neq 1 \qquad 12)$$

The first term in the right hand side is sensibly constant in the temperature range used in the calculations so that a plot of the left hand side of one of the two equations versus 1/T must be a straight line of slope $-E/2.3\,R$. The order of reaction is not calculated directly. In fact, the calculations have to be performed using several values of n in order to retain the value leading to the best linear relationship.

Values calculated with this method are reported in table V.

It can be observed that the values obtained for the activation energy of the second step of wood pyrolysis tend to be lower than the values calculated for pure cellulose. With poplar, it has been necessary to increase the ratio $(m_o)_2/m_o$ up to .82 in order to obtain a straight line. This value is abnormally elevated even if it lead to satisfactorily results with the maximum point method.

BROIDO method :

Using a different assumption for performing the integration of equation 4, BROIDO derived the following expression, valid only for a first order reaction

$$\log \left(\log \frac{1}{1-Y}\right) = -\frac{E}{2.3\,RT} + \text{constant} \qquad 13)$$

In view of the results obtained with the other methods for the order of reaction, it has not been possible to apply the BROIDO method to both steps of wood pyrolysis (table VI).

This method and the COATS-REDFERN method, often called integral methods are very sensitive to the values chosen for $(m_o)_s$ and $(m_f)_s$ when calculating the conversion factor. This is illustrated by the three curves corresponding to different values of $(m_o)_s$ for the second step of fir pyrolysis (figure 4).

CONCLUSION :

An examination of the results obtained for cellulose pyrolysis in nitrogen

shows that the five techniques of kinetic calculations lead to results very similar : the mass loss rate can be interpreted in term of one reaction of first order of activation energy close to 250 kJ/mole.

For wood pyrolysis, we have distinguished two steps in the thermograms. By calculating a specific conversion factor for each step it has been possible to apply the same calculation techniques. However, calculation of this specific conversion factor introduces an error related to the estimation of the mass range over which each step is observed. Owing to this fact, the accuracy of the different calculation techniques is directly related to the degree at which the boundary values $(m_o)_s$ and $(m_f)_s$ are involved. From this point of view, the FREEMAN and CARROLL method and the ratio method are the most suitable. It is interesting to notice that these two techniques have confirmed that kinetic parameters of the second step of wood pyrolysis, corresponding to the maximum mass loss rate, have the same values than those obtained for pure cellulose.

REFERENCES :

1 - ROBERTS, A.F., Comb. and Flame 14, 261-272 (1970)

2 - WELKER, J.R., J. Fire Flammability 1, (1970), 12.

3 - ANTAL, M.J., FRIEDMAN, H.L., ROGERS, F.E., Comb. Sci. and Technol. (1980), Vol. 24, 141-152.

4 - VOVELLE, C., MELLOTTEE, H., and DELBOURGO, R., Nineteenth Symposium (International) on Combustion, The Combustion Institute, to be published

5 - FREEMAN, E.S., and CARROLL, B., J. Phys. Chem. 62, (1958), 394.

6 - FUOSS, R.M., SALVER, I.O., and WILSON, H.S., J. Polym. Sci. A2, (1964), 3147.

7 - MICHELSON, R.W., and EINHORN, I.N., Thermochimica Acta, 1, (1970), 147-158.

8 - COATS, A.W., and REDFERN, J.P., Nature, Vol. 201, (1964), 68-69.

9 - BROIDO, A., J. Polymer Sci.,7,(1969) p. 1761.

Fig. 1 : Thermograms obtained in nitrogen (120 ml/min)

——— cellulose (16.2°C/min)

····· fir (13.0°C/min)

-·-·- poplar (23.2°C/min)

—·—·— oak (12.9°C/min)

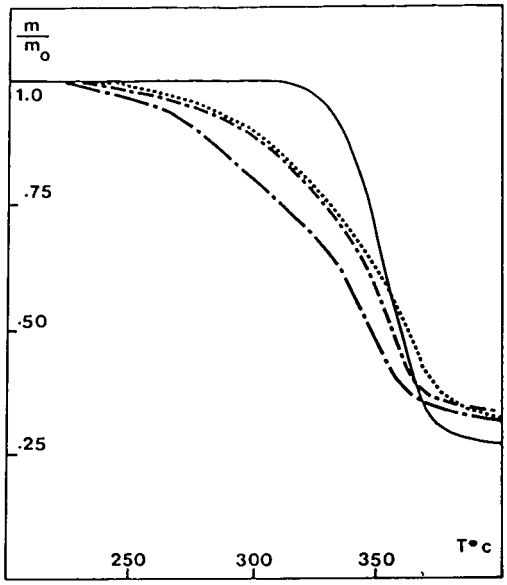

Fig. 2 : FREEMAN and CARROLL method.
First step of fir thermal degradation

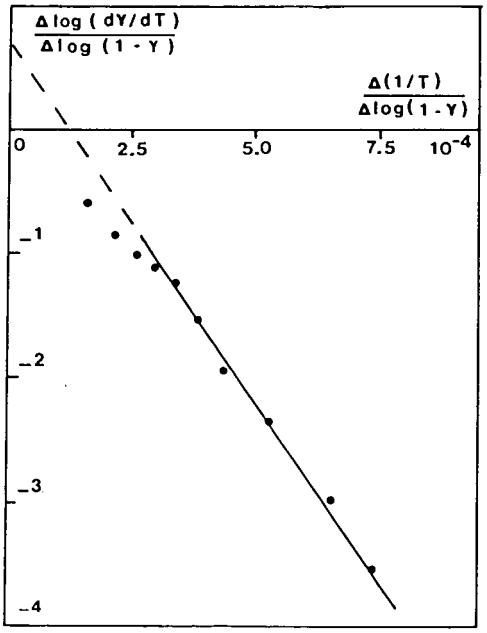

Fig. 3 : FREEMAN and CARROLL method.
Second step of fir thermal degradation

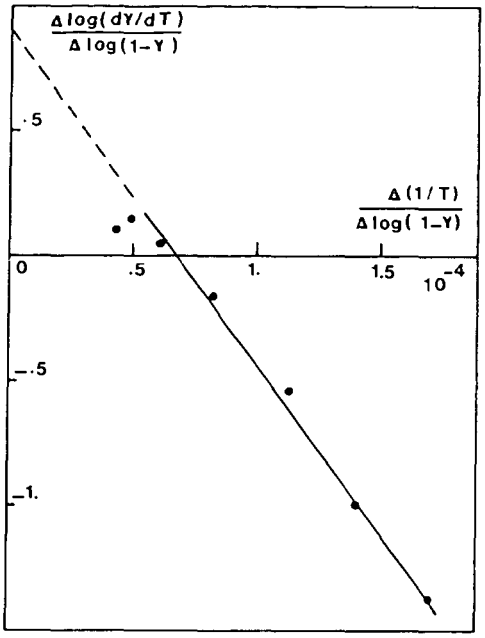

Fig. 4 : BROIDO method.
Second step of fir thermal degradation

▲ $\frac{(m_o)_2}{m_o} = .7$

● $\frac{(m_o)_2}{m_o} = .75$

■ $\frac{(m_o)_2}{m_o} = .8$

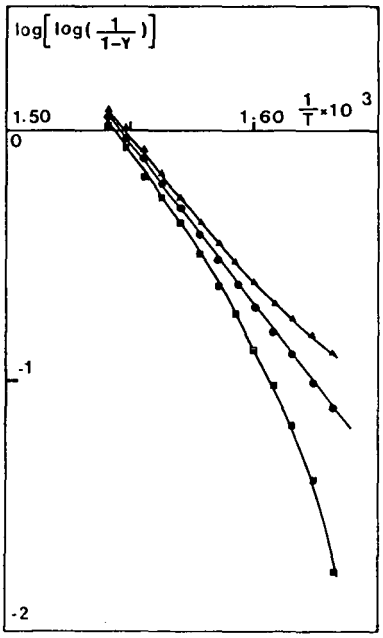

material		n	$A(s^{-1})$	E(kJ/mole)	α_o	α_f
cellulose		1	$1.\ 10^{19}$	250	1	.29
fir	50% cellulose	1	$4.\ 10^{18}$	250	1	.27
	50% 2nd component	1	$1.3\ 10^{5}$	84	1	.40
oak	50% cellulose	1	$1.4\ 10^{19}$	250	1	.27
	50% 2nd component	1	$2.6\ 10^{5}$	84	1	.40
poplar	50% cellulose	1	$1.5\ 10^{19}$	250	1	.30
	50% 2nd component	1	$2.2\ 10^{5}$	84	1	.40

Table I : kinetic parameters obtained in a previous study (4) by means of a simulation model

material		n	$A(s^{-1})$	E(kJ/mole)	$\frac{(m_o)_s}{m_o}$	$\frac{(m_f)_s}{m_o}$
cellulose		1.1	$1.\ 10^{18}$	238	1	.26
fir	1st step	.7	$3.4\ 10^{7}$	109	1	.75
	2nd step	.9	$1.4\ 10^{19}$	257	.75	.33
oak	1st step	1	$1.5\ 10^{7}$	100	1	.73
	2nd step	1.4	$3.\ 10^{19}$	253	.73	.33
poplar	1st step	.25	$4.3\ 10^{4}$	76	1	.71
	2nd step	1.1	$3.9\ 10^{19}$	255	.71	.34

Table II : kinetic parameters calculated with the FREEMAN and CARROLL method

material	$1-Y_m$	T_m (K)	n	$A\ (s^{-1})$	E (kJ/mole)	$\frac{(m_o)_s}{m_o}$	$\frac{(m_f)_s}{m_o}$
cellulose	.368	630	1	$2.3\ 10^{18}$	243	1	.26
fir	.356	636	.93	$5.8\ 10^{18}$	252	.75	.33
oak	.430	619	1.4	$6.5\ 10^{20}$	269	.73	.33
poplar	.380	626	1.07	$7.7\ 10^{17}$	234	.82	.34

Table III : kinetic parameters calculated with the maximum point method

material		r	n	A (s^{-1})	E (kJ/mole)	$\frac{(m_f)_s}{m_o}$
cellulose		1.5	1.1	2.9 10^{17}	232	.26
fir	1st step	1.2	.7	5.2 10^{7}	111	.75
	2nd step	2	.91	4.6 10^{18}	250	.33
oak	1st step	1.2	.99	1.5 10^{7}	100	.73
	2nd step	2	1.3	1.1 10^{19}	248	.33
poplar	1st step	1.25	.3	2. 10^{4}	72	.71
	2nd step	2	1.12	1.7 10^{18}	238	.34

Table IV : kinetic parameters calculated with the ratio method

material		n	A (s^{-1})	E (kJ/mole)	$\frac{(m_o)_s}{m_o}$	$\frac{(m_f)_s}{m_o}$
cellulose		1.1	1.1 10^{20}	263	1	.26
fir	1st step	.7	9.9 10^{6}	104	1	.75
	2nd step	1	6.3 10^{17}	239	.75	.33
oak	1st step	1	5.9 10^{7}	106	1	.73
	2nd step	1.4	1. 10^{16}	211	.79	.33
poplar	1st step	.3	1.8 10^{5}	83	1	.71
	2nd step	1	3. 10^{15}	205	.82	.34

Table V : kinetic parameters calculated with the COATS-REDFERN method

material		n	A (s^{-1})	E (kJ/mole)	$\frac{(m_o)_s}{m_o}$	$\frac{(m_f)_s}{m_o}$
cellulose		1	5. 10^{19}	259	1	.26
fir	2nd step	1	9.1 10^{18}	254	.75	.33
oak	1st step	1	5.5 10^{8}	117	1	.73
poplar	2nd step	1	4.8 10^{16}	220	.82	.34

Table VI: kinetic parameters calculated with the BROIDO method

The Effect of Pressure on the Pyrolysis of Newsprint

Ravindra K. Agrawal and Richard J. McCluskey

Department of Chemical Engineering, Clarkson College, Potsdam, New York 13676

Introduction

There is national concern over the disposal of solid municipal waste. Several pyrolysis plants designed to convert such waste into useful products have proven uneconomical. To help provide a stronger data base for improved pyrolysis processes, we have been studying the thermal chemistry of newsprint, the principle cellulosic material in urban waste. Previously, we have reported on the rate of degradation at low pressure, where secondary reactions of pyrolysis products are negligible (1). This paper discusses the influence of ambient pressure on newsprint pyrolysed at 340°C.

Since a dilute acid wash pre-treatment has been shown to significantly alter product yields from newsprint pyrolysis (2), we have examined both untreated and 1% HCl washed newsprint.

Pyrolysis of any lignocellulosic material gives a host of different products which are usually classified as either chars, tars, or gases depending upon their volatility. Chars are carbonaceous products, such as charcoal, that are not volatile. Tars are relatively high molecular weight compounds that are volatile only at pyrolysis temperatures; and gases are those products having readily measureable vapor pressures at room temperature.

Several investigators have shown, using a variety of cellulosic materials, ranging from cotton cellulose to wood, that pyrolysis in nitrogen at atmospheric pressure results in lower tar yields and greater gas and char formation than pyrolysis in a strong vacuum (3 , 4). This difference in yields has been interpreted as due to secondary decomposition of tar molecules whose ability to escape from the reacting substrate is reduced at higher pressures. While the effect of ambient pressure on pyrolysis yields is qualitatively understood, there exists little quantitative information that allows mathematical modeling of this phenomena and, thereby, a clear link between low pressure pyrolysis experiments, used to study fundamental reaction kinetics, and industrial pyrolysis processes carried out at atmospheric pressure.

Experimental Procedures

A sketch of our experimental apparatus is shown in Figure 1. Since a detailed account of our procedures is provided in reference (1), only a brief outline will be given here.

100 mg samples of dry, shredded newsprint are weighed into a small aluminum foil boat. The boat is sealed into a cool end of the reactor and a vacuum is drawn on the system. If we are examining the effects of ambient pressure, nitrogen is bled slowly into the system. Then the pyrolysis chamber is brought to a temperature slightly above that of pyrolysis. Next, power is reduced to that necessary for maintaining pyrolysis temperature and the sample boat is quickly brought to the center of the pyrolysis zone by means of a hand held magnet. Sample temperature is continuously monitored by a thermocouple embedded in the newsprint.

After a set time period, the boat is quickly withdrawn from the pyrolysis chamber, the cold traps are sealed off, and the reactor is allowed to cool.

The weight of residue in the sample boat is measured, and the tar products are rinsed off the cool glass walls of the reactor's side arms into tared vials. In this manner we can measure the weights of residue and tar as a function of pyrolysis time and pressure.

Theory

Our basic assumptions are that secondary decomposition of tar molecules is negligible in pyrolysis experiments below one torr, and that, ΔW_t, the difference between W_t, the weight of tar obtained below one torr, and W_t', the weight of tar formed at higher pressure, is a direct measure of the amount of secondary reaction.

A tar molecule may undergo two types of secondary reactions, decomposition to char and gases and repolymerization with the substrate. If each type of reaction is homogeneous and first order in tar, the rate of secondary reaction is

$$\frac{d\,\Delta W_t}{dt} = (k_d + k_r)\, W_t'' \qquad 1)$$

where k_d and k_r are the rate constants for decomposition and repolymerization, respectively, and W_t'' is the weight of tar molecules within the heated newsprint.

Diffusion coefficients in low pressure gases are inversely proportional to pressure. Therefore, if the tars rate of escape from the newsprint is taken as proportional to the amount of tar in the newsprint and inversely proportional to pressure, then

$$\frac{d\,W_t'}{dt} = \frac{\varkappa}{P}\, W_t'' \qquad 2)$$

where $\varkappa$ is the escape rate per unit weight per unit pressure.

If k_d, k_r and $\varkappa$ are independent of time, then the ratio of equations 1 and 2 implies that for any time interval during which the amount of repolymerized tar is unimportant relative to the amount of unreacted newsprint

$$\frac{\Delta W_t}{W_t'} = \frac{(k_d + k_r)}{\varkappa}\, P \qquad 3)$$

Similarly, when reaction of repolymerized tar is unimportant, the fractional conversion to char via secondary decomposition may be expressed

$$\frac{\Delta R}{\Delta W_t} = \frac{f_d k_d + k_r}{k_d + k_r} \qquad 4)$$

For longer pyrolysis times, when the fate of repolymerized tar molecules must be considered

$$\frac{\Delta R}{\Delta W_t} = \frac{f_d k_d + f_r k_r}{k_d + k_r} \qquad 5)$$

where ΔR is the difference in the weight of residue (char) between higher and very low pressure pyrolyses, f_d is the weight fraction of any tar molecule undergoing secondary decomposition that becomes char, and f_r is the average weight of char resulting from repolymerization of one tar molecule. If the repolymerization reaction disrupts the tar molecule's ring structure, the repolymerized compound may be predisposed to form char and gases.

An interesting parameter to consider is the ratio of the amount of tar escaping from the substrate during any given time interval at higher pressure to the amount of tar formed in the same time interval at very low pressure. If all repolymerized material eventually decomposes to char and gases, then this ratio is

$$\frac{W_t'}{W_t} = \frac{\alpha/P}{(\alpha/P) + k_d + k_r} \qquad 6)$$

If a repolymerized tar molecule can be regenerated, then this ratio will be larger than the value predicted by equation 6. However, should the breakdown to char of the repolymerized material induce or catalyze substrate conversion to char, then the W_t'/W_t ratio will be less than predicted by equation 6 .

Results

The influence of ambient pressure on pyrolysis yields is illustrated in Figure 2. The weight of tar products and the weight of sample residue is plotted versus time, comparing 700 torr and below one torr pyrolyses of 100 mg of acid washed newsprint at 340°C. The ultimate tar yield at 700 torr is 34 % less than at very low pressure, while the final weight of residue (char) is 32 % greater at 700 torr. Notice that at both pressures there is an initial rapid generation of tar.

In our previous paper we noted that the thermal degradation of newsprint occurs in two stages: a fast initial degradation, that can be modeled as a zeroth order reaction; and a subsequent, slower degradation that is first order in remaining newsprint. At 340°C, the rapid, early degradation is over within three minutes of the sample's entry into the pyrolysis zone. This initial reaction accounts for 68 % of the ultimate tar production. As seen in Figure 2, the remaining 32 % of the tar is produced largely during the next sixty minutes of pyrolysis, while the degradation reaction follows a first order rate law.

Table 2 gives data describing the secondary decomposition during the first three minutes of pyrolysis. The fractional extent of secondary tar decomposition and $\Delta R/\Delta W_t$ are listed for both acid washed and untreated newsprint. For each substrate, the extent of secondary decomposition increases uniformly with ambient pressure. The change in the sample residue is nearly a constant fraction of the change in weight of recovered tar. $\Delta R/\Delta W_t$ is not a function of ambient pressure.

The ratio of the amount of secondary reaction to the amount of recovered tar is plotted versus pressure in Figure 3, for the initial degradation of both acid washed and untreated newsprint. As predicted by equation 3 , the data are well fit by a straight line passing through the origin. Linear least square fits to the data that are constrained to pass through the origin are included in Figure 3. The slopes of these lines are reported in Table 1 along with their 95% confidence limits. From equation (3), these slopes represent the ratio of the rate of secondary tar reaction to the rate of tar escape per unit pressure. The larger value obtained for the acid washed newsprint suggests that the tars produced from acid washed newsprint are more reactive than the tars arising from untreated newsprint.

As seen from equation 4 , the magnitude of the $\Delta R/\Delta W_t$ ratio depends on two factors, f_d, the fractional char yield during secondary decomposition, and k_d/k_r, the ratio of the rate of decomposition to the rate of repolymerization.

If we arbitrarily adopt a value for f_d of 0.2, the ultimate char yield in low pressure pyrolyses, then the k_d/k_r ratios implied by the R/W_t results are 7.0 and 0.6 for the acid washed and untreated newsprint, respectively. The point is that, irrespective of the f_d value, the repolymerization reactions are relatively more important in the untreated than in the acid washed newsprint.

Insight into the types of secondary reactions that occur at longer pyrolysis times can be gathered from the data in Table 2. At longer times the amount of repolymerized material will no longer be small in regard to the amount of remaining substrate. The ultimate $\Delta R/\Delta W_t$ ratios are given in Table 2 for both acid washed and untreated substrates. These ratios show no pressure dependence, but they are slightly higher than the corresponding ratios at the end of only three minutes pyrolysis time. This suggests that char forming reactions are more prevalent at longer pyrolysis times.

Table 2 also lists the ratio of the amount of tar recovered in higher pressure experiments to the amount of tar formed in low pressure pyrolyses for pyrolysis times greater than three minutes. Also included in Table 2 is the value predicted for this ratio by equation 6, based on the assumption that all repolymerized material eventually forms either char or gases. Agreement between the experimental and predicted quantities is poor only for the lowest pressures, where the measured values fall below those given by equation 6. This implies some ability of the repolymerized material to catalyze char formation in the substrate, although the effect is subtle and readily masked at higher loadings of repolymerized tar.

Summary

We have developed a simple model, based upon homogeneous first order reactions, for describing the influence of ambient pressure on newsprint pyrolysis. Values for the relative rates of secondary tar reaction to tar escape per unit pressure have been obtained for acid washed and untreated newsprint. Tars from the acid washed material are more apt to decompose while tars from untreated newsprint have a greater likelihood of repolymerizing and then catalyzing char formation.

References

1. R.K. Agrawal and R.J. McCluskey, J. Appl. Poly. Sci., 27, 367 (1983).
2. F. Shafizadeh, R.H. Furneaux, T.G. Cochran, J.P.Scholl and Y. Sakai, J. Appl. Poly. Sci., 23, 3525 (1979).
3. A. Roberts, Combust. Flame, 14, 261 (1970).
4. F. Shafizadeh, T.G. Cochran and Y. Sakai, AIChE Symp. Ser. No. 184, 75, 24 (1979).

Table 1 - Early Secondary Decomposition Reactions

Pressure (torr)	Acid Washed Newsprint $\frac{\Delta W_t}{W_{t\ 3min}}$	Acid Washed Newsprint $\frac{\Delta R}{\Delta W_{t'\ 3min}}$	Untreated Newsprint $\frac{\Delta W_{t'}}{W_{t'\ 3\ min}}$	Untreated Newsprint $\frac{\Delta R}{\Delta W_{t'\ 3\ min}}$
100	.072	.33	.026	.80
175	.13	.30	.036	.64
400	.27	.28	.11	.73
700	.35	.29	.18	.73

$\frac{k_d + k_r}{\chi}$ $(torr^{-1})$ $8.15 \pm .33 \times 10^{-4}$ $3.07 \pm .07 \times 10^{-4}$

Table 2 - Longer Time Secondary Reaction Data

Pressure (torr)	$\frac{\Delta R}{\Delta W_{t'\infty}}$	$\frac{W_{t'\infty} - W_{t'3}}{W_{t\infty} - W_{t3}}$	$\frac{\chi/P}{\frac{\chi}{P} + k_d + k_r}$	
100	.37	.75	.93	Acid Washed Newsprint
400	.36	.77	.75	
700	.40	.69	.64	
175	.76	.90	.95	Untreated Newsprint
400	.81	.88	.89	
700	.84	.82	.82	

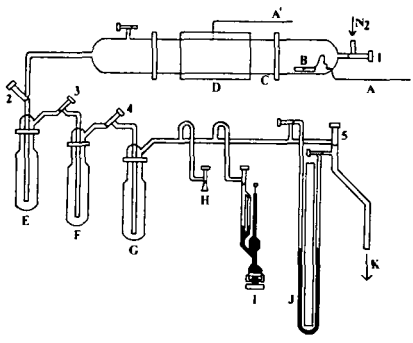

Fig. 1. Experimental apparatus: (A,A') thermocouple wires; (B) sample boat; (C) Pyrex cylinder; (D) insulated, quartz pyrolysis zone; (E, F, G) cold traps; (H) sample port; (I) McLeod gauge; (J) manometer; (K) connection to vacuum pump; (1-5) PTFE valves.

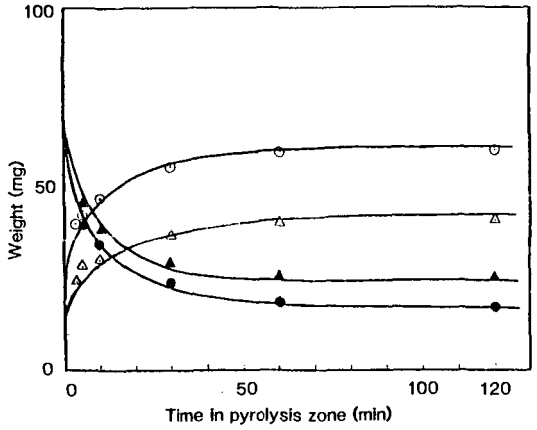

Fig 2. Influence of ambient pressure on pyrolysis yields at 340 C. Open figures represent tars and solids represent residue. Pressures are 1 torr (○) and 700 torr (△).

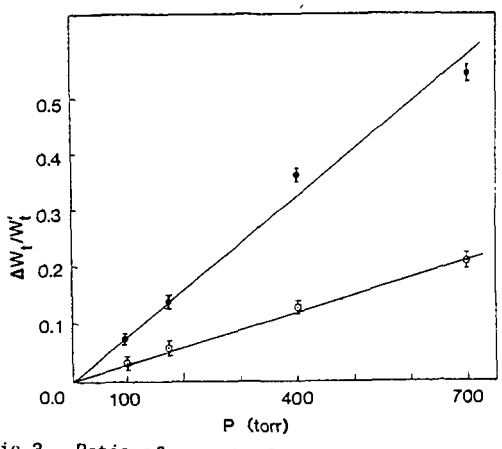

Fig 3. Ratio of amount of secondary reaction to the amount of recovered tars versus pressure. Open figures represent unwashed newsprint and solids represent 1% HCl washed newsprint.

LIGNIN PYROLYSIS IN HEATED GRID APPARATUS: EXPERIMENT AND THEORY

Eitan Avni and Robert W. Coughlin

University of Connecticut, Storrs, CT 06268

Peter R. Solomon and Hsiang Hui King

Advanced Fuel Research, Inc., 87 Church Street, East Hartford, CT 06108

Introduction

The study of lignin pyrolysis has a vitsl importance since all lignin conversion processes, namely; combustion, liquefaction and gasification, are initiated by this step. Lignin, a major component of biomass is a potential source of aromatic chemicals through the pyrolysis process. Important recent reviews of lignin conversion processes have been published by Goldstein (1), Drew (2), Goheen (3) and Coughlin and Avni, et.al., (4).

Very few kinetic studies of lignin pyrolysis have been carried out recently. Gavsiss, et.al., (5) studied the pyrolysis of Kraft lignin using the captive sample technique. At 400-650°C for 10-120 sec, he claimed that a fundamental kinetic description of lignin pyrolysis was not possible at the time. Klein (6) modeled lignin pyrolysis based on its model components and compared his simulations to previously published data (7). In a recent study by Avni, et.al., (8-9), the pyrolysis behavior of Iotech lignin was studied at different ambient pressures and heating rates.

This paper considers the application of a recently developed pyrolysis model of coal pyrolysis (10-12) applied to a heated grid as well as an entrained flow reactor, to the pyrolysis of lignin. Flash pyrolysis as well as slow heating rate pyrolysis was carried out in a heated grid (13), in which on-line, in-situ gas and tar analysis is performed by Fourier Transform Infrared (FT-IR) Spectroscopy. The model has proved to be successful in simulating the results of vacuum flash pyrolysis and slow heating rate pyrolysis for a variety of lignins.

Experimental

Lignin Samples

Seven lignins were used in the study; Table 1 compares the different lignins and their sources. Four of them were received from manufacturers while the last three were extracted in our laboratory. Table 2 shows the elemental composition and methoxy content of the lignins. All lignin samples were dried for 48 hours at 108°C under vacuum before the experiments.

Flash Pyrolysis Experiments

The flash pyrolysis apparatus is illustrated in Fig. 1. It consists of a heated grid pyrolyzer located in the center of a large gas cell with KBr windows to allow FT-IR (Nicolet) analysis (13). The lignin is evenly distributed between two layers of stainless-steel or tungsten screen which is electrically heated. Lignin temperatures of 1800°C and heating rates in excess of 10,000°C/sec for the highest temperatures can be achieved using a tungsten screen. When flash pyrolysis is performed in vacuum, the tar molecules quickly escape the grid and land on the cold glass.

Evolution kinetics for gaseous species are determined with the FT-IR which permits low resolution spectra (8 wavenumbers) to be taken at 80 msec intervals. The low resolution analysis can determine CO, CO_2, H_2O, CH_4, SO_2, CS_2, C_2H_2, C_2H_4, C_3H_6, benzene, and heavy paraffins and olefins. The time-temperature evolution for

each species can be determined from such scans as indicated in Fig. 2 which shows the CO yield as a function of time at several temperatures.

The distribution of major products is determined by weighing the lignin, the char (which remains on the screen) and the tar (which accumulates on a glass tube surrounding the grid) and by quantitative analysis of 0.5 wavenumber, FT-IR spectra of the evolved gas taken at the completion of a run. The high resolution spectra can quantitatively determine all of the above species plus C_2H_6, C_3H_8, C_4H_8, NH_3 and potentially many other species which have not yet been observed. Calibration of the FT-IR was made using pure gases or prepared gas mixtures. Analysis of the solids was performed with the FT-IR and by elemental analysis.

Constant Heating Rate Experiment

Slow constant heating rate experiments with evolved gas analysis by Mass Spectrometry (MS) or Gas Chromatography (GC) has been used by several investigators to study coal (14-17). Gas analysis by FT-IR, as used in the experiments here, offers advantages over GC in speed and over MS in the ability to identify heavy tar materials.

Constant heating rate experiments were performed for lignin using the apparatus shown in Fig. 1. The sample is heated at a constant rate (30°C/min) while gas evolution is monitored by FT-IR. The pyrolysis gas is swept from the cell with a constant flow of nitrogen (700 ml/min) at a pressure of 1 atm.

Pyrolysis Model

The pyrolysis model assumes a lignin structure constisting of substituted phenyl-propane subunits linked by C-O and C-C bonds. During thermal decomposition the relatively weak bonds break, releasing the tar which is comprised of monomers, dimers and trimers of phenyl-propane subunits. The FT-IR spectra of the lignin tar show a remarkable similarity to the parent lignin. Figure 3a-c shows such a comparison. Such similarity has also been observed for pyrolysis of coals and model polymers.

A pyrolysis model should simulate the evolution of tar fragments and competitive cracking of substituted groups and ring clusters to form the light molecular species of the gas. The yield of each gas species should depends on the functional group distribution in the original lignin. At low temperatures there is very little rearrangement of the lignin polymer but there is decomposition of the substituted groups and aliphatic structures resulting in CO_2 release from the carbonyl, H_2O from hydroxyl, hydrocarbon gases from aliphatic and methoxy groups, and CO from weakly bound oxygen groups such as aldehyde groups. At high temperatures there is breaking and rearrangement of the aromatic rings. Late in the pyrolysis, the rearrangment of the lignin subunits permits H_2 to be evolved from the aromatic hydrogen. Additional CO form tightly bound oxygen functionalities. As this process continues the char becomes more graphitic. At high temperatures the FT-IR spectra of lignin char and coal char are remarkably similar, (see Figure 3d) both are highly aromatic. A striking feature of thermal decomposition which was observed for a variety of coals and lignins in the heated grid experiments is that the temperature dependent evolution rate of CO_2 and CO are similar for all lignins and coals while the evolution rates of H_2O, CH_4, paraffins and tar from lignin vary slightly from coal, due to the different bridges between the ring clusters. The rate of evolution of a specie will depend on the nature of the functional group which is its source but appears relatively insensitive to lignin source or extraction processes. The insenitivity of kinetic rates to coal rank has been reported in other investigations (14,18-21).

The mathematical description of the pyrolysis used here has been presented previously (10-12). The model considers the removal of functional groups by a parallel independent evolution of the light species in competition with the tar evolution.

To model these two competing paths with one path yielding a product which is similar in composition to the parent coal, the dry, ash-free (DAF) coal or lignin ia

represented as a rectangular area. As shown in Fig. 4a, the Y dimension is divided according to the chemical composition of the coal or lignin. Y°_i represents the initial fraction of a particular component (carboxyl, aromatic hydrogen, etc) and the sum of the Y°_i's equals 1. The evolution of each component into the gas (carbonxyl into CO_2, aromatic hydrogen into H_2, etc) is represented by the first order diminishing of the Y_i dimension, $Y_i = Y^\circ_i \exp(-k_i t)$. The X dimension is divided into a potential tar forming fraction X° and a non-tar forming fraction $1-X^\circ$. The evolution of the tar is represented by the first order diminishing of the X dimension $X = X^\circ \exp(-k_t t)$.

Figure 4-a shows the initial state of the coal. Values for Y° are obtained from elemental and FT-IR analysis and from the heated grid pyrolysis experiments (10,12,22). The value of X° is at present a parameter of the model. It is controlled by the oxygen and aliphatic or hydroaromatic hydrogen content of the lignin and can be influenced by pressure, particle size, bed geometry and the transport properties of the pyrolysis medium.

Figure 4-b shows the initial stage of thermal decomposition during which the volatile components, H_2O, CO-loose and CO_2, evolve from the hydroxyl, ether-loose and carboxyl groups, respectively, along with aliphatics and tar. At a later stage (Fig. 4-c) CO-tight and H_2 are evolved from the ether-tight and aromatic hydrogen. Figure 4-d shows the final state of the char, tar and gas.

Table 3 presents the kinetic rates used in the model and the functional group composition of Iotech Aspen lignin. A distributed activation energy is used for species evolution kinetics. Such models were used by Pitt (23) and by Anthony, et.al. (24) for describing coal weight loss. Weimer and Nagan (14) employed Anthony's model to describe individual species evolution. This model was used in the present study.

Results and Discussion

Figure 5 shows the evolution rates of the major gas species and tar from Iotech lignin at a constant heating rate pyrolysis of 30°C/min. The simulations of the evolution rates, using the parameters in Table 3 agree well with the experimental results. As was mentioned previously, the kinetic rates of CO and CO_2 are similar for coal and lignin. The experimental CO evolution rates (Fig. 6) of several lignins indicate a high temperature tight-CO and show the insensitivity of the evolution rate to the lignin source or the extraction processes used.

The methane evolution rate suggests a tightly and loosely bound precursor. The loose methane is probably from the methoxy group of the phenylpropane subunit. The methoxy content of Iotech lignin is 17.01 weight percent, much higher then any coal methoxy content. Figure 8 compares the experimental evolution rate of methane from Iotech lignin and Pittsburgh Seam coal, the only difference between the two is the loose methane in the lignin. The similarity between the two can be explained in light of the similar FT-IR spectra (see Fig. 3-d) of lignin char and coal char at 500°C and higher temperatures. In both cases the char is highly aromatic relative to the starting materials. The relative ratio of the area under the aliphatic peaks near 2900 cm^{-1} to the aromatic peaks near 800^{-1} decreased drastically in the lignin char at 500°C compared to the ratio in the lignin. In both coal and lignin the residual oxygen appears to be predominantly ether type oxygen. Figure 7 compared the methane evolution rate of several lignins, again the rate is insensitive to the lignin source and extraction process. The ratio of the loose methane to tight methane peaks is changing from one lignin to another. The ratio seems to increase with an increase in the methoxy content of the lignin (see Table 2 for methoxy content).

The predicted tar evolution rate is in excellent agreement with the experimental data. The activation energy used for the simulations of tar evolution (48 kcal/mole $\pm$ 1500 cal/mole) is in a very good agreement with the estimated activation energy of the ether linkage (48 kcal/mole) connecting the phenylypropane subunits. The activation energies have been calculated using the group additivity theory of S. W. Benson (25,26). The DTGA of Iotech lignin confirms the location and shape of the tar rate curve on the temperature scale. The differences in the tar rates between

coal and lignin are due to the weak ether linkages that exist in the lignin between the polymer subunits; such weak linkages do not exist in coal.

Figure 9 shows the gas yield versus pyrolysis time in a flash pyrolysis. The major gas species evolved were CO, CO_2, H_2O and paraffins, at a final static temperature of 500°C for 80 seconds. The simulations of the gas species obtained with the parameters in Table 3 are in good agreemet with the data presented within the experimental errors. The methane evolution in the slow heating rate experiments shows a higher fraction of tight-methane than is observed in the flash pyrolysis. There is no such indication with the rest of the gas species.

Yield of CO versus pyrolysis time in a flash pyrolysis at different temperatures of flash pyrolysis are shown in Fig. 2 where it is evident that the agreeement between theory and experiment is good.

Conclusions

The experiments have shown that lignin pyrolysis kinetics are insensitive to lignin source or extracting process. Theory and experiment agree well for both slow and fast heating rates, using the given model parameters. The lignin parameters of the model are related to the functional group composition of the lignin.

References

1. Goldstein, I.S., Applied Polymer Symposium, 28, 256-267, (1975).
2. Drew, S., AIChE Symposium Series, 181,, Vol. 79, pp. 21-25, (1978).
3. Goheen, D.W., Chapter in Organic Chemicals from Biomass, Ed. by Goldstein, I.S. CRC Press, (1981).
4. Coughlin, R.W., Avni, E. and Sundstrom, D.W., Conversion of Lignin to Useful Chemical Products, Chap., Ed. by Wise, D.L. CRC Press, (1983).
5. Gavalas, G.R., et.al., Ind. Eng. Chem. Prod. Res. Dev., 18, (2), 127, (1979).
6. Klein, M.T. and Kirk, R.S., Preprint, Div. of Fuel Chem., ACS, (1981).
7. Klein, M.T., Sc.D. Thesis, Dept. Chem. Eng.,M.I.T., Cambridge, MA (1981).
8. Avni, E., Devoudzadeh, F. and Coughlin, R.W., International Conference, Fundamentals of Thermochemical Biomass Conversion, October, (1982).
9. Avni, E. and Coughlin, R.W., Presented at AIChE Meeting, Los Angeles, Nov. (1982).
10. Solomon, P.R. and Colket, M.B., 17th Symposium (International) in Combustion, The Combustion Institute, Pittsburgh, PA pp. 131-143, (1979).
11. Solomon, P.R., Prepr., Div. of Fuel Chem., ACS, 2, 24, 179-184, (1979).
12. Solomon, P.R., Fuel 60, 3, (1981).
13. Solomon, P.R., Hamblen, D.G. and Carangelo, R.M., Coal Pyrolysis, AIChE Symposium on Coal Pyrolysis, Nov. (1981).
14. Weimer, R.F. and Nagan, D.Y., ACS Div. of Fuel, Chem. Prepr., 24, (3),
15. Juntgen, H. and van Heek, K.H., Fuel Processing Technology, 2, 261,
16. Fitzgerald, D. and van Krevelen, D.W., Fuel, 38, 17, (1959).
17. Campbell, J.H., Fuel, 57, 217, (1978).
18. Tyler, R.J., Fuel, 59, 218, (1980).
19. Freihaut, J.D., Solomon, P.R. and Seery, D.J., ACS Division of Fuel Chemistry Preprints, 25, Sept. (1980).
20. Suuberg, E.M., Peters, W.A. and Howard, J.B., Ind. Eng. Chem. Process. Des. Devel., 17, 37, (1978).
21. Solomon, P.R. and Hamblen, D.G., Coal Gasification Reactions wtih On-Line In-Situ FT-IR Analysis, 1st Quaterly Report, DOE Contract #DE-AC21-FE05122.
22. Solomon, P.R., Preprints, Div. of Fuel Chem., ACS, 24, 3, 1514, (1979).
23. Pitt, G.J., Fuel, 41, 267, (1962).
24. Anthony, D.B., Howard, J.B., Meissner, H.P. and Hottel, H.G., 15th Symposium (International) on Combustion, p 1303, Aug. 25-31, (1975).
25. Benson, S.W. and Oneal, H.E., Kinetic Data on Gas Phase Unimolecular Reactions, NSRDS-NBS, 21, (1970).
26. Benson, S.W., Thermochemical Kinetics, Wiley, NY, (1978).

TABLE 1

LIGNIN SOURCE

Lignin	Wood	Manufacturer	Pretreatment
Iotech	Aspen	Iotech Corp.	steam explosion
Stake	Aspen	Stake Tech. Ltd.	autohydrolysis
BEC	Aspen	Biological Energy Corp.	---
Indulin	Pine	Westvaco	---
Ethanol	Aspen	b	[a] steam explosion
HCl	Aspen	c	[a] steam explosion
H_2SO_4	Aspen	d	[a] steam explosion

a) The Aspen wood was steam-exploded by Iotech Corp. and extracted in our laboratory.

b) 25 g of wood is mixed with 250 g of 43 Wt% ethanol in water mixture at pH 6. The reaction is carried out in autoclave at 185°C for 1 hour.

c) 25 g of wood was stirred for 4 hours with 500 g conc. HCl at room temperature. After 20 hours water is added and the mixture is filtered and washed with soda solution.

d) 25 g of wood is treated with 250 ml of 72% H_2SO_4 and stirred at room temperature for 2 hours, 2 volumes of water is added and the mixture is filtered. The lignin is reflex for 1 hour in 125 ml 3% H_2SO_4.

TABLE 2

ELEMENTAL COMPOSITION AND METHOXY CONTENT OF LIGNINS

Lignin	Iotech	Indulin	BEC	Stake	Ethanol	HCl	H_2SO_4
C	63.44	64.35	66.84	60.61	65.57	52.33	61.54
H	5.87	5.71	6.09	5.31	5.76	5.75	5.14
O	29.94	27.69	27.04	33.39	28.37	40.08	31.83
S	-	1.3	-	-	-	-	0.5
Mineral	0.75	0.95	0.03	0.69	0.30	0.56	0.99
Methoxyl	17.01	13.95	19.32	12.58	17.41	6.93	10.99

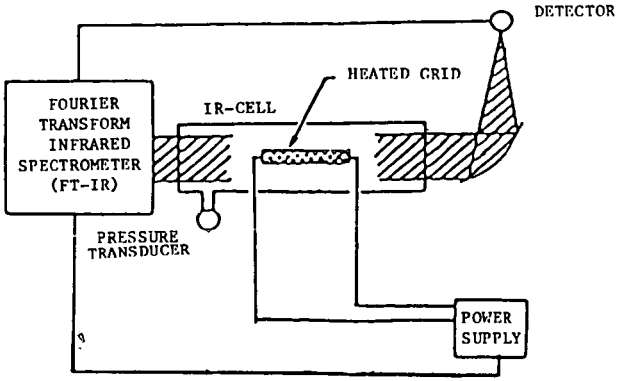

Figure 1. Pyrolysis Apparatus.

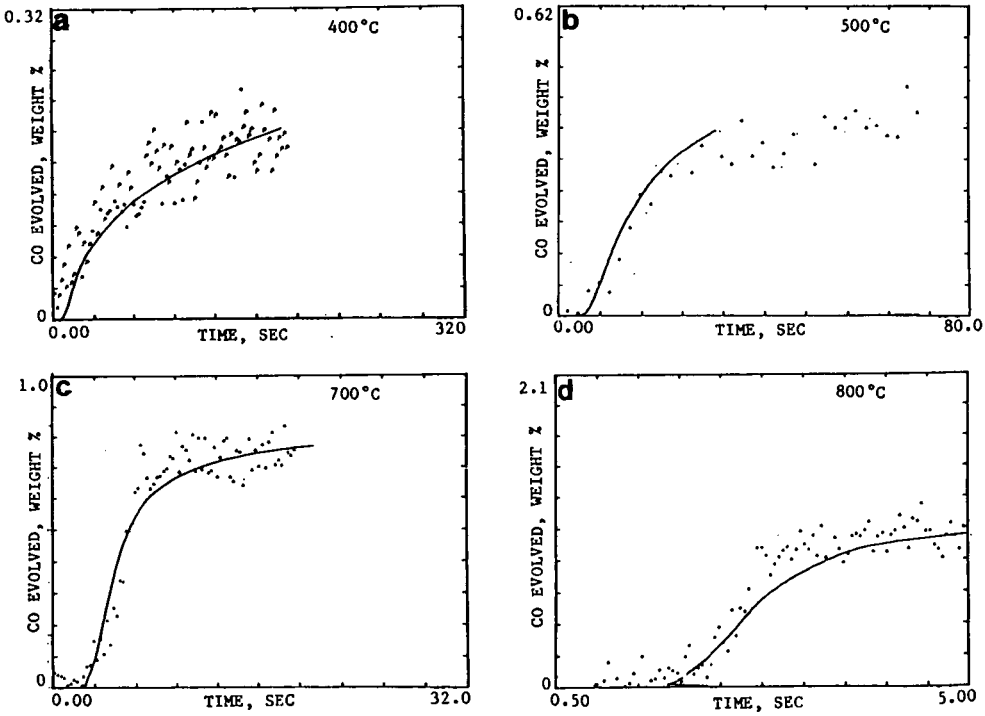

Figure 2. CO Yield from Iotech Lignin at Different Temperatures of Flash Pyrolysis, (points) experiment and (solid line) simulation.

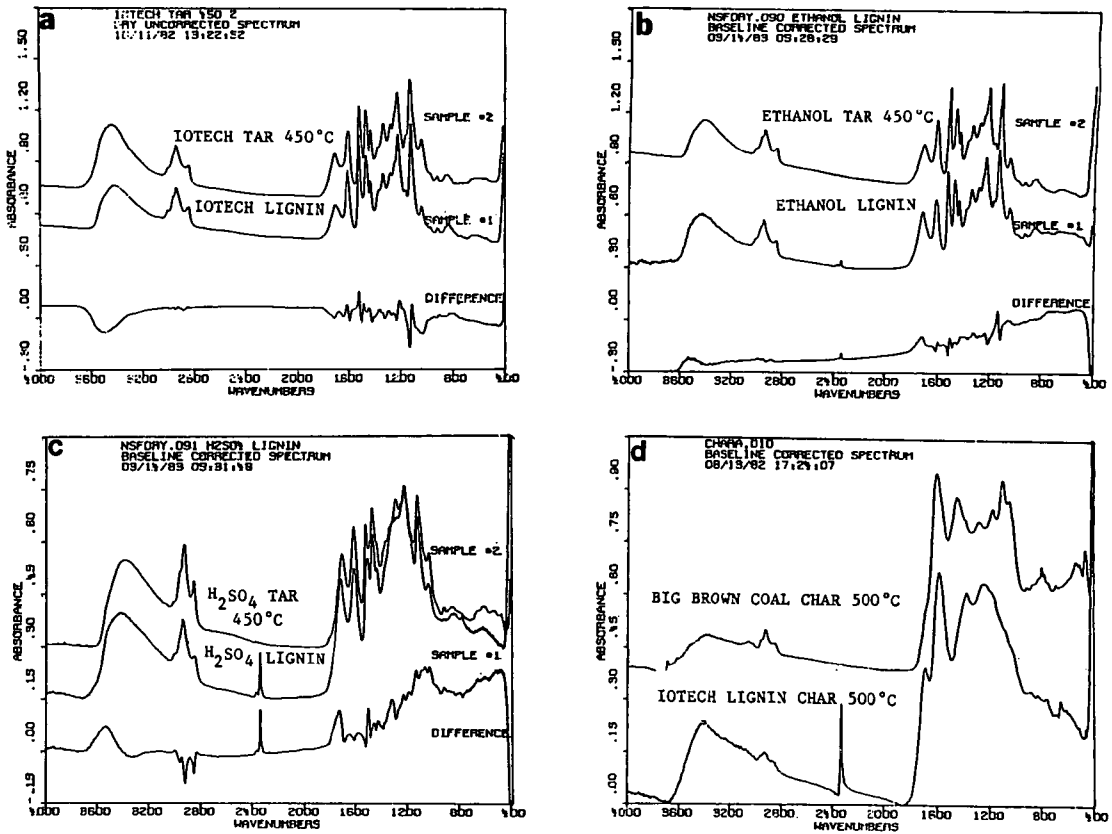

Figure 3. Infrared Spectra showing Comparison of Lignin and Tar as well as Coal Char and Lignin Char.

TABLE 3

Kinetic Rates and Functional Group Compositions

Composition Parameter		Iotech Lignin (WTX DAF)	Kinetic Rate Constants (sec^{-1})
C		0.634	
H		0.059	
N		0.000	
S(organic)		0.000	
O		0.307	
		1.000	
Y^o_1	CO_2 - Extra-loose	0.0068	k_1 = 0.10E+15 exp((23900. ± 2500.)/T)
Y^o_2	CO_2 - Loose	0.0036	k_2 = 0.10E+15 exp((27900. ± 1400.)/T)
Y^o_3	CO_2 - Tight	0.0026	k_3 = 0.10E+15 exp((32900. ± 3300.)/T)
Y^o_4	H_2O	0.0654	k_4 = 0.10E+14 exp((23000. ± 2000.)/T)
Y^o_5	CO - Ether Loose	0.0300	k_5 = 0.17E+12 exp((25000. ± 2500.)/T)
Y^o_6	CO - Ether Tight	0.3889	k_6 = 0.10E+16 exp((54900. ± 5000.)/T)
Y^o_7	HCN - Loose	0.0000	k_7 = 0.54E+04 exp((8850. ± 0.)/T)
Y^o_8	HCN - Tight	0.0000	k_8 = 0.70E+08 exp((32000. ± 0.)/T)
Y^o_9	NH_3	0.0000	k_9 = 0.12E+13 exp((27300. ± 2400.)/T)
Y^o_{10}	CH_x-Aliphatic	0.0942	k_{10} = 0.17E+15 exp((30000. ± 1500.)/T)
Y^o_{11}	Methane-loose	0.0049	k_{11} = 0.50E+16 exp((30000. ± 1500.)/T)
Y^o_{12}	Methane-tight	0.0100	k_{12} = 0.20E+14 exp((30000. ± 3000.)/T)
Y^o_{13}	H-Aromatic	0.0130	k_{13} = 0.16E+08 exp((23000. ± 2300.)/T)
Y^o_{14}	C-Non Volatile	0.3804	k_{14} = 0
Y^o_{15}	S-Organic	0.0000	
	Total	1.0000	
X^o	Tar	0.6200	K_T = 0.10E+15 exp((24000. ± 1500.)/T)

Cracking Rates:

Paraffins - Olefins	k_{OL} = 0.15E+12 exp((27600.)/T)
Olefin - Acetylene	k_{AC} = 0.21E+08 exp((22000.)/T)

*Distributed rates have not yet been determined.

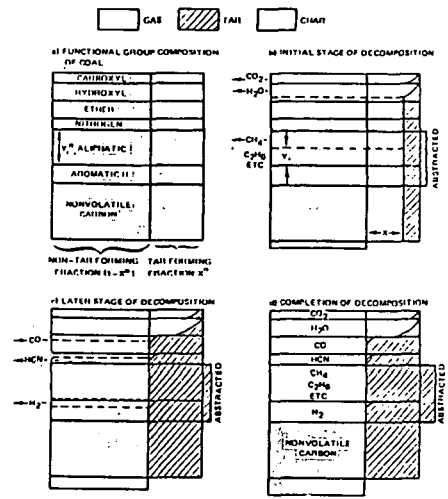

Figure 4. Progress of Thermal Decomposition According to Model. a) Functional Group Composition of Lignin, b) Initial State of Decomposition, c) Later Stage of Decomposition, d) Completion of Decomposition.

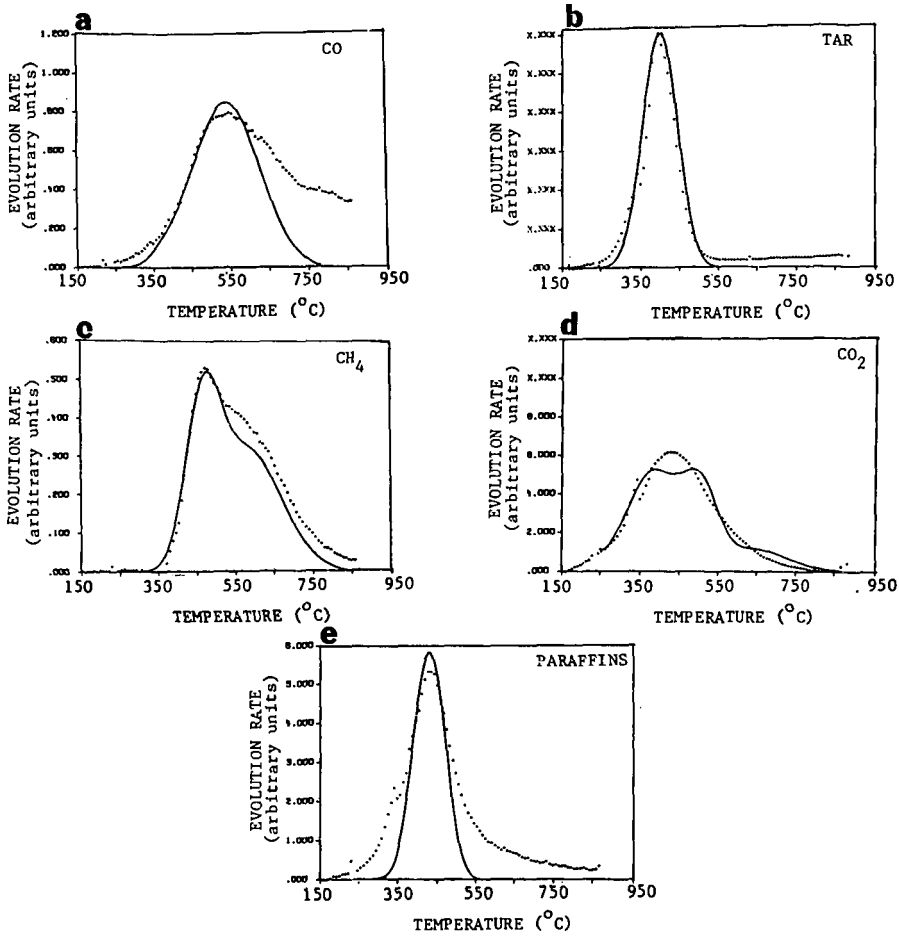

Figure 5. Evolution Rate of Major Volatile Species from Iotech Lignin in a Heating Rate of 30°C/min, Experiment (points) and Simulations (solid line).

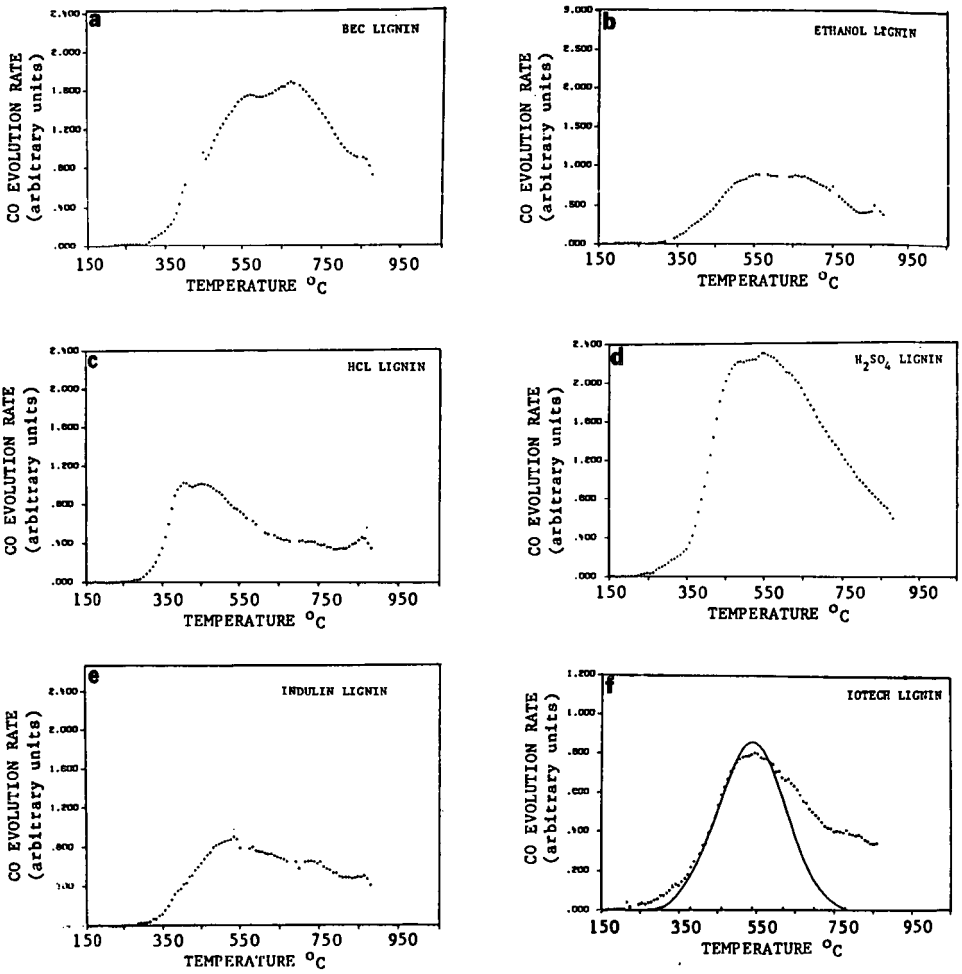

Figure 6. Evolution Rate of CO from Different Lignins at a Heating Rate of 30°C/min, experiment (points) and simulation (solid line).

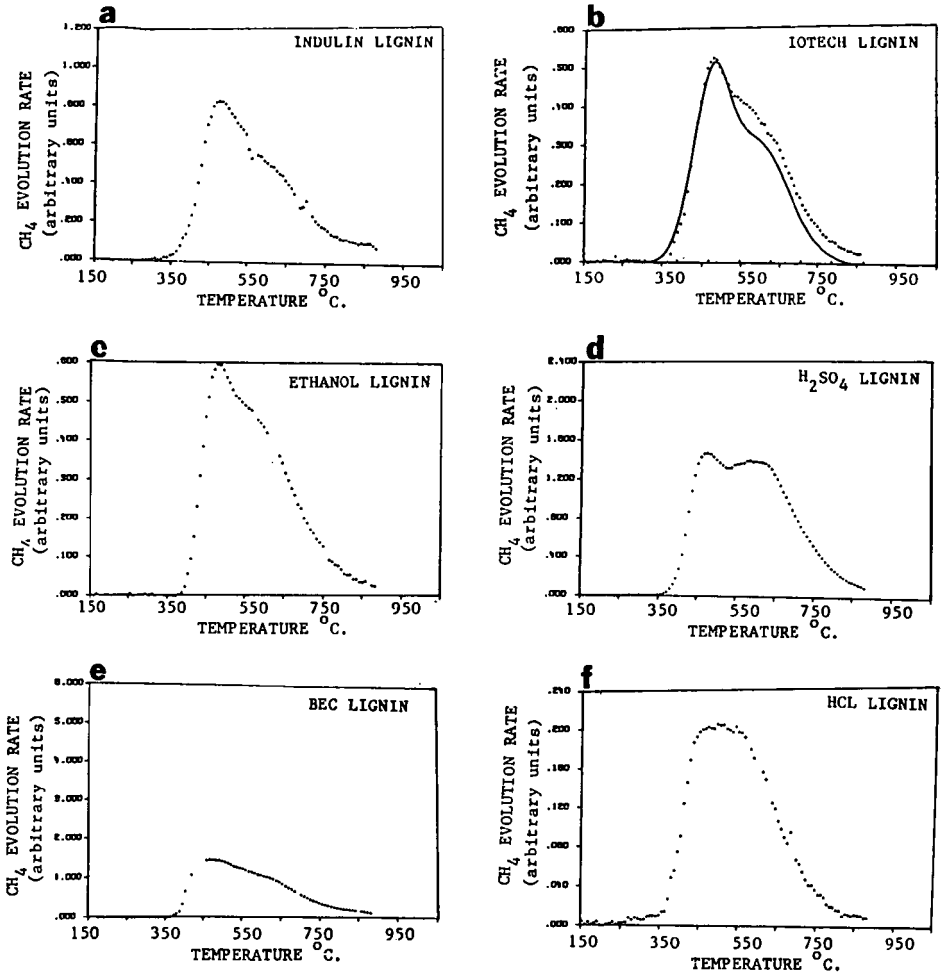

Figure 7. Evolution Rate of Methane from Different Lignins at a Heating Rate of 30°C/min.

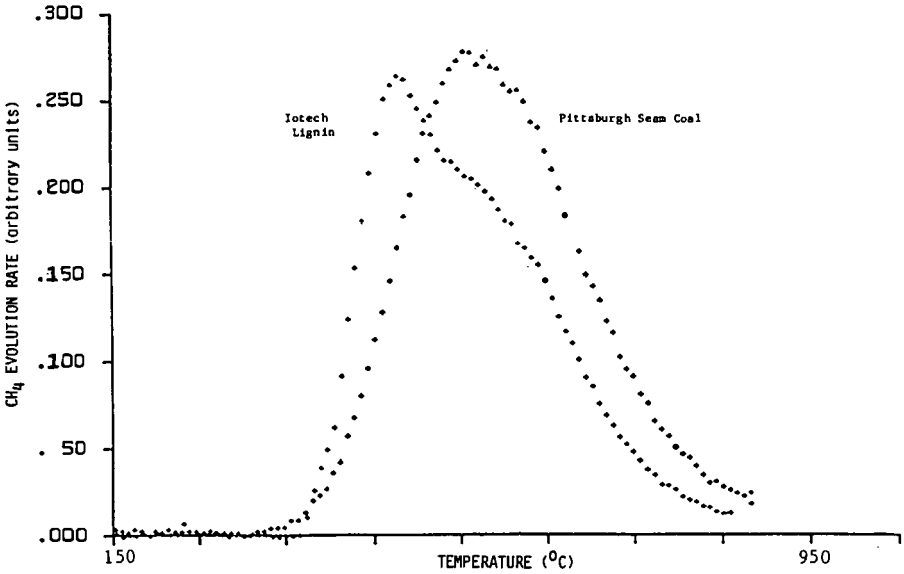

Figure 8. Evolution Rate of Methane from Pittsburgh Seam Coal and Lignin at a Heating Rate of 30°C/min.

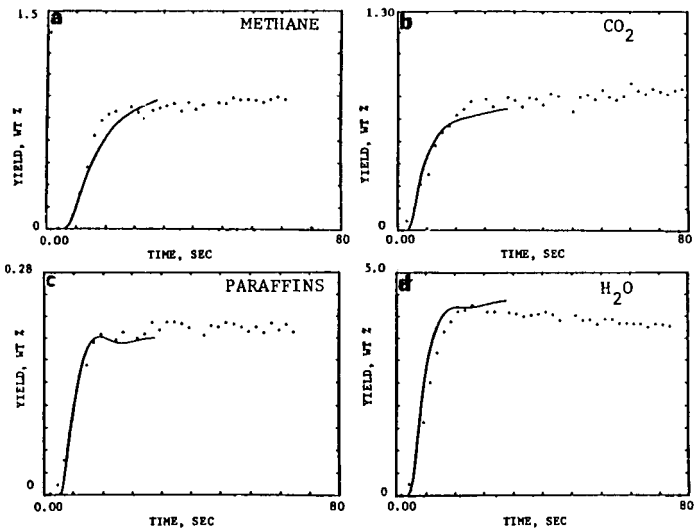

Figure 9. Major Gas Species Versus Time in a Flash Pyrolysis at 500°C, experiment (points) and simulation (solid line).

MODELING TAR COMPOSITION IN LIGNIN PYROLYSIS*

Hsiang-Hui King and Peter R. Solomon

Advanced Fuel Research, 87 Church Street, East Hartford, CT 06108

Eitan Avni and Robert W. Coughlin

University of Connecticut, Storrs, CT 06268

Lignin is an integral constituent in all vascular plants and an important alternative source of fuel and chemical feedstock. Pyrolysis depends strongly on the properties of the substrate and is the initial step in any thermal process. A better understanding of lignin pyrolysis, just as in the case of coal, is essential for developing lignin conversion processes.

Lignin can be viewed as a coploymer consisting of phenylpropane units linked together by carbon-carbon and carbon-oxygen bonds (1). A depolymerization model has been developed recently to predict tar yield and composition for the pyrolysis of model homopolymers which simulate individual structural features of coal (2). In this paper, the depolymerization model is expanded to predict the pyrolysis behavior of a copolymer comprising up to seven different and randomly distributed monomers and applied to simulate the pyrolysis of an Aspen lignin. The effects of pyrolysis temperature and pressure on tar yield are examined. More importantly, this model predicts the molecular weight distributions for pyrolysis tars in detail and the predictions agree reasonably with the experimental results.

EXPERIMENTAL

An alkaline soluble lignin extracted from a steam-exploded Aspen wood was obtained from Iotech Corporation, Canada. The elemental composition is 63.4% C, 5.9% H, 30.0% O (by difference), and 0.7% ash. The pyrolysis experiments, including constant heating rate and flash pyrolysis, were performed in an apparatus which employs an electrically heated grid within an infrared cell to provide on-line, in-situ analysis of evolved products by Fourier Transform Infrared (FT-IR) Spectrometry as presented in Fig. 1. In the constant heating rate experiments the cell was swept by a constant flow (700 ml/sec) of nitrogen gas to keep the cell pressure at 1 atm. In the flash pyrolysis experiments the cell was closed. The FT-IR spectra were recorded on a Nicolet model 7199 FT-IR spectrometer. Both tar and char yields were obtained gravimetrically. The field ionization mass spectrometry (FIMS) and elemental analysis were performed at SRI International and Galbraith Laboratories, respectively.

THEORY FOR POLYMER PYROLYSIS

Thermal depolymerization of macromolecules to produce volatile products requires: 1) cleavage of weak bonds, 2) stabilization of the free radicals by donatable hydrogen atoms, and 3) transport of the products away from the reaction zone. To understand the effect of these three factors, consider first the case in which the donatable hydrogen is unlimited. In pyrolysis, the depolymerization proceeds with the random breaking of weak bonds until the fragments are small enough to vaporize. With unlimited hydrogen, the polymer will decompose completely into volatile products if at least the monomer can be vaporized under the reaction conditions. The actual distribution of monomer, dimer, trimer and higher molecular weight oligomers in the

*Work supported by the National Science Foundation under Contract #CPE-8107453

products will depend in detail on the rate of bond breaking relative to the rate of transport of the fragments formed. Conditions which enhance transport relative to bond breaking will increase the average molecular weight of the volatile products. In cases where donatable hydrogen is limited, the volatile yield will depend on the demand for hydrogen; i.e., the amount of hydrogen employed for stabilization of products which are carried away. For a given polymer, the higher the average molecular weight of the volatile products the fewer the broken bonds requiring stabilization, and the lower the hydrogen demand per weight of volatile product.

The theory combines random cleavage of weak bonds with transport of depolymerization fragments by vaporization and diffusion to predict product yield and composition. The assumptions in this theory include: 1) the bonds between the monomer units in the polymer molecule are the only weak bonds and equally likely to be cleaved; 2) during an infinitesimal period of time the probability of cleaving simultaneously two weak bonds in one molecule is so small that it can be ignored, 3) the melt is homogeneous, i.e., there is no concentration and temperature gradient in the particle; and 4) the particle is spherical and its radius shrinks proportionally to the cubic root of its mass as the reaction proceeds. The theory has been developed for the geometry indicated in Fig. 2, where spherical particles (located within the heated grid), are at the pyrolysis temperature while the temperature of the cell wall, where tar is condensed and collected, is only slightly above room temperature. The particle size and cell diameter are not shown to scale in Fig. 2, the cell diameter is 5 cm and the mean particle size is 0.3 mm.

The theory considers the molecular weight distribution Q_i in the reacting polymer and the molecular weight distribution N_i of the tar, where Q_i and N_i are the molar quantities of the polymeric component with DP = i in the reacting polymer and in the tar. DP (degree of polymerization) is defined as the number of monomer units in a polymer molecule. The rate of change of Q_i is

$$dQ_i/dt = (dF_i/dt) - (dB_i/dt) - (dN_i/dt) \qquad 1)$$

where dF_i/dt is the rate of formation for the component with DP = i from the decomposition of components with DP > i in the reacting polymer, dB_i/dt is the rate of disappearance by decomposition for the component with DP = i in the reacting polymer, and dN_i/dt is the rate of transport of fragments with DP = i from the particle as tar or gas.

In the following paragraphs we develop the equations for the terms on the right hand side of eq. 1.

The terms dF_i/dt and $dB_i dt$ are the rate of creating and distruction of oligomers with DP = i through the cleavage of weak bonds. The cleavage of these weaks bonds is assumed to be a first order process with a rate constant k, i.e., the rate at which bonds break is k times the number of breakable bonds. Since there are (i - 1) weak bonds in the polymeric component with DP = i and the breaking of any one of them will remove that component from the distribution parameter Q_i. The rate of distribution for the component i may be written,

$$dB_i/dt = (i - 1)\ k\ Q_i \qquad 2)$$

The creation of component i can occur by the distribution of all components j with j > i. For each component with DP = j > i in the reacting polymer, there are two ways of breaking weak bonds to form component with DP = i, thus, the rate at which component i is created from component j ia

$$(dF_i/dt)_j = 2\ k\ Q_j \qquad 3)$$

and

$$dF_i/dt = 2\,k \sum_{j=i+1}^{a} Q_j \qquad 4)$$

where the DP of the starting homopolyer is a.

As illustrated in Fig. 2, there are five weak bonds in the hexamer which decomposes to pentamer plus monomer by cleaving two different bonds, to tetramer plus dimer by cleaving another two different bonds, or to a pair of trimers by cleaving the middle bond. Comparing equations 2 and 4, it is obvious that $(dF_i/dt)_6 = (2/5)(dB_6/dt)$ where i range from 1 to 5.

For component i to leave a particle as tar it must be volatile and be available within the particle (Q_i greater than 0). The maximum possible transport rate for component with DP = i is

$$dN_i/dt = [W/((4/3)\pi r_o^3 d)][dV_i/dt] \qquad 5)$$

$$= [\text{number of particles}][\text{transport rate for component i from each particle}]$$

where w, r_o and d are the starting weight of polymer, the particle radius and the density of the original polymer, respectively. The transport rate for oligomer with DP = i from a particle of radius r_p at any given time is approximately given by the following equation (2)

$$dV_i/dt = 4\pi r_p D_i (P_i/RT)(Q_i/\sum_{m=1}^{a} Q_m) \qquad 6)$$

where D_i and P_i are the diffusion coefficient and the vapor pressure for oligomer with DP = i, R is the gas constant, and T is temperature in K. D_i and P_i can be estimated by the following equations (2,3,7)

$$D_i(T,P) = 1.585 M_i^{-0.675} (T/273)^{1.08} (1/P) \quad cm^2/sec \qquad 7)$$

$$P_i = (1.23\times10^5 \text{ atm}) \exp(-236 M_i^{-0.654}/T) \qquad 8)$$

where M_i is the molecular weight of component i

The tar fraction Y, is defined as

$$Y = (M/Wa)\sum_{i=1}^{a} (iN_i) \qquad 9)$$

where M is the molecular weight of the polymer.

This theory has been expanded to predict the pyrolysis behavior of a copolymer comprising up to seven different and randomly distributed monomers. The expanded theory is not included because of page limit. In each simulation, an activation energy (E) and a frequency factor (A) were given to calculate the rate constant, k, using the following equation

$$k = A \exp(-E/RT) \qquad 10)$$

Other initial inputs include a, M, W, r_o, d, molecular weights of monomers, reaction pressure and the temperature of the particle as a function of time. At time zero,

$$Q_a = W/M$$

$$Q_i = 0 \qquad \text{if } i \neq a$$

and

$$N_i = 0$$

The simulation is carried out by keeping track of Q_i, N_i, Y, k, and r_p at each time step using equations 1 to 9. The time increment is kept very small. All computations were performed on a PDP 11/23 computer.

INPUT INFORMATION

Aspen is a hardwood and its milled wood lignin was reported to contain 57% of guaiacylpropane units and 43% syringylpropane units (4). As indicated by FIMS results for lignin tars presented in Figs. 3a and 4a, in addition to the formation of coniferyl alcohol (MW = 180), 3-guaiacyl-1-propanol (MW = 182), sinapaldehyde (MW = 208) and sinapyl alcohol (MW = 210), other products derived from these compounds with concurrent formation of CO, CO_2, H_2O, CH_4, C_2H_6, etc. were also detected in lignin tars. One of the most probable structures for each molecular weight is presented in Table 1. The compound with MW = 418 is probably dehydrobis-sinapyl alcohol with biphenyl type linkage. Although it is a dilignol, it is treated as a monomer in this simulation because the linkage between the two C_9 units is very stable under the pyrolysis conditions. Therefore, compounds with MW $\leqslant$ 210 and the compound with MW = 418 are viewed as monomers in this simulation.

Equation 8 was originally used to estimate vapor pressures for hydrocarbons. Since lignin and its tar contain fairly large amounts of oxygen, adjustment in the estimation of vapor pressure is necessary. Boiling points and molecular weights for selected relevant compounds are presented in Table 2. By comparing a pair of compounds, one hydrocarbon and one oxygen-containing compound, with the same boiling point and assuming that compounds with the same boiling point show the same temperature dependence for vapor pressure, adjustments in molecular weights for selected groups are estimated and presented in Table 3. Accordingly, the adjusted molecular weights for the compounds in Table 1 are estimated and used in eq. 8 to estimate the vapor pressure. In this simulation, monomers with very similar molecular weights are treated as one entity and the molecular weights for the seven monomers are included in Table 4. The mole fractions for these compounds are assumed so that theoretical prediction can fit the FIMS result for lignin tar produced at 500°C (Fig. 3a). The monomers with MW = 154, 196 and 210 contain one syringyl group and the monomer with MW = 418 contains two syringyl groups. Thus, guaiacyl to syringyl ratio among these monomers is 40 to 60. This ratio is lower than that reported (4) for the milled wood lignin of Aspen (57% to 43%) and suggests that the bonds connected to syringyl units are more reactive than those to guaiacyl units. The thermally most labile bond in lignin is the α-O-4 bond as shown below

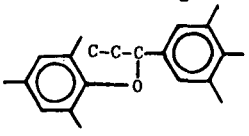

The rate constant for homolysis of the carbon-oxygen bond in benzyl phenyl ether has been reported as $5 \times 10^{14} \exp(-25{,}400/T)$ (5). An alkyl substituent at the benzylic position reduces the activation energy by about 3 Kcal according to some reported activation energies (5). Consequently, the rate constant for lignin pyrolysis is estimated as $10^{14} \exp(-24{,}000/T)$.

A correlation between coal density and elemental composition on a dry mineral matter free (dmmf) basis has been developed (6).

$$D_{He(dmmf)} = 0.023\ C_{dmmf} + 0.0292\ O_{dmmf} - 0.0261\ H_{dmmf} + 0.0225\ S_{org(dmmf)} - 0.765 \quad 11)$$

From this expression, the density for the Aspen lignin used in this study is estimated to be 1.43 g/cm^3. The particle radius of 0.03 mm is used in this simulation. DP of the original polymer, a, is assumed to be 50 and the molecular weight of the original polymer

$$M = 50\ (0.4 \times 180 + 0.6 \times 210) = 9900\ g/mole$$

RESULTS AND DISCUSSION

Fraction of Potentially Depolymerized Bonds (F_{pdb})

The fraction of potentially depolymerized bonds (F_{pdb}) is defined as the fraction of weak bonds whose resulting free radicals can be stabilized by donatable hydrogen atoms. In the pyrolysis of lignin, some weak bonds convert to much stronger bonds, e.g., conversion of carbon-carbon single bond to double bond as a result of hydrogen donation, thus, F_{pdb} is usaully less than one. F_{pdb} depends on the structure of lignin and on the reaction conditions and is one of the most important factors in determining the chsr yield. F_{pdb} should be regarded as an adjustable parameter in the simulation. In each computer simulation, a certain value is used for F_{pdb}. When x_c becomes equal to F_{pdb} then there will be no additional bond cleavage, i.e., dF_i/dt and dB_i/dt in equation 1 are zeros.

Effect of Reaction Temperature

The molecular weight distribution of tar is determined by the competition between transport and decomposition for all possible components. For a certain component, if transport is much faster than decomposition, it transports away to tar fraction before it decomposes, otherwise, a fraction or all of this component remains on the heated grid and decomposes to smaller components. An increase in temperature accelerates both transport and decomposition, however, the increase in decomposition rate is more significant. Consequently, a higher reaction temperature favors the formation of tar components with higher volatilities or lower molecular weights.

The effect of reaction temperature has been examined experimentally. Pyrolyais experiments of Aspen lignin were performed at 500°C and 650°C. FIMS results for the tar samples are presented in Figs. 3a and 4a. The major products are monolignols and dilignols along with small amounts of trilignols. The number average molecular weight ($\bar{M}_n$) decreases from 388 to 333 as reaction temperature increases from 500°C to 650°C. The yielda of dilignols and trilignols at 650°C are less than those at 500°C. Theoretical predictions (assuming $F_{pdb} = 0.5$) presented in Figs. 3b and 4b show the same patterns of molecular weight distributions although the predicted number average molecular weights are smaller than the experimental ones.

Effect of External Pressure

The transport rate decreasea as the external pressure increases at a constant temperature while the decomposition rate is independent of the pressure of inert gas. Consequently, a higher external pressure suppresses the formations of tar components with higher molecular weights. Theoretical prediction at 550°C and 4 atm of inert gas pressure is presented in Fig. 5b. Under 4 atm of nitrogen, only compounds MW $\ll$ 210 are produced in significant amounts. The FIMS spectrum for the tar sample produced under these conditions is presented in Fig. 5a. The predicted reduction in molecular weight is observed but is not as drastic as predicted. The data show a smaller ratio of dimer to monomer and ver little trimer compared to a tar obtained at slightly lower temperature at 2 torr, Fig. 3a. But the theory

predicts no dimers or trimers, suggesting some modifications of the pressure and molecular weight dependence of the diffusion coefficient and vapor pressure, equations 7 and 8, may be required.

A higher external pressure results in a smaller average molecular weight for volatile products and therefore an increased usage of donatable hydrogen per weight of volatile products. Because the donatable hydrogen is limited in lignin pyrolysis, the increased hydrogen usage results in a higher char yield. This effect has been verified experimentally. At 550°C, the char yield increases from 33% to 44% as the pressure of nitrogen increases from 2 torr to 4 atm. Theoretical predictions of the char yields are 44% at 2 torr (assuming $F_{pdb} = 0.5$) and 55% at 4 atm (assuming $F_{pdb} = 0.75$, a smaller value of F_{pdb} leads to an even higher char yield) and agree reasonably with the experimental results.

Constant Heating Rate Experiment

The heating rate for lignin pyrolysis is 30°C/min and the pressure of nitrogen is 1 atm. The time and temperature dependent tar evolution rate, monitored by the baseline scattering in the FT-IR spectra, is presented in Fig. 6. The solid line in Fig. 6 is the theoretical fit and its width is about 1/5 of that for the experimental data. This difference is due to the fact that there are different types of bonds between the C_9 units in lignin and indicates the need to expand this theory to include a distribution of activation energies. In addition, this theory in its present form can not predict the evolutions of gaseous products. The theory described in the following paper has these capabilities. Thus, incorporation of these two theories will provide the much needed tool to predict the behavior of lignin in pyrolysis reactions.

SUMMARY

A depolymerization theory has been developed to predict the molecular weight distributions for lignin tars produced in various pyrolysis reactions. It can also predict the char yield semiquantitatively. Incorporation of this theory with the theory described in the following paper will provide the much needed predicting capability for lignin pyrolysis.

REFERENCES

1. Freudenberg, K. and Neish, A.C. "Constitution and Biosynthesis of Lignin", Springer-Verlag, New York, 1968

2. Solomon, P.R. and King, H.-H. Pyrolysis of Model Polymers: Theory and Experiments, submitted to Fuel

3. Unger, P.E. and Suuberg, E.M. "Eighteenth Symposium (International) on Combustion", The Combustion Institute, Pittsburgh, PA, 1981, p. 1203

4. Sarkanen, K.V. and Hergert, H.L. "Lignins", (Ed. Sarkanen, K.V. and Ludwig, C.H.), Wiley Interscience, New York, 1971, p. 43

5. Stein, S.E. "New Approaches in Coal Chemistry", (Ed. Blaustein, B.D., Bockrath, B.C. and Friedman, S.) Am. Chem. Soc. Symp. Series, 169, Am. Chem. Soc., Washington, DC, 1981, p.97

6. Neavel, R.C., Hippo, E.J., Smith, S.E. and Miller, R.N. Preprints Am. Chem. Soc. Div. Fuel Chem., 1980, 25 (3), 246

7. Perry, R.H. and Chilton, C.H. "Chemical Engineer's Handbook", Fifth Ed., McGraw-Hill, New York, 1973, Section 3

TABLE 1

MONOMERS IN LIGNIN TAR

Molecular Weight	Possible Structure (name)	Adjusted Molecular Weight
138	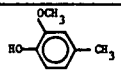 4-methylguaiacol	162
140	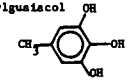 5-methylpyrogallol	252
152	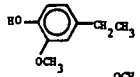 4-ethylguaiacol	176
154	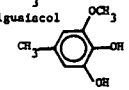 3-methoxy-5-methylcatechol	218
166	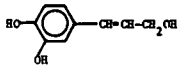 3-(3,4-dihydroxyphenyl)-2-propen-1-ol	278
168	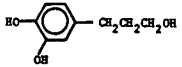 3-(3,4-dihydroxyphenyl)-1-propanol	280
180	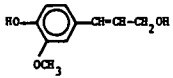 coniferyl alcohol	244

TABLE 1 (continued)

182	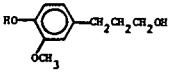 3-guaiacyl-1-propanol	246
194	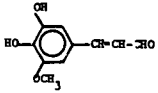 3-(3,4-dihydroxy-5-methoxyphenyl)-2-propenal	272
196	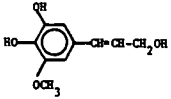 3-(3,4-dihydroxy-5-methoxyphenyl)-2-propen-1-ol	310
208	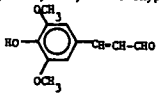 sinapaldehyde	258
210	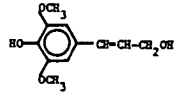 sinapyl alcohol	286
418	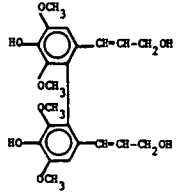 dehydrobis-sinapyl alcohol	570

TABLE 2

BOILING POINTS FOR SELECTED COMPOUNDS

Compound	Structure	Boiling Point (°C)	Molecular Weight
2,6-dimethoxyphenol		261	154
1-phenyloctane	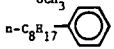	262	190
guaiacol		205	124
1-phenylpentane	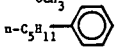	205	148
2-phenylpropionaldehyde	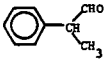	203	134
3-phenyl-1-propanol	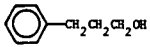	235	136
1-phenylheptane	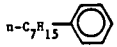	233	176
phenol		181	94
1-phenylbutane	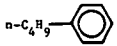	183	134
catechol		245	110

TABLE 3

ADJUSTMENTS IN MOLECULAR WEIGHTS FOR SELECTED GROUP

Group	ΔMW
	36
—OH	40
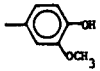	24
—CH=O	14
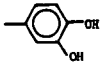	72

TABLE 4

MONOMERS USED IN SIMULATION

Molecular Weight	Adjusted Molecular Weight	Mole Fraction
138	187	0.11
154	206	0.14
168	280	0.185
182	246	0.16
196	291	0.10
210	272	0.155
418	570	0.15

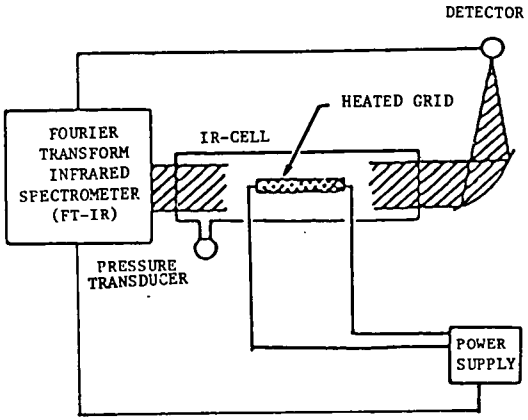

Figure 1. Heated Grid Pyrolysis Apparatus.

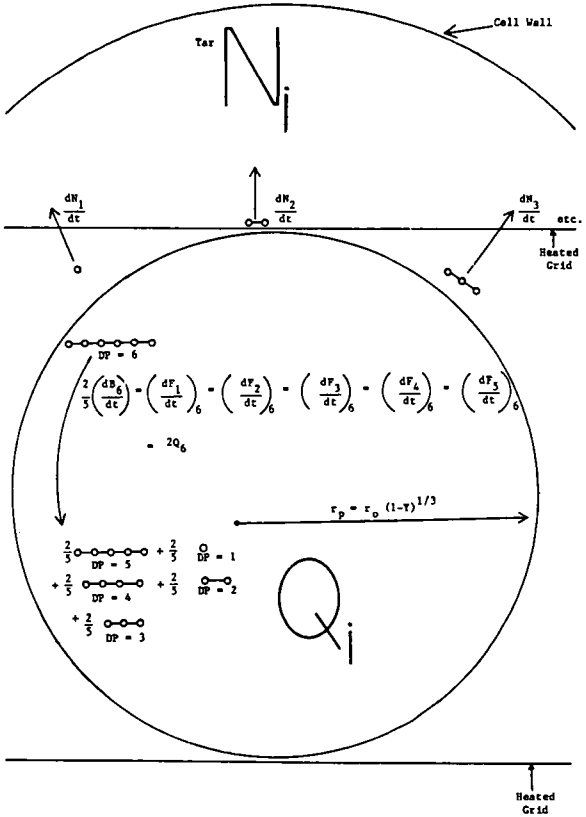

Figure 2. Typical Features Considered in the Depolymerization Theory.

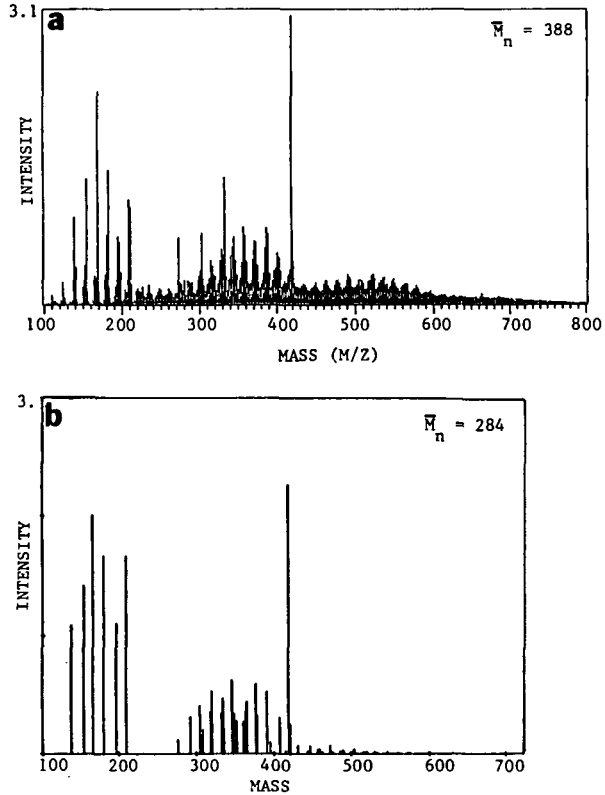

Figure 3. Molecular Weight Distribution for Lignin Tar Produced at 500°C and 2 torr. a) FIMS Result, b) Theoretical Prediction.

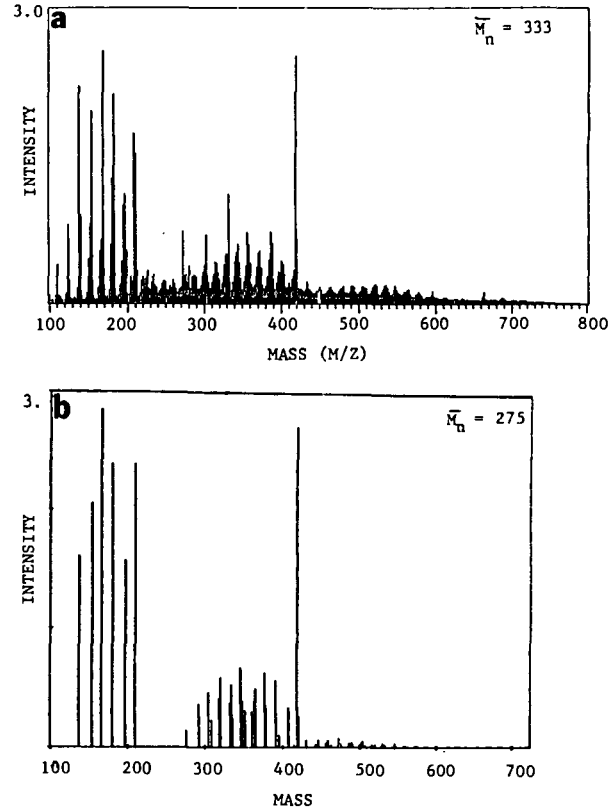

Figure 4. Molecular Weight Distribution for Lignin Tar Produced at 650°C and 2 torr. a) FIMS Result, b) Theoretical Prediction.

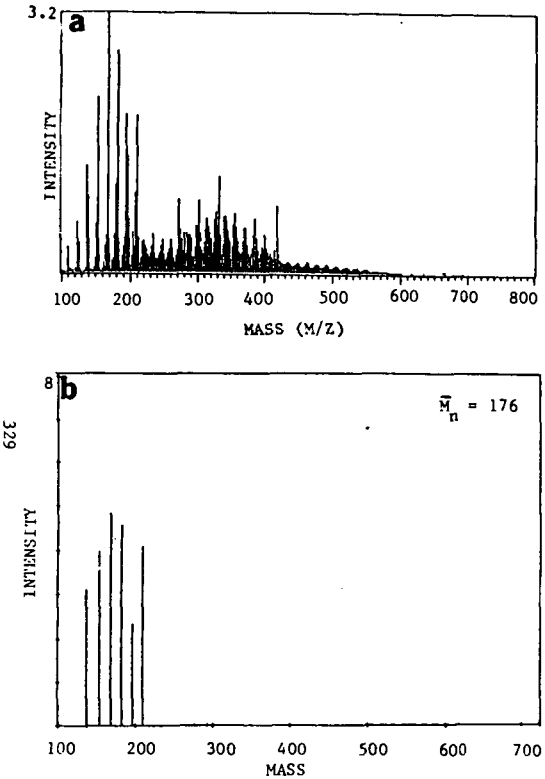

Figure 5. Predicted Molecular Weight Distributions for Lignin Tars Produced at 550°C. a) P = 2 torr, b) P = 4 atm.

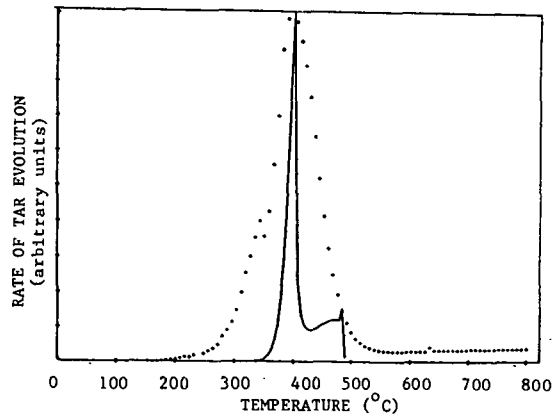

Figure 6. Constant Heating Rate Pyrolysis of Lignin. Heating Rate = 30°C/min. Solid Line is Theoretical Prediction.

MODELING OF PHYSICAL AND CHEMICAL PROCESSES DURING PYROLYSIS OF A LARGE BIOMASS PELLET WITH EXPERIMENTAL VERIFICATION

R. Chan and B.B. Krieger
Dept. of Chemical Engineering, Univ. of Washington
Benson Hall BF-10 Seattle, WA 98195

INTRODUCTION

A desire for optimal energy recovery from biomass has led to furnace simulation (1) and interest in chemicals production has led to biomass gasifier modeling (2). However, global considerations employed in these models give little insight into fundamental physical and chemical processes occuring in individual biomass particles during devolatilization. In previous studies addressing these processes, the emphasis has been on burning times (3), heat transfer rates (4), and weight loss rates (5) rather than detailed prediction of volatiles composition during pyrolysis. Detailed intrinsic kinetics studies of small biomass particles to determine pyrolysis product distribution as a function of temperature and time have been conducted (6,7). However, the results were correlated with Arrhenius type equations using best-fit parameters rather than parameters related to chemical structure. The latter is a difficult task given the diverse physical nature of biomass (8) and the complex molecular structure of the natural polymers of which it is composed (9). Indeed, the effects of particle size and physical microstructure (anisotropy) on devolatilization have not been systematically investigated in experiments, nor modeled using fundamental principles. To what extent the internal geometry of the wood influences the rates of heat and mass transfer, and thus the reaction products' composition, is largely unknown. Of particular importance is the ability to predict the relative proportions of char, tar, and gas (and components therein) that result from a given biomass thermal conversion process and given feedstock.

The goal of this work is to use fundamental considerations to predict changes in biomass pyrolysis product composition. The approach taken is to model a single, well-characterized biomass pellet under varying conditions during pyrolysis. This model can then be used to refine the gasifier and combustor models when a suitable distribution function for the feedstock characteristics is determined. Independent variables are feedstock characteristics (particle size, density, moisture, composition) and thermal conversion process characteristics (heating rate, diluent gas composition). Dependent variables predicted are instantaneous particle temperature and density profiles, gas and tar release rates, and char yields as well as ultimate yields.

For verification of the model, experiments were conducted according to a Box-Behnken design(10). A 1-D model is presented here for comparison with the experiments, and a 2-D model is being developed. Understanding gained from this model will aid in process design for biomass gasification, wood combustor design, as well as aid in fire safety.

BRIEF EXPERIMENTAL DESCRIPTION

The experimental apparatus is described in detail elsewhere (11-13). Briefly, it is a single particle, 1-D reactor. One face of a well-characterized cylinder of wood, compressed sawdust, cellulose, or lignin is heated by a combustion- level radiant heat source (4-12 cal/cm^2-s). As the temperature front at which reaction occurs moves inward, volatile species flow toward the heated face under a slight pressure gradient. The escaping volatiles reduce the incident radiation and the time- dependent magnitude of this effect is

quantified (11). The progress of the temperature front is monitored by 3 thermocouples at 2, 4, and 6 mm from the surface and the surface temperature is measured with an infra red pyrometer. Density profiles along the length of the pellet (integrated over the diameter) are taken via an X-ray technique.

Outflowing volatiles are rapidly quenched by helium and swept to a cold trap where water and tars are collected and analyzed in detail (11) as a time-integrated sample . Uncondensed gases are sampled every 3-15 sec by an automatic gas chromatographic sampling valve which also triggers the X-ray device. Char and gases are also analyzed in detail.

Although the experimental results are intriguing, especially the effects of anisotropy, they are described elsewhere (11). The major emphasis in this preprint is on the formulation and validation of the mathematical model. Other modeling details and aspects such as sensitivity analysis are also presented elsewhere (11,13).

MATHEMATICAL MODEL

An analysis similar to that of Russel, et al (14) was done (11,13) to determine the characteristic times for physical and chemical rate processes in a devolatilizing wood particle. For a 1 cm particle, conduction heat transfer to the interior is two orders of magnitude slower than chemical reaction at high temperature. However, the devolatilization reaction rate is comparable to the heat transfer rate at low temperature. Because the net conduction rate is strongly influenced by reaction product outflow and therefore the reaction rate, a fully unsteady model with variable properties was developed.

Heat Transfer Model

A one dimensional energy balance on the devolatilizing particle is schematically shown in Fig. 1. A time-varying radiant heat flux (Q_1), uniform in the radial direction, heats the face of the particle. Conduction (Q_4) is offset by volatiles outflow (Q_6). The volatiles are assumed to be in thermal equilibrium with the solid behind the reaction front as they flow outward, and are assumed to flow in one direction only[1].

The heats of reaction for wood are not well-known and they have been observed to be functions of particle size (15). In this model, the latent heat of water is treated as a heat of reaction(Q_5), and the heat of the devolatilization reaction (lumped with Q_5) is treated as a parameter using published values as bounds (16).

In the radial direction, the cylinder is considered insulated and impermeable. The heated face boundary condition includes radiation heat loss (Q_3) and convection heat loss (Q_2) which is described using the carrier gas flowrate. The outflowing CO_2 and H_2O absorb the incident radiation. This phenomena is treated using an estimated absorption coefficient for water in the model, and the incident radiation is reduced by an amount corresponding to the instantaneous water outflow.[2] The unheated face is considered impermeable to volatiles owing to the imposed pressure. Radiative (Q_8) and convective heat loss (Q_7) at this surface are treated, however. The film heat transer coefficient at each face was calculated using Nusselt number correlations and the properties and flowrate of helium at conditions of the experiments.

---

[1] It has been verified by Lee, et al, (17).

[2] Experimental verification of the net radiation arriving at the surface during a typical run was accomplished using a Medtherm heat flux gauge. These results were matched to the model using a value for the absorption coefficient which was a best-fit parameter.

For most previous modeling studies, the thermal conductivity and heat capacity of wood were modeled as linear functions of the initial and final (char) values (18) using either the porosity or density change (18-21). It should be observed, however, that these models require a final char density, heat capacity, and conductivity for every case considered, restricting their utility and predetermining the calculated char yield. Additionally, in this study experimental measurements of temperature profiles as a function of time indicated that the thermal conductivity was an order of magnitude higher than would be predicted if it were a function of density alone. Unfortunately, few measurements of wood thermal properties have been made at high temperature because of the attendant chemical reaction. Thermal conductivity was measured for our samples at low temperatures and a model analogous to Birkebak and Ozil (22) was developed to describe a radiation contribution to the temperature variation (11,13). The heat capacity and porosity of wood were described by linear functions of the density(11,13).

Chemical Reaction Model

A schematic of the chemical reactions considered and the lumping scheme for gas, tar, and secondary gases is given in Table 1. Rate coefficients for reactions 1,2 and 4 were taken from Ref. (6). Tar cracking reaction rates (k_5) were taken from Refs. (23) and (24) and alpha and beta are adjustable. The char production rate (k_3) is estimated from the work of Shafizadeh, who has measured the arithmetic sum of char production and gas production (25). In this work k_3 must be viewed as a parameter, and as discussed below, the model is extremely sensitive to its value. Water production by evaporation and dehydration reactions are lumped (k_4) and treated as an activated process. The generation term in the energy equation contains the heat of vaporization of water, since it is larger than the heats of reaction measured for wood (15,16).

Mass Transfer Model

In previous models, with a single reaction step (weight loss kinetics), the product distribution is unaltered by the presence or absence of a finite mass transfer rate (26) since only a lumped gas species is described. The only possible implication of a slow mass transfer step is a delayed appearance of the volatiles. The experimental studies (11) indicated that a mass transfer resistance was not significant for heating parallel to the grain direction. Since the model is one dimensional, anisotropy is not treated and inclusion of a mass transfer resistance at this stage is not warranted. The previous analysis of characteristic times for mass transfer is consistent with this observation and the rather open porous structure of wood. For comparison to experiment, the volatiles mass flux is computed as the instantaneous integral over the pellet length of the local total change in density (11,13).

Numerical Method and Equations

Limited space in the preprint prevents the presentation of the detailed equations. However, earlier versions of the model equations appear in Ref. (11) and the current model will be detailed in a forthcoming publication (13). The coupled partial differential equations for the pellet temperature, and species concentrations are solved in dimensionless form using a GEARB package (Finlayson,1980). For ease of comparison with experimental results, in this paper model predictions are given in dimensional form. The cases of thick pellets heated by high heat flux result in very sharp temperature and reaction fronts which lead to "stiff" systems of equations. Computation times and comments appear in Refs. 11 and 13.

RESULTS AND DISCUSSION

Comparison of the measurements to model predictions of the unsteady temperature profile as a function of time at 3 locations are shown in Fig. 2 for the case of an intermediate heat flux and the thinnest particle, 0.5 cm. The model overpredicts the temperature at short reaction times, but satisfactorily predicts the pseudo-steady temperatures at several depths after 200-300 secs. For other cases, similar overprediction occurs early in the pyrolysis, but the steady state temperatures are in agreement with experiment even for the highest heat flux and thickest particle. Previous studies (5,18) reported only predictions of steady state temperatures. It is felt that refinement of the absorption model for the net radiant heating of the wood surface will enhance agreement of temperature profiles in the early reaction period (11).

Fig. 3 presents the comparison of predicted gas release rate to experimental measurements for the same case as Fig. 2. Only uncondensed gas flux (not tar and water) is presented in the figure. As can be seen both the magnitude and shape of the volatiles release curve agree rather well with experiment. Correction of the temperature overprediction discussed earlier will delay the predicted gas release, in better agreement with experiment.

Extensive comparisons between model and experiment cannot be presented; however, similar agreement to that shown in Figs. 2 and 3 exists for most cases studied by experiment. Numerical difficulties are encountered for the cases with the sharpest fronts, i.e., steepest temperature gradients resulting from high heat flux and thick samples. Oscillations in the temperature and density profiles occur and a refinement of the numerical methods is indicated (27). However, these oscillations have little effect on the prediction of ultimate product distribution. As shown in Table 2, there is satisfactory agreement between predicted and measured gas, tar, and char yield for most cases. Agreement between these values was substantially improved when the experimental mass balance on water was very carefully analyzed and when the moisture release rate in the chemical reaction model and the energy balance was included.

A significant advance resulting from this modeling approach is that it is unnecessary to assume or measure a final value for char yield and thermal properties. Since char deposition is explicitly treated in the chemical reaction model, it is of interest to examine Fig. 4 in which the local density of char is presented as a function of reaction time for a case similar to those previously discussed. There is a slightly greater fraction of char produced when the reaction front is deeper in the sample, owing to the reduced heating rate experienced there. This is consistent with general observations in coal and wood pyrolysis that indicate char yield increases with slower heating. Since no char gasification reactions are currently incorporated into the reaction model, the char deposited near the surface of the sample retains its initial density throughout the reaction period. While it was foreseen that predictions of this nature could be confirmed with the X-ray density profiles, the resolution of this method is not sufficient to confirm this prediction.

The rate coefficient used for the char deposition reaction is estimated from the work of Shafizadeh (25). Behind the reaction front the deposited char insulates the unreacted wood and char thermal conductivity determines the subsequent temperature profile and rate of pyrolysis. Thus, the model is quite sensitive to both the value of the rate coefficient for char deposition as well as the model for the variation of wood and char thermal conductivity with density and temperature. If too little char is predicted, the char density is too low resulting in too slow a pyrolysis. If the char thermal properties are

incorrect as a function of temperature, the reaction can terminate prematurely or runaway can occur. A definite need exists for information on char deposition rates from carbonizing various fuel species (28), as well as on char thermal properties over a wide range of temperatures and porosities.

SUMMARY

A mathematical model of wood pyrolysis has been presented that is in satisfactory agreement with experimental reaction product distributions over a range of conditions of practical importance for gasification and combustion. Both chemical and physical processes are described using fundamental principles. Inclusion of water release and char deposition chemical reactions results in predictions of ultimate product distributions (gas, tar, and char yields) that are in good agreement with experiment and can aid in optimization of processes to maximize or minimize tar production. Predictions of products instantaneously released from a single wood pellet are in fair agreement with experiment. Computational difficulties are encountered for the cases with the steepest temperature gradients.

Previous studies (29) using a complex kinetic mechanism and heat transfer in a wood slab made no comparison to experimental results. Thus, this study provides both a data base (11) and a fundamental modeling approach that will enhance the understanding of the effects of physical properties and processes on the chemistry of devolatilizing biomass. Presentation of sensitivity analyses and further verification comparisons of the model are presented in a forthcoming article (13). Currently, pyrolysis product distribution as a function of particle size can be predicted only for the 1-D case. Extension of the model and experiments to realistic cases using 2-D samples is planned.

ACKNOWLEDGEMENTS

The authors would like to acknowledge the financial support of the Department of Energy, Solar Energy Research Institute. In addition, the helpful suggestions of Prof. Bruce Finlayson are gratefully acknowledged.

LITERATURE CITED

(1) Adams, T.N., Comb. and Flame, 1979, 34, 47-61.
(2) Bacon, D.W. J. Downie, J.C. Hsu, J. Peters, paper presented at "Fundamentals of Thermochemical Biomass Conversion: An Intl. Conference," Solar Energy Research Institute, Estes Park, Colo., Oct. 1982. To be published as a book, 1983.
(3) Phillips, A.M. and H.A. Becker, Comb. and Flame, 1982, 46, 221-251.
(4) Kanury, A.M., and P.L. Blackshear, Jr., Comb. Sci. and Tech., 1970, 18, 339.
(5) Kung, H.C., Comb. and Flame, 1972, 18, 185-195.
(6) Hajaligol,M.R., W.A. Peters, J.B., Howard and J.P. Longwell, Proc. - Specialists Workshop on Fast Pyrolysis of Biomass, Solar Energy Res. Inst., Golden, Colo., 1980.
(7) Iatriadis, B., and G.R. Gavalas, I.E.C. Prod. Res. Dev., 1979, 18, 127.
(8) Bain, R., "Beneficiation of Biomass for Gasification and Combustion", SERI/TR-33-239, A Survey of Biomass Gasification, Vol. II, 1979.
(9) Milne, T., "Pyrolysis - Thermal Behavior of Biomass Below 600 C", SERI/TR-33-239, A Survey of Biomass Gasification, Vol. II, 1979.
(10) Box, G.E.P. and D.W. Behnken, Technometrics, 1960, 2(4), 455.
(11) Chan, W.C.R., Ph.D. Thesis, University of Washington, Dept. Chem. Engrg., 1983.

(12) Chan, W.C.R., and B.B. Krieger, Chemical Reaction Engineering - Boston, 1982, ACS Symp. Ser. 196, 459.
(13) Chan, W.C.R., and B.B. Krieger, Mathematical Modeling of Biomass Pyrolysis, to be published, 1983.
(14) Russel, W.A., D.A. Saville, and M.I. Greene, AICHE J., 1979, 25, 65.
(15) Roberts, A.F., 13th Symp. (Intl.) on Combustion, Comb. Inst., 1971, 893.
(16) Tang, W.K., Ph.D. Dissertation, University of Wisconsin, 1964.
(17) Lee, C.K., R.F. Chaiken, and J.M. Singer, 16 Symp. on Combustion, Comb. Inst., 1976, 1459.
(18) Kansa, E.J., H.E. Perlee and R.F. Chaiken, Comb. and Flame, 1977, 29, 311.
(19) Kung, H.C. and A. Kalelkar, Comb. and Flame, 1973, 20, 91.
(20) McClean, J.D., Amer. Soc. of Heat and Vent. Eng. Trans., 1941, 47.
(21) Wong, P.T.Y., For. Prod. J., May, 1964, 195-198.
(22) Birkebak , R.C. and E. Ozil, Studies in Heat Transfer, McGraw-Hill, 1979.
(23) Sakai, T. I.E.C. Prod. Des. Dev., 1971, 10, 305.
(24) Froment, G.F., Chem. Eng. Sci., 1981, 36, 1271-1282.
(25) Shafizadeh, F., personal communications, 1977-1983.
(26) Fan, L., L.S. Fan, K. Tojo and W.P. Walawender, Can. J. Chem. Engrg., 1978, 56, 603.
(27) Finlayson, B.A., Non-Linear Analysis in Chem. Engrg., McGraw-Hill, N.Y., 1981.
(28) MacKay, D. M. and P.V. Roberts, Carbon, 1982, 20(2), 87-94; and 95-104.
(29) Panton, R.L. and J.G. Rittman, 13th Symp. on Combustion, Combustion Institute, 1970, 881.

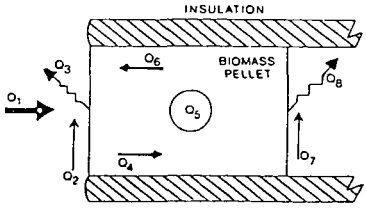

Fig. 1 - Schematic diagram of the heat transfer model.

TABLE 1

CHEMICAL REACTION MODEL

Reaction	Frequency Factor, s^{-1}	E_A, kcal/mol
$S \rightarrow G_1$	1.3×10^8	33.5
$S \rightarrow T_1$	2.0×10^8	31.79
$S \rightarrow C$	1.08×10^7	29.
$M \rightarrow W$	5.13×10^6	21.
$T_1 \rightarrow \alpha G_2 + \beta T_2$	1.48×10^6	27.29

Lumped Species Symbol	Identification
S	solid wood
C	char, high molecular weight tar (non-volatile)
M	moisture and chemically bound water in wood
W	vaporized water and released water
G_1	primary gases, e.g., CO_2, some CO, CH_4(?)
T_1	primary tar, e.g., phenols, levoglucosan
G_2	secondary gases, e.g., some CO, C_2H_4, C_2H_2, etc.
T_2	secondary tars, e.g., condensed aromatics (volatile)

α, β are adjustable parameters (stoichiometric coefficients).

TABLE 2
ULTIMATE PRODUCT DISTRIBUTION COMPARISON
EXPERIMENTAL RESULTS AND MODEL PREDICTIONS

1) For L = 0.5 cm, Heat Flux = 4 cal/cm^2-sec.

	Char	Tar*	Gas
Model	21.45	54.78	23.77
Expt.	18.05	62.33	19.63

2) For L = 1.0 cm, Heat Flux = 2 cal/cm^2-sec.

	Char	Tar*	Gas
Model	28.65	58.47	12.88
Expt.	25.12	62.37	12.52

3) For L = 1.5 cm, Heat Flux = 4 cal/cm^2-sec.

	Char	Tar*	Gas
Model	27.49	51.78	20.73
Expt.	22.82	53.98	23.20

* The tar yield includes water produced from the reactions but excludes water from the moisture evaporation.

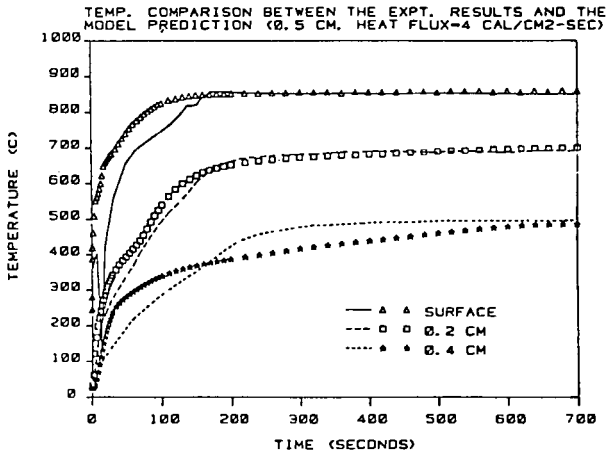

Fig. 2 - Temperature profile comparison - experiment (dashed lines) and model prediction (symbols) - 0.5 cm; ρ = .37 g/cc; initial thermal conductivity = 3.8 x 10^{-4} cal/cm-s-^{o}K

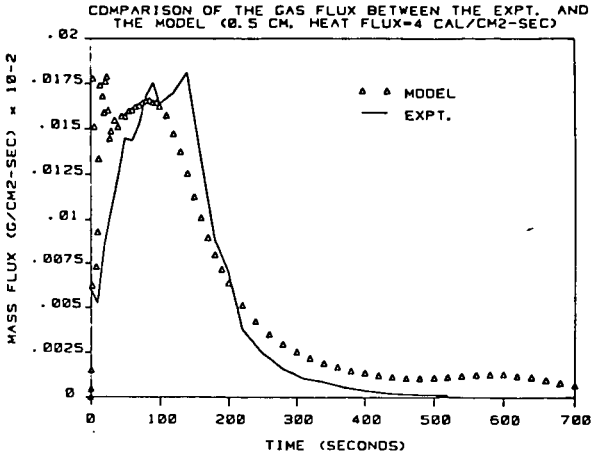

Fig. 3 - Total gas flux comparison - same conditions as Fig. 2

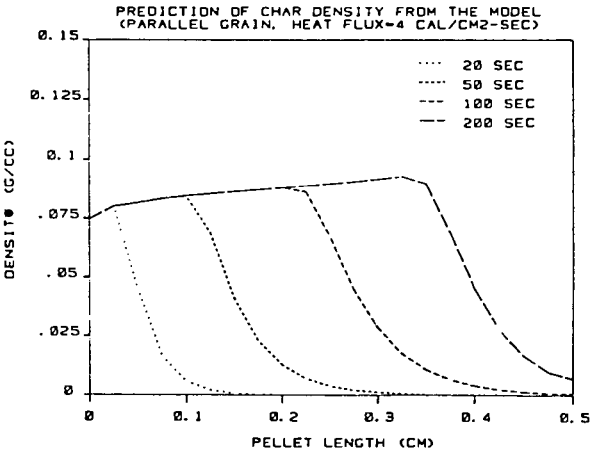

Fig. 4 - Predicted char deposition as a function of time - same conditions as Figs. 2 & 3.

A PHASE-CHANGE APPROACH TO MACRO-PARTICLE PYROLYSIS OF CELLULOSIC MATERIALS.

R. E. DEROSIERS and R. J. LIN

Chemical Engineering Department, Texas Tech University, Lubbock, TX 79409

INTRODUCTION

Biomass is a solid fuel with a high content (approx. 80%) of volatile matter (VM) as defined by standard proximate analyses. As a result, the devolatilization of the material introduced into any thermal conversion device is the most significant process occurring on a mass basis. From the viewpoint of reactor design, it would be convenient to have closed form expressions for the rate of pyrolysis of large particles of cellulosic materials suitable for the convective-heat-transfer environment of the packed or fluidized bed reactor.

The state of knowledge of the fundamental aspects of the pyrolysis "reaction" is advancing rapidly through kinetic studies on small, finely-divided samples in which physical transport considerations are minimized. The Arrhenius rate expressions resulting from these studies are reflective, it is hoped, of the intrinsic chemical reaction rates of pyrolysis processes. The high cost of comminution of feedstock to small mesh sizes however, dictates against the large scale conversion of biomass in this form. Thermal conversion of cellulosic materials in packed or fluidized beds will most likely be accomplished with particle sizes in the range of one to eight cm. With dimensions of that magnitude, the relative rates of chemical and transport processes must be considered.

An indication of the disparity in chemical versus heat transfer rates is afforded by the observation of "advancing front" behavior in the pyrolysis of cylindrical samples of biomass materials (Blackshear, Murty, 1966). The low thermal conductivity and high reactivity of biomass result in a narrow, advancing, reacting zone of pyrolysis. The sharply peaked reaction rate profile results from the depletion of VM in the char and a low temperature level in the virgin solid. The validity of this reaction rate profile is supported by experimental density and temperature profiles. If the reaction rate was slower,

the density profile would be less sharply stepped. The acceleration of the heat transfer rate in the virgin solid would likewise result in a more gradual transition.

Several pyrolysis models have been proposed (Bamford (1946), Roberts (1963), Blackshear (1966), Maa (1973), Lee (1982)) in order to faithfully reproduce the detailed pyrolysis behavior of large samples of cellulosic materials. These usually involve the solution of coupled partial differential equations (PDE's) representing mass, energy, and momentum balances. These models may be classified into two general categories. Volumetric models (Fan, 1978) are the most sophisticated and complex. The rate of decomposition is calculated at the local temperature throughout the solid. Shrinking core models (Maa, 1973) take the advancing front behavior to the limit of an infinitesimally thin reaction zone. In the former case, the reaction is a source term in the conservation equations while in the latter case, the reaction rate appears as a boundary condition. The continuing effort to describe ever more accurately the complicated phenomena of pyrolysis will doubtless give rise to more complex models.

The complexity of the single-particle model used to describe the pyrolysis process will be augmented however, when this model is integrated into the simulation of a gasification reactor. Thus it is our goal to move in the direction of simpler, albeit less precise, models of macro-particle pyrolysis. Consider the computational burden involved in the simulation of a packed-bed reactor. The conservation equations for the bed require an iterative solution because of split boundary conditions. (For example, solid temperature at one terminus, and gas temperature at the other.) For each iteration of the equations for the bed, many evaluations of the reaction rate for the particle must be made. If the evaluation of this rate at each point requires a finite-difference solution of a set of coupled PDE's for the particle, then the calculation time becomes excessive.

The model considered below may be called kinetics-free in that no explicit consideration is given to the rate of pyrolysis. The controlling influence on the rate of decomposition is the heat transfer rate. The progress of the pyrolysis is followed by the rate of advance of a sharp boundary defined as the locus of points at a fixed pyrolysis temperature, T_p. The resulting model is similar in many respects to a phase change problem. In fact, the process may be considered as a change in phase from one solid form (wood) to another (char).

We have been investigating the suitability of such a model in decribing the pyrolysis of 0.5 to 2.5 cm cylindrical samples of natural and densified wood. The objectives of the work are:

1. Develop the proper forms of the relevant equations of change; select an appropriate set of dimensionless variables.
2. Develop efficient numerical schemes to integrate the coupled partial-differential equations and to generate temperature profiles and rate vs time curves.
3. Determine if the model can even crudely reproduce experimental temperature profiles and pyrolysis times without extensive curve fitting. That is, by selecting realistic values of physical parameters, can an a priori calculation produce feasible results.
4. Perform a sensitivity analysis to determine which parameters have the greatest influence on the rate of advance of the pyrolysis front.
5. Determine to what extent the model is capable of faithfully reproducing the details of pyrolysis phenomena even if some parameters must be curve-fitted.

THE PHENOMENA OF PYROLYSIS

Before considering the development of the phase-change model of pyrolysis, it is worthwhile to list some of the more important processes occurring in pyrolysis in order to assess their relevance to any simulation.

Reaction: The primary events of pyrolysis are being intensively studied and it is clear that considering pyrolysis as a single reaction with a fixed product slate is a gross oversimplification. The classification of species as primary and secondary products is far from complete. The expertise to predict in detail even the overall ("final") products of the process is not available. It is not even possible to predict in advance for any feed the precise char yield under different heating rates. It is therefore entirely reasonable to represent pyrolysis crudely as

$$\text{wood} = c \text{ char} + b \text{ volatiles}$$

Heat of Reaction: Thermodynamic arguments indicate quite clearly that the overall pyrolysis process is exothermic. TGA studies support this contention. There is some doubt however concerning the amount of char produced by primary and secondary events. The exothermicity is directly proportional to char production. It could be possible for example to have an endothermic primary reaction producing some char and mostly reduced gases such as CO, followed by an exothermic conversion to CO_2 and more carbon at a different location. Since the heat of pyrolysis depends on the spectrum of products, and the spectrum of products depends strongly on the conditions imposed to cause pyrolysis, it is not unreasonable to assume that the primary decomposition is endothermic. Indeed, when carried out under inert atmospheres, some differential scanning calorimetry studies have indicated that this is the case (Muhlenkamp (1975)).

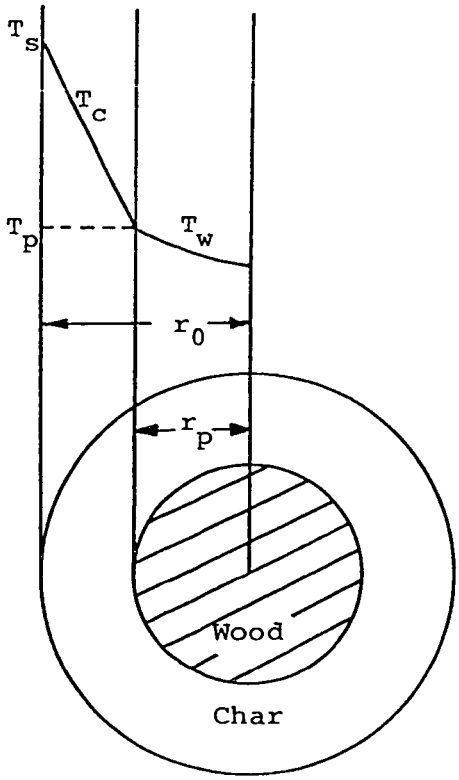

Figure 1: Pyrolysis Scheme of a Single Particle Under the Boundary Condition of First Kind

Reaction Rate: The possibility of representing the rate of decomposition of a mixture of linear polysaccharides and a cross-linked phenylpropane polymer with a single Arrhenius rate expression appears remote. At best it seems likely that a distribution of activation energies would be required. It is assumed below that the rate of decomposition is fast relative to the rate of heat transfer necessary to sustain the pyrolysis.

Geometry: Some shrinkage does occur during pyrolysis as evidenced by checking and pitting of char layers. But this effect will be ignored and constant diameter assumed. Of more importance is the porosity of chars and the resulting effects on density and resistance to gas flow. In this work, the porosity is assumed sufficiently great that the hydrodynamics of gas flow can be ignored. A cylindrical particle geometry has been used in this study.

Gas Flow: A unidirectional, outward flow of non-condensible gases must occur during pyrolysis. But condensible species such as water may be forced inward and result in a net flow towards the cooler, inner region of the cylinder. Water condensing in the layers immediately adjacent to the pyrolysis zone has been proposed by some investigators to explain the delay in the development of the inner temperature profile of samples of pressed cellulose. This inward flow of condensibles has not as yet been considered in the development of the phase-change model but could crudely be accommodated by using a higher effective heat capacity for the unpyrolyzed solid. A better approximation could be made by considering two "phase" changes: in effect, a drying wave and a pyrolysis wave passing through the sample.

THE PHASE CHANGE MODEL OF PYROLYSIS

The simulation of pyrolysis proposed here seeks to avoid the mathematical complexity of the volumetric model as well as the pre-selection of the pyrolysis rate inherent in the steady-state, moving-boundary approach. Maa (1973), for example, uses a kinetic expression for the rate of pyrolysis, but fixes the temperature at which it is evaluated, resulting in a steady state. The pseudo steady-state is probably a reasonable assumption for a large piece of wood (a log or beam) but is probably not valid for a one-cm particle.

To proceed, we make the following assumptions:

1. The pyrolysis reaction may be considered simply as:

   $$\text{Feed} = b\ \text{Gas} + c\ \text{Char}$$

   Here "Gas" refers to all volatile products, and "char" to the completely devolatilized solid. The reaction occurs instantaneously when the solid is raised to a fixed temperature, T_p.
2. Heat is conducted through the char layer to a surface separating char and unpyrolyzed solid. This surface is defined as the locus of points at $T = T_p$. At this surface, the temperature is continuous, but a jump occurs in the temperature gradient, the magnitude of which is determined by the heat of pyrolysis and the thermal properties of the two solids.
3. The temperature of escaping volatiles is always equal to the local char temperature, T_c.

Although not necessary, the following assumptions have been made for convenience in this initial development:

4. Thermal properties (heat capacity, conductivity) and density are assumed constant at an effective or average value.
5. Cylindrical geometry.
6. Specified surface temperature (B.C. of 1st kind).

The mathematical formulation of the model is derived from the equation of change for energy. In the char layer

$$\frac{\partial}{\partial t}(\rho_c\, c_{pc}\, T_c) + \frac{\partial}{\partial \underline{r}} \cdot (-k_c \frac{\partial T}{\partial \underline{r}} + \rho_g\, c_{pg}\, T_c\, \underline{u}_g) = 0$$

The third term is the convective flux of gas. A mass balance at any radial location yields an expression for the gas flux.

$$\rho_g\, u_g = -\, b \rho_w \frac{r_p}{r} \frac{dr_p}{dt}$$

where r_p is the location of the advancing front. Ordinary conduction occurs in the fresh solid region. (Hereafter referred to as wood.) The system of equations to be solved in each region in cylindrical geometry are

$$\frac{\partial T_c}{\partial t} = \alpha_c \left(\frac{\partial^2 T_c}{\partial r^2} + \frac{1}{r} \frac{\partial T_c}{\partial r} \right) + b \frac{\rho_w}{\rho_c} \frac{C_{pg}}{C_{pc}} \frac{r_p}{r} \frac{dr_p}{dt} \frac{\partial T_c}{\partial r} \qquad r_p < r < r_o \quad t > 0$$

With no gas flux in the core:

$$\frac{\partial T_w}{\partial t} = \alpha_w \left(\frac{\partial^2 T_w}{\partial r^2} + \frac{\partial T_w}{r \partial r} \right) \qquad 0 < r < r_p \quad t > 0$$

$$\text{IC:}\quad T_w = T_i \qquad 0 < r < r_o \qquad t = 0$$

$$\text{BC: (1)}\quad T_c = T_s \qquad r = r_o \qquad t > 0$$

$$\text{(2)}\quad T_c = T_w = T_p \qquad r = r_p \qquad t > 0$$

$$\text{(3)}\quad k_w \frac{\partial T_w}{\partial r} - k_c \frac{\partial T_c}{\partial r} = \rho_w (\Delta H) \frac{dr_p}{dt} \qquad r = r_p \qquad t > 0$$

$$\text{(4)}\quad \frac{\partial T_w}{\partial r} = 0 \qquad r = 0 \qquad t > 0$$

The system of equations is non-linear because of the convective term as well as the third boundary condition (Carslaw, Jaeger, 1959). It is of the same form as a simple phase change problem, with the exception of the convective term. Exact solutions on infinite domains are available (Stefan, 1891; Ockendon and Hodgkins, 1975). Comparable problems on finite geometries are usually solved numerically. Extensive bibliographies are available (Selim, Roberts, 1981; Wilson, et. al., 1978). The numerical procedure developed by Roberts (1981) is used here. This procedure is facilitated by the introduction of the following dimensionless parameters:

$$R = 1 - r/r_o \qquad \tau = \alpha_c\, t/r_o^{\,2}$$

$$U = \left(\frac{k_c}{k_w}\right) \frac{T_c - T_p}{T_p - T_i} \qquad V = \frac{T_w - T_p}{T_p - T_i}$$

$$T_s{}^* = \frac{k_c}{k_w}\ \frac{T_s - T_p}{T_p - T_i} \qquad T_i{}^* = \frac{T_i - T_p}{T_p - T_i} = -1$$

$$\alpha^* = \alpha_c/\alpha_w \qquad \Delta H^* = \frac{\alpha_c}{\alpha_w}\frac{\Delta H}{C_{pw}(T_p - T_i)}$$

$$B = 1 + b\frac{\rho_w}{\rho_c}\frac{C_{pg}}{C_{pc}}(R_p - 1)\frac{dR_p}{d\tau}$$

The dimensionless form of the system of equations is

$$\frac{\partial U}{\partial \tau} = \frac{\partial^2 U}{\partial R^2} + \frac{B}{R-1}\frac{\partial U}{\partial R} \qquad 0 < R < R_p \quad \tau > 0 \qquad (1)$$

$$\frac{\partial V}{\partial \tau} = \frac{1}{\alpha^*}\frac{\partial^2 V}{\partial R^2} + \frac{1}{R-1}\frac{\partial V}{\partial R} \qquad R_p < R < 1 \quad \tau > 0 \qquad (2)$$

$$\text{IC} \quad V = -1 \qquad 0 < R < 1 \quad \tau = 0 \qquad (3)$$

$$\text{BC} \quad U = T_s^* \qquad R = 0 \quad \tau > 0 \qquad (4)$$

$$U = V = 0 \qquad R = R_p \quad \tau > 0 \qquad (5)$$

$$\frac{dR_p}{d\tau} = \left(\frac{\partial V}{\partial R} - \frac{\partial U}{\partial R}\right)\frac{1}{\Delta H^*} \qquad R = R_p \quad \tau > 0 \qquad (6)$$

$$\frac{\partial V}{\partial R} = 0 \qquad R = 1 \quad \tau > 0 \qquad (7)$$

Finite Difference Formulation

The finite difference form of the numerical algorithm requires a finite, non-zero value of R_p. If a fixed surface temperature is imposed with $T_s > T_p$, then the Stefan analytical solution is used to obtain a starting position of the pyrolysis front. A standard explicit finite difference scheme is used to advance through the first time step and a Dufort Frankel scheme (which requires

temperatures at a previous time) is used for all subsequent time steps. If a time dependent surface temperature, beginning with $T_s < T_p$ is imposed, then the numerical integration of the straight-forward conduction problem with no pyrolysis front is implemented until the temperature at a finite value of R reaches T_p, at which time the Dufort Frankel scheme with a moving boundary is begun. Temperatures at points adjacent to either terminus R = 0 or R = 1, or the moving boundary are calculated with the usual approximations. The details are presented below.

In order to approximate the solution of the parabolic partial differential equations, (1) and (2), a network of grid points with equal size in the R-direction and equal size in the time step is established throughout the region $0 < R < 1$, $0 < \tau$.

A DuFort-Frankel scheme (Carnahan, 1969) was chosen to obtain a finite difference solution to the parabolic partial differential equations. Adequate accuracy was obtained with 21 grid points and $\Delta t/(\Delta R)^2 < 0.5$.

The DuFort-Frankel Scheme requires data from two previous time levels. The standard explicit scheme is used as a starting method to provide the required data. Eqs. (1) and (2) expressed in the standard explicit scheme (see Figure 2) are given by

$$\frac{U_{i,j+1} - U_{i,j}}{\Delta\tau} = \frac{U_{i-1,j} - 2U_{i,j} + U_{i+1,j}}{(\Delta R)^2} + \frac{B}{(i\Delta R - 1)} \frac{(U_{i+1,j} - U_{i-1,j})}{2\Delta R} \qquad i = 1,2,\ldots,M-1 \tag{8}$$

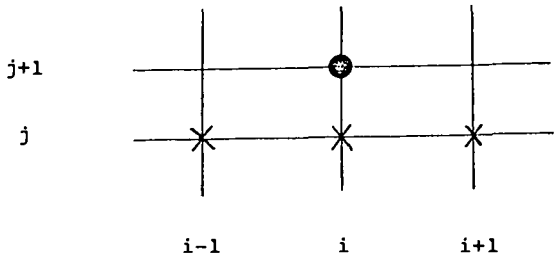

Standard Explicit Scheme

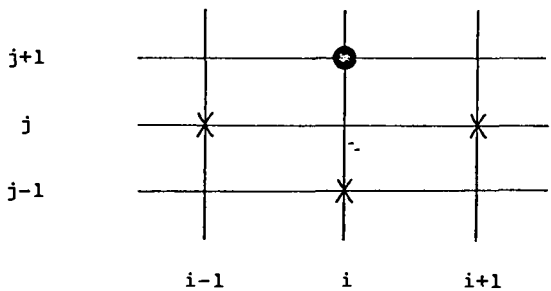

DuFort-Frankel Scheme

Figure 2: Graphic Description of Finite-Difference Scheme.

$$\frac{V_{i,j+1} - V_{i,j}}{\Delta\tau} = \frac{1}{\alpha^*} \frac{V_{i-1,j} - 2V_{i,j} + V_{i+1,j}}{(\Delta R)^2} +$$

$$\frac{1}{(i\Delta R - 1)} \frac{(V_{i+1,j} - V_{i-1,j})}{2\Delta R} \qquad i = M+2, M+3, \ldots, N-1 \qquad (9)$$

and M indicates the nearest grid point to the left of the pyrolyzing front (see Figure 3). These two equations are rearranged and solved for the unknown terms $U_{i,j+1}$ and $V_{i,j+1}$ to give:

$$U_{i,j+1} = (1 - 2\lambda)U_{i,j} + \lambda\left[(1 - \frac{B}{2(i - \frac{1}{R})})U_{i-1,j} + \right.$$

$$\left.(1 + \frac{B}{2(i - \frac{1}{R})})U_{i+1,j}\right] \qquad i = 1,2,\ldots,M-1 \qquad (10)$$

$$V_{i,j+1} = (1 - \frac{2\lambda}{\alpha^*})V_{i,j} + \frac{\lambda}{\alpha^*}\left[(1 - \frac{1}{2(i - \frac{1}{\Delta R})})V_{i-1,j} + \right.$$

$$\left.(1 + \frac{1}{2(i - \frac{1}{\Delta R})})V_{i+1,j}\right] \qquad i = M+2, M+3, \ldots, N-1 \qquad (11)$$

where $\lambda = \Delta\tau/(\Delta R)^2$.

Expressed in the DuFort-Frankel Scheme, Equations (1), (2) become

$$\frac{U_{i,j+1} - U_{i,j-1}}{2\,\Delta\tau} = \frac{U_{i-1,j} - U_{i,j+1} - U_{i,j-1} + U_{i+1,j}}{(\Delta R)^2} +$$

$$\frac{B}{(i\Delta R - 1)} \frac{(U_{i+1,j} - U_{i-1,j})}{2\Delta R} \qquad i = 1,2,\ldots,M-1 \qquad (12)$$

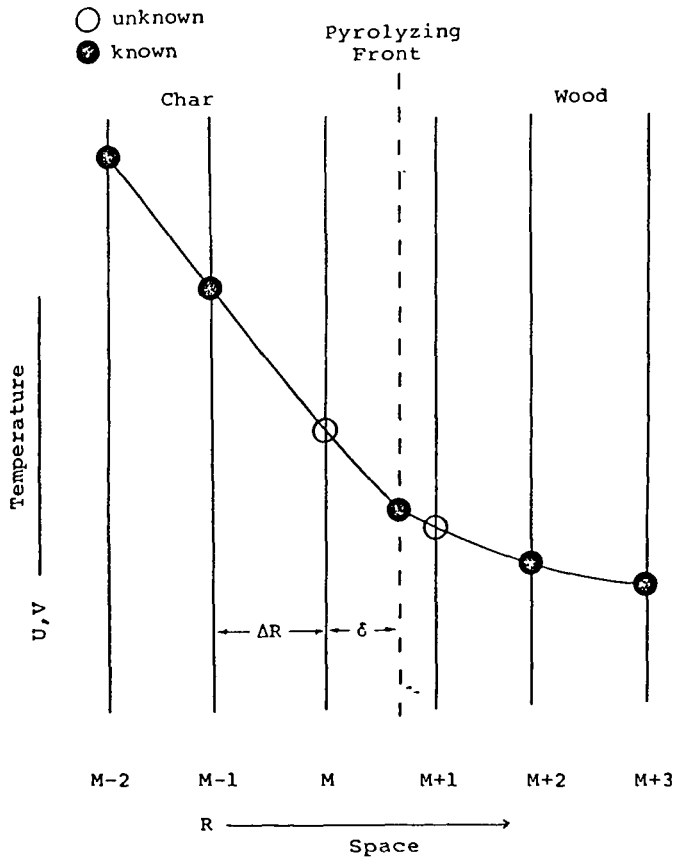

Figure 3: 3-Point Lagrangian Interpolation for the unknow temperature U_M, V_{M+1} Adjacent to the pyrolysis front.

$$\frac{V_{i,j+1} - V_{i,j-1}}{2\Delta\tau} = \frac{1}{\alpha^*}\frac{V_{i-1,j} - V_{i,j+1} - V_{i,j-1} + V_{i+1,j}}{(\Delta R)^2} +$$

$$\frac{1}{(i\Delta R - 1)}\frac{(V_{i+1,j} - V_{i-1,j})}{2\Delta R} \qquad i = M+1, M+2, \ldots, N \qquad (13)$$

Equations (12) and (13) are rearranged and solved for the unknown terms $U_{i,j+1}$, $V_{i,j+1}$ to give

$$U_{i,j+1} = \frac{1 - 2\lambda}{1 + 2\lambda} U_{i,j-1} + \frac{2\lambda}{1 + 2\lambda}\left[\left(1 - \frac{B}{2(i - \frac{1}{\Delta R})}\right)U_{i-1,j} + \right.$$

$$\left.\left(1 + \frac{1}{2(i - \frac{1}{\Delta R})}\right)U_{i+1,j}\right] \qquad i = 1, 2, \ldots, M-1 \qquad (14)$$

$$V_{i,j+1} = \frac{1 - \frac{2\lambda}{\alpha^*}}{1 + \frac{2\lambda}{\alpha^*}} V_{i,j-1} + \frac{\frac{2\lambda}{\alpha^*}}{1 + \frac{2\lambda}{\alpha^*}}\left[\left(1 - \frac{1}{2(i - \frac{1}{\Delta R})}\right)V_{i-1,j} + \right.$$

$$\left.\left(1 + \frac{1}{2(i - \frac{1}{\Delta R})}\right)V_{i+1,j}\right] \qquad i = M+1, M+2, \ldots, N \qquad (15)$$

The singularity of Equation (2) at R = 1 is prevented by using L'Hopital's rule to yield

$$\frac{\partial V}{\partial \tau} = -\frac{2}{\alpha^*}\frac{\partial^2 V}{\partial R^2} \qquad R = 1 \quad \tau > 0 \qquad (16)$$

This equation written in the standard explicit form is given by

$$\frac{V_{i,j+1} - V_{i,j}}{\Delta\tau} = \frac{2}{\alpha^*}\frac{(V_{i-1,j} - 2V_{i,j} + V_{i+1,j})}{(\Delta R)^2} \qquad (17)$$

and in the Dufort-Frankel Scheme by

$$\frac{V_{i,j+1} - V_{i,j-1}}{2\Delta\tau} = -\frac{2}{\alpha^*}\frac{(V_{i-1,j} - V_{i,j+1} - V_{i,j-1} + V_{i+1,j})}{(\Delta R)^2} \qquad i = N \qquad (18)$$

Equation (7) can be written in finite-difference form using a central difference approximation to give

$$\frac{V_{N+1,j} - V_{N-1,j}}{2\Delta R} = 0.$$

Combined with Equation (18) this yields an expression for the center-line dimensionless temperature

$$V_{N,j+1} = (1 - \frac{4\lambda}{\alpha^*})V_{N,j} + \frac{4\lambda}{\alpha^*} V_{N-1,j} \qquad R = 1 \qquad (19)$$

in the standard explicit form and

$$V_{N,j+1} = \frac{1 - \frac{4\lambda}{\alpha^*}}{1 + \frac{4\lambda}{\alpha^*}} V_{N,j-1} \quad \frac{\frac{8\lambda}{\alpha^*}}{1 + \frac{4\lambda}{\alpha^*}} V_{N-1,j} \qquad R = 1 \qquad (20)$$

in the DuFort-Frankel Scheme.

Grid Points M, M+1

The temperatures at grid points immediately adjacent to the pyrolyzing front (grid points M and M+1 in Figure 3) cannot be calculated by Equations (10)-(11) and (14)-(15). Instead, a three-point Lagrangian interpolation is used to determine these unknown temperatures.

$$U_{M,j} = \frac{-\delta}{(2\Delta R + \delta)} U_{M-2,j} + \frac{2\delta}{(\Delta R + \delta)} U_{M-1,j} \qquad i = M \qquad (21)$$

$$V_{M+1,j} = \frac{2(\Delta R - \delta)}{(2\Delta R - \delta)} V_{M+2,j} + \frac{(\Delta R - \delta)}{(3\Delta R + \delta)} V_{M+3,j} \qquad i = M+1 \tag{22}$$

Where

$$\delta = R_p - R_M = R_p - M\Delta R$$

Grid Points M = 1,2

When the pyrolyzing front is located within the first grid space, Equation (21) is not required, since the boundary value $U_{0,j}$ is already known.

If the pyrolyzing front is located within the second grid space, Equation (21) cannot be used because the required three points are not available. By assuming that the temperature profile within the char layer is quadratic in R, the derivatives U/ t, U/ R, ^{2}U/ R^2 in equation (1) can be approximated to yield.

$$\frac{U_{2,t+1} - U_{2,t}}{\Delta\tau} = \frac{2}{\Delta R(\Delta R + \delta)} U_{1,t} - \frac{2}{\Delta R(\delta)} U_{2,t+1} - \left(\frac{B}{\Delta R - 1}\right)\left(\frac{\delta}{\Delta R(\Delta R + \delta)}\right) U_{1,t}$$

$$- \left(\frac{\Delta R - \delta}{\Delta R(\delta)}\right) U_{2,t+1} \tag{23}$$

which can be solved for $U_{2,t+1}$

Advancing the Pyrolysis Front

Euler's method (Carnahan, 1969) is used to solve the energy balance across the pyrolyzing surface, Eq. 9. The march of the pyrolysis front is computed from the following finite difference form of Eq. 9.

$$R_p\Big|_{\tau=\tau+\Delta\tau} - R_p\Big|_{\tau} = \Delta R_p = \frac{\Delta\tau}{\Delta H^*}\left(\frac{\partial U}{\partial R} - \frac{\partial V}{\partial R}\right)\Bigg|_{R=R_p},$$

The temperature gradients are approximated by differentiation of the three-point Lagrangian interpolation formulas, Equations (21) and (22), to give

$$\left.\frac{\partial U}{\partial R}\right|_{R=R_p} = \frac{(\Delta R + \delta)}{(2\Delta R + \delta)\Delta R} U_{M-2,j} - \frac{(2\Delta R + \delta)}{(\Delta R + \delta)\Delta R} U_{M-1,j} \tag{24}$$

$$\left.\frac{\partial V}{\partial R}\right|_{R=R_p} = \frac{(3\Delta R - \delta)}{(2\Delta R - \delta)\Delta R} U_{M+2,j} - \frac{(2\Delta R - \delta)}{(3\Delta R - \delta)\Delta R} U_{M+3,j} \tag{25}$$

When the pyrolyzing front is within the first grid space, two point interpolation formulas are used to approximate the temperature gradient in the char layer.

$$\left.\frac{\partial U}{\partial R}\right|_{R=R_p} = - \frac{U_{1,j}}{R_p} \tag{26}$$

When the pyrolyzing front is located within the second grid space, a quadratic polynomial is used to approximate the temperature gradient in the char layer. The gradient at the pyrolyzing front is

$$\left.\frac{\partial U}{\partial R}\right|_{R=R_p} = \frac{-\delta}{\Delta R(\Delta R + \delta)} U_{1,j} - \frac{\Delta R + \delta}{\Delta R(\delta)} U_{2,j} \tag{27}$$

Since the temperature of the unreacted core is so close to the pyrolysis temperature when the pyrolyzing front moves into the last two grid spaces, a two point interpolation formula is used to approximate the temperature gradient in the wood layer. The temperature of the unreacted core is taken equal to the pyrolysis temperature and the temperature gradient in the wood layer at $R = R_p$ becomes equal to zero thereafter.

Since the advance of the front during the last time step may place it beyond $R = 1$, a three point Lagrangian interpolation formula is used to find the time required for complete the pyrolysis.

$$\tau_p = \frac{(1 - R_{p2})(1 - R_{p3})}{(R_{p1} - R_{p2})(R_{p1} - R_{p3})}\tau_1 + \frac{(1 - R_{p1})(1 - R_{p3})}{(R_{p2} - R_{p1})(R_{p2} - R_{p3})}\tau_2 + \frac{(1 - R_{p1})(1 - R_{p2})}{(R_{p3} - R_{p1})(R_{p3} - R_{p2})}\tau_3$$

Where R_{p1}, R_{p2}, R_{p3} = the last three computed R_p values.

τ_1, τ_2, τ_3 = the three times corresponding to the above values.

SENSITIVITY STUDY

Using the numerical procedures described above, temperature profiles at various times were generated. Sample profiles are illustrated in figure 4. The time required for the pyrolysis front to reach the centerline of the cylinder was defined as t_{pyr}.

The effect of each model parameter on the time required for complete pyrolysis was studied in order to determine its relative importance. A base case was constructed by selecting average values for the parameters (as listed in Table 1) and calculating the pyrolysis time. Values of t_{pyr} were then determined for several cases in which each parameter was varied individually. Sensitivity was defined as $\Delta t_{pyr}/\Delta p$, where Δp is the change in the value of the parameter studied from its base value. A negative sensitivity indicates increasing p will decrease t_{pyr}.

The results of the sensitivity study are summarized in Table 2 and illustrated in Figure 5.

Temperature Profile

With Convection Term.

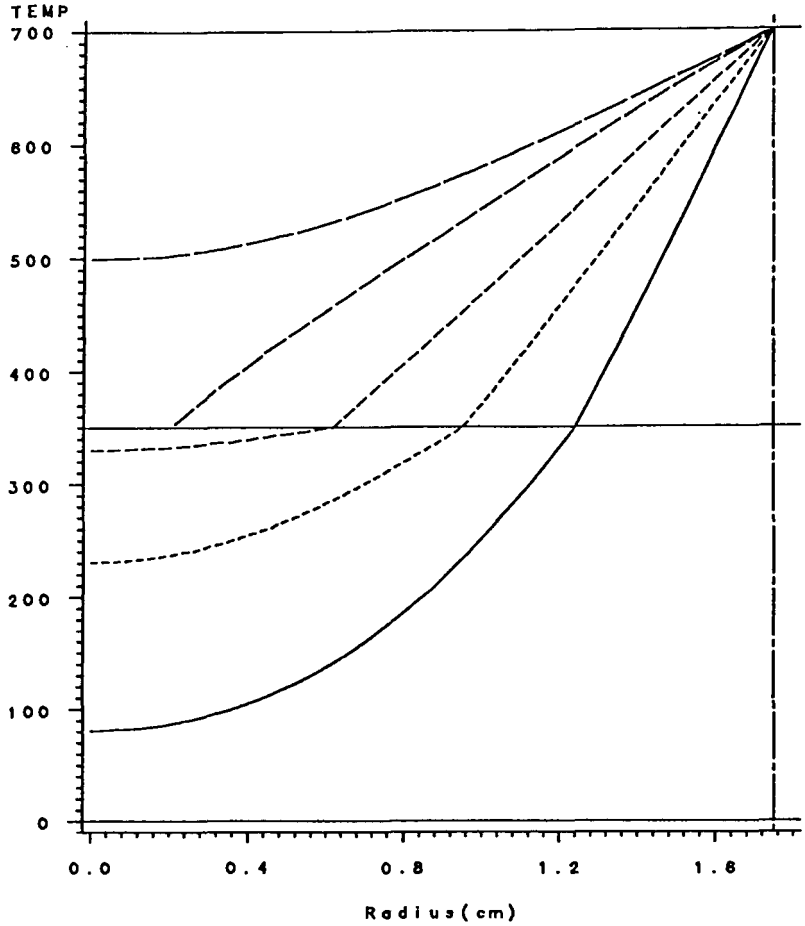

LEGEND: TIME ——— 1.978 ------- 3.892 ----- 5.806 ——— 7.72 ——— 9.634

Figure 4

Table 1

Typical Values of Model Parameters Used in Sensitivity Study

ρ_w	= 1230.0	Kg/M^3
ρ_c	$= \rho_w(1-b)$	
C_{pw}	= 1318.0	Joule/Kg
C_{pc}	= 991.6	Joule/Kg
k_w	= 0.2000	Joule/M-Sec-K
k_c	= 0.20	Joule/M-Sec-K
r_o	= 0.01	m
T_s	= 700.0	C
T_p	= 350.0	C
T_i	= 25.0	C
b	= 0.7	
ΔH	= 368200	Joule/kg of wood

Table 2

Relative Importance of Model Parameters for a Particle 2 cm in Diameter

Parameter	Sensitivity Range	Parameter Range Studied	Relative Importance
r_o	1.5 -- 3.0	0.5 - 2.0 cm	1
T_s	-38.1 -- -0.73	360 - 1050 C	2
k_c	-1.73 -- -0.46	0.1 - 0.4 Joule/M-Sec-K	3
ρ_w	1.0	615 - 2460 (Kg/M^3)	4
T_p	-0.66 -- -1.54	175 - 525 C	5
ΔH	0.5 -- 0.47	184100 - 763640 Joule/Kg	6
C_{pw}	0.28 -- 0.30	659 - 2636 Joule/Kg-K	7
k_w	-0.14 -- -0.07	0.1 - 0.4 Joule/M-Sec-K	8
C_{pg}	0.14 -- 0.13	600 - 2400 Joule/Kg-K	9
C_{pc}	0.07 -- 0.06	495.8 - 1983.2 Joule/Kg-K	10
b	-0.012 -- - 0.027	0.3 - 0.9	11
T_i	-0.0144 -- -0.015	0 - 300 C	12

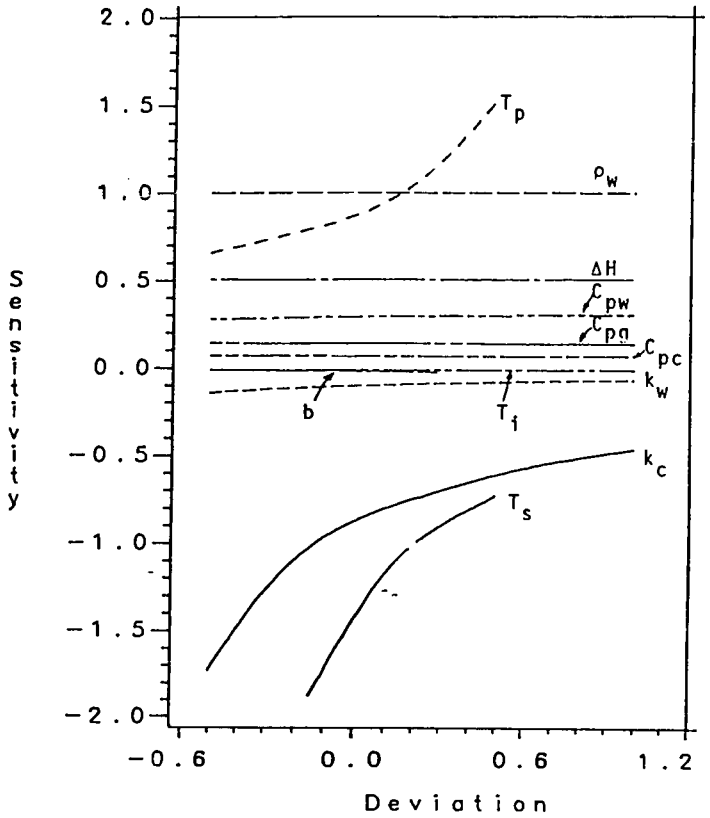

Figure 5 : Sensitivity of Model Parameters for a Particle of 2cm in Diameter

Particle Size and Density (r_o, ρ_w)

As expected, the pyrolysis time varied approximately quadratically with r (cylindrical geometry) and linearly with ρ_w indicating that for the size range studied, t_{pyr} is proportional to the mass of the sample.

Characteristic Temperatures (T_s, T_p, T_i)

For a particle 2 cm diameter, the imposed surface temperature has the greatest effect of all parameters in the determining pyrolysis time. When T_s is 525, 700, 875°C, the corresponding pyrolysis times are 8.8, 5.6, and 4.3 minutes. The pyrolysis temperature has a moderate influence on t_{pyr} when varied over a physically meaningful range. When T_p is varied from 263 to 350°C, t_{pyr} increases from 4.5 to 5.6 minutes. The initial temperature, T_i, has a negligible effect. The sensitivities of these parameters are illustrated in Figure 5. Plots of front position vs. time for a wide range of the parameters T_s, T_p, and T_i appear in Figures 6, 7, and 8.

Thermal Conductivities (k_c, k_w)

Due to the nature of the model, the thermal conductivity of the char is the most sensitive of all the physical properties considered. The thermal conductivity of the virgin solid however, has a negligible influence on the time required for complete pyrolysis. The comparison is best illustrated by the front position vs. time plots when the above parameters are varied (Figures 9, 10).

When k_c is varied from .1 to .4 J/msK t_{pyr} varies from 10 to 3 minutes. Over the same range of values for k_w, t_{pyr} varies from 6 to 5.2 minutes.

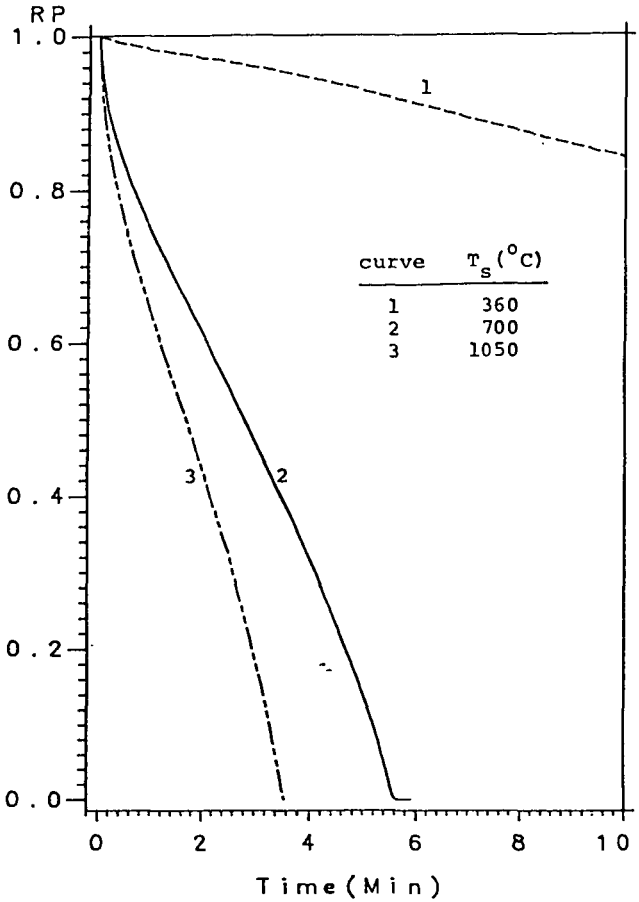

Figure 6: Pyrolyzing Front vs. Time curves at Three Surface Temperatures for a Particle of 2 cm Diameter

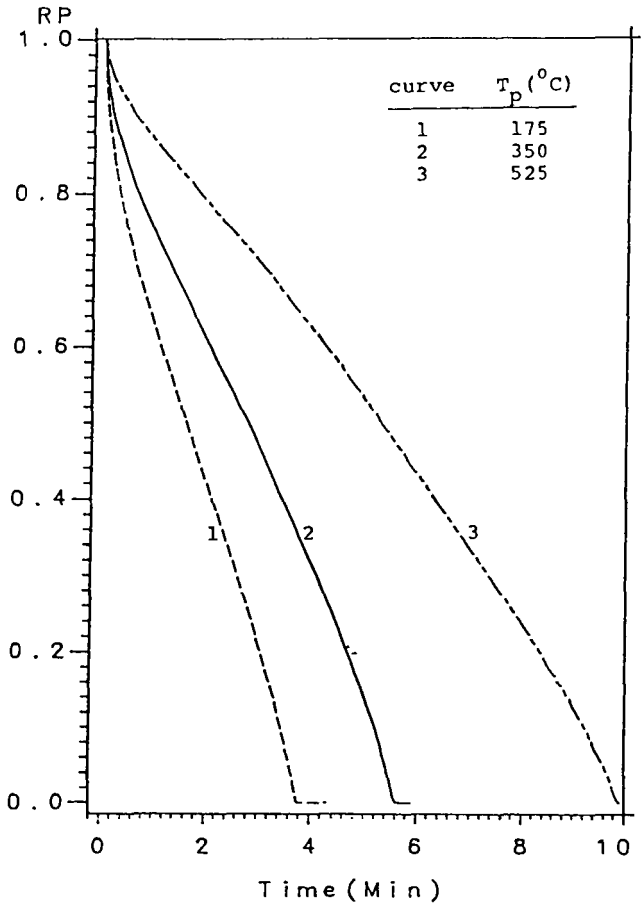

Figure 7 : Pyrolyzing Front vs. Time curves at Three Pyrolysis Temperatures for a Particle of 2 cm Diameter

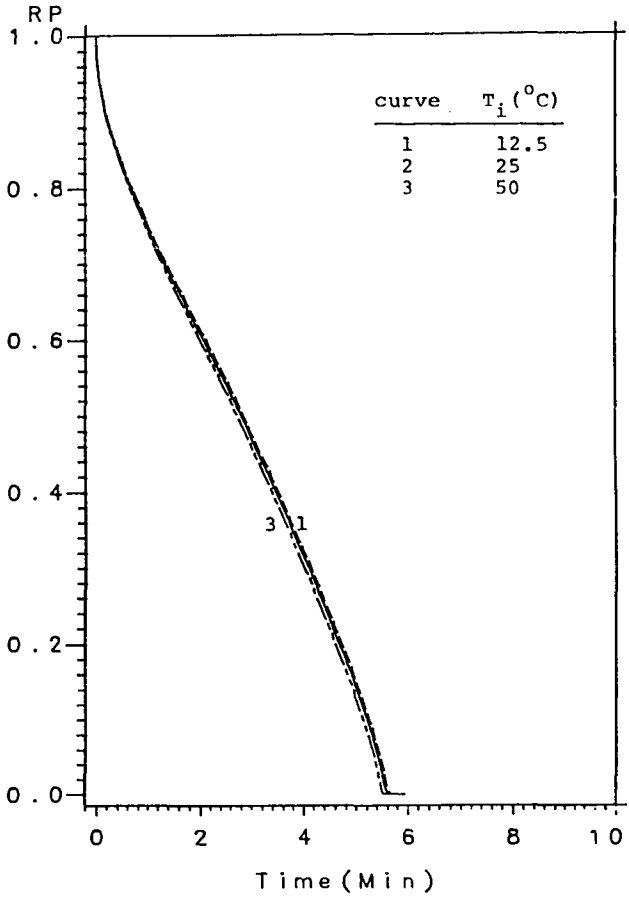

Figure 8: Pyrolyzing Front vs. Time Curves at Three Values of Initial Temperatures for a Particle of 1 cm Radius

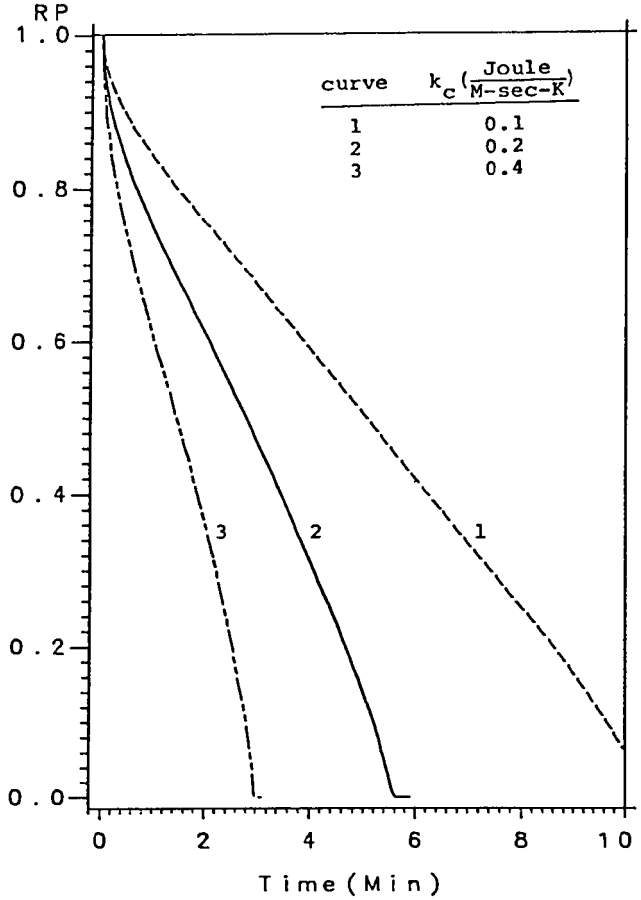

Figure 9 : Pyrolyzing Front vs. Time Curves at Three Values of Char Thermal Conductivity for a Particle of 1 cm Radius

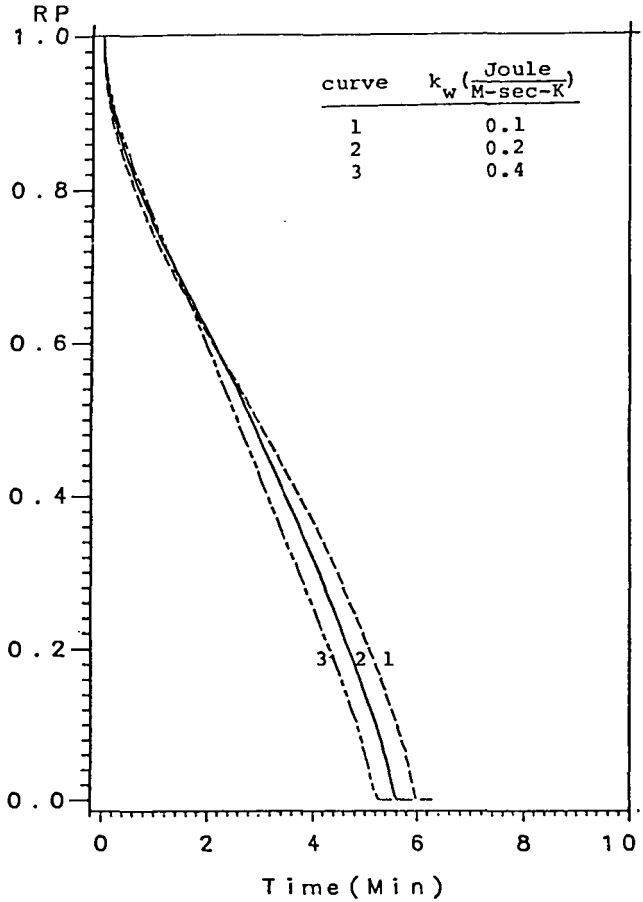

Figure 10: Pyrolyzing Front vs. Time Curves at Three Values of Thermal conductivity of Wood for a Particle of 1 cm Radius

Heat Capacities (C_{pc}, C_{pw})

The heat capacity of the unpyrolyzed solid, C_{pw}, has a greater influence on the rate of pyrolysis than the corresponding property for the resultant char, C_{pc}. The comparison is most directly illustrated in Figures 11 and 12.

Stoichiometric Coefficient (b)

When the stoichiometric coefficient of the gaseous product in the reaction

$$\text{wood} = b \text{ gas} + c \text{ char}$$

is varied over a wide range, there is virtually no change in the time required for pyrolysis (see Figure 13). It appears that the changing density of the char $\rho_c = \rho_w(1-b)$ counteracts the effect of the convective term in the energy balance.

Heat of Pyrolysis (H)

As illustrated in Figure 14, when the endothermic heat of primary pyrolysis varied from 184.1 to 736.4 J/g, the pyrolysis time increased from 4.2 to 8.4 minutes.

Summary

The results of any simulation using the phase-change model of pyrolysis are most significantly affected by the values of pyrolysis temperature, char thermal conductivity, and heat of pyrolysis.

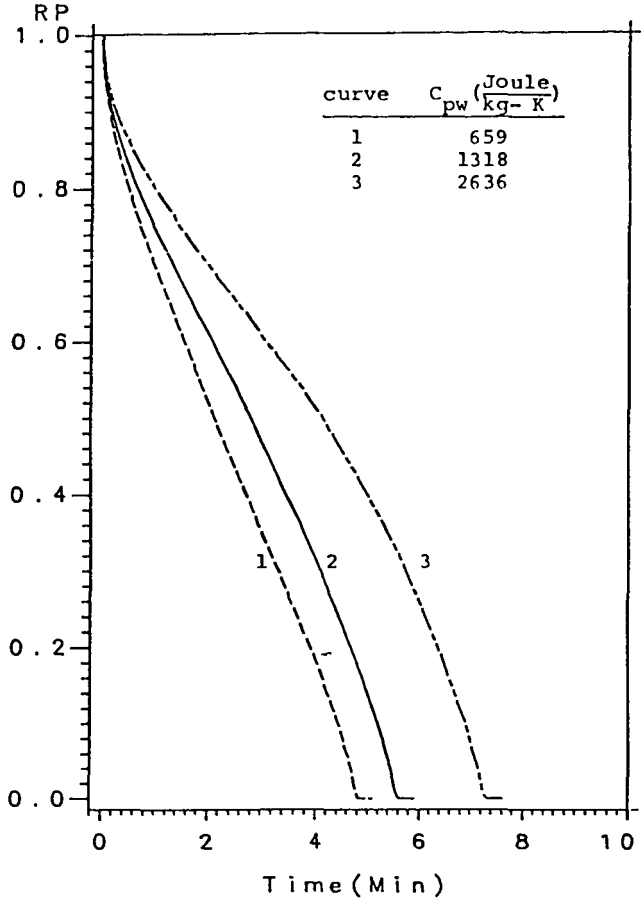

Figure 11: Pyrolyzing Front vs. Time Curves at Three Values of Heat Capacity of Wood for a Particle of 1 cm Radius

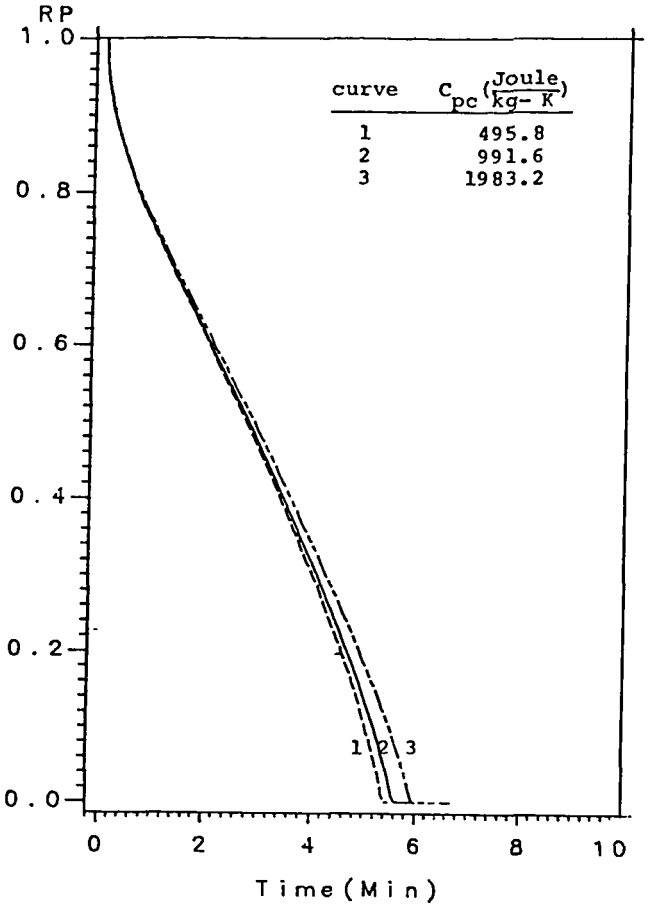

Figure 12: Pyrolyzing Front vs. Time Curves at Three Values of Heat Capacity of Char for a Particle of 1 cm Radius

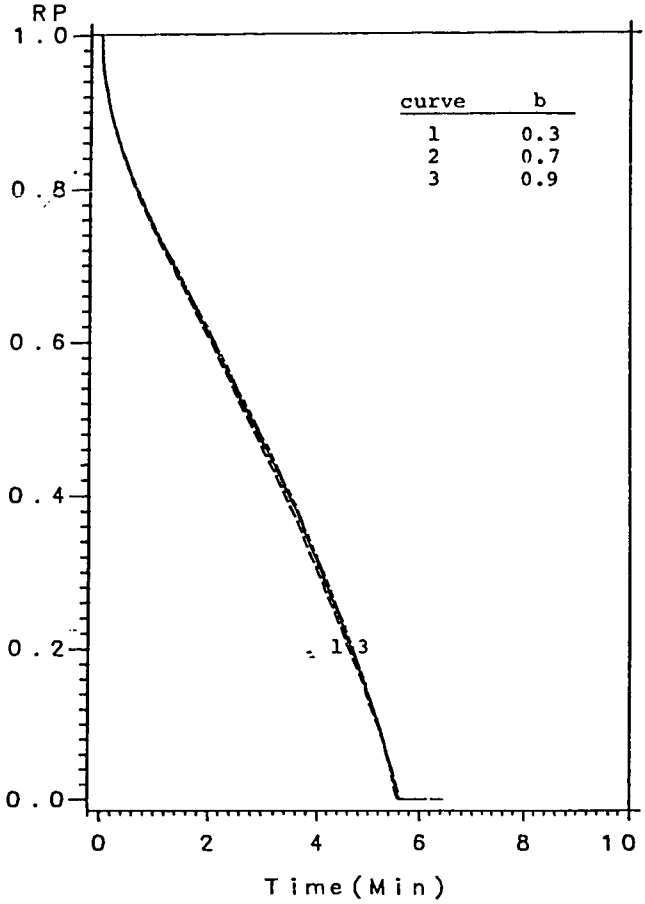

Figure 13: Pyrolyzing Front vs. Time Curves at Three Values of Stoichiometric Coefficient of Pyrolysis Gas for a Particle of 1 cm Radius

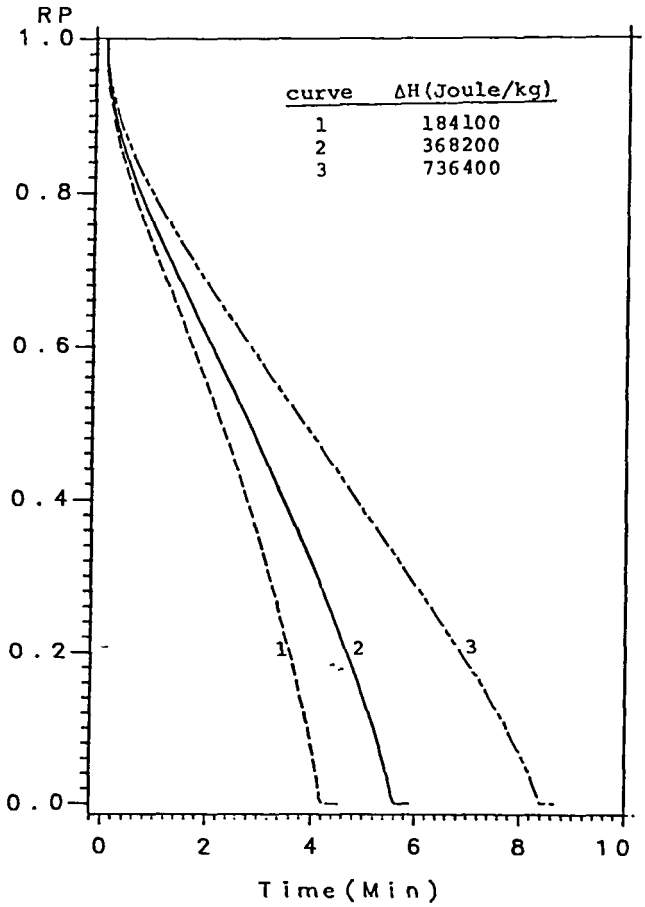

Figure 14: Pyrolyzing Front vs. Time Curves at Three Values of Heat of Pyrolysis for a Particle of 1 cm Radius

SINGLE PARTICLE SIMULATIONS

Up to the present time we have investigated only the case of a boundary condition of the first kind, in which the surface temperature is specified. The more useful case of a convective boundary condition (B.C. of 3rd kind) is currently under study. The choice to study the former problem was made on the basis of available experimental data. Investigators performing pyrolysis experiments on single particles usually measure and report surface temperature.

In one experiment (Kanury, 1966) a cylindrical specimen 1.75 cm in radius of pressed α-cellulose was placed in an externally-heated, rotating copper tube. Temperature profiles were recorded by thermocouples embedded at various radii. Measured surface and centerline temperatures are plotted in Figure 15. Using the parameters listed in Table 3 and the measured surface temperature as a boundary condition, the centerline temperature was calculated using the phase-change model. The calculated profile is also plotted in Figure 15.

The experimental profile displays plateaus at 120°C and 380°C corresponding to drying and pyrolysis temperatures. The calculated profile cannot reproduce the drying plateau because no phase change corresponding to drying was incorporated in the model. The plateau corresponding to pyrolysis however, was clearly observed. The measured surface temperature after complete pyrolysis was erratic because the thermocouple at the surface was not tightly bonded to the char.

In a second experiment (Roberts and Clough, 1963) the weight loss history of a 1 cm (radius) beech cylinder was recorded during pyrolysis in a nitrogen atmosphere. Using the parameters in Table 4 and the measured surface temperature, the weight vs. time curve was calculated. The results are shown in Figure 16. The heating rate of the oven used in the experiment was 20°C/min. Since the model predicts no weight loss until the surface temperature reaches the assumed

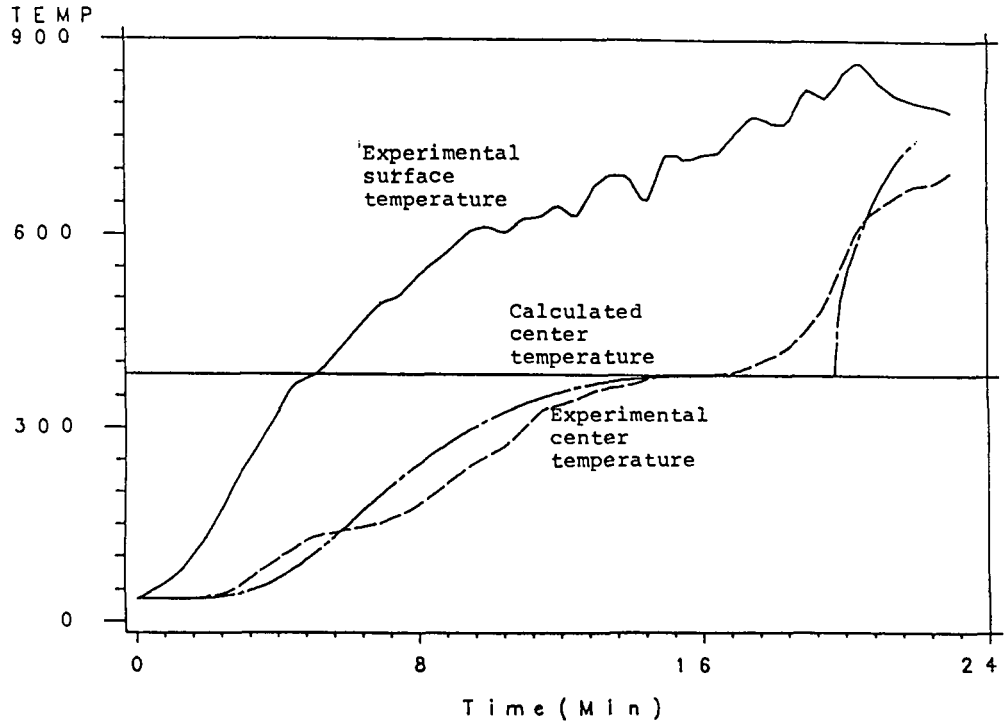

Figure 15 : Comparison between Experimental and Calculated Temperature History.

Table 3

Parameters and Properties Used to Simulate Kannry's Experiment

$\rho_w = 605$	(Kg/M^3)
$\rho_c = (1-b)\ _w$	(Kg/M^3)
$k_w = 0.14$	(Joule/M-Sec-K)
$k_c = 0.06$	(Joule/M-Sec-K)
$C_{pc} = 991.6$	(Joule/Kg-K)
$C_{pw} = 1318.0$	(Joule/Kg-K)
$C_{pg} = 1200$	(Joule/Kg-K)
$b = 0.80$	
$H = 100000$	(Joule/Kg)
$T_p = 382$	C
$T_i = 35$	C

Table 4

Representative Values of Parameters and Properties Used in Model Calculation for Beech Cylinder

ρ_w	= 600.0	(Kg/M^3)
ρ_c	= (1-b) $_w$	(Kg/M^3)
k_w	= 0.14	(Joule/M-Sec-K)
k_c	= 0.04	(Joule/M-Sec-K)
C_{pw}	= 1318.0	(Joule/M-Sec-K)
C_{pc}	= 991.6	(Joule/Kg-K)
C_{pg}	= 1200.0	(Joule/Kg-K)
b	= 0.61	
ΔH	= 100000	(Joule/Kg)
T_p	= 290	ˆC
T_i	= 25	C

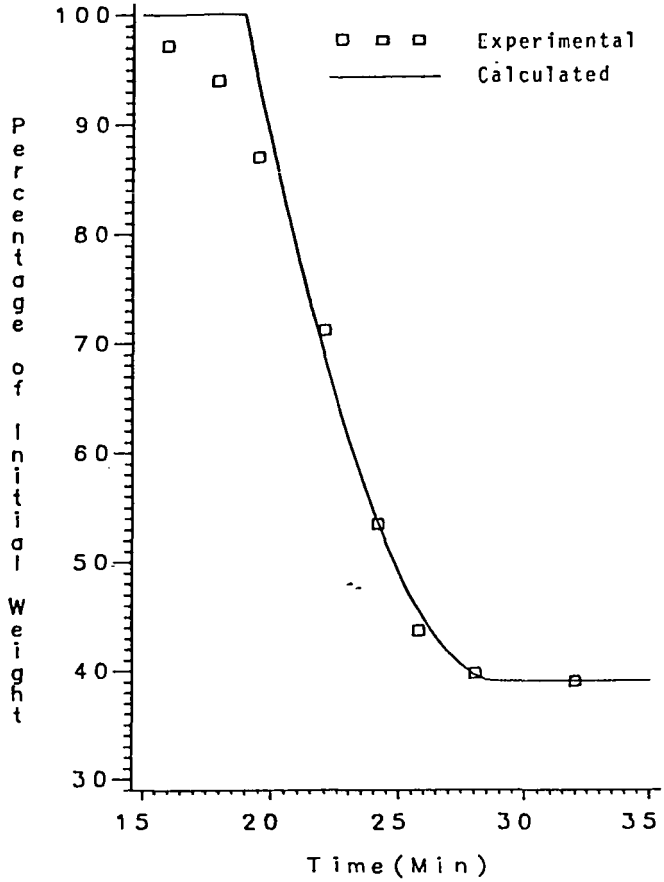

Figure 16: Comparison between Calculated and Experimental Weight/Time Curves for a Pyrolyzing Beech Cylinder.

pyrolysis temperature, it cannot reproduce that portion of the measured curve corresponding to low temperature pyrolysis.

PYROLYSIS ZONE OF A PACKED-BED GASIFIER

In order to simulate the pyrolysis zone of a packed-bed gasifier, the reactor was treated conceptually as two ideal reactors: one, a char combustor/gasifier and the second, a feed pyrolyzer. The gas temperature and flowrate exiting the gasification zone were used as input parameters for the pyrolysis simulation. The other boundary conditions were the offgas and feed temperatures.

The pyrolysis reaction is

$$\text{Feed} \longrightarrow \text{Char} + \text{Oil} + H_2O + \text{Gas}$$

The reaction is driven by the sensible heat in the char-derived gases from the combustion zone. The char-derived gas is considered inert and the offgas composition is obtained by simply mixing the char-derived gas flow with the volatile products of the pyrolysis reaction. The temperature of the gas, which is assumed to be the same as the surface temperature of the solid pellets, is used as the boundary condition of the kinetics-free model. We also assume that the pyrolysis portion of the reactor is characterized by plug flow, with no important radial gradients of mass or temperature.

Material balances were taken over the gas and solid phases.

$$dG_g/dZ = R_g \qquad\qquad dG_s/dZ = R_s$$

The energy balance was taken as

$$\frac{d}{dZ}(G_g C_{pg} T_g) = Q_s a + R_s \; H_2$$

The generation terms are the flux ($Q_s a$) into the pellets and $R_s \Delta H_2$, the exothermic heat of reaction of the volatiles, both based on unit volume of reactor. ΔH_2 is the difference between the exothermic heat of the overall pryolysis reaction and the endothermic heat of the primary pyrolysis step used in the phase change model.

A Runge Kutta method was used to integrate the system of equations. An axial temperature profile for the bed was assumed. This profile was used in the phase change model to calculate the reaction rate and heat flux as a function of time. The velocity of the solid phase was constant (no particle shrinkage) so time was proportional to distance along the bed. The bed temperature was calculated and the process repeated until the boundary conditions were satisfied.

For the conditions listed in Table 5, the calculated profile illustrated in Figure 17 was obtained.

FUTURE WORK

A convective boundary condition (B.C. of 3rd kind) using effective heat transfer coefficients will be investigated. The heat transfer correlations for particles in packed beds will be modified to account for the escape of volatiles from the surface of the char. Single particle experiments are being planned in which the convective environment (gas temperature and velocity) of the sample will be controlled. Gas temperatures can be measured more easily than solid surface temperatures. In addition, packed-bed experiments with thermocouple-studded samples are planned.

Table 5

Operating Conditions for the Test Run on the Biomass Gasifier

Wood Pellett Feed Rate (Kg/Hour)	15.8
Air Feed Rate (Kg/Hour)	9.678
Steam Feed Rate (Kg/Hour)	1.941

Parameters of Char and Wood Pellets Used to Simulate the Test Run of the Biomass Gasifier

ρ_w	= 1230.0	Kg/M^3
ρ_c	= $\rho_w(1-b)$	Kg/M^3
C_{pw}	= 1318.0	Joule/Kg
C_{pc}	= 991.6	Joule/Kg
k_w	= 0.03	Joule/M-Sec-K
k_c	= 0.005	Joule/M-Sec-K
r_o	= 0.003175	m
T_p	= 300.0	C
T_i	= 25.0	C
b	= 0.8	
ΔH	= 62760	Joule/Kg of wood
ΔH_2	= -368200	Joule/Kg of wood

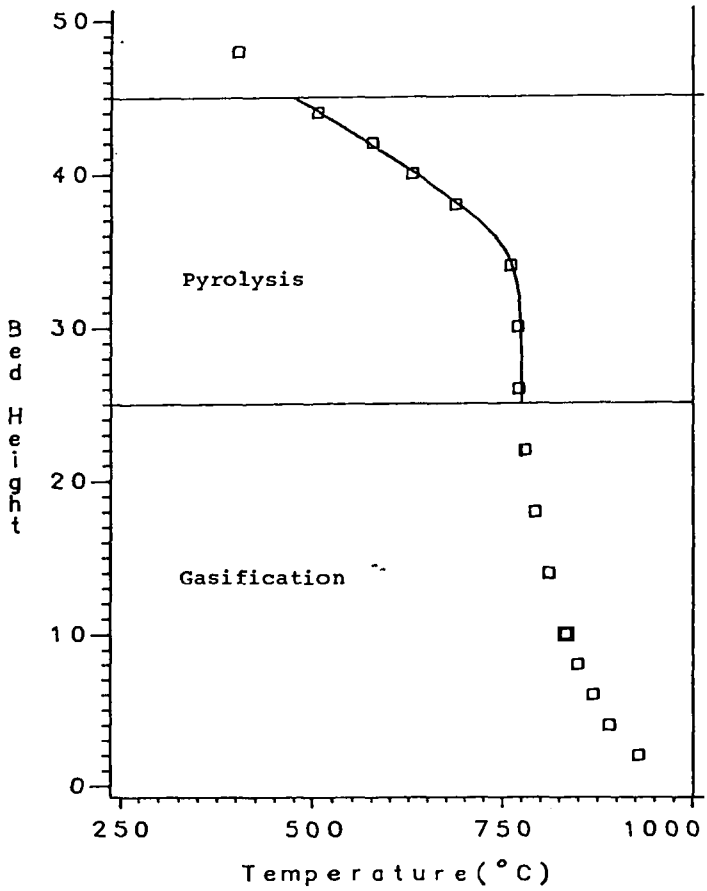

Figure 17: Comparison Between Calculated and Experimental Temperature Profiles in a Packed-Bed Gasifier.

Nomenclature

α	Thermal diffusivity
b	Stoichiometric coefficient of char in the pyrolysis reaction
B	Dimensionless parameter arising from the convective term in the char layer
c_p	Heat capacity
	Distance of pyrolyzing front from nearest grid point in the char layer
k	Thermal conductivity
M	Index of grid point in the char layer nearest the pyrolyzing front
N	Number of grid points
	Density
r	Radial position (r = 0 at center)
r_o	Cylinder radius at surface
R	Dimensionless radial distance (R = 0 at surface, R = 1 at center)
T	Temperature
	Dimensionless time
U,V	Dimensionless temperature
u_g	Velocity of exiting volatiles

Subscripts:

w	Wood layer, virgin solid
c	Char layer
p	Pyrolysis
s	Surface
g	Gas

References

Ackendon, J. R.; Hodgkins, W. R., Moving Boundary Problems in Heat Flow and Diffusion, Clarendon Press, Oxford (1975).

Bamford, C. H., Crank, J. and Malan, D. H., "The Combustion of Wood, Part I," Proc. of Cambridge Phil. Soc., 42, 166-184 (1946).

Carnahan, B., Luther, H. A., Wilkes, J. O., Applied Numerical Method, John Wiley and Sons, New York (1969).

Carslaw, H. S., Jaeger, J. C., Conduction of Heat in Solids, Oxford University Press, London (1959).

Fan, L. S., Fan, L. T., Tojo, K., Walawender, W. P., "Volume Reaction Model for Pyrolysis of a Single Solid Particle Accompanied by a Complex Reaction," Can. J. of Chem. Engr., 56, 603-609 (1978).

Maa, Sheng-Shyong P., "Influence of Particle Size and Environmental Condition on High Temperature Pyrolysis of the Cellulosic Material--I (Theoretical)," Combustion Science and Technology, 7, 257-269 (1973).

Muhlenkamp, S. P., "Pyrolysis of Living Wildland Fuels," Ph.D. Dissertation, University of Oklahoma, Norman, Oklahoma (1975).

Murty, K. A., Blackshear, P. L., "An X-Ray Photographic Study of the Reaction Kinetics of O-Cellulose Decomposition," Pyrodynamics, 4, 285-298 (1966).

Murty, K. A., "An Evaluation of The Physico-Chemical Factors Influencing the Burning Rate of Cellulosic Fuels and a Comprehensive Model for Solid Fuel Pyrolysis and Combustion," Ph.D. Dissertation, University of Minnesota (1969).

Roberts, A. F., Clough, G., "Thermal Decomposition of Wood in an Inert Atmosphere," Ninth Symposium (International) on Combustion, 158-166 (1963).

Roberts, D. L., "Numerical Solution of Heat Conduction Problem with a Change of Phase," Master Thesis, Texas Tech University (1981).

Stefan, Ann. Phys. u. Chem., N.F., 42, 269 (1891).

Wilson, D. G., Solomon, A. D., Boggs, P. T., Moving Boundary Problems, Academic Press (1978).

EXPERIMENTAL MEASUREMENT OF ABLATION RATE OF WOOD PIECES, UNDERGOING FAST PYROLYSIS BY CONTACT WITH A HEATED WALL.

J. LEDE, J. PANAGOPOULOS and J. VILLERMAUX

Laboratoire des Sciences du Génie Chimique, CNRS-ENSIC, 1 rue Grandville 54042 NANCY (France)

1. INTRODUCTION

The conventional pyrolysis of biomass yields about equal amounts of gases, char and tar. When pyrolysis is carried out in severe heating conditions, the reaction products can be almost entirely gaseous and contain significant amounts of light unsaturated hydrocarbons. Authors involved in such research, generally recommend several types of conditions : small wood particles, high temperatures, high heating rates, high heat fluxes, etc. Few of them [1,3,5,6] have associated the idea of ablation regime, to the observation of the fast pyrolysis reaction. Actually, the apparent rate of reaction is a function of two competitive processes within the wood particle : the rate of heat transfer and the rate of chemical decomposition of wood itself. If chemical processes are very fast, the heat transfer is rate controlling: this is the so called ablation regime characterized by a thin superficial layer of reacting wood). Such a regime can be represented by the rate at which the reacting layer moves towards the cold unreacted core of the piece of wood (ablation rate v) and the thickness of this reacting layer (e).

2. EXPERIMENTAL SET UP (Fig. 1)

The experimental system consists in a stainless steel disks (diameter: 7.5 x 10^{-2} m) spinning at a constant velocity (of the order of 1 $m.s^{-1}$) and heated by four gas burners located under the disk. The mean temperature is measured with a thermocouple pressed on the upper face. Rods of beech wood (2,3,4,6 and 10 x 10^{-3} m diameter) are vertically applied on the hot surface under known and variable pressures. A jet of argon is directed towards the contact surface in order to prevent spontaneous inflammation in air. No significant rise of wood temperature and no subsequent reaction is observed when the spinning disk is not heated. This eliminates the possibility of frictional heating effects. The experiments reported here are carried out in conditions of independence of reaction rate upon disk velocity. It is to be noticed that no change in the apparent rate was observed when a notched disk was used. The reaction produces gases and liquids undergoing further gasification on the disk surface. The presence of intersticial fluid between wood and steel acts as a kind of lubricant making the frictional contacts smoother.

The apparent rate of reaction **v** is obtained by direct measurement of the time required for a known length of rod to be consumed. The thickness of the ablation layer e is estimated by microscopic measurement of the extent of the uniformly darkened zone near the surface.

3. EXPERIMENTAL RESULTS

The variations of v and e were studied as a function of disk temperature (T_W), rod diameter (d), and pressure (P) under which the rods were pressed onto the disk. The pressure was controlled by placing known weights on the upper part of the rod (Fig. 1).

3.1. Variations of e with v

Fig. 2 shows some typical values of e as a function of **v** for T_W = 873 K and d = 3 x 10^{-3} m. The large dispersion of points is explained by the difficulty of measurement of e:: wood is a very heterogeneous material and the boundary between fresh and partially reacted wood cannot be defined with accuracy. This boundary is also blurred by capillary migration of strongly coloured liquid between the grains

of the wood (this liquid is mainly water couloured by traces of tar). Despite this lack of accuracy, Fig. 2 shows that the ablation thickness roughly decreases as ablation rate increases. For high values of v, e is two small to be accurately measured (extreme ablation conditions).

3.2. Variations of v with P

A logarithmic plot of v against P shows that v can be represented by a simple relationship

$$v = a\,P^{\beta} \qquad 1)$$

The accuracy of experiments is not sufficient to detect any influence of d. This shows that fast pyrolysis can be carried out with large pieces of wood and not only with small particles, as often stated in the literature. From figure 3 a straight line fitting yields the following β values: $\beta = 0.99$ ($T_w = 873$ K), $\beta = 0.97$ ($T_w = 973$ K), $\beta = 1.02$ ($T_w = 1073$ K), $\beta = 1.01$ ($T_w = 1173$ K). Therefore, we may adopt a linear dependence $v = aP$.

Fig. 3 also shows that under high temperature and pressure, the ablation rate becomes very high and may exceed 3×10^{-2} m s^{-1} in agreement with other determinations [1]. In these conditions, the apparent massic rate of wood consumption reaches 0.24 kg hr^{-1} ($d = 2 \times 10^{-3}$ m) and 6 kg hr^{-1} ($d = 10^{-2}$ m).

4. INTERPRETATION AND DISCUSSION OF RESULTS

4.1. Signification of a

In the same manner as the ablation reaction is controlled by heat transfer inside the wood, it will be supposed that the reaction is also limited by heat transfer from the disk to the surface of wood. The variations of v will be attributed to the variations of the heat flux with T_w and P. It will be also assumed that the temperature T_d of the surface of pyrolyzing wood is constant whatever the experimental conditions. In these conditions :

$$\phi = h(T_w - T_d) = v\,\rho\,C_p(T_d - T_o) + \rho v \Delta H \qquad 2)$$

It is difficult to select an accurate value for the reaction enthalpy ΔH. Direct measurements [7] by rapid pyrolysis of wood have given values close to zero around 773 K. Reed et al. [2] proposed a model assuming that the reaction occurs in several steps: the wood is first sensibly heated without any transformation up to the reaction temperature where it is depolymerized to yield a solid which subsequently melts before vaporizing. If the tars are mechanically wiped away the heat input corresponds to sensible heat and heat of fusion. The latter has been estimated to about 4×10^4 J kg^{-1} at 773 K, which represents only 3.6% of the heat required to heat the wood from 373 to 773 K. Thence:

$$\phi = h(T_w - T_d) = v\,\rho C_p(T_d - T_o) \qquad 3)$$

Thanks to 1) with $\beta = 1$ and 3) it can be deduced that h is proportional to P:

$$h = KP \qquad 4)$$

3) and 4) show that $\frac{v}{P}$ is a linear function of T_w, allowing the calculation of T_d and K :

$$\frac{v}{P} = \frac{K}{\rho C_p}\left(\frac{T_w}{T_d - T_o} - \frac{T_d}{T_d - T_o}\right) \qquad 5)$$

As expected, Fig. 4 shows that the variation is linear. With $T_o = 373$ K, $\rho = 700$ kg s^{-1} and $C_p = 2800$ J kg^{-1} K^{-1} the following values are deduced:

$$K = 0.02\ W\,m^{-2}\,K^{-1}\,Pa^{-1} \quad \text{and} \quad T_d = 753 \pm 30\ K$$

4.2. Discussion

4.2.1. About the heat transfer coefficient h

The variations of h deduced from relation 3) and from experimental measurements are reported in Fig. 5. It appears that h is independant of d and T_w and is only a function of P. Of course, a best fitted straight line leads to the same values of K (0.02 W m^{-2} K^{-1} Pa^{-1}) and β (0,998) as previously optimized.

The three significant modes of heat transfer are convection, radiation and more or less direct contact with the disk. There are few chances that convection may occur significantly because of transpirational cooling effect. The radiation heat transfer coefficient can be defined as: $h_R = \sigma\varepsilon(T_w^2 + T_d^2)(T_w + T_d)$. Assuming $\varepsilon = 0.5$ and $T_d = 753$ K, h_R(W m^{-2} K^{-1}) has the following values:: 62 (873 K), 74 (973 K), 89 (1073 K), 106 (1173K). These are much lower than the experimental values of h, especially at high pressure (Fig. 5).

Direct heat transfer by interface contact between the disk and the rod can take place by combined mechanisms of conduction across true contact points and conduction across entrapped intersticial fluid. The prediction of theoretical h values is difficult: they depend on the thermal conductivity of fluid and solids, surface finish, and hardness, contact pressure, etc. Extreme values of h compiled by Rohsenow et al. [8] have been reported in Fig. 5 (dashed lines). In spite of very different experimental conditions (contact materials are metals, gap materials are metals or gases). The order of magnitude is correct. However, it is difficult to find a physical justification to the linear variation of h with P. For explaining this, theories of lubrication might be invoked if the whole heat transfer was supposed to take place across a continuous layer of insulating fluid between the two solid surfaces.

In anyway, the coefficient h is very high, showing that the mechanisms of heat transfer by contact must not be underestimated in the study of reactors where solid particles are pyrolysed by contact on the hot walls of the vessel (cyclone reactor for instance [3,8,10]).

4.2.2. About the surface temperature T_d

T_d has been assumed independent of T_w and P. The good linearity observed in Fig. 4 is a first confirmation of this. Fig. 4 also shows that v = 0 for T_w = 753 K, in good agreement with the experimental observation that no fast reaction significantly occurs when T_w < 753 K. These observations are also in agreement with thermogravimetric measurements showing that pyrolysis of dry wood is essentially complete at 773 K [4]. Let us also remind the model proposed in [2] assimilating fast pyrolysis to a three phases reaction: heating to 773 K, melting at 773 K, vaporization of tars.

Thus it seems fairly reasonable to assume that the temperature of the wood surface is of the order of 753 K whatever T_w and P. According to this mechanism, it could be wrong to say that wood is heated at the temperature of the walls of a reactor before decomposing.

4.3. Relationship between v and e

There are three differents ways for establishing a simple relationship between v and e.

. Let us suppose that e is the distance between the two isothermal surfaces T = 473 K, T_d = 773 K, and that the heat transferred is used to increase the wood temperature:

$$v\rho C_p(T_d - T) = \frac{\lambda}{e}(T_d - T) \quad \text{or} \quad ve = \frac{\lambda}{\rho\, C_p} = \alpha \qquad 6)$$

where α is the thermal diffusivity of wood.

. Assuming that penetration of heat into the rod takes place by simple one-dimension conduction, the expression giving T as a function of depth z in the solid at steady state is [8]:

$$\frac{T - T_o}{T_d - T_o} = \exp\left(-\frac{vz}{\alpha}\right) \qquad 7)$$

Taking T = 437 K, T_o = 373 K and T_d = 773 K, z is considered to be equal to e and then:

$$ve = 1.39\ \alpha \qquad 8)$$

. A model has been proposed [5] for representing the thermal volatilization of solid particles, where the equations of simultaneous heat and mass balances are numerically solved. Assuming a constant surface temperature, this model yields:

$$v = \frac{1}{b\rho}\left(\frac{\lambda r}{C_p}\right)^{1/2} \quad \text{and} \quad e = \frac{5}{b}\left(\frac{\lambda r}{rC_p}\right)^{1/2} \qquad 9)$$

b is a constant number close to 2.6 when $\Delta H = 0$, r is the chemical rate of reaction and e is the thickness of the solid layer where 99 % of the reaction occurs. From expressions 9) we obtain:

$$ve = \frac{5}{b^2}\frac{\lambda}{\rho\ C_p} \simeq 0.74\ \alpha \qquad 10)$$

. From the three methods above it can be deduced that

$$0.7\ \alpha < ve < 1.4\ \alpha \qquad 11)$$

Several values of α have been proposed in the litterature: 10^{-7} m^2 s^{-1} [6], 0.82 x 10^{-7} m^2 s^{-1} [2], 0.6 to 1.5 x 10^{-7} m^2 s^{-1} [11], 1.4 x 10^{-7} to 3.4 x 10^{-7} m^2 s^{-1} [12]. These different estimations lead to: 0.4 x 10^{-7} < ve (m^2s^{-1}) < 5 x 10^{-7}.

Fig. 2 shows that the experimental results (mean value ve = 0.8 x 10^{-7} m^2s^{-1}) are in agreement with this rough estimation (dashed lines).

As an illustration, for the highest ablation rate measured (fig. 3): 32.5 x 10^{-3} m s^{-1}, the thickness of the ablation layer e is predicted to be about 3 x 10^{-6} m.

5. CONDITIONS REQUIRED FOR THE OBSERVATION OF ABLATION

Relation 3) shows that fast pyrolysis in ablation regime (high value of v and small value of e) is expected when high heat fluxes are available as for example in solar concentrators or image furnaces. A few experiments have been done with an image furnace (mean flux density:: 5 x 10^5 W m^{-2}) focused on the end of a beech wood rod (d = 8 x 10^{-3} m), automatically adjusted as the reaction proceeds. The rod is placed inside a transparent glass vessel in steam atmosphere.

The apparent rate of reaction is measured to about 2 x 10^{-4} m s^{-1} while the theoretical value is 8.5 x 10^{-3} m s^{-1} (calculated on the basis of 3) with ρ = 700 kg m^{-3}, C_p = 2800 J kg^{-1} s^{-1}, $T_d - T_o$ = 400 K). The reaction produces also large amounts of char. How can this discrepancy be explained? The primary products remain for some time at the surface (there is no mechanical elimination) until they disappear by partial decomposition under the effect of high local temperature and by gasification with steam. This relatively thick layer of products partially prevents the radiation to reach fresh parts of wood and a part of the flux is consumed by the endothermal reaction of char gasification. Consequently, the overall reaction takes place in slow pyrolysis regime.

As a conclusion, it appears that fast pyrolysis of wood in ablation regime is observed if two conditions are fulfilled: high available heat flux density and efficient elimination of primary products from the surface of wood.

REFERENCES

[1] J.P. DIEBOLD. Proceedings of Specialists' Workshop on Fast Pyrolysis of Biomass

Copper Mountain Co (USA), October 19-22 (1980), p. 237
[2] T.B. REED, J.P. DIEBOLD and R. DESROSIERS. Ibid., p. 7
[3] J. LEDE, F. VERZARO, B. ANTOINE and J. VILLERMAUX. Ibid. p. 327
[4] F. SHAFIZADEH. Ibid. p. 79
[5] J. VILLERMAUX and B. ANTOINE. Rev. Gen. Therm. Fr. 227 (1980), 851
[6] J. VILLERMAUX, J. LEDE and F. VERZARO. Rev. Gén. Therm. Fr. 227 (1980), 861
[7] A. ROLIN. Thesis. Centre agréé régional CNAM, Nancy (F) (1981)
[8] W.R. ROHSENOW and J.P. HARTNETT. Handbook of Heat Transfer. McGraw Hill (1973)
[9] J. LEDE et J. VILLERMAUX. La Recherche 134 (1982) 787
[10] J.P. DIEBOLD and J. SCAHILL. Fundamentals of Thermochemical Biomass Conversion YMCA of the Rockies, Estes Park Co (USA) October 18-22 (1982)
[11] G. LESGOURGUES and J.L. HOUZELOT. Private communication. Laboratoire des Sciences du Génie Chimique. Nancy (F) (1981)
[12] R. CHARUEL, J.C. ROSSELET and J.M. SERRA-TOSIO. Colloque Sciences et Industries du Bois. Grenoble 20-22 Septembre (1982)

NOMENCLATURE

a,b,k	Constants
C_p	Heat capacity of wood
d	Rod diameter
e	Thickness of ablation layer
h, h_R	Heat transfer coefficient: Experimental, by pure radiation
P	Pressure
r	Chemical rate of reaction
T_o, T_d, T_w	Temperatures: initial (373 K), of the surface of pyrolysing wood, of the disk
v	Ablation rate
z	Depth in the rod
α	Thermal diffusivity of wood
β	Exponent
ΔH	Enthalpy of the reaction
ε	Emissivity
ϕ	Density of flux
λ	Thermal conductivity of wood
ρ	Mass density of wood
σ	Boltzmann constant (5.67×10^{-8} W m^{-2} K^{-4})

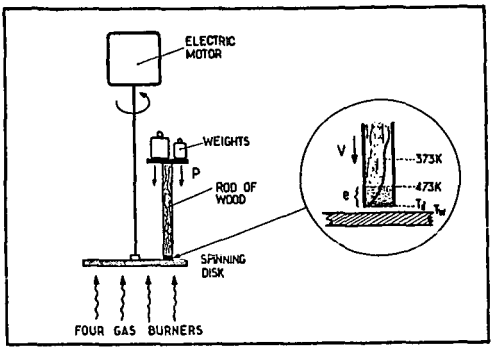

Figure 1. Scheme of experimental set-up

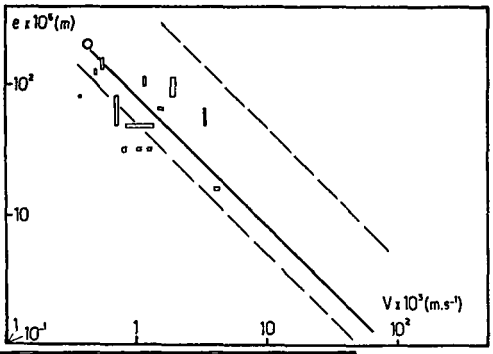

Figure 2. Variations of the thickness of ablation layer e as a function of ablation rate v.

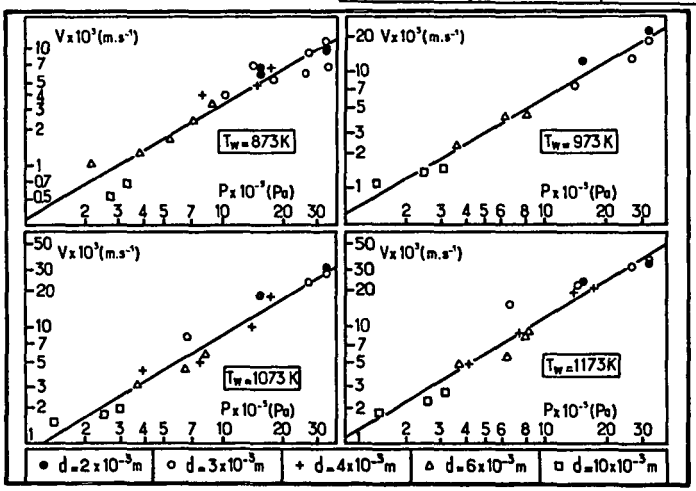

Figure 3. Experimental variations of ablation rate v as a function of pressure P for four values of disk temperature T_w.

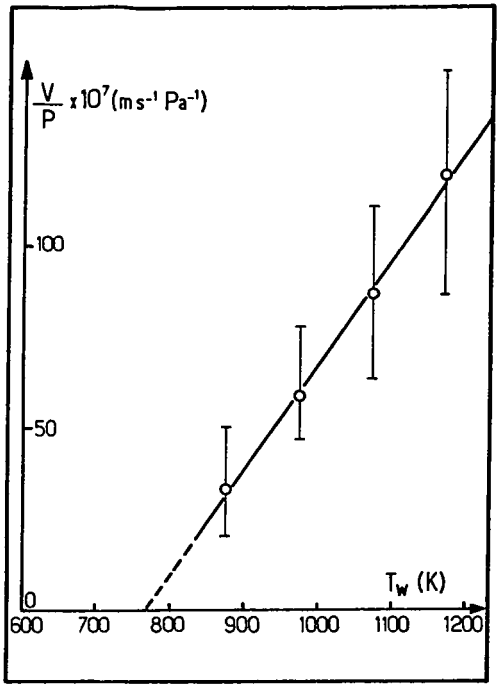

Figure 4. Variations of the ratio $\frac{\text{Ablation rate } v}{\text{Pressure } P}$ as a function of disk temperature T_w.

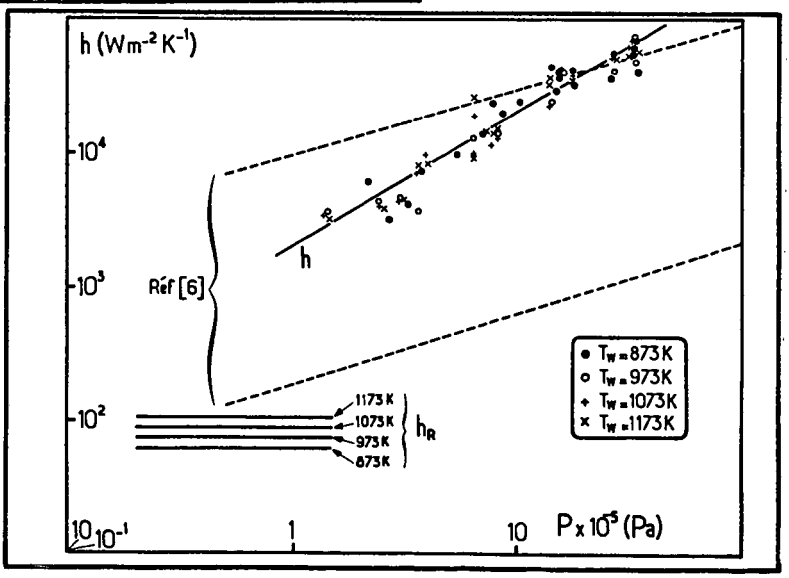

Figure 5. Variations of heat transfer coefficient h as a function of pressure p.

A NEW MODEL FOR THERMAL VOLATILIZATION OF SOLID PARTICLES UNDERGOING FLASH-PYROLYSIS

J. Villermaux, B. Antoine, J. Lédé and F. Soulignac

Laboratoire des Sciences du Génie Chimique, CNRS-ENSIC Nancy-France

Many industrial processes involve the consumption of solid particles immersed in a reacting medium. Among these, the gasification of coal and biomass in fixed, fluidized or moving beds is of special interest. A great number of models describing gas-solid reactions can be found in the literature [1] [2] [3] [4] [5]. Models dealing with the thermal volatilization of a solid controlled by heat transfer between the surrounding medium and the inner volume of the particle are more scarce. In addition, existing models often rely on the concept of a "surface reaction", which is questionable, because deeper layers also contribute to the reaction as heat penetrates into the solid.

We propose below a new model describing the volatilization of a solid by thermal penetration (VTP model). This model was initially imagined for interpreting flash-pyrolysis of sawdust particles. Actually, it could be applied to any kind of solid reactions where volatilization is controlled by heat conduction from the outer surface. Only a few preliminary but significant results are presented in this paper. More extensive and accurate simulations will be published later.

1. Assumptions and model equations

The basic assumptions of the model are :

- The solid is homogeneous and its mean density ρ is constant and independent of temperature.

- Heat transfer takes place by conduction in the solid, heat conductivity λ and heat capacity c_p are assumed to be constant.

- The rate of volatilization of the solid is $\mathfrak{R}$. $\mathfrak{R}$ is the mass of solid transformed into gas per unit time and per unit solid volume. $\mathfrak{R}$ increases with temperature according to Arrhenius law $\mathfrak{R} = k_o \exp(-E/R_gT)$.

- The reaction is endothermic, the reaction enthalpy per unit mass of solid is $\Delta H > 0$ (the case of $\Delta H < 0$ can also be treated by this model, but it will not be discussed here). It is assumed that $\Delta H = \Delta H_1 + \Delta c_p(T - T_1)$ where T_1 is a reference temperature.

- The gaseous products escape freely towards the surface without any diffusional resistance (this is possible if the remaining solid has a porous structure allowing free gas permeation).

- However, it is assumed that the remaining solid shrinks so that it conserves a constant density. The result is that, seen from the center, all the points in the solid seem to move nearer to each other. Conversely, seen from the surface, it is the center which seems to come nearer. This linear shrinking velocity will be denoted as u.

- The solid particle is initially at constant temperature T_o where the reaction is negligible. It is suddenly immersed in a hot medium. Four kinds of boundary conditions can be imagined :

a) Constant surface temperature $T_s = T_p$ (Cauchy condition).

b) Constant surface heat flux q_o

c) Convective heat transfer from a gas at constant temperature T_p (Fourier condition)

d) Radiative heat transfer from a wall at constant temperature T_p.

Only conditions a) and c) will be considered here.

- The particles may have different initial shapes. The case of infinite slabs and spheres will be treated below but this is not a limitation of the model. Actually, a unified treatment valid for any shape can be developed, especially in the so-called "ablation regime". The situation is very similar to that encountered in the study of diffusion-controlled reactions in catalyst pellets.

- Volatilization thus causes shrinking along one single dimension. One wants to calculate the decay of thickness L as a function of time and the time t_F for total consumption of the particle.

Depending on the problem, coordinate axis may be attached to the outer surface of the particle (Oz normal to the surface, directed towards the center and thus moving as volatilization proceeds). This is especially convenient for a slab and for the study of the "ablation regime". This will be referred to below as convention I. Conversely, the axis may be attached to the center of the particle (Or normal to the outer surface); this is more convenient for a sphere and a cylinder, and will be referred to below as convention II.

At any time, there exist a temperature profile T (z,t) or T (r,t) and a shrinking velocity profile u (z,t) or u (r,t). The mass and energy balances are easily written as follows:

Dimensional units, infinite slab, convention I:

Mass balance:

$$\rho \frac{\partial u}{\partial z} + \mathfrak{R} = 0 \tag{1}$$

$$\mathfrak{R} = k_o \exp(-E/R_g T) \tag{2}$$

Initial and boundary conditions:

$$\left.\begin{array}{l} t = 0,\ u = 0,\ L = L_o \\ z = 0,\ u = 0 \\ z = L,\ u_L = \dfrac{dL}{dt} < 0 \end{array}\right\} \tag{3}$$

Heat balance:

$$\lambda \frac{\partial^2 T}{\partial z^2} = \mathfrak{R}\Delta H + \rho u\, c_p \frac{\partial T}{\partial z} + \rho c_p \frac{\partial T}{\partial t} \tag{4}$$

Initial and boundary conditions:

$$\left.\begin{array}{lll} t = 0,\ T = T_o & & \\ z = 0, & \text{a) } T = T_p & \text{b) } -\lambda\dfrac{\partial T}{\partial z} = q_o \\ \text{c) } -\lambda \dfrac{\partial T}{\partial z} = h(T_p - T) & & \text{d) } -\lambda \dfrac{\partial T}{\partial z} = \varepsilon\sigma(T_p^4 - T^4) \\ z = L & \dfrac{\partial T}{\partial z} = 0 & \end{array}\right\} \tag{5}$$

Infinite slab (p = 0), infinite cylinder (p = 1), sphere (p = 2), convention II:

$$\frac{1}{r^p}\frac{\partial}{\partial r}(r^p \rho u) + \mathfrak{R} = 0 \text{ , } \mathfrak{R} \text{ given by (2)} \tag{1'}$$

Initial and boundary conditions :

$$\left.\begin{array}{l} t = 0,\ u = 0,\ r = R_o \\ r = 0,\ u = 0 \\ r = R,\ u_R = \dfrac{dR}{dt} < 0 \end{array}\right\} \tag{3'}$$

Heat balance:

$$\frac{\lambda}{r^p}\frac{\partial}{\partial r}\left(r^p\frac{\partial T}{\partial r}\right) = \mathfrak{R}\,\Delta H + \rho u c_p\frac{\partial T}{\partial r} + \rho c_p\frac{\partial T}{\partial t} \qquad (4')$$

Initial and boundary conditions:

$$\left.\begin{array}{lll} t = 0,\ T = T_o;\ r = 0,\ \dfrac{\partial T}{\partial r} = 0 & & \\ r = R \quad a)\ T = T_p & b)\ \lambda\dfrac{\partial T}{\partial r} = q_o & \\ c)\ \lambda\dfrac{\partial T}{\partial r} = h(T_p - T) & d)\ \lambda\dfrac{\partial T}{\partial r} = \varepsilon\sigma(T_p^4 - T) & \end{array}\right\} \qquad (5')$$

It is interesting to write the model equations in reduced form. For the slab case, convention I, dimensionless quantities are defined as follows: $x = z/L_o$, $\theta = t\mathfrak{R}^*/\rho$, $v = \rho u/(L_o\mathfrak{R}^*)$, $Y = T/T^*$, $W = \mathfrak{R}/\mathfrak{R}^*$, $A = E/(R_gT^*)$, $M = \mathfrak{R}^*L_o^2c_p/\lambda$, $\ell = L/L_o$, $H = \Delta H_1/(c_pT^*)$, $K = \Delta c_p/c_p$, $B = hL_o/\lambda$, $Q_o = q_oL_o/(\lambda T^*)$, $S = \varepsilon\sigma L_oT^{*3}/\lambda$. ($R_g$ is the gas constant).

T^* is a reference temperature (in the numerical examples treated here $T^* = T_1 = T_p$), and $\mathfrak{R}^*$ is the rate of reaction at T^*.

Equations (1) to (5) are then written:

$$\frac{\partial v}{\partial x} + W = 0 \qquad (6)$$

$$W = \exp\left(-A\left(\frac{1 - Y}{Y}\right)\right) \qquad (7)$$

$$\theta = 0,\ v = 0;\quad x = 0,\ v = 0;\quad x = \ell,\ v = \frac{d\ell}{d\theta} \qquad (8)$$

$$\frac{1}{M}\frac{\partial^2 Y}{\partial x^2} = (H + K(Y - Y_1))W + v\frac{\partial Y}{\partial x} + \frac{\partial Y}{\partial \theta} \qquad (9)$$

$$\left.\begin{array}{lll} \theta = 0,\ Y = Y_o & & \\ x = 0 \quad a)\ Y = Y_o & b)\ -\dfrac{\partial Y}{\partial x} = Q_o & \\ c)\ -\dfrac{\partial Y}{\partial x} = B(Y_p - Y) & d)\ -\dfrac{\partial Y}{\partial x} = S(Y_p^4 - Y^4) & \end{array}\right\} \qquad (10)$$

A similar reduction can be performed on equations (1') to (5'), the characteristic length R_o replacing L_o. The important parameters are the activation criterion A, the thermicity criterion H, the thermal BIOT number B, and especially M, which appears as a THERMAL THIELE MODULUS

$$M = \frac{\mathfrak{R}^*L_o^2}{\alpha\rho} = \frac{t_T}{t_R} \qquad (11)$$

where $\alpha = \lambda/(\rho c_p)$ is the thermal diffusivity

$t_R = \rho/\mathfrak{R}^*$ is a characteristic reaction time and $t_T = L_o^2/\alpha$ is a characteristic heat penetration time. If $M \ll 1$, $t_T \ll t_R$ so that heat has the time to penetrate into the particle before it volatilizes. Volatilization is thus controlled by the chemical reaction, this is the so-called CHEMICAL REGIME. If $M \gg 1$, $t_T \gg t_R$, heat has not the time to reach the particle core and volatilization takes place in a thin layer close to the surface. The rate of volatilization is controlled by an irreducible coupling between reaction and heat diffusion: this is the so-called ABLATION REGIME. We shall see below that shrinking then proceeds at a constant linear velocity.

2. Examples of simulations

Equations (6) to (10) and their equivalent for a sphere were solved numerically, yielding internal velocity and temperature profiles and time θ_F for total consumption as a function of physical parameters.

In the simulations reported here, the following values were selected:

$Y_p = Y_1 = 1$, $Y_o = 0.25$ (for instance $T_o = 300$ K and $T_p = T^* = 1200$ K)

$H = 0.5$, A variable (1, 10, 100)

M and B variable.

Figure 1 shows internal temperature profiles, mainly for a 50 % linear size reduction (e.g. $\ell = 0.5$) in the case of Fourier (c) and Cauchy (a) conditions. The influence of M is obvious. When M is small, the temperature tends to become uniform whereas when M is large ($M > 100$), a steep temperature profile exists close to the surface. This is especially clear for constant surface temperature (Cauchy condition, $B = \infty$). In this case, a comparison between curves drawn for $\ell = 0.75$ and $\ell = 0.5$ shows that the temperature profile is simply translated as a function of time when volatilization proceeds, the core of the particle remaining cold. The influence of the Biot number B is also interesting: it appears that the ablation regime is more difficult to reach (even for large M) if the rate of heat transfer at the surface is slow (small B). Figures 2 to 4 show the reduction of size of particles (L/L_o or R/R_o) as a function of reduced time θ. Starting from the chemical regime ($M = 0$), where $L/L_o = \exp(-\theta)$, the decay curves tend to become straight lines in frankly established ablation regime ($M > 100$, $B = \infty$): $L/L_o = 1 - \theta/\theta_F$. Times for total consumption θ_F are reported as a function of M in figures 5 and 6. Several interesting remarks can be made by inspection of these figures:

- θ_F increases when M augments and when B diminishes (Fourier condition).

- Curves for different shapes are very close to each other for equal values of the Biot number B.

- As $B \to \infty$, the Fourier condition tends to the Cauchy condition. In ablation regime, θ_F then tends to be proportional to $\sqrt{M}$.

For $A = 10$ and $H = 0.5$, one finds approximately

$$\theta_F \approx 3\sqrt{M} \tag{12}$$

In dimensional variables,

$$t_F \approx 3\sqrt{t_R t_T} = 3\, L_o \frac{\overline{t_R}}{\alpha} \tag{13}$$

This means that the time for total consumption is proportional to the initial size and that the shrinking velocity is constant (a clue for the ablation regime). This also makes it possible to determine the true value of the reaction time t_R even in the presence of a severe heat transfer control. A value for the thickness of the reaction zone may be obtained as the ratio $e = \alpha/|u| \approx \alpha t_F/L_o$ of the heat diffusivity to the shrinking velocity. Then,

$$e \approx 3\sqrt{\alpha t_R} \tag{14}$$

and

$$e/L_o \approx 3\, L_o/\sqrt{M} \tag{15}$$

For instance, if $M = 10\,000$, $e \approx 0.03\, L_o$

- Coefficient 3 in relationships (12), (13), (14), (15) obviously depends on the numerical values of A, H and Y_o selected for simulations. Figure 6 shows that the absolute value of θ_F depends on A but that the curves are roughly parallel. It can be expected that in ablation regime, the $\sqrt{M}$ dependency still holds whatever the value of A.

In a previous paper [6], an empirical expression for θ_F in ablation regime and variable H has been established:

$$\theta_F \approx 1.13\,(H + 2.3)\sqrt{M} \tag{16}$$

($A = 10$, $Y_o = 0.25$, Cauchy condition)

However, this relationship should be checked by more careful numerical studies.

3. Conclusion

Although relying on very simple assumptions, the VTP model makes it possible to estimate the rate of consumption of solid particles as a function of physicochemical parameters. Evidence for the existence of two volatilization regimes is provided, depending on the value of the thermal Thiele Modulus M and the thermal Biot number B. The ablation regime is achieved if both $M = t_T/t_R$ and $B = hL_o/\lambda$ are large (M, B > 100). In this regime, the shrinking velocity is constant and the reaction takes place only in a thin layer at the solid surface. Experimental data on wood pyrolysis obtained with sawdust or with massive rods confirm the existence of these two regimes (see companion paper). Total consumption times estimated in a cyclone reactor or direct measurement of ablation velocities are in agreement with theoretical predictions of the VPT model.

Example: For wood particles, $\lambda = 0.2\ W\ m^{-1}\ K^{-1}$, $c_p = 2800\ J.kg^{-1}.K^{-1}$, $\rho = 500\ kg.m^{-3}$, $\alpha = 1.4 \times 10^{-7} m^2\ s^{-1}$, $H = 0.5$ corresponds to $\Delta H = 1680\ kJ.kg^{-1}$ at $T^* = 1200$ K. Then, $t_T = L_o^2/\alpha = 7 \times 10^{-2}$ s. For particles of $L_o = 10^{-4}$ s, the ablation regime requires that (M > 100) $t_R < 7 \times 10^{-4}$ s. If $t_R = 7 \times 10^{-4}$ s, then $t_F = 3\ t_R \sqrt{M} = 30\ t_R = 21 \times 10^{-3}$ s.

These preliminary results have been obtained with very simple numerical methods which are not best adapted to the "stiff" conditions encountered in the ablation regime (M and B both large). Further improvements are in progress, which will make it possible to perform more accurate simulations in a broader range of variation of parameters.

Literature cited

[1] Szekelly J., Evans J.W. and John H.Y. Gas Solid Reactions, Academic Press, 1976

[2] Levenspiel O. The Chemical Reactor Omnibook O.S.U., Corvallis, Oregon USA, 1979

[3] Hicks B.L. Theory of ignition considered as a thermal reaction. J. Chem. Phys. 22, (1954), 414

[4] Kindelan M., and Williams F.A. Theory for endothermic gasification of a solid by a constant energy flux. Comb. Sci. Technology, 10 (1975), 1

[5] Bradley H.H. Jr. Theory of ignition of a reactive solid by constant energy flux. Comb. Sci. Technol. 2 (1970), 11

[6] Villermaux J. and Antoine B. Pyrolyse éclair de solides divisés dans un réacteur continu. 1. Un nouveau modèle de volatilisation thermique de particules solides. Rev. Gen. Therm. Fr. n° 227, Nov. 1980, 851

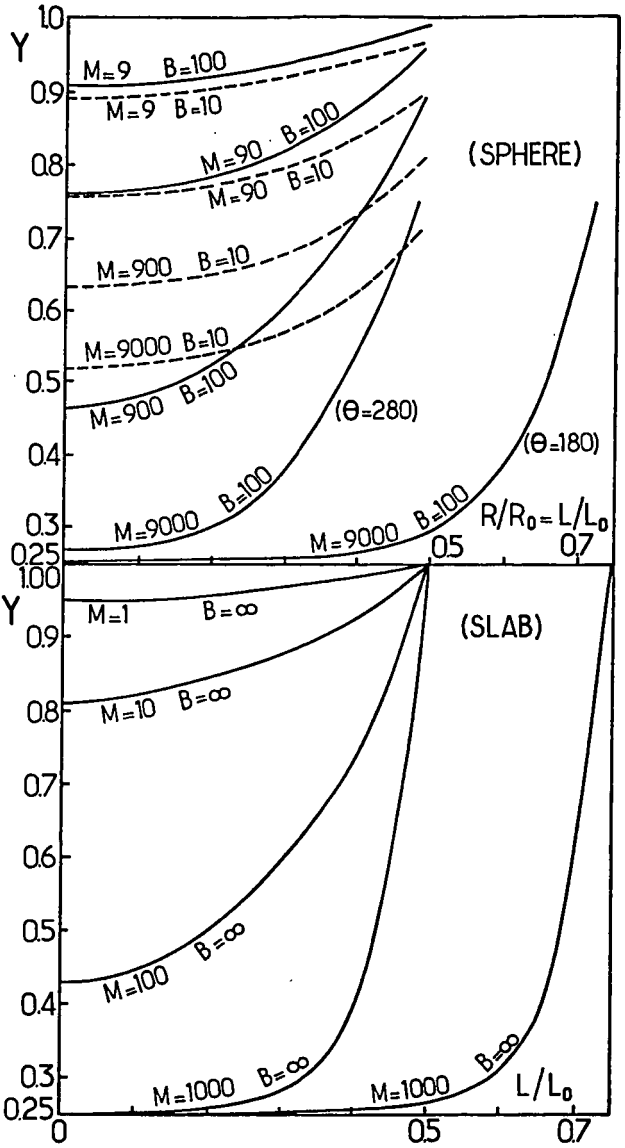

Fig. 1. Internal temperature profiles as a function of M and B (sphere and slab), mainly for $L/L_0 \approx 0.5$. Notice the translation of the profile in ablation regime ($L/L_0 = 0.75 \rightarrow L/L_0 = 0.5$). A = 10, H = 0.5, $Y_0 = 0.25$

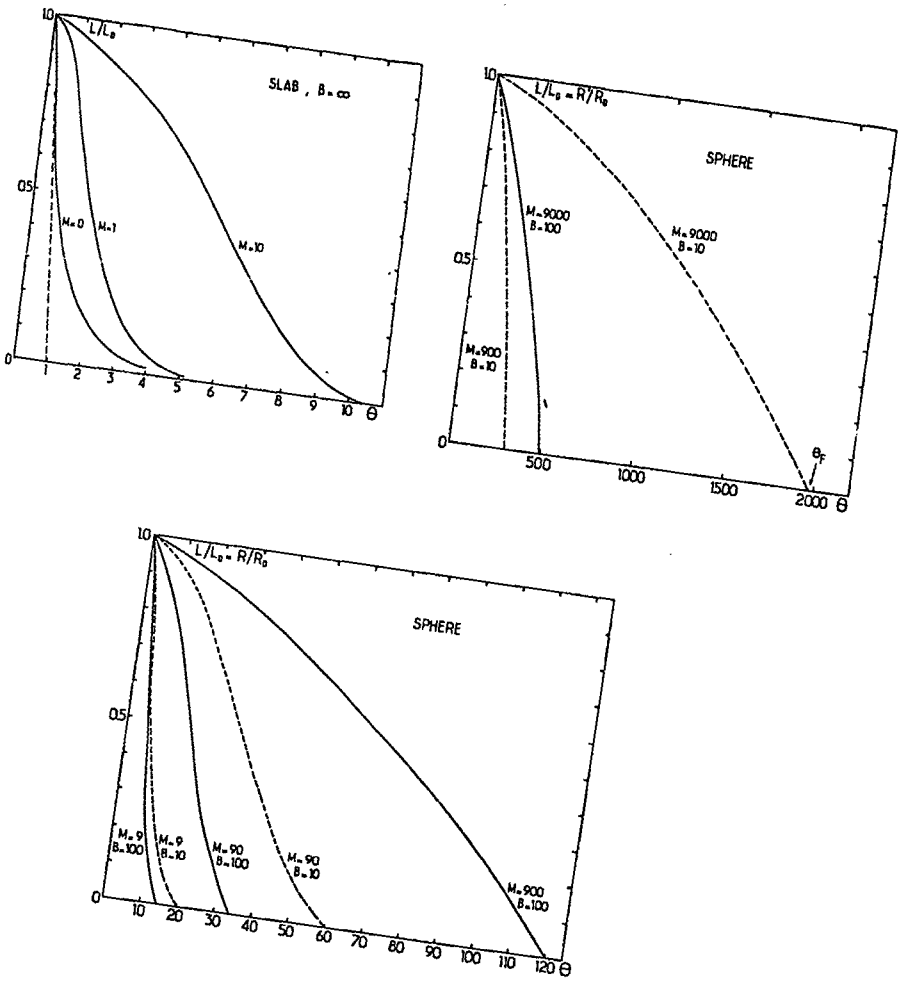

Fig. 2,3,4. Decrease of the particle size (L/L_o) as a function of time θ. Various shapes and conditions. $A = 10$, $H = 0.5$, $Y_o = 0.25$.

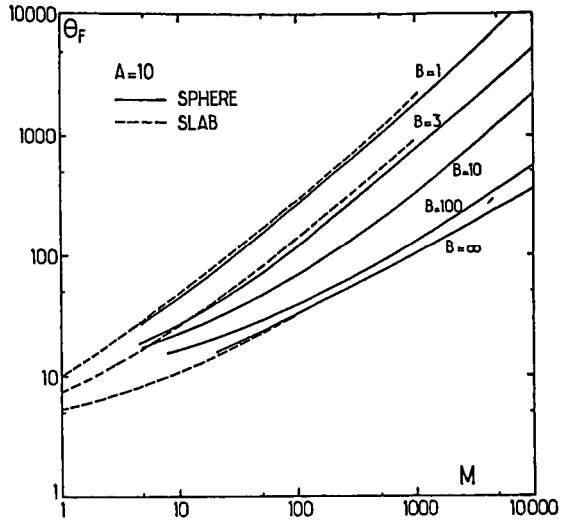

Fig. 5. Time for total consumption θ_F as a function of thermal Thiele modulus M. Various shapes and Biot numbers B (Fourier and Cauchy conditions). Notice the $\sqrt{M}$ dependency in ablation regime. A = 10, H = 0.5, Y_o = 0.25.

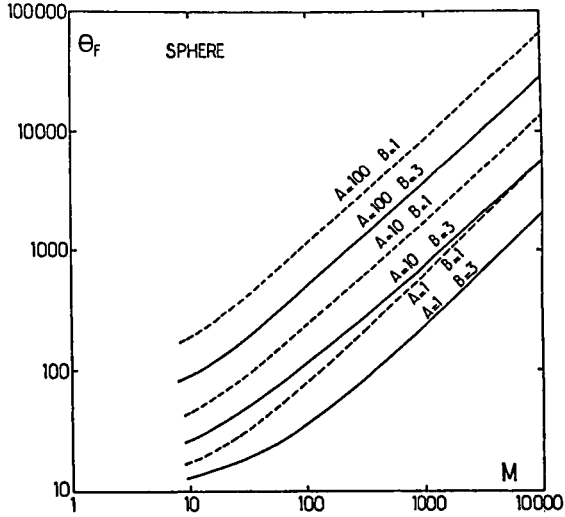

Fig. 6. Time for total consumption $_F$ as a function of thermal Thiele modulus M. Influence of activation parameter A. H = 0.5, Y_o = 0.25.

Numerical Studies of the Radiant Flash Pyrolysis of Cellulose

Virendra Kothari and Michael J. Antal, Jr.*

Department of Mechanical & Aerospace Engineering
Princeton University
Princeton, New Jersey 08544

INTRODUCTION

When biomass particles are heated very rapidly (>1000°C/s) in an oxygen free environment, they undergo pyrolysis with the formation of little or no char (1,2). If concentrated solar energy is used to rapidly heat the particles (3), their temperature may exceed that of the surrounding gaseous environment by several hundred degrees Celsius when pyrolysis occurs (4,5). This "two temperature" effect gives rise to the formation of high yields of sirups from the pyrolyzing biomass (6-8). Our interest in the selective formation of sirups during the radiative flash pyrolysis of biomass caused us to initiate numerical explorations of the combined effects of heat and mass transfer on the radiative flash pyrolysis phenomena. These explorations are described in this paper.

An earlier work (9) presented the derivation of the general equations governing chemical reaction, species, energy, and momentum conservation, as well as the appropriate boundary conditions, for a spherical particle of cellulose undergoing rapid pyrolysis in an intense radiative flux. The following section discusses three simplified sets of equations, which represent three different levels of physical complexity, and offer some insight into the more complex problem.

SIMPLIFIED PYROLYSIS MODELS

The general pyrolysis model (9) is specified by a coupled set of two ordinary and three partial differential equations, as well as the appropriate boundary conditions. The three "level" problems discussed in this section simplify the general problem by representing only the effects of: (1) chemical reaction and external heat transfer, (2) chemical reaction, external and internal heat transfer, and (3) chemical reaction, external heat transfer and internal mass transfer.

The major assumptions underlying the Level 1 problem are that the resistances to heat and mass transfer within the particle are negligible. Hence the particle is assumed to sustain no temperature or pressure gradients within it. We also assume that only a single vapor phase species (levoglucosan) is present within the particle, and we neglect the kinetic energy of the vapor as well as the rate of change of its enthalpy relative to that of the cellulose. Integrating over the volume of the particle, the energy conservation equation becomes

$$V_p(\rho_s c_{ps}+\rho_c c_{pc})\frac{dT}{dt} = V_p\Delta H(-W_s) + A_p\alpha FI + A_p\bar{h}(T_f-T) + A_p\varepsilon\sigma(T_w^4-T^4) \qquad 1)$$

The reaction rate W_s is given by

$$W_s = \frac{-d\rho_s}{dt} = A' e^{-E/R_g T}\left(\frac{V^*}{\rho_{so}}\right)^{n-1}\rho_s^n \qquad 2)$$

*Author to whom correspondence should be sent.
Present address: Department of Mechanical Engineering
University of Hawaii
Honolulu, Hawaii 96822

where

$$\rho_c = a(\rho_{so} - \rho_s) \qquad 3)$$

with $\rho_{so}, \rho_c = 0$ and $T = T_i$ at $t = o$. In previous studies, a constant value for the heat transfer coefficient $\bar{h}$ was assumed. As discussed in Reference 7, the outward bulk flow of voltatiles generated by pyrolysis effectively reduces the rate at which heat is transferred from the surrounding gaseous environment to the particle. The corrected heat transfer coefficient $\bar{h}$ is related to the uncorrected value h by

$$\frac{\bar{h}}{h} = \frac{\phi_h}{e\phi_{h-1}} \qquad 4)$$

To nondimensionalize equations 1 -4 we take as a reference temperature T_p the temperature at which the devolatilization rate is maximum. A reference time is chosen to be $(T_p - T_i)/\beta$ where β is a characteristic average heating rate. Table 1 summarizes the six dimensionless parameters Θ_1-Θ_6 which result from a nondimensionalization of Eq. 1. A further discussion of the significance of these parameters is given in the following section.

The Level 2 problem accounts for the existence of temperature gradients within "large" particles undergoing rapid heating, or particles with a low thermal diffusivity. The resistance to mass transfer is still presumed to be negligible; pyrolytic vapors exit the particle without holdup. With these assumptions, the energy equation becomes

$$(\rho_s c_{ps} + \rho_c c_{pc})\frac{\partial T}{\partial t} = \Delta H(-w_s) + \frac{1}{r^2}\frac{\partial}{\partial r}\left(r^2 k_e \frac{\partial T}{\partial r}\right) - N\frac{\partial}{\partial r}(c_p T) \qquad 5)$$

wherein the molar flux of volatiles N is given by the species continuity equation

$$\frac{1}{r^2}\frac{\partial}{\partial r}(r^2 WN) = bw_s \qquad 6)$$

The initial and boundary conditions associated with Eqs. 2, 3, 5, and 6, which specify the Level 2 problem, are given by

$$\begin{aligned} t = 0 \quad & \rho_s = \rho_{so}, \rho_c = 0,\ T = T_i,\ N = 0 \\ r = 0 \quad & \frac{\partial T}{\partial r} = 0 \\ r = R \quad & k_e \frac{\partial T}{\partial r} = \alpha FI + \bar{h}(T_f - T) + \sigma\epsilon(T_w^4 - T^4) \end{aligned} \qquad 7)$$

The nondimensionalization of Eqs. 2, 3, and 5-7 introduces the two new dimensionless parameters Θ_7 and Θ_8 given in Table 1.

The Level 3 problem attempts to account for the effects of mass transfer on the Level 1 problem. Two major assumptions are made: (1) the resistance to heat transfer within the particle is negligible; hence the particle is considered to be isothermal, and (2) the mass flux is given by the hydrodynamic flow expression

$$N_i = \left(-p_i \frac{B_o}{\mu}\right)\frac{dc_i}{dr} \qquad 8)$$

Equation 8 presumes viscous flow to be much greater than the diffusive flow, which would be the case if the permeability B_o is large compared to the diffusivity of the gas within the solid. An evaluation of the mass transfer peclet number $\frac{pB_o}{\mu D}$

for this problem results in a value exceeding 4000 (7), justifying assumption (2). With these assumptions, the equation governing the concentration of volatiles within the particle becomes

$$\frac{\partial}{\partial t}(\varepsilon_p cW) - \frac{1}{r^2}\frac{\partial}{\partial r}\left(r^2 pW \frac{Bo}{\mu}\frac{\partial c}{\partial r}\right) = b\dot{w}_s \qquad 9)$$

with $p = cR_gT$. The initial and boundary conditions are given by

$$t = 0 \qquad \rho_s = \rho_{so},\ \rho_c = 0,\ T = T_i, c = p_o/R_gT_i$$

$$r = 0 \qquad \frac{\partial T}{\partial r} = 0 \quad , \quad \frac{\partial c}{\partial r} = 0 \qquad 10)$$

$$r = R \qquad k_e\frac{\partial T}{\partial r} = \alpha FI + \bar{h}\,(T_f - T) + \varepsilon\sigma(T_W^4 - T^4)$$

$$N = \bar{K}\,(c - c_\infty)$$

where $\bar{K}$ is the corrected mass transfer coefficient given by

$$\frac{\bar{K}}{K} = \frac{\phi_m}{e^{\phi_m} - 1} \qquad 11)$$

Thus the Level 3 problem is specified by Eqs. 1-3 and 9-11, whose nondimensionalization introduces the new parameter θ_g (see Table 1). The reader should note that the Level 3 problem is more mathematically complex then its predecessors due to the coupled boundary conditions in Eq. 10, reflected in the dependence of $\bar{h}$ and $\bar{K}$ on ϕ_h and ϕ_m, which are both functions of the unknown flux of volatiles N at the surface of the particle.

RESULTS

The coupled set of ODE's and PDE's making up the Level 1-3 problems were solved using the method of lines (10) as implemented in a modified form (9) of the algorithm PDEONE developed by Sincovec and Madsen (11). The coupled system of ODE's obtained from the method of lines was integrated using the GEARB package developed by Hindmarsh (12). Numerous tests were performed to ensure the integrity (accuracy and precision) of the results, as described in detail in Reference 9.

The influence of the particle diameter, the incident intensity of solar radiation, and the freestream fluid temperature on the time dependent volatilization of the cellulose particle was studied in a variety of numerical simulations. Table 2 catalogues values of the parameters selected for study. Due to space limitations, only a small fraction of the results will be discussed here. The interested reader is referred to Reference 9 for a more complete presentation.

Figures 1 and 2 display the weight loss of a particle as a function of time (as would be measured using a TGA) for particles with diameters of 100 and 500 μm surrounded by steam at 500°C, when exposed to flux densities of 50, 100, 200, 400 and 1600 W/cm^2. Figure 3 shows the temperature histories of a 100 μm diameter subjected to a variety of flux densities with a freestream temperature of 800°C. It is seen that the pyrolysis of the particle can be considered to take place in two stages - a heatup stage and a devolatilization stage. In the heatup stage, the particle heats up rapidly without a significant loss of weight. As the temperature of the particle increases, the reaction rate increases considerably and the devolatilization stage sets in. As a general trend, it is observed that the time taken for complete devolatilization of the particle decreases with increasing solar flux, increasing fluid temperature and decreasing particle size. However, as evidenced in Figure 3, smaller particles subject to lower flux densities reach a stagnation temperature slightly above the freestream temperature after which little temperature change occurs until pyrolysis is complete. This causes the time for volatilization of the smaller particles subject to lower flux densities in cooler environments to increase considerably.

To calculate the values of the dimensionless numbers θ_1-θ_6 associated with the Level 1 problem, T_p and β must be evaluated. An estimate of T_p (1) may be obtained using

$$T_p \cong E/(R_g \ln(A' R_g T_p^2/\beta E)) \qquad 12)$$

where the value β can be estimated using the following formulae for the initial values of the heating rate due to radiation and convection

$$\beta_r = \frac{4\pi R^2 \alpha F I}{\frac{4\pi R^3}{3} \rho_{so} c_{pso}} \qquad 13)$$

$$\beta_c = 4\pi R^2 \frac{h}{2}\left(\frac{T_f - T_i}{2}\right) / \frac{4\pi R^3}{3} \rho_{so} c_{pso} \qquad 14)$$

with $\beta = \beta_r + \beta_c$. As discussed earlier, the value of β decreases during heatup and volatilization. This penomena is illustrated in Figure 4. If the value of β estimated above is reduced by 50%, values for T_p estimated using Eq. 12 usually differ from the exact values by less than 50°C. Larger errors are encountered for small particles and low fluxes, when a stagnation temperature is reached. For these cases, the value $T_p = T_f$ would be more appropriate.

Tables 3 and 4 present representative values of the nondimensional numbers θ_1-θ_6 based on values for T_p and β calculated using the above procedure. Increasing values of θ_1 and θ_2 reflect the decreasing ability of solar radiation to provide both the sensible heat and the endothermic heat of reaction requirements. The anomalous behavior of θ_3 reflects errors associated with our method for approximating the value of β used to calculate T_p. Negative values of θ_4 occur when $T_p > T_f$. For $\theta_4 < -1$ the particle should reach a stagnation temperature, in which case $T_p \cong T_f$ and θ_4 is artificially assigned the value $\theta_4 = 0$. As expected, values of θ_5 and θ_6 are influenced by β and T_p.

If heat transfer to the particle during devolatilization is rate limiting, then a characteristic time t_{dh} for devolatilization can be estimated using

$$t_{dh} = \frac{\Delta H \rho_{so} R}{\alpha F I + h(T_f - T_p)/2} \qquad 15)$$

Similarly, a characteristic heatup time t_{hh} can be defined based on the sensible heat requirement:

$$t_{hh} = \frac{\rho_{so} C_{pso} (T_p - T_i) R}{\alpha F I + h\left(\frac{(T_f - T_i) + (T_f - T_p)}{2}\right)} \qquad 16)$$

Figures 5 and 6 display the relationship between the actual values for t_h and t_d and the estimated values t_{hh} and t_{dh} using Eqs. 15 and 16 above. The evident linear relationship between the estimated and actual values of t_h and t_d provides an algorithm (using Eqs. 15 and 16, and Figures 5 and 6) which accurately estimates t_h, t_d and the total time $t_t = t_h + t_d$ required for pyrolysis without resort to numerical integration of the Level 1 ODE's.

For all of the cases studied in this work $t_h \leq t_d$; consequently chemical kinetics control the total time required for the pyrolysis of the particle. Only for extremely high heating rates does $t_h \leq t_d$.

Figure 7 displays representative results for the Level 2 problem. In general, internal conduction and convection increase the time required for devolatilization, but have little effect on heatup. The increase in t_d is more prominent for larger particles, and higher heating rates. The fact that t_h is not dependent on internal conduction and convection may be understood in terms of the characteristic time for conduction $t_c = R^2/\alpha_s$, which takes on values 4.17, 16.7 and 417 ms for particles with diameters of 50, 100 and 500 μm (respectively). These values of t_c are comparable to the heatup times t_h for the Level 1 problem; hence the value of Θ_7 is close to unity for all the cases studied. Consequently, pyrolysis does not occur at the same time throughout the particle; rather the particle's surface rapidly heats and undergoes pyrolysis while the inside remains "cool." Thus pyrolysis occurs by ablation in all the cases studied, and t_h is unaffected by internal conduction and convection.

Table 5 displays values of Θ_8 calculated using the approximate characteristic temperature T_p defined earlier for the Level 1 problem. Values of Θ_8 indicate that for large particles and higher heating rates the internal convective heat flux (which tends to cool the particle) becomes comparable in magnitude to the conductive heat flux. This effect tends to increase t_d by counteracting heat flow into the particle during pyrolysis. Figure 8 displays the dependence of t_d (Level 2)/t_d (Level 1) vs. Θ_8. The observed linear dependence permits one to correct the estimated value of t_d (obtained by methods discussed earlier for the Level 1 problem) by simply evaluating Θ_8 and multiplying t_d (Level 1) by the appropriate correction factor obtained from Figure 8.

Values of Θ_9 were estimated for the range of parameters studied in this work. In almost all cases $\Theta_9 \geq 10$ (in the worst case $\Theta_9 \approx 1$); consequently for the cases studied volatiles do not accumulate within the particle and no pressure gradients are generated. For this reason, no attempt was made to solve the Level 3 problem.

CONCLUSIONS

For all the cases treated in this work, chemical kinetics control the time required to achieve devolatilization of the particle. Because of ablation, the time required for intraparticle heat transfer plays a less significant role. Mass transfer limitations were not significant for any of the cases studied.

Simple formulae were derived which facilitate rapid accurate estimates of t_h, t_d and t_t for many problems of interest. Evaluation of the nondimensional parameters Θ_1 - Θ_9 should enable other workers to apply the specific results of this work to their own problems.

Table 1

Dimensionless Parameters

Parameter	Expression	Significance
θ_1	$\frac{\rho_{so} c_{pso} R\beta}{\alpha F I}$	sensible heat requirement / heat supplied by incident solar radiation
θ_2	$\frac{\Delta H_o}{c_{pso}(T_p - T_i)}$	heat of reaction / sensible heat
θ_3	$\left(\frac{T_p - T_i}{\beta}\right) / \frac{1}{(V^*)^{n-1} A' \exp(-E/R_g T_p)}$	heatup time / pyrolysis time
θ_4	$\frac{h(T_f - T_p)}{\alpha F I}$	convective heat transfer / incident solar radiation
θ_5	$\frac{\epsilon \sigma T_w^4}{\alpha F I}$	wall radiation / incident solar radiation
θ_6	$\frac{\epsilon \sigma T_p^4}{\alpha F I}$	particle radiation / incident solar radiation
θ_7	$\frac{T_p - T_i}{\beta} \Big/ \frac{R^2 \rho_{so} c_{pso}}{k_{eo}}$	Heatup time / conduction time
θ_8	$R^2 \left(\frac{\rho_{so}}{W}\right) V^{*n-1} A' \exp(-E/R_g T_p) c_{po} / k_{eo}$	internal convection / conduction
θ_9	$\frac{P_o^2 \kappa B_o}{R^2 R_g T_p \mu} \Big/ b \rho_{so} (V^*)^{n-1} A' \exp(-E/R_g T_p)$	volatiles flow rate / volatiles generation rate

Table 2

Selected Values of Parameters
Used in the Simulations

Particle diameter	=	50, 100 and 500 μm
Flux density	=	50, 100 200, 400 and 1600 W/cm^2
Freestream temperature	=	500° and 800°C

Table 3

Values of dimensionless parameters
100 μ diameter, T_f = 500°C

I (W/cm^2)	θ_1	θ_2	θ_3	θ_4	θ_5	θ_6
1600	1.635	-0.0245	10.282	-0.275	0.003	0.051
400	2.041	-0.0273	10.651	-0.877	0.036	0.153
200	2.583	-0.0285	11.046	-1.598	0.072	0.274
100	3.667	-0.0510	?	?	0.144	0.144
50	5.834	-0.0510	?	?	0.283	0.288

Table 4

Values of dimensionless parameters
500 μ diameter, T_f = 500°C

I (W/cm^2)	θ1	θ2	θ3	θ4	θ5	θ6
1600	1.526	-0.0285	10.434	-0.004	0.009	0.034
400	1.607	-0.0318	11.372	-0.122	0.036	0.104
200	1.715	-0.0336	11.532	-0.210	0.072	0.182
100	1.931	-0.0354	11.451	-0.358	0.144	0.321
50	2.363	-0.0370	11.419	-0.612	0.288	0.578

Table 5

Values of the dimensionless parameter, θ_8

T_f = 800°C

I	Particle diameter		
(W/cm^2)	50 μ	100 μ	500 μ
1600	0.252	0.531	2.78
200	0.084	0.155	0.54
50	0.063	0.108	0.232

T_f = 500°C

I	Particle diameter		
(W/cm^2)	50 μ	100 μ	500 μ
1600	0.236	0.488	2.74
200		0.108	0.485
50			0.169

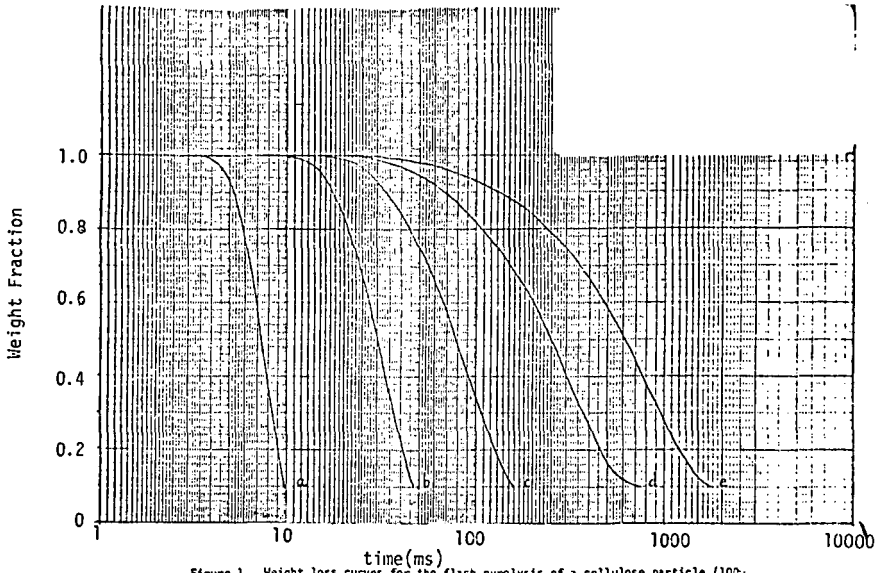

Figure 1. Weight loss curves for the flash pyrolysis of a cellulose particle (100μ diameter) in steam (T_f=500°C) at varying flux levels.

Curve	a	b	c	d	e
Flux(W/cm^2)	1600	400	200	100	50

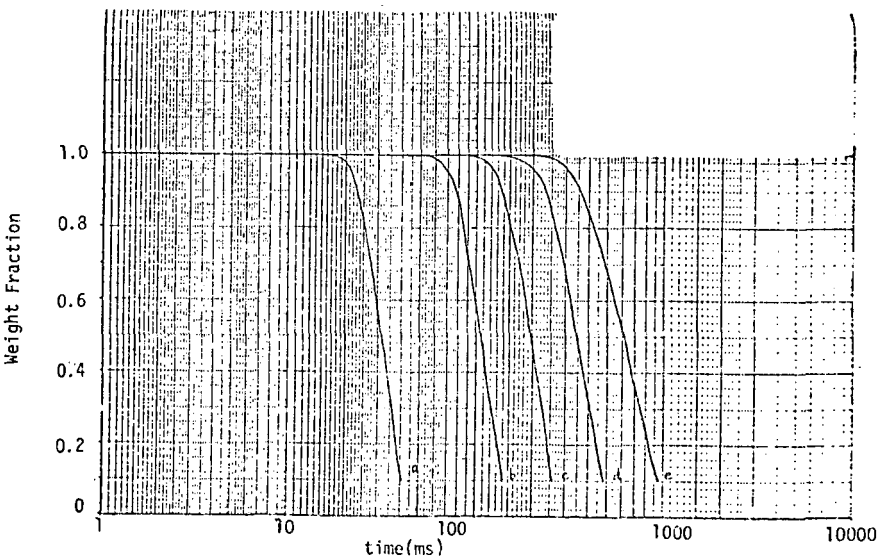

Figure 2. Weight loss curves for the flash pyrolysis of a cellulose particle (500μ diameter) in steam (T_f=500°C) at varying flux levels.

Curve	a	b	c	d	e
Flux(W/cm^2)	1600	400	200	100	50

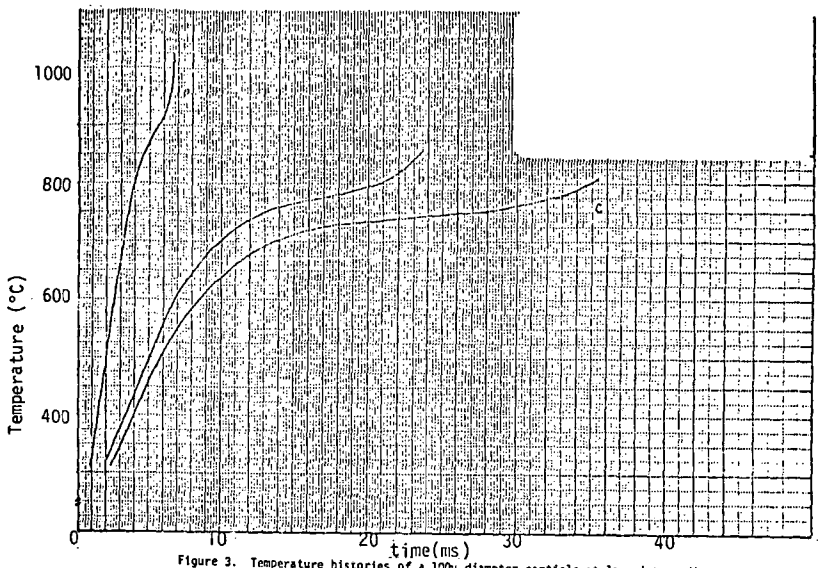

Figure 3. Temperature histories of a 100μ diameter particle at low, intermediate and high fluxes. T_f=800°C

Curve	a	b	c
Flux(W/cm^2)	1600	200	50

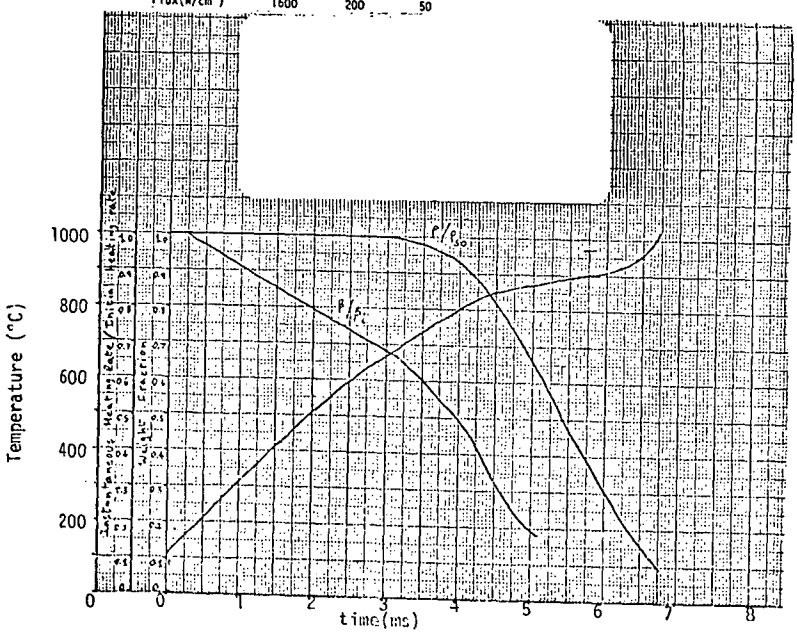

Figure 4. Weight loss, Temperature and heating rate for a 100μ diameter particle, T_f=800°C, I=1600W/cm^2

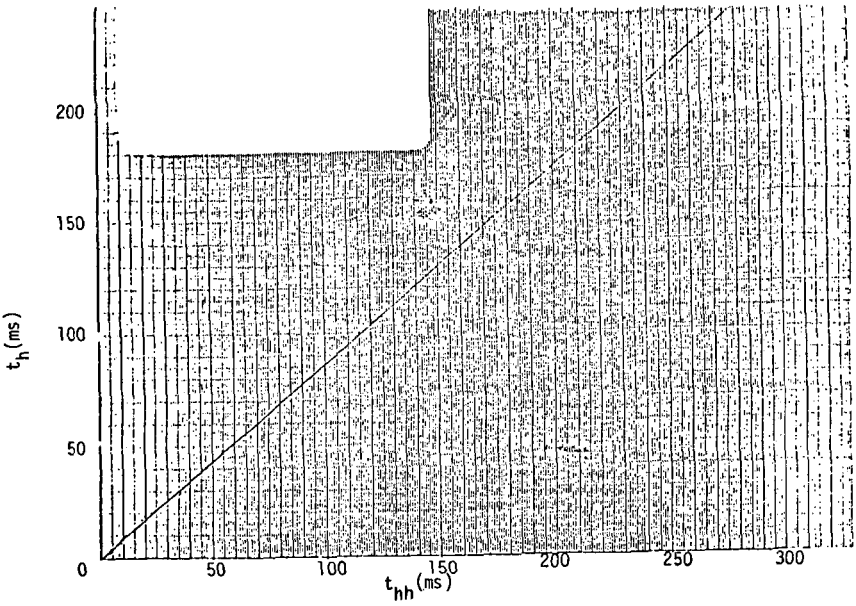

Figure 5. Plot of numerically computed heatup time, t_h, vs. characteristic heatup time, t_{hh}

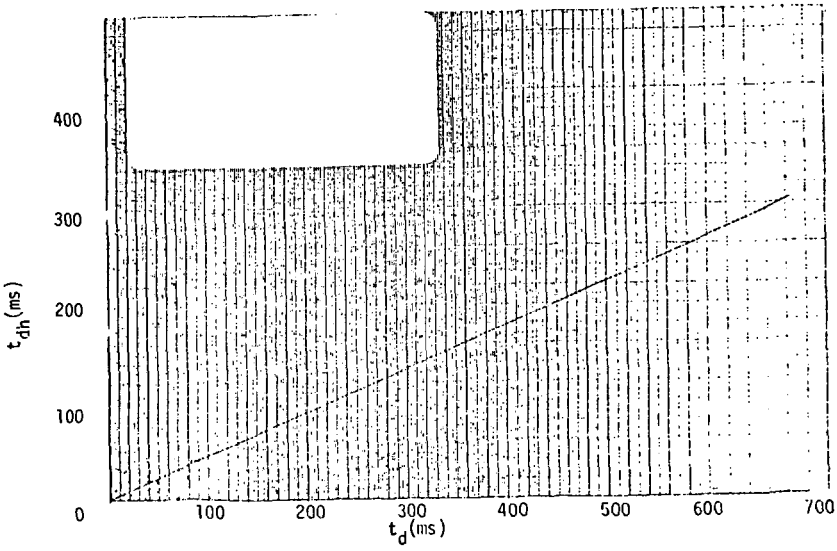

Figure 6. Plot of numerically computed devolatilization time, t_d, vs. characteristic devolatilization time, t_{dh}

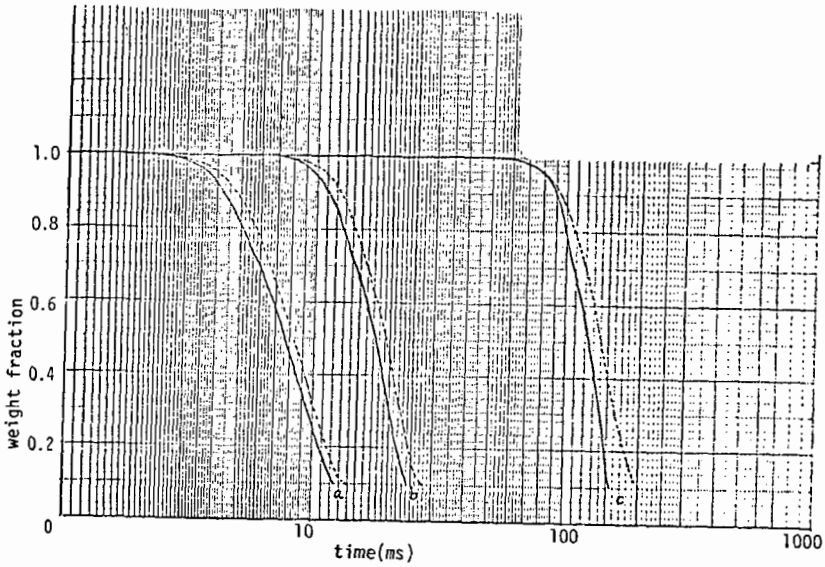

Figure 7. Plot of numerically computed heatup time, t_h, vs. characteristic heatup time, t_{hh}

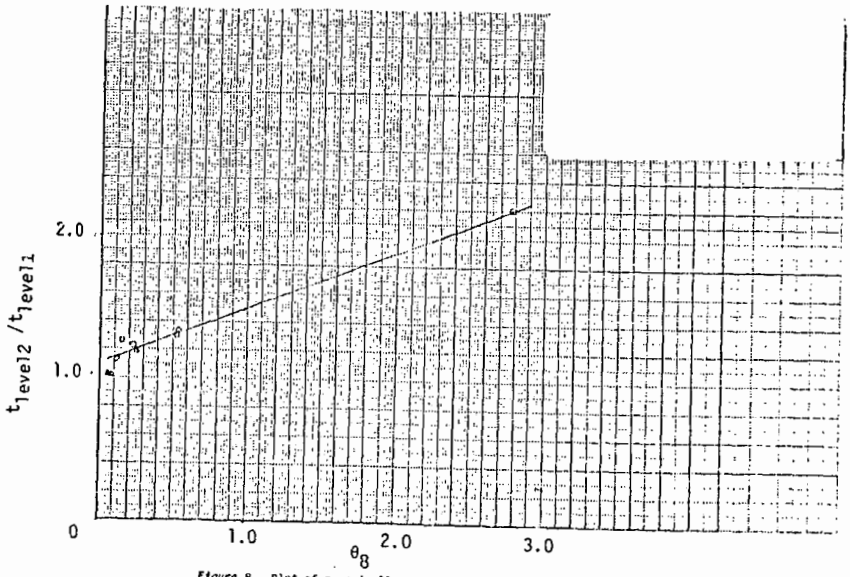

Figure 8. Plot of numerically computed devolatilization time, t_d, vs. characteristic devolatilization time, t_{dh}

REFERENCES

1. M.J. Antal, Jr. "The Effects of Residence Time, Temperature and Pressure on the Steam Gasification of Biomass" in "Biomass as a Non Fossil Fuel Source" D.E. Klass ed. A.C.S. Symposium Series No. 144, American Chemical Society, Washington, D.C. 1981 pp 313-334.

2. M.W. Hopkins, M.J. Antal, Jr., and J.G. Kay, "Radiant Flash Pyrolysis of Biomass Using a Xenon Flashtube", J. Applied Polym. Scie., in press.

3. M.J. Antal, L. Hofmann, J.R. Moreira, C.T. Brown, and R. Steenblick, "Design and Operation of a Solar Fired Biomass Flash Pyrolysis Reactor", Solar Energy, 30, pp 299-312, 1983.

4. L. Hofmann, "Experimental and Theoretical Simulations of Solar Powered Biomass Pyrolysis Reactors", MSE thesis, Princeton University, Princeton, N.J. 1981.

5. L. Hofmann and M.J. Antal, Jr., "Numerical Simulations of Solar Fired Biomass Pyrolysis Reactors", submitted for publication in Solar Energy.

6. C.I. DeJenga, M.J. Antal and M. Jones, "Yields and Composition of Sirups Resulting from the Flash Pyrolysis of Cellulosic Materials Using Radiant Energy", J. Applied Polym. Scie., 27, pp 4313-4322 (1982).

7. M.W. Hopkins, "Investigations of the Flash Pyrolysis of Biomass Using Simulated Solar Radiation", MSE thesis, Princeton University, Princeton, N.J. 1982.

8. M.W. Hopkins, C.I. DeJenga, and M.J. Antal, "The Flash Pyrolysis of Cellulosic Materials Using Concentrated Visible Light", Solar Energy, in press.

9. V.S. Kothari, "Numerical Studies of the Flash Pyrolysis of Cellulose", MSE thesis, Princeton University, Princeton, N.J. 1980.

10. O.A. Liskovets, "The method of Lines (review)." Differential Equations, 1, 1308. (English Translation). (1965).

11. R.F. Sincovec and N.K. Madesen, "Software for nonlinear partial differential equations." ACM Trans. Math. Software 1, 232. (1975).

12. A.C. Hindmarsh, "GEAR: Ordinary differential equation system solver." Report UCID-30001 Rev. 2, Lawrence Livermore Lab., Livermore, California. (1974).

A MATHEMATICAL MODEL FOR STRATIFIED DOWNDRAFT GASIFIERS

Thomas B. Reed, Benjamin Levie, and Michael L. Markson
Solar Energy Research Institute, Golden, CO 80401

Michael S. Graboski
Colorado School of Mines, Golden, CO 80401

INTRODUCTION

The downdraft gasifier originating from World War II Swedish designs has proven to be successful in generating a clean product gas when operated in an air blown mode. Such gas producers are useful for generating an essentially tar free boiler gas or engine fuel from renewable resources such as wood and agricultural waste. Recently, a new generation of stratified downdraft gasifiers (1, 2) has been studied. A successful model of this type of gasification process should be able to clearly show the interdependency of operating variables in order to optimize both cost of gasifier and performance. Such a process model would be useful in determining the proper gasification conditions when input conditions or design parameters change.

Figure 1 shows the important features of the gasifier. Biomass fuel and oxidizer are fed cocurrently to the top of the gas generator where pyrolysis of the fuel takes place. The pyrolysis reaction is driven by heat transfer from the gas and hot char bed below. As the fresh solid is heated it dries and devolatilizes. The volatiles evolved contain combustible species which react with oxygen/air to produce heat, CO, CO_2, H_2, H_2O and light hydrocarbons. During pyrolysis, the gas and solid are at vastly different temperatures because pyrolysis cools the solid while oxidation heats the gas. (At the end of pyrolysis the gas may be more than 500K hotter than the solid.) In this zone of the reactor, about 80% to 90% of the solid weight loss occurs.

Once oxygen is consumed and pyrolysis is completed, reduction of char by CO_2 and H_2O can occur in the gasification zone. The reactions occurring are endothermic so that the gas and solid temperatures fall as carbon conversion proceeds. The reactions tend to quit at about 1000K due to kinetic limitations.

In the steady-state operation of the downdraft gasifier, a specific oxygen to fuel ratio exists for a given feedstock and carbon conversion level. In practice it is found that gasifier throughput does not affect the required O_2/fuel ratio and the product gas composition for a sufficiently deep char bed. Also, it is found that the majority of hydrocarbons are destroyed in the pyrolysis zone. These data suggest that the pyrolysis and gasification zones are to a good approximation separate and that the whole char bed in downdraft gasifiers is not truly active.

In the char gasification zone three reactions dominate (neglecting the cracking of residual tars and hydrocarbon gases from the pyrolysis zone):

Boudouard Reaction

$$\text{Char} + CO_2 \rightarrow 2CO \quad \Delta H = +40{,}778 \text{ kcal/mol}$$

Water Gas Reaction

$$\text{Char} + H_2O \rightarrow CO + H_2 \quad \Delta H = +32{,}472 \text{ kcal/mol}$$

Water Gas Shift Reaction

$$H_2O + CO \rightleftharpoons H_2 + CO_2 \quad \Delta H = -8306 \text{ kcal/mol}$$

The kinetics and thermodynamics of these reactions determine the conversion of char to gas and the subsequent gas composition at any point in the char gasification zone.

In the reaction scheme, the water-gas and Boudouard reactions are coupled by the shift reaction. Therefore, only two of these reactions can be considered to be truly independent. The water-gas shift reaction is fairly rapid over carbon surfaces at gasification temperatures and is assumed to be in equilibrium in this investigation. In our model we have assumed that Edrich et al. (3) kinetics for the Boudouard reaction over ponderosa pine charcoal approximates the carbon reduction reaction occurring in the gasifier. Since the activation energy for carbon reduction by CO_2 is about 35 kcal, kinetics in error by a factor of 2 will be equivalent to a 50°C offset. This offset is within the accuracy of data available for bed temperature. At atmospheric pressure, this reaction sequence should adequately describe the kinetic processes. At elevated pressure, methane forming kinetics should probably be considered. For char particles with minor dimensions up to 3/4 inch, Edrich et al. (3) also show that intraparticle mass transfer is not important. Therefore, the same rate expression for char gasification applies regardless of particle size (if less than 3/4 inch).

The reactor design conditions which affect the char gasification zone include initial conditions, such as char and gas temperatures, flow rate and composition of the incoming gas, and gasifier parameters, such as char gasification kinetics, cross-sectional area of reactor, heat transfer from the gas to the solids, and the density and void fraction of the char. An adequate model must account for changes in these initial conditions and parameters.

To date the most extensive modelling of the char zone of the stratified downdraft gasifier has been developed by Reed (1). Reed's model of the char gasification zone assumes equal molar feed rates of CO_2 and carbon (char). This zone is assumed to be adiabatic, yielding a change in temperature of about 24°K per 1% of reaction of carbon. Coupling the temperature change to the kinetics of the Boudouard reaction then yields the conversion of carbon and temperature of the reaction versus time and position (depending on feed rate). The model gives a good first approximation of the gasifier behavior leading the way towards the use of theory for practical predictions.

MODEL FORMULATION

The overall gasifier model consists of two parts; these are a pyrolysis model and a gasification model. The pyrolysis model is used to provide a starting gas composition, flow rate, and temperature for the char gasification zone. To initiate the modelling, the air/fuel or O_2/fuel ratio, feed ultimate and proximate analysis and a methane leakage from the gasifier are specified. The model generates pyrolysis gas composition and temperature along with carbon conversion gas composition and temperature along the char bed length.

Pyrolysis Model

Biomass is assumed to be artificially composed of fixed carbon (char) and volatile matter. Upon pyrolysis, for biomass under downdraft gasifier conditions, the char yield is assumed to be equal to that from the proximate yield. The char is treated as pure carbon. With the specification of an air or O_2/fuel ratio and feed composition, an adiabatic reaction calculation around the pyrolysis zone will yield temperature, gas composition and flow rate. It is further assumed that any methane escaping pyrolysis is not cracked in the char bed. Therefore, the mass and energy balance around the pyrolysis zone allows for the methane leakage specified as a model input.

In order to calculate the adiabatic flame temperature of the pyrolysis gas, when it is oxidized by the air or oxygen, first the energy released by the combustion is determined.

$$\Delta H_{298} = HHV - \Delta H_{combustion}$$

where ΔH_{298} is the energy released from the pyrolysis and partial combustion assuming N_2, CO, CO_2, H_2, H_2O, CH_4, and char are the only products, HHV is the high heating value of the biomass (calculated by the ITG method), and $\Delta H_{combustion}$ is the sum of the moles of the products of pyrolysis times their heats of combustion. In the model predictions presented below, a typical biomass composition of 51 percent carbon, 6 percent hydrogen and 43 percent oxygen by weight was assumed for the material balance calculation.

The adiabatic flame temperature can then be determined by the following equation

$$\int_{T_{298}}^{T_{flame}} \Sigma m_i Cp_i = \Delta H_{298}$$

In this model an integral average value of C_{Pi} for each of the gas constituents is utilized. The calculated adiabatic flame temperature is then used to determine the correct K_p and gas composition in a second iteration. Since the flame temperature varies little with changes in K_p, only two iterations are necessary for accurate gas composition and adiabatic flame temperature predictions. Specifying the amount of fixed carbon yielded from the biomass and the oxygen to fuel ratio gives a unique gas composition and temperature.

Char Gasification Model

The char gasification model described below assumes that the char gasification zone is adiabatic and, as in the pyrolysis zone, the water gas shift reaction is at equilibrium. Char gasification kinetics are employed to compute the conversion/length profile. Heat balances on the gas and solid are used to determine temperature profiles. Material balances written for gas and char in the reactor assume plug flow; however, the gas and char move at different rates down the reactor. The fractional conversion of the char, X, is defined as follows:

$$X = (\dot{m}_c(0) - \dot{m}_c(z))/\dot{m}_c(0)$$

where $\dot{m}_c(0)$ = molar flow rate of carbon at top of gasification zone, and $\dot{m}_c(z)$ = molar flow rate of carbon at position "z" in the gasification zone. The carbon mass balance is then:

$$\dot{m}_c(0)dX/dz = r_c S$$

where X is the fractional conversion of the char, z is the distance down the reactor, r_c is the rate of conversion of in moles char/min, S is the cross sectional area of the reactor, and $\dot{m}_c(0)$ is the char feed rate in moles char/min. The rate is computed from kinetic data.

For the Boudouard reaction:

$$-r_c = (k_1 \cdot PCO_2)/(1 + k_2 \cdot PCO)$$

$$k_1 = \exp(-E_1/RT + 12.3091)$$

$$k_2 = \exp(-E_2/RT - 28.4295)$$

where r_c is in units of 1/min, $E_1 = 43870 - 19811/T_p$ (pretreatment) cal/mol, $E_2 = -67,300$ cal/mol and PCO and PCO_2 are partial pressures of CO and CO_2 respectively. The pretreatment temperature is the temperature at which the biomass is pyrolyzed. In this model it is assumed to be 1000K. For the purpose of this model, the bed voidage and particle size are assumed constant. Shift kinetics are assumed to be rapid. Thus, the gas composition is brought to a water gas shift equilibrium at each position in the reactor. To account for kinetics the equilibrium constant is displaced from the gas temperature by 50°C.

The energy balance includes individual equations for the char, and one for the gas phase. In the gas phase:

$$\Sigma m_g cp_g \frac{dT_g}{dz} = h \cdot A_p \ (T_s - T_g) \ \rho \ (1-\varepsilon) S$$

where m_g is the mass flow rate of the gas, cp_g is the heat capacity of the gas, T_g is the gas temperature, h is the heat transfer coefficient between the gas and the char, A_p is the surface area per gram char, T_s is the char temperature. ρ is the char density and ε is the void fraction in the bed.

For the solid phase

$$\Sigma m_s cp_s \frac{dT_s}{dz} = - \Sigma m_g cp_g \frac{dT_g}{dz} - \left(\dot{m}_c(0) \cdot \frac{dX}{dz} \cdot \Delta H_B + \dot{m}_{H_2O}(0) \frac{dY}{dz} \cdot \Delta H_{WGS}\right)$$

where X is the conversion of char, H_B is the heat of reaction for the Boudouard, Y is the conversion of steam to hydrogen, and H_{WGS} is the heat of reaction for the water gas shift reaction. The mass and energy balances are coupled and solved using a Runge Kutta integration routine in an interactive mode.

The model results are very dependent on initial conditions, including the input from the pyrolysis model calculations of temperature and composition of the gas. The average temperature of the solid is not known exactly but is assumed to be somewhere between the flame temperature and the pyrolysis front temperature. The solid temperature is not critical, since the heat transfer coefficient is large and the heat capacity of the solid phase is small relative to the gas phase.

The heat transfer coefficient in the energy balance has been calculated by an empirical correlation of Satterfield (4) for fixed bed reactors. The model needs the area to volume ratio of the feedstock to calculate the heat transfer coefficient, h, and the particle area to weight ratio, A_p.

EXPERIMENTAL DATA

To compare the prediction of the model with experimental gasifier results, a quartz tube gasifier 54 mm outer diameter, shown in Fig. 2, was employed. A type K 1/16-in. thermocouple was used for temperature measurement through the pyrolysis and gasification zones. A 1/16-in. 304 SS tube was placed directly alongside the thermocouple, through which gas samples were pulled. A 10 cc syringe (+ needle) was used to evacuate the tube and to take the sample. Gas analysis was done with a Carle #111H gas chromatograph, with a hydrogen transfer tube and a ten ft Carbosieve column. Integration of analysis was performed with a Varian # CDS111 integrator.

Two samples were taken for each level measured. Once a steady state conditon in the gasifier was achieved, the probes were inserted to the specified level and the gas sampling temperature recording procedure begun. The probes were then moved at 2 cm intervals up through the bed until the temperature read below gasification pyrolysis temperatures (100°C). The time interval in between each sample was approximately 1 minute.

RESULTS

Table 1 presents results of the pyrolysis material and energy balance model. The adiabatic flame temperatures of the pyrolysis products, assuming fractions of fixed carbon from 0.05 to 0.20 when burned with various ratios of O_2/fuel has been calculated. The model also yields the gas composition at the end of pyrolysis for each fixed carbon and O_2/fuel ratio. The gas temperature and composition is then input into the gasification model. For predictions of the laboratory data, the fixed carbon is assumed to be 15% and the O_2/fuel ratio is set at 0.45. For the oxygen runs the O_2/fuel ratio is assumed to be 0.40. The results presented yield varying char loss through the grate. An alternate calculation is to iterate on the air/fuel ratio to consume a specified amount of fixed carbon.

Table 1. Pyrolysis Model Calculations

Feed Gas	O_2/Fuel	Fraction Fixed Carbon	Adiabatic Flame Temperature (K)
Air (O_2)	0.4	0.05	575 (888)
		0.10	764 (1182)
		0.15	955 (1475)
		0.20	1146 (1765)
	0.45	0.05	745 (1201)
		0.10	924 (1490)
		0.15	1104 (1775)
		0.20	1282 (2055)
	0.50	0.05	897 (1504)
		0.10	1067 (1785)
		0.15	1236 (2061)
		0.20	1403 (2330)

Figure 3 shows the model predictions of the char and gas phase temperature profiles through the gasifiction zone for air gasification. The solid phase is represented by the solid line, the gaseous phase is represented by the dotted line and the experimental data are represented by stars. Excellent agreement with the data is observed throughout the char gasification zone, with the exception of the data point at the grate. This discrepancy is caused by heat loss (conduction and radiation) at the grate, resulting in lower temperature measurements than expected. In a reactor with a layer of ceramic balls above the grate it would be expected that heat loss would not be important.

Figure 4 shows predictions and experimental data of the CO/CO_2 ratio down the reactor. The agreement between model predictions and experimental data is good

confirmation of the model. Since no adjustable parameters were input into the model to make the temperature profile and CO/CO_2 ratio predictions, the model appears successful at simulating laboratory conditions.

The effect of varying throughput on char conversion is shown in Fig. 5. In this figure, the result of inputting into the model ten times normal, normal, and one tenth normal air thorughput is illustrated. Quantitatively, after the solid and gas have come to the same temperature, the conversion of char for a given distance is linearly dependent on the throughtput. Although an increase in throughput increases the heat transfer from the gas to the solid, the net effect on char conversion, as yielded by model calculations, is the same char conversion for equivalent residence times, regardless of throughput. Increasing the surface area/volume ratio for the feedstock also increases heat transfer from gas to char, but again no significant difference in conversion occurs for various ratios, after the gas and solid temperatures approach the same point.

Figure 5 also shows the char conversion for a throughput consisting of oxygen instead of air. An interesting outcome from using oxygen in the model calculations is that the temperature of the char only rises about 50K above the peak temperature of the air gasification case, as depicted in Fig. 6. This is in spite of the initial gas temperature of the oxygen run of 1750K, compared to 1400K for the air case. Similar results have been observed in the laboratory for the oxygen gasifier. The reason for this phenomenon is the buffering effect of the endothermic gasification reactions which increase their rates at higher temperatures, thus converting greater amounts of sensible heat to chemical energy. The end result then is not higher temperatures in the reactor but higher conversion of the char in the gasification zone.

CONCLUSIONS

(1) A pyrolysis model has been developed which yields gas temperature and composition for both air and oxygen gasification. The results of this model are then input into a separate char gasification model.

(2) A char gasification model has been developed which utilizes no adjustable parameters to predict design parameters and gasifier process conditons.

(3) The two models yield realistic temperature profiles of the solid and gas phases down the reactor. Predictions compare very well with laboratory data.

(4) The CO/CO_2 ratio predicted agree well with laboratory data.

(5) The model shows an essentially linear correlation between throughput and char conversion for a given reactor length.

(6) The model predicts equivalent conversions of char for various surface to volume ratios of the same feedstock.

(7) The model demonstrates the buffering effect of the endothermic gasification reactions in keeping down the char temerpature in an oxygen gasifier.

RECOMMENDATIONS

(1) A model should be incorporated to give the residence time and integral average temperature of the char after pyrolysis. This addition would allow determinations of the appropriate reactor length for complete gasification, and remove the estimation of initial particle temperature in the char gasification zone.

(2) Experimental data shold be taken with various gasifier conditions and designs to check model predictions and assumptions.

ACKNOWLEDGEMENTS

Support for this project from the Office of Alcohol fuels of the United States Department of Energy is gratefully acknowledged. Review of this paper by J. Diebold and T. Milne is sincerely appreciated.

REFERENCES

1. Reed, T.B., M. Markson, "A Predictive Model for Stratified Downdraft Gasification of Biomass," Proceedings of the 14th Biomass Thermochemical conversion contractors Meeting. Atlanta, GA, 1982.

2. Walawender, Walter P., S. M. Chern and L. T. Fan, "Wood Chip Gasification in a Commercial Downdraft Gasifier," Presented at the International Conference on Fundamentals of Thermochemical Biomass Conversion. Estes Park, CO, 18-22 October 1982.

3. Edrich, R., T. Bradley, and M. S. Graboski, "The Gasification Kinetics of Ponderosa Pine Charcoal," Presented at the International Conference on Fundamentals of Thermochemical Biomass Conversion. Estes Park, CO, 18-22 October 1982.

4. Satterfield, C. N. Mass Transfer in Heterogeneous Catalysis. MA: MIT Press, 1970.

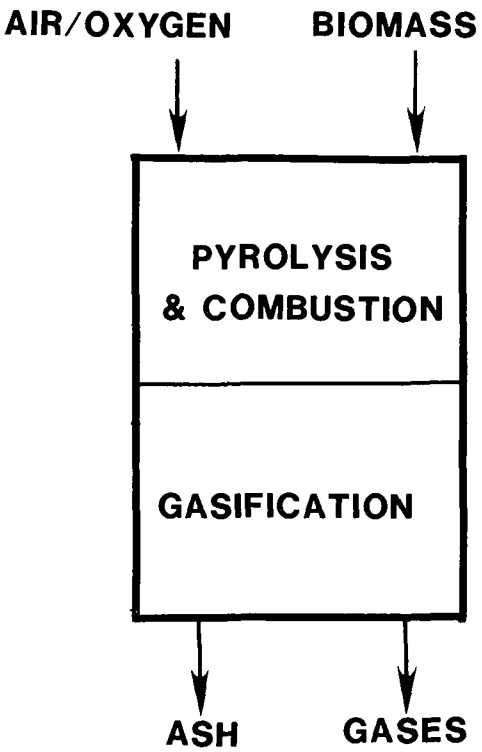

Figure 1. Stratified Downdraft Gasifier.

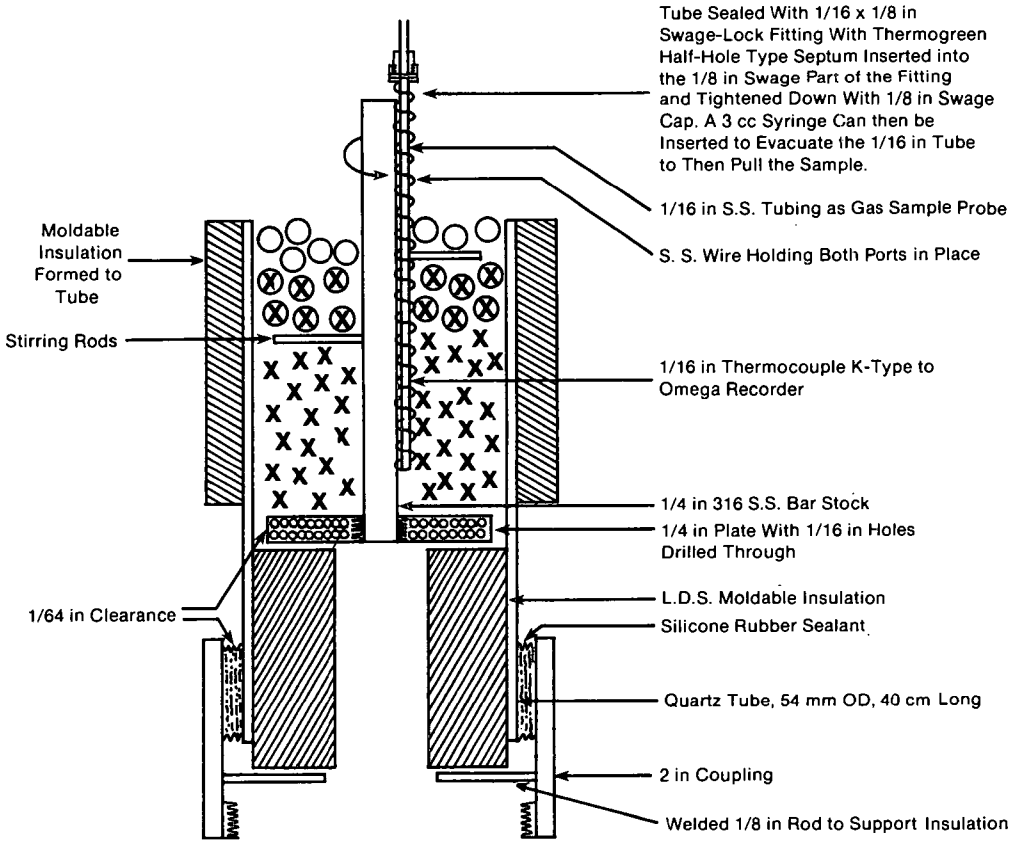

Figure 2. Quartz Tube Gasifier and Measurement Apparatus.

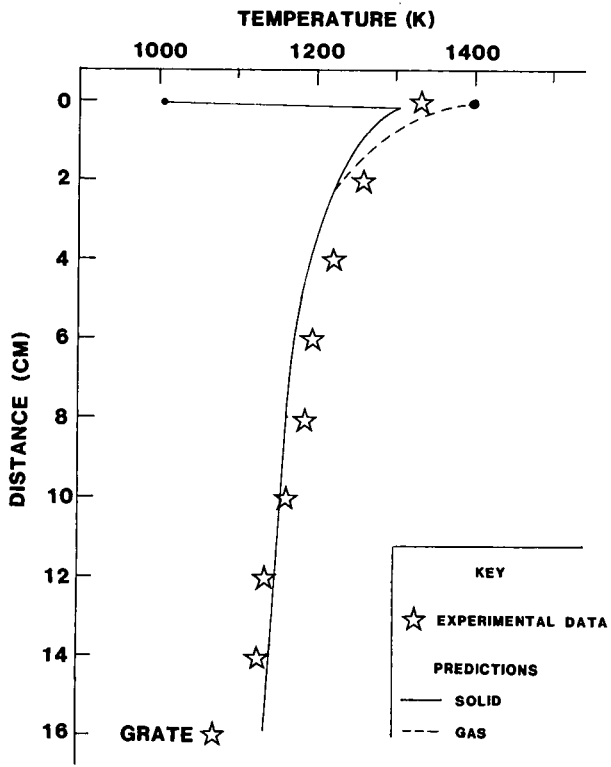

Figure 3. Char Gasification Zone Solid and Gas Temperature Predictions and Experimental Data for Air Gasifier with 1/4-in. Wood Chips.

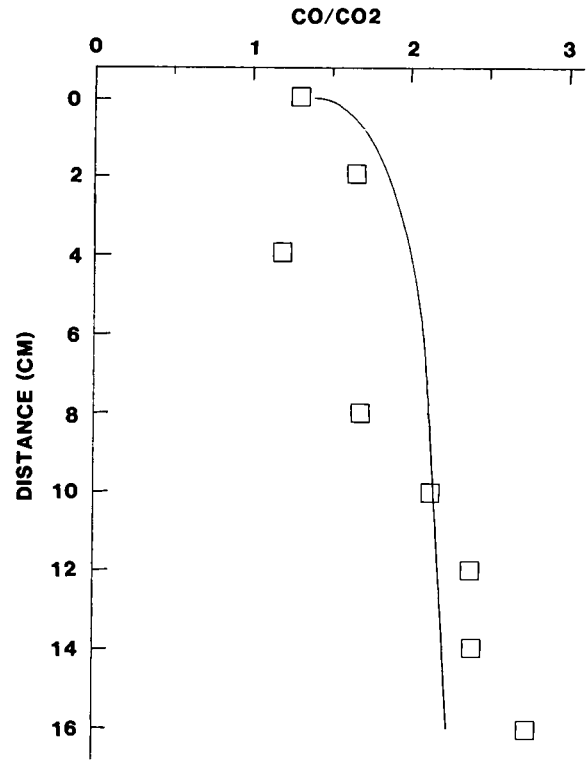

Figure 4. Char Gasification Zone CO/CO_2 Prediction and Experimental Data for Air Gasifier with 1/4-in. Wood Chips.

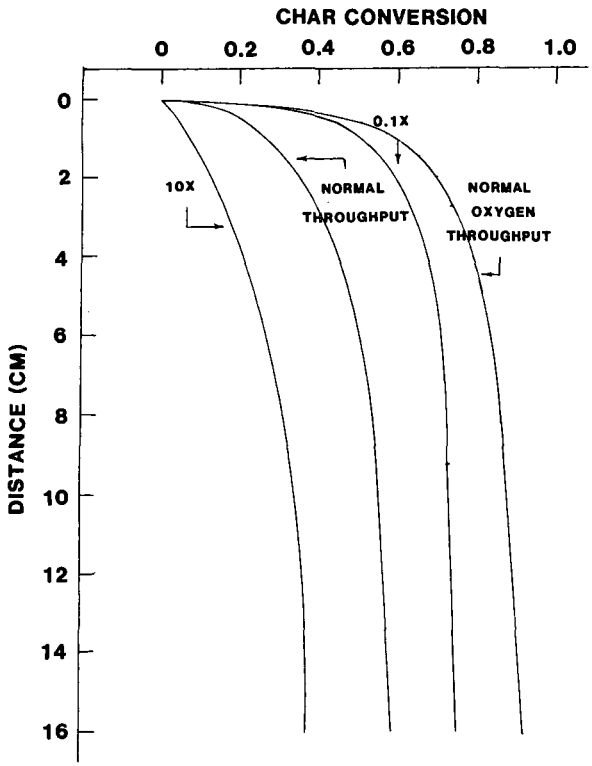

Figure 5. Char Gasification Zone Fractional Char Conversion for Various Air and Oxygen Throughputs.

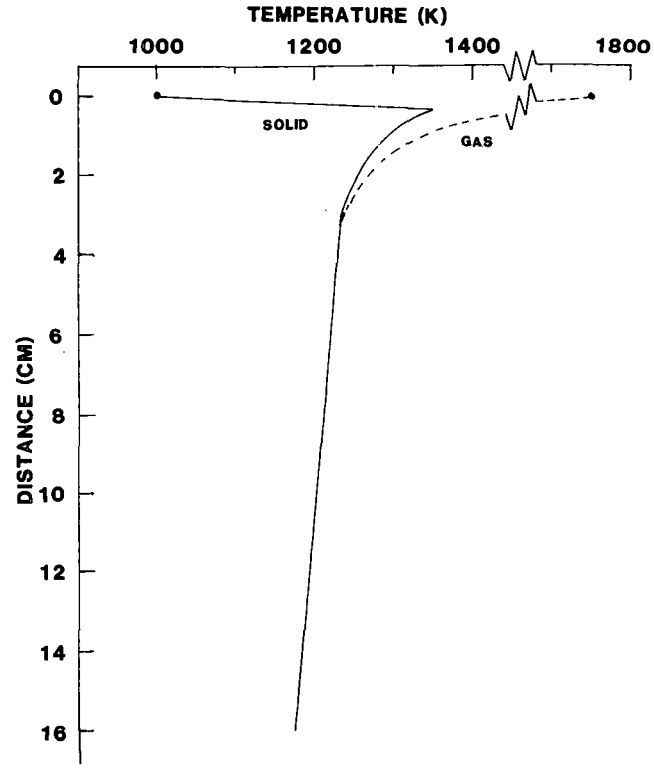

Figure 6. Char Gasification Zone Solid and Gas Temperature Predictions for Oxygen Gasifier with 1/4-in. Wood Chips.